

**Signaling Mechanism in Regulating Vasculogenic Mimicry of
Oral Squamous Cell Carcinoma and Combating with
Phytochemicals at Transcription and Post Transcription Level**

A THESIS

Submitted to

JADAVPUR UNIVERSITY



*in partial fulfillment of the requirements
for the award of the degree of*

DOCTOR OF PHILOSOPHY (Science)

BY

DEPANWITA SAHA

(INDEX NO: 111/19/Life Sc./26)

Department of Signal Transduction and Biogenic Amines

Chittaranjan National Cancer Institute

37, S.P Mukherjee Road, Kolkata -700026

India

DR. NABENDU MURMU, PhD

Senior Scientific Officer, Assistant Director Grade
Head-Dept. of Signal Transduction and Biogenic Amines



Chittaranjan National Cancer Institute

An autonomous body under the Ministry of Health
and Family Welfare, Govt. of India

37, S. P. Mukherjee Road, Kolkata - 700026

Phone: 2475 9313, 2476 5101 (Extn. 322)

Fax: 2475 7606;

Email: nabendu.murmu@cnci.ac.in
nabendu64@gmail.com

CERTIFICATE FROM THE SUPERVISOR

This is to certify that the thesis entitled, “**Signaling Mechanism in Regulating Vasculogenic Mimicry of Oral Squamous Cell Carcinoma and Combating with Phytochemicals at Transcription and Post Transcription Level**” submitted by Ms. Depanwita Saha, who got her name registered on 25th September, 2019 for the award of Ph.D. (Science) degree of Jadavpur University, is absolutely based upon her own work under my supervision and that neither this thesis nor any part of it has been submitted for either any degree/ diploma or any other academic award anywhere before.

Nabendu Murmu 16.02.2023

(DR. NABENDU MURMU)

डॉ० नबेंदु मुरुमु / Dr. Nabendu Murmu Ph.D
वरिष्ठ वैज्ञानिक अधिकारी, सहायक संचालक ग्रेड
Sr. Scientific Officer, Assistant Director Grade
विभाग प्रमुख सिग्नल ट्रांसडक्शन और बायोजेनिक एमाइंस/
Head. Department of Signal Transduction and Biogenic Amines
चितरंजन राष्ट्रीय कैंसर संस्थान
Chittaranjan National Cancer Institute
स्वास्थ्य और परिवार कल्याण मंत्रालय
Ministry of Health & Family Welfare
कोलकाता-700 026 / Kolkata-700 026

DECLARATION

I hereby declare that the thesis entitled, “**Signaling Mechanism in Regulating Vasculogenic Mimicry of Oral Squamous Cell Carcinoma and Combating with Phytochemicals at Transcription and Post Transcription Level**” submitted to Jadavpur University, for the award of Ph.D. (Science) degree, is a record of original research work carried out by me under the supervision of Dr. Nabendu Murmu, Head of the department, Senior Scientific Officer, Assistant Director Grade, Department of Signal Transduction & Biogenic Amines (STBA), Chittaranjan National Cancer Institute, 37, S. P. Mukherjee Road, Kolkata- 700026, India. This work has not been submitted elsewhere for any other degree/ diploma or any academic award.

Place: Kolkata

Depanwita Saha,

Date: 16.02.2023

(DEPANWITA SAHA)

DEDICATION

This thesis is dedicated to my beloved parents

Mrs. Lily Saha

&

Dr. Nerod Chandra Saha

*Who have always been sources of inspiration, encouragement
throughout my entire life, believed in me and motivated me constantly to complete
the work with enthusiasm and determination*

ACKNOWLEDGEMENT

I would like to express my deepest gratitude to my supervisor **Dr. Nabendu Murmu**, Head, Department of Signal Transduction and Biogenic Amines, Chittaranjan National Cancer Institute, Kolkata for giving me the opportunity to work in his lab, providing valuable guidance and feedback throughout my entire journey. His timely advice, meticulous scrutiny, scholarly advice and scientific approach have helped me to a great extent to accomplish the work.

I am extremely grateful to **Dr. Biswanath Majumder**, Oncology Division, Bugworks Research, C-CAMP, Bangalore and **Dr. Pradip K. Majumder**, Department of Cancer Biology, Praesidia Biotherapeutics, 1167 Massachusetts Avenue, Arlington, MA for their valuable suggestions and contributions in planning and designing various aspects of the research work.

A special thanks to **Dr. Neyaz Alam** and **Dr. Sagar Sen**, Department of Surgical Oncology, Chittaranjan National Cancer Institute for providing clinical specimens and **Dr. Saunak Mitra Mustafi**, Department of Pathology, Chittaranjan National Cancer Institute for his valuable clinical insights. I want to thank **Dr. Syamsundar Mandal**, Department of Epidemiology and Biostatistics, Chittaranjan National Cancer Institute for helping with statistical analysis.

I am thankful to **Dr. Jayanta Chakrabarti**, Director of Chittaranjan National Cancer Institute for his support during the entire curriculum.

I had the pleasure of working with my amazing lab members **Dr. Gaurav Das** (DST-INSPIRE Faculty), **Mr. Debarpan Mitra** (SRF), **Dr. Paramita Ghosh**, **Dr. Sayantan Bhattacharyya**, **Dr. Sudipta Ray**, **Dr. Sreyashi Mitra**, **Ms. Rimi Mukherjee** (JRF), **Mr. Debojit Talukdar** (JRF), **Ms. Aritri Bhattacharjee** (JRF), **Mr. Subhabrata Guha** (JRF) and **Mr. Sayandeep Mukherjee** (Project Intern) .

I gratefully acknowledge the funding received towards my PhD from the Science and Engineering Research Board (SERB) and Senior Research Fellowship (SRF) from Indian Council of Medical Research (ICMR), Government of India (Sanction No: 3/2/2/112/2022-NCD-III).

I would like to acknowledge the Doctoral Committee of Jadavpur University for evaluating my work.

Lastly I would be remiss in not mentioning my family members especially my parents (*Mrs. Lily Saha & Dr. Nerod Chandra Saha*), sister (*Dr. Tanusree Saha*) and spouse (*Dr. Rajib Roy*).

Their belief in me has kept my spirits and motivation high during this process.

ABBREVIATIONS

5-FU	-	5-fluorouracil
ACC	-	Adenoid cystic carcinoma
ADCC	-	Antibody dependent cellular cytotoxicity
AJCC	-	American Joint Committee on Cancer
ANOVA	-	Analysis of variance
BCA	-	Bicinchoninic Acid
BM	-	Basement membrane
BPIFB1	-	BPI Fold Containing Family B Member 1
CD-31	-	Cluster of differentiation 31
CDK2	-	Cyclin-dependent kinase 2
CI	-	Confidence interval
C_{max}	-	Maximum concentration
COX2	-	Cyclooxygenase-2
CSC	-	Cancer stem cell
DAB	-	3,3-diaminobenzidine
DFS	-	Disease free survival
DMSO	-	Dimethyl sulfoxide
DR3	-	Death receptor 3
EBV	-	Epstein barr virus
ECM	-	Extracellular matrix
EDTA	-	Ethylenediaminetetraacetic acid

EGFR	-	Epidermal growth factor receptor
EMT	-	Epithelial–mesenchymal transition
EPC	-	endothelial precursor cell
EphA2	-	Erythropoietin producing hepatocellular receptor A2
ERK	-	Extracellular signal-regulated kinase
FAK	-	Focal adhesion kinase
FBS	-	Fetal bovine serum
FC	-	Flow cytometry
FFPE		Formalin Fixed Paraffin Embedded
FGF	-	Fibroblast growth factor
FITC	-	Fluorescein isothiocyanate
HIF-1α	-	Hypoxia inducing factor-1 α
HNC	-	Head and neck cancer
HNSCC	-	Head and neck squamous cell carcinoma
HPV	-	Human papillomavirus
HR	-	Hazards radio
HRP	-	Horseradish peroxidase
IFS	-	Immunofluorescence
IHC	-	Immunohistochemistry
IL-17F	-	Interleukin-17F
LGR5	-	Leucine-rich repeat-containing G-protein coupled receptor 5
LMP1	-	Latent membrane protein 1
LSCC	-	Laryngeal squamous cell carcinoma

MDSC	-	Myeloid derived suppressor cell
miRNA	-	Micro RNA
MMP	-	Matrix metalloproteinase
mRNA	-	Messenger RNA
MTDH	-	Metadherin
NAC	-	N-Acetyl cysteine
NAD	-	Nicotinamide adenine dinucleotide
NEAT1	-	Nuclear Enriched Abundant Transcript 1
NFκB	-	Nuclear factor kappa B
NPC	-	Nasopharyngeal carcinoma
OS	-	Overall survival
OSCC	-	Oral squamous cell carcinoma
PAS	-	Periodic acid schiff
PBS	-	Phosphate buffer saline
PCNA	-	Proliferating cell nuclear antigen
PD	-	Pharmacodynamics
PECAM	-	Platelet endothelial cell adhesion molecule
PI	-	Propidium iodide
PI3-K	-	phosphatidylinositol-3-kinase
PK	-	Pharmacokinetics
PMD	-	Potentially malignant disorder
PPI	-	Protein protein interaction
PVDF	-	Polyvinylidene difluoride

ROS	-	Reactive oxygen species
SACC	-	Salivary adenoid cystic carcinoma
SDS-PAGE	-	Sodium dodecyl sulfate-Polyacrylamide gel electrophoresis
SIRT1	-	Sirtuin 1
SNSCC	-	Sinonasal squamous cell carcinoma
SOX7	-	SRY-box 7
TAZ	-	Tafazzin
TBS	-	Tris Buffer saline
TF	-	Tissue factor
TFPI	-	Tissue factor pathway inhibitor
TICs	-	tumor initiating cells
TNM	-	Tumor node metastasis
TS	-	Tumor stromal interface
TUNEL	-	Terminal deoxynucleotidyl transferase dUTP nick end labeling
VE-cadherin	-	Vascular endothelial cadherin
VEGF	-	Vascular endothelial growth factor
VEGFR	-	Vascular endothelial growth factor receptor
VM	-	Vasculogenic mimicry
WB	-	Western Blot
WHO	-	World Health Organization

TABLE OF CONTENTS

Content	Page No
<i>Acknowledgement</i>	iii
<i>List of Abbreviations</i>	v
<i>Abstract</i>	1-5
<i>Chapter 1: Introduction</i>	6-11
<i>Chapter 2: Review of Literature</i>	12-40
2.1. Histology and potentially malignant changes in Oral squamous cell carcinoma	13
2.2. Structural evolution of Vasculogenic mimicry	14
2.3. Molecular phenotype in regulating vasculogenic mimicry	16
2.4. Signaling pathways and molecular factors associated with VM in head and neck cancer	17
2.4.1. Role of EMT and Cancer stem (like) cell (CSC)	19
2.4.2. JAK-2/STAT-3 pathway	20
2.4.3. EBV-LMP1/ VEGFA axis	21
2.4.4. Foxq1	21
2.4.5. BPIFB1	22
2.4.6. MTDH/VEGFA-165/Flt-1 axis	22
2.4.7. Myeloid derived suppressor cells (MDSC)	23
2.4.8. Role of miRNAs	23
2.4.8.1. miR-124	23
2.4.8.2. miR195-5p	23
2.4.8.3. miR-125a	24
2.4.9. Additional molecular markers regulating VM in Head and Neck Cancer	24
2.5. Chemotherapy against oral cancer	26
2.5.1. Paclitaxel	26
2.5.1.1. Chemical structure of Paclitaxel	26
2.5.1.2. Mechanism of action of Paclitaxel	27
2.5.1.3. Side effects of Paclitaxel	28
2.6. Phyto-chemicals against cancer treatment	29
2.6.1. Therapeutic potential of phytochemicals targeting VM	30
2.6.2. Lupeol	31

2.6.2.1. Chemical structural analysis of Lupeol	32
2.6.2.2. Mechanistic activity of Lupeol against different cancer models	33
2.6.2.3. Pharmacological and toxicity study of Lupeol	34
2.7. Therapeutic strategies targeting VM in Head and Neck Cancer	36
2.7.1. Niclosamide	36
2.7.2. Melatonin	37
2.7.3. Curcumin	37
2.7.4. Silibinin	38
2.7.5. Ginsenoside Rg3	39
2.7.6. Axitinib	39
Chapter 3: Objective of the thesis	41-43
Chapter 4: Scope of the thesis	44-47
Chapter 5: Evaluation of the functional association and prognostic significance of vasculogenic mimicry (VM) with HIF-1 α induced EphA2 signaling cascade, EMT and CSC markers in oral squamous cell carcinoma (OSCC)	48-76
Chapter 6: Role of hypoxia in inducing vasculogenic mimicry in oral squamous cell carcinoma via HIF-1 α /EphA2/Laminin-5 γ 2 signalling cascade	77-92
Chapter 7: Evaluation of synergistic effect of Lupeol and Paclitaxel in attenuating vasculogenic mimicry in <i>in vitro</i> and <i>ex vivo</i> oral squamous cell carcinoma	93-126
Chapter 8: Summary & Conclusion	127-130
Bibliography	131-183
Conferences/Workshops attended	184-186
List of Publications	187-189

LIST OF TABLES

Table No	Table Name	Page No
1	Molecular markers regulating VM in different subtypes of Head and Neck cancer	18
2	Head and Neck cancer associated signaling molecules regulating VM in several other types of cancers	25
3	Evidences of anti-tumor efficacy of Paclitaxel in Oral Cancer	28
4	Phytochemicals targeting VM related proteins in different cancer models	30
5	Lupeol content in Different fruits and plants	32
6	Mechanism of action of Lupeol in various cancer models	33
7	IHC score calculation and determination of inter-observer and inter-method agreement	55
8	Demographic and clinicopathological profile of OSCC patients	59
9	Correlation of VM and HIF-1 α with the molecular markers involved in EphA2/ Laminin5 γ 2 cascade, EMT and CSC phenomenon in OSCC patients	65
10	Association between the expression of VM, HIF-1 α and Laminin-5 γ 2 with the clinico-pathological characteristics of oral squamous cell carcinoma (OSCC) patients	67
11	Association between the expression of VM-HIF-1 α dual expression and VM-Laminin-5 γ 2 dual expression with the clinico-pathological characteristics of oral squamous cell carcinoma (OSCC) patients	68
12	Results of univariate analyses of disease free survival (DFS) and overall survival (OS) time	70
13	Assessment of prognostic factors of disease free survival (DFS) and Overall survival (OS) by univariate analysis of Cox- Proportional Hazards model	73
14	Assessment of prognostic factors of Disease Free Survival (DFS) and overall survival (OS) by multivariate analysis of Cox- Proportional Hazards model	74
15	Determination of effective combinatorial dose of Lupeol and Paclitaxel using the method of Chou et al, 2010	106
16	Demographic and clinicopathological profile of OSCC patients for explant culture	119

LIST OF FIGURES

Figure No	Figure Name	Page No
1	Structural differentiation among VM, conventional blood vessel and lymph vessel	16
2	Overview of the signaling crosstalk implicated in the formation of VM networks in different subtypes of head and neck cancers	18
3	Chemical structure of Paclitaxel	27
4	Chemical structure of Lupeol	33
5	Proposed VM inhibitors with the approved standard of care chemotherapeutic drugs against Head and Neck cancers	39
6	Schematic representation of patients' selection criteria	52
7	Normalization of the digital image analysis with the pathologists' manual analysis	57
8	CD31-PAS staining showing VM (with different score) and endothelial structures in OSCC.	61
9	Representative images for immuno-histochemical status (coupled with PAS staining) of HIF-1 α , VE-Cadherin, EphA2, pERK1/2, MMP2 and Laminin-5 γ 2 in VM positive and VM negative OSCC cohorts	63
10	Representative images for immuno-histochemical status (coupled with PAS staining) of E-Cadherin, Vimentin, Snail, Twist and CD133 in VM positive and VM negative OSCC cohorts	64
11	Kaplan Meir analysis of the disease free survival (DFS) rate of patients with OSCC in relation to differential expressional status of VM, HIF-1 α , Laminin-5 γ 2, VM- HIF-1 α dual status and VM- Laminin-5 γ 2 dual status	71
12	Kaplan Meir analysis of the overall survival (OS) rate of patients with OSCC in relation to differential expressional status of VM, HIF-1 α , Laminin-5 γ 2, VM- HIF-1 α dual status and VM- Laminin-5 γ 2 dual status	72
13	Standardization of hypoxia induction and dose of HIF-1 α siRNA in OSCC cell lines.	85
14	siRNA against HIF-1 α inhibits vasculogenic mimicry formation in vitro	86
15	siRNA against HIF-1 α inhibits the expression of vasculogenic mimicry related genes in vitro	87
16	siRNA against HIF-1 α inhibits transwell migration, invasion, sphere	88

	formation in vitro	
17	siRNA against HIF-1 α inhibits the expression of EMT and CSC related genes in vitro	89
18	Effect of Lupeol and paclitaxel in hypoxia induced cellular proliferation in-vitro	107
19	Effect of Lupeol and paclitaxel in hypoxia induced colony formation and wound healing potential in vitro	108
20	Effect of Lupeol and paclitaxel in inducing apoptosis in-vitro	110
21	Effect of Lupeol and paclitaxel in hypoxia induced vasculogenic mimicry in vitro	111
22	Effect of Lupeol and paclitaxel in the expression of hypoxia induced vasculogenic mimicry related genes in vitro	113
23	Effect of Lupeol and Paclitaxel in the expression of HIF-1 α using Immunofluorescence staining and flow cytometry	114
24	Effect of Lupeol and paclitaxel in hypoxia induced migration, invasion, sphere formation in vitro	115
25	Effect of Lupeol and paclitaxel in hypoxia induced EMT and CSC related genes in vitro	116
26	Effect of Lupeol and Paclitaxel in the expression of E-Cadherin, Vimentin and CD133 using Immunofluorescence	117
27	Effect of Lupeol and paclitaxel in regulating the expression of proliferating marker (Ki-67) and apoptotic marker (Caspase-3) in Ex-vivo platform of OSCC	119
28	Effect of Lupeol and paclitaxel in regulating the expression of VM associated genes in Ex-vivo platform of OSCC	120
29	Effect of Lupeol and paclitaxel in regulating the expression of VM associated EMT and CSC markers in Ex-vivo platform of OSCC	121
30	Model depicting the involvement of HIF1 α and key interacting partners in VM and intervention by Lupeol and Paclitaxel	123

Abstract

Background

Vasculogenic mimicry (VM) is an angiogenesis independent alternative mechanism of tumor perfusion through generating blood containing pseudo-vascular channels, associated with high tumor grade, metastasis, chemo-resistance and prone to poor prognosis in genetically dysregulated and highly aggressive cancers including oral squamous cell carcinoma (OSCC). Understanding the underlying mechanism associated with VM and combating with phytochemicals may help scientists and clinicians for better prognosis and development of new anticancer therapy against OSCC.

Objectives

Our work aims to solve three major problems in oral oncology.

The *first objective* of our study is to demonstrate the functional association of vasculogenic mimicry with HIF-1 α induced EphA2 signaling cascade in correlation with the clinicopathological traits in oral squamous cell carcinoma (OSCC) and subsequently to evaluate their orchestrated expression as promising prognostic marker which will offer a novel therapeutic target for OSCC which will be helpful to understand responsiveness of tumor to different drugs in near future.

Our *second objective* focused on the in vitro mechanistic exploration of hypoxia in facilitating Vasculogenic mimicry in human oral squamous cell carcinoma cells through HIF-1 α /EphA2/Laminin 5 γ 2 signaling which may be a potential therapeutic target against the malignant phenotypes of OSCC.

Our *third objective* emphasized on the evaluation of the possible mitigating properties of phytochemical Lupeol in combination with a common chemo-therapeutic drug Paclitaxel in regulating the pseudo-vascularization in hypoxic conditions using different OSCC cell lines and

patient derived ex vivo platform which may emerge a new treatment strategy for aggressive oral cancers.

Materials and Methods

Our study includes 116 clinically diagnosed OSCC patients from Chittaranjan National Cancer Institute, Kolkata. The formalin fixed paraffin embedded (FFPE) blocks were prepared from the surgically resected OSCC tumor specimens obtained from the patients with ethical consent. From the FFPE blocks the VM structures were identified using CD31/PAS immunohistochemistry and the total patients were stratified into VM positive (VM+) and VM negative (VM-) cohorts. Characterization of VM associated signaling molecules including HIF-1 α , EphA2, pERK1/2, MMP2, Laminin 5 γ 2 were done using immunohistochemistry to compare the VM+ and VM- cohorts followed by their correlation with the clinico-pathological parameters and survival end points of OSCC cohorts. Kaplan Meir and Cox regression analysis were performed to assess the survivability and prognostic implications. For the in vitro studies two OSCC cell lines UPCI:SCC154 and UPCI:SCC090 were chosen and the hypoxic condition was stimulated by incubating cells in a hypoxic chamber flushed with a gas mixture of 1% O₂/ 5% CO₂/94%N₂. 3D matrigel mediated tube forming assay was performed to evaluate the VM forming potential of OSCC cell lines Transfection with HIF-1 α siRNA resulted in gene knockdown. The in vitro proliferation, invasion/migration and stemness property were detected using MTT, transwell migration and sphere forming assays with the treatment of the phytochemical Lupeol and conventional chemotherapeutic drug Paclitaxel. Annexin-V/PI staining was used to detect apoptosis. The expression levels of molecular markers were analyzed by immunohistochemistry, western blot and real time PCR. Patient derived tumor explant culture was established to manifest ex vivo OSCC model.

Results

Our investigations with the patient samples indicated that based on the CD31/PAS staining, vasculogenic mimicry (VM) was identified in 29.31% of OSCC tissue specimens and the total patient population was stratified into VM+ and VM- cohorts. The presence of VM had a significant correlation ($P < 0.0001$) with the expression of HIF-1 α as well as its downstream players involved in ECM remodeling (VE-Cadherin, EphA2, pERK1/2, MMP2 and Laminin-5 γ 2), EMT and cancer stemness which was also reflected by their significant expressional alterations in the VM + and VM- cohorts. Additionally, the expression of HIF-1 α , Laminin-5 γ 2, and VM-HIF-1 α and VM-Laminin-5 γ 2 was strongly correlated with the TNM stage, lymph node metastasis, tumor grade, and primary tumor size but not with the patients' age, gender, or cigarette or alcohol using habits. It is also noteworthy that the disease-free survival (DFS) and overall survival (OS) rates were significantly lower in the VM-HIF-1 α and VM-Laminin-5 γ 2 double positive cohorts. Interestingly the individual expression of VM, Laminin-5 γ 2 and their subsequent dual expression also proved to be independent prognostic indicators for DFS and OS in OSCC patients.

In the next part of the work, we have shown that the extracellular matrix (ECM) remodeling and EMT traits that are mechanistically related to the propensity for VM formation were enhanced by the hypoxia-induced overexpression of HIF-1 α . Experimental HIF-1 α stimulation significantly changed the expression of EMT and CSC markers (E-Cadherin, Vimentin, Snail, Twist, CD133) and improved cell migration/invasion and spheroid formation effectiveness. The disruption of matrigel-mediated tube formation and Laminin-5 γ 2 expression that followed the targeted reduction of HIF-1 α caused by siRNA transfection was synchronized with the down-regulation of VE-Cadherin, total and phosphorylated (S-897) EphA2, pERK1/2,

and MMP2. Next, we discovered that Paclitaxel and Lupeol together caused in vitro apoptosis with alteration of VM-associated phenotypes and pertinent molecular signalling. In a patient-derived tumour explant culture model of oral malignancy, we further confirmed the effectiveness of this unique interventional strategy. By inhibiting the HIF-1/EphA2/Laminin5/2 cascade, the ex vivo tumour model replicated the in vitro anti-VM capability of the Lupeol-Paclitaxel combination.

Conclusion

In conclusion our research work revealed that the expression of HIF-1 α and the extracellular matrix protein Laminin-5 γ 2 coordinated with VM are significantly associated with tumor grade, primary tumor size, lymph node metastasis and TNM stage. Co-expression of vasculogenic mimicry with HIF-1 α and Laminin-5 γ 2 significantly correlates with the decreased disease free and overall survival in OSCC patients with the more specific emphasis on VM- Laminin-5 γ 2 duality as an independent prognostic biomarker for OSCC. The study also concluded HIF-1 α as a key regulator of vasculogenic mimicry formation by modulating EphA2-Laminin 5 γ 2 cascade in the hypoxic microenvironment of OSCC and being a phytochemical with no side effects whatsoever Lupeol in synergistic association with Paclitaxel will emerge as a new direction of cancer treatment for OSCC progression and after series of clinical trials this potential drug combination may be used as an effective and definitive therapeutic modality against OSCC.

Chapter 1

Introduction

Oral squamous cell carcinoma (OSCC) is specifically defined as the heterogeneous group of malignant neoplasm occurring as the ulcero-proliferative lesions originating from the epithelium of mucosal surface affecting the oropharynx, together with the lips, cheeks, tongue, sinuses, hard and soft palate, and the base of the mouth (Borse et al., 2020; PIRES et al., 2013; Usman et al., 2021). The most common anatomical sites include gingivobuccal sulcus of mandible followed by tongue and floor of mouth (Deshmukh & Shekar, 2021). It is well known that some potentially malignant conditions (PMDs) such as lichen, dyskeratosis congenita, inflammatory oral submucosa, fibrosis, erythroplakia, leukoplakia, candidal leukoplakia, and leukoplakia precede the onset of OSCC. (Mortazavi et al., 2014; Mustafa et al., 2021; Warnakulasuriya et al., 2021). OSCC contributes more than 90% of oral cancer subtypes and worldwide it ranks 6th among all types of cancers (Borse et al., 2020; Puneeta et al., 2022). Globally it accounts for over 6,50,000 new cases and 3,30,000 deaths annually (Sung et al., 2021). About one-fourth of all cases worldwide roughly in India, there are 77,000 new cases and 52,000 fatalities per year (Basak & Ara, 2022; Gupta, n.d.; Kshersagar et al., 2020). In India, oral cancer is a much bigger worry than it is in the west since over 70% of cases are reported to be at an advanced stage. Long term use of tobacco in smoke and smokeless form, chewing of areca nut, betel quid, alcohol consumption, human papillomavirus (HPV) infection (for oropharyngeal cancer) are the major risk factors associated with OSCC (Dhull et al., 2018; Maasland et al., 2014). During the past few decades the overall survival rate (OS) of oral cancer didn't improve significantly due to the detection in the advanced age followed by local lymph node metastasis and/or uncontrolled post-operative recurrence (Ferlito et al., 2001; Nigro et al., 2017).

It is widely acknowledged that angiogenesis is a critical process for tumor invasion, metastasis and recurrence (Teleanu et al., 2019), however the routine anti-angiogenic therapy is still

unsatisfactory for patients' survival due to the complex tumor vasculature as well as the alternative mechanism of re-vascularization (Vasudev & Reynolds, 2014). Traditionally solid tumors require sufficient blood supply for tumor growth and accessibility to oxygen and nutrients. The term "vasculogenic mimicry" was initially put forth in this context by (Maniotis et al., 1999) in genetically dysregulated and aggressive uveal melanoma cells which facilitates tumor perfusion through generating blood containing pseudo-vascular channels de-novo, independent of surrounding endothelial blood vessels. VM has been identified as lumen like small vesicular structures (surrounded by tumor cells on the non-luminal side) which is Periodic acid-Schiff (PAS) positive but CD31/CD34 negative (Maniotis et al., 1999; B. Sun et al., 2004, 2006, 2008; Valdivia et al., 2019). Vasculogenic mimicry has been described in two distinctive types including tubular type (resembles with endothelial cell lined blood vessels) and patterned matrix type (does not resemble with blood vessels morphologically). The pseudo-vascular structures have since been shown to be rich in several glycoproteins including type I, IV, VI collagen, fibronectin, laminin and glycosaminoglycans specially heparan sulfate proteoglycan. In oral squamous cell carcinoma (OSCC) tissue specimens the VM structure was observable in linear, tubular and network pattern (Wang et al., 2018). The absence of CD31/CD34 staining eliminated the involvement of endothelial cells on the luminal side of the VM structures. In some cases the presence of red blood cells were observed in the lumen (Liu et al., 2008) but no microscopic field with inflammatory infiltrates, necrosis and hemorrhage near VM structures was considered for evaluation (Wu et al., 2017). VM is associated with the worse prognostic clinico-pathological attributes such as tumor grade, tumor size, lymph node metastasis and TNM stage considering it as an independent prognostic factor for overall and disease free survival rate in various cancer models including OSCC considering VM as a new molecular target for

therapeutic intervention. Numerous research shed new light on the molecular complexity of VM involving different underlying potential mechanism such as Epithelial–mesenchymal transition (EMT) (Liu et al., 2016), Cancer stem cells (CSCs) (Murugesan et al., 2021; Seftor et al., 2001) and various molecular pathways which include vascular (VE-Cadherin, EphA2, VEGFR) (Hendrix et al., 2003; Hess et al., 2007; Koch et al., 2011; Wang et al., 2018), Embryonic/stem cells (Nodal, Notch4, Wnt) (Gong et al., 2016; Hardy et al., 2010), hypoxia (HIF-1 α , Twist1) (Gustafsson et al., 2005; Li et al., 2016; Sun et al., 2010) tyrosine kinase (FAK, PI3-K) (Chiablaem et al., 2014), extracellular matrix (ECM) remodelers including MMPs, Laminin5 γ 2, tissue factor (TF), tissue factor pathway inhibitor (TFPI) promoting cellular invasion, migration matrix remodeling and the aggressive metastatic phenotypes (Ruf et al., 2003; Seftor et al., 2001).

Under tumor microenvironment, hypoxia plays a pivotal role in different cancer types including OSCC through contributing vast oxygen and energy consumption of tumor cells (Emami Nejad et al., 2021; Muz et al., 2015). When the volume of solid tumor exceeds 2mm³, the cells in the region are exposed to hypoxic environment due to the starvation of oxygen and nutrients. Hypoxia inducing factor-1 (HIF-1) is one of the most critical regulatory molecules orchestrating tumor metabolism, immune escape, angiogenesis and cell survival (Jing et al., 2019; Walsh et al., 2014). Under hypoxia, α subunit of HIF-1 (HIF-1 α) can be translocated into nucleus, where it combines with the β subunit of HIF-1 to form HIF-1 heterodimer (Ziello et al., 2007). One of the major drivers of VM has been attributed to hypoxia in several cancer models (Du et al., 2014; Jin-lu et al., 2011; Li et al., 2017; Mao et al., 2013; Sun et al., 2007), however, very limited work has been focused on oral squamous cell carcinoma (OSCC). VE-cadherin, Ephrin type-A receptor 2, platelet endothelial cell adhesion molecule (PECAM), vascular endothelial growth

factor (VEGF) (Saito et al., 2015) and focal adhesion kinase (FAK) up-regulations are followed by the induction of VM channel-forming cells by HIF-1 α in hypoxic conditions. This cascade of cellular responses leads to the formation of VM channels by invasive cancer cells through matrix metallo-proteases (MMPs) (Ju et al., 2014). When exposed to a hypoxic condition, cancer cells start expressing the HIF (Hypoxia Inducing Factor) -the protein which further activates the Ephrin family of proteins (Zhou & Sakurai, 2017). The entire mechanism is believed to be triggered by two major signaling proteins i.e. ERK $\frac{1}{2}$ and PI3-K. Once these two proteins get activated via various upstream signaling axis including the VE- Cadherin, FGF and VEGF, both of them are able to activate pro-MMP 14 to active MMP-14 (Miao et al., 2001) which, in turn cleaves Laminin and creates the vascular like structures (Delgado-Bellido et al., 2017).

In patients with locally advanced primary OSCC often get chemotherapeutic treatment or ionizing radiation at a high dose (Ko & Citrin, 2009; Minhas et al., 2017). It is a well established fact that these chemotherapeutic drugs and radiotherapy come with their limitations and adverse side effects which may lead to poor prognosis of the patient (Mittal et al., 2015; Nguyen et al., 2006). This necessitates developing alternative strategies that may overcome chemotherapy resistance and prove to be more effective while minimizing toxicity.

Photochemical, a diverse group of naturally occurring metabolites, have been reported to be effective as anticancer drugs with limited toxicity to normal cells of the body. They act primarily by suppressing abnormal cell proliferation, inducing apoptosis and inhibiting metastasis and angiogenesis (Shu et al., 2010). Lupeol is a naturally occurring triterpene (phytosterol) that is pharmacologically active and can be found in a variety of fruits and vegetables (e.g., olive, mango, strawberry, and grapes) as well as in a number of therapeutic plants (Ojewole, 2005). In mouse melanoma and human leukaemia cells, Lupeol therapy has been shown to induce tumor

differentiation and decrease tumor growth (Hata et al., 2002; Aratanechemuge et al., 2004). The effect of Lupeol as an effective EGFR signaling inhibitor in OSCC has been studied by Rauth et al., 2016 to implicate its role in triggering antitumor efficacy (Rauth et al., 2016). A very recent study by (Bhattacharyya et al., 2019) also indicated that Lupeol can become a proficient agent in treating the progression of murine melanoma by inhibiting vasculogenic mimicry. The effect of Lupeol on the hypoxia induced and ephrinA2 pathway mediated VM has not been evaluated in any cancer model yet. So our study also aims to establish Lupeol as an alternative chemotherapeutic drug with no side effects and more efficacies in treating aggressive oral cancers. We further delineated the mechanistic consequences emanating from the synergistic cooperation of Lupeol and Paclitaxel in the coordinated regulation of HIF-1 α induced EphA2 pathway and epithelial mesenchymal transition (EMT) and cancer stemness in OSCC cell lines as well as in patient-derived ex vivo system.

Chapter 2
Review of Literature

2.1. Histology and potentially malignant changes in oral squamous cell carcinoma

Oral squamous cell carcinoma may be defined as the invasive neoplasm of the epithelial layer with varying degrees of differentiation. Tobacco and alcohol abuse are the predominant risk factors of oral squamous cell carcinoma (OSCC) (Mayne et al., 2009). In India and other South-east Asian countries smokeless-tobacco or chewing tobacco is a major cause of OSCC specially when consumed in the form of betel-quid with areca nut and slaked lime (Gupta et al., 1996). Human papillomavirus infection is also responsible for a fraction of OSCCs (Gillison et al., 2000). Histological grading of neoplasm based on cellular differentiation, has been a traditional tool used by pathologists for descriptively categorizing OSCCs and this is known as Broder's classification (Akhter et al., 2011). The tumors are graded as well differentiated (containing <25% undifferentiated cells) having abundant pink cytoplasm with proper nuclear to cytoplasmic ratio, mild to moderate atypia, well developed keratinisation, moderately differentiated (<50% undifferentiated cells) showing focal keratinization, poorly differentiated (<75% undifferentiated cells) containing no/minimal keratinization, high nuclear to cytoplasmic ratio, markedly atypical or anaplastic cells. Some scientists believed that well-differentiated oral neoplasm usually metastasizes to regional lymph nodes while the poorly differentiated type is more aggressive and causes not only regional metastasis but subsequently distant metastasis as well (Fortin et al., 2001). But it has been well established that there is lack of correlation between degree of differentiation and prognosis of the carcinoma mainly because OSCCs comprise of a heterogeneous population of cells with marked differences in invasiveness, differentiation and metastatic potential (Anneroth et al., 1987). The TNM clinical classification (T, tumor size; N, regional lymph node compromise; M, metastasis) authorized by the American Joint Committee on Cancer (AJCC) is mainly used for prognostic evaluation.

Pre-neoplastic alterations, such as mild, moderate, and severe dysplasia, can occur before the onset of an invasive carcinoma and are distinguished from reactive epithelial changes, such as hyperkeratosis, hyperplasia, and acanthosis, by their histological appearance (Wang et al., 2009; Rivera & Venegas, 2014; Sagheer et al., 2021). Oral cancer develops from an epithelial dysplasia and is defined by abnormal squamous cell proliferation on the epithelial layer's surface, which leads to the breakdown of the subepithelial basement membrane (BM). Local devastation and distant invasion through metastasis are brought about by BM degradation. The epithelial cells in the islets and cords invade the underlying tissue locally (Fuentes et al., 2012). Similar to how neoplastic tissue architecture and healthy epithelium are correlated with neoplastic tissue, the ability to metastasize is directly correlated with the differential grade of tumor cells.

2.2. Structural evolution of Vasculogenic mimicry

The growth of solid tumors depends on vascular networks to supply blood, nutrients and oxygen (Nishida et al., 2006; Ribatti et al., 1999). Conventionally, sprouting angiogenesis was considered to be the exclusive route of tumor vascularization (Hillen & Griffioen, 2007). However, over the years it has been accepted that tumors have several other mechanisms of neo-vascularization including endothelial precursor cells (EPCs), Intussusceptions or vessel splitting, Vessel cooption and Vasculogenic mimicry (VM) (Belotti et al., 2021; Dunleavey & Dudley, 2012). In 1999, Vasculogenic mimicry was first identified by (Maniotis et al., 1999) in highly aggressive and genetically dysregulated melanoma cells to describe their unique ability to form vascular like matrix embedded networks containing plasma and red blood cells without the involvement of endothelial cells. The term “Vasculogenic mimicry” was coined because “vasculogenic” indicates formation of pseudovascular channels, not from the pre-existing vessels and in spite of not being true blood vessels they mimic the function of blood vessels by

distributing plasma and red blood cells, hence the term “mimicry” has been devised (Folberg & Maniotis, 2004). Several matrix proteins including collagens IV and VI, laminin, heparan sulfate proteoglycan have been identified in this pseudo vascular architecture (Fernández-Cortés et al., 2019; Luo et al., 2020). Although angiogenesis, lymph vessels and VM share the fluid conducting features, VM vessels exhibit some unique features in comparison with traditional blood vessels and lymph vessels. Both the blood vessels and lymph vessels contain a single layer of endothelial cells surrounding the inner layer of basement membrane (luminal side), where as the VM structures contain cancer cells surrounding to the non-luminal side of glycoprotein rich matrix (Valdivia et al., 2019). Two unique subtypes of VM have been identified, including tubular type and patterned matrix type. While the patterned matrix type of VM has tumour cells and tissue that are wrapped in several PAS-positive matrix proteins like laminin, heparan sulphate proteoglycan, and collagens IV and VI, the tubular type of VM has tubular channels lined by tumor cells rather than endothelial cells and covered by secretory glycoprotein. VM has been identified as a lumen like small vesicular structure (surrounded by tumor cells on the non-luminal side) which is PAS positive but CD31/CD34 negative (Maniotis et al., 1999; Valdivia et al., 2019; Sun et al., 2004, 2006, 2008). In oral squamous cell carcinoma (OSCC) tissue specimens the VM structure was observable in linear, tubular and network pattern (Wang et al., 2018). The absence of CD31/CD34 staining eliminated the involvement of endothelial cells on the luminal side of the VM structures. In some cases the presence of red blood cells were observed in the lumen (Liu et al., 2008) but no microscopic field with inflammatory infiltrates, necrosis and hemorrhage near VM structures was considered for evaluation (Wu et al., 2017). In Laryngeal squamous cell carcinoma (LSCC), Wang et al., 2010 and Lin et al., 2012 have detected VM structures where the PAS positive substances lining the VM channels form a

basement membrane like structure. The review of Salem & Salo, 2021 and Hujanen et al., 2021 evaluated a comprehensive phenotypic characterization of VM in the aggressive HNSCC tumors. It has been also well established by several groups of investigators that VM is associated with the worse prognostic clinico-pathological attributes such as tumor grade, tumor size, lymph node metastasis and TNM stage (Wang et al., 2010; Wang et al., 2018; Wu et al., 2017) considering it as an independent prognostic factor for overall and disease free survival rate specifically in OSCC and LSCC. The systemic review and meta-analysis by Hujanen et al., 2020 assessed the prognostic implications of VM on the overall survival (OS) and other survival endpoints with its correlation with the clinico-pathological characteristics in different HNSCC models confirming VM as a new molecular target for therapeutic intervention.

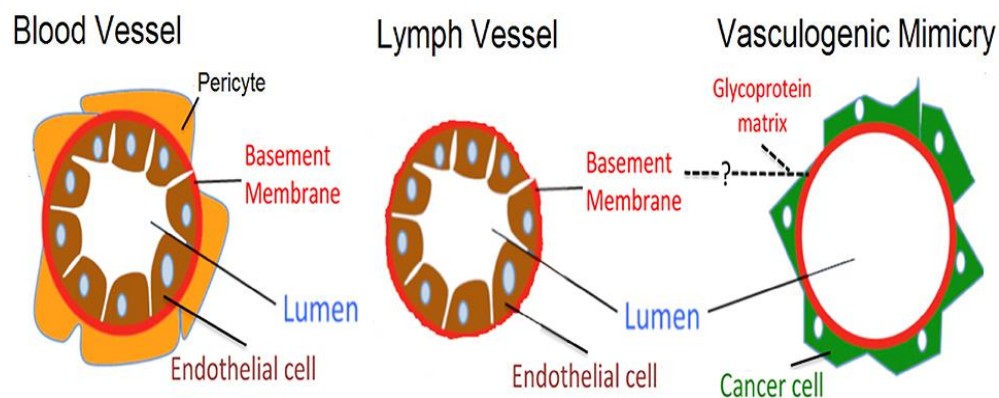


Figure 1: Structural differentiation among VM, conventional blood vessel and lymph vessel (adapted from Valdivia et al., 2019)

2.3. Molecular phenotype in regulating vasculogenic mimicry

Cancer metastasizes to other parts of the body in order to evade the hostile environment within the tumor mass created by hypoxia. When exposed to a hypoxic condition, cancer cells start expressing the HIF (Hypoxia Inducing Factor), the protein which further activates the Ephrin family of proteins (Hess et al., 2007). The entire mechanism is believed to be triggered by two major signaling proteins i.e. ERK $\frac{1}{2}$ and PI3-K. Once these two proteins get activated via various

upstream signaling axis including the VE- Cadherin, FGF and VEGF, both of them are able to activate pro-MMP 14 to active MMP-14 (Davis et al., 1994) which, in turn cleaves Laminin and creates the vascular like structures. Typically, the cell-cell adhesion feature of normal epithelial cells is extremely stable. The result is significant because tyrosine-phosphorylated EphA2 negatively affects cell growth and invasion and binds ligands that are attached to the cell membrane (Zantek et al., 1999; Zelinski et al., 2001; Miao et al., 2000, 2001; Zschiesche et al., 1997). In cancerous cells, things change drastically. Cancer cells commonly have unstable intercellular connections, which reduces the duration and intensity of EphA2 ligand binding (Ben-Ze'ev et al., 1994; Zelinski et al., 2001). As a result, EphA2 is typically not tyrosine phosphorylated in cancerous cells. Notably, this EphA2 still has enzymatic function, but the unphosphorylated EphA2 encourages tumor cell proliferation, invasion, and survival (rather than inhibiting these processes) (Pratt & Kinch, 2003).

2.4. Signaling pathways and molecular factors associated with VM in head and neck cancer

The narrative review of Yue et al., 2021 emphasized on the effect of Epstein Barr virus, immune cells in VM formation along with the involvement of a few molecular markers including HIF-1 α , EphA2, JAK-2/STAT3 where as our review incorporated several other recent articles to portray a more comprehensive interconnected signaling axis including crosstalk among more diversified molecular markers regulating VM formation in different subtypes of HNC. The regulatory mechanism of VM proposed by several groups of investigators in different HNC subtypes has been described below and outlined in Figure 1 and Table 1.

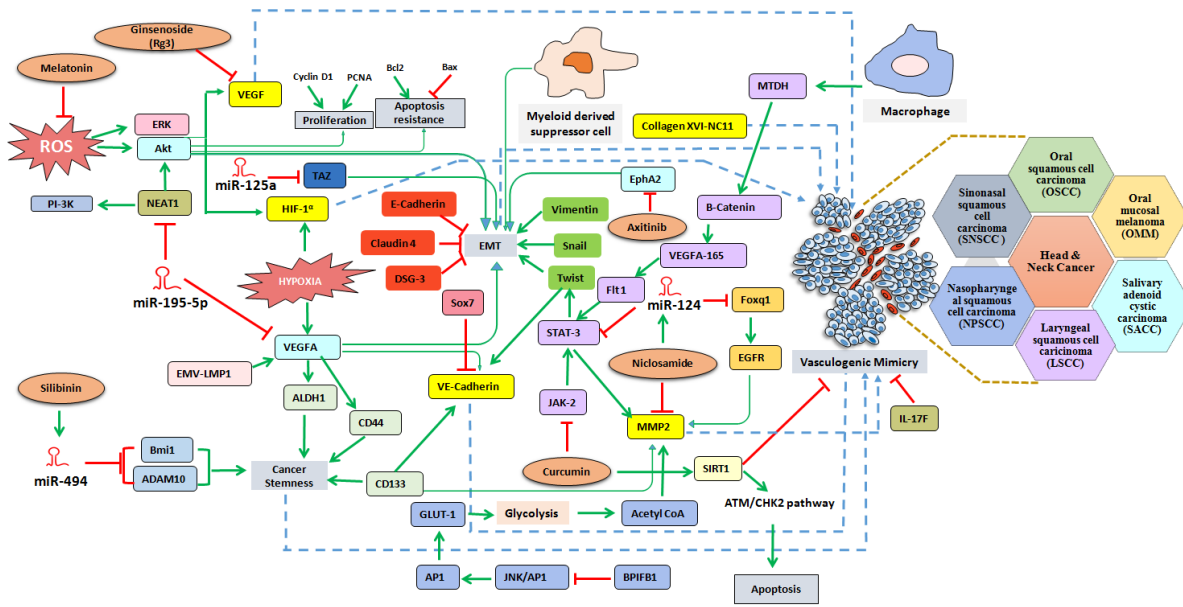


Figure 2: Overview of the signaling crosstalk implicated in the formation of VM networks in different subtypes of head and neck cancers

Table 1: Molecular markers regulating VM in different subtypes of Head and Neck cancer

Molecular regulators	Molecular target	Types of HNC	Effect on VM formation	References
	EMT associated molecules			
EphA2	including E-cadherin, vimentin, Twist, Claudin4, DSG3	HNSCC	Promote	Wang et al., 2014
Mac-MTDH	VEGFA-Fit1	HNSCC	Promote	Liu et al., 2021
Collagen XVI-NC11	VEGFR1, VEGFR2, uPAR	OSCC	Promote	Bedal et al., 2015
	EMT associated molecules			
MDSC	including E-cadherin, vimentin, N-Cadherin, Twist, Snail, Slug	OSCC	Promote	Pang et al., 2020
IL-17F	-	OSCC	Inhibit	Almahmoudi et al., 2021
SOX-7	VE-Cadherin	OSCC	Inhibit	Hong et al., 2021
Hypoxia/ HIF-1α	VEGFA	SACC	Promote	Wang et al., 2019

CD133	VE-Cadherin, MMP2, MMP9	SACC	Promote	Wang et al., 2016
JAK2/STAT-3	MMP2, VEGF	LSCC	Promote	Hu, , et al., 2015
EBV-LMP1	VEGFA/VEGFR1	NPC	Promote	Xu et al., 2018
Foxq1	EGFR, VE-Cadherin, MMP2, MMP9	NPC	Promote	Luo et al., 2021
BPIFB1	GLUT1	NPC	Inhibit	Jiang et al., 2022
miR-124	STAT-3	OSCC	Inhibit	Li et al., 2018
	Foxq1	NPC	Inhibit	Luo et al., 2021
miR-195-5p	NEAT-1, VEGFA	SNSCC	Inhibit	Lu & Kang, 2020
miR-125a	TAZ	NPC	Inhibit	Wan et al., 2022

2.4.1. Role of EMT and Cancer stem (like) cell (CSC)

In HNSCC, EphA2 plays a major role in the formation of VM through regulating the Epithelial-Mesenchymal transition (EMT). The correlation of EphA2 and EMT associated molecules such as E-cadherin, vimentin, Twist, Claudin4, DSG3 with VM was deduced by (Wang et al., 2014) in the surgical tissue specimens and in vitro HNSCC model. The siRNA mediated knockdown of EphA2 impaired the formation of channel like networks in matrigel matrix and after rescuing the EphA2 expression, the tubular structure was retrieved, which interpreted the contribution of EphA2 molecule in VM formation. The disruption of EphA2 expression also led to the reversal of EMT associated molecules which indicated that EMT may be an alternative mechanism of VM formation in HNSCC (different from the remodeling of extracellular matrix) regulated by EphA2.

VEGFA is also a significant downstream component that promoted the hypoxia induced VM through regulating EMT and stemness in SACC (Wang et al., 2019). Their study first demonstrated that under hypoxic niche, VEGFA expression was noticeably upregulated in the SACC tube-forming cells. The expression of VE-Cadherin in accordance with VEGFA was also

assessed in the hypoxic microenvironment. In hypoxia, the exogenous VEGFA enhanced the mRNA and protein level of VE-Cadherin, while the VEGFA inhibitor (Bevacizumab) reversed the changes indicating the possible downstream target of VEGFA in the regulation of hypoxia inducing VM formation in SACC. Moreover, the VEGFA stimulation enhanced mesenchymal markers (N-Cadherin, Vimentin) and stemness marker (CD44, ALDH1) in the VM forming cells whereas on contrary VEGFA inhibitor led to the reversal of the expressional status of EMT markers and stemness markers indicating that the VM formation in SACC can be mediated through Cancer stem cells and the EMT process. The positive association of VM in SACC specimens with another CSC marker CD133 was previously proved by the same group of investigators (Wang et al., 2016). Their study indicated that compared to the CD133- ACC cells the CD133+ cancer stem like cells exhibited enhanced migration, invasion and tube forming capability in vitro. Their study further demonstrated that the expression of the endothelial cell markers VE-Cadherin, MMP2, MMP9 in CD133+ cancer stem like cells and xenograft tumors of CD133+ cell injected nude mice was significantly higher than in CD133- ACC cells, interpreting the capacity of CD133+ cancer stem like ACC cells in trans-differentiation and acquiring the endothelial cell phenotype through expressing VE-Cadherin to promote VM structures.

2.4.2. JAK-2/STAT-3 pathway

The involvement of JAK-2/STAT-3 pathway in the VM formation of laryngeal SCC has already been studied by (Hu et al., 2015). Their study indicated that the potent inhibitor of JAK2 (AG490) downregulated pSTAT-3 production and significantly disrupted the tube forming ability in type I collagen consisting 3D matrix as well as other VM associated events such as growth, proliferation and migration of Hep2 cells. Blocking of the JAK-2/STAT-3 pathway also

resulted in consecutive downregulation and suppression of MMP2 and VEGF protein associated with VM formation.

2.4.3. EBV-LMP1/ VEGFA axis

The VEGFA/VEGFR1 signaling is associated with VM formation in nasopharyngeal carcinoma involving the onco-viral protein EBV-LMP1 (Xu et al., 2018). The relevance of VEGFR subtype VEGFR1 on the tubular network formation, induced by EBV-LMP1 in nasopharyngeal cancer cells has been investigated in this study. The significant correlation of LMP1 expression with VEGFR1 and occurrence of VM in primary NPCs has been observed by (Xu et al., 2018). On the other hand, the siRNA mediated knockdown of LMP1, VEGFR1 and VEGFA distinctly disrupted the tubular network formation in NPC cells, whereas the downregulation of VEGFR2 didn't cause any significant observable change in the main geometrical features of the tubular structures, indicating that VEGFR1, but not VEGFR2 signaling was associated with VM formation in NPC. Moreover, the LMP1- siRNA transfected cells exhibited reduced expression of LMP1 accompanied with decreased VEGFA expression which confirms the involvement of LMP1/ VEGFA axis in association with VM in NPC.

The induction of VM by EBV infection has been reported by (Xiang et al., 2018). They have indicated that the EBV induced VM formation is associated with HIF-1 α accumulation via involvement of PI3K/AKT signaling pathway which is also partly mediated by LMP2A.

2.4.4. Foxq1

The study of (Luo et al., 2021) indicated the role of Foxq1 in regulating VM formation in NPC via up-regulating EGFR signaling followed by VM associated genes including AKT, MMP2 and MMP9. Foxq1 and EGFR expression was found to be positively correlated with the expression of VM in 114 NPC patients. The contribution of Foxq1 in VM formation was confirmed by

characterizing the loss of VM forming capability in Foxq1 depleted NPC cells (5-8F and CNE1) as well as the VM promoting capacity in Foxq1 over-expressing cells and in-vivo BALB/C nude mice xenograft model. Furthermore, the abrogation of Foxq1 induced VM formation by EGFR inhibitor Erlotinib confirmed the VM promoting effect of Foxq1 through EGFR. Moreover, the luciferase reporter gene and CHIP assay showed that Foxq1 directly binds to the EGFR promoter and regulates its transcription which further stimulates NPC growth, metastasis and VM formation.

2.4.5. BPIFB1

In NPC, BPIFB1 plays an important role in VM formation through regulating metabolic reprogramming. For the first time (Jiang et al., 2022) reported the specific mechanism of BPIFB1 as a tumor suppressor gene involving in reduction of VM formation via inhibiting GLUT1 mediated H3K27 acetylation and glycolysis in in vitro and in-vivo NPC model. Through the comprehensive analysis they also elucidated that GLUT1 could be inhibited by BPIFB1 through JNK/AP1 pathway to reduce the acetyl CoA production in glycolysis and subsequent decrease in the acetylation of H3K27 and expression of VM associated VEGFA, VE-Cadherin and MMP2.

2.4.6. MTDH/VEGFA-165/Flt-1 axis

The effect of macrophage derived MTDH on VM formation has been depicted by (Liu et al., 2021) in the in vitro and in vivo HNSCC model. Over-expression of MTDH triggered the tumor associated macrophage polarization into M2 type and secretion of VEGFA-165 isoform to activate Flt1 which further transmit signal through pSTAT-3/Twist/VE-Cadherin cascade and promotes VM formation, migration, invasion and metastasis of cancer cells.

2.4.7. Myeloid derived suppressor cells (MDSC)

The study of (Pang et al., 2020) reported the role of tumor associated MDSCs in modulating VM formation through induction of EMT in OSCC cells. Cells treated with MDSCs derived from OSCC patients exhibited typical vascular architecture along with the upregulated expression of VE-Cadherin and mesenchymal markers (Vimentin, N-Cadherin) and downregulation of E-Cadherin expression indicating MDSC a novel inducer of EMT in OSCC.

2.4.8. Role of miRNAs

2.4.8.1. miR-124: The miR-124/STAT-3/VM axis has been established in oral cancer using in vitro as well as in vivo xenograft mouse model by (Li et al., 2018). To assess the interplay of miR-124 and STAT-3 signaling pathway in VM formation the stably expressing miR-124 oral cancer cell line (HN6-miR-124) was generated through transfecting WSU-HN6 cell line with the plasmid carrying miR-124 overexpression cassette which exhibited reduced number of VM channels as well as the downregulated expression pSTAT-3 compared to the control cells. miR-124 also targets Foxq1 to downregulate EGFR signaling pathway and relevant VM associated molecules to inhibit the metastasis of NPC.

2.4.8.2. miR195-5p: In a very recent study (Lu & Kang, 2020) found that via miR195-5p/VEGFA axis, the downregulation of NEAT1 inhibited the viability and VM formation in sinonasal SCC. They investigated that miR195-5p was negatively correlated with both NEAT1 and VEGFA in SNSCC patients' tissue. NEAT1 and VEGFA were silenced, which decreased the survival of SNSCC cells and prevented them from forming capillary-like tubes. They have also discovered that miR195-5p can competitively bind to NEAT1 and target VEGFA. Since VEGFA is a miR195-5p target, overexpressing VEGFA reversed the effects of miR195-5p, and vice versa, downregulating miR195-5p reversed the effects of silencing NEAT1 on the expressional

status of NEAT1, miR195-5p, tube-forming capacity, and the downstream activation of PI3K/Akt pathway, which details the role of NEAT1 at the molecular level in SNSCC via the miR195-5p/VEGFA axis.

2.4.8.3. miR-125a: The inhibitory role of miR-125a in the NPC VM formation has been demonstrated by (Wan et al., 2022) and identified TAZ, which is the key functional component of Hippo pathway as the direct downstream target of miR-125a. miR-125a containing exosomes isolated from artificially engineered human mesenchymal stem cell inhibited VM formation in the in vitro and in vivo NPC model.

2.4.9. Additional molecular markers regulating VM in Head and Neck Cancer

A very interesting study of (Bedal et al., 2015) suggested that the NC11 domain of collagen XVI triggers VM in 2D and 3D OSCC cells via up-regulated expression of endothelial receptors VEGFR1, VEGFR2 and uPAR. The study of (Wu et al., 2017) indicated the positive association of LGR5 (a regulated target of Wnt signaling pathway) with VM in OSCC patients and (Wang et al., 2018) also reported a positive correlation of VM with ALDH1 (CSC marker) and Beclin 1 (Autophagy marker) but the underlying molecular mechanism is still unexplored. Our study (Saha et al., 2022) recently reported a significant positive correlation of VM with matrix proteins MMP2 and Laminin-5 γ 2 in OSCC patients' specimen with the establishment of VM-Laminin-5 γ 2 orchestration as a prognostic marker of OSCC. A recent study by (Hong et al., 2021) revealed an inverse relationship between the expression of SOX7, a member of the sex determining region Y box family, and the presence of VM channels in OSCC specimens. By inhibiting the expression of VE-Cadherin, SOX7 could be a potential regulator of OSCC metastasis. The investigation of (Almahmoudi et al., 2021) confirmed that Extracellular

Interleukin-17F (IL-17F) exhibited in vitro VM inhibitory potential in the OSCC cell line HSC3 but its mechanistic approach remained unexplained.

Table 2: Head and Neck cancer associated signaling molecules regulating VM in several other types of cancers

Signaling Molecules	Mechanisms regulating VM	Cancer types other than Head and Neck Cancer	References
HIF-1 α	Promotes VM by modulating VE-Cadherin-EphA2-Ln5 γ 2 Signaling pathway	Esophageal	Tang et al., 2014
	Directly targets the EMT regulator LOXL2 which in turn represses E-Cadherin expression and promotes metastasis and EMT	Hepatocellular	Shao et al., 2019
	Through inducing phosphorylation of Akt	Liver	Nishida et al., 2006; Ribatti et al., 1999
	Directly targets transmembrane glycoprotein NRP1 and further promotes VE-Cadherin, MMP2 and Vimentin	Lung adenocarcinoma	Fu et al., 2021
	Induces the expression of pro-tumoral c-MYC and anti-apoptotic Bcl2 protein	Breast Cancer	Scatozza et al., 2020
EphA2	Promotes VM through phosphorylation at Ser897 residue, regulated by PI3-K	Prostate	Wang et al, 2016
	Induces EphA2-FAK-Paxillin pathway	Gallbladder	Lu et al, 2013
VEGF	Induces VM by activating PI3K/Akt signal transduction pathway	Choroidal Melanoma	Xu et al, 2019
	Induces VM by activating VEGF-EphA2-MMPs signaling cascade	Ovarian	Wang et al, 2008
VE-Cadherin	FAK dependent phosphorylation of VE –Cadherin (Y-658) upregulates Kaiso dependent genes such as CCDN1 , WNT11 to accelerate VM	Melanoma	Bellido et al, 2018
	VE-Cadherin fusion protein (consisting of VE-Cadherin extracellular domain and IgG- Fc region) elevates the expression of endogenous VE-Cadherin and activates VE-cadherin/PI3K/MMPs and VE-cadherin/EphA2/FAK/p-VE- cadherin axes to promote VM.	Hepatocellular	Shuai et al, 2012
	Induces VM under hypoxia regulated by Bcl2	Melanoma	Zhao et al, 2012
	Regulates the ligand mediated phosphorylation of EphA2 to induce VM	Melanoma	Hess et al, 2006

CSC markers	CD133+ cells upregulates VM mediators MMP2 , MMP9 and promotes VM	Breast Cancer	Liu et al, 2012
STAT3	p-STAT3 influences VM by affecting EMT marker Vimentin	Colorectal Cancer	Han et al, 2017

2.5. Chemotherapy against oral cancer

Standard chemotherapeutic regime for metastatic OSCC contains Cisplatin or Carboplatin in combination with other chemotherapy agents, such as 5-FU, Docetaxel, and Paclitaxel (Hartner, 2018). Cisplatin is a heavy metal which is believed to cause DNA cross-linking. In determining dose-intensity of Cisplatin, renal toxicity and neurotoxicity act as the most important limiting factors. Nowadays Cisplatin is applied with pre- and post-therapy hydration along with mannitol infusion that protect against renal toxicity. 5-fluorouracil (5-FU) is a pyrimidine analogue which is converted to fluorodeoxyuridine monophosphate in the cells. This inhibits thymidylate synthase which is required for thymidine formation thus in turn blocking DNS synthesis. 5-FU also produces fluorouridine triphosphate that hampers RNA synthesis.

2.5.1. Paclitaxel

Paclitaxel is the first microtubule stabilizing antitumor drug that exhibits promising activity in human malignancies including breast, ovarian, lung, head and neck cancers (Nawara et al., 2021; Weaver, 2014). Paclitaxel was identified as an active ingredient of the crude extract from the bark of the western yew tree *Taxus brevifolia* (Wall, 1998; Wall & Wani, 1995, 1996; Wani et al., 1971). The research group of Robert A Holton developed a four step procedure to convert 10-deacetylbaccatin into Paclitaxel (Holton, 1992, 1998).

2.5.1.1. Chemical structure of Paclitaxel

Paclitaxel is a tetracyclic diterpenoid. Its empirical formula is $C_{47}H_{51}NO_{14}$ and the molecular weight is 853.9 units. A four-member oxetan ring connected to a taxane ring structure at

positions C-4 and C-5 makes up the alkaloid ester Paclitaxel and its taxane rings are linked to an ester at C-13 (Mekhail & Markman, 2002). It is highly lipophilic in nature and the melting point is around 216-217°C (K & U, 2012).

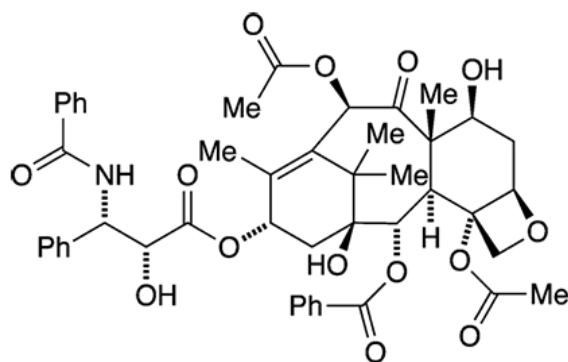


Figure 3: Chemical structure of Paclitaxel

2.5.1.2. Mechanism of action of Paclitaxel

Paclitaxel is a microtubule stabilizing drug. It binds to the N terminal 31 amino acids of the β tubulin subunit of the microtubule (Parness & Horwitz, 1981). Microtubules are very vital in forming the mitotic spindle during cell division as well as maintenance of cellular shape, motility, intracellular signal transduction and transport (Kl & Dh, 1981; Rowinsky et al., 1990). Paclitaxel causes the polymerization of tubulins, resulting into the formation of extraordinarily stable and dysfunctional microtubules, promoting cell death by disrupting the microtubule dynamics required for the conventional cell division and interphase (Bharadwaj & Yu, 2004; Brito et al., 2008; Ganguly et al., 2010; K & U, 2012). So Paclitaxel protects and stabilizes microtubule against disassembly and even at higher dose it suppresses the detachment of the minus end of microtubules from centrosomes. More elaborately (Gard & Kirschner, 1985) showed that Paclitaxel stimulates the phosphorylation of β tubulin in both differentiated and undifferentiated N15 cells leading to the stabilization and polymerization of microtubule

causing cell death. Furthermore (Horwitz, 1992) found that Paclitaxel also stabilizes microtubules and arrests somatic cell mitosis at G2/M phase of cell cycle. In human oral squamous cell carcinoma (OSCC) cell line, OECCM-1, Paclitaxel showed synergistic cytotoxic activity with Cisplatin whereas it acted additively in combination with Carboplatin and 5-FU. Thus, Taxol/cisplatin was more effective against these OSCC cells than Taxol/Carboplatin or Taxol/5-FU therapy. (Huang et al., 2004) .The mechanism of action of Paclitaxel in different models of head and neck cancers have been described in Table 3.

Table 3: Evidences of anti-tumor efficacy of Paclitaxel in Oral Cancer

Mechanistic involvement of Paclitaxel	References
Enhanced apoptosis via increasing the expression of Bim and Bid protein.	Choi et al., 2020; Hu et al., 2015; Nonaka et al., 2006;
Growth inhibition via downregulating EGFR cascade.	Okamoto et al., 2015
Enhanced immune function and inflammatory response of patients via increased expression of IL-2, IFN- γ , CD3+, CD4+, CD4/CD8.	Zhang & Zhao, 2022
Anti-angiogenic efficacy via reduced expression of VEGF and CD31	Myoung et al., 2001
Induction of antibody dependent cellular cytotoxicity (ADCC)	Sawatani et al., 2020

2.5.1.3. Side effects of Paclitaxel

Chemotherapeutic drugs work by killing rapidly dividing cells. However, along with cancer cells several other essential cells of our body divide rapidly including cells of the skin, scalp, lining of the stomach and bone marrow, which results in a serious deleterious effects on one's health (Coates et al., 1983; Griffin et al., 1996). It has been reported that patients who are receiving chemotherapy experience an average of almost 20 symptoms, most of which are physical while some are psychosocial. The major physical side effects of chemotherapy that have been reported

are nausea, vomiting, tiredness, difficulty in sleeping, hair loss, loss of taste and appetite, frequent passing of urine, sore mouth and dry skin. Besides these side effects Paclitaxel induced toxicity includes several major hypersensitive reactions (dyspnea, bronchospasm, urticaria, and hypotension) and minor hypersensitive reactions (flushing and rashes) (Eisenhauer & Vermorken, 1998; Rowinsky et al., 1990). Though it can be dealt with the lower infusion rate of Paclitaxel and dexamethasone treatment (Peereboom et al., 1993), but this approach is not always successful. Another principal toxic effect of Paclitaxel is neutropenia (Rowinsky, Eisenhauer, et al., 1993) which arises after 8-10 days of treatment and recovery is completed within 15-21 days. Paclitaxel at higher doses ($\geq 250\text{mg/m}^2$) may cause neurotoxic effects showing peripheral neuropathy characterized by several sensory symptoms including numbness and paresthesia (Gelmon et al., 1999; Rowinsky, Chaudhry, et al., 1993). Furthermore, Paclitaxel may also cause muscular and cardiac toxicity (IMAI et al., 2012; Rowinsky et al., 1991). This compels the need for developing alternative strategies that may overcome chemotherapy resistance and prove to be more effective and less toxic against the disease.

2.6. Phytochemicals against cancer treatment

Phytochemicals are the plant derived naturally occurring biologically active compounds, which serve as promising resources for novel drugs to improve treatment efficacy and decrease adverse reactions of cancer therapy. Phytochemicals possess anticancer mechanism via scavenging free radicals to increase the antioxidant (Lee et al., 2013), suppression of cellular proliferation through induction of cell cycle arrest and apoptosis (Zhao et al., 2017), inhibition of angiogenesis and invasiveness of tumor cells (Zhang et al., 2020). Several taxol analogues, vinca alkaloids, podophyllotoxin analogues are some of the examples of typical phytochemicals. The different molecular targets of phytochemicals include several membrane receptors, kinases,

transcriptional factors, miRNAs, cyclins etc (Cojocneanu Petric et al., 2015; Deleu et al., 2004; Deng et al., 2017).

2.6.1. Therapeutic potential of phytochemicals targeting VM

The resistance of VM towards the anti-angiogenic therapy causes the treatment evasion in several aggressive tumors and leads to the poor prognosis of cancer patients (Potente et al., 2011; Qiao et al., 2015) which potentially may establish VM as a novel target for cancer therapeutic strategy. Phytochemicals targeting several signaling cascades related to the vascular network formation have been enlisted in Table 4.

Table 4: Phytochemicals targeting VM related proteins in different cancer models

Name of Phytochemicals	Category of Phytochemicals	Source of the photochemical	Types of Cancer	Mechanism of action of VM inhibition	References
Resveratrol	Non flavonoid polyphenol	Grapes, Apples, Blueberries, Plums, Peanuts	Prostate cancer	Inhibits EphA2/Twist/VE-Cadherin/AKT cascade	Han et al., 2022
			Melanoma	Inhibits VEGF, VEGF-R, VEGF-R2	Vartanian et al., 2007
Curcumin	Polyphenol	Turmeric (<i>Curcuma longa</i>)	LSCC	Inhibits JAK2 and pSTAT-3expression Reduces the expression of MMP2 and VEGF.	Hu et al., 2015
			HNSCC	Activates SIRT1, ATM/CHK2 pathway and inhibits NFκβ.	Hu et al., 2015
			Glioblastoma	Inhibits EphA2, PI-3K and MMP2	Liang et al., 2014
			Hepatocellular Carcinoma	Inhibits STAT3, PI-3K /AKT	Chiablaem et al., 2014
Breast cancer	Inhibition of PI-3K /AKT and EMT	Morales-Guadarrama et al., 2022			

Dehydroeffusol	Phenanthrene	Traditional Chinese Medicine (TCM) <i>Juncus effuses</i>	Non small cell lung cancer Gastric cancer	Inhibits hypoxia induced EMT and inactivation of Wnt/ β -Catenin Inhibits VE-Cadherin and MMP2	Wei et al., 2020 Liu et al., 2015
Crocin	Diterpenoid	Saffron	Gastric cancer	Inhibits Sonic Hedgehog pathway	Zang et al., 2021
Celastrrol	Triterpenoid	Chinese herbal medicinal plant <i>Tripterygium wilfordii</i> Hook F	Glioblastoma	Inhibits PI-3K/AKT/mTOR	Zhu et al., 2020
Thymoquinone	Monoterpene	Black cumin (<i>Nigella sativa</i>)	Breast cancer	Inhibits PI-3K, Wnt 3a, VE-Cadherin	Haiaty et al., 2021
Epigallocatechin-3-Gallate	Flavonoid	Green tea	Prostate cancer Breast Cancer	Inhibits Twist/VE-Cadherin/AKT Inhibits STAT-3 phosphorylation	Yeo et al., 2020 Gonzalez Suarez et al., 2021
Luteolin	Flavonoid	Vegetables and fruits such as celery, parsley, broccoli, onion leaves, carrots, peppers, cabbages, apple skins, and chrysanthemum flowers	Gastric cancer	Inhibits Notch-1-VEGF signalling	Zang et al., 2017
Ginsenoside Rg3	Tetracyclic triterpenoid	Korean Red Ginseng root (<i>Panax ginseng</i>)	NPC Pancreatic cancer	Downregulates the expression of VEGF Downregulation of VE-Cadherin, EphA2	Wang et al., 2010 JingQiang et al., 2017
Silibinin	Flavonolignan	Milk thistle seeds (<i>Silybum marianum</i>)	HNSCC	Activates miR-494 and inhibits Bmi1 and ADAM10	Chang et al., 2015

2.6.2. Lupeol

Lupeol is a naturally occurring, pharmacologically active pentacyclic triterpenoid that is found in many edible fruits (olive, fig, mango, strawberry, red grapes) and vegetables (white cabbage, pepper, cucumber, tomato) as well as some medicinal plants (American ginseng, Shea butter

plant, *Tamarindus indica*, *Allanblackia monticola*, *Himatanthus sukuuba*, *Celastrus paniculatus*, *Zanthoxylum riedelianum*, *Leptadenia hastata*, *Crataeva nurvala*, *Bombax ceiba* and *Sebastiania adenophora*). Native Americans use American ginseng, Shea butter plant, *Tamarindus indica*, *Allanblackia monticola*, *Himatanthus sukuuba*, *Celastrus paniculatus*, *Zanthoxylum riedelianum*, *Leptadenia hastata*, *Crataeva nurvala*, Bomba Under in vitro and in vivo circumstances, Lupeol has demonstrated a number of advantageous pharmacological effects against inflammation, cancer, arthritis, diabetes, cardiac problems, renal toxicity, and hepatic toxicity. (Beserra et al., 2019; Huang et al., 2021; Li et al., 2022; Saha et al., 2020; Song et al., 2022; Tiwari et al., 2019). The content of Lupeol in different fruits and vegetables has been summarized in Table 5.

Table 5: Lupeol content in Different fruits and plants

Name of Plant	Lupeol ($\mu\text{g/g}$)
Olive Fruit	3 μg / g of fruit
Mango fruit	1.80 μg / g mango pulp
Aloe Leaves	280 μg / g dry leaf
Elm Plant	880 μg / g bark
Japanese Pear (shinko)	175 $\mu\text{g/g}$ twig bark
Ginseng Oil	15.2.mg/100 g of oil

2.6.2.1. Chemical structural analysis of Lupeol

The chemical formula of Lupeol is $\text{C}_{30}\text{H}_{50}\text{O}$, with a molecular weight of 426.7174 g/mol (PubChem, NIH library, Compound ID 259846). Properties evaluated from the chemical structure exhibited its melting point of 215–216 °C. The infra-red spectrum of Lupeol depicted the presence of hydroxyl spectrum at 3235 cm^{-1} and an olefinic moiety at 1640 cm^{-1} . The presence of seven methyl singlets and an olefinic function in the $^1\text{H-NMR}$ spectrum confirmed that Lupeol is pentacyclic triterpenoid in nature. Furthermore, the HPLC and mass spectroscopy

(MS) data revealed the presence of a parent ion peak at m/z 409 $[M+H-18]^{+}$ for Lupeol. The chemical structure of Lupeol has been represented in Figure 4.

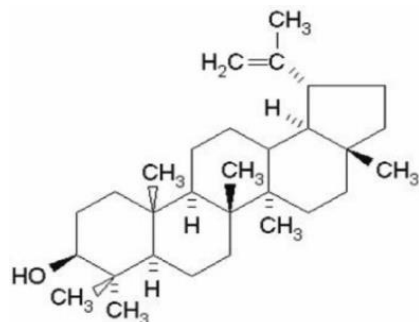


Figure 4: Chemical structure of Lupeol

2.6.2.2. Mechanistic activity of Lupeol against different cancer models

Lupeol is a multi-target agent with an enormous anti-inflammatory potential targeting key molecular signaling involving nuclear factor kappa B (NF κ B), cFLIP, Fas, Kras, phosphatidylinositol-3-kinase (PI3K)/Akt and Wnt/ β -catenin in various cells. The molecular mechanism indicating the anticancer potential of Lupeol in various cancer models has been summarized in Table 6.

Table 6: Mechanism of action of Lupeol in various cancer models

Cancer model	Mechanism of action of Lupeol	References
Gastric Cancer	Promotes the proliferation of NK cells through increasing the expression of PEP, IFN- γ and CD107a via the activation of PI3K/Akt and Wnt/ β -catenin signaling pathways.	Wu et al., 2013
Lung Cancer	Inhibition of MAPK/ERK pathway along with the expression of N-Cadherin and Vimentin. Induction of apoptosis, ROS generation and downregulation of mTOR/PI-3K/AKT signaling pathway	Bhatt et al., 2021 He et al., 2018
Cervical cancer	Induction of S phase cell cycle arrest and apoptosis	Prasad et al., 2018
Head and Neck	Triggers G1 cell cycle arrest through upregulating the expression of	Bhattacharyya et

cancer	CDKN2A and inhibition of CyclinD1.	al., 2017
	Inhibition of NF- κ B activity	Lee et al., 2007
Pancreatic cancer	Reduces the expression of Ras oncoprotein, and NF- κ B signaling cascade via modulating the expression of PKC α /ODC, PI3K/Akt and MAPK pathways.	Saleem et al., 2005
Prostate cancer	Disruption of microtubule assembly via decreased expression of stathmin, cFLIP, and survivin.	Saleem et al., 2009
	Reduction of the expression of β -Catenin, TCF and MMP2	Saleem et al., 2009
Melanoma	Induction of apoptosis by arresting G1-S cell cycle phase, increased Bax/Bcl ₂ ratio, increased expression of Caspase and p21 and decreased expression of Cyclin D1, Cyclin D2 and CDK2.	Saleem et al., 2008
Oral cancer	Reduction of expression of EGFR, COX2 and NF κ B	Rauth et al., 2016
Breast cancer	Induction of autophagic cell death by inhibiting Akt-mTOR pathway and reversal of EMT	Zhang et al., 2022
	Induction of apoptosis via upregulated expression of Caspase 3 and anti-migratory effect via decreased expression of MMP9	Malekinejad et al., 2022
Liver cancer	Induction of apoptosis via decreased expression of Bcl ₂ and the increased expression of active Caspase 3.	Eldohaji et al., 2021
	Downregulation of Death receptor (DR3) and elevated expression of FADD to induce apoptosis	Zhang et al., 2009
Renal cancer	Modulation of mitochondrial dynamics	Sinha et al., 2019
Retinoblastoma	Promotes autophagy and apoptosis by inhibiting PI-3K/AKT/mTOR pathway.	Che et al., 2022
Osteosarcoma	modulation of miR-212-3p/HMGA2 axis	Zhong et al., 2020

2.6.2.3. Pharmacological and toxicity study of Lupeol

The physiologic concentration of Lupeol (in blood) through diet can be analyzed through pharmacokinetic parameters from the concentration vs. time profile of the drug in the living

system. Though the study of (Saleem, 2009) reported that the Lupeol content in per gram of fruits (Mango and olives) is 1.80-3 µg, the specific and direct pharmacokinetic studies concerning Lupeol has not been performed yet in humans as the compound is still at early preclinical study phase. However, there is a good amount of work to provide indirect evidence in this regard. For example, the study of (Cháirez-Ramírez et al., 2019) determined the plasma level of Lupeol in CD1 mice strain after oral administration of 200 mg/kg body weight dose, which revealed a maximum Lupeol concentration (C_{max}) of 6.12 ± 2.17 ng/µL in plasma at 8 h post-administration. Another study conducted by (Priyanka et al., 2017) reported that after oral administration of a *Ficus religiosa* L. extract, which is equivalent to 50 mg/kg of Lupeol in Wistar Rat model, the C_{max} in rat plasma was 178.61 ± 24.6 ng/mL. Similarly, (Khatal & More, 2019) also indicated that after oral (30mg/kg) and intravenous (1mg/kg) administration of Lupeol in Wistar Rats, the C_{max} in plasma were 133.33 ng/ml and 12,485.69 ng/ml respectively. They have also reported that the bioavailability in oral route was <1%. Furthermore, the study of Zhang et al., 2019 exhibited that the intravenous administration of Lupeol loaded liposomes at a dose of 10mg/Kg body weight in SD male rat, the C_{max} in plasma was found to be 64.96 ± 6.66 µg/mL. One can attribute the difference in the findings mainly to the model systems used. To get a more comprehensive profile, the bioavailability of Lupeol in experimental animal models can be further extended to phase-I human pharmacokinetic study after feedback from PK/PD and toxicity profiling in large experimental animals like dogs as an integrated part of developmental pipeline.

Several *in vitro* studies have reported about the cytotoxicity of Lupeol within the dose range of ~15-100 µM, including breast carcinoma, lung cancer, renal carcinoma and melanoma and head and neck cancer (Malekinejad et al., 2022; Min et al., 2019; Pitchai et al., 2014; Sinha et al.,

2019; Bociort et al., 2021; Lee et al., 2007). There are several other in vitro and in vivo studies indicating the off-tumor non-toxicity of Lupeol in non-malignant cells. For example, the study (Nyaboke et al., 2018; Pitchai et al., 2014) reported the non-toxic nature of Lupeol towards normal breast epithelial cells (MCF-10A) and normal hepatocytes AML-12. Similarly, the study of Al-Rehaily et al., 2001; Bani et al., 2006; Lee et al., 2007; Patočka, 2003; Saleem, 2009 also reported the non-toxicity of Lupeol, providing the further evidence of no mortality and systemic toxicity (as defined by key parameters like infection, diarrhea, loss of body weight etc) in experimental animal models at a dose of 2-2000 mg/kg body weight.

2.7. Therapeutic strategies targeting VM in Head and Neck Cancer

Though the conventional chemotherapeutic drugs including Cisplatin, 5-Fu, Paclitaxel/Docetaxel improve the treatment outcome of head and neck cancers, the chemoresistance due to DNA damage repair, evasion of apoptosis, activation of growth factor receptors, drug efflux reveal critical challenge for clinicians (Kanno et al., 2021). The study of Li et al., 2014 reported the VM inhibitory property of Paclitaxel loaded liposomes modified with multifactorial tandem peptide [R8-c(RGD)] in Glioma. The investigation by Peri et al., 2021 indicated that 5-FU chemoresistance can enhance vasculogenic capacity in gastric cancer cell lines but no evidence has been established regarding the anti-VM property of the conventional chemotherapeutic drugs in head and neck cancers. Several evidences of novel anti-cancer agents targeting VM-related molecules inhibiting VM formation in different HNC subtypes including OSCC have been described below.

2.7.1. Niclosamide

It has been proposed by Li et al., 2018 that the FDA approved oral anti helminthic drug Niclosamide exerts an anti VM property in oral cancer in vitro and in vivo through the

upregulation of miR-124 and downregulation of STAT-3. Moreover, Niclosamide markedly inhibited the expression of VM associated genes VEGFA, MMP2, ROCK1, Cdc42 at mRNA and protein level. The authors also demonstrated that in Niclosamide treated WSU-HN6 cells, there was significant protein-level downregulation of pSTAT-3 and mRNA-level upregulation of miR-124 which ultimately exhibited reduced mobility, invasiveness and VM forming ability compared to the control cells.

2.7.2. Melatonin

The study of Liu et al., 2018 proved the inhibitory effect of melatonin (secreted by pineal gland and involved in chrono-biological rhythm regulation) in ROS driven cellular proliferation, apoptosis resistance, EMT as well as VM through the blockage of ROS reliant AKT/ERK signaling pathways involving HIF-1 α . Moreover at molecular level, melatonin also downregulated the expression of pro-survival proteins (cyclin D1, PCNA, Bcl2) and upregulated the expression of pro-apoptotic protein Bax. Melatonin induced inactivation of ROS reliant Akt signaling also significantly abolished the invasion and migration of oral cancer cells and altered the expression of EMT associated molecules (E-cadherin, Vimentin and Snail). The employment of ROS scavenger (NAC) and ERK and PI3K/AKT inhibitors (U026 and LY294002 respectively) also exhibited the significant downregulation of HIF-1 α and VEGF in Cal27 and FaDu cells which confirmed the inhibitory role of melatonin in tumor progression and vasculogenic mimicry formation through targeting ROS induced ERK/AKT signaling.

2.7.3. Curcumin

Curcumin (polyphenol derived from turmeric) has been found to be associated with the suppression of VM formation in LSCC (Hu, et al., 2015) in vitro through the inhibition of JAK-2/STAT-3 pathway. Additionally, the potent dose of Curcumin also hindered the other VM

associated phenotypes including cellular growth, proliferation and migration. Corresponding with the selective inhibitor of JAK 2 (AG490), pretreatment of Hep2 cells with Curcumin significantly inhibited JAK 2 and pSTAT-3. Furthermore, the inhibition of JAK-2/STAT-3 pathway also resulted into the downregulation of MMP2 at mRNA and protein level which is a crucial player of extracellular matrix degradation. In addition to the direct effects on VM, Curcumin also exerted its anti-angiogenic effect through the inhibition of endothelial nitric oxide synthase (eNOS) and VEGF expression of Hep2 cells.

The anti-migratory and anti-vasculogenic mimicry potential of Curcumin has also been observed by (Hu et al., 2015) in HNSCC cell lines (FaDu and Cal27) through the induction of SIRT1 activity which catalyzes NAD⁺ dependent protein deacetylation yielding nicotinamide and O- acetyl ADP-ribose. They have also demonstrated that the anticancer activity of Curcumin relies upon the induction of apoptosis through the activation of ATM/CHK2 pathway and inhibition of NFK β as well as triggering the extrinsic (Caspase 8) and intrinsic (Caspase 9) apoptotic pathways. Interestingly they have also reported that the inhibition of SIRT1 pathway resulted in the suppression and downregulation of MMP2 and VEGF proteins which are associated with VM formation.

2.7.4. Silibinin

The study of (Chang et al., 2015) indicated Silibinin (polyphenolic flavonoid isolated from milk thistle plant *Silybum marianum*) to cause inhibition of vasculogenic mimicry in the tumor initiating cells (TICs) of HNSCC in a dose dependent manner. In this study CD44⁺ and ALDH1⁺ tumor infiltrating cells (TICs) were isolated which resulted in the relapse and metastasis of HNC. The suppression of their self-renewal, tumor initiation and chemoresistance properties by the dose dependent treatment of Silibinin has been reported through activation of

miR-494 and inhibition of Bmi1(Chromatin structure regulator) and ADAM10 (responsible for angiogenesis, tumorigenesis). The in vivo validation using xenograft model also confirmed Silibinin, a potential anticancer drug for the treatment of HNC.

2.7.5. Ginsenoside Rg3

In nasopharyngeal carcinoma, there is evidence of inhibition of VM in vitro by Ginsenoside Rg3 (biologically active steroid saponin groups). Wang et al., 2010 indicated the negative correlation of number of tube like structures of human nasopharyngeal carcinoma HNE-1 cells on matrigel and the concentration of ginsenoside Rg3 in association with the down regulation of VEGF protein expression in HNE-1 cells.

2.7.6. Axitinib

The study of Duo et al., 2018 indicated that in oral mucosal melanoma the tyrosin kinase inhibitor Axitinib could modulate vasculogenic mimicry in patient derived xenograft models. With the reduction of tumor volume and number of vasculogenic mimicry the protein expression of Epha2 and MMP2 was found to be decreased in Axitinib treated group.

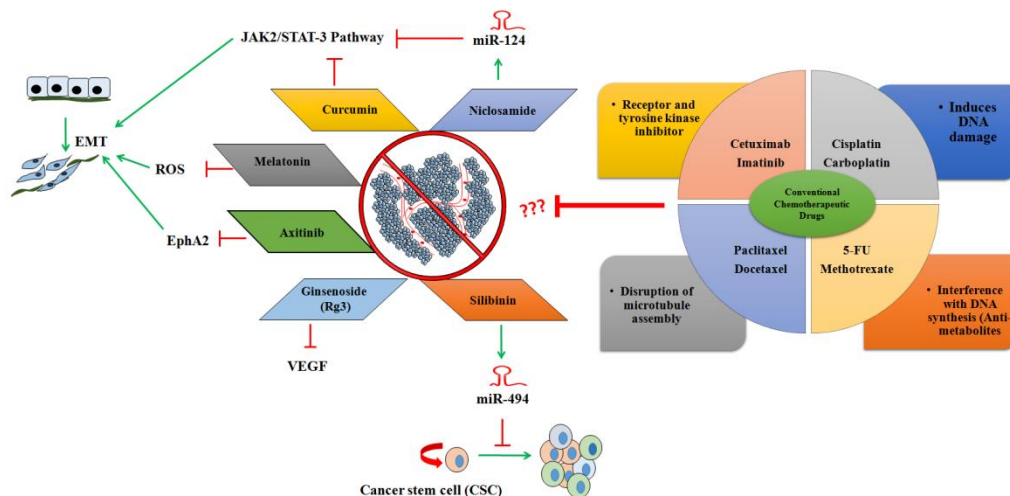


Figure 5: Proposed VM inhibitors with the approved standard of care chemotherapeutic drugs against Head and Neck cancers

Since the limited efficacy and treatment with conventional anti-angiogenic agents didn't significantly improve patients' survival time hence the discovery of VM provides a new therapeutic strategy for patients confronting aggressive cancers. Here we have encapsulated several investigations focusing on the VM associated key regulators involved in cellular adhesion, hypoxia, EMT, CSC and microRNA mediated post-transcriptional regulation of VM related proteins in different head and neck cancer models however deciphering the critical molecular mechanism underlying VM formation in HNCs deserves further studies.

The exploration and development of new and specific molecular imaging techniques might be helpful for investigating the true structural and functional relevance of VM structures in tumors. Finally the discovery of novel and potent anti-VM agents and their combination with other therapeutic strategies such as anti-angiogenesis, anti-lymphangiogenesis, and chemotherapy will provide an avenue to improve the treatment modalities and clinical outcomes of head and neck cancer patients

Chapter 3

Objective of Research

The aim of our work is to decipher the effect of hypoxia in modulating EphrinA2 signaling pathway and inducing epithelial-mesenchymal transition (EMT) and in association with vasculogenic mimicry in OSCC and to establish Lupeol as an alternative chemotherapeutic agent targeting VM with no side effects and more efficacies.

It is a well-established fact that to treat the cancer patient, the delivery of chemotherapeutic drugs and radiotherapy comes with their limitations and adverse side effects which may lead to poor prognosis of the patient. The elucidation of the underlying molecular mechanism leading to VM formation may provide a viable therapeutic target in OSCC. With no side effects and more efficacies, the establishment of the anti-VM property of phytochemical Lupeol can indicate a novel therapeutic regimen in treating very aggressive oral cancer.

The molecular mechanism involved in VM progression through hypoxia induced EphrinA2 and EMT signaling is yet to be explored in OSCC. Elucidation of the anti VM property of Lupeol in combination with common therapeutic drug Paclitaxel may lead to a novel therapeutic regimen in combating OSCC.

The proposed research work has been subdivided into three main objectives-

1. To decipher the expressional status of the HIF-1 α induced EphA2 pathway molecules in correlation with vasculogenic mimicry in OSCC tissues and their probable prognostic significance.
2. Deterministic investigation of the role of HIF-1 α in modulating EphA2 pathway and the induction of EMT in correlation with vasculogenic mimicry in OSCC cell lines.
3. Evaluation of the possible mitigating properties of phytochemical Lupeol in combination with a common chemo-therapeutic drug in regulating the HIF-1 α induced pseudo-

vascularization using different OSCC cell lines and ex vivo platform (patient derived cancer tissue culture) at transcription and post- transcriptional level.

Chapter 4

Scope of Thesis

Oral cancer is one of the most important health related crises in our country which is emerging rapidly among men and women due to the tobacco addiction habit in urban as well as in rural India. Since neoplastic transformation and progression is a multistep process that involves various stages and molecular changes in aggressive tumor microenvironment, in this regard vasculogenic mimicry (VM) highlights the aggressive tumor behavior in a new and exciting way. It has been observed that the presence of VM is mostly abundant in aggressive and genetically dysregulated tumors including melanoma, glioblastoma, breast cancer, prostate cancer, which make this phenomenon an obvious target to investigate clinical prognosis and responsiveness to chemotherapy and radiotherapy in cancer patients. However the underlying molecular mechanism of VM influencing the prognosis and therapeutic intervention in oral cancer is still less elusive. Therefore the thesis work aims to solve three major problems in the field of oral oncology.

The *first part* of the thesis intended to establish VM as a unique prognostic indicator for oral squamous cell cancer (OSCC). It emphasized on the morphological characterization of VM structures using CD31/PAS staining in OSCC microenvironment, in association with the expressional status of the associated biomarkers. Furthermore the significant association of the simultaneous existence of VM and relevant biomarkers in the tumor microenvironment with the clinico-pathological parameters will be helpful in specifying their relevance in the malignant and metastatic progression of OSCC. Moreover after following up the patients up to 5 years, it has also been evident that the dual expression of VM with Laminin-5 γ 2 and MMP2 correlated with decreased disease free and overall survival with the independent prognostic impact of Laminin-5 γ 2 which will be helpful in providing better therapeutic guidance against OSCC.

The *second part* of the study provided a novel regulatory mechanism of VM formation in the OSCC model which is still a less explored area. HIF-1 α was found to induce VM channel-forming cells in hypoxic conditions, which was followed by up-regulations of VE-cadherin and ephrin type-A receptor 2 (EphA2). This cascade of cellular responses led to the formation of VM channels in invasive cancer cells via matrix metallo-proteinases (MMPs) and cleavage of Laminin-5 into pro-migratory $\gamma 2x$ and $\gamma 2'$ fragments. Furthermore, targeting HIF-1 α and its downstream signaling cascade is a possible therapeutic target for the treatment of OSCC has been justified given that the hypoxic milieu has also been shown to play a significant role in controlling VM development by retaining stemness and inducing EMT.

A standard chemotherapeutic regime for OSCC contains Cisplatin or Carboplatin in combination with other chemotherapy drugs, such as 5-fluorouracil (5-FU), taxanes (Paclitaxel or Docetaxel) and Cetuximab (a humanized monoclonal epidermal growth factor receptor antibody). Taxol (Paclitaxel) and taxotere (Docetaxel) act as chemotherapeutic agents by stabilizing microtubules and enable the assembly of cytoplasmic free microtubules, thus inhibiting cell division. However these chemotherapeutic drugs target rapidly dividing cells and in turn damage several rapidly proliferating non-malignant healthy cells essential for our body mainly in the skin, mucous membrane, scalp, lining of the stomach and bone marrow and often attribute to serious adverse effects. This necessitates developing alternative strategies that may overcome chemotherapy resistance and prove to be more effective while minimizing toxicity.

Therefore the *third part* of our study explored the synergistic effect of Lupeol and Paclitaxel in obstructing VM as well as its associated aggressive phenotypes in the in vitro and ex vivo OSCC model.

Hence the thesis will contribute to the existing knowledge for better understanding the molecular basis of the association of HIF-1 α induced vasculogenic mimicry via modulating extracellular matrix remodeling along with EMT and CSC phenotypes in oral cancer. Being a phytochemical with no side effects whatsoever, the restorative effect of Lupeol in reversing the vasculogenic mimicry will emerge a new field of cancer treatment for aggressive oral cancers and after series of clinical trials, the drug may be used as a chemotherapeutic as well as chemopreventive agent against OSCC.

Chapter 5

Evaluation of the functional association and prognostic significance of vasculogenic mimicry (VM) with HIF-1 α induced EphA2 signaling cascade in oral squamous cell carcinoma (OSCC)

5.1. Background

Oral Cancer is the 6th most common malignancy in the world (Borse et al., 2020). Oral squamous cell carcinoma (OSCC) accounting for over 90% of oral cancers (Tandon et al., 2017), is one of the most common causes of cancer related deaths in the developing countries including India and the South East Asia. The estimated incidence and mortality due to lip, oral cavity cancer in the world is 2.0% and 1.8% respectively (Sung et al., 2021). Annually 75000-80000 new oral cancer cases are being reported in India (Mishra, 2019). Use of tobacco in various forms including cigarette, bidi, hookah, betel nut, betel quid is the major risk factor for OSCC (Tenore et al., 2020). Severe alcoholism, HPV infection, dietary deficiencies and poor oral hygiene are the other common identified risk factors (Sun et al., 2022). Metastasis and postoperative recurrence are the most common reasons for poor 5 year survival (Sun et al., 2019) that further increases failure of treatment. There are multiple clinico-pathological factors responsible for this poor outcome. Growing tumors survive in the nutrients and oxygen deficit state using diverse strategies. In 1999, Maniotis et al demonstrated that when blood supply cannot meet the need of rapid tumor growth, some aggressive, metastatic and genetically dysregulated cancer cells mimic the endothelial cells and form pseudo-vascular channel like structures called vasculogenic mimicry (VM) (Maniotis et al., 1999). It was first described in human uveal melanoma as Periodic acid Schiff (PAS) positive patterned vascular network and enables the tumors to form matrix-embedded vascular structures carrying plasma and blood cells to fulfill the increasing nutrient and metabolic demands in tumor microenvironment (Folberg et al., 2000). Core matrix proteins such as laminin, heparan sulfate proteoglycan, and collagens IV and VI have been identified in these patterns (Folberg & Maniotis, 2004). Though Vasculogenic mimicry is considered as an established prognostic marker in melanoma (Bhattacharyya et al., 2019; Zhang

et al., 2019), breast cancer (Andonegui-Elguera et al., 2020; Mitra et al., 2020), glioblastoma (Yue & Chen, 2005), ovarian cancer (Yu et al., 2017), lung cancer (Wang, Yang, et al., 2018), prostate cancer (Sharma et al., 2002), digestive cancers (Ren et al., 2019) the underlying molecular phenotypes inducing it in OSCC and their prognostic significance is poorly understood.

When exposed to a hypoxic condition, cancer cells start expressing the HIF (Hypoxia Inducing Factor), the protein which further activates the Ephrin family of proteins (Hess et al., 2007). The entire mechanism is believed to be triggered by two major signaling proteins i.e. ERK ½ and PI3-K. Once these two proteins get activated via various upstream signaling axis including the VE- Cadherin both of them are able to activate pro-MMP 14 to active MMP-14 (Seftor et al., 2001) which, in turn cleaves Laminin and creates the vascular like structures. Normal epithelial cells generally have highly stable cell- cell adhesion properties.

Laminin-5 (Ln-5), a component of extracellular matrix (ECM) adhesion molecules, is expressed predominantly in the epithelial basal membrane structure that promotes static adhesion and hemidesmosome formation (Giannelli & Antonaci, 2000). However, the cleavage of short arm of $\gamma 2$ subunit of Laminin-5 by matrix metalloproteinases (MMPs) such as MMP-2 and MT1-MMP leads to its switching from static to migratory form resulting in cell migration and/or invasion (Malina et al., 2004; Rousselle & Scoazec, 2020). In the context of the molecular mechanism influencing VM, the downstream signaling of VE Cadherin, EphA2 and VEGF choreographs the cleavage of Laminin-5 in to the pro-migratory $\gamma 2x$ and $\gamma 2'$ fragments through activated MMP2, implicating the roles of the extracellular matrix remodeling in positively regulating the formation of VM network (Delgado-Bellido et al., 2017).

Here we aim to investigate the phenotypic characteristics of VM structures in OSCC tumor tissues and evaluate the expression of HIF-1 α and its downstream modulator Laminin-5 γ 2 as well as their correlation in the process of the acquisition of VM structure in OSCC microenvironment. Finally, we have undertaken the survival and risk factor assessment of VM-HIF-1 α and VM-Laminin-5 γ 2 coordination in a defined patient cohort to enlighten a novel and promising therapeutic target of OSCC.

5.2. Materials and methods

5.2.1. Patients and tissue samples

The surgical and clinically confirmed OSCC tissue specimens from a sum total of 116 patients (median age: 54 years, range: 28-80 years) were obtained from Chittaranjan National Cancer Institute, Kolkata during May, 2014 - April, 2015. Patients with history of recurrence or preoperative chemotherapy, radiotherapy were excluded (Figure 6). Informed written consents were obtained from all the patients prior to specimen collection. The study was approved by the Institutional Ethics committee (IEC Ref: A-4.311/53/2014) in accordance with the ethical guidelines of Declaration of Helsinki (1964) and its later amendments. Tumor-node-metastasis stages were evaluated according to the 8th edition of American Joint Committee on Cancer (AJCC) and tumor grade was classified according to World Health Organization (WHO) standards. For OSCC patients with complete clinico-pathological information and follow-up data, the overall survival (OS) time was calculated as the time interval from the date of surgery of the patients to their oral cancer related death and disease free survival (DFS) was noted as the time interval from the date of surgery to the first documentation of local recurrences or distant metastasis.

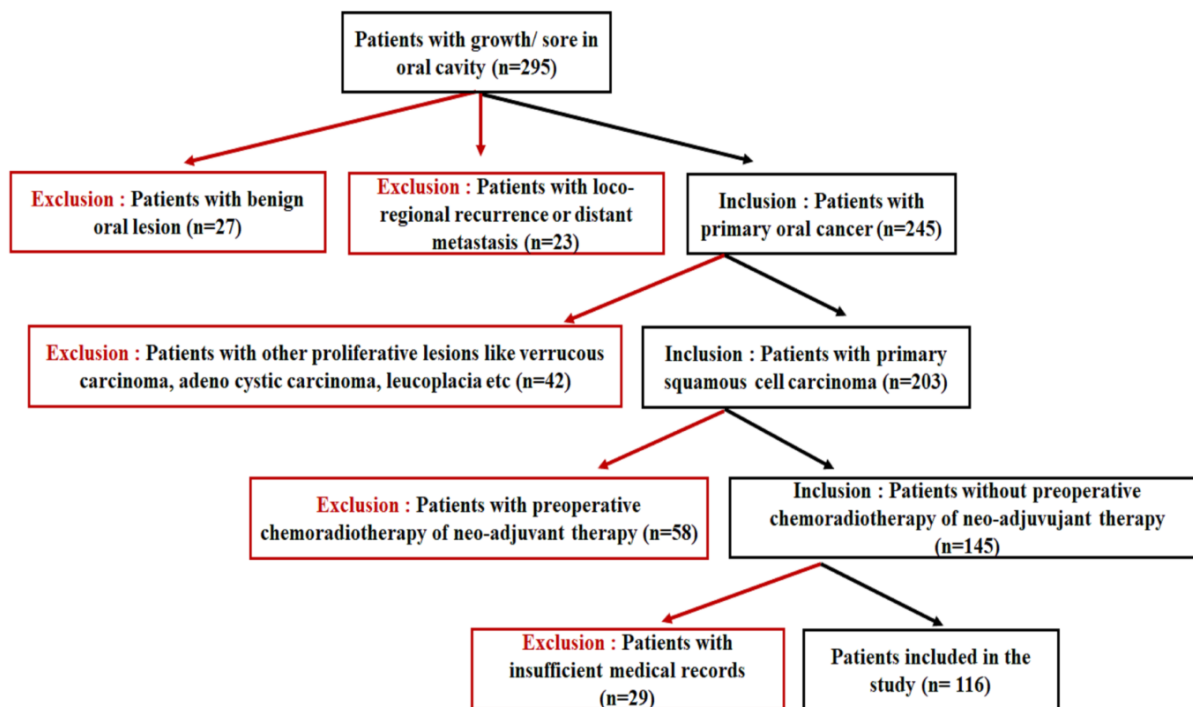


Figure 6: Schematic representation of patients' selection criteria

5.2.2. Antibodies

The primary antibodies used for Immuno-histochemistry (IHC) are as follows. Rabbit polyclonal anti-HIF1 α [Novus Biologicals, Cat# NB100-479, dilution: 1:100], Mouse monoclonal anti-VE-Cadherin [Novus Biologicals, Cat# NB600-1409, dilution: 1:100], Rabbit monoclonal anti-EphA2 [Cell signaling technology, Cat#6997, Clone : D4A2, dilution: 1:100], Rabbit monoclonal anti phospho p44/42 MAPK (Erk1/2) (Thr202/Tyr204) [Cell signaling technology, Cat#4370, Clone : D13.14.4E, dilution: 1:100], , Mouse monoclonal anti- MMP2 [Novus Biologicals, Cat #NB200-114,Clone 8B4,dilution: 1:100], mouse monoclonal anti-Laminin-5 (Y2 chain) [Merck, Cat #MAB19562, Clone D4B5, dilution: 1:100 (IHC)], Rabbit monoclonal anti CD-31 or PECAM-1 (Santa Cruz Biotechnology, Cat # sc-1506-R, Clone M-20,

dilution:1:100], Rabbit monoclonal anti-E-Cadherin [Novus Biologicals, Cat #NBP2-67540, Clone ST54-01,dilution: 1:100], Mouse monoclonal anti- Vimentin [Santa Cruz Biotechnology, Cat # sc-6260, Clone V9, dilution: 1:100], Mouse monoclonal anti-Snail [Novus Biologicals, Cat #NBP2-50300, Clone 20C8, dilution: 1:200], Mouse monoclonal anti-Twist1 [Novus Biologicals, Cat #NBP2-37364, Clone 10E4E6, dilution: 1:200], Rabbit polyclonal anti-CD133 [Novus Biologicals, Cat # NB120-16518, dilution: 1:100 were used as primary antibodies in this study.

5.2.3. CD-31/PAS staining and Immunohistochemistry

Immuno-histochemistry (IHC) was performed according to the manufacturer's instruction of Millipore IHC Select DAB150 Immuno-peroxidase secondary detection system kit. 4 μ M tissue sections from Formalin Fixed Paraffin Embedded (FFPE) tissue blocks were deparaffinized in xylene and sequentially rehydrated using graded ethanol solutions. Antigen retrieval in Sodium citrate buffer (10mM sodium citrate, 0.05% Tween-20, pH-6), followed by exhaustion of endogenous peroxidase activity was performed by immersing the tissue sections into 3% hydrogen peroxide in methanol. Subsequently the tissue sections were incubated with respective primary antibodies for 1 hour at room temperature. The tissue sections were incubated with biotinylated secondary antibody and followed by HRP tagged streptavidin. Finally, the immunoreactivity of the tissue sections was visualized by chromogenic reagent DAB (3,3-diaminobenzidine) and counterstained with Mayer's hematoxylin. For PAS staining coupled with IHC (Sun et al., 2008), the tissue sections were immersed for 10 mins with 0.5% periodic acid solution, after the application of DAB and then stained with Schiff's reagent (Merck) for 10 mins in dark condition, followed by washing in lukewarm water and counterstaining with hematoxylin

solution for 2 min. Ultimately the sections were examined under 200X and 400X magnification using the bright field microscope (Carl Zeiss, model: Primo Star).

5.2.4. Evaluation of Vasculogenic mimicry and IHC markers

The immuno-histochemical score of our studied markers was determined by considering intensity of staining and proportion (%) of stained cells (Gkouveris et al., 2017; Krajewska et al., 1996; Kukita et al., 2019; McCarty et al., 1986; Wu et al., 2018; Zhou et al., 2021). All the staining results were blindly evaluated by two experienced pathologists in a semi quantitative manner. To account the intra-tumoral heterogeneity of antibody expression, ten randomly selected represented fields (under 400X magnification) from different areas of each slide was evaluated by two qualified pathologists (manual method). The staining intensity was determined on the following scale: 0-negative, 1- mild, 2-moderate, 3-strong staining and the percentage (proportion) of positively stained cells per field was scored as follows: 0- <10%, 1- <25% of positively stained cells, 2- <50% positively stained cells, 3- >50% positive cells (Dong et al., 2018; Sun et al., 2008; Sun et al., 2017). The final immuno-histochemical staining score of each sample was determined by summation of staining intensity and percentage (proportion) of positively stained cells, which ranged from 0-6. The final staining score 0-3 was considered as negative staining and that of 4-6 was considered as positive staining (Shao et al., 2008; Wang et al., 2018). The semi-quantitative evaluation of pathologists was further validated by IHC profiler plugin (Varghese et al., 2014) compatible with Image J (Figure 7). To normalize the digital image analysis with the pathologists' manual analysis, the IHC profiler generated four tier staining pattern was scored from 0-3 scale (0- Negative, 1- Low positive, 2-Moderately positive, 3-High positive) similar to the manual assessment. Further the total percentage of positive staining (1- Low positive, 2-Moderately positive, 3-High positive) was determined from their

individual percentage contribution and also scored from 0-3 scale in accordance with the pathologists' consideration of score for proportion (%) of stained cells (Dong et al., 2018; Sun et al., 2008; Sun et al., 2017). The final immuno-histochemical score (0-6) of each sample was determined by summation of the percentage score of total positive staining and the total intensity score contributed by different degree of positive staining pattern to harmonize the digital assessment with the manual findings inferring the final score ≤ 3 as negative staining and that of >3 as positive staining. The figure 7 showed the significantly positive correlation (R square > 0.9 , $P < 0.001$) between the IHC scoring of two pathologists as well as between digital and manual methods. Kappa statistics was used to assess the inter-observer and inter method agreement which revealed almost perfect strength of agreement ($\kappa = 0.81-1.00$) between the scoring of two pathologists and substantial strength of agreement ($\kappa = 0.61-0.80$) (Landis & Koch, 1977) between digital and manual methods confirming the reliability of our IHC scoring method.

Table 7: IHC score calculation and determination of inter-observer and inter-method agreement

Image	Digital (IHC Profiler)				Manual (Pathologist)			Kappa Score (P value)	
	Degree of staining pattern (assigned score)	of Percentage score (0-3) contributed by different staining pattern	Intensity score (0-3) contributed by different staining pattern	Final Score (0-6)	Percentage score (0-3) contributed by different staining pattern	Intensity score (0-3) contributed by different staining pattern	Final Score (0-6)	Agreement (Pathologist 1 vs Pathologist 2)	Agreement (Digital vs Manual)
Laminin 5γ2 positive	Pixel count	4915200	5	Not determined	5	Almost perfect ($\kappa=0.817$), $P<0.001^*$	Substantial ($\kappa=0.761$), $P<0.001^*$		
Total positive	56.3805 (3)	1.759 (~2)	53.78 (3)	1.866 (~2)					
High Positive (3)	13.8183	0.735	16.19	0.903					
Moderately positive (2)	15.2055	0.539	14.25	0.529					
Low positive (1)	27.3567	0.485	23.34	0.434					
Negative (0)	43.6195	0	46.22	0					

Laminin	Pixel count	133668		2	Not determined		2		
5γ2	Total positive	15.0047 (1)	1.238 (~1)		11.02 (1)	1.172 (~1)			
Negative	High Positive (3)	0.6757	0.135		0.23	0.062			
	Moderately positive (2)	2.2185	0.296		1.45	0.263			
	Low positive (1)	12.1105	0.807		9.34	0.847			
	Negative (0)	84.9954	0		88.98	0			
MMP2	Pixel count	133668		5	Not determined		5	Almost perfect	Substantial
Positive	Total positive	80.1754 (3)	2 (2)		79.53(3)	2.059 (~2)		(κ=0.837),	(κ=0.754),
	High Positive (3)	22.5078	0.842		25.23	0.952		P<0.001*	P<0.001*
	Moderately positive (2)	35.2948	0.880		33.76	0.849			
	Low positive (1)	22.3728	0.279		20.54	0.258			
	Negative (0)	19.8246	0		20.47	0			
MMP2	Pixel count	134091		1	Not determined		1		
Negative	Total positive	9.3678 (0)	1.385 (~1)		4.46 (0)	1.318 (~1)			
	High Positive (3)	1.0412	0.333		0.43	0.289			
	Moderately positive (2)	1.5314	0.327		0.56	0.251			
	Low positive (1)	6.7952	0.725		3.47	0.778			
	Negative (0)	90.6321	0		95.54	0			

Intensity score contributed by total positive staining pattern = Sum of (Percentage contribution for degree of positive staining/Percentage contribution for total positive staining) X Assigned score for degree of positive staining pattern

Final Score = Percentage score (0-3) for total positive staining pattern + Intensity score (0-3) contributed by total positive staining pattern

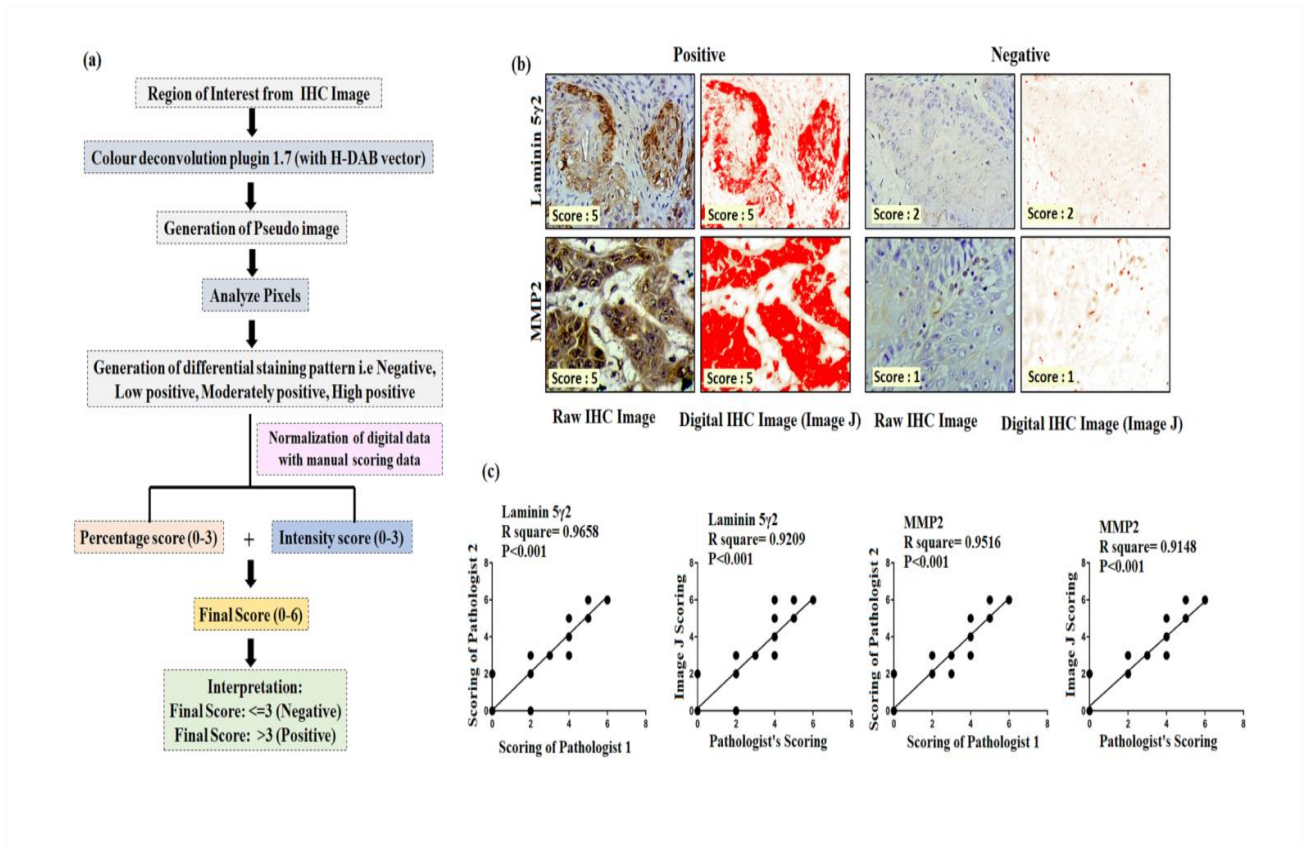


Figure 7: Normalization of the digital image analysis with the pathologists' manual analysis

(a) Flowchart demonstrating the steps involved in the quantification of IHC image using Image J (IHC profiler) and its normalization with manual method. (b) Example of computed IHC score of raw image and digital (Image J generated) image for Laminin-5γ2 and MMP2 marker. (c) Linear correlation between the IHC scoring of two pathologists and two methods for Laminin-5γ2 and MMP2 marker.

5.2.5. Statistical analysis

Association between clinico-pathological parameters and VM, Laminin5γ2, HIF-1α was analyzed using two tailed Chi-square (χ^2) tests and correlation among Laminin5γ2, HIF-1α expression and VM was determined by Spearman Correlation. Statistical analysis of differences between VM positive and VM negative groups were performed by paired Student's *t*-test. The

5year survival rate was determined by Kaplan- Meier method and differences in mean survival time (months) were compared by Log rank tests. The patients' death caused by oral cancer (in case of OS) and loco-regional recurrence or development of distant metastasis (in case of DFS) were considered as outcomes and death by other causes unrelated to oral cancer or lost to follow-up cases were considered as censored. Independent prognostic factors were analyzed using Univariate and Multivariate Cox Proportional Hazard Regression Model. All the statistical analyses were performed using SPSS 17 software (SPSS Inc, Chicago, IL, USA) and Graph-pad Prism version 7.00 software (California, USA). A value of $P < 0.05$ was regarded as statistically significant.

5.3. Results

5.3.1. Clinico-pathological features of OSCC patients

The demographic and clinico-pathological details of the total 116 patients (median age: 54 years, range: 28-80 years) have been recorded in Table 8. Parameters which are correlated with diagnosis, prognosis and treatment of OSCC such as age at the time of diagnosis, anatomic location of primary tumor, histological grade, habit of tobacco and alcohol consumption, tumor size, lymph node metastasis, TNM stage group have been considered. At the end of the of follow-up period (median follow up period was 56 months with a range of 16-60 months), 36 patients (31.03%) were dead due to local recurrence or metastasis after surgery and 62 (53.45%) patients were alive with the rest being lost to follow up or died due to other diseases unrelated to OSCC. they were considered censored for further analysis.

Table 8: Demographic and clinicopathological profile of OSCC patients

Patients' characteristics	n (%)
Age (Years)	
<55	62 (53.45)
>=55	54 (46.55)
Gender	
Male	85 (73.28)
Female	31 (26.72)
Tobacco consumption	
Yes	50 (43.10)
No	66 (56.90)
Alcohol consumption	
Yes	10 (8.62)
No	106 (91.38)
Tumor location	
Lip	8 (6.89)
Tongue	17 (14.65)
Buccal Mucosa	39 (33.62)
Gingiva	24 (20.69)
Floor of Mouth	4 (3.45)
Retromolartriangle (RMT)	5 (4.31)
Others ^a	19 (16.38)
Grade	
Well	73 (62.93)
Moderate	41 (35.34)
Poor	2 (1.72)
Primary Tumor status	
T1	64 (55.17)
T2	8 (6.89)
T3	18 (15.52)
T4	26 (22.41)
Lymph Node metastasis	
N0	66 (56.89)
N1	27 (23.27)
N2	21 (18.10)
N3	2 (1.72)
TNM stage group	
I (T1N0M0)	50 (43.10)
II (T2N0M0)	5 (4.31)
III (T3N0M0, T1-3N1M0)	23 (19.83)
IV (T4N0M0-T1-4N1-3M0)	38 (32.76)

Others^a include alveolar mucosa, hard palate, soft palate

5.3.2. Evaluation of VM in OSCC tissue specimens

Vasculogenic mimicry (VM) was identified through the detection of CD-31 negative and PAS positive lumen like structures surrounded by tumor cells (but not with endothelial cells) with or without red blood cells inside the lumen (Liu et al., 2012; Meng et al., 2019; You et al., 2021) (Figure 8). The vascular structures were observed for structural integrity with no incidence of hemorrhage, necrosis or inflammatory cell infiltration in close proximity (Cheng et al., 2020; B. Shao et al., 2019; Sun et al., 2006; Yu et al., 2021). The VM density with respect to the overall vascular density has been assessed according to the modified method described by (Shao et al., 2008; Weidner et al., 1991; Zhou et al., 2019). The total number of CD31+ and CD31- lumen like vascular structures, surrounded by tumor cells or endothelial cells were considered as the overall vascular density. The areas of highest vascular density were found by observing the slides at 200X magnification. VM vessels were individually counted in 5 randomly selected 200X magnification field. The average percentage of VM has been evaluated relative to the overall vascular density and graded on the basis of following score 0: negative, 1: <20%, 2: 20-<40%, 3: 40-<60%, 4: \geq 60%). Vasculogenic mimicry (VM) was identified in 29.31% of OSCC tissue specimens. Based on the CD31/PAS staining, the total patient population was stratified into VM positive (VM+) and VM negative (VM-) cohorts (Figure 8). Total 34 of 116 (29.31%) cases were VM positive and 82 (70.69%) cases were VM negative.

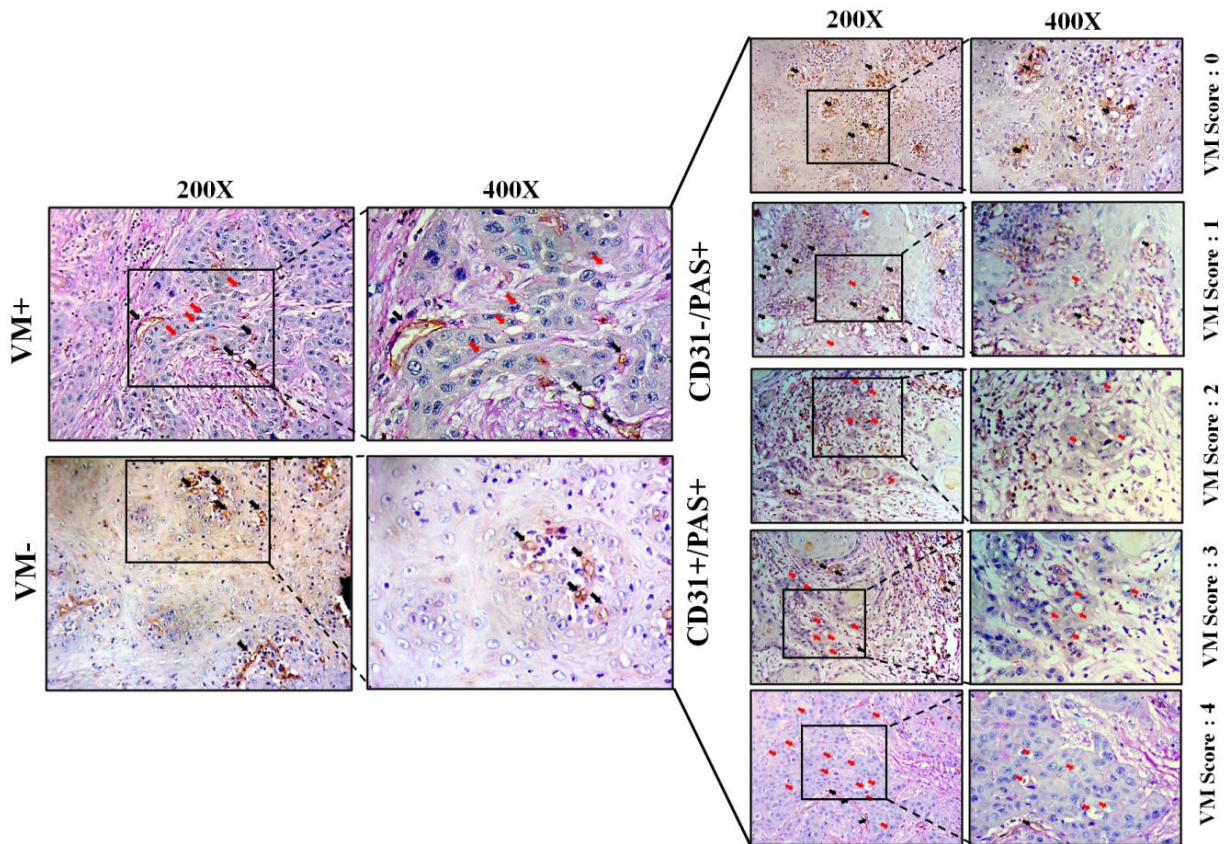


Figure 8: CD31-PAS staining showing VM (with different score) and endothelial structures in OSCC. Red arrows indicate PAS positive and CD31 negative VM architecture (200X and 400X magnifications). Black arrows represent endothelial structure showing CD31 positive staining with or without PAS staining (200X and 400X magnifications)

5.3.3. Differential expression pattern of HIF-1 α along with its downstream EphA2 signaling molecules, EMT and CSC markers in VM stratified OSCC cohorts

The immuno-histochemical staining pattern of HIF-1 α , VE-Cadherin, EphA2, pERK1/2, HIF-1 α and Laminin-5 γ 2 were represented in Figure 9. HIF-1 α and pERK1/2 exhibited both nuclear and cytoplasmic expression. EphA2 expression was widely distributed in tumor cytoplasm. VE-

Cadherin expression was observed around the tumor cytoplasm and vascular architectures. The expression of Laminin-5 γ 2 and MMP2 was observed in OSCC tumor cell cytoplasm as well as in tumor stroma. In most of the cases, Laminin-5 γ 2 showed positive expression to the tumor cells, adjacent to the stroma (S) or tumor stromal interfaces (TS). On the other hand, the expression of MMP2 was distributed in the lining of basement cells around the nests of tumor cells, which in some cases, has been overlapped with the signal of PAS staining. The quantitative data indicated the significantly elevated expression of the above markers in VM positive cohorts ($P < 0.0001$) compared to the VM- specimens. Similarly the differential immuno-histochemical expression of EMT markers (E-Cadherin, Vimentin, Snail Twist) and CSC marker (CD133) was also analyzed among the VM stratified cohorts (Figure 10). Strong positive expression of Vimentin was observed in cytoplasm and infiltrative margin of OSCC tissue. E-Cadherin and CD133 expression was observed in cell cytoplasm whereas Snail and Twist exhibited both cytoplasmic and nuclear expression. All the mesenchymal markers (Vimentin, Snail Twist) and CD133 expression was found to be significantly higher in VM+ cohorts whereas E-Cadherin exhibited significantly reduced expression in VM+ cohorts compared to the VM- group.

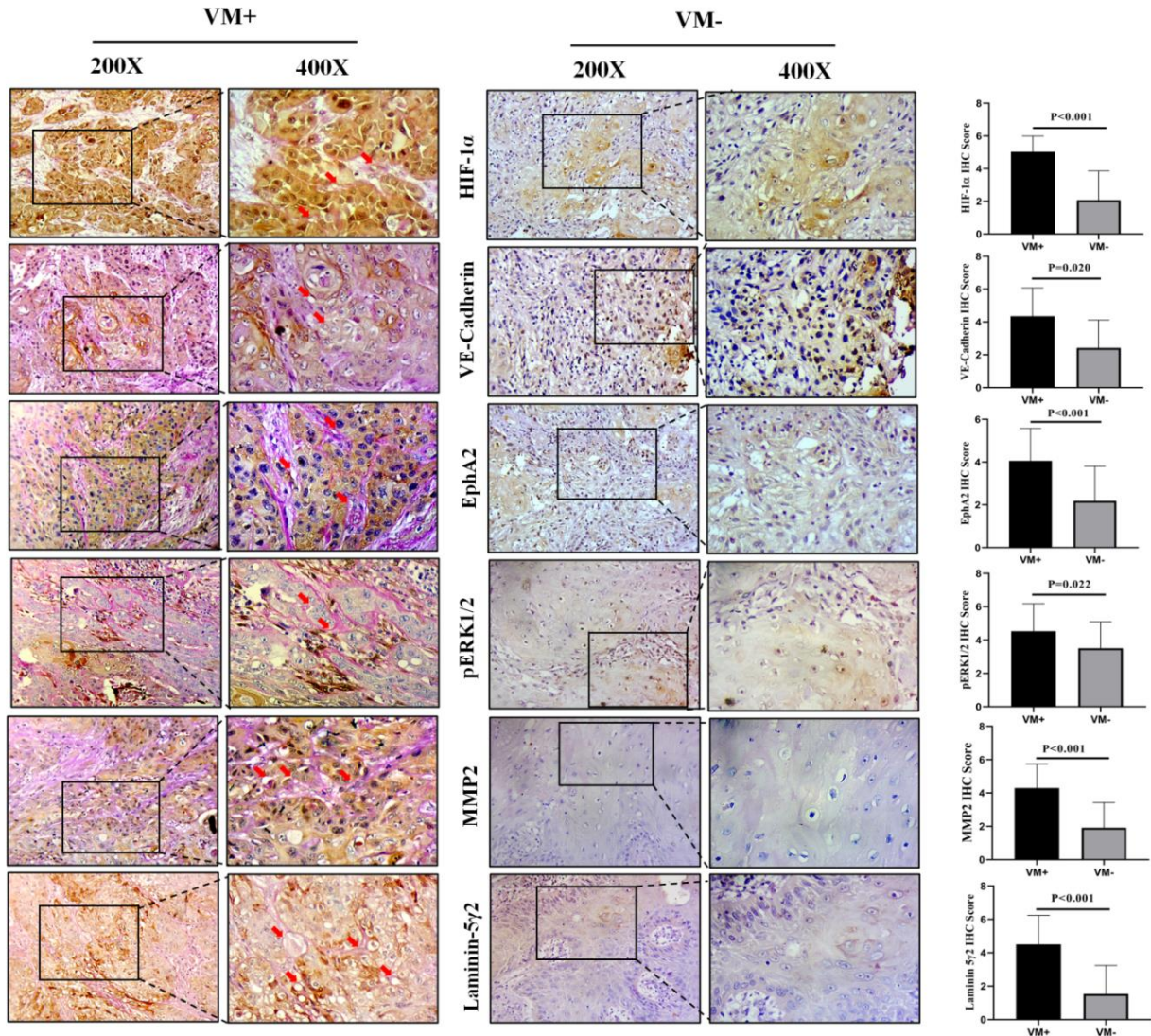


Figure 9: Representative images for immuno-histochemical status (coupled with PAS staining) of HIF-1 α , VE-Cadherin, EphA2, pERK1/2, MMP2 and Laminin-5 γ 2 in VM positive and VM negative OSCC cohorts (200X and 400X magnifications) with their comparative immuno-histochemical scores. Red arrows indicate PAS positive networks. The differences between VM positive and VM negative groups were calculated by paired Student's *t* test ($P<0.0001$).

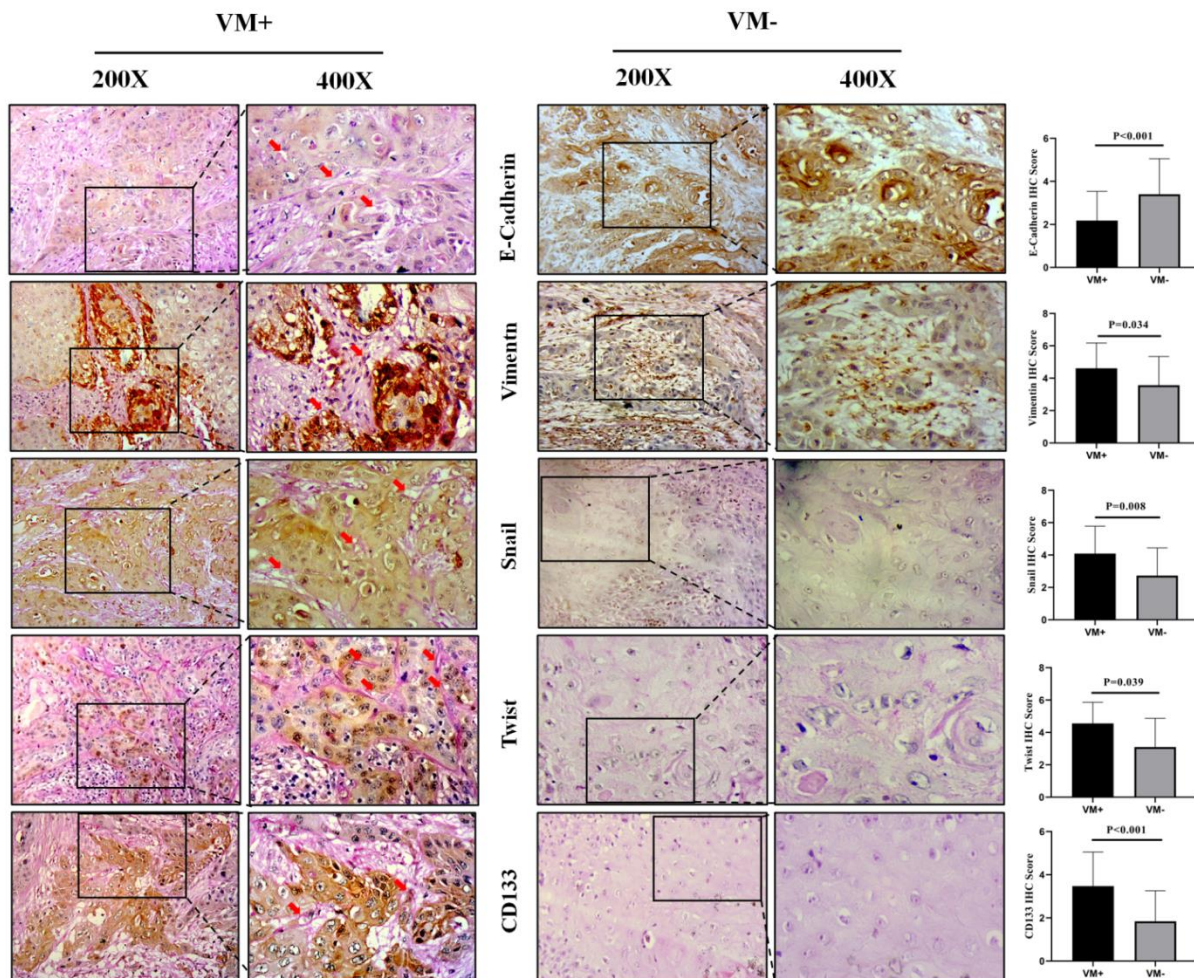


Figure 10: Representative images for immuno-histochemical status (coupled with PAS staining) of E-Cadherin, Vimentin, Snail, Twist and CD133 in VM positive and VM negative OSCC cohorts (200X and 400X magnifications) with their comparative immuno-histochemical scores. Red arrows indicate PAS positive networks. The differences between VM positive and VM negative groups were calculated by paired Student's *t* test ($P < 0.0001$).

5.3.4. Correlation between VM, HIF-1 α and its downstream effectors molecules in OSCC

The correlation of VM with the relevant molecules, i.e., HIF-1 α , VE-Cadherin, EphA2, pERK 1/2, HIF-1 α and Laminin 5Y2 as well as EMT markers (E-Cadherin, Vimentin, Snail Twist) and CSC marker (CD133) are depicted in Table 9. Data revealed significant positive correlation of

the presence of VM with the expression of all of the downstream molecules except E-Cadherin. Unlike E-Cadherin all of the markers were also significantly correlated with the positive expression status of HIF-1 α . These data indicate that HIF-1 α along with the downstream effector molecules may act as a deterministic factor in OSCC progression and VM occurrence.

Table 9: Correlation of VM and HIF-1 α with the molecular markers involved in EphA2/Laminin5 γ 2 cascade, EMT and CSC phenomenon in OSCC patients.

EphA2/ Laminin5 γ 2 cascade		VM	HIF-1 α
HIF-1α	r	0.6511	-
	P value	<0.001	-
VE-Cadherin	r	0.5103	0.5765
	P value	<0.001	<0.001
EphA2	r	0.5290	0.4584
	P value	<0.001	<0.001
Perk1/2	r	0.4167	0.4201
	P value	<0.001	<0.001
MMP2	r	0.6008	0.4997
	P value	<0.001	<0.001
Laminin5γ2	r	0.5743	0.7369
	P value	<0.001	<0.001
EMT markers			
E-Cadherin	r	-0.3796	-0.2152
	P value	<0.001	<0.001
Vimentin	r	0.3900	0.3702
	P value	<0.001	<0.001
Snail	r	0.4097	0.4393
	P value	<0.001	<0.001
Twist	r	0.3519	0.4406
	P value	<0.001	<0.001
CSC marker			
CD133	r	0.5099	0.3233
	P value	<0.001	<0.001

5.3.5. Association between VM, HIF-1 α , Laminin-5 γ 2 expression and patients' clinico-pathological characteristics

The association of VM and expression of HIF-1 α , Laminin 5 γ 2 with the clinico-pathological characteristics of patients has been summarized in Table 10. The presence of VM in OSCC was significantly associated with tumor grade (P=0.002), primary tumor status (P=<0.001) and lymph node metastasis (P=0.005) and TNM stage group (P=<0.001) but not with patient's age, sex and tobacco or alcohol consumption habit. It has been significantly found that 50% (1/2) cohort of the poorly differentiated tumor grade developed VM whereas 48.78% (20/41) of the moderately differentiated group and 17.80% (13/73) of the well differentiated group were found to be VM positive. It is also noteworthy that 59.09% (26/44) patients of T3 and T4 primary tumor status significantly developed VM compared to T1 and T2 group [11.11% (8/72)]. Similarly the occurrence of VM was also significantly prevalent in the patients with positive nodal status compared to the negative ones [46 % (23/50) vs 16.66% (11/66) as well as in the patients with TNM stage group III and IV [47.54% (29/61)] compared to I and II TNM stage group [9.09% (5/55)] . The positive rate of VM was also significantly associated with the expression of HIF-1 α and Laminin-5 γ 2 OSCC. 41.38% (48/116) showed higher expression (staining score: >3) of HIF-1 α and 43.9% of the patients (51/116) showed higher expression (staining score: >3) of Laminin-5 γ 2. Among them the VM positive group was found to have significantly increased level of expression of HIF-1 α (91.18%, P<0.001) and Laminin-5 γ 2 (88.23%, P<0.001) compared to the VM negative counterparts. The associations of patients' clinico-pathological attributes were also analyzed with the expressional status of HIF-1 α and Laminin-5 γ 2. The expression of both HIF-1 α and Laminin-5 γ 2 were significantly associated with primary tumor status (P<0.001 and P<0.001, respectively) and TNM stage group (P=0.002 and P<0.001 respectively). However,

Laminin-5 γ 2 exhibited significant association with no other clinico-pathological parameters but positive rate of HIF-1 α expression was significantly associated with tumor grade (P=0.002) and nodal status (P=0.005).

Table 10: Association between the expression of VM, HIF-1 α and Laminin-5 γ 2 with the clinico-pathological characteristics of oral squamous cell carcinoma (OSCC) patients

Patients' characteristics	VM		χ^2	P value	HIF-1 α		χ^2	P value	Laminin-5 γ 2		χ^2	P value
	Positive n (%)	Negative n (%)			Positive n (%)	Negative n (%)			Positive n (%)	Negative n (%)		
Age (Years)												
<55	17 (14.65)	45 (38.79)	0.230	0.632	23 (19.83)	39 (33.62)	1.007	0.315	23 (19.83)	39 (33.62)	2.55	0.110
\geq 55	17 (14.65)	37 (31.89)			25 (4.31)	29 (25)			28 (24.14)	26 (22.41)		
Gender												
Male	23 (19.83)	62 (53.45)	0.778	0.378	35 (30.17)	50 (43.10)	0.005	0.941	37 (31.89)	48 (41.38)	0.246E	0.875
Female	11 (9.48)	20 (17.24)			13 (11.20)	18 (15.52)			14 (12.07)	17 (14.65)	-01	
Tobacco consumption												
Yes	12 (10.34)	38 (32.76)	1.20	0.274	15 (12.93)	35 (30.17)	4.691	0.030	19 (16.37)	31 (26.72)	1.27	0.260
No	22 (18.96)	44 (37.93)			33 (28.45)	33 (28.45)			32 (27.59)	34 (29.31)		
Alcohol consumption												
Yes	2 (1.72)	8 (6.89)	0.458	0.499	2 (1.72)	8 (6.89)	2.062	0.151	2 (1.72)	8 (6.89)	2.55	0.110
No	32 (27.59)	74 (63.79)			46 (39.65)	60 (51.72)			49 (42.24)	57 (49.14)		
Grade												
Well	13 (11.21)	60 (51.72)	12.6	0.002*	26 (22.41)	47 (40.52)	2.697	0.259	28 (24.14)	45 (38.79)	2.53	0.283
Moderate	20 (17.24)	21 (18.10)			21 (18.10)	20 (17.24)			22 (18.96)	19 (16.38)		
Poor	1 (0.86)	1 (0.86)			1 (0.8)	1(0.8)			1 (0.86)	1 (0.86)		
Primary Tumor status												
T1	5 (4.31)	59 (50.86)	33.6	<0.001*	12 (10.34)	52 (44.83)	32.024	<0.001	17 (14.65)	47 (40.52)	18.5	<0.001*
T2	3 (2.59)	5 (4.31)			4 (34.48)	4 (3.45)			4 (3.45)	4 (3.45)		
T3	10 (8.62)	8 (6.90)			12 (10.34)	6 (5.17)			12 (10.34)	6 (5.17)		
T4	16 (13.79)	10 (8.62)			20 (17.24)	6 (5.17)			18 (15.52)	8 (6.89)		
Lymph Node metastasis												
N0	11 (9.48)	55 (47.41)	12.9	0.005*	16 (13.79)	50 (43.10)	17.221	<0.001	20 (17.24)	46 (39.65)	6.91	0.075
N1	14 (12.07)	13 (11.21)			16 (13.79)	11 (9.48)			16 (13.79)	11 (9.48)		
N2	8 (6.89)	13 (11.21)			14 (12.07)	7 (6.03)			14 (12.07)	7 (6.03)		
N3	1 (0.86)	1 (0.86)			2 (1.72)	0			1 (0.86)	1 (0.86)		
TNM stage group												
I+II	5 (4.31)	50 (43.10)	20.6	<0.001*	11 (9.48)	44 (37.93)	19.708	0.001	16 (13.79)	39 (33.62)	9.39	0.002*
III+IV	29 (25)	32 (27.59)			37 (31.89)	24 (20.69)			35 (30.17)	26 (22.41)		
VM												
Positive	-	-	-	-	31 (26.72)	3 (2.59)	49.169	<0.001	30 (25.86)	4 (3.45)	38.3	<0.001*
Negative	-	-			17 (14.65)	65 (56.03)			21 (18.10)	61 (52.59)		

5.3.6. Association of VM- HIF-1 α and VM-Laminin-5 γ 2 dual positive expression with the clinico-pathological characteristics of patients

The relationship of patients' clinico-pathological parameters with VM-HIF-1 α and VM-Laminin-5 γ 2 double positive status have been shown in Table 11. The result showed 31 (26.72%) VM-HIF-1 α double positive cases, 3 (2.59%) VM positive and HIF-1 α negative group, 17 (14.65%) VM negative and HIF-1 α positive cases and 65 (56.03%) VM-HIF-1 α double negative cases. Similarly, 30 (25.86%) cases belong to VM-Laminin-5 γ 2 double positive group, 4 (3.44%) cases belong to VM positive Laminin-5 γ 2 negative group, 21 (18.10%) cases belong to VM negative Laminin-5 γ 2 positive group and 61 (52.58%) cases belong to VM-Laminin-5 γ 2 double negative group. Interestingly, double positive expressional status of VM- HIF-1 α and VM- Laminin-5 γ 2 were significantly associated with tumor grade (P=0.018 and P=0.010), primary tumor status (P<0.001 and P<0.001), lymph node metastasis (P=0.013 and P<0.001) and TNM stage group (P<0.001, P<0.001).

Table 11: Association between the expression of VM-HIF-1 α dual expression and VM-Laminin-5 γ 2 dual expression with the clinico-pathological characteristics of oral squamous cell carcinoma (OSCC) patients

Patients' characteristics	VM & HIF-1 α dual expression				VM & Laminin-5 γ 2 dual expression			
	Positive n(%)	Negative n (%)	χ^2	P value	Positive n (%)	Negative n (%)	χ^2	P value
Age (Years)								
<55	15 (12.93)	47 (40.52)	0.4355	0.509	14 (12.07)	48 (41.38)	0.748	0.387
>=55	16 (13.79)	38 (32.76)			16 (13.79)	38 (32.76)		
Gender								
Male	22 (18.96)	63 (54.31)	0.1151	0.7344	20 (17.24)	65 (56.03)	0.903	0.342
Female	9 (7.76)	22 (18.96)			10 (8.62)	21 (18.10)		
Tobacco consumption								
Yes	10 (8.62)	40 (34.48)	2.029	0.1543	12 (10.34)	38 (32.76)	0.159	0.690
No	21(18.10)	45 (38.79)			18 (15.52)	48 (41.38)		
Alcohol								

consumption								
Yes	2 (1.72)	8 (6.89)			2 (1.72)	8 (6.89)		
No	29 (25)	77 (66.38)	0.2527	0.615	28 (24.14)	78 (67.24)	0.196	0.658
Grade								
Well	60 (51.72)	13 (11.20)			12 (10.34)	61 (52.59)		
Moderate	24 (20.69)	17 (14.65)	8.0653	0.018	17 (14.65)	24 (20.69)	9.19	0.010*
Poor	1(0.8)	1(0.8)			1 (0.86)	1 (0.86)		
Primary Tumor status								
T1	5 (4.31)	59 (50.86)			4 (3.45)	60 (51.72)		
T2	3 (2.59)	5 (4.31)			3 (2.59)	5 (4.31)		
T3	8 (6.89)	10 (8.62)	27.782	<0.001	8 (6.89)	10 (8.62)	30.4	<0.001*
T4	15 (12.93)	11 (9.48)			15 (12.93)	11 (9.48)		
Lymph Node metastasis								
N0	10 (8.62)	56 (48.27)			8 (6.89)	58 (50)		
N1	12 (10.34)	15 (12.93)			13 (11.21)	14 (12.07)		
N2	8 (6.89)	13 (11.21)	10.783	0.013	8 (6.89)	13 (11.21)	15.7	0.001*
N3	1 (0.86)	1 (0.86)			1 (0.86)	1 (0.86)		
TNM Stage Group								
I+II	5 (4.31)	50 (43.10)			4 (3.45)	51 (43.96)		
III+IV	26 (22.41)	35 (30.17)	16.607	<0.001	26 (22.41)	35 (30.17)	18.9	<0.001*

5.3.7. Survival analysis correlating positive expression of VM, HIF-1 α and Laminin 5 γ 2 with 5 years of disease free survival and overall survival

To understand the collaborative prognostic significance of VM and its associated markers, the 5 year survival rate was calculated for total 116 patients with respect to the survival endpoints including DFS and OS. The Kaplan Meier plot of DFS and OS in OSCC patients with differential status of VM, HIF-1 α , Laminin-5 γ 2 as well as their dual existence has been shown in Figure 11 and Figure 12. The follow up data demonstrated that the mean DFS of VM positive cohort (31.735 ± 2.605 months), HIF-1 α positive cohort (39.272 ± 2.488 months), Laminin-5 γ 2 positive cohort (39.814 ± 2.455 months) were significantly inferior to that of VM negative (58.255 ± 0.451 months, log rank= 92.052, P<0.001), HIF-1 α negative (58.472 ± 0.569 months, log rank= 48.646, P<0.001), Laminin-5 γ 2 negative (58.786 ± 0.357 months, log rank=40.575,

P<0.001) ones. VM- HIF-1 α and VM-Laminin-5 γ 2 double positive cohort also had significantly worse DFS compared to the respective double negative cohorts (30.548 \pm 2.695 months vs 59.028 \pm 0.367 months, log rank= 100.758, P<0.001 respectively and 27.633 \pm 2.006 months vs 58.964 \pm 0.344 months, log rank= 125.283, P<0.001). The distinguishing DFS rate among these groups was also reflected with the OS time. The mean OS of VM positive cohort (41.206 \pm 2.077 months), HIF-1 α positive cohort (46.359 \pm 1.841 months), Laminin-5 γ 2 positive cohort (46.666 \pm 1.798 months), VM- HIF-1 α double positive cohort (40.509 \pm 2.204 months) and VM- Laminin-5 γ 2 double positive cohort (37.583 \pm 1.527 months) was significantly poorer than that of VM negative (58.906 \pm 0.322, log rank= 80.363, P<0.001), HIF-1 α negative (59.058 \pm 0.399 months, log rank= 55.852, P<0.001), Laminin-5 γ 2 negative (59.261 \pm 0.288, log rank=45.209, P<0.001), VM- HIF-1 α double negative (59.465 \pm 0.263 months, log rank = 97.133, P<0.001) and VM- Laminin-5 γ 2 double negative (59.349 \pm 0.280 months, log rank= 114.464, P<0.001) cohorts respectively. These results implied that VM, HIF-1 α and Laminin5 γ 2 either alone or together are indicators of DFS and OS with oral cancer.

Table 12: Results of univariate analyses of disease free survival (DFS) and overall survival (OS) time

Variables	n (%)	Disease free survival (DFS)			Overall Survival (OS)		
		Mean DFS (Months) \pm SE	Log rank	P value	Mean OS (Months) \pm SE	Log rank	P value
VM							
Negative	82 (70.69)	58.255 \pm 0.451	92.052	0.000*	58.906 \pm 0.322	80.363	0.000*
Positive	34 (29.31)	31.735 \pm 2.605			41.206 \pm 2.077		
HIF-1α							
Negative	68 (58.62)	58.472 \pm 0.569	48.646	0.000*	59.058 \pm 0.399	48.317	0.000*
Positive	48 (41.38)	39.272 \pm 2.488			46.359 \pm 1.841		
VM and HIF-1α combined							
Both VM and HIF-1 α negative	65 (56.03)	59.028 \pm 0.367	100.758	0.000*	59.465 \pm 0.263	89.147	0.000*
VM positive and HIF-1 α	3 (18.75)	44.000 \pm 8.083			48.333 \pm 4.234		

negative

VM negative and HIF-1 α positive 17 (14.65) 55.357 \pm 1.416 56.861 \pm 1.010

Both VM and HIF-1 α positive 31(26.72) 30.548 \pm 2.695 40.509 \pm 2.204

Laminin 5 γ 2

Negative 65 (56.03) 58.786 \pm 0.357 40.575 **0.000*** 59.261 \pm 0.288

Positive 51 (43.96) 39.814 \pm 2.455 46.666 \pm 1.798 45.209 **0.000***

VM and Laminin 5 γ 2**combined**

Both VM and Laminin 5 γ 2 negative 61 (52.59) 58.964 \pm 0.344 59.349 \pm 0.280

VM positive and Laminin 5 γ 2 negative 4 (3.45) 56.250 \pm 1.949 125.283 **0.000*** 58.000 \pm 1.732

VM negative and Laminin 5 γ 2 positive 21 (18.10) 56.139 \pm 1.364 57.589 \pm 0.910 114.464 **0.000***

Both VM and Laminin 5 γ 2 positive 30 (25.86) 27.633 \pm 2.006 37.583 \pm 1.527

Abbreviation: SE, Standard error

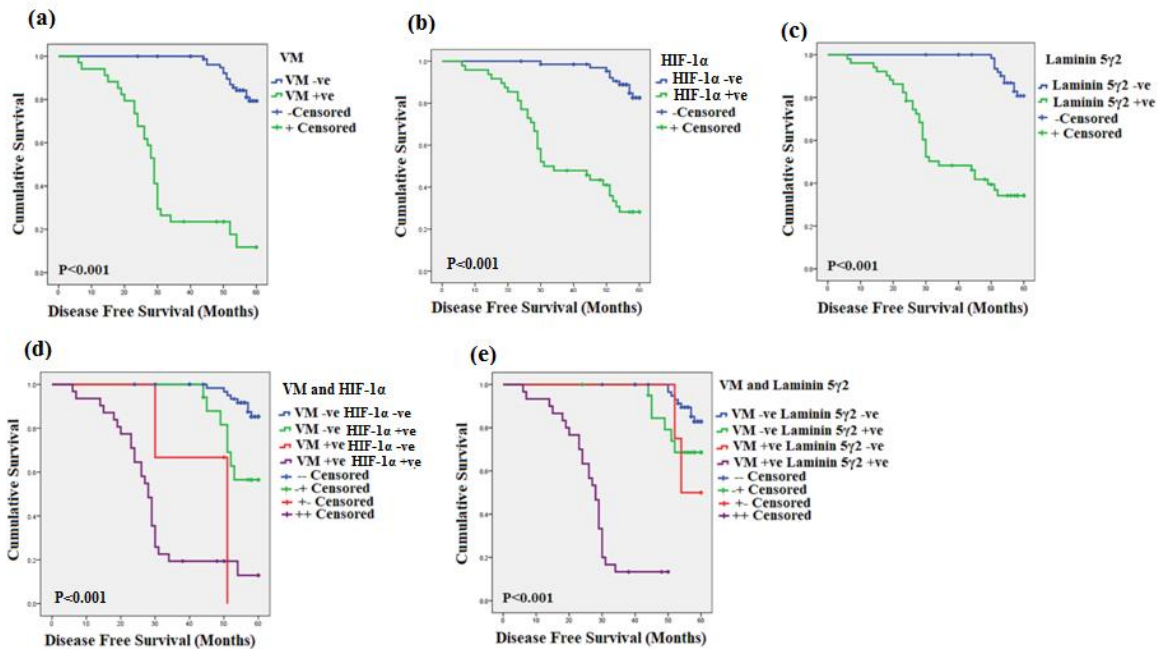


Figure 11: Kaplan Meir survival analysis for disease free survival. Kaplan Meir analysis of the disease free survival (DFS) rate of patients with OSCC in relation to (a) differential expressional

status of (a) VM, (b) HIF-1 α , (c) Laminin-5 γ 2, (d) VM-HIF-1 α dual status and (e) VM-Laminin-5 γ 2 dual status

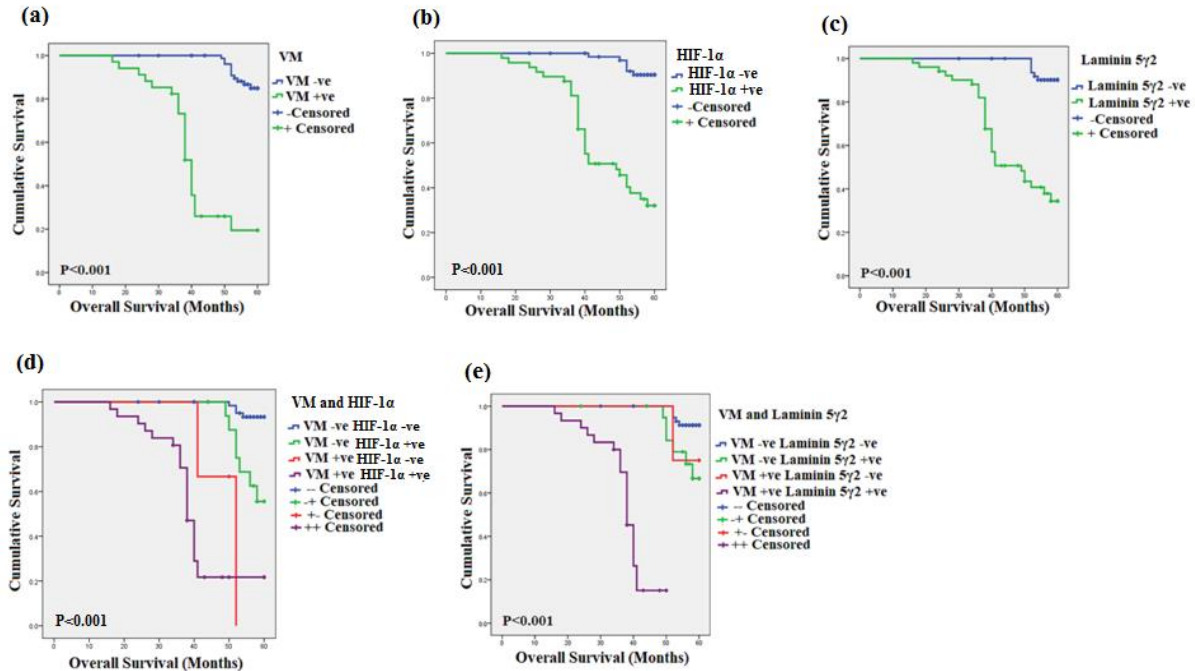


Figure 12: Kaplan Meir survival analysis for overall survival. Kaplan Meir analysis of the overall survival (OS) rate of patients with OSCC in relation to (a) differential expressional status of (a) VM, (b) HIF-1 α , (c) Laminin-5 γ 2, (d) VM-HIF-1 α dual status and (e) VM-Laminin-5 γ 2 dual status

5.3.8. Prognostic impact of paired VM-Laminin-5 γ 2 positivity on disease free and overall survival

Based on the significant findings of univariate analysis (Table 13), indicating the significance of clinicopathological parameters such as tumor grade, primary tumor status, lymph node metastasis, TNM stage group and occurrence of VM independently as well as in conjunction with the expression of Laminin-5 γ 2 in DFS and OS, the multivariate Cox proportional hazards regression model was applied to assess their role as independent survival risk factors (Table 14).

The multivariate analysis revealed that in addition to primary tumor status and lymph node metastasis, the occurrence of VM [Hazard ratio (HR) : 1.696; 95% CI :1.030-2.791; P=0.038], positive expression of Laminin-5 γ 2 (HR: 1.327; CI:1.013-1.739; P=0.040) and VM- Laminin 5 γ 2 double positive status (HR: 9.896; CI: 1,286-76.173; P=0.028) were proved to be independent risk factors for DFS. Similar to DFS, the occurrence of VM (HR: 3.081; CI: 1.428-6.651; P=0.004), positive expression of Laminin-5 γ 2 (HR: 1.424; CI: 1.043-1.945; P=0.026) and the simultaneous double positive expression of VM- Laminin-5 γ 2 (HR: 21.401; CI: 1.276-358.980; P=0.033) were also found to be independent risk factor for OS. In support of the significant findings on the survival endpoints, the positive expression of HIF-1 α and its co-existence with VM were also considered for the analysis of risk factor assessment but neither of them proved to be the independent prognostic factor for DFS and OS in our OSCC cohorts.

Table 13: Assessment of prognostic factors of disease free survival (DFS) and Overall survival (OS) by univariate analysis of Cox- Proportional Hazards model

Variables	Disease Free Survival (DFS)				Overall Survival (OS)			
	HR	P Value	95%CI		HR	P Value	95%CI	
			Lower	Upper			Lower	Upper
Age	1.016	0.225	0.990	1.043	1.029	0.056	0.999	1.060
Gender	1.303	0.094	0.956	1.775	1.339	0.087	0.958	1.872
Tobacco consumption	1.169	0.323	0.858	1.593	1.108	0.549	0.792	1.550
Alcohol consumption	0.948	0.839	0.566	1.586	0.877	0.621	0.521	1.475
Grade	2.893	0.000*	1.690	4.953	2.723	0.001*	1.534	4.832
Primary tumor status	2.102	0.000*	1.648	2.680	2.408	0.000*	1.799	3.224
Lymph node metastasis	2.417	0.000*	1.761	3.317	2.844	0.000*	2.008	4.027
TNM stage group	4.995	0.000*	2.387	10.454	9.632	0.000*	3.399	27.300
VM only	3.112	0.000*	2.402	4.033	5.198	0.000*	3.384	7.984
Laminin 5 γ 2 only	2.025	0.000*	1.632	2.512	2.553	0.000*	1.883	3.461
VM and Laminin 5 γ 2 double positive	44.191	0.000*	16.038	121.763	63.366	0.000*	17.805	225.519

Table 14: Assessment of prognostic factors of Disease Free Survival (DFS) and overall survival (OS) by multivariate analysis of Cox- Proportional Hazards model

Variables	Disease Free Survival (DFS)				Overall Survival (OS)			
	HR	P Value	95%CI		HR	P Value	95%CI	
			Lower	Upper			Lower	Upper
Grade	1.759	0.099	0.900	3.439	1.219	0.625	0.551	2.699
Primary tumor status	1.821	0.003*	1.221	2.717	1.559	0.054	0.992	2.449
Lymph node metastasis	2.944	<0.001*	1.632	5.311	2.865	0.002*	1.478	5.554
TNM stage group	0.307	0.123	0.068	1.379	0.494	0.486	0.068	3.589
VM only	1.696	0.038*	1.030	2.791	3.081	0.004*	1.428	6.651
Laminin 5 γ 2 only	1.327	0.040*	1.013	1.739	1.424	0.026*	1.043	1.945
VM and Laminin 5 γ 2 double positive	9.896	0.028*	1.286	76.173	21.401	0.033*	1.276	358.980

5.4. Discussion

Alternative vascularization influences the poor prognosis of cancer patients (Cao et al., 2013; Hujanen et al., 2020), evoking tumor resistance towards anti-angiogenic and anti-neoplastic therapy (Belotti et al., 2021). Vasculogenic mimicry is a leading pathological entity representing this state to which prompted us for a more comprehensive evaluation of VM and associated prognostic biomarkers underpinning in OSCC.

In this present study, we have evaluated the correlation of VM with expression of HIF-1 α and Laminin-5 γ 2 in predicting the survival and prognosis of OSCC. We have inferred that the occurrence of VM is significantly prevalent in the poorly differentiated tumor with increased primary tumor size, higher lymph-node metastasis and TNM stage which reflected the mechanistic link of VM to the invasion and metastasis attributing the aggressive and malignant progression of OSCC. Contextually, commonalities have been observed in other malignant tumors (Yang et al., 2016). HIF-1 α plays a major role in the cellular response to hypoxia, which is correlated with poor prognosis in several cancers (Birner et al., 2000; Sivridis et al., 2002).

Hypoxia is also an inducer of epithelial-mesenchymal transition (EMT), characterized by loss of cell junction and gain of migratory behavior (Ahmed et al., 2010). So there is the evidence of hypoxic tumor microenvironment to induce EMT and promoting VM progression (Salnikov et al., 2012). Laminin-5 γ 2 complements ECM remodeling, and considered to be one of the most common downstream signaling proteins in molecular cascades associated with VM i.e., TGF- β (Ling et al., 2011), VE-Cadherin, EphA2, PI3-K (Hess et al., 2006), MMP2 (Larson et al., 2014; Lu et al., 2013). Moreover, Laminin receptor Integrin β 1 mediated FAK signaling has also been associated with VM like network formation in human fibrosarcoma cells (Kawahara et al., 2018). On the other hand, the cooperative interaction of MMP2 and Laminin-5 γ 2 has been well established in a number of malignancies including glioblastoma (Ling et al., 2011) and aggressive melanoma when cultured on a three-dimensional ECM (Seftor et al., 2001). Our study delineated a significant interrelation of VM, HIF-1 α and Laminin5 γ 2 along with their coordinated alignment with the histological and conventional prognostic parameters like tumor grade, primary tumor size, lymph node metastasis and TNM stage group highlighting the impact of integrating multiple facets of these markers that may benefit while assessing the risk factors in OSCC. The double positivity of VM -HIF-1 α and VM -Laminin-5 γ 2 as well as their individual positive expression also had the significantly poorer DFS and OS in our study which may act as a tool to predict a worse prognostic indication. Although a few recent studies indicated the individual prognostic significance of some VM associated biomarkers including LGR5 (Wu et al., 2017), ALDH1, Beclin1, p16 (Wang, et al., 2018) and extracellular IL17-F (Almahmoudi et al., 2021), the combinatorial approach of VM with its associated biomarkers (Mitra et al., 2020; Xing et al., 2018) is still a less explored area in OSCC. In this context, our investigation confirmed for the first time that both VM and Laminin-5 γ 2 in combination, provide better

prognostic significance with higher statistical power including increased hazard ratio [(HR)= 9.896, P=0.028 (DFS) and HR= 21.401, P=0.033 (OS)] compared to individual expression of VM [(HR)= 1.696, P=0.038 (DFS) and HR= 3.081, P=0.004 (OS)] and Laminin-5 γ 2 [(HR)= 1.327, P=0.040 (DFS) and HR= 1.424, P=0.026 (OS)]. Collectively, these findings indicate the complementarity of VM and Laminin-5 γ 2 as powerful risk factor of DFS and OS in OSCC. We further validated the manual quantification data with the inputs from automatic profiler and showed a linear pattern (Miles et al., 2021). Indeed, digital quantitative pathology is an evolving modality and needs further validation before its routine adoption as stand-alone method. Knowing the therapeutic challenges of late refractory oral malignancies and roles of novel prognostic biomarkers in informed treatment decisions, these findings will provide important contextual guidance for defining appropriate clinical strategies.

5.5. Conclusion

In conclusion, from this chapter, it can be revealed that the expression of the hypoxia induced HIF-1 α and extracellular matrix protein Laminin-5 γ 2 coordinated with VM are significantly associated with tumor grade, primary tumor size, lymph node metastasis and TNM stage. Furthermore, co-expression of vasculogenic mimicry with HIF-1 α and Laminin-5 γ 2 underlined the independent prognostic impact and correlated with the decreased disease free and overall survival in OSCC patients.

Chapter 6

Role of hypoxia in inducing vasculogenic mimicry in oral squamous cell carcinoma via HIF-1^α/EphA2/Laminin-5γ2 signaling cascade

6.1. Background

Hypoxia is one of the most common phenomenon within the tumor microenvironment of solid tumors including OSCC which is orchestrated by hypoxia inducible factor (HIF-1 α) contributing to tumor metabolism, cellular survival and resistance towards chemotherapy and radiotherapy (Balamurugan, 2016; Patel et al., 2020; Pezzuto & Carico, 2018) in association with tumor metastasis, recurrence and poor survival rate (Eckert et al., 2010; Lee et al., 2007; Zhou et al., 2017). Under hypoxic condition vasculogenic mimicry (VM) serves as an unique strategy of blood and essential nutrient supply to the genetically dysregulated and aggressive tumor cells (Folberg & Maniotis, 2004; Maniotis et al., 1999; Wei et al., 2021) independent of angiogenesis and is associated with tumor invasion, metastasis and poor prognosis of several cancers (Mitra et al., 2020; Ren et al., 2019; Sun, et al., 2018; Yu et al., 2017; Zhang et al., 2019) including OSCC (Hujanen et al., 2021; Wang, et al., 2018; Wu et al., 2017). Although a variety of proteins and micro-environmental factors have been found to contribute VM formation under hypoxic condition in several cancer models including breast cancer (Li et al., 2017; Maroufi et al., 2020; Sun, et al., 2018) hepatocellular carcinoma (Chen et al., 2019; Wang et al., 2017; Zhang et al., 2020), lung adenocarcinoma (Fu et al., 2021), melanoma (Li & Zhou, 2019), colorectal cancer (Li et al., 2016), glioma (Duan, 2018), its underlying molecular mechanistic approach in OSCC remains poorly understood. In the hypoxic malignant tumor microenvironment HIF-1 α enhances the differentiation potential of cancer stem cells (CSC) (Emami Nejad et al., 2021; Li et al., 2016) and promotes their transformation into more mobile cells through epithelial mesenchymal transition (EMT) process (Fan et al., 2013; Hernández de la Cruz et al., 2019) including the remodeling of extracellular matrix (ECM) (Winkler et al., 2020) via the degradation of laminin with the recruitment of matrix metalloproteases (Rousselle & Scoazec, 2020) (Delgado-Bellido

et al., 2017) through a series of intracellular signaling pathways and results into the formation of PAS+/CD31- infiltrating pseudo-vascular VM network to transport red blood cells and nutrients to the tumor cells (Yue et al., 2021). Previous studies had demonstrated that VM channel forming cells could be fueled by upregulated expression of VE-Cadherin, EphA2, ERK1/2, MMP2, Laminin 5 γ 2 genes (Hendrix et al., 2001; Hess et al., 2001, 2006; Larson et al., 2014; Lu et al., 2013; Seftor et al., 2001) in several cancer models but their interconnected cascade and simultaneous induction through HIF-1 α has not been established yet in OSCC. In our previous study we have depicted the prognostic significance of VM in coordination with Laminin 5 γ 2 expression in OSCC patient cohorts (Saha et al., 2022) and based on that findings we further aim to investigate the mechanistic link between HIF-1 α and Laminin 5 γ 2 involving the classical intracellular signaling cascade for reshaping and degradation of ECM and simultaneous formation of VM architecture in OSCC model which may be a potential therapeutic target against the malignant phenotypes of OSCC.

6.2. Materials and methods

6.2.1. Antibodies

The primary and secondary antibodies used for Western blot (WB) are as follows. Rabbit polyclonal anti-HIF1 α (Novus Biologicals, Cat# NB100-479, dilution: 1:500, Mouse monoclonal anti-VE-Cadherin (Novus Biologicals, Cat# NB600-1409, dilution: 1:100, Rabbit monoclonal anti-EphA2 (Cell signaling technology, Cat# 6997, Clone : D4A2, dilution:1:1000, Rabbit monoclonal anti-pEphA2 (S-897) (Cell signaling technology, Cat# 6347, Clone : D9A1, dilution:1:1000, Rabbit monoclonal anti phospho p44/42 MAPK (Erk1/2) (Thr202/Tyr204) (Cell signaling technology, Cat# 4370, Clone : D13.14.4E, dilution:1:2000, Rabbit polyclonal anti Erk1+Erk2 (Abcam, Cat# ab17942, dilution:1:1000), Mouse monoclonal anti- MMP2 (Novus

Biologicals, Cat# NB200-114, Clone 8B4,dilution:1:1000), mouse monoclonal anti-Laminin-5 (Y2 chain) (Merck, Cat# MAB19562, Clone D4B5, dilution:1:1000), Rabbit monoclonal anti-E-Cadherin [Novus Biologicals, Cat# NBP2-67540, Clone ST54-01,dilution:1:1000), Mouse monoclonal anti- Vimentin (Santa Cruz Biotechnology, Cat# sc-6260, Clone V9, dilution:1:200), Mouse monoclonal anti-Snail (Novus Biologicals, Cat# NBP2-50300, Clone 20C8, dilution:1:1000), Mouse monoclonal anti-Twist1 (Novus Biologicals, Cat# NBP2-37364, Clone 10E4E6, dilution: 1:1000), Rabbit polyclonal anti-CD133 (Novus Biologicals, Cat# NB120-16518, dilution: 1:1000), Mouse monoclonal anti β -Actin (Santa Cruz Biotechnology, Cat # sc-47778, Clone C4, dilution:1:200) were used as primary antibodies in this study. Horseradish peroxidase (HRP) conjugated Goat Anti Rabbit polyclonal IgG (Sigma Aldrich, Cat# A0545) and Rabbit Anti Mouse IgG (Sigma Aldrich, Cat# A9044) were used as secondary antibodies.

6.2.2. Cell lines and culture condition

Human oral squamous cell carcinoma cell lines UPCI:SCC154 (ATCC[®]CRL-3241[™]) and UPCI:SCC090 (ATCC[®]CRL-3239[™]) were obtained from American Type Culture Collection (Manassas, VA, USA). All the cell lines were maintained in Minimum Essential Medium (Gibco, Life Technologies, USA) supplemented with 10% heat inactivated Fetal Bovine Serum (FBS) (Gibco, Life Technologies, USA) and 2 mM L-glutamine (Thermo-Fisher Scientific) at 37°C in a humidified incubator with 5% CO₂. All the experiments were performed after 3rd passage of cell lines which were maintained in an exponential growing phase. Hypoxic condition was stimulated by incubating cells in a hypoxic chamber flushed with a gas mixture of 1% O₂/ 5% CO₂/94%N₂ and the induction of HIF-1 α expression was assessed by Western blot analysis.

6.2.3. Transfection of siRNA

The ON-TARGETplusSMARTpool siRNA targeting HIF-1 α (siRNA#1: GAACAAAUACAUGGGAUUA, siRNA#2: AGAAUGAAGUGUACCCUAA, siRNA#3: GAUGGAAGCACUAGACAAA, siRNA#4: CAAGUAGCCUCUUUGACAA) as well as the ON-TARGETplus Non-targeting siRNA (sicontrol) (siControl#1: UGGUUUACAUGUCGACUAA, siControl#2: UGGUUUACAUGUUGUGUGA, siControl#3: UGGUUUACAUGUUUUCUGA, siControl#4: UGGUUUACAUGUUUCCUA) were purchased from Dharmacon (Horizon). The siRNA dried pellet was resuspended in RNase free 1X siRNA buffer to prepare a 20 μ M stock solution. Finally, 100 nM of HIF-1 α siRNA were used to transfect cells. For transfection, cells were seeded into 6 well plates at 1.5×10^5 cells/well (2ml) and cultured overnight. Afterwards when the cells reached 50-60% confluency they were transfected with siRNAs using Jetprime (Polyplus) reagents for 48 hours according to manufacturer's instructions and then characterized by Western blot to assess the level of silencing of HIF-1 α . The silencing experiments and the downstream assays were performed both under normoxia and hypoxia.

6.2.4. In vitro Tube formation assay

Pre-chilled 96 well culture plate was evenly coated with 50 μ l of matrigel matrix (354262, Corning, USA) and incubated at 37 $^{\circ}$ C for 30 mins to solidify. Tumor cells [2×10^4 cells/well (200 μ l)] were seeded in the matrigel coated plate and incubated overnight. In case of transfected cells, after 48 hours of transfection, cells were trypsinized, and then seeded on the matrigel coated plate. The VM channels were observed under inverted microscope and the images were captured at 100X magnification. The images were analyzed to calculate the tube length and number of master junctions using Angiogenesis Analyzer compatible with Image J.

6.2.5. Transwell Migration and Invasion assay

The migration and invasion assay was carried out using 24 well plate containing transwell chambers with the polycarbonate filters of 6.5mm diameter and 8µm pore size (3422, Corning, USA). Cells suspended in 100µl of serum free media were seeded into the upper chambers at a density of 1×10^4 /well for migration and 2×10^4 /well for invasion. For the invasion assays, the growth factor reduced Matrigel (356231, Corning, USA) was diluted with serum-free medium according to the manufacturer instructions at a ratio of 1:5 and 100µl/well was added to the upper chambers and incubated at 37°C for 1 h before seeding cells. The lower chambers were filled with 600µl of complete media containing 10% FBS as chemoattractant. After the incubation of 24 hours the membranes were fixed with methanol for 15 mins and after washing with PBS the membranes were stained with Giemsa stain. The non- migrating or non-invading cells on the upper surface of the membrane were removed using cotton swabs. The no of migrating or invading cells were counted and the images were captured at 100X magnification.

6.2.6. Sphere formation assay

For sphere formation assay single cell suspension in the tumor sphere media (serum free media supplemented with 1X B27, 20ng/ml epidermal growth factor, 10ng/ml basic fibroblast growth factor, 5µg/ml insulin, 0.4% FBS) were seeded at a density of 1000 cells/well (200µl) in a 96-well ultra-low attachment plate. After one week of incubation the sphere forming cells were observed under inverted microscope and the sphere forming efficiency was determined by dividing the number of oral spheres by the number of cells seeded and the images were captured at 100X magnification.

6.2.7. Western blot analysis

Western blot analysis was performed as described earlier (Rauth et al., 2016). Cells were lysed in ice-cold cell lysis buffer (15 mM Tris, 2 mM EDTA, 50 mM 2-mercaptoethanol, 20% glycerol, 0.1% Triton X-100, 1 mM PMSF, 1 mM sodium fluoride, 1 mM sodium orthovanadate, 1 µg/ml aprotinin, 1 µg/ml leupeptin, and 1 µg/ml pepstatin). The total cell lysates were centrifuged at 13,500 rpm at 4°C for 15 min, and the supernatant was aliquoted in separate tubes. The protein concentration was measured using BCA kit (Thermo Scientific) as per the manufacturer's protocol. 50µg of total cell lysate was resolved by 10% SDS-PAGE and then electro-transferred to polyvinylidenedifluoride (PVDF) membrane. After blocking with 5% non-fat dry milk in Tris-buffered saline (20 mM Tris HCl and 137 mM NaCl, pH 7.5) for 1 hour at room temperature the membranes were incubated with different dilutions of primary antibodies overnight at 4°C. Next day, the membranes were washed using Tris-buffered saline (TBS) with 0.5 % Tween 20 and incubated with appropriate secondary antibodies conjugated with horse radish peroxidase (HRP) for 1 hour at room temperature. The signal was visualized using enhanced chemiluminescence kit (BioRad) and the resulting bands were acquired using Image Lab 5.2.1 software (BioRad) and the band density was quantified by Image J software. β -actin was used as a loading control.

6.2.8. Real Time PCR

For gene expression analysis total RNA was extracted with Trizol reagent according to manufacturer's protocol. The complementary DNA (cDNA) was synthesized from 2µg of total RNA using Roche Evoscript Universal cDNA master kit. Quantitative analysis of cDNA amplification was assessed by incorporating SYBR green nucleic acid stain (Roche FastStart Essential DNA Green Master kit) into double stranded DNA. The specific primers for investigating gene expression are as follows: HIF-1 α Forward -5'

GTCTGCAACATGGAAGGTATTG-3', HIF-1 α Reverse- 5'-GCAGGTCATAGGTGGTTTCT - 3', Laminin 5 γ 2 Forward -5' GATGGCATTCACTGCGAGAAG-3', Laminin 5 γ 2 Reverse- 5'-TCGAGCACTAAGAGAACCTTTGG-3', GAPDH Forward- 5'-GTCAACGGATTTGGTCGTATTG-3', GAPDH Reverse- 5'-TGTAGTTGAGGTCAATGAAGGG-3'. The PCR condition included denaturation at 95°C for 1 min, Annealing at 52°C for 1 min and Extension at 72°C for 2 mins. All the samples were evaluated in triplicates using Roche Light cycler 96. GAPDH was used as an endogenous control. Quantitative evaluation of data was carried out using $2^{-\Delta\Delta CT}$ method and Ct (cycle threshold) values were standardized with respect to GAPDH expression.

6.2.9. Statistical analysis

All the statistical analysis was performed using GraphPad Prism 7 (GraphPad, USA) software. All the experiments were repeated independently three times and the data were recorded as mean \pm SD. One way Analysis of variance (ANOVA) followed by post-hoc comparisons with Tukey test was carried out to assess the significant difference between each treated group and untreated control. P<0.05 was considered as statistically significant.

6.3. Results

6.3.1. HIF-1 α escalates VM forming ability in oral cancer in vitro

To investigate the role of HIF-1 α in the enhancement of VM formation, the tube forming ability of OSCC cell lines in 3D tumor culture was monitored by stabilizing HIF-1 α under hypoxia and also silencing HIF-1 α expression with HIF-1 α siRNA. The hypoxic condition triggered the formation of vascular architecture (characterized by the interconnected loops and tubular networks) in all the OSCC cell lines. Further the cells transfected with HIF-1 α siRNA significantly inhibited the tube forming capacity of OSCC cell lines in both normoxia and

hypoxia compared to the non-transfected cells and control siRNA transfected cells demonstrating the fracturing in the tubular structure as well as the significant decrease in the length and number of tubes along with the reduced number of tubular junctions (Figure 14). The non-transfected cells and control siRNA transfected cells did not reveal any significant differences in their VM forming ability either in normoxia or in hypoxia.

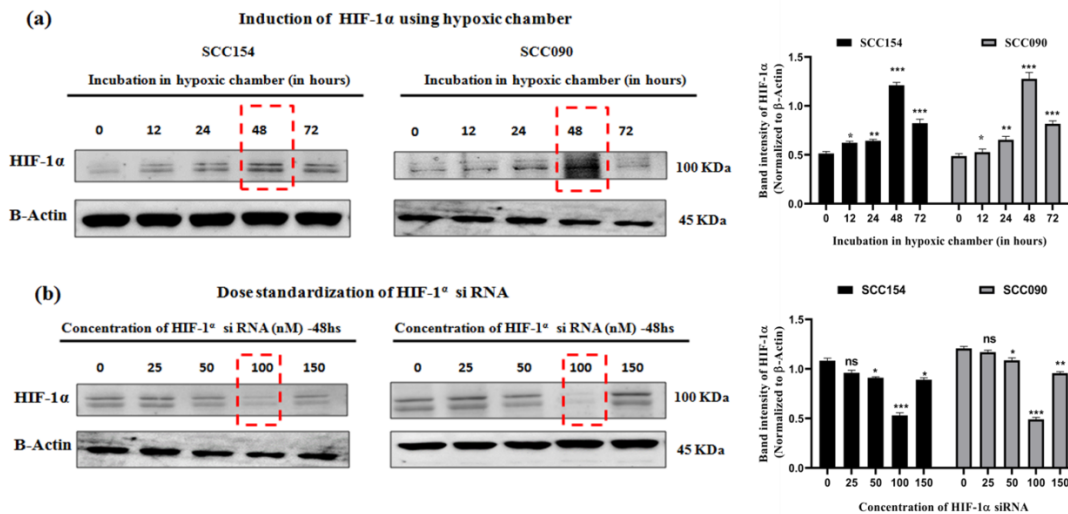


Figure 13: Standardization of (a) hypoxia induction and (b) dose of HIF-1 α siRNA in OSCC cell lines and the representative bar graphs. Each experiment was performed in triplicates. * P value < 0.05, ** P value < 0.01 and * P value < 0.0001 denote statistically significant changes compared to corresponding control by One Way ANOVA test (P ANOVA < 0.0001) followed by post hoc Tukey's test.**

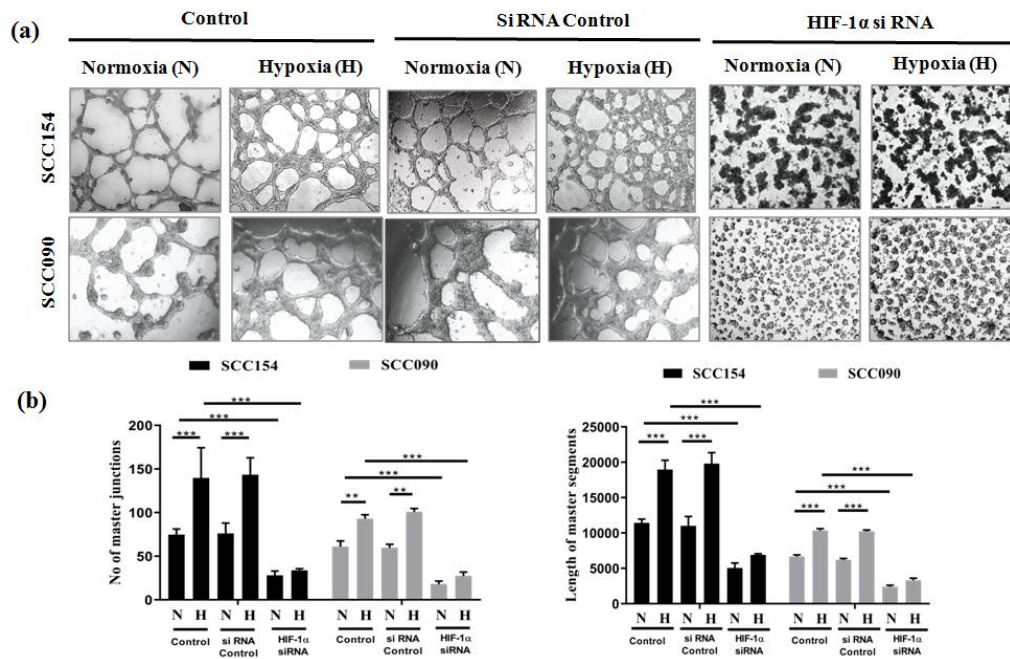


Figure 14: siRNA against HIF-1 α inhibits vasculogenic mimicry formation in vitro (a) Effect of silencing of HIF-1 α on the formation of VM in OSCC cells (Magnification 100X) under normoxia and hypoxia. (b) Quantification of VM formation with respect to the number of master junctions and length of master segments in OSCC cells treated with HIF-1 α siRNA under normoxia and hypoxia. Each experiment was performed in triplicates. * P value <0.05 , ** P value <0.01 and *** P value <0.0001 denote statistically significant changes compared to corresponding control by One Way ANOVA test (P ANOVA < 0.0001) followed by post hoc Tukey's test.

6.3.2. HIF-1 α regulates VM associated EphA2/Laminin 5 γ 2 axis

The expressional alteration of VM associated signaling molecules with the induced and silenced expression of HIF-1 α was evaluated using western blot analysis. Under hypoxia the protein expression of HIF-1 α and its downstream VE-Cadherin, EphA2, pEphA2 (S897), pERK1/2, MMP2 and Laminin 5 γ 2 was significantly increased whereas the knock-down of HIF-1 α notably

downregulated the expression of these VM associated signaling molecules both under normoxic and hypoxic condition in the OSCC cells (Figure 15a) indicating the role of HIF-1 α in regulating the VM promoting EphA2/Laminin 5 γ 2 signaling cascade. Similarly the mRNA expression of HIF-1 α and Laminin 5 γ 2 was also markedly reduced in the HIF-1 α silenced cells under normoxia and hypoxia (Figure 15b).

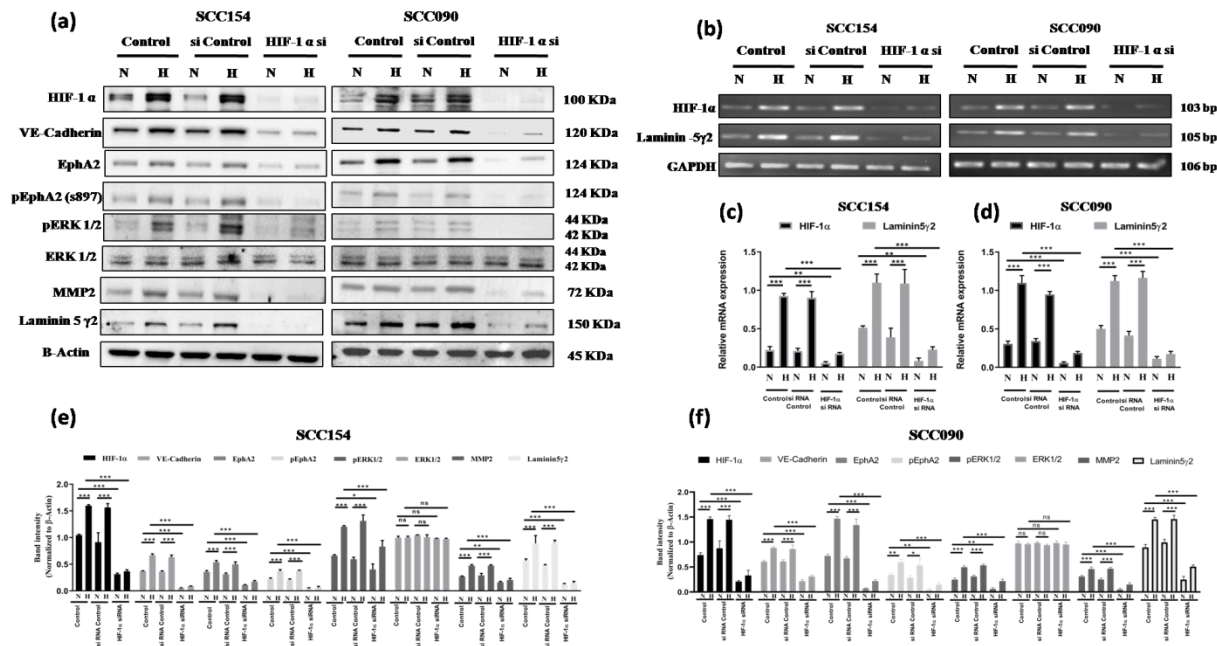


Figure 15: siRNA against HIF-1 α inhibits the expression of vasculogenic mimicry related genes in vitro. (a,e,f) Effect of silencing of HIF-1 α on the protein expression of VM related genes. (b,c,d) Effect of silencing of HIF-1 α on the mRNA expression of VM related genes.

6.3.3. HIF-1 α regulates VM related aggressive phenotype and expression of EMT and CSC markers

Since VM is closely associated with the migration and invasion of tumor cells hence the migratory and invading potential of OSCC cells were assessed using transwell migration and invasion assay in HIF-1 α induced condition and after performing HIF-1 α knockdown respectively (Figure 16). Induction of hypoxia significantly increased the number of migrating

and invading cells whereas the HIF-1 α siRNA transfected cells exhibited significant decrease in tumor cell migration and invasion through transwell chambers compared to the non-transfected cells and control siRNA transfected cells. Hypoxia induced HIF-1 α also heightened the stemness property of tumor cells characterized by the formation of spherical and non-adherent tumor spheres. Sphere forming assay revealed the significant increase in the number and volume of the spheres in hypoxic cells followed by the reduction in sphere formation and downregulation of CD133 with the HIF-1 α knockdown. Furthermore the amelioration of EMT phenomenon through HIF-1 α induction was also investigated by assessing the expressional alteration of EMT markers such as E-Cadherin, Vimentin, Snail and Twist. Hypoxia induced HIF-1 α significantly decreased the expression of E-Cadherin and increased the expression of other mesenchymal markers (Vimentin, Snail and Twist). HIF-1 α siRNA consistently reversed the effect of hypoxia evaluating the expressional alteration of the EMT markers in all the OSCC cell lines (Figure 17).

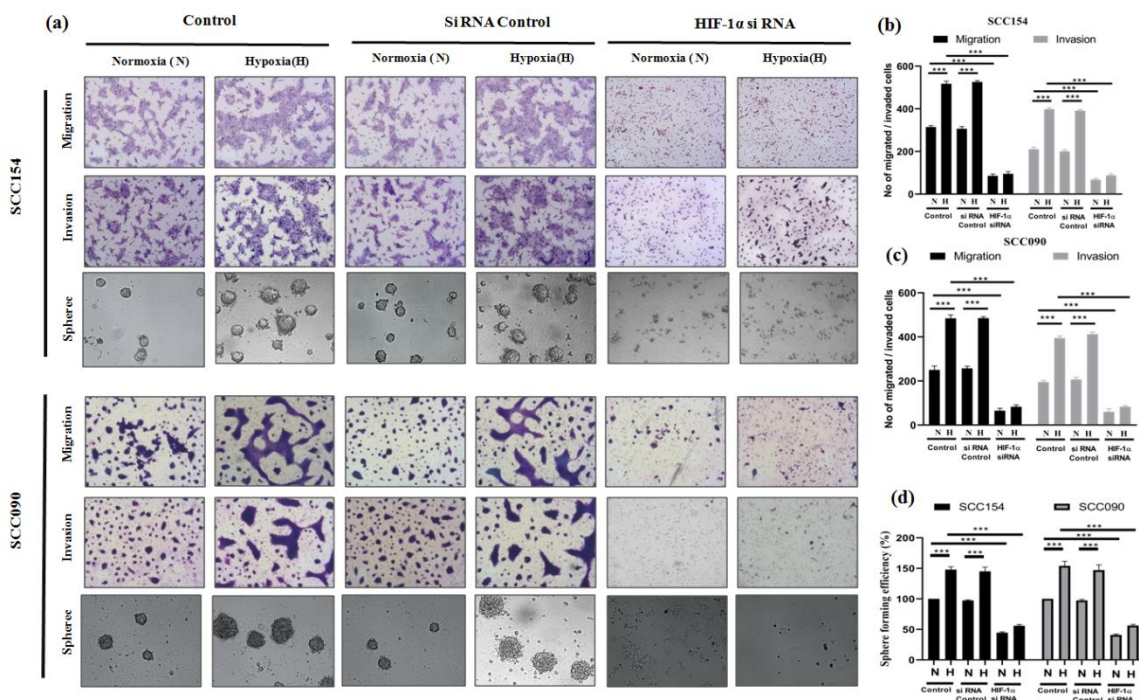


Figure 16: siRNA against HIF-1 α inhibits transwell migration, invasion, sphere formation and expression of EMT and CSC related genes in vitro. (a) Effect of silencing of HIF-1 α on the transwell migration, invasion and sphere formation in OSCC cells (Magnification 100X) under normoxia and hypoxia. (b) Quantification of migrated and invaded OSCC cells and CSC enriched spheres treated with HIF-1 α siRNA under normoxia and hypoxia

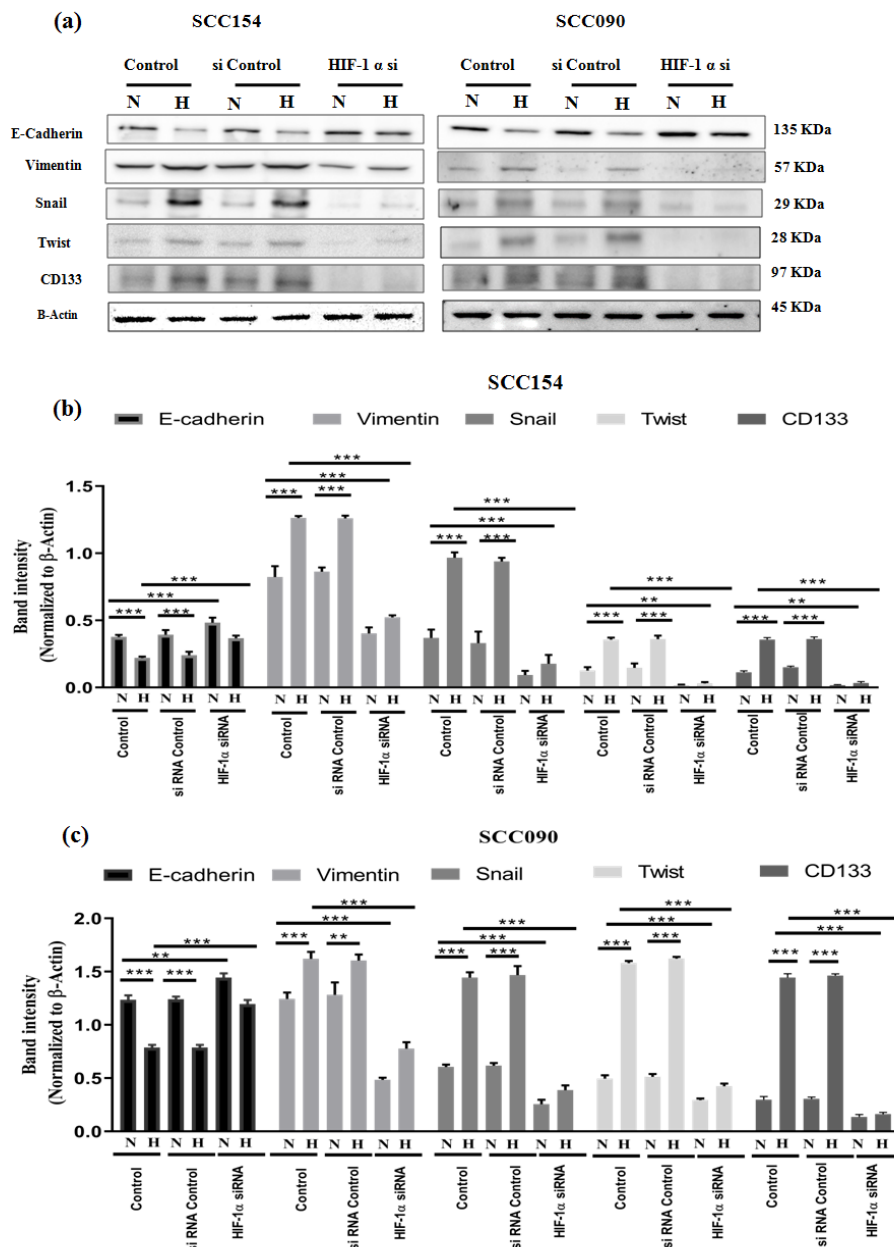


Figure 17: siRNA against HIF-1 α inhibits the expression of EMT and CSC related genes in vitro. (a) Effect of silencing of HIF-1 α on the protein expression of EMT and CSC related genes. (b,c) Quantification of alteration of protein expression in HIF-1 α silenced cells compared to untreated control.

6.4. Discussion

A few recent studies indicated the prognostic significance of some VM associated biomarkers including SOX7 (Hong et al., 2021), LGR5 (Wu et al., 2017), ALDH1, Beclin1, p16 (Wang, et al., 2018) NC11 domain of Collagen XVI (Bedal et al., 2015) in OSCC but the molecular mechanistic approach behind the VM formation in coordination with other intracellular factors has not been explored yet. The current study linked the hypoxic induction of HIF-1 α and OSCC-VM formation through modulating the expression of Laminin-5 γ 2 which is an indicator of extracellular matrix remodeling via the consequential up-regulation of VE-Cadherin, EphA2, pEphA2 (S-897), pERK1/2 and MMP2. The siRNA mediated knockdown of HIF-1 α disrupted VM formation and inhibited the potential of cellular migration, invasion and stemness under both normoxia and hypoxia in SCC154 and SCC090 cell lines. Hypoxic induction of VM has been reported in lung adenocarcinoma through NRP1 up regulation (Fu et al., 2021) and hepatocellular carcinoma through upregulation of LOXL2 (Wang et al., 2017) as well as triggering HIF-1 α stabilization and elevation of Vimentin expression via RhoA/ROCK and RAC1/PAK signaling (Zhang et al., 2020). Macrophage migration inhibitory factor (MIF) also augmented the hypoxia induced VM formation through CXCR4-AKT pathway in glioblastoma cells (Guo et al., 2017). Hypoxia induced VM formation has also been explained in breast cancer via ROS mediated GSK-3 β /Snail signaling (Sun, et al., 2018) but none of the studies have focused upon the hypoxia induced changes in ECM components. In this regard our study

suggests a narrative of multifactorial signaling in the hypoxic tumor microenvironment that might converge to influence the orchestration of ECM degradation and metastatic VM formation in OSCC model. Earlier the study of (Tang et al., 2014) demonstrated that HIF-1 α up-regulated the expression of VE-Cadherin to modulate VM in esophageal squamous cell carcinoma but did not emphasize on the intermediate players of EphA2 signaling including pEphA2 (S-897) and pERK1/2 which are found to be correlated with VM expression in liver (Huang et al., 2014), prostate (Wang et al., 2016) and breast cancer (Mitra et al., 2020). We further demonstrated that the hypoxic induction of HIF-1 α augmented the EMT along with stem like phenotype in OSCC cells through notable expressional alteration of E-Cadherin, Vimentin, Snail, Twist and CD133. Our findings have been supported by (Wang et al., 2019) who investigated the role of VEGFA in hypoxia induced VM formation through regulating EMT and stemness in salivary adenoid cystic carcinoma (SACC). Another study from their group also indicated the VM forming potential of CD133+ cancer stem like cells in SACC (Wang et al., 2016). Several recent studies including breast cancer (Maroufi et al., 2020), liver cancer (Chen et al., 2019), melanoma (Li & Zhou, 2019) demonstrated the crucial role of EMT in hypoxia induced VM formation and the study of Wang et al., 2014 and Kang et al., 2021 revealed the mechanism of VM formation via EphA2 as well as Tenascin C and ERK mediated EMT phenotype in head and neck squamous cell carcinoma and gastric cancer but no evidence of hypoxia inducing VM formation via EMT has been reported yet in OSCC. In that context our study revealed that hypoxic induction caused enhancement of VM forming ability in OSCC cells and on the other hand silencing of HIF-1 α resulted into the significant reduction of VM forming capacity followed by the inhibition of downstream signaling components including EphA2, pERK1/2, MMP2, Laminin-5 γ 2 under normoxic and hypoxic condition. Furthermore silencing of HIF-1 α also significantly reduced the

invasion, migration and sphere forming efficiency in the in vitro OSCC model as well the alteration of subsequent EMT and CSC markers, revealing their mechanistic involvement in the OSCC VM formation.

6.5. Conclusion

From this chapter it can be concluded that HIF-1 α plays an important role in the hypoxia induced VM formation in the in vitro oral cancer model. The possible mechanism is that the hypoxic microenvironment causes induced expression of HIF-1 α which leads to the simultaneous upregulation of the downstream targets including VE-Cadherin, pEphA2 (S-897), pERK1/2, MMP2, Laminin-5 γ 2 causing extracellular matrix remodeling and enhancement of Mesenchymal phenotype and cancer stemness in OSCC cells.

Chapter 7

**Evaluation of synergistic effect of Lupeol and
Paclitaxel in attenuating vasculogenic mimicry in in
vitro and ex vivo oral squamous cell carcinoma**

7.1. Background

Despite the advances in diagnosis and various treatment modalities, the 5 year survival of OSCC patients did not improve for more than 50%, mostly because of the treatment failure due to the loco-regional recurrence and distant metastasis (Thavarool et al., 2019). The poor survival outcome is also influenced by alternative vascularization strategies which evokes tumor resistance towards anti-angiogenic and anti-neoplastic therapies (Belotti et al., 2021). Since traditional anti-angiogenic therapy could not inhibit the formation of VM, finding a new treatment regimen specifically targeting VM holds a great challenge to the researchers and clinicians. Platinum based drugs like Cisplatin and Carboplatin, in combination with Fluorouracil have been considered as conventional chemotherapeutic regimens for locally advanced OSCC (Gibson et al., 2005; Hartner, 2018). To improve prognosis, administration of taxane based drugs such as Paclitaxel in conjunction with the platinum drugs or Cetuximab have recently been reported to be effective with lower cytotoxicity and higher tolerability (Ahn et al., 2016; Hitt et al., 2012; Sawatani et al., 2020). Paclitaxel is a mitotic inhibitor which stabilizes cytoplasmic microtubules and causes interference of cellular replication, arresting cells from entering to G2/M phases of the cell cycle, and apoptosis (Horwitz, 1994). However its adverse side effects on non-malignant healthy cells is a concerning factor to develop alternative treatment scheme. Combining the cancer preventive phytochemicals with the conventional chemotherapeutic agents has become an emerging strategy of treating cancer to augment the efficacy and response rate of the anticancer drug and concurrently to overcome the drug resistance, dose induced toxicity and adverse side effects. Hence our goal is to elucidate the anti-VM efficacy of phytochemical Lupeol via modulating hypoxia induced ECM remodeling and simultaneous EMT and CSC phenotypes. Lupeol is a pharmacologically active natural triterpene widely found in edible fruits

and vegetables (Liu et al., 2021; Saleem, 2009) including mango, strawberry, olive, red grapes, white cabbage, cucumber, pepper, tomato and reported to have extensive anti-inflammatory, mutagenesis-inhibiting, anti-neoplastic, anti-arthritis, and anti-diabetic properties in both in vitro and in vivo studies (Bociort et al., 2021; Che et al., 2022; Malekinejad et al., 2022). Moreover, data from in vitro (Nyaboke et al., 2018; Pitchai et al., 2014) and animal studies (Al-Rehaily et al., 2001; Patočka, 2003; Saleem, 2009) provided convincing evidences regarding safety profile of Lupeol. In this regard our study aims to explore the possible chemo-sensitization effect of Lupeol to potentiate the anti-neoplastic effect of conventional chemotherapeutic drug Paclitaxel in terms of obstructing VM and its associated aggressive phenotypes in the in vitro and ex vivo OSCC platform and through establishing the synergistic cooperation of Lupeol with lower doses of Paclitaxel, our study may indicate a novel and promising therapeutic strategy against human OSCC.

7.2. Materials and methods

7.2.1. Reagents

A 30 mM stock solution of Lupeol (Sigma, S957712) was prepared by dissolving in warm alcohol followed by dilution with DMSO (Sigma, D2650) at a ratio of 1:1. For all the treatment protocols the final concentration of DMSO was <0.01% which is nontoxic to cells. A 50mM stock solution of Paclitaxel (Sigma, T1912) was prepared by dissolving in DMSO.

7.2.2. Antibodies

The primary and secondary antibodies used for Western blot (WB), Immuno-histochemistry (IHC), Immunofluorescence (IFS) and Flow cytometry (FC) are as follows. Rabbit polyclonal anti-HIF1 α (Novus Biologicals, Cat# NB100-479, dilution: 1:500 for WB; 1:100 for IHC; 1:100 for IFS; 1:100 for FC), Mouse monoclonal anti-VE-Cadherin (Novus Biologicals, Cat# NB600-

1409, dilution: 1:100 for WB ; 1:100 for IHC), Rabbit monoclonal anti-EphA2 (Cell signaling technology, Cat#6997, Clone: D4A2, dilution: 1:1000 for WB; 1:100 for IHC), Rabbit monoclonal anti-pEphA2 (S-897, Cell signaling technology, Cat#6347, Clone: D9A1, dilution: 1:1000 for WB; 1:100 for IHC), Rabbit monoclonal anti phospho p44/42 MAPK (Erk1/2) (Thr202/Tyr204), from Cell signaling technology, Cat#4370, Clone: D13.14.4E, dilution: 1:2000 for WB; 1:100 for IHC), Rabbit polyclonal anti Erk1+Erk2 (Abcam, Cat# ab17942, dilution: 1:1000 for WB), Mouse monoclonal anti-MMP2 (Novus Biologicals, Cat #NB200-114, Clone: 8B4, dilution: 1:1000 for WB; 1:100 for IHC), mouse monoclonal anti-Laminin-5 (Y2 chain) from Merck (Cat #MAB19562, Clone: D4B5, dilution: 1:1000 for WB; 1:100 for IHC), Rabbit monoclonal anti CD-31 or PECAM-1 (Santa Cruz Biotechnology, Cat# sc-1506-R, Clone: M-20, dilution: 1:100 for IHC), Rabbit monoclonal anti-E-Cadherin (Novus Biologicals, Cat#NBP2-67540, Clone: ST54-01, dilution: 1:1000 for WB; 1:100 for IHC; 1:100 for IFS), Mouse monoclonal anti- Vimentin (Santa Cruz Biotechnology, Cat# sc-6260, Clone:V9, dilution: 1:200 for WB; 1:100 for IHC; 1:100 for IFS), Mouse monoclonal anti-Snail (Novus Biologicals, Cat#NBP2-50300, Clone: 20C8, dilution: 1:1000 for WB; 1:200 for IHC), Mouse monoclonal anti-Twist1 (Novus Biologicals, Cat# NBP2-37364, Clone: 10E4E6, dilution: 1:1000 for WB; 1:200 for IHC), Rabbit polyclonal anti-CD133 (Novus Biologicals, Cat# NB120-16518, dilution: 1:1000 for WB; 1:100 for IHC; 1:100 for IFS), Rabbit monoclonal anti -Bcl2 (Novus Biologicals, Cat# NBP2-07182, Clone: JF104-8, dilution: 1:1000 for WB), mouse monoclonal anti-Bax (Santa Cruz Biotechnology, Cat #sc-7480, Clone: B9, dilution: 1:200 for WB), Mouse monoclonal anti β -Actin (Santa Cruz Biotechnology, Cat# sc-47778, Clone: C4, dilution: 1:200 for WB) were used as primary antibodies in this study. Horseradish peroxidase (HRP) conjugated Goat Anti Rabbit polyclonal IgG (Sigma Aldrich, Cat# A0545) and Rabbit Anti

Mouse IgG (Sigma Aldrich, Cat# A9044) were used as secondary antibodies for performing western blot and Goat anti-Rabbit IgG F(ab')₂ secondary antibody with FITC conjugate (Invitrogen, Cat# 31573) and Goat anti-Mouse F(ab')₂ IgG (H+L) secondary antibody with PE conjugate (Invitrogen, Cat# 12-4010-82) were used for performing Immunofluorescence and Flow cytometry.

7.2.3. Cell lines and culture condition

Human oral squamous cell carcinoma cell lines UPCI:SCC154 (ATCC®CRL-3241™) and UPCI:SCC090 (ATCC®CRL-3239™) were obtained from American Type Culture Collection (Manassas, VA, USA). All the cell lines were maintained in Minimum Essential Medium (Gibco, Life Technologies, USA) supplemented with 10% heat inactivated Fetal Bovine Serum (FBS) (Gibco, Life Technologies, USA) and 2 mM L-glutamine (Thermo-Fisher Scientific) at 37°C in a humidified incubator with 5% CO₂. All the experiments were performed after 3rd passage of cell lines which were maintained in an exponential growing phase. Hypoxic condition was stimulated by incubating cells in a hypoxic chamber flushed with a gas mixture of 1% O₂/5% CO₂/94%N₂ and the induction of HIF-1α expression was assessed by Western blot analysis.

7.2.4. Cell viability assay

7.2.4.1. MTT assay

Cell viability was determined by MTT assay. Cells were seeded at a density of 1x10⁴/well (200μl) in a 96 well plate and then exposed to Lupeol (0-200 μM), Paclitaxel (0-150 nM) and Lupeol+ Paclitaxel for 48 hours under hypoxic condition. Thereafter 10μl of MTT solution (2mg/ml) was added in each well and incubated for 2-4 hours at 37°C. Then 100μl of DMSO was added to dissolve the formazan crystal and OD was measured at 570 nm using microplate reader. The percentage cell viability was determined with respect to the untreated control.

7.2.4.2. Determination of Combination Index (CI)

After the determination of individual and combinatorial inhibitory effects of Lupeol and Paclitaxel the combination index was calculated according to the meth described by (Chou, 2010). The value of CI implies the quantitative measure of degree of interaction between two drugs. $CI < 1$ denotes synergistic, $CI=1$ denotes additive and $CI >1$ denotes antagonistic effects. The dose reduction index (DRI) is the measure of dose reduction of each drug in a synergistic combination of a given level compared with the doses of individual drugs.

7.2.5. Clonogenic assay

Approximately 500 cells / well (2ml) were seeded in a 6 well plate and after overnight incubation cells were treated with designated doses of Lupeol and Paclitaxel and were then grown in fresh medium for another 3 days at 37°C until the colonies were formed. Cell colonies were fixed with 10% methanol for 15 mins. After that colonies were washed with 1X PBS and stained with Harry's hematoxylin. Then the number of colonies (a single colony denotes >50 cells) were counted under the bright field microscope and photographs were captured at 4X magnification and the percentage of colonies were calculated with respect to the untreated control.

7.2.6. Wound healing assay:

For wound healing assay, cells were seeded at a density of 1×10^6 cells/well in a 6 well plate. When the cells reached more than 80% confluency a vertical wound was created through cell monolayer using 200 μ l pipette tip. Cellular debris and smooth edges of scratch were removed by washing the cells once and replaced with serum free media containing different concentrations of Lupeol and Paclitaxel. Wound closure was observed at different time points and photographs were captured at 4X magnification under bright field microscope and the scratch area was analyzed using Image J software.

7.2.7. Evaluation of apoptosis

7.2.7.1. AnnexinV/PI assay

Cell apoptosis was detected using Annexin V Apoptosis detection kit (Santa Cruz Biotechnology Inc, sc-4252 AK). Briefly after treatment of individual and combined doses of Lupeol and Paclitaxel for 48 hours the cells were harvested by centrifugation and dissolved in 1X assay buffer. Cells were then stained with Annexin-V-FITC and propidium iodide (PI), incubated at room temperature for 15 minutes in the dark and then data were acquired by BD FACSVerserTM flow cytometer. Cells without Annexin V-FITC and PI stains were considered as negative control. Total 10000 events were considered during acquisition. The dual parameter dot plot considering the logarithmic fluorescence intensity of FL1-H (X axis- FITC fluorescence) and FL2-H (Y axis- PI fluorescence) was obtained using FlowJoTM v10 software to determine the percentage of total apoptosis (consisting of early apoptosis and late apoptosis).

7.2.7.2. TUNEL assay

Apoptotic cells that undergo DNA degradation were detected using TUNEL assay using TACS - 2 TdT-Fluor Insitu Apoptosis detection kit (R&D systems, Cat #4812-30K) according to the manufacturer's protocol. After fixation with 3.7% buffered formaldehyde, the cells on the sterile coverslips were digested with protease K for 15 minutes at room temperature. The cells were then washed and incubated with TUNEL reaction mix (TdT enzyme solution and labeling solution) for 60 minutes at 37°C in humidified chamber. The cells on the coverslips were mounted on clean glass slides and the TUNEL positive apoptotic cells were detected with the fluorescence microscope at 400X magnification.

7.2.8. In vitro Tube formation assay

Pre-chilled 96 well culture plate was evenly coated with 50 μ l of matrigel matrix (354262, Corning, USA) and incubated at 37°C for 30 mins to solidify. Tumor cells [2 X 10⁴ cells/well (200 μ l)] were seeded in the matrigel coated plate and incubated overnight. In case of transfected cells, after 48 hours of transfection, cells were trypsinized, and then seeded on the matrigel coated plate. The VM channels were observed under the inverted microscope and the images were captured at 100X magnification. The images were analyzed to calculate the tube length and number of master junctions using Angiogenesis Analyzer compatible with Image J.

7.2.9. Transwell Migration and Invasion assay

The migration and invasion assay was carried out using 24 well plate containing transwell chambers with the polycarbonate filters of 6.5mm diameter and 8 μ m pore size (3422, Corning, USA). Cells suspended in 100 μ l of serum free media were seeded into the upper chambers at a density of 1 \times 10⁴/well for migration and 2 \times 10⁴/well for invasion. For the invasion assays, the growth factor reduced Matrigel (356231, Corning, USA) was diluted with serum-free medium according to the manufacturer instructions at a ratio of 1:5 and 100 μ l/well was added to the upper chambers and incubated at 37°C for 1 h before seeding cells. The lower chambers were filled with 600 μ l of complete media containing 10% FBS as chemo-attractant. After the incubation of 24 hours the membranes were fixed with methanol for 15 mins and after washing with PBS the membranes were stained with Giemsa stain. The non-migrating or non-invading cells on the upper surface of the membrane were removed using cotton swab. The number of migrating or invading cells were counted and the images were captured at 100X magnification.

7.2.10. Sphere formation assay

For sphere formation assay single cell suspension in the tumor sphere media (serum free media supplemented with 1X B27, 20ng/ml epidermal growth factor, 10ng/ml basic fibroblast growth factor, 5µg/ml insulin, 0.4% FBS) were seeded at a density of 1000 cells/well (200µl) in a 96-well ultra-low attachment plate. After one week of incubation the sphere forming cells were observed under inverted microscope and the sphere forming efficiency was determined by dividing the number of oral spheres by the number of cells seeded and the images were captured at 100X magnification.

7.2.11. Western blot analysis

Western blot analysis was performed as previously described method (Rauth et al., 2016) in chapter 6. 50µg of total cell lysates were resolved by 10% SDS-PAGE and then electro-transferred to polyvinylidenedifluoride (PVDF) membrane. After blocking with 5% non-fat dry milk for 1 hour at room temperature the membranes were incubated with different dilutions of primary antibodies overnight at 4°C followed by the exposure with appropriate secondary antibodies conjugated with horse radish peroxidase (HRP) for 1 hour at room temperature. The signal was visualized using enhanced chemiluminescence kit (BioRad) and the resulting bands were acquired using Image Lab 5.2.1 software (BioRad) and the band density was quantified by Image J software. β -actin was used as a loading control.

7.2.12. Real Time PCR

For gene expression analysis, total RNA was extracted with Trizol reagent according to the manufacturer's protocol. The complementary DNA (cDNA) was synthesized from 2µg of total RNA using Roche Evoscript Universal cDNA master kit. Quantitative analysis of cDNA amplification was assessed by incorporating SYBR green nucleic acid stain (Roche FastStart

Essential DNA Green Master kit) into double stranded DNA. The specific primers for investigating gene expression are as follows: HIF-1 α Forward -5'-GTCTGCAACATGGAAGGTATTG-3', HIF-1 α Reverse- 5'-GCAGGTCATAGGTGGTTTCT-3', Laminin 5 γ 2 Forward -5'-GATGGCATTCACTGCGAGAAG-3', Laminin 5 γ 2 Reverse 5'-TCGAGCACTAAGAGAACCTTTGG-3', GAPDH Forward- 5'-GTCAACGGATTTGGTCGTATTG-3', GAPDH Reverse- 5'-TGTAGTTGAGGTCAATGAAGGG-3'. The PCR condition included denaturation at 95°C for 1 min, Annealing at 52°C for 1 min and Extension at 72°C for 2 mins. All the samples were evaluated in triplicates using Roche Light cycler 96. GAPDH was used as an endogenous control. Quantitative evaluation of data was carried out using $2^{-\Delta\Delta CT}$ method and Ct (cycle threshold) values were standardized with respect to GAPDH expression.

7.2.13. Immunofluorescence assay

For Immunofluorescence assay tumor cells [$\sim 1-1.5 \times 10^4$ cells/well (2ml)] were seeded on the sterile coverslips in 6-well plates and cultured overnight. After the treatment with Lupeol and Paclitaxel cells were fixed with methanol. Next the cells were incubated with appropriate primary antibodies for 1 hour after permeabilization with 0.5% Triton-X 100 and 5% BSA. After washing with PBS containing 0.5% Tween-20, cells were incubated with FITC and PE Conjugated secondary antibodies for 1 hour followed by incubation with DAPI for nuclear localization. After the staining the coverslips were mounted with glycerol and imaging was performed by fluorescence microscope (Olympus,) and the data were analyzed by Image J software.

7.2.14. Flow cytometry analysis

For flow cytometry analysis cells were seeded at a density of 2×10^5 cells/well (2ml) of 6 well plates and after the treatment with Lupeol and Paclitaxel, cells were washed with PBS, trypsinized and centrifuged at 4000 rpm for 5 minutes. Cells were then incubated with appropriate primary antibodies for 1 hour followed by incubation with FITC and PE Conjugated secondary antibodies for 30 mins. After that cells were fixed with paraformaldehyde and data were acquired by BD FACSVerse™ flow cytometer. Total 10000 events were acquired and the dot plot considering the logarithmic fluorescence intensity of FL1-H (X axis- FITC fluorescence) /FL2-H (Y axis- PE fluorescence) was obtained using FlowJo™ v10 software to determine the percentage of gated population in order to evaluate the expressional alteration of the studied markers. An unstained sample was prepared without primary and secondary antibodies.

7.2.15. Patient derived tumor explant culture

The patient derived tumor explant culture was established as described by (Majumder et al., 2015). Fresh OSCC tumor specimens were collected from a total of 5 patients (details mentioned in Table 16) immediately after surgical resection from Chittaranjan National Cancer Institute, Kolkata. For each patient, non-heparinized blood was collected and serum was separated and stored at -80°C for further use. The study was approved by the Institutional Ethics Committee (IEC Ref: A-4.311/53/2014) in accordance with the ethical guidelines of Declaration of Helsinki (1964) and its later amendments. Patients have no history of recurrence, preoperative chemotherapy or radiotherapy. Surgically removed fresh tumor tissues were cut into $\sim 2\text{-}3\text{mm}^3$ sections and cultured into 24 well culture plates coated with tumor matrix proteins and RPMI medium (Gibco, Life Technologies, USA) supplemented with 2% autologous serum and 8% FBS. Tumor slices were treated with individual and combinatorial doses of Lupeol and Paclitaxel

or with DMSO (vehicle control) for 48 hours. The formalin fixed paraffin embedded (FFPE) tumor blocks were then used for histological examination.

7.2.16. Immunohistochemistry/PAS dual staining

Immuno-histochemistry (IHC) was performed according to the manufacturer's instruction of Millipore IHC Select DAB150 Immuno-peroxidase secondary detection system kit from the FFPE tumor blocks as per our previously described methods (Mitra et al., 2020; Saha et al., 2022) in Chapter 5. Primary antibodies against CD-31 or PECAM-1, HIF-1 α , VE-Cadherin, EphA2, pERK1/2, MMP2, Laminin 5 γ 2, E-Cadherin, Vimentin, Snail, Twist, CD133 were used for IHC. The final IHC score was determined by considering intensity of staining and proportion (%) of stained cells as described earlier (Saha et al., 2022).

7.2.17. Protein-protein interaction (PPI) and network analysis

For STRING protein-protein interaction (PPI) network analysis (<https://string-db.org>), all input markers were selected from current study and queried in setting that involves full network (type), confidence (edge meaning), multiple active interaction sources/channels in combination spanning text mining, database, experiments, co-expression, neighborhood, gene fusion and co-occurrence. Minimum required interaction score with high confidence or 0.700 was selected for final analysis. We restricted the maximum number of interactions only to queried proteins that have been profiled in the study and no additional layer or second shell was added.

7.2.18. Statistical analysis

All the statistical analysis was performed using GraphPad Prism 7 (GraphPad, USA) software. All the experiments were repeated independently three times and the data were recorded as mean \pm SD. One way Analysis of variance (ANOVA) followed by post-hoc comparisons with

Tukey test was carried out to assess the significant difference between each treated group and untreated control. $P < 0.05$ was considered as statistically significant.

7.3. Results

7.3.1. Effect of Lupeol and Paclitaxel on the viability and proliferation of OSCC cells under hypoxia

MTT assay results indicated the potential cytotoxic effect of Lupeol and Paclitaxel on the OSCC cell lines. The dose dependent cytotoxicity of Lupeol did not differ significantly in 24 and 48 hours in both the UPCI:SCC154 and UPCI:SCC090 cell lines whereas treatment with varying doses of Paclitaxel exhibited notable differences in the cell viability during 48 hours in comparison with 24 hours. Hence for further assays the treatment duration of 48 hours was considered for both Lupeol and Paclitaxel. Individual treatment of Lupeol attained the IC₅₀ value of 79.43 μ M in UPCI:SCC154 cells and 91.25 μ M in UPCI:SCC090 cells during 48 hours whereas the treatment of Paclitaxel alone derived the IC₅₀ value of 83nM in UPCI:SCC154 cells and 67nM in UPCI:SCC090 cells. The simultaneous treatment of cells with Lupeol and sub IC₅₀ doses of Paclitaxel attained a stronger inhibitory effect on cellular viability compared to their individual treatment (details mentioned in Table 15 and Figure 18). The CI value for the combinatorial treatment was found to be 0.737 for UPCI:SCC154 cells and 0.815 for UPCI:SCC090 cells indicating the synergistic effects of Lupeol and Paclitaxel in cell viability inhibition. Finally the combination of 39.43 μ M of Lupeol + 20nM of paclitaxel (for UPCI:SCC154 cells) and 52.58 μ M of Lupeol + 16nM of Paclitaxel (for UPCI:SCC090 cells) indicated the best synergistic inhibition potential (Figure 18i), which was designated for further investigations. The combinatorial dose exhibited a significantly decreased percentage of colonies

(Figure 19a) and reduced wound healing potential compared to the individual treatment (Figure 19b).

Table 15: Determination of effective combinatorial dose of Lupeol and Paclitaxel using the method of Chou et al, 2010

	SCC154	SCC090
Factors	Lupeol+ Paclitaxel (C1)	Lupeol+ Paclitaxel (C2)
Dose selection (μM)	Lupeol : 20,40,60,80,100 Paclitaxel : 0.020, 0.040	Lupeol : 20,40,60,80,100 Paclitaxel : 0.016, 0.033
IC 50 for individual compound treatment (μM)	Lupeol : 79.43 Paclitaxel : 0.083	Lupeol : 91.25 Paclitaxel : 0.067
IC 50 for combined treatment (μM) (Effective Dose)	Lupeol : 39.43, when Paclitaxel : 0.020	Lupeol : 52.58, when Paclitaxel : 0.016
Combination Index (CI) (Paclitaxel :)	$C1 = (39.43/79.43) + (0.020/0.083) = 0.737$	$C2 = (52.58/91.25) + (0.016/0.067) = 0.815$
CI= ($D_{\text{Lupeol, Comb}}/D_{\text{Lupeol}} + D_{\text{Paclitaxel, Comb}}/D_{\text{Paclitaxel}}$)		
Dose reduction Index (DRI) $D_{\text{Drug}}/D_{\text{Drug, Comb}}$	Lupeol : $(79.43/39.43) = 2.014$ Paclitaxel : $(0.083/0.020) = 4.15$	Lupeol : $(91.25/52.58) = 1.746$ Paclitaxel : $(0.067/0.016) = 4.187$
Combination effect	Synergistic	Synergistic

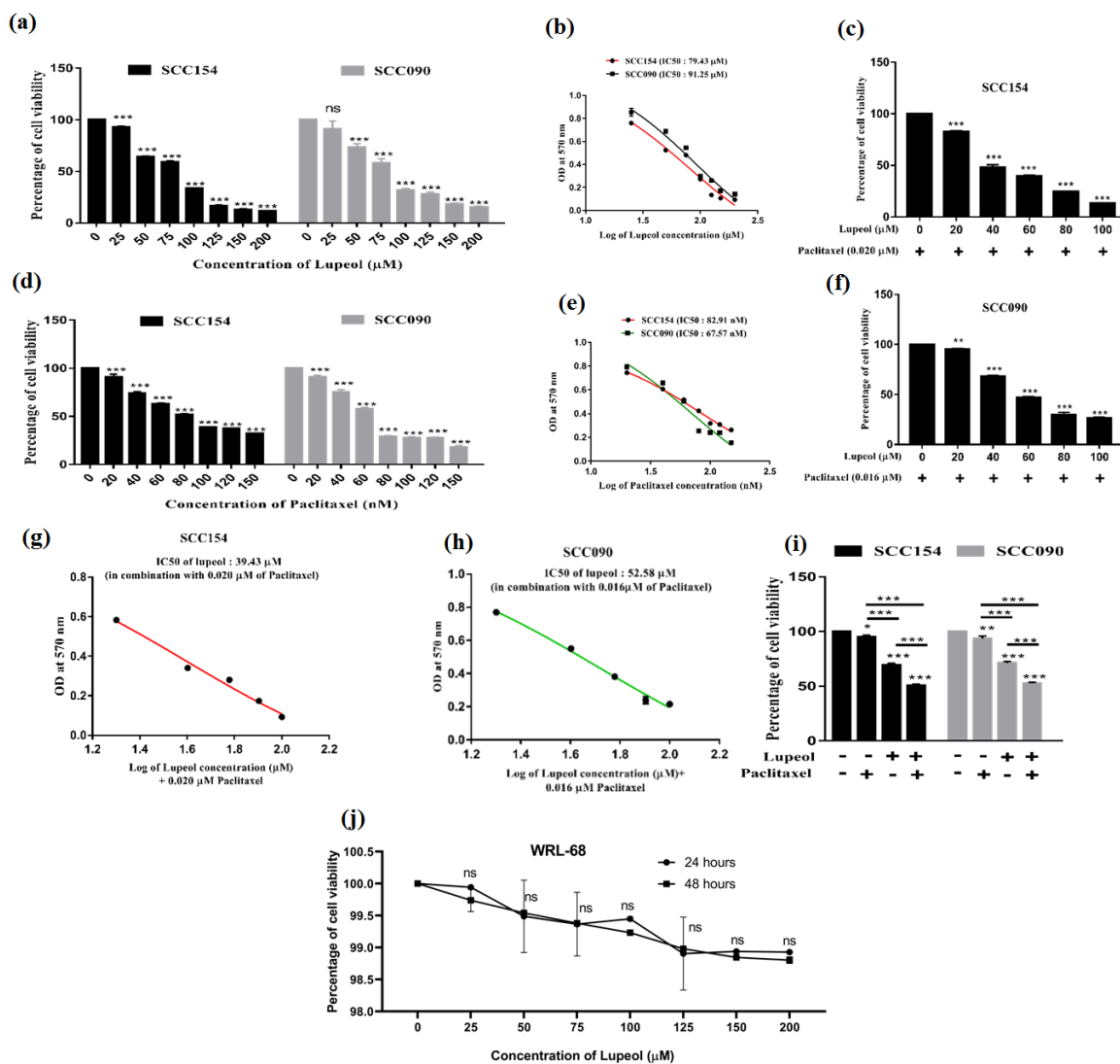


Figure 18: Effect of Lupeol and Paclitaxel in hypoxia induced cellular proliferation in vitro
 (a) & (c) Percentage of cell viability with increasing doses of individual treatment of Lupeol and Paclitaxel in OSCC cells. (b) & (d) IC_{50} dose of Lupeol and Paclitaxel calculated using nonlinear regression curve fit followed by log (inhibition) vs response equation. (e) & (g) Percentage of cell viability with varying doses of Lupeol in combination with sub IC_{50} dose of Paclitaxel in OSCC cells. (f) & (h) IC_{50} dose of Lupeol in combination with Paclitaxel

calculated using nonlinear regression curve fit followed by log (inhibition) vs response equation.

(i) Percentage of cell viability in Lupeol and Paclitaxel treated OSCC cells with respect to untreated control. (j) Percentage of cell viability in Lupeol and Paclitaxel treated normal liver cell line WRL-68. Each experiment was performed in triplicates. *P value<0.05, **P value <0.01 and ***P value <0.0001 denote statistically significant changes compared to corresponding control by One Way ANOVA test (P ANOVA< 0.0001) followed by post hoc Tukey's test.

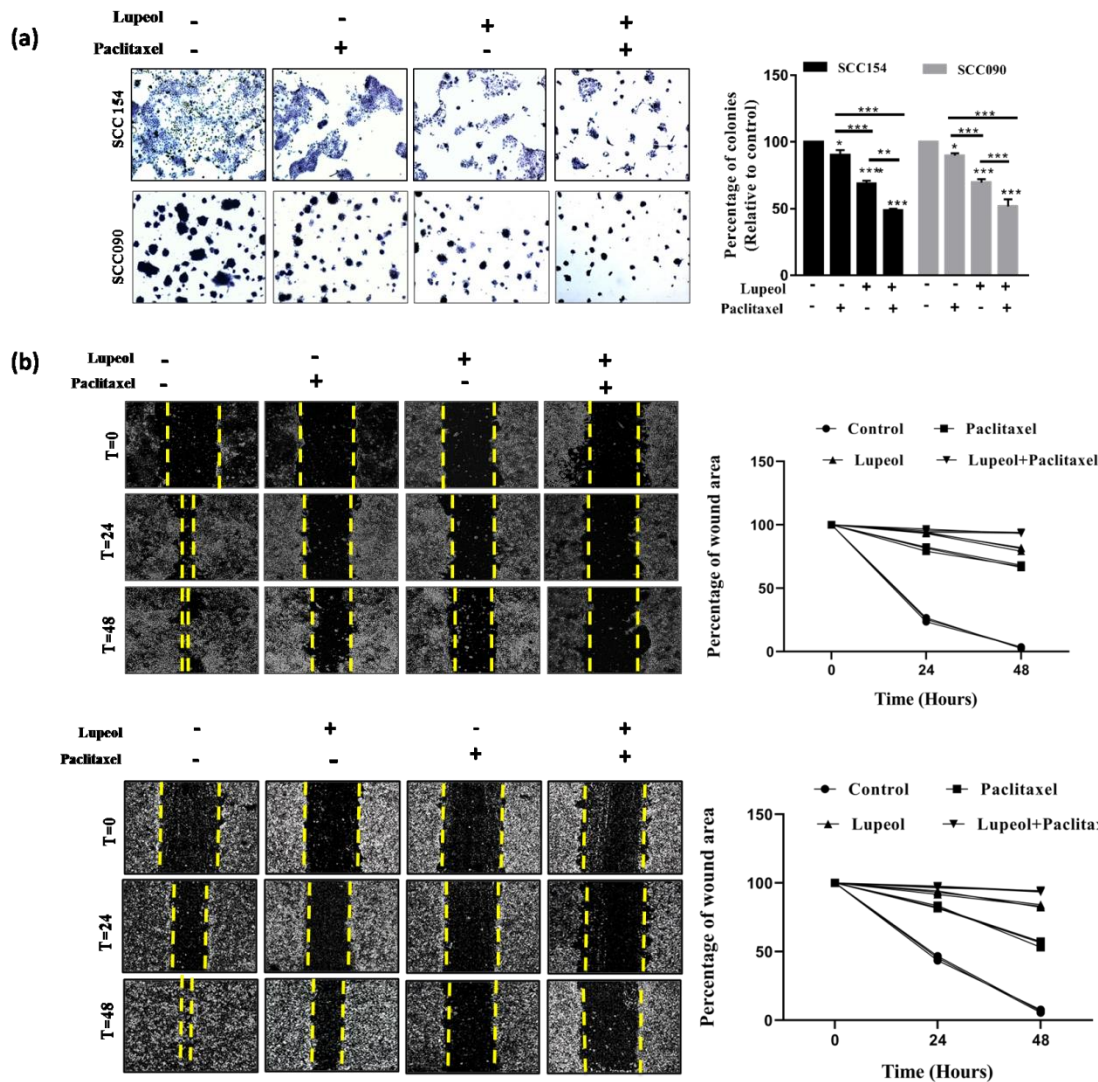


Figure 19: Effect of Lupeol and Paclitaxel in hypoxia induced colony formation and wound healing potential in vitro. (a) Individual and combinatorial effect of Lupeol and Paclitaxel on the hypoxia induced colony formation in OSCC cells (Magnification 40X) and quantification of the percentage of colony formation (relative to control). (b) Kinetics of wound closure of OSCC cells treated with Lupeol alone and in combination with Paclitaxel (Magnification 40X). Each experiment was performed in triplicates. **P* value <0.05, ***P* value <0.01 and ****P* value <0.0001 denote statistically significant changes compared to the corresponding control by One Way ANOVA test (*P* ANOVA < 0.0001) followed by post hoc Tukey's test.

7.3.2. Lupeol enhanced Paclitaxel induced apoptosis in OSCC cell lines under hypoxia

In order to evaluate whether the anticancer properties of Lupeol and Paclitaxel are exerted through inducing apoptotic signals, the rate of apoptosis was quantified by flow cytometry using Annexin V-FITC and PI labelling. In both of the OSCC cell lines either Lupeol or Paclitaxel alone induced apoptosis but their combinatorial treatment demonstrated the significant enhancement of the percentage of apoptotic cells (Figure 20a). In case of UPCI:SCC154 cells the total apoptosis rate was increased by 52.88% and in case of UPCI:SCC090 cells the same was enhanced by 24.63% through the synergistic combination of Lupeol and Paclitaxel during 48 hours of hypoxic incubation. Moreover to understand the underlying molecular mechanisms the protein expression level of the key regulators of apoptosis (Bax, Bcl₂) were investigated, which revealed significant upregulated expression of Bax and downregulated expression of Bcl₂ in the cells treated with Lupeol and/or Paclitaxel in both of the cell lines (Figure 20c). It is also noteworthy that the expressional alteration of the apoptotic regulators was found to be more pronounced when both of the compounds were used together than their individual treatment.

TUNEL assay data also indicated significantly increased fluorescence intensity of the apoptotic cells in Lupeol and Paclitaxel treated groups (Figure 20b).

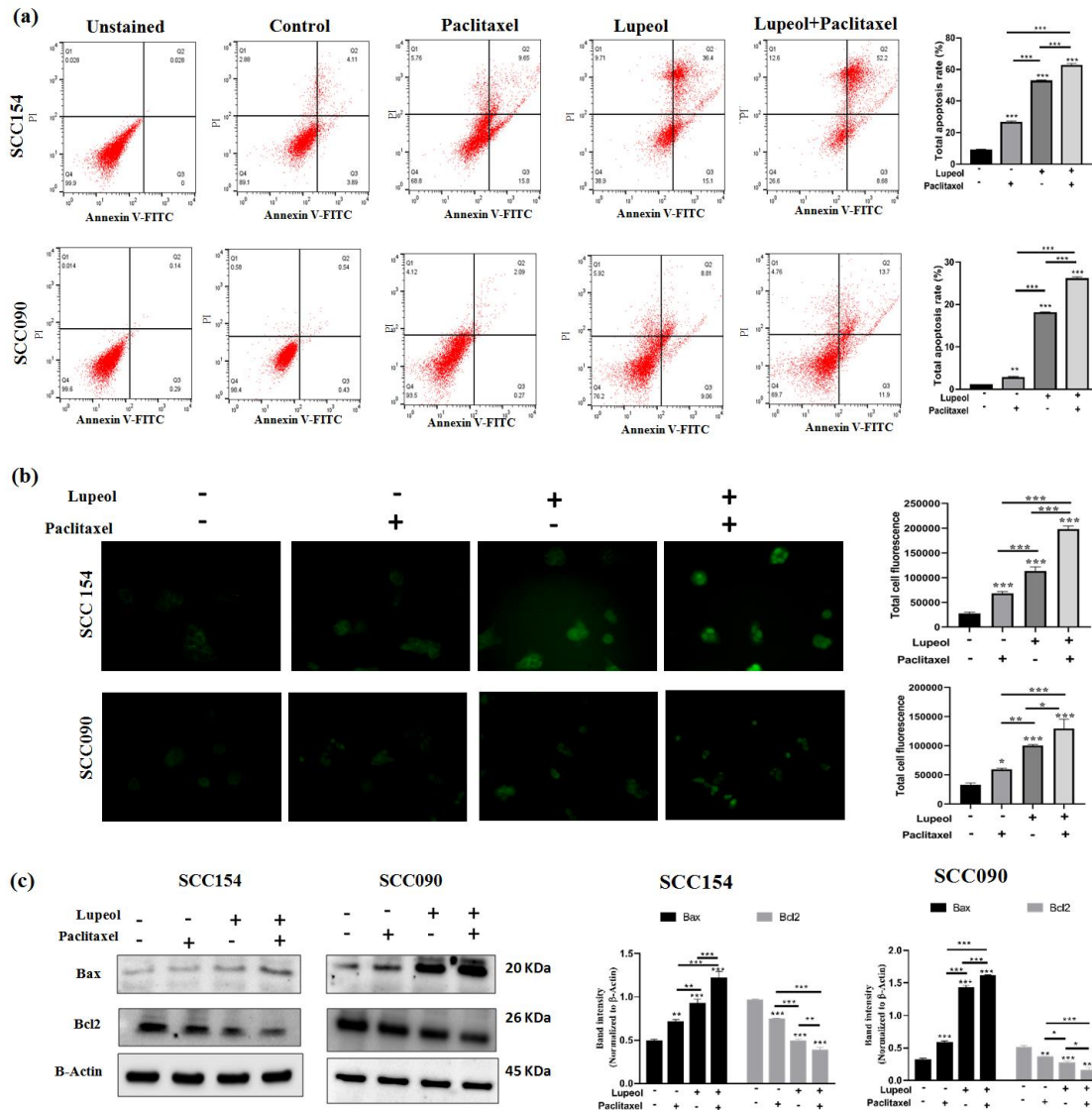


Figure 20: Effect of Lupeol and Paclitaxel in inducing apoptosis in vitro. (a) Annexin V/PI staining indicating total apoptosis rate in OSCC cells treated with individual and combinatorial effects of Lupeol and Paclitaxel. (b) TUNEL assay indicating total fluorescence intensity of apoptotic cells with the treatment of Lupeol and Paclitaxel in comparison with untreated control. (c) Effect of Lupeol and Paclitaxel on the apoptotic protein expression. Each experiment was

performed in triplicates. **P* value <0.05, ***P* value <0.01 and ****P* value <0.0001 denote statistically significant changes compared to the corresponding control by One Way ANOVA test (*P* ANOVA < 0.0001) followed by post hoc Tukey's test.

7.3.3. Combination treatment of Lupeol and Paclitaxel hindered the hypoxia induced VM formation

In chapter 6 (Figure 14) it has been observed that hypoxia facilitated the VM forming ability of UPCI:SCC154 and UPCI:SCC090 cells. We further investigated the potential role of Lupeol and Paclitaxel on regulating the hypoxia induced VM forming capacity of the OSCC cells (Figure 21) which revealed the significant disruption of VM structures resulting into the remarkable reduction of length and number of tubular junctions in the cells co-treated with Lupeol and Paclitaxel. Though the individual treatment of the compounds notably fractured the in vitro vascular architecture, their combinatorial effect is more evident inferring their synergistic anticancer potential through inhibiting the VM channel formation.

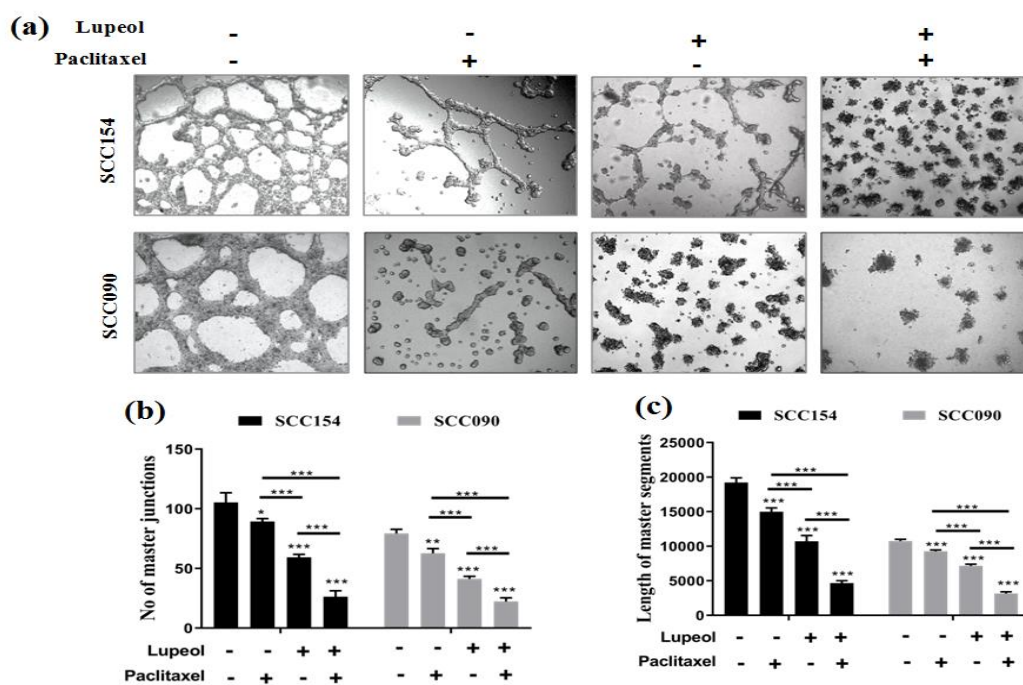


Figure 21: Effect of Lupeol and Paclitaxel in hypoxia induced vasculogenic mimicry in vitro
(a) Individual and combinatorial effect of Lupeol and Paclitaxel on the hypoxia induced VM formation in OSCC cells (Magnification 100X). Quantification of VM formation with respect to (b) number of master junction and (c) length of master segments in OSCC cells treated with Lupeol alone and in combination with Paclitaxel. Each experiment was performed in triplicates. **P* value <0.05, ***P* value <0.01 and ****P* value <0.0001 denote statistically significant changes compared to the corresponding control by One Way ANOVA test (*P* ANOVA < 0.0001) followed by post hoc Tukey's test.

7.3.4. Combination of Lupeol and Paclitaxel inhibited the hypoxia induced HIF-1 α /EphA2/Laminin 5 γ 2 signaling cascade

To elucidate the molecular mechanism involved in the reversing effect of Lupeol and Paclitaxel on the hypoxia induced VM formation the expressional alteration of HIF-1 α and its downstream signaling components were also investigated. The western blot analysis interpreted the significant downregulation of hypoxia induced HIF-1 α and its downstream VM associated regulators such as VE-Cadherin, pEphA2 (S-897), pERK1/2, MMP2 and Laminin 5 γ 2 in the cells treated with Lupeol alone and in combination with Paclitaxel (Figure 22a). No significant change was observed in the expression of total EphA2 and total ERK1/2 proteins. The synergistic association of Lupeol and Paclitaxel also significantly suppressed the hypoxia induced upregulation of the mRNA expression of HIF-1 α and Laminin 5 γ 2, the downstream indicator of extracellular matrix remodeling indicating their VM inhibiting potential at the transcription level (Figure 22d).

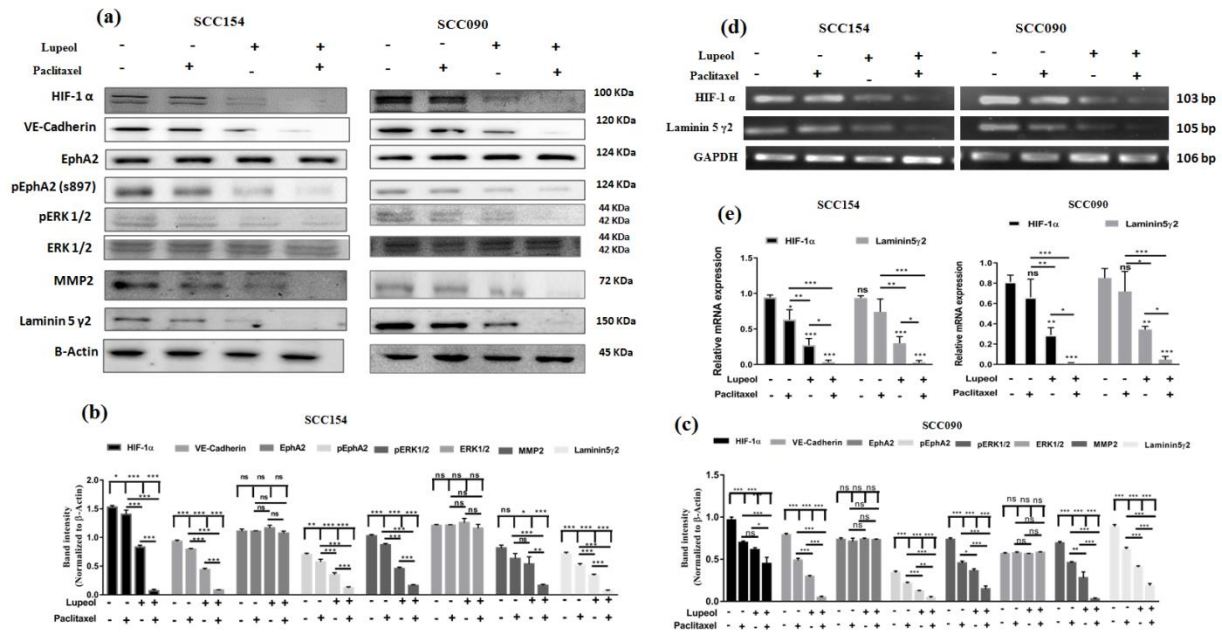


Figure 22: Effect of Lupeol and Paclitaxel in the expression of hypoxia induced vasculogenic mimicry related genes in vitro. (a,b,c) Individual and combinatorial effect of Lupeol and Paclitaxel on the protein expression of VM associated genes. (d,e) Individual and combinatorial effect of Lupeol and Paclitaxel on the mRNA expression of VM associated genes. Each experiment was performed in triplicates. **P* value <0.05, ***P* value <0.01 and ****P* value <0.0001 denote statistically significant changes compared to the corresponding control by One Way ANOVA test (*P* ANOVA < 0.0001) followed by post hoc Tukey's test.

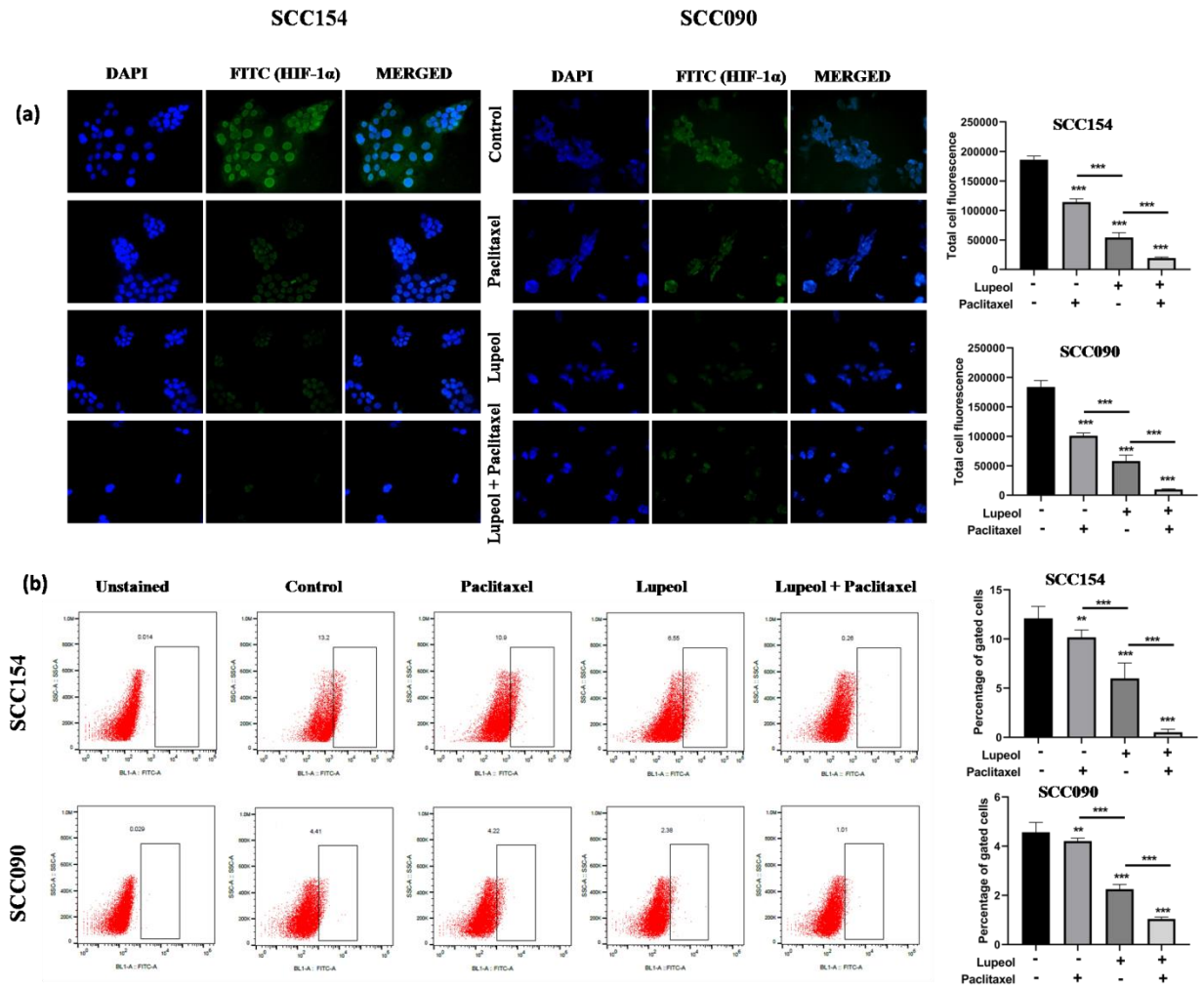


Figure 23: Effect of Lupeol and Paclitaxel in the expression of HIF-1 α using Immunofluorescence staining (a) and flow cytometry (b) and the comparative quantification with respect to the untreated control. Each experiment was performed in triplicates. * P value <0.05 , ** P value <0.01 and * P value <0.0001 denote statistically significant changes compared to the corresponding control by One Way ANOVA test (P ANOVA < 0.0001) followed by post hoc Tukey's test.**

7.3.5. Lupeol and Paclitaxel synergism reversed hypoxia influenced EMT and CSC phenomenon

In chapter 6 (Figure: 16) we have investigated that the induction of HIF-1 α enhanced EMT and CSC phenomenon in OSCC cells which plays a crucial role in the VM formation. The Figure 24 depicted a significantly reduced number of migrated and invaded cells through transwell when co-treated with Lupeol and Paclitaxel indicating their indispensable role in regulating VM associated migration and invasion potential. The combinatorial treatment also caused a significant decrease in the sphere forming potential with the downregulation of CD133 marker. Furthermore Lupeol alone and in combination with Paclitaxel significantly upregulated the expression of E-Cadherin and also consistently downregulated the mesenchymal markers such as vimentin, Snail and twist deducing their reversing effect in the hypoxia promoting EMT (Figure 25).

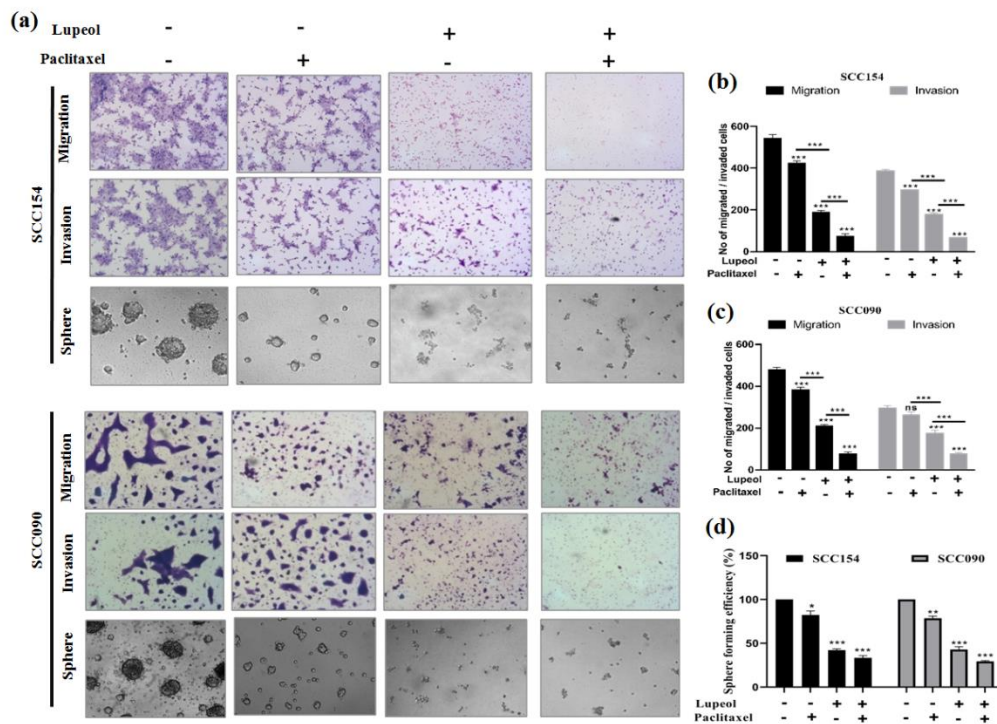


Figure 24: Effect of Lupeol and Paclitaxel in hypoxia induced migration, invasion, sphere formation in vitro. (a) Individual and combinatorial of Lupeol and Paclitaxel on the hypoxia induced transwell migration, invasion and sphere formation in OSCC cells (Magnification 100X) and (b,c,d) quantification of migrated and invaded OSCC cells and CSC rich sphere forming cells treated with Lupeol alone and in combination with Paclitaxel. Each experiment was performed in triplicates. **P* value <0.05, ***P* value <0.01 and ****P* value <0.0001 denote statistically significant changes compared to the corresponding control by One Way ANOVA test (*P* ANOVA < 0.0001) followed by post hoc Tukey's test.

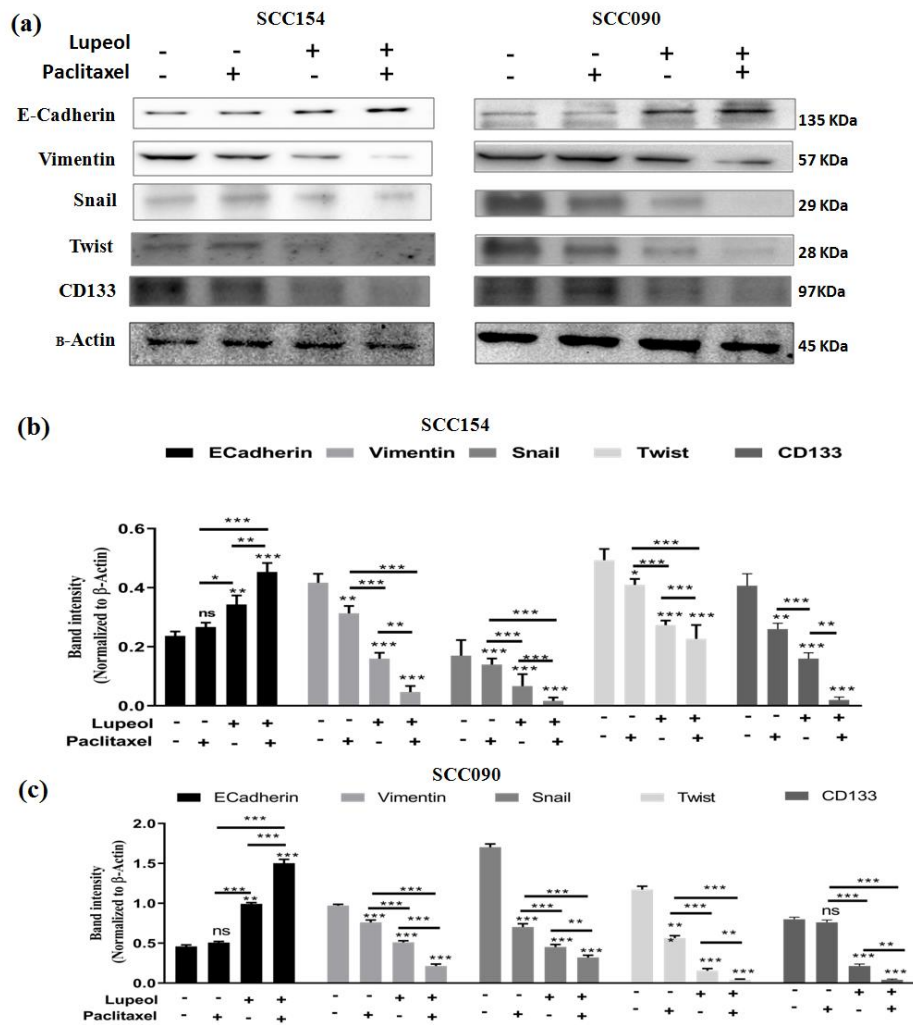


Figure 25: Effect of Lupeol and Paclitaxel in hypoxia induced EMT and CSC related genes in vitro. Individual and combinatorial effect of Lupeol and Paclitaxel on the protein expression of EMT and CSC associated genes. Each experiment was performed in triplicates. **P* value <0.05, ***P* value <0.01 and ****P* value <0.0001 denote statistically significant changes compared to the corresponding control by One Way ANOVA test (*P* ANOVA < 0.0001) followed by post hoc Tukey's test.

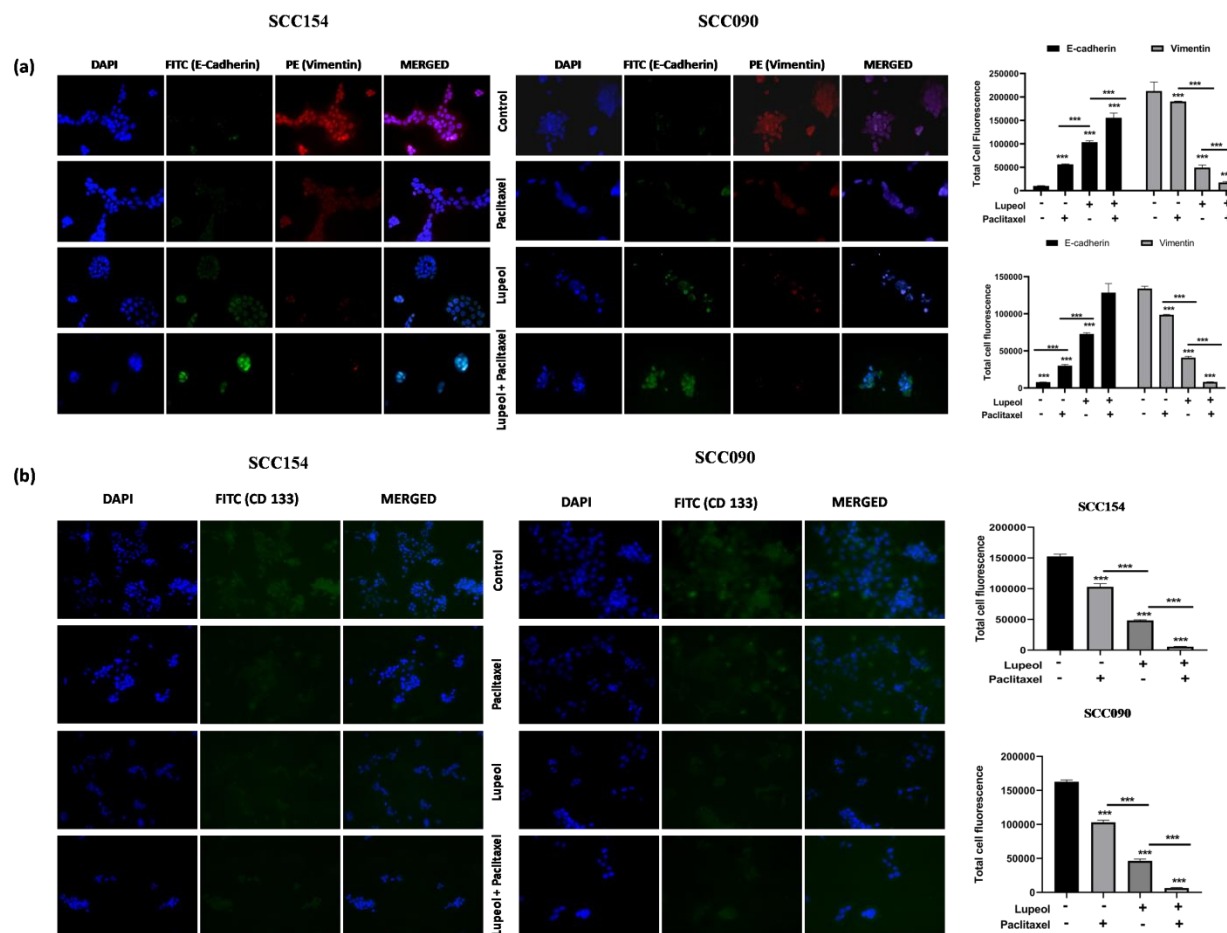


Figure 26: Effect of Lupeol and Paclitaxel in the expression of E-Cadherin, Vimentin (a) and CD133 (b) using Immunofluorescence and the comparative quantification with respect to the untreated control. Each experiment was performed in triplicates. **P* value <0.05, ***P* value <0.01 and ****P* value <0.0001 denote statistically significant changes compared to the

corresponding control by One Way ANOVA test (P ANOVA < 0.0001) followed by post hoc Tukey's test.

7.3.6. Synergistic effect of Lupeol and Paclitaxel in regulating hypoxia induced vasculogenic mimicry in patient derived ex vivo platform

In order to elucidate the efficacy of the combinatorial drug in ex vivo system the expressional alteration of VM associated regulators along with the proliferative and apoptotic markers was assessed at 48 hours of post treatment. Post 48 hours of cultured condition the tissue architecture of untreated control exhibited compact tumor cells whereas the Lupeol and Paclitaxel co-treated group was found to have more damaged structures with sparse and separated nuclei from each other. CD31/PAS staining showed a significantly decreased number of VM structures in Lupeol and Paclitaxel treated specimens compared to the untreated control (Figure 28). Lupeol + Paclitaxel treatment group indicated significant decrease in the expression of the proliferative marker ki67 (Figure 27) as well as VM associated HIF-1 α and its downstream regulators VE-Cadherin, pEphA2 (S-897), pERK1/2, MMP2 and Laminin 5 γ 2 compared to the untreated control (Figure 28). The significantly upregulated expression of Caspase3 (Figure 27) in Lupeol and Paclitaxel treated group confirmed their anticancer potential exerted by the induction of apoptosis. Furthermore the immuno-histochemical expression of EMT and CSC markers were also evaluated which showed the reduced expression of CSC inducing CD133 and mesenchymal markers such as Vimentin, Snail, Twist and significantly increased expression of the epithelial marker E-Cadherin (Figure 29) in the tissue section treated with Lupeol alone and in combination with Paclitaxel indicating the potential of the drug combination in altering the EMT phenomenon in personalized ex vivo setting.

Table 16: Demographic and clinicopathological profile of OSCC patients for explant culture

Patients' characteristics	#1	#2	#3	#4	#5
Age (Years)	50	60	60	54	58
Gender	Male	Male	Female	Male	Male
Tobacco consumption	Yes	Yes	No	Yes	Yes
Alcohol consumption	Yes	No	No	No	No
Tumor location	Tongue	Buccal Mucosa	Lip	Buccal Mucosa	Buccal Mucosa
Grade	Poor	Moderate	Moderate	Moderate	Well
Primary Tumor status	T4	T4	T3	T3	T2
Lymph Node metastasis	N2	N1	N0	N1	N1
TNM stage group	IV	IV	III	III	III

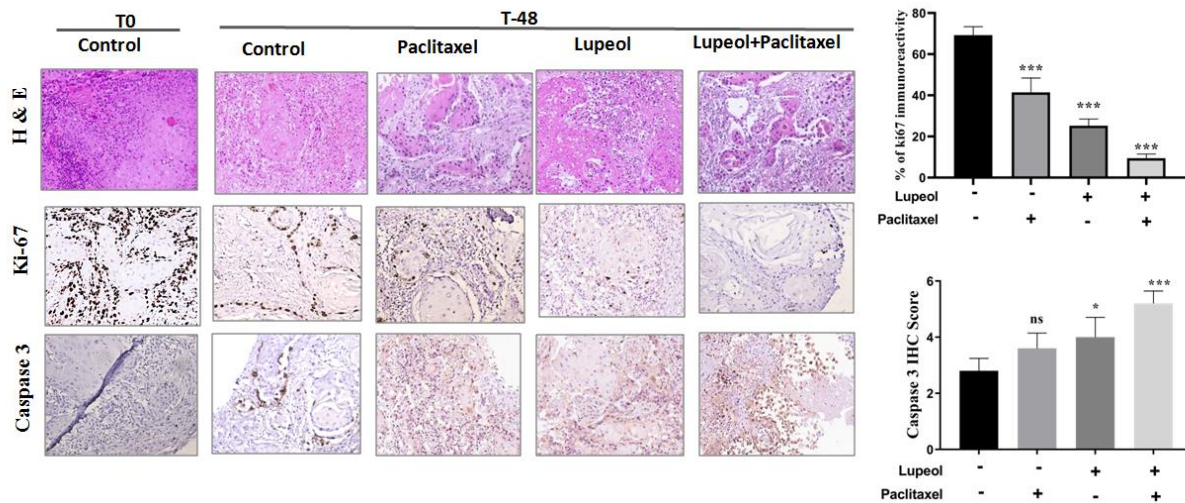


Figure 27: Effect of Lupeol and Paclitaxel in regulating the expression of proliferating marker (Ki-67) and apoptotic marker (Caspase-3) in Ex vivo platform of OSCC. Immunohistochemical expression of markers (200X magnification, left) and comparative analysis of their IHC scores in Lupeol and Paclitaxel treated tissue specimens (right). T0 specimens have been shown to represent the baseline expression of markers. Each experiment was performed in triplicates. *P value <0.05, **P value <0.01 and ***P value <0.0001 denote

statistically significant changes compared to the corresponding control by One Way ANOVA test (P ANOVA < 0.0001) followed by post hoc Tukey's test.

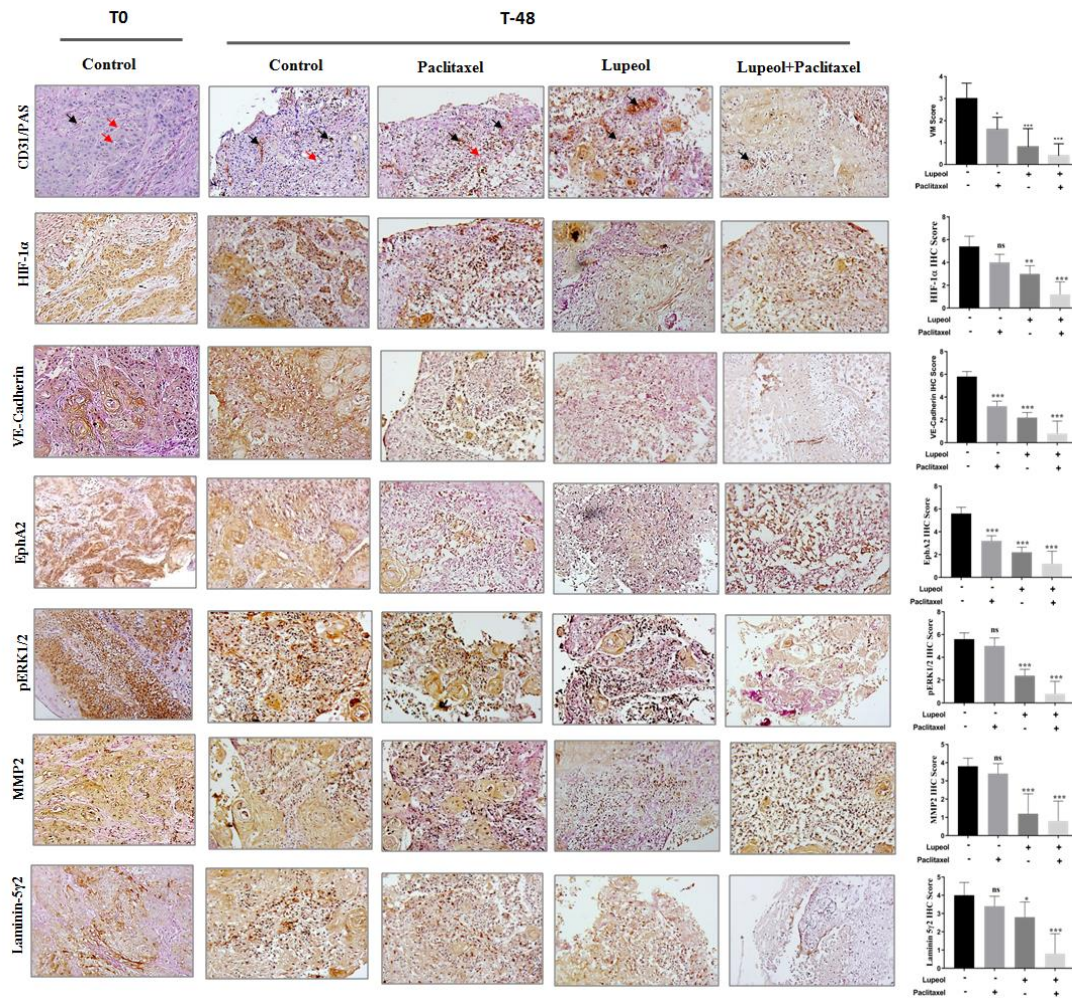


Figure 28: Effect of Lupeol and Paclitaxel in regulating the expression of VM associated genes in Ex vivo platform of OSCC. Red arrows in the CD31/PAS staining indicate PAS positive VM architecture and black arrows indicate endothelial structures. Immunohistochemical expression of markers (200X magnification, left) and comparative analysis of their IHC scores in Lupeol and Paclitaxel treated tissue specimens (right). T0 specimens have been shown to represent the baseline expression of markers. Each experiment was performed in triplicates. *P

value <0.05 , ** P value <0.01 and *** P value <0.0001 denote statistically significant changes compared to the corresponding control by One Way ANOVA test (P ANOVA < 0.0001) followed by post hoc Tukey's test.

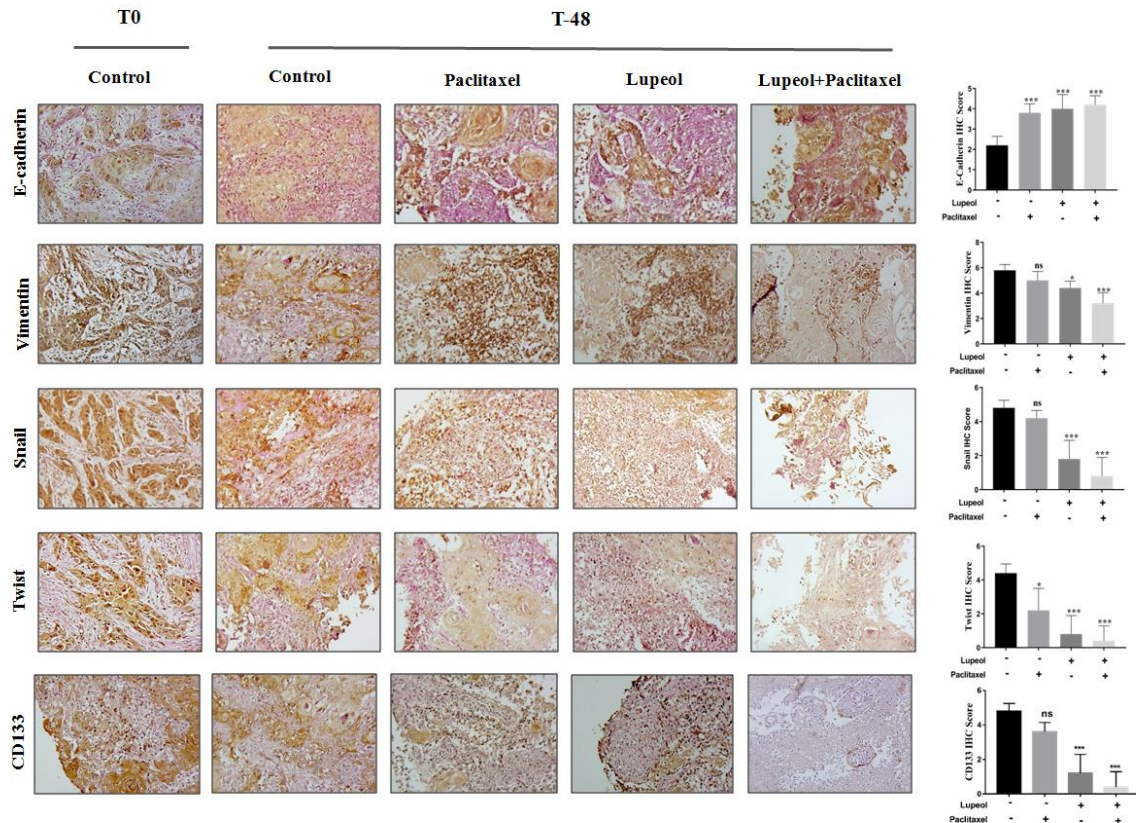


Figure 29: Effect of Lupeol and Paclitaxel in regulating the expression of VM associated EMT and CSC markers in *Ex vivo* platform of OSCC. Immunohistochemical expression of markers (200X magnification, left) and comparative analysis of their IHC scores in Lupeol and Paclitaxel treated tissue specimens (right). T0 specimens have been shown to represent the baseline expression of markers. Each experiment was performed in triplicates. * P value <0.05 , ** P value <0.01 and *** P value <0.0001 denote statistically significant changes compared to the corresponding control by One Way ANOVA test (P ANOVA < 0.0001) followed by post hoc Tukey's test.

7.3.7. PPI analysis of VM interacting proteins

To investigate the functional link among the differentially expressed proteins in the hypothesized network, protein- protein interactions (PPI) were analyzed via STRING. In our study the STRING analysis identified the main network proteins implicated in cellular proliferation, extracellular matrix remodeling, EMT, CSC phenotype and apoptosis. The different grade of association was denoted via confidence level (low-0.150, medium-0.400, high-0.700, highest-0.900) and edge thickness. Our key network protein HIF-1 α exhibited the highest degree of association with Twist (0.979), followed by the same with MMP2 (0.754) and Snail (0.727). Laminin also indicated strong association (0.925) with MMP2 and Caspase 3 (0.907). All other possible associations are depicted in Figure 30a.

7.4. Discussion

Despite the recent advances in diagnosis and treatment the prognosis of OSCC patients remains poor. Resistance to anti-angiogenesis and anti-metastatic drugs due to the tumor perfusion through alternative vascularization pathways emerged a new treatment challenge to the clinicians. VM has been shown to be associated with tumor size, grade, lymph node metastasis and poor prognosis in OSCC patients which emphasizes the necessity for developing anti-vascular therapeutic agents that specifically target VM.

Our findings revealed the combinatorial effect of Lupeol and Paclitaxel in weakening the hypoxia enhancing VM tube formation through the down-regulation of HIF-1 α mediated and Laminin-5 γ 2 driven signaling cascade both in the in vitro and patient derived ex vivo network.

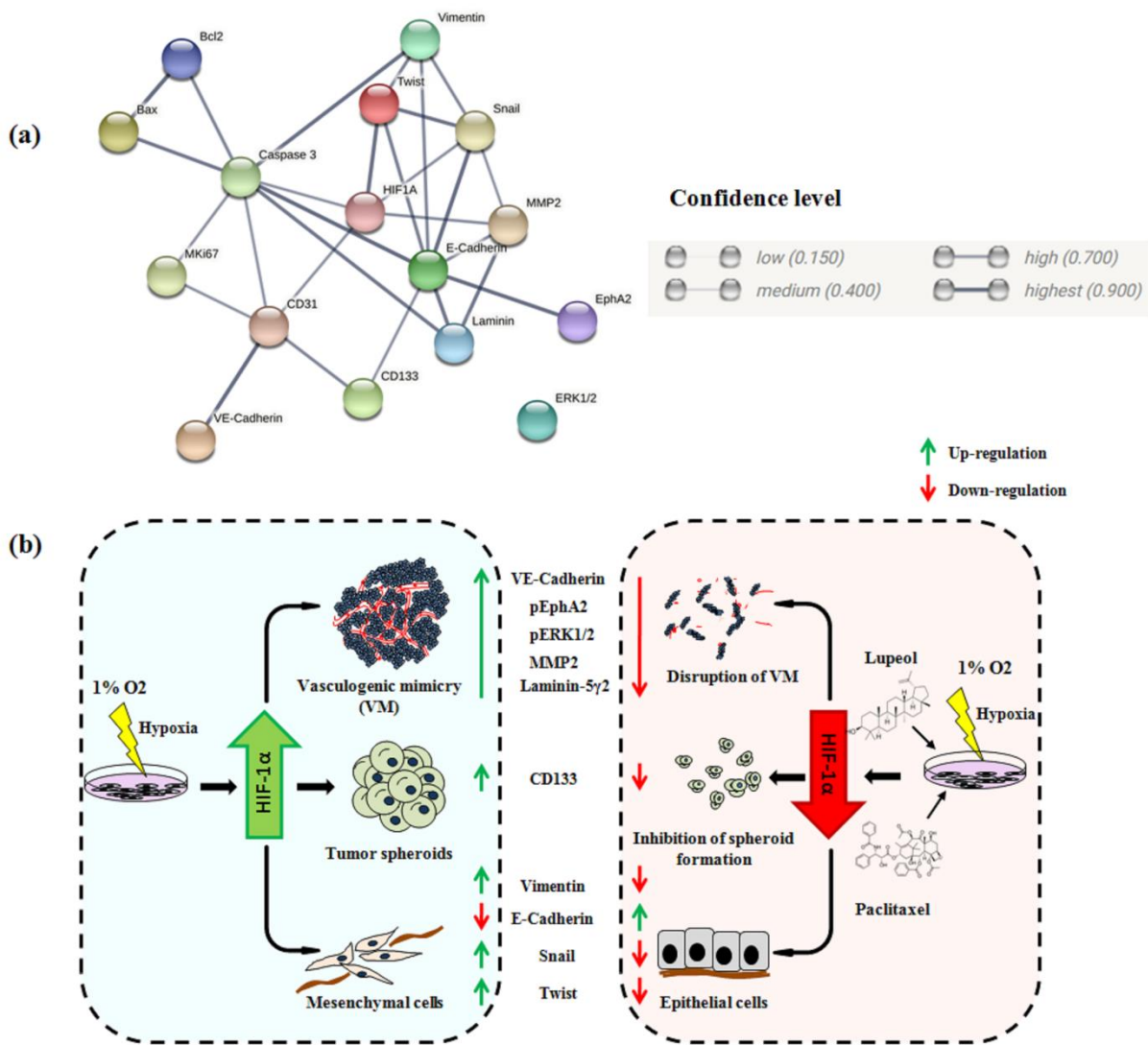


Figure 30: Model depicting the involvement of HIF1 α and key interacting partners in VM and intervention by Lupeol and Paclitaxel (a) Protein-protein interaction network analysis using input proteins from the present study on STRING platform showing interacting molecules and confidence level in the network. Legends of confidence level have been taken from the STRING database. (b) Schematic diagram representing cellular phenotypes, molecular drivers and synergistic effect of Lupeol and Paclitaxel on perturbing hypoxia induced Vasculogenic mimicry in OSCC.

Several studies have demonstrated that phytochemicals and active compounds from dietary supplements such as green tea extract, AT-101, epigenin, hyperforin, silibinin synergistically enhance Paclitaxel toxicity in different cancer models including breast cancer (Barathan et al., 2021; Karaca et al., 2010), ovarian cancer (Panji et al., 2021), lung cancer (Xu et al., 2011), gastric cancer (Zhang et al., 2018) and the anticancer activity of Lupeol has been explored in head and neck cancer by inhibiting oncogenic EGFR cascade (Rauth et al., 2016), inducing the intrinsic apoptotic pathway (Bhattacharyya et al., 2017) and downregulating NF- κ B activity (Lee et al., 2007). However the chemo-sensitization potential of Lupeol to amplify the effectiveness of Paclitaxel has not been elucidated yet. To the best of our knowledge our investigation is the first preclinical study assessing the synergistic potential of phytochemical Lupeol and common anti-neoplastic drug Paclitaxel in suppressing the induced by hypoxia in the in vitro and ex vivo OSCC model. In this study we have shown that Lupeol and Paclitaxel individually exhibited growth inhibitory activities on OSCC cells in a dose dependent manner and the combination index analysis demonstrated that the combination regimen with Lupeol and lower dose of Paclitaxel produced significant anti-cancer synergistic effect (CI <1) with approximately 2 fold reduction of IC₅₀ dose of Lupeol and 4 fold reduction of Paclitaxel IC₅₀ dose. The flow cytometric analysis using Annexin-V/PI staining, fluorescence microscopy of TUNEL assay validated that the combined cytotoxic effect of Lupeol/Paclitaxel is causally associated with apoptotic cell death pathway which was consistent with the western blot results showing the alteration of Bax/Bcl2 ratio with the combined treatment of Lupeol and Paclitaxel. Our study further revealed that Lupeol individually had the potential to inhibit hypoxia induced VM in the in vitro and patient derived ex vivo OSCC model and its cooperation with Paclitaxel exhibited an enhanced anti VM effect against OSCC. Earlier the study of Bhattacharyya et al., 2019 indicated

the reversing effect of Lupeol in the progression of VM in murine melanoma model by downregulating CD133 expression and Paclitaxel also exhibited an in vitro VM inhibitory potential in murine glioma model (Liu et al., 2015) but the molecular mechanistic approach behind the destruction of VM tubes remained unexplored. In this regard for the first time our study portrayed that along with the structural disruption of VM tubes in SCC154 and SCC090 cell lines, Lupeol decreased the expression of HIF-1 α leading to the simultaneous inhibition of VE-Cadherin, pEphA2 (S-897), pERK1/2, MMP2 and Laminin 5 γ 2 and its co-treatment with lower dose of Paclitaxel enhanced the down-regulation of the protein levels suggesting that Lupeol/Paclitaxel synergism hinders hypoxia induced VM formation in OSCC model and the possible mechanism may be related to inhibition of HIF-1 α mediated EphA2-Laminin 5 γ 2 axis. Previously the study of Li et al., 2018 reported the VM inhibitory effect of Niclosamide and Melatonin in OSCC via up-regulation of miR-124, downregulation of STAT-3 and through the blockage of ROS reliant AKT/ERK signaling pathways respectively. The recent investigation of Almahmoudi et al., 2021 indicated that IL-17F also inhibited the in vitro VM formation of OSCC cells. Corresponding to these findings our study designated an additional novel therapeutic intervention targeting our hypothesized signaling pathway leading to the pseudo-vascular features pertaining to the aggressive OSCC. Furthermore our research also exerted that compared to the individual treatment the combinatorial dose of Lupeol and Paclitaxel revealed pronounced inhibitory effect in the expression of markers related to EMT (Vimentin, Snail, Twist) and CSC (CD133) phenotypes which are the essential factors for VM formation (Fan et al., 2013; Jue et al., 2017; Sun et al., 2019). Consistent with the outcomes of in vitro model we also demonstrated that combined treatment of Lupeol and Paclitaxel can proficiently reduce the formation of VM channels in patient derived ex vivo platform via CD31/PAS staining and the

immuno-histochemical expression of VM associated markers were also significantly down-regulated in the co-treated group compared to the individually treated groups which will be beneficial for the prediction of therapeutic response in a personalized strategy and identifying the most appropriate treatment regimen for individual patient. We conjectured from the above findings that Paclitaxel accompanied with Lupeol may inhibit hypoxia induced VM formation via down-regulating HIF-1 α -EphA2-Laminin 5 γ 2 cascade and associated EMT and CSC phenomenon in OSCC and further investigation in in-vivo model is critically essential to exert their anti-VM potential for OSCC treatment.

7.5. Conclusion

From this chapter we may conclude that HIF-1 α is a key regulator of OSCC in terms of VM formation and targeting its downstream signaling components, the synergistic combination of Lupeol and Paclitaxel will emerge a new direction of cancer treatment for aggressive oral cancers and after series of clinical trials this potential drug combination may be used as an effective and definitive therapeutic modality against OSCC.

Chapter 8

Summary & Conclusion

Oral squamous cell carcinoma, one of the major subtypes of head and neck cancer, is a heterogenous, aggressive and complex entity. In spite of the advanced treatment modalities, the five year survival rate is still <50% in advanced cases. Since neoplastic transformation and progression is a multistep process that involves various stages and molecular changes in tissue environment and there is considerable progress in our understanding of the pathogenesis; recent research sheds light on new properties explaining consequences of aggressive tumor microenvironment (TME). Tumors require a blood supply for growth and metastasis. So far most of the studies have drawn attention on the role of angiogenesis. When Maniotis et.al.1999 first described the formation of vasculogenic mimicry as endothelial cell independent vessel- like structures in the Uveal melanoma model, an entirely new field of cancer research emerged. Although a variety of proteins and micro environmental factors contribute to VM formation, but the molecular mechanisms underlying its formation are still unclear in OSCC. Since the cellular induction of hypoxia may promote the plastic and trans-endothelial phenotype of tumor cells which are capable of VM formation by maintaining stemness and EMT induction, so understanding the linkage between the hypoxia related and VM including molecular signaling may provide crucial new therapeutic strategies for the development of novel tumor targeted treatments in OSCC. On the other hand it is a well-established fact that chemotherapeutic drugs and high doses of radiotherapy come with their limitations and adverse side effects which may lead to the poor prognosis of oral cancer patients. Keeping that in mind a possible alternative has always been the key interest for scientists as well as clinicians.

In this context ***Part 1 (Chapter 5)*** of the thesis work indicated that the presence of VM exhibited positive correlation with HIF-1 α as well as its downstream signaling components including VE-Cadherin, EphA2, pERK1/2, MMP2 and Laminin 5 γ 2 as well as the mesenchymal (Vimentin,

Snail, Twist) and CSC (CD133) markers, revealing their significant expressional alteration among VM+ and VM- OSCC cohorts. Positive expression of HIF-1 α and the extracellular matrix protein Laminin-5 γ 2 coordinated with the simultaneous existence of VM are significantly associated with tumor grade, primary tumor size, lymph node metastasis and TNM stage in OSCC indicating their relevance in the malignant and metastatic progression of OSCC. Furthermore, OSCC patients with positive expression of HIF-1 α and Laminin-5 γ 2 in coordination with VM also exhibited poor disease free and overall survival rate. In addition, most promisingly our study reported for the first time that Laminin-5 γ 2 and VM either alone or together were significantly represented as the independent risk factors in OSCC which might support the rationale for developing the VM-Laminin5 γ 2 orchestration as the successful prognostic and therapeutic target.

Next the **Part 2 (Chapter 6)** of the thesis established the molecular regulatory axis mediating the formation of pseudovascular VM structures in the in vitro OSCC model. HIF-1 α plays a major role in hypoxia inducing VM formation in OSCC. Hypoxic treatment enhanced the number of matrigel mediated tubular junctions, whereas the silencing of HIF-1 α resulted in the disruption of vascular structures with the simultaneous reduction of relevant downstream signaling components associated with extracellular matrix remodeling, EMT and cancer stemness.

Finally, the **Part 3 (Chapter 7)** of the thesis aims to establish the combination of Lupeol and chemotherapeutic drug Paclitaxel as an alternative treatment regimen with minimum side effects and more efficacies. Though the cytotoxic effect of both of these agents is well known, but their anti-VM property in oral cancer model has not been evaluated yet.

Hence, for the first time in our study, the effective dose of phytochemical Lupeol in combination with the sub-therapeutic dose of Paclitaxel exhibited the anti VM property in in

vitro and ex vivo OSCC model. With the inhibition of VM, the Lupeol-Paclitaxel combination also promoted apoptosis, interrupted the invasion, migration potential, tumor sphere forming ability of cancer stem like cells and the EMT property of OSCC cells. The ex vivo platform in a pilot scale also validated the anti-VM property of Lupeol–Paclitaxel combination through the structural disruption as well as the inhibition of VM associated signaling molecules.

So in a nutshell the thesis work has enlightened HIF-1 α mediated interconnecting signaling pathways, their clinical implications and prognostic significance to understand the possible regulatory mechanism in modulation of Vasculogenic mimicry in OSCC which will provide a clear outline for the future investigations regarding the identification and targeting of VM related molecules for better understanding and discovering the advanced therapeutic modalities of OSCC. Furthermore the reversing effect of phytochemical Lupeol in combinatorial settings with standard chemotherapeutic agents on vasculogenic mimicry via suppressing HIF-1 α - Laminin5 γ 2 axis along with the EMT and CSC phenotypes will emerge a new field of cancer treatment for aggressive oral cancers.

Bibliography

- Ahmed, N., Abubaker, K., Findlay, J., & Quinn, M. (2010). Epithelial mesenchymal transition and cancer stem cell-like phenotypes facilitate chemoresistance in recurrent ovarian cancer. *Current Cancer Drug Targets*, *10*(3), 268–278. <https://doi.org/10.2174/156800910791190175>
- Ahn, M.-J., D’Cruz, A., Vermorken, J. B., Chen, J.-P., Chitapanarux, I., Dang, H. Q. T., Guminski, A., Kannarunimit, D., Lin, T.-Y., Ng, W. T., Park, K.-U., & Chan, A. T. C. (2016). Clinical recommendations for defining platinum unsuitable head and neck cancer patient populations on chemoradiotherapy: A literature review. *Oral Oncology*, *53*, 10–16. <https://doi.org/10.1016/j.oraloncology.2015.11.019>
- Akhter, M., Hossain, S., Rahman, Q. B., & Molla, M. R. (2011). A study on histological grading of oral squamous cell carcinoma and its co-relationship with regional metastasis. *Journal of Oral and Maxillofacial Pathology: JOMFP*, *15*(2), 168–176. <https://doi.org/10.4103/0973-029X.84485>
- Almahmoudi, R., Salem, A., Hadler-Olsen, E., Svineng, G., Salo, T., & Al-Samadi, A. (2021). The effect of interleukin-17F on vasculogenic mimicry in oral tongue squamous cell carcinoma. *Cancer Science*, *112*(6), 2223–2232. <https://doi.org/10.1111/cas.14894>
- Al-Rehaily, A. J., ElTahir, K. E. H., Mossa, J. S., & Rafatullah, S. (2001). Pharmacological Studies of Various Extracts and the Major Constituent, Lupeol, obtained from Hexane Extract of *Teclea nobilis* in Rodents. *Natural Product Sciences*. <https://www.scinapse.io/papers/2404020843>
- Andonegui-Elguera, M. A., Alfaro-Mora, Y., Cáceres-Gutiérrez, R., Caro-Sánchez, C. H. S., Herrera, L. A., & Díaz-Chávez, J. (2020). An Overview of Vasculogenic Mimicry in Breast Cancer. *Frontiers in Oncology*, *10*, 220. <https://doi.org/10.3389/fonc.2020.00220>

- Anneroth, G., Batsakis, J., & Luna, M. (1987). Review of the literature and a recommended system of malignancy grading in oral squamous cell carcinomas. *Scandinavian Journal of Dental Research*, 95(3), 229–249. <https://doi.org/10.1111/j.1600-0722.1987.tb01836.x>
- Aratanechemuge, Y., Hibasami, H., Sanpin, K., Katsuzaki, H., Imai, K., & Komiya, T. (2004). Induction of apoptosis by lupeol isolated from mokumen (*Gossampinus malabarica* L. Merr) in human promyelotic leukemia HL-60 cells. *Oncology Reports*, 11(2), 289–292.
- Balamurugan, K. (2016). HIF-1 at the crossroads of hypoxia, inflammation, and cancer. *International Journal of Cancer*, 138(5), 1058–1066. <https://doi.org/10.1002/ijc.29519>
- Bani, S., Kaul, A., Khan, B., Ahmad, S. F., Suri, K. A., Gupta, B. D., Satti, N. K., & Qazi, G. N. (2006). Suppression of T lymphocyte activity by Lupeol isolated from *Crataeva religiosa*. *Phytotherapy Research: PTR*, 20(4), 279–287. <https://doi.org/10.1002/ptr.1852>
- Barathan, M., Zulpa, A. K., Mee Hoong, S., Vellasamy, K. M., & Vadivelu, J. (2021). Synergistic effect of hyperforin and Paclitaxel on growth inhibition, apoptotic mediator activation in MCF-7 human breast cancer cells. *Journal of Taibah University for Science*, 15(1), 918–927. <https://doi.org/10.1080/16583655.2021.2010910>
- Basak, J., & Ara, S. A. (2022). Liquid biopsy as a diagnostic and prognostic tool—A systematic review. *IP International Journal of Maxillofacial Imaging*, 7(4), 174–182. <https://doi.org/10.18231/j.ijmi.2021.031>
- Bedal, K. B., Grässel, S., Spanier, G., Reichert, T. E., & Bauer, R. J. (2015). The NC11 domain of human collagen XVI induces vasculogenic mimicry in oral squamous cell carcinoma cells. *Carcinogenesis*, 36(11), 1429–1439. <https://doi.org/10.1093/carcin/bgv141>

- Belotti, D., Pinessi, D., & Taraboletti, G. (2021). Alternative Vascularization Mechanisms in Tumor Resistance to Therapy. *Cancers*, *13*(8), 1912. <https://doi.org/10.3390/cancers13081912>
- Ben-Ze'ev, A., Rodríguez Fernández, J. L., Glück, U., Salomon, D., & Geiger, B. (1994). Changes in adhesion plaque protein levels regulate cell motility and tumorigenicity. *Advances in Experimental Medicine and Biology*, *358*, 147–157. https://doi.org/10.1007/978-1-4615-2578-3_14
- Beserra, F. P., Vieira, A. J., Gushiken, L. F. S., de Souza, E. O., Hussni, M. F., Hussni, C. A., Nóbrega, R. H., Martinez, E. R. M., Jackson, C. J., de Azevedo Maia, G. L., Rozza, A. L., & Pellizzon, C. H. (2019). Lupeol, a Dietary Triterpene, Enhances Wound Healing in Streptozotocin-Induced Hyperglycemic Rats with Modulatory Effects on Inflammation, Oxidative Stress, and Angiogenesis. *Oxidative Medicine and Cellular Longevity*, *2019*, e3182627. <https://doi.org/10.1155/2019/3182627>
- Bharadwaj, R., & Yu, H. (2004). The spindle checkpoint, aneuploidy, and cancer. *Oncogene*, *23*(11), 2016–2027. <https://doi.org/10.1038/sj.onc.1207374>
- Bhatt, M., Patel, M., Adnan, M., & Reddy, M. N. (2021). Anti-Metastatic Effects of Lupeol via the Inhibition of MAPK/ERK Pathway in Lung Cancer. *Anti-Cancer Agents in Medicinal Chemistry- Anti-Cancer Agents*, *21*(2), 201–206. <https://doi.org/10.2174/1871520620666200424131548>
- Bhattacharyya, S., Mitra, D., Ray, S., Biswas, N., Banerjee, S., Majumder, B., Mustafi, S. M., & Murmu, N. (2019). Reversing effect of Lupeol on vasculogenic mimicry in murine melanoma progression. *Microvascular Research*, *121*, 52–62. <https://doi.org/10.1016/j.mvr.2018.10.008>

- Bhattacharyya, S., Sekar, V., Majumder, B., Mehrotra, D. G., Banerjee, S., Bhowmick, A. K., Alam, N., Mandal, G. K., Biswas, J., Majumder, P. K., & Murmu, N. (2017). CDKN2A-p53 mediated antitumor effect of Lupeol in head and neck cancer. *Cellular Oncology*, *40*(2), 145–155. <https://doi.org/10.1007/s13402-016-0311-7>
- Birner, P., Schindl, M., Obermair, A., Plank, C., Breitenecker, G., & Oberhuber, G. (2000). Overexpression of hypoxia-inducible factor 1alpha is a marker for an unfavorable prognosis in early-stage invasive cervical cancer. *Cancer Research*, *60*(17), 4693–4696.
- Bociort, F., Macasoi, I. G., Marcovici, I., Motoc, A., Grosu, C., Pinzaru, I., Petean, C., Avram, S., & Dehelean, C. A. (2021). Investigation of Lupeol as Anti-Melanoma Agent: An In Vitro-In Ovo Perspective. *Current Oncology*, *28*(6), Art. 6. <https://doi.org/10.3390/curroncol28060425>
- Borse, V., Konwar, A. N., & Buragohain, P. (2020). Oral cancer diagnosis and perspectives in India. *Sensors International*, *1*, 100046. <https://doi.org/10.1016/j.sintl.2020.100046>
- Brito, D. A., Yang, Z., & Rieder, C. L. (2008). Microtubules do not promote mitotic slippage when the spindle assembly checkpoint cannot be satisfied. *The Journal of Cell Biology*, *182*(4), 623–629. <https://doi.org/10.1083/jcb.200805072>
- Cao, Z., Bao, M., Miele, L., Sarkar, F. H., Wang, Z., & Zhou, Q. (2013). Tumour vasculogenic mimicry is associated with poor prognosis of human cancer patients: A systemic review and meta-analysis. *European Journal of Cancer (Oxford, England: 1990)*, *49*(18), 3914–3923. <https://doi.org/10.1016/j.ejca.2013.07.148>
- Cháirez-Ramírez, M. H., Gallegos-Infante, J. A., Moreno-Jiménez, M. R., González-Laredo, R. F., & Rocha-Guzmán, N. E. (2019). Absorption and distribution of Lupeol in CD-1

- mice evaluated by UPLC–APCI+–MS/MS. *Biomedical Chromatography*, 33(3), e4432. <https://doi.org/10.1002/bmc.4432>
- Chang, Y.-C., Jan, C.-I., Peng, C.-Y., Lai, Y.-C., Hu, F.-W., & Yu, C.-C. (2015). Activation of microRNA-494-targeting Bmi1 and ADAM10 by silibinin ablates cancer stemness and predicts favourable prognostic value in head and neck squamous cell carcinomas. *Oncotarget*, 6(27), 24002–24016. <https://doi.org/10.18632/oncotarget.4365>
- Che, S., Wu, S., & Yu, P. (2022). Lupeol induces autophagy and apoptosis with reduced cancer stem-like properties in retinoblastoma via phosphoinositide 3-kinase/protein kinase B/mammalian target of rapamycin inhibition. *Journal of Pharmacy and Pharmacology*, 74(2), 208–215. <https://doi.org/10.1093/jpp/rgab060>
- Chen, Q., Lin, W., Yin, Z., Zou, Y., Liang, S., Ruan, S., Chen, P., Li, S., Shu, Q., Cheng, B., & Ling, C. (2019). Melittin Inhibits Hypoxia-Induced Vasculogenic Mimicry Formation and Epithelial-Mesenchymal Transition through Suppression of HIF-1 α /Akt Pathway in Liver Cancer. *Evidence-Based Complementary and Alternative Medicine: ECAM*, 2019, 9602935. <https://doi.org/10.1155/2019/9602935>
- Cheng, L., Wang, Q., Tao, X., Qin, Y., Wu, Q., Zheng, D., Chai, D., Zhang, Y., Lu, D., Ci, H., Wang, Z., Ma, J., Wang, D., Cheng, Z., Wu, S., & Tao, Y. (2020). FOXM 1 induces Vasculogenic mimicry in esophageal cancer through β -catenin /Tcf4 signaling. *Diagnostic Pathology*, 15(1), 14. <https://doi.org/10.1186/s13000-020-00929-9>
- Chiablaem, K., Lirdprapamongkol, K., Keeratichamroen, S., Surarit, R., & Svasti, J. (2014). Curcumin suppresses vasculogenic mimicry capacity of hepatocellular carcinoma cells through STAT3 and PI3K/AKT inhibition. *Anticancer Research*, 34(4), 1857–1864.

- Choi, H. S., Kim, Y.-K., Hwang, K.-G., & Yun, P.-Y. (2020). Increased FOXM1 Expression by Cisplatin Inhibits Paclitaxel-Related Apoptosis in Cisplatin-Resistant Human Oral Squamous Cell Carcinoma (OSCC) Cell Lines. *International Journal of Molecular Sciences*, *21*(23), Art. 23. <https://doi.org/10.3390/ijms21238897>
- Chou, T.-C.(2010). Drug combination studies and their synergy quantification using the Chou-Talalay method.*Cancer Research*, *70*(2), 440–446. <https://doi.org/10.1158/0008-5472.CAN-09-1947>
- Coates, A., Abraham, S., Kaye, S. B., Sowerbutts, T., Frewin, C., Fox, R. M., & Tattersall, M. H. (1983). On the receiving end—Patient perception of the side-effects of cancer chemotherapy. *European Journal of Cancer & Clinical Oncology*, *19*(2), 203–208. [https://doi.org/10.1016/0277-5379\(83\)90418-2](https://doi.org/10.1016/0277-5379(83)90418-2)
- Cojocneanu Petric, R., Braicu, C., Raduly, L., Zanoaga, O., Dragos, N., Monroig, P., Dumitrascu, D., & Berindan-Neagoe, I. (2015). Phytochemicals modulate carcinogenic signaling pathways in breast and hormone-related cancers. *OncoTargets and Therapy*, *8*, 2053–2066. <https://doi.org/10.2147/OTT.S83597>
- Davis, S., Gale, N. W., Aldrich, T. H., Maisonpierre, P. C., Lhotak, V., Pawson, T., Goldfarb, M., & Yancopoulos, G. D. (1994). Ligands for EPH-related receptor tyrosine kinases that require membrane attachment or clustering for activity. *Science (New York, N.Y.)*, *266*(5186), 816–819. <https://doi.org/10.1126/science.7973638>
- Deleu, D., Hanssens, Y., & Northway, M. G. (2004). Subcutaneous apomorphine: An evidence-based review of its use in Parkinson’s disease. *Drugs & Aging*, *21*(11), 687–710.

- Delgado-Bellido, D., Serrano-Saenz, S., Fernández-Cortés, M., & Oliver, F. J. (2017). Vasculogenic mimicry signaling revisited: Focus on non-vascular VE-cadherin. *Molecular Cancer*, *16*(1), 65. <https://doi.org/10.1186/s12943-017-0631-x>
- Deng, Q.-P., Wang, M.-J., Zeng, X., Chen, G. G., & Huang, R.-Y. (2017). Effects of Glycyrrhizin in a Mouse Model of Lung Adenocarcinoma. *Cellular Physiology and Biochemistry: International Journal of Experimental Cellular Physiology, Biochemistry, and Pharmacology*, *41*(4), 1383–1392. <https://doi.org/10.1159/000467897>
- Deshmukh, V., & Shekar, K. (2021). Oral Squamous Cell Carcinoma: Diagnosis and Treatment Planning. In K. Bonanthaya, E. Panneerselvam, S. Manuel, V. V. Kumar, & A. Rai (Eds.), *Oral and Maxillofacial Surgery for the Clinician* (pp. 1853–1867). Springer Nature. https://doi.org/10.1007/978-981-15-1346-6_81
- Dhull, A. K., Atri, R., Dhankhar, R., Chauhan, A. K., & Kaushal, V. (2018). Major Risk Factors in Head and Neck Cancer: A Retrospective Analysis of 12-Year Experiences. *World Journal of Oncology*, *9*(3), 80–84. <https://doi.org/10.14740/wjon1104w>
- Dong, W.-W., Li, J., Li, J., Zhang, P., Wang, Z.-H., Sun, W., & Zhang, H. (2018). Reduced expression of oestrogen receptor- β is associated with tumour invasion and metastasis in oestrogen receptor- α -negative human papillary thyroid carcinoma. *International Journal of Experimental Pathology*, *99*(1), 15–21. <https://doi.org/10.1111/iep.12266>
- Du, J., Sun, B., Zhao, X., Gu, Q., Dong, X., Mo, J., Sun, T., Wang, J., Sun, R., & Liu, Y. (2014). Hypoxia promotes vasculogenic mimicry formation by inducing epithelial–mesenchymal transition in ovarian carcinoma. *Gynecologic Oncology*, *133*(3), 575–583. <https://doi.org/10.1016/j.ygyno.2014.02.034>

- Duan, S. (2018). Silencing the autophagy-specific gene Beclin-1 contributes to attenuated hypoxia-induced vasculogenic mimicry formation in glioma. *Cancer Biomarkers: Section A of Disease Markers*, 21(3), 565–574. <https://doi.org/10.3233/CBM-170444>
- Dunleavey, J. M., & Dudley, A. C. (2012). Vascular Mimicry: Concepts and Implications for Anti-Angiogenic Therapy. *Current Angiogenesis*, 1(2), 133–138. <https://doi.org/10.2174/2211552811201020133>
- Duo, H., Zi-yue, G. U., Jiang, L. I., & Zhi-yuan, Z. (2018). Axitinib inhibits oral mucosal melanoma growth through modulating vasculogenic mimicry in a patient-derived xenograft model. *China Journal of Oral and Maxillofacial Surgery*, 16(4), 296. <https://doi.org/10.19438/j.cjoms.2018.04.002>
- Eckert, A. W., Lautner, M. H. W., Schütze, A., Bolte, K., Bache, M., Kappler, M., Schubert, J., Taubert, H., & Bilkenroth, U. (2010). Co-expression of Hif1alpha and CAIX is associated with poor prognosis in oral squamous cell carcinoma patients. *Journal of Oral Pathology & Medicine: Official Publication of the International Association of Oral Pathologists and the American Academy of Oral Pathology*, 39(4), 313–317. <https://doi.org/10.1111/j.1600-0714.2009.00829.x>
- Eisenhauer, E. A., & Vermorken, J. B. (1998). The taxoids. Comparative clinical pharmacology and therapeutic potential. *Drugs*, 55(1), 5–30. <https://doi.org/10.2165/00003495-199855010-00002>
- Eldohaji, L. M., Fayed, B., Hamoda, A. M., Ershaid, M., Abdin, S., Alhamidi, T. B., Mohammad, M. G., Omar, H. A., & Soliman, S. S. M. (2021). Potential targeting of Hep3B liver cancer cells by Lupeol isolated from *Avicennia marina*. *Archiv Der Pharmazie*, 354(9), 2100120. <https://doi.org/10.1002/ardp.202100120>

- Emami Nejad, A., Najafgholian, S., Rostami, A., Sistani, A., Shojaeifar, S., Esparvarinha, M., Nedaeinia, R., Haghjooy Javanmard, S., Taherian, M., Ahmadlou, M., Salehi, R., Sadeghi, B., & Manian, M. (2021). The role of hypoxia in the tumor microenvironment and development of cancer stem cell: A novel approach to developing treatment. *Cancer Cell International*, 21(1), 62. <https://doi.org/10.1186/s12935-020-01719-5>
- Fan, Y.-L., Zheng, M., Tang, Y.-L., & Liang, X.-H. (2013). A new perspective of vasculogenic mimicry: EMT and cancer stem cells (Review). *Oncology Letters*, 6(5), 1174–1180. <https://doi.org/10.3892/ol.2013.1555>
- Ferlito, A., Shaha, A. R., Silver, C. E., Rinaldo, A., & Mondin, V. (2001). Incidence and sites of distant metastases from head and neck cancer. *ORL; Journal for Oto-Rhino-Laryngology and Its Related Specialties*, 63(4), 202–207. <https://doi.org/10.1159/000055740>
- Fernández-Cortés, M., Delgado-Bellido, D., & Oliver, F. J. (2019). Vasculogenic Mimicry: Become an Endothelial Cell “But Not So Much.” *Frontiers in Oncology*, 9, 803. <https://doi.org/10.3389/fonc.2019.00803>
- Folberg, R., & Maniotis, A. J. (2004). Vasculogenic mimicry. *APMIS*, 112(7–8), 508–525. <https://doi.org/10.1111/j.1600-0463.2004.apm11207-0810.x>
- Folberg, R., Hendrix, M. J., & Maniotis, A. J. (2000). Vasculogenic mimicry and tumor angiogenesis. *The American Journal of Pathology*, 156(2), 361–381. [https://doi.org/10.1016/S0002-9440\(10\)64739-6](https://doi.org/10.1016/S0002-9440(10)64739-6)
- Fortin, A., Couture, C., Doucet, R., Albert, M., Allard, J., & Tetu, B. (2001). Does histologic grade have a role in the management of head and neck cancers? *Journal of Clinical*

- Oncology: Official Journal of the American Society of Clinical Oncology*, 19(21), 4107–4116. <https://doi.org/10.1200/JCO.2001.19.21.4107>
- Fu, R., Du, W., Ding, Z., Wang, Y., Li, Y., Zhu, J., Zeng, Y., Zheng, Y., Liu, Z., & Huang, J. (2021). HIF-1 α promoted vasculogenic mimicry formation in lung adenocarcinoma through NRP1 upregulation in the hypoxic tumor microenvironment. *Cell Death & Disease*, 12, 394. <https://doi.org/10.1038/s41419-021-03682-z>
- Fuentes, B., Duaso, J., Droguett, D., Castillo, C., Donoso, W., Rivera, C., Venegas, B., & Kemmerling, U. (2012). Progressive Extracellular Matrix Disorganization in Chemically Induced Murine Oral Squamous Cell Carcinoma. *International Scholarly Research Notices*, 2012, e359421. <https://doi.org/10.5402/2012/359421>
- Ganguly, A., Yang, H., & Cabral, F. (2010). Paclitaxel-dependent cell lines reveal a novel drug activity. *Molecular Cancer Therapeutics*, 9(11), 2914–2923. <https://doi.org/10.1158/1535-7163.MCT-10-0552>
- Gard, D. L., & Kirschner, M. W. (1985). A polymer-dependent increase in phosphorylation of beta-tubulin accompanies differentiation of a mouse neuroblastoma cell line. *The Journal of Cell Biology*, 100(3), 764–774. <https://doi.org/10.1083/jcb.100.3.764>
- Gelmon, K., Eisenhauer, E., Bryce, C., Tolcher, A., Mayer, L., Tomlinson, E., Zee, B., Blackstein, M., Tomiak, E., Yau, J., Batist, G., Fisher, B., & Iglesias, J. (1999). Randomized phase II study of high-dose paclitaxel with or without amifostine in patients with metastatic breast cancer. *Journal of Clinical Oncology: Official Journal of the American Society of Clinical Oncology*, 17(10), 3038–3047. <https://doi.org/10.1200/JCO.1999.17.10.3038>

- Giannelli, G., & Antonaci, S. (2000). Biological and clinical relevance of Laminin-5 in cancer. *Clinical & Experimental Metastasis*, 18(6), 439–443. <https://doi.org/10.1023/a:1011879900554>
- Gibson, M. K., Li, Y., Murphy, B., Hussain, M. H. A., DeConti, R. C., Ensley, J., Forastiere, A. A., & Eastern Cooperative Oncology Group. (2005). Randomized phase III evaluation of cisplatin plus fluorouracil versus cisplatin plus Paclitaxel in advanced head and neck cancer (E1395): An intergroup trial of the Eastern Cooperative Oncology Group. *Journal of Clinical Oncology: Official Journal of the American Society of Clinical Oncology*, 23(15), 3562–3567. <https://doi.org/10.1200/JCO.2005.01.057>
- Gillison, M. L., Koch, W. M., Capone, R. B., Spafford, M., Westra, W. H., Wu, L., Zahurak, M. L., Daniel, R. W., Viglione, M., Symer, D. E., Shah, K. V., & Sidransky, D. (2000). Evidence for a causal association between human papillomavirus and a subset of head and neck cancers. *Journal of the National Cancer Institute*, 92(9), 709–720. <https://doi.org/10.1093/jnci/92.9.709>
- Gkouveris, I., Nikitakis, N., Avgoustidis, D., Karanikou, M., Rassidakis, G., & Sklavounou, A. (2017). ERK1/2, JNK and STAT3 activation and correlation with tumor differentiation in oral SCC. *Histology and Histopathology*, 32(10), 1065–1076. <https://doi.org/10.14670/HH-11-868>
- Gong, W., Sun, B., Zhao, X., Zhang, D., Sun, J., Liu, T., Gu, Q., Dong, X., Liu, F., Wang, Y., Lin, X., & Li, Y. (2016). Nodal signaling promotes vasculogenic mimicry formation in breast cancer via the Smad2/3 pathway. *Oncotarget*, 7(43), 70152–70167. <https://doi.org/10.18632/oncotarget.12161>

- Gonzalez Suarez, N., Rodriguez Torres, S., Ouanouki, A., El Cheikh-Hussein, L., & Annabi, B. (2021). EGCG Inhibits Adipose-Derived Mesenchymal Stem Cells Differentiation into Adipocytes and Prevents a STAT3-Mediated Paracrine Oncogenic Control of Triple-Negative Breast Cancer Cell Invasive Phenotype. *Molecules*, 26(6), Art. 6. <https://doi.org/10.3390/molecules26061506>
- Griffin, A. M., Butow, P. N., Coates, A. S., Childs, A. M., Ellis, P. M., Dunn, S. M., & Tattersall, M. H. (1996). On the receiving end. V: Patient perceptions of the side effects of cancer chemotherapy in 1993. *Annals of Oncology: Official Journal of the European Society for Medical Oncology*, 7(2), 189–195. <https://doi.org/10.1093/oxfordjournals.annonc.a010548>
- Guo, X., Xu, S., Gao, X., Wang, J., Xue, H., Chen, Z., Zhang, J., Guo, X., Qian, M., Qiu, W., & Li, G. (2017). Macrophage migration inhibitory factor promotes vasculogenic mimicry formation induced by hypoxia via CXCR4/AKT/EMT pathway in human glioblastoma cells. *Oncotarget*, 8(46), 80358–80372. <https://doi.org/10.18632/oncotarget.18673>
- Gupta, P. C., Murti, P. R., & Bhonsle, R. B. (1996). Epidemiology of cancer by tobacco products and the significance of TSNA. *Critical Reviews in Toxicology*, 26(2), 183–198. <https://doi.org/10.3109/10408449609017930>
- Gupta. (n.d.). *Trends and patterns of head-and-neck cancer among a cohort of bidi smokers: A clinical study*. Retrieved November 21, 2022,
- Gustafsson, M. V., Zheng, X., Pereira, T., Gradin, K., Jin, S., Lundkvist, J., Ruas, J. L., Poellinger, L., Lendahl, U., & Bondesson, M. (2005). Hypoxia requires notch signaling to maintain the undifferentiated cell state. *Developmental Cell*, 9(5), 617–628. <https://doi.org/10.1016/j.devcel.2005.09.010>

- Haiaty, S., Rashidi, M.-R., Akbarzadeh, M., Bazmani, A., Mostafazadeh, M., Nikanfar, S., Zibaei, Z., Rahbarghazi, R., & Nouri, M. (2021). Thymoquinone inhibited vasculogenic capacity and promoted mesenchymal-epithelial transition of human breast cancer stem cells. *BMC Complementary Medicine and Therapies*, *21*(1), 83. <https://doi.org/10.1186/s12906-021-03246-w>
- Han, D.-S., Lee, H.-J., & Lee, E.-O. (2022). Resveratrol suppresses serum-induced vasculogenic mimicry through impairing the EphA2/twist-VE-cadherin/AKT pathway in human prostate cancer PC-3 cells. *Scientific Reports*, *12*(1), Art. 1. <https://doi.org/10.1038/s41598-022-24414-z>
- Hardy, K. M., Kirschmann, D. A., Seftor, E. A., Margaryan, N. V., Postovit, L.-M., Strizzi, L., & Hendrix, M. J. C. (2010). Regulation of the embryonic morphogen Nodal by Notch4 facilitates manifestation of the aggressive melanoma phenotype. *Cancer Research*, *70*(24), 10340–10350. <https://doi.org/10.1158/0008-5472.CAN-10-0705>
- Hartner, L. (2018). Chemotherapy for Oral Cancer. *Dental Clinics of North America*, *62*(1), 87–97. <https://doi.org/10.1016/j.cden.2017.08.006>
- Hata, K., Hori, K., & Takahashi, S. (2002). Differentiation- and apoptosis-inducing activities by pentacyclic triterpenes on a mouse melanoma cell line. *Journal of Natural Products*, *65*(5), 645–648. <https://doi.org/10.1021/np0104673>
- He, W., Li, X., & Xia, S. (2018). Lupeol triterpene exhibits potent antitumor effects in A427 human lung carcinoma cells via mitochondrial mediated apoptosis, ROS generation, loss of mitochondrial membrane potential and downregulation of m-TOR/PI3Ksol;AKT signalling pathway. *Journal of B.U.ON.: Official Journal of the Balkan Union of Oncology*, *23*(3), 635–640.

- Hendrix, M. J. C., Seftor, E. A., Hess, A. R., & Seftor, R. E. B. (2003). Vasculogenic mimicry and tumour-cell plasticity: Lessons from melanoma. *Nature Reviews. Cancer*, 3(6), 411–421. <https://doi.org/10.1038/nrc1092>
- Hendrix, M. J., Seftor, E. A., Meltzer, P. S., Gardner, L. M., Hess, A. R., Kirschmann, D. A., Schatteman, G. C., & Seftor, R. E. (2001). Expression and functional significance of VE-cadherin in aggressive human melanoma cells: Role in vasculogenic mimicry. *Proceedings of the National Academy of Sciences of the United States of America*, 98(14), 8018–8023. <https://doi.org/10.1073/pnas.131209798>
- Hernández de la Cruz, O. N., López-González, J. S., García-Vázquez, R., Salinas-Vera, Y. M., Muñoz-Lino, M. A., Aguilar-Cazares, D., López-Camarillo, C., & Carlos-Reyes, Á. (2019). Regulation Networks Driving Vasculogenic Mimicry in Solid Tumors. *Frontiers in Oncology*, 9, 1419. <https://doi.org/10.3389/fonc.2019.01419>
- Hess, A. R., Margaryan, N. V., Seftor, E. A., & Hendrix, M. J. C. (2007). Deciphering the signaling events that promote melanoma tumor cell vasculogenic mimicry and their link to embryonic vasculogenesis: Role of the Eph receptors. *Developmental Dynamics: An Official Publication of the American Association of Anatomists*, 236(12), 3283–3296. <https://doi.org/10.1002/dvdy.21190>
- Hess, A. R., Seftor, E. A., Gardner, L. M., Carles-Kinch, K., Schneider, G. B., Seftor, R. E., Kinch, M. S., & Hendrix, M. J. (2001). Molecular regulation of tumor cell vasculogenic mimicry by tyrosine phosphorylation: Role of epithelial cell kinase (Eck/EphA2). *Cancer Research*, 61(8), 3250–3255.
- Hess, A. R., Seftor, E. A., Gruman, L. M., Kinch, M. S., Seftor, R. E. B., & Hendrix, M. J. C. (2006). VE-cadherin regulates EphA2 in aggressive melanoma cells through a novel

- signaling pathway: Implications for vasculogenic mimicry. *Cancer Biology & Therapy*, 5(2), 228–233. <https://doi.org/10.4161/cbt.5.2.2510>
- Hillen, F., & Griffioen, A. W. (2007). Tumour vascularization: Sprouting angiogenesis and beyond. *Cancer Metastasis Reviews*, 26(3–4), 489–502. <https://doi.org/10.1007/s10555-007-9094-7>
- Hitt, R., Irigoyen, A., Cortes-Funes, H., Grau, J. J., García-Sáenz, J. A., Cruz-Hernandez, J. J., & Spanish Head and Neck Cancer Cooperative Group (TTCC). (2012). Phase II study of the combination of cetuximab and weekly Paclitaxel in the first-line treatment of patients with recurrent and/or metastatic squamous cell carcinoma of head and neck. *Annals of Oncology: Official Journal of the European Society for Medical Oncology*, 23(4), 1016–1022. <https://doi.org/10.1093/annonc/mdr367>
- Holton, R. A. (1992). *Method for preparation of taxol using β -lactam* (United States Patent No. US5175315A). <https://patents.google.com/patent/US5175315A/en>
- Holton, R. A. (1998). *Method for preparation of taxol* (European Union Patent No. EP0400971B1). <https://patents.google.com/patent/EP0400971B1/en>
- Hong, K.-O., Oh, K.-Y., Yoon, H.-J., Swarup, N., Jung, M., Shin, J.-A., Kim, J.-H., Chawla, K., Lee, J.-I., Cho, S.-D., & Hong, S.-D. (2021). SOX7 blocks vasculogenic mimicry in oral squamous cell carcinoma. *Journal of Oral Pathology & Medicine: Official Publication of the International Association of Oral Pathologists and the American Academy of Oral Pathology*, 50(8), 766–775. <https://doi.org/10.1111/jop.13176>
- Horwitz, S. B. (1992). Mechanism of action of taxol. *Trends in Pharmacological Sciences*, 13(4), 134–136. [https://doi.org/10.1016/0165-6147\(92\)90048-b](https://doi.org/10.1016/0165-6147(92)90048-b)

- Horwitz, S. B. (1994). Taxol (Paclitaxel): Mechanisms of action. *Annals of Oncology: Official Journal of the European Society for Medical Oncology*, 5 Suppl 6, S3-6.
- Hu, A., Huang, J.-J., Jin, X.-J., Li, J.-P., Tang, Y.-J., Huang, X.-F., Cui, H.-J., Xu, W.-H., & Sun, G.-B. (2015). Curcumin suppresses invasiveness and vasculogenic mimicry of squamous cell carcinoma of the larynx through the inhibition of JAK-2/STAT-3 signaling pathway. *American Journal of Cancer Research*, 5(1), 278–288.
- Hu, A., Huang, J.-J., Li, R.-L., Lu, Z.-Y., Duan, J.-L., Xu, W.-H., Chen, X.-P., & Fan, J.-P. (2015). Curcumin as therapeutics for the treatment of head and neck squamous cell carcinoma by activating SIRT1. *Scientific Reports*, 5, 13429. <https://doi.org/10.1038/srep13429>
- Hu, J., Zhang, N., Wang, R., Huang, F., & Li, G. (2015). Paclitaxel induces apoptosis and reduces proliferation by targeting epidermal growth factor receptor signaling pathway in oral cavity squamous cell carcinoma. *Oncology Letters*, 10(4), 2378–2384. <https://doi.org/10.3892/ol.2015.3499>
- Huang, B., Xiao, E., & Huang, M. (2014). MEK/ERK pathway is positively involved in hypoxia-induced vasculogenic mimicry formation in hepatocellular carcinoma which is regulated negatively by protein kinase A. *Medical Oncology*, 32(1), 408. <https://doi.org/10.1007/s12032-014-0408-7>
- Huang, G.-C., Liu, S.-Y., Lin, M.-H., Kuo, Y.-Y., & Liu, Y.-C. (2004). The synergistic cytotoxicity of cisplatin and taxol in killing oral squamous cell carcinoma. *Japanese Journal of Clinical Oncology*, 34(9), 499–504. <https://doi.org/10.1093/jjco/hyh091>
- Huang, S., Mo, C., Zeng, T., Lai, Y., Zhou, C., Xie, S., Chen, L., Wang, Y., Chen, Y., Huang, S., Gao, L., & Lv, Z. (2021). Lupeol ameliorates LPS/D-GalN induced acute

- hepatic damage by suppressing inflammation and oxidative stress through TGF β 1-Nrf2 signal pathway. *Aging (Albany NY)*, *13*(5), 6592–6605. <https://doi.org/10.18632/aging.202409>
- Hujanen, R., Almahmoudi, R., Karinen, S., Nwaru, B. I., Salo, T., & Salem, A. (2020). Vasculogenic Mimicry: A Promising Prognosticator in Head and Neck Squamous Cell Carcinoma and Esophageal Cancer? A Systematic Review and Meta-Analysis. *Cells*, *9*(2), 507. <https://doi.org/10.3390/cells9020507>
- Hujanen, R., Almahmoudi, R., Salo, T., & Salem, A. (2021). Comparative Analysis of Vascular Mimicry in Head and Neck Squamous Cell Carcinoma: In Vitro and In Vivo Approaches. *Cancers*, *13*(19), 4747. <https://doi.org/10.3390/cancers13194747>
- IMAI, A., MATSUNAMI, K., TAKAGI, H., & ICHIGO, S. (2012). Proposed medications for taxane-induced myalgia and arthralgia (Review). *Oncology Letters*, *3*(6), 1181–1185. <https://doi.org/10.3892/ol.2012.651>
- J, A.-R.A., E.h, E.-T.K., S, M. J., & Syed, R. (2001). Pharmacological Studies of Various Extracts and the Major Constituent, Lupeol, obtained from Hexane Extract of *Teclea nobilis* in Rodents. *Natural Product Sciences*, *7*(3), 76–82.
- Jiang, X., Deng, X., Wang, J., Mo, Y., Shi, L., Wei, F., Zhang, S., Gong, Z., He, Y., Xiong, F., Wang, Y., Guo, C., Xiang, B., Zhou, M., Liao, Q., Li, X., Li, Y., Li, G., Xiong, W., & Zeng, Z. (2022). BPIFB1 inhibits vasculogenic mimicry via downregulation of GLUT1-mediated H3K27 acetylation in nasopharyngeal carcinoma. *Oncogene*, *41*(2), 233–245. <https://doi.org/10.1038/s41388-021-02079-8>

- Jing, X., Yang, F., Shao, C., Wei, K., Xie, M., Shen, H., & Shu, Y. (2019). Role of hypoxia in cancer therapy by regulating the tumor microenvironment. *Molecular Cancer*, *18*(1), 157. <https://doi.org/10.1186/s12943-019-1089-9>
- JingQiang, G., & ShengZhang, L. (2017). Inhibitory effect of ginsenoside Rg3 on the vasculogenic mimicry formation in the pancreatic cancer sw-1990 cell line in vitro. *China Journal of Traditional Chinese Medicine and Pharmacy*, *32*(3), 1310–1312.
- Jin-lu, M., Su-xia, H., Qing, Z., Jing, Z., Dan, Z., Li, W., & Yi, L. (2011). Role of Twist in vasculogenic mimicry formation in hypoxic hepatocellular carcinoma cells in vitro. *Biochemical and Biophysical Research Communications*, *408*(4), 686–691. <https://doi.org/10.1016/j.bbrc.2011.04.089>
- Ju, R.-J., Li, X.-T., Shi, J.-F., Li, X.-Y., Sun, M.-G., Zeng, F., Zhou, J., Liu, L., Zhang, C.-X., Zhao, W.-Y., & Lu, W.-L. (2014). Liposomes, modified with PTD(HIV-1) peptide, containing epirubicin and celecoxib, to target vasculogenic mimicry channels in invasive breast cancer. *Biomaterials*, *35*(26), 7610–7621. <https://doi.org/10.1016/j.biomaterials.2014.05.040>
- Jue, C., Lin, C., Zhisheng, Z., Yayun, Q., Feng, J., Min, Z., Haibo, W., Youyang, S., Hisamitsu, T., Shintaro, I., Shiyu, G., & Yanqing, L. (2017). Notch1 promotes vasculogenic mimicry in hepatocellular carcinoma by inducing EMT signaling. *Oncotarget*, *8*(2), 2501–2513. <https://doi.org/10.18632/oncotarget.12388>
- K, P., & U, K. A. (2012). Paclitaxel Against Cancer: A Short Review. *Medicinal Chemistry*, *2*(7), 1–3. <https://doi.org/10.4172/2161-0444.1000130>
- Kang, X., Xu, E., Wang, X., Qian, L., Yang, Z., Yu, H., Wang, C., Ren, C., Wang, Y., Lu, X., Xia, X., Guan, W., & Qiao, T. (2021). Tenascin-c knockdown suppresses

- vasculogenic mimicry of gastric cancer by inhibiting ERK- triggered EMT. *Cell Death & Disease*, 12(10), 890. <https://doi.org/10.1038/s41419-021-04153-1>
- Kanno, Y., Chen, C.-Y., Lee, H.-L., Chiou, J.-F., & Chen, Y.-J. (2021). Molecular Mechanisms of Chemotherapy Resistance in Head and Neck Cancers. *Frontiers in Oncology*, 11, 640392. <https://doi.org/10.3389/fonc.2021.640392>
- Karaca, B., Muslu, U., Cakar, B., Kisim, A., Atmaca, H., Purcu, D., Uzunoglu, S., & Uslu, R. (2010). Synergistic cytotoxic/apoptotic effects of AT-101, a phytochemical with BH3-mimetic property, in combination with Paclitaxel in human breast cancer cells. *Journal of Clinical Oncology*, 28, e21082–e21082. https://doi.org/10.1200/jco.2010.28.15_suppl.e21082
- Kawahara, R., Niwa, Y., & Simizu, S. (2018). Integrin β 1 is an essential factor in vasculogenic mimicry of human cancer cells. *Cancer Science*, 109(8), 2490–2496. <https://doi.org/10.1111/cas.13693>
- Khatal, L., & More, H. (2019). Development and validation of a liquid chromatography-tandem mass spectrometry method for quantification of Lupeol in plasma and its application to pharmacokinetic study in rats. *Journal of Chromatography B*, 1121, 58–65. <https://doi.org/10.1016/j.jchromb.2019.05.008>
- Kl, C., & Dh, C. (1981). Microtubule stabilization by taxol inhibits initiation of DNA synthesis by thrombin and by epidermal growth factor. *Cell*, 27(2 Pt 1). [https://doi.org/10.1016/0092-8674\(81\)90417-7](https://doi.org/10.1016/0092-8674(81)90417-7)
- Ko, C., & Citrin, D. (2009). Radiotherapy for the management of locally advanced squamous cell carcinoma of the head and neck. *Oral Diseases*, 15(2), 121–132. <https://doi.org/10.1111/j.1601-0825.2008.01495.x>

- Koch, S., Tugues, S., Li, X., Gualandi, L., & Claesson-Welsh, L. (2011). Signal transduction by vascular endothelial growth factor receptors. *The Biochemical Journal*, *437*(2), 169–183. <https://doi.org/10.1042/BJ20110301>
- Krajewska, M., Krajewski, S., Epstein, J. I., Shabaik, A., Sauvageot, J., Song, K., Kitada, S., & Reed, J. C. (1996). Immunohistochemical analysis of bcl-2, bax, bcl-X, and mcl-1 expression in prostate cancers. *The American Journal of Pathology*, *148*(5), 1567–1576.
- Kshersagar, J., Bedge, P., Jagdale, R., Toro, Y., Sharma, S., & Joshi, M. (2020). A review on current scenario of oral cancer in india with special emphasis on modern detection systems and biomarkers. *International Journal of Applied Pharmaceutics*, 1–10. <https://doi.org/10.22159/ijap.2020.v12s4.40098>
- Kukita, A., Sone, K., Oda, K., Hamamoto, R., Kaneko, S., Komatsu, M., Wada, M., Honjoh, H., Kawata, Y., Kojima, M., Oki, S., Sato, M., Asada, K., Taguchi, A., Miyasaka, A., Tanikawa, M., Nagasaka, K., Matsumoto, Y., Wada-Hiraike, O., ... Fujii, T. (2019). Histone methyltransferase SMYD2 selective inhibitor LLY-507 in combination with poly ADP ribose polymerase inhibitor has therapeutic potential against high-grade serous ovarian carcinomas. *Biochemical and Biophysical Research Communications*, *513*(2), 340–346. <https://doi.org/10.1016/j.bbrc.2019.03.155>
- Landis, J. R., & Koch, G. G. (1977). The measurement of observer agreement for categorical data. *Biometrics*, *33*(1), 159–174.
- Larson, A. R., Lee, C.-W., Lezcano, C., Zhan, Q., Huang, J., Fischer, A. H., & Murphy, G. F. (2014). Melanoma Spheroid Formation Involves Laminin-Associated Vasculogenic Mimicry. *The American Journal of Pathology*, *184*(1), 71–78. <https://doi.org/10.1016/j.ajpath.2013.09.020>

- Lee, T. K., Poon, R. T. P., Wo, J. Y., Ma, S., Guan, X.-Y., Myers, J. N., Altevogt, P., & Yuen, A. P. W. (2007). Lupeol Suppresses Cisplatin-Induced Nuclear Factor- κ B Activation in Head and Neck Squamous Cell Carcinoma and Inhibits Local Invasion and Nodal Metastasis in an Orthotopic Nude Mouse Model. *Cancer Research*, *67*(18), 8800–8809. <https://doi.org/10.1158/0008-5472.CAN-07-0801>
- Lee, W.-L., Huang, J.-Y., & Shyur, L.-F. (2013). Phytoagents for cancer management: Regulation of nucleic acid oxidation, ROS, and related mechanisms. *Oxidative Medicine and Cellular Longevity*, *2013*, 925804. <https://doi.org/10.1155/2013/925804>
- Li, D., Guo, Y., Cen, X., Qiu, H., Chen, S., Zeng, X., Zeng, Q., Xu, M., & Tang, Q. (2022). Lupeol protects against cardiac hypertrophy via TLR4-PI3K-Akt-NF- κ B pathways. *Acta Pharmacologica Sinica*, *43*(8), Art. 8. <https://doi.org/10.1038/s41401-021-00820-3>
- Li, S., Meng, W., Guan, Z., Guo, Y., & Han, X. (2016). The hypoxia-related signaling pathways of vasculogenic mimicry in tumor treatment. *Biomedicine & Pharmacotherapy* *Biomedecine & Pharmacotherapie*, *80*, 127–135. <https://doi.org/10.1016/j.biopha.2016.03.010>
- Li, S., Zhang, Q., Zhou, L., Guan, Y., Chen, S., Zhang, Y., & Han, X. (2017). Inhibitory effects of compound DMBT on hypoxia-induced vasculogenic mimicry in human breast cancer. *Biomedicine & Pharmacotherapy*, *96*, 982–992. <https://doi.org/10.1016/j.biopha.2017.11.137>
- Li, W., & Zhou, Y. (2019). LRIG1 acts as a critical regulator of melanoma cell invasion, migration, and vasculogenic mimicry upon hypoxia by regulating EGFR/ERK-triggered epithelial-mesenchymal transition. *Bioscience Reports*, *39*(1), BSR20181165. <https://doi.org/10.1042/BSR20181165>

- Li, W., Zong, S., Shi, Q., Li, H., Xu, J., & Hou, F. (2016). Hypoxia-induced vasculogenic mimicry formation in human colorectal cancer cells: Involvement of HIF-1a, Claudin-4, and E-cadherin and Vimentin. *Scientific Reports*, 6(1), Art. 1. <https://doi.org/10.1038/srep37534>
- Li, X., Yang, Z., Han, Z., Wen, Y., Ma, Z., & Wang, Y. (2018). Niclosamide acts as a new inhibitor of vasculogenic mimicry in oral cancer through upregulation of miR-124 and downregulation of STAT3. *Oncology Reports*, 39(2), 827–833. <https://doi.org/10.3892/or.2017.6146>
- Li, X.-Y., Zhao, Y., Sun, M.-G., Shi, J.-F., Ju, R.-J., Zhang, C.-X., Li, X.-T., Zhao, W.-Y., Mu, L.-M., Zeng, F., Lou, J.-N., & Lu, W.-L. (2014). Multifunctional liposomes loaded with paclitaxel and artemether for treatment of invasive brain glioma. *Biomaterials*, 35(21), 5591–5604. <https://doi.org/10.1016/j.biomaterials.2014.03.049>
- Liang, Y., Huang, M., Li, J., Sun, X., Jiang, X., Li, L., & Ke, Y. (2014). Curcumin inhibits vasculogenic mimicry through the downregulation of erythropoietin-producing hepatocellular carcinoma-A2, phosphoinositide 3-kinase and matrix metalloproteinase-2. *Oncology Letters*, 8(4), 1849–1855. <https://doi.org/10.3892/ol.2014.2401>
- Lin, P., Wang, W., Sun, B.-C., Cai, W.-J., Li, L., Lu, H.-H., Han, C.-R., & Zhang, J.-M. (2012). Vasculogenic mimicry is a key prognostic factor for laryngeal squamous cell carcinoma: A new pattern of blood supply. *Chinese Medical Journal*, 125(19), 3445–3449.
- Ling, G., Wang, S., Song, Z., Sun, X., Liu, Y., Jiang, X., Cai, Y., Du, M., & Ke, Y. (2011). Transforming growth factor- β is required for vasculogenic mimicry formation in glioma

- cell line U251MG. *Cancer Biology & Therapy*, 12(11), 978–988.
<https://doi.org/10.4161/cbt.12.11.18155>
- Liu, K., Zhang, X., Xie, L., Deng, M., Chen, H., Song, J., Long, J., Li, X., & Luo, J. (2021). Lupeol and its derivatives as anticancer and anti-inflammatory agents: Molecular mechanisms and therapeutic efficacy. *Pharmacological Research*, 164, 105373.
<https://doi.org/10.1016/j.phrs.2020.105373>
- Liu, Q., Qiao, L., Liang, N., Xie, J., Zhang, J., Deng, G., Luo, H., & Zhang, J. (2016). The relationship between vasculogenic mimicry and epithelial-mesenchymal transitions. *Journal of Cellular and Molecular Medicine*, 20(9), 1761–1769.
<https://doi.org/10.1111/jcmm.12851>
- Liu, R., Wang, H., Deng, M., Wen, X., Mo, Y., Chen, F., Zou, C., Duan, W., Li, L., & Nie, X. (2018). Melatonin Inhibits Reactive Oxygen Species-Driven Proliferation, Epithelial-Mesenchymal Transition, and Vasculogenic Mimicry in Oral Cancer. *Oxidative Medicine and Cellular Longevity*, 2018, 1–13. <https://doi.org/10.1155/2018/3510970>
- Liu, R., Yang, K., Meng, C., Zhang, Z., & Xu, Y. (2012). Vasculogenic mimicry is a marker of poor prognosis in prostate cancer. *Cancer Biology & Therapy*, 13(7), 527–533.
<https://doi.org/10.4161/cbt.19602>
- Liu, S.-Y., Chang, L.-C., Pan, L.-F., Hung, Y.-J., Lee, C.-H., & Shieh, Y.-S. (2008). Clinicopathologic significance of tumor cell-lined vessel and microenvironment in oral squamous cell carcinoma. *Oral Oncology*, 44(3), 277–285.
<https://doi.org/10.1016/j.oraloncology.2007.02.007>
- Liu, W., Meng, M., Zhang, B., Du, L., Pan, Y., Yang, P., Gu, Z., Zhou, Q., & Cao, Z. (2015). Dehydroeffusol effectively inhibits human gastric cancer cell-mediated vasculogenic

- mimicry with low toxicity. *Toxicology and Applied Pharmacology*, 287(2), 98–110.
<https://doi.org/10.1016/j.taap.2015.05.003>
- Liu, X., Lv, Z., Zhou, S., Kan, S., Liu, X., Jing, P., & Xu, W. (2021). MTDH in macrophages promotes the vasculogenic mimicry via VEGFA-165/Flt-1 signaling pathway in head and neck squamous cell carcinoma. *International Immunopharmacology*, 96, 107776.
<https://doi.org/10.1016/j.intimp.2021.107776>
- Liu, Y., Mei, L., Yu, Q., Xu, C., Qiu, Y., Yang, Y., Shi, K., Zhang, Q., Gao, H., Zhang, Z., & He, Q. (2015). Multifunctional Tandem Peptide Modified Paclitaxel-Loaded Liposomes for the Treatment of Vasculogenic Mimicry and Cancer Stem Cells in Malignant Glioma. *ACS Applied Materials & Interfaces*, 7(30), 16792–16801.
<https://doi.org/10.1021/acsami.5b04596>
- Lo Nigro, C., Denaro, N., Merlotti, A., & Merlano, M. (2017). Head and neck cancer: Improving outcomes with a multidisciplinary approach. *Cancer Management and Research*, 9, 363–371. <https://doi.org/10.2147/CMAR.S115761>
- Lu, H., & Kang, F. (2020). Down-regulating NEAT1 inhibited the viability and vasculogenic mimicry formation of sinonasal squamous cell carcinoma cells via miR-195-5p/VEGFA axis. *Bioscience Reports*, 40(11), BSR20201373. <https://doi.org/10.1042/BSR20201373>
- Lu, X.-S., Sun, W., Ge, C.-Y., Zhang, W.-Z., & Fan, Y.-Z. (2013). Contribution of the PI3K/MMPs/Ln-5γ2 and EphA2/FAK/Paxillin signaling pathways to tumor growth and vasculogenic mimicry of gallbladder carcinomas. *International Journal of Oncology*, 42(6), 2103–2115. <https://doi.org/10.3892/ijo.2013.1897>
- Luo, Q., Wang, J., Zhao, W., Peng, Z., Liu, X., Li, B., Zhang, H., Shan, B., Zhang, C., & Duan, C. (2020). Vasculogenic mimicry in carcinogenesis and clinical applications.

- Journal of Hematology & Oncology*, 13(1), 19. <https://doi.org/10.1186/s13045-020-00858-6>
- Luo, Y., Wang, J., Wang, F., Liu, X., Lu, J., Yu, X., Ma, X., Peng, X., & Li, X. (2021). Foxq1 promotes metastasis of nasopharyngeal carcinoma by inducing vasculogenic mimicry via the EGFR signaling pathway. *Cell Death & Disease*, 12(5), 411. <https://doi.org/10.1038/s41419-021-03674-z>
- Maasland, D. H. E., van den Brandt, P. A., Kremer, B., Goldbohm, R. A. S., & Schouten, L. J. (2014). Alcohol consumption, cigarette smoking and the risk of subtypes of head-neck cancer: Results from the Netherlands Cohort Study. *BMC Cancer*, 14, 187. <https://doi.org/10.1186/1471-2407-14-187>
- Majumder, B., Baraneedharan, U., Thiagarajan, S., Radhakrishnan, P., Narasimhan, H., Dhandapani, M., Brijwani, N., Pinto, D. D., Prasath, A., Shanthappa, B. U., Thayakumar, A., Surendran, R., Babu, G. K., Shenoy, A. M., Kuriakose, M. A., Bergthold, G., Horowitz, P., Loda, M., Beroukhim, R., ... Majumder, P. K. (2015). Predicting clinical response to anticancer drugs using an ex vivo platform that captures tumour heterogeneity. *Nature Communications*, 6, 6169. <https://doi.org/10.1038/ncomms7169>
- Malekinejad, F., Kheradmand, F., Khadem-Ansari, M. H., & Malekinejad, H. (2022). Lupeol synergizes with doxorubicin to induce anti-proliferative and apoptotic effects on breast cancer cells. *DARU Journal of Pharmaceutical Sciences*, 30(1), 103–115. <https://doi.org/10.1007/s40199-022-00436-w>
- Malina, R., Motoyama, S., Hamana, S., & Maruo, T. (2004). Laminin-5 gamma2 chain and matrix metalloproteinase-2 expression in the neoplastic changes of uterine cervical squamous epithelium. *The Kobe Journal of Medical Sciences*, 50(3–4), 123–130.

- Maniotis, A. J., Folberg, R., Hess, A., Seftor, E. A., Gardner, L. M., Pe'er, J., Trent, J. M., Meltzer, P. S., & Hendrix, M. J. (1999). Vascular channel formation by human melanoma cells in vivo and in vitro: Vasculogenic mimicry. *The American Journal of Pathology*, *155*(3), 739–752. [https://doi.org/10.1016/S0002-9440\(10\)65173-5](https://doi.org/10.1016/S0002-9440(10)65173-5)
- Mao, X., Xue, X., Wang, L., Zhang, X., Yan, M., Tu, Y., Lin, W., Jiang, X., Ren, H., Zhang, W., & Song, S. (2013). CDH5 is specifically activated in glioblastoma stemlike cells and contributes to vasculogenic mimicry induced by hypoxia. *Neuro-Oncology*, *15*(7), 865–879. <https://doi.org/10.1093/neuonc/not029>
- Maroufi, N. F., Amiri, M., Dizaji, B. F., Vahedian, V., Akbarzadeh, M., Roshanravan, N., Haiaty, S., Nouri, M., & Rashidi, M.-R. (2020). Inhibitory effect of melatonin on hypoxia-induced vasculogenic mimicry via suppressing epithelial-mesenchymal transition (EMT) in breast cancer stem cells. *European Journal of Pharmacology*, *881*, 173282. <https://doi.org/10.1016/j.ejphar.2020.173282>
- Mayne, S. T., Morse, D. E., & Winn, D. M. (2009). Cancers of the Oral Cavity and Pharynx. In *Cancer Epidemiology and Prevention*. Oxford University Press. <https://doi.org/10.1093/acprof:oso/9780195149616.003.0035>
- McCarty, K. S., Szabo, E., Flowers, J. L., Cox, E. B., Leight, G. S., Miller, L., Konrath, J., Soper, J. T., Budwit, D. A., & Creasman, W. T. (1986). Use of a monoclonal anti-estrogen receptor antibody in the immunohistochemical evaluation of human tumors. *Cancer Research*, *46*(8 Suppl), 4244s–4248s.
- Mekhail, T. M., & Markman, M. (2002). Paclitaxel in cancer therapy. *Expert Opinion on Pharmacotherapy*, *3*(6), 755–766. <https://doi.org/10.1517/14656566.3.6.755>

- Meng, J., Chen, S., Lei, Y.-Y., Han, J.-X., Zhong, W.-L., Wang, X.-R., Liu, Y.-R., Gao, W.-F., Zhang, Q., Tan, Q., Liu, H.-J., Zhou, H.-G., Sun, T., & Yang, C. (2019). Hsp90 β promotes aggressive vasculogenic mimicry via epithelial-mesenchymal transition in hepatocellular carcinoma. *Oncogene*, *38*(2), 228–243. <https://doi.org/10.1038/s41388-018-0428-4>
- Miao, H., Burnett, E., Kinch, M., Simon, E., & Wang, B. (2000). Activation of EphA2 kinase suppresses integrin function and causes focal-adhesion-kinase dephosphorylation. *Nature Cell Biology*, *2*(2), 62–69. <https://doi.org/10.1038/35000008>
- Miao, H., Wei, B.-R., Peehl, D. M., Li, Q., Alexandrou, T., Schelling, J. R., Rhim, J. S., Sedor, J. R., Burnett, E., & Wang, B. (2001). Activation of EphA receptor tyrosine kinase inhibits the Ras/MAPK pathway. *Nature Cell Biology*, *3*(5), Art. 5. <https://doi.org/10.1038/35074604>
- Miles, G. J., Powley, I., Mohammed, S., Howells, L., Pringle, J. H., Hammonds, T., MacFarlane, M., & Pritchard, C. (2021). Evaluating and comparing immunostaining and computational methods for spatial profiling of drug response in patient-derived explants. *Laboratory Investigation*, *101*(3), Art. 3. <https://doi.org/10.1038/s41374-020-00511-3>
- Min, T.-R., Park, H.-J., Ha, K.-T., Chi, G.-Y., Choi, Y.-H., & Park, S.-H. (2019). Suppression of EGFR/STAT3 activity by Lupeol contributes to the induction of the apoptosis of human non-small cell lung cancer cells. *International Journal of Oncology*, *55*(1), 320–330. <https://doi.org/10.3892/ijo.2019.4799>
- Minhas, S., Kashif, M., Altaf, W., Afzal, N., & Nagi, A. H. (2017). Concomitant-chemoradiotherapy-associated oral lesions in patients with oral squamous-cell carcinoma.

Cancer Biology & Medicine, 14(2), 176–182. <https://doi.org/10.20892/j.issn.2095-3941.2016.0096>

Mishra, N. (2019). Oral cancer: A study in retrospection. *National Journal of Maxillofacial Surgery*, 10(1), 1. https://doi.org/10.4103/njms.NJMS_28_19

Mitra, D., Bhattacharyya, S., Alam, N., Sen, S., Mitra, S., Mandal, S., Vignesh, S., Majumder, B., & Murmu, N. (2020). Phosphorylation of EphA2 receptor and vasculogenic mimicry is an indicator of poor prognosis in invasive carcinoma of the breast. *Breast Cancer Research and Treatment*, 179(2), 359–370. <https://doi.org/10.1007/s10549-019-05482-8>

Mittal, B. B., Pauloski, B. R., Rademaker, A. W., Discekici-Harris, M., Helenowski, I. B., Mellot, A., Agulnik, M., & Logemann, J. A. (2015). Effect of induction chemotherapy on swallow physiology and saliva production in patients with head and neck cancer: A pilot study. *Head & Neck*, 37(4), 567–572. <https://doi.org/10.1002/hed.23635>

Morales-Guadarrama, G., Méndez-Pérez, E. A., García-Quiroz, J., Avila, E., García-Becerra, R., Zentella-Dehesa, A., Larrea, F., & Díaz, L. (2022). Endothelium-Dependent Induction of Vasculogenic Mimicry in Human Triple-Negative Breast Cancer Cells Is Inhibited by Calcitriol and Curcumin. *International Journal of Molecular Sciences*, 23(14), Art. 14. <https://doi.org/10.3390/ijms23147659>

Mortazavi, H., Baharvand, M., & Mehdipour, M. (2014). Oral Potentially Malignant Disorders: An Overview of More than 20 Entities. *Journal of Dental Research, Dental Clinics, Dental Prospects*, 8(1), 6–14. <https://doi.org/10.5681/joddd.2014.002>

Murugesan, A., Sekar, B., Saranyan, R., Manivannan, E., & Rajmohan, M. (2021). A Review on Cancer Stem Cells in Vasculogenic Mimicry Formation: A New Dimension for

- Targeted Therapy. *Journal of Advanced Oral Research*, 12(1), 34–41.
<https://doi.org/10.1177/2320206820960862>
- Mustafa, E., Parmar, S., & Praveen, P. (2021). Premalignant Lesions and Conditions of the Oral Cavity. In K. Bonanthaya, E. Panneerselvam, S. Manuel, V. V. Kumar, & A. Rai (Eds.), *Oral and Maxillofacial Surgery for the Clinician* (pp. 1845–1852). Springer Nature. https://doi.org/10.1007/978-981-15-1346-6_80
- Muz, B., de la Puente, P., Azab, F., & Azab, A. K. (2015). The role of hypoxia in cancer progression, angiogenesis, metastasis, and resistance to therapy. *Hypoxia*, 3, 83–92.
<https://doi.org/10.2147/HP.S93413>
- Myoung, H., Hong, S.-D., Kim, Y.-Y., Hong, S.-P., & Kim, M.-J. (2001). Evaluation of the anti-tumor and anti-angiogenic effect of paclitaxel and thalidomide on the xenotransplanted oral squamous cell carcinoma. *Cancer Letters*, 163(2), 191–200.
[https://doi.org/10.1016/S0304-3835\(00\)00701-1](https://doi.org/10.1016/S0304-3835(00)00701-1)
- Nawara, H. M., Afify, S. M., Hassan, G., Zahra, M. H., Seno, A., & Seno, M. (2021). Paclitaxel-Based Chemotherapy Targeting Cancer Stem Cells from Mono- to Combination Therapy. *Biomedicines*, 9(5), 500.
<https://doi.org/10.3390/biomedicines9050500>
- Nguyen, N. P., Moltz, C. C., Frank, C., Vos, P., Smith, H. J., Karlsson, U., Nguyen, L. M., Rose, S., Dutta, S., & Sallah, S. (2006). Evolution of chronic dysphagia following treatment for head and neck cancer. *Oral Oncology*, 42(4), 374–380.
<https://doi.org/10.1016/j.oraloncology.2005.09.003>
- Nishida, N., Yano, H., Nishida, T., Kamura, T., & Kojiro, M. (2006). Angiogenesis in Cancer. *Vascular Health and Risk Management*, 2(3), 213–219.

- Nonaka, M., Ikeda, H., Fujisawa, A., Uehara, M., & Inokuchi, T. (2006). Induction of apoptosis by paclitaxel in human oral carcinoma cells. *International Journal of Oral and Maxillofacial Surgery*, 35(7), 649–652. <https://doi.org/10.1016/j.ijom.2006.01.011>
- Nyaboke, H. O., Moraa, M., Omosa, L. K., Mbaveng, A. T., Vaderament-Alexe, N.-N., Masila, V., Okemwa, E., Efferth, T., & Kuete, V. (2018). *Cytotoxicity of Lupeol from the Stem Bark of Zanthoxylum gillettii against Multi-factorial Drug Resistant Cancer Cell Lines*. 6.
- Ojewole, J. a. O. (2005). Antiinflammatory, analgesic and hypoglycemic effects of *Mangifera indica* Linn. (Anacardiaceae) stem-bark aqueous extract. *Methods and Findings in Experimental and Clinical Pharmacology*, 27(8), 547–554. <https://doi.org/10.1358/mf.2005.27.8.928308>
- Okamoto, A., Higo, M., Shiiba, M., Nakashima, D., Koyama, T., Miyamoto, I., Kasama, H., Kasamatsu, A., Ogawara, K., Yokoe, H., Tanzawa, H., & Uzawa, K. (2015). Down-Regulation of Nucleolar and Spindle-Associated Protein 1 (NUSAP1) Expression Suppresses Tumor and Cell Proliferation and Enhances Anti-Tumor Effect of Paclitaxel in Oral Squamous Cell Carcinoma. *PLOS ONE*, 10(11), e0142252. <https://doi.org/10.1371/journal.pone.0142252>
- Pang, X., Fan, H., Tang, Y., Wang, S., Cao, M., Wang, H., Dai, L., Wang, K., Yu, X., Wu, J., Tang, Y.-J., & Liang, X. (2020). Myeloid derived suppressor cells contribute to the malignant progression of oral squamous cell carcinoma. *PLOS ONE*, 15(2), e0229089. <https://doi.org/10.1371/journal.pone.0229089>
- Panji, M., Behmard, V., Zare, Z., Malekpour, M., Nejadbiglari, H., Yavari, S., Nayerpour Dizaj, T., Safaeian, A., Bakhshi, A., Abazari, O., Abbasi, M., Khanicheragh, P., &

- Shabanzadeh, M. (2021). Synergistic effects of green tea extract and Paclitaxel in the induction of mitochondrial apoptosis in ovarian cancer cell lines. *Gene*, 787, 145638. <https://doi.org/10.1016/j.gene.2021.145638>
- Parness, J., & Horwitz, S. (1981). Taxol binds to polymerized tubulin in vitro. *The Journal of Cell Biology*, 91(2), 479–487.
- Patel, U., Pandey, M., Kannan, S., Samant, T. A., Gera, P., Mittal, N., Rane, S., Patil, A., Noronha, V., Joshi, A., Patil, V. M., Prabhash, K., & Mahimkar, M. B. (2020). Prognostic and predictive significance of nuclear HIF1 α expression in locally advanced HNSCC patients treated with chemoradiation with or without nimotuzumab. *British Journal of Cancer*, 123(12), 1757–1766. <https://doi.org/10.1038/s41416-020-01064-4>
- Patočka, J. (2003). Biologically active pentacyclic triterpenes and their current medicine signification. *Journal of Applied Biomedicine*, 1(1), 7–12. <https://doi.org/10.32725/jab.2003.002>
- Peereboom, D. M., Donehower, R. C., Eisenhauer, E. A., McGuire, W. P., Onetto, N., Hubbard, J. L., Piccart, M., Gianni, L., & Rowinsky, E. K. (1993). Successful re-treatment with taxol after major hypersensitivity reactions. *Journal of Clinical Oncology: Official Journal of the American Society of Clinical Oncology*, 11(5), 885–890. <https://doi.org/10.1200/JCO.1993.11.5.885>
- Peri, S., Biagioni, A., Versienti, G., Andreucci, E., Staderini, F., Barbato, G., Giovannelli, L., Coratti, F., Schiavone, N., Cianchi, F., Papucci, L., & Magnelli, L. (2021). Enhanced Vasculogenic Capacity Induced by 5-Fluorouracil Chemoresistance in a Gastric Cancer Cell Line. *International Journal of Molecular Sciences*, 22(14), 7698. <https://doi.org/10.3390/ijms22147698>

- Pezzuto, A., & Carico, E. (2018). Role of HIF-1 in Cancer Progression: Novel Insights. A Review. *Current Molecular Medicine*, 18(6), 343–351. <https://doi.org/10.2174/1566524018666181109121849>
- PIRES, F. R., RAMOS, A. B., de OLIVEIRA, J. B. C., TAVARES, A. S., da LUZ, P. S. R., & dos SANTOS, T. C. R. B. (2013). Oral squamous cell carcinoma: Clinicopathological features from 346 cases from a single Oral Pathology service during an 8-year period. *Journal of Applied Oral Science*, 21(5), 460–467. <https://doi.org/10.1590/1679-775720130317>
- Pitchai, D., Roy, A., & Ignatius, C. (2014). In vitro evaluation of anticancer potentials of Lupeol isolated from *Elephantopus scaber* L. on MCF-7 cell line. *Journal of Advanced Pharmaceutical Technology & Research*, 5(4), 179–184. <https://doi.org/10.4103/2231-4040.143037>
- Potente, M., Gerhardt, H., & Carmeliet, P. (2011). Basic and therapeutic aspects of angiogenesis. *Cell*, 146(6), 873–887. <https://doi.org/10.1016/j.cell.2011.08.039>
- Prasad, N., Sabarwal, A., Yadav, U. C. S., & Singh, R. P. (2018). Lupeol induces S-phase arrest and mitochondria-mediated apoptosis in cervical cancer cells. *Journal of Biosciences*, 43(2), 249–261. <https://doi.org/10.1007/s12038-018-9743-8>
- Pratt, R. L., & Kinch, M. S. (2003). Ligand binding up-regulates EphA2 messenger RNA through the mitogen-activated protein/extracellular signal-regulated kinase pathway. *Molecular Cancer Research: MCR*, 1(14), 1070–1076.
- Priyanka, K., Kosuru, R., Sharma, R. P., Sahu, P. L., & Singh, S. (2017). Assessment of pharmacokinetic parameters of Lupeol in *Ficus religiosa* L. extract after oral

- administration of suspension and solid lipid nanoparticles to Wistar rats. *Journal of Drug Delivery Science and Technology*, *41*, 58–67. <https://doi.org/10.1016/j.jddst.2017.06.019>
- Puneeta, N., Santosh, T., Mishra, I., Gaikwad, P., & Sahu, A. (2022). Evaluation of e-cadherin and vimentin expression for different grades of oral epithelial dysplasia and oral squamous cell carcinoma – An immunohistochemical study. *Journal of Oral and Maxillofacial Pathology*, *26*(2), 285. https://doi.org/10.4103/jomfp.JOMFP_166_20
- Qiao, L., Liang, N., Zhang, J., Xie, J., Liu, F., Xu, D., Yu, X., & Tian, Y. (2015). Advanced research on vasculogenic mimicry in cancer. *Journal of Cellular and Molecular Medicine*, *19*(2), 315–326. <https://doi.org/10.1111/jcmm.12496>
- Rauth, S., Ray, S., Bhattacharyya, S., Mehrotra, D. G., Alam, N., Mondal, G., Nath, P., Roy, A., Biswas, J., & Murmu, N. (2016). Lupeol evokes anticancer effects in oral squamous cell carcinoma by inhibiting oncogenic EGFR pathway. *Molecular and Cellular Biochemistry*, *417*(1), 97–110. <https://doi.org/10.1007/s11010-016-2717-y>
- Ren, H.-Y., Shen, J.-X., Mao, X.-M., Zhang, X.-Y., Zhou, P., Li, S.-Y., Zheng, Z.-W., Shen, D.-Y., & Meng, J.-R. (2019). Correlation Between Tumor Vasculogenic Mimicry and Poor Prognosis of Human Digestive Cancer Patients: A Systematic Review and Meta-Analysis. *Pathology Oncology Research: POR*, *25*(3), 849–858. <https://doi.org/10.1007/s12253-018-0496-3>
- Ribatti, D., Vacca, A., & Dammacco, F. (1999). The Role of the Vascular Phase in Solid Tumor Growth: A Historical Review. *Neoplasia (New York, N.Y.)*, *1*(4), 293–302.
- Rivera, C., & Venegas, B. (2014). Histological and molecular aspects of oral squamous cell carcinoma (Review). *Oncology Letters*, *8*(1), 7–11. <https://doi.org/10.3892/ol.2014.2103>

- Rousselle, P., & Scoazec, J. Y. (2020). Laminin 332 in cancer: When the extracellular matrix turns signals from cell anchorage to cell movement. *Seminars in Cancer Biology*, 62, 149–165. <https://doi.org/10.1016/j.semcancer.2019.09.026>
- Rowinsky, E. K., Cazenave, L. A., & Donehower, R. C. (1990). Taxol: A novel investigational antimicrotubule agent. *Journal of the National Cancer Institute*, 82(15), 1247–1259. <https://doi.org/10.1093/jnci/82.15.1247>
- Rowinsky, E. K., Chaudhry, V., Cornblath, D. R., & Donehower, R. C. (1993). Neurotoxicity of Taxol. *Journal of the National Cancer Institute. Monographs*, 15, 107–115.
- Rowinsky, E. K., Eisenhauer, E. A., Chaudhry, V., Arbuck, S. G., & Donehower, R. C. (1993). Clinical toxicities encountered with paclitaxel (Taxol). *Seminars in Oncology*, 20(4 Suppl 3), 1–15.
- Rowinsky, E. K., McGuire, W. P., Guarnieri, T., Fisherman, J. S., Christian, M. C., & Donehower, R. C. (1991). Cardiac disturbances during the administration of taxol. *Journal of Clinical Oncology: Official Journal of the American Society of Clinical Oncology*, 9(9), 1704–1712. <https://doi.org/10.1200/JCO.1991.9.9.1704>
- Ruf, W., Seftor, E. A., Petrovan, R. J., Weiss, R. M., Gruman, L. M., Margaryan, N. V., Seftor, R. E. B., Miyagi, Y., & Hendrix, M. J. C. (2003). Differential role of tissue factor pathway inhibitors 1 and 2 in melanoma vasculogenic mimicry. *Cancer Research*, 63(17), 5381–5389.
- Sagheer, S. H., Whitaker-Menezes, D., Han, J. Y. S., Curry, J. M., Martinez-Outschoorn, U., & Philp, N. J. (2021). Chapter 6 - 4NQO induced carcinogenesis: A mouse model for oral squamous cell carcinoma. In L. Galluzzi & A. Buqué (Eds.), *Methods in Cell Biology* (Vol. 163, pp. 93–111). Academic Press. <https://doi.org/10.1016/bs.mcb.2021.01.001>

- Saha, D., Mitra, D., Alam, N., Sen, S., Mitra Mustafi, S., Mandal, S., Majumder, B., & Murmu, N. (2022). Orchestrated expression of vasculogenic mimicry and laminin-5 γ 2 is an independent prognostic marker in oral squamous cell carcinoma. *International Journal of Experimental Pathology*, 103(2), 54–64. <https://doi.org/10.1111/iep.12430>
- Saha, S., Profumo, E., Togna, A. R., Riganò, R., Saso, L., & Buttari, B. (2020). Lupeol Counteracts the Proinflammatory Signalling Triggered in Macrophages by 7-Keto-Cholesterol: New Perspectives in the Therapy of Atherosclerosis. *Oxidative Medicine and Cellular Longevity*, 2020, e1232816. <https://doi.org/10.1155/2020/1232816>
- Saito, S., Lin, Y.-C., Tsai, M.-H., Lin, C.-S., Murayama, Y., Sato, R., & Yokoyama, K. K. (2015). Emerging roles of hypoxia-inducible factors and reactive oxygen species in cancer and pluripotent stem cells. *The Kaohsiung Journal of Medical Sciences*, 31(6), 279–286. <https://doi.org/10.1016/j.kjms.2015.03.002>
- Saleem, M. (2009). Lupeol, A Novel Anti-inflammatory and Anti-cancer Dietary Triterpene. *Cancer Letters*, 285(2), 109–115. <https://doi.org/10.1016/j.canlet.2009.04.033>
- Saleem, M., Kaur, S., Kweon, M.-H., Adhami, V. M., Afaq, F., & Mukhtar, H. (2005). Lupeol, a fruit and vegetable based triterpene, induces apoptotic death of human pancreatic adenocarcinoma cells via inhibition of Ras signaling pathway. *Carcinogenesis*, 26(11), 1956–1964. <https://doi.org/10.1093/carcin/bgi157>
- Saleem, M., Maddodi, N., Abu Zaid, M., Khan, N., bin Hafeez, B., Asim, M., Suh, Y., Yun, J.-M., Setaluri, V., & Mukhtar, H. (2008). Lupeol Inhibits Growth of Highly Aggressive Human Metastatic Melanoma Cells In vitro and In vivo by Inducing Apoptosis. *Clinical Cancer Research*, 14(7), 2119–2127. <https://doi.org/10.1158/1078-0432.CCR-07-4413>

- Saleem, M., Murtaza, I., Tarapore, R. S., Suh, Y., Adhami, V. M., Johnson, J. J., Siddiqui, I. A., Khan, N., Asim, M., Hafeez, B. B., Shekhani, M. T., Li, B., & Mukhtar, H. (2009). Lupeol inhibits proliferation of human prostate cancer cells by targeting β -catenin signaling. *Carcinogenesis*, *30*(5), 808–817. <https://doi.org/10.1093/carcin/bgp044>
- Salem, A., & Salo, T. (2021). Vasculogenic Mimicry in Head and Neck Squamous Cell Carcinoma—Time to Take Notice. *Frontiers in Oral Health*, *2*. <https://www.frontiersin.org/article/10.3389/froh.2021.666895>
- Salnikov, A. V., Liu, L., Platen, M., Gladkich, J., Salnikova, O., Ryschich, E., Mattern, J., Moldenhauer, G., Werner, J., Schemmer, P., Büchler, M. W., & Herr, I. (2012). Hypoxia induces EMT in low and highly aggressive pancreatic tumor cells but only cells with cancer stem cell characteristics acquire pronounced migratory potential. *PloS One*, *7*(9), e46391. <https://doi.org/10.1371/journal.pone.0046391>
- Sawatani, Y., Komiyama, Y., Nakashiro, K., Uchida, D., Fukumoto, C., Shimura, M., Hasegawa, T., Kamimura, R., Hitomi-Koide, M., Hyodo, T., & Kawamata, H. (2020). Paclitaxel Potentiates the Anticancer Effect of Cetuximab by Enhancing Antibody-Dependent Cellular Cytotoxicity on Oral Squamous Cell Carcinoma Cells In Vitro. *International Journal of Molecular Sciences*, *21*(17), Art. 17. <https://doi.org/10.3390/ijms21176292>
- Scatozza, F., D'amore, A., Fontanella, R. A., Cesaris, P. D., Marampon, F., Padula, F., Ziparo, E., Riccioli, A., & Filippini, A. (2020). Toll-like Receptor-3 Activation Enhances Malignant Traits in Human Breast Cancer Cells Through Hypoxia-inducible Factor-1 α . *Anticancer Research*, *40*(10), 5379–5391. <https://doi.org/10.21873/anticancer.14546>

- Seftor, R. E., Seftor, E. A., Koshikawa, N., Meltzer, P. S., Gardner, L. M., Bilban, M., Stetler-Stevenson, W. G., Quaranta, V., & Hendrix, M. J. (2001). Cooperative interactions of laminin 5 gamma2 chain, matrix metalloproteinase-2, and membrane type-1-matrix/metalloproteinase are required for mimicry of embryonic vasculogenesis by aggressive melanoma. *Cancer Research*, *61*(17), 6322–6327.
- Shao, B., Zhao, X., Liu, T., Zhang, Y., Sun, R., Dong, X., Liu, F., Zhao, N., Zhang, D., Wu, L., Wang, Y., Wang, M., Meng, J., Lin, X., & Sun, B. (2019). LOXL2 promotes vasculogenic mimicry and tumour aggressiveness in hepatocellular carcinoma. *Journal of Cellular and Molecular Medicine*, *23*(2), 1363–1374. <https://doi.org/10.1111/jcmm.14039>
- Shao, Z., Zhang, W.-F., Chen, X.-M., & Shang, Z.-J. (2008). Expression of EphA2 and VEGF in squamous cell carcinoma of the tongue: Correlation with the angiogenesis and clinical outcome. *Oral Oncology*, *44*(12), 1110–1117. <https://doi.org/10.1016/j.oraloncology.2008.01.018>
- Sharma, N., Seftor, R. E. B., Seftor, E. A., Gruman, L. M., Heidger, P. M., Cohen, M. B., Lubaroff, D. M., & Hendrix, M. J. C. (2002). Prostatic tumor cell plasticity involves cooperative interactions of distinct phenotypic subpopulations: Role in vasculogenic mimicry. *The Prostate*, *50*(3), 189–201. <https://doi.org/10.1002/pros.10048>
- Shu, L., Cheung, K.-L., Khor, T. O., Chen, C., & Kong, A.-N. (2010). Phytochemicals: Cancer chemoprevention and suppression of tumor onset and metastasis. *Cancer Metastasis Reviews*, *29*(3), 483–502. <https://doi.org/10.1007/s10555-010-9239-y>
- Sinha, K., Chowdhury, S., Banerjee, S., Mandal, B., Mandal, M., Majhi, S., Brahmachari, G., Ghosh, J., & Sil, P. C. (2019). Lupeol alters viability of SK-RC-45 (Renal cell carcinoma

- cell line) by modulating its mitochondrial dynamics. *Heliyon*, 5(8), e02107.
<https://doi.org/10.1016/j.heliyon.2019.e02107>
- Sivridis, E., Giatromanolaki, A., Gatter, K. C., Harris, A. L., Koukourakis, M. I., & Tumor and Angiogenesis Research Group. (2002). Association of hypoxia-inducible factors 1alpha and 2alpha with activated angiogenic pathways and prognosis in patients with endometrial carcinoma. *Cancer*, 95(5), 1055–1063. <https://doi.org/10.1002/cncr.10774>
- Song, T., Shi, R., Vijayalakshmi, A., & Lei, B. (2022). Protective effect of Lupeol on arthritis induced by type II collagen via the suppression of P13K/AKT signaling pathway in Sprague dawley rats. *Environmental Toxicology*, 37(7), 1814–1822.
<https://doi.org/10.1002/tox.23529>
- Sun, B., Qie, S., Zhang, S., Sun, T., Zhao, X., Gao, S., Ni, C., Wang, X., Liu, Y., & Zhang, L. (2008). Role and mechanism of vasculogenic mimicry in gastrointestinal stromal tumors. *Human Pathology*, 39(3), 444–451.
<https://doi.org/10.1016/j.humpath.2007.07.018>
- Sun, B., Zhang, D., Zhang, S., Zhang, W., Guo, H., & Zhao, X. (2007). Hypoxia influences vasculogenic mimicry channel formation and tumor invasion-related protein expression in melanoma. *Cancer Letters*, 249(2), 188–197.
<https://doi.org/10.1016/j.canlet.2006.08.016>
- Sun, B., Zhang, S., Zhang, D., Du, J., Guo, H., Zhao, X., Zhang, W., & Hao, X. (2006). Vasculogenic mimicry is associated with high tumor grade, invasion and metastasis, and short survival in patients with hepatocellular carcinoma. *Oncology Reports*, 16(4), 693–698.

- Sun, B., Zhang, S., Zhang, D., Li, Y., Zhao, X., Luo, Y., & Guo, Y. (2008). Identification of metastasis-related proteins and their clinical relevance to triple-negative human breast cancer. *Clinical Cancer Research: An Official Journal of the American Association for Cancer Research*, *14*(21), 7050–7059. <https://doi.org/10.1158/1078-0432.CCR-08-0520>
- Sun, B., Zhang, S., Zhao, X., Zhang, W., & Hao, X. (2004). Vasculogenic mimicry is associated with poor survival in patients with mesothelial sarcomas and alveolar rhabdomyosarcomas. *International Journal of Oncology*, *25*(6), 1609–1614.
- Sun, H., Yao, N., Cheng, S., Li, L., Liu, S., Yang, Z., Shang, G., Zhang, D., & Yao, Z. (2019). Cancer stem-like cells directly participate in vasculogenic mimicry channels in triple-negative breast cancer. *Cancer Biology & Medicine*, *16*(2), 299–311. <https://doi.org/10.20892/j.issn.2095-3941.2018.0209>
- Sun, H., Zhang, D., Yao, Z., Lin, X., Liu, J., Gu, Q., Dong, X., Liu, F., Wang, Y., Yao, N., Cheng, S., Li, L., & Sun, S. (2017). Anti-angiogenic treatment promotes triple-negative breast cancer invasion via vasculogenic mimicry. *Cancer Biology & Therapy*. <https://doi.org/10.1080/15384047.2017.1294288>
- Sun, L., Chin, R.-I., Gastman, B., Thorstad, W., Yom, S. S., Reddy, C. A., Nussenbaum, B., Wang, S. J., Knackstedt, T., Vidimos, A. T., Koyfman, S. A., & Manyam, B. V. (2019). Association of Disease Recurrence With Survival Outcomes in Patients With Cutaneous Squamous Cell Carcinoma of the Head and Neck Treated With Multimodality Therapy. *JAMA Dermatology*, *155*(4), 442–447. <https://doi.org/10.1001/jamadermatol.2018.5453>
- Sun, T., Zhao, N., Zhao, X.-L., Gu, Q., Zhang, S.-W., Che, N., Wang, X.-H., Du, J., Liu, Y.-X., & Sun, B.-C. (2010). Expression and functional significance of Twist1 in

- hepatocellular carcinoma: Its role in vasculogenic mimicry. *Hepatology (Baltimore, Md.)*, 51(2), 545–556. <https://doi.org/10.1002/hep.23311>
- Sun, Z., Sun, X., Chen, Z., Du, J., & Wu, Y. (2022). Head and Neck Squamous Cell Carcinoma: Risk Factors, Molecular Alterations, Immunology and Peptide Vaccines. *International Journal of Peptide Research and Therapeutics*, 28(1), 19. <https://doi.org/10.1007/s10989-021-10334-5>
- Sung, H., Ferlay, J., Siegel, R. L., Laversanne, M., Soerjomataram, I., Jemal, A., & Bray, F. (2021). Global Cancer Statistics 2020: GLOBOCAN Estimates of Incidence and Mortality Worldwide for 36 Cancers in 185 Countries. *CA: A Cancer Journal for Clinicians*, 71(3), 209–249. <https://doi.org/10.3322/caac.21660>
- Tandon, P., Dadhich, A., Saluja, H., Bawane, S., & Sachdeva, S. (2017). The prevalence of squamous cell carcinoma in different sites of oral cavity at our Rural Health Care Centre in Loni, Maharashtra—A retrospective 10-year study. *Contemporary Oncology (Poznan, Poland)*, 21(2), 178–183. <https://doi.org/10.5114/wo.2017.68628>
- Tang, N.-N., Zhu, H., Zhang, H.-J., Zhang, W.-F., Jin, H.-L., Wang, L., Wang, P., He, G.-J., Hao, B., & Shi, R.-H. (2014). HIF-1 α induces VE-cadherin expression and modulates vasculogenic mimicry in esophageal carcinoma cells. *World Journal of Gastroenterology : WJG*, 20(47), 17894–17904. <https://doi.org/10.3748/wjg.v20.i47.17894>
- Teleanu, R. I., Chircov, C., Grumezescu, A. M., & Teleanu, D. M. (2019). Tumor Angiogenesis and Anti-Angiogenic Strategies for Cancer Treatment. *Journal of Clinical Medicine*, 9(1), 84. <https://doi.org/10.3390/jcm9010084>

- Tenore, G., Nuvoli, A., Mohsen, A., Cassoni, A., Battisti, A., Terenzi, V., Della Monaca, M., Raponi, I., Brauner, E., De Felice, F., Musio, D., Di Gioia, C. R. T., Messineo, D., Mezi, S., Di Carlo, S., Botticelli, A., Valentini, V., Marchetti, P., Tombolini, V., ... Romeo, U. (2020). Tobacco, Alcohol and Family History of Cancer as Risk Factors of Oral Squamous Cell Carcinoma: Case-Control Retrospective Study. *Applied Sciences*, *10*(11), Art. 11. <https://doi.org/10.3390/app10113896>
- Thavarool, S. B., Muttath, G., Nayanar, S., Duraisamy, K., Bhat, P., Shringarpure, K., Nayak, P., Tripathy, J. P., Thaddeus, A., Philip, S., & B, S. (2019). Improved survival among oral cancer patients: Findings from a retrospective study at a tertiary care cancer centre in rural Kerala, India. *World Journal of Surgical Oncology*, *17*(1), 15. <https://doi.org/10.1186/s12957-018-1550-z>
- Tiwari, A., Gandhi, S., & Joshi, M. (2019). Effect of Lupeol in Diabetic Nephropathy and Its Anti-oxidant Mechanism. *International Journal of Advanced Science and Technology*, *28*, 1404–1413.
- Usman, S., Jamal, A., Teh, M.-T., & Waseem, A. (2021). Major Molecular Signaling Pathways in Oral Cancer Associated With Therapeutic Resistance. *Frontiers in Oral Health*, *1*. <https://www.frontiersin.org/articles/10.3389/froh.2020.603160>
- Valdivia, A., Mingo, G., Aldana, V., Pinto, M. P., Ramirez, M., Retamal, C., Gonzalez, A., Nualart, F., Corvalan, A. H., & Owen, G. I. (2019). Fact or Fiction, It Is Time for a Verdict on Vasculogenic Mimicry? *Frontiers in Oncology*, *9*, 680. <https://doi.org/10.3389/fonc.2019.00680>
- Varghese, F., Bukhari, A. B., Malhotra, R., & De, A. (2014). IHC Profiler: An open source plugin for the quantitative evaluation and automated scoring of immunohistochemistry

- images of human tissue samples. *PloS One*, 9(5), e96801.
<https://doi.org/10.1371/journal.pone.0096801>
- Vartanian, A. A., Burova, O. S., Stepanova, E. V., Baryshnikov, A. Y., & Lichinitser, M. R. (2007). Melanoma vasculogenic mimicry is strongly related to reactive oxygen species level. *Melanoma Research*, 17(6), 370–379.
<https://doi.org/10.1097/CMR.0b013e3282f1d2ec>
- Vasudev, N. S., & Reynolds, A. R. (2014). Anti-angiogenic therapy for cancer: Current progress, unresolved questions and future directions. *Angiogenesis*, 17(3), 471–494.
<https://doi.org/10.1007/s10456-014-9420-y>
- Wall, M. E. (1998). Camptothecin and taxol: Discovery to clinic. *Medicinal Research Reviews*, 18(5), 299–314. [https://doi.org/10.1002/\(sici\)1098-1128\(199809\)18:5<299::aid-med2>3.0.co;2-o](https://doi.org/10.1002/(sici)1098-1128(199809)18:5<299::aid-med2>3.0.co;2-o)
- Wall, M. E., & Wani, M. C. (1995). Camptothecin and Taxol: Discovery to Clinic—Thirteenth Bruce F. Cain Memorial Award Lecture1. *Cancer Research*, 55(4), 753–760.
- Wall, M. E., & Wani, M. C. (1996). Camptothecin and taxol: From discovery to clinic. *Journal of Ethnopharmacology*, 51(1), 239–254. [https://doi.org/10.1016/0378-8741\(95\)01367-9](https://doi.org/10.1016/0378-8741(95)01367-9)
- Walsh, J. C., Lebedev, A., Aten, E., Madsen, K., Marciano, L., & Kolb, H. C. (2014). The Clinical Importance of Assessing Tumor Hypoxia: Relationship of Tumor Hypoxia to Prognosis and Therapeutic Opportunities. *Antioxidants & Redox Signaling*, 21(10), 1516–1554. <https://doi.org/10.1089/ars.2013.5378>
- Wan, F., Zhang, H., Hu, J., Chen, L., Geng, S., Kong, L., & Lu, J. J. (2022). Mesenchymal Stem Cells Inhibits Migration and Vasculogenic Mimicry in Nasopharyngeal Carcinoma

- Via Exosomal MiR-125a. *Frontiers in Oncology*, 12, 781979.
<https://doi.org/10.3389/fonc.2022.781979>
- Wang, H., Huang, B., Li, B. M., Cao, K. Y., Mo, C. Q., Jiang, S. J., Pan, J. C., Wang, Z. R., Lin, H. Y., Wang, D. H., & Qiu, S. P. (2018). ZEB1-mediated vasculogenic mimicry formation associates with epithelial-mesenchymal transition and cancer stem cell phenotypes in prostate cancer. *Journal of Cellular and Molecular Medicine*, 22(8), 3768–3781. <https://doi.org/10.1111/jcmm.13637>
- Wang, H., Lin, H., Pan, J., Mo, C., Zhang, F., Huang, B., Wang, Z., Chen, X., Zhuang, J., Wang, D., & Qiu, S. (2016). Vasculogenic Mimicry in Prostate Cancer: The Roles of EphA2 and PI3K. *Journal of Cancer*, 7(9), 1114–1124. <https://doi.org/10.7150/jca.14120>
- Wang, H., Lin, Y., Zeng, D., Lin, W., Hong, C., Lin, W., & Chen, J. (2010). [Inhibitory effect of ginsenoside Rg3 on the tube-like structure formation in human nasopharyngeal carcinoma HNE-1 cell line in vitro]. *Zhonghua Zhong Liu Za Zhi [Chinese Journal of Oncology]*, 32(10), 739–742.
- Wang, H.-F., Wang, S.-S., Zheng, M., Dai, L.-L., Wang, K., Gao, X.-L., Cao, M.-X., Yu, X.-H., Pang, X., Zhang, M., Wu, J.-B., Wu, J.-S., Yang, X., Tang, Y.-J., Chen, Y., Tang, Y.-L., & Liang, X.-H. (2019). Hypoxia promotes vasculogenic mimicry formation by vascular endothelial growth factor A mediating epithelial-mesenchymal transition in salivary adenoid cystic carcinoma. *Cell Proliferation*, 52(3), e12600. <https://doi.org/10.1111/cpr.12600>
- Wang, M., Zhao, X., Zhu, D., Liu, T., Liang, X., Liu, F., Zhang, Y., Dong, X., & Sun, B. (2017). HIF-1 α promoted vasculogenic mimicry formation in hepatocellular carcinoma through LOXL2 up-regulation in hypoxic tumor microenvironment. *Journal of*

- Experimental & Clinical Cancer Research: CR*, 36(1), 60.
<https://doi.org/10.1186/s13046-017-0533-1>
- Wang, S., Gao, X., Liu, X., Gao, S., Fan, Y., Jiang, Y., Ma, X., Jiang, J., Feng, H., Chen, Q., Tang, Y., Tang, Y., & Liang, X. (2016). CD133+ cancer stem-like cells promote migration and invasion of salivary adenoid cystic carcinoma by inducing vasculogenic mimicry formation. *Oncotarget*, 7(20), 29051–29062.
<https://doi.org/10.18632/oncotarget.8665>
- Wang, W., Lin, P., Han, C., Cai, W., Zhao, X., & Sun, B. (2010). Vasculogenic mimicry contributes to lymph node metastasis of laryngeal squamous cell carcinoma. *Journal of Experimental & Clinical Cancer Research: CR*, 29, 60. <https://doi.org/10.1186/1756-9966-29-60>
- Wang, W., Lin, P., Sun, B., Zhang, S., Cai, W., Han, C., Li, L., Lu, H., & Zhao, X. (2014). Epithelial-mesenchymal transition regulated by EphA2 contributes to vasculogenic mimicry formation of head and neck squamous cell carcinoma. *BioMed Research International*, 2014, 803914. <https://doi.org/10.1155/2014/803914>
- Wang, Y., Sun, H., Zhang, D., Fan, D., Zhang, Y., Dong, X., Liu, S., Yang, Z., Ni, C., Li, Y., Liu, F., & Zhao, X. (2018). TP53INP1 inhibits hypoxia-induced vasculogenic mimicry formation via the ROS/snail signalling axis in breast cancer. *Journal of Cellular and Molecular Medicine*, 22(7), 3475–3488. <https://doi.org/10.1111/jcmm.13625>
- Wang, Y., Wang, X., Zhang, Y., Yu, L., Zhu, B., Wu, S., & Wang, D. (2018). Vasculogenic mimicry and expression of ALDH1, Beclin1, and p16 correlate with metastasis and prognosis in oral squamous cell carcinoma. *International Journal of Clinical and Experimental Pathology*, 11(3), 1599–1609.

- Wang, Y., Yang, R., Wang, X., Ci, H., Zhou, L., Zhu, B., Wu, S., & Wang, D. (2018). Evaluation of the correlation of vasculogenic mimicry, Notch4, DLL4, and KAI1/CD82 in the prediction of metastasis and prognosis in non-small cell lung cancer. *Medicine*, 97(52), e13817. <https://doi.org/10.1097/MD.00000000000013817>
- Wang, Z., Zhang, B., Jiang, L., Zeng, X., Chen, Y., Feng, X., Guo, Y., & Chen, Q. (2009). RACK1, an excellent predictor for poor clinical outcome in oral squamous carcinoma, similar to Ki67. *European Journal of Cancer (Oxford, England: 1990)*, 45(3), 490–496. <https://doi.org/10.1016/j.ejca.2008.11.012>
- Wani, M. C., Taylor, H. L., Wall, M. E., Coggon, P., & McPhail, A. T. (1971). Plant antitumor agents. VI. Isolation and structure of taxol, a novel antileukemic and antitumor agent from *Taxus brevifolia*. *Journal of the American Chemical Society*, 93(9), 2325–2327. <https://doi.org/10.1021/ja00738a045>
- Warnakulasuriya, S., Kujan, O., Aguirre-Urizar, J. M., Bagan, J. V., González-Moles, M. Á., Kerr, A. R., Lodi, G., Mello, F. W., Monteiro, L., Ogden, G. R., Sloan, P., & Johnson, N. W. (2021). Oral potentially malignant disorders: A consensus report from an international seminar on nomenclature and classification, convened by the WHO Collaborating Centre for Oral Cancer. *Oral Diseases*, 27(8), 1862–1880. <https://doi.org/10.1111/odi.13704>
- Weaver, B. A. (2014). How Taxol/paclitaxel kills cancer cells. *Molecular Biology of the Cell*, 25(18), 2677. <https://doi.org/10.1091/mbc.E14-04-0916>
- Wei, H., Zhang, F., Wang, J., Zhao, M., Hou, T., & Li, L. (2020). Dehydroeffusol inhibits hypoxia-induced epithelial–mesenchymal transition in non-small cell lung cancer cells through the inactivation of Wnt/β-catenin pathway. *Bioscience Reports*, 40(5), BSR20194284. <https://doi.org/10.1042/BSR20194284>

- Wei, X., Chen, Y., Jiang, X., Peng, M., Liu, Y., Mo, Y., Ren, D., Hua, Y., Yu, B., Zhou, Y., Liao, Q., Wang, H., Xiang, B., Zhou, M., Li, X., Li, G., Li, Y., Xiong, W., & Zeng, Z. (2021). Mechanisms of vasculogenic mimicry in hypoxic tumor microenvironments. *Molecular Cancer*, *20*, 7. <https://doi.org/10.1186/s12943-020-01288-1>
- Weidner, N., Semple, J. P., Welch, W. R., & Folkman, J. (1991). Tumor angiogenesis and metastasis—Correlation in invasive breast carcinoma. *The New England Journal of Medicine*, *324*(1), 1–8. <https://doi.org/10.1056/NEJM199101033240101>
- Winkler, J., Abisoye-Ogunniyan, A., Metcalf, K. J., & Werb, Z. (2020). Concepts of extracellular matrix remodelling in tumour progression and metastasis. *Nature Communications*, *11*(1), 1–19.
- Wu, D.-H., Wang, T.-T., Ruan, D.-Y., Li, X., Chen, Z.-H., Wen, J.-Y., Lin, Q., Ma, X.-K., Wu, X.-Y., & Jia, C.-C. (2018). Combination of ULK1 and LC3B improve prognosis assessment of hepatocellular carcinoma. *Biomedicine & Pharmacotherapy = Biomedecine & Pharmacotherapie*, *97*, 195–202. <https://doi.org/10.1016/j.biopha.2017.10.025>
- Wu, X.-T., Liu, J.-Q., Lu, X.-T., Chen, F.-X., Zhou, Z.-H., Wang, T., Zhu, S.-P., & Fei, S.-J. (2013). The enhanced effect of Lupeol on the destruction of gastric cancer cells by NK cells. *International Immunopharmacology*, *16*(2), 332–340. <https://doi.org/10.1016/j.intimp.2013.04.017>
- Wu, Z., Song, W., Cheng, Z., Yang, D., & Yu, L. (2017). Expression of LGR5 in oral squamous cell carcinoma and its correlation to vasculogenic mimicry. *International Journal of Clinical and Experimental Pathology*, *10*(11), 11267–11275.

- Xiang, T., Lin, Y.-X., Ma, W., Zhang, H.-J., Chen, K.-M., He, G.-P., Zhang, X., Xu, M., Feng, Q.-S., Chen, M.-Y., Zeng, M.-S., Zeng, Y.-X., & Feng, L. (2018). Vasculogenic mimicry formation in EBV-associated epithelial malignancies. *Nature Communications*, 9(1), Art. 1. <https://doi.org/10.1038/s41467-018-07308-5>
- Xing, P., Dong, H., Liu, Q., Zhao, T., Yao, F., Xu, Y., Chen, B., Zheng, X., Wu, Y., Jin, F., & Li, J. (2018). ALDH1 Expression and Vasculogenic Mimicry Are Positively Associated with Poor Prognosis in Patients with Breast Cancer. *Cellular Physiology and Biochemistry: International Journal of Experimental Cellular Physiology, Biochemistry, and Pharmacology*, 49(3), 961–970. <https://doi.org/10.1159/000493227>
- Xu, S., Bai, J., Zhuan, Z., Li, B., Zhang, Z., Wu, X., Luo, X., & Yang, L. (2018). EBV-LMP1 is involved in vasculogenic mimicry formation via VEGFA/VEGFR1 signaling in nasopharyngeal carcinoma. *Oncology Reports*, 40(1), 377–384. <https://doi.org/10.3892/or.2018.6414>
- Xu, Y., Xin, Y., Diao, Y., Lu, C., Fu, J., Luo, L., & Yin, Z. (2011). Synergistic Effects of Apigenin and Paclitaxel on Apoptosis of Cancer Cells. *PLoS ONE*, 6(12), e29169. <https://doi.org/10.1371/journal.pone.0029169>
- Yang, J. P., Liao, Y. D., Mai, D. M., Xie, P., Qiang, Y. Y., Zheng, L. S., Wang, M. Y., Mei, Y., Meng, D. F., Xu, L., Cao, L., Yang, Q., Yang, X. X., Wang, W. B., Peng, L. X., Huang, B. J., & Qian, C. N. (2016). Tumor vasculogenic mimicry predicts poor prognosis in cancer patients: A meta-analysis. *Angiogenesis*, 19(2), 191–200. <https://doi.org/10.1007/s10456-016-9500-2>
- Yeo, C., Han, D.-S., Lee, H.-J., & Lee, E.-O. (2020). Epigallocatechin-3-Gallate Suppresses Vasculogenic Mimicry through Inhibiting the Twist/VE-Cadherin/AKT Pathway in

- Human Prostate Cancer PC-3 Cells. *International Journal of Molecular Sciences*, 21(2), 439. <https://doi.org/10.3390/ijms21020439>
- You, B., Sun, Y., Luo, J., Wang, K., Liu, Q., Fang, R., Liu, B., Chou, F., Wang, R., Meng, J., Huang, C.-P., Yeh, S., Chang, C., & Xu, W. (2021). Androgen receptor promotes renal cell carcinoma (RCC) vasculogenic mimicry (VM) via altering TWIST1 nonsense-mediated decay through lncRNA-TANAR. *Oncogene*, 40(9), 1674–1689. <https://doi.org/10.1038/s41388-020-01616-1>
- Yu, L., Zhu, B., Wu, S., Zhou, L., Song, W., Gong, X., & Wang, D. (2017). Evaluation of the correlation of vasculogenic mimicry, ALDH1, KiSS-1, and MACC1 in the prediction of metastasis and prognosis in ovarian carcinoma. *Diagnostic Pathology*, 12(1), 23. <https://doi.org/10.1186/s13000-017-0612-9>
- Yu, P., Zhu, X., Zhu, J.-L., Han, Y.-B., Zhang, H., Zhou, X., Yang, L., Xia, Y.-Z., Zhang, C., & Kong, L.-Y. (2021). The Chk2-PKM2 axis promotes metabolic control of vasculogenic mimicry formation in p53-mutated triple-negative breast cancer. *Oncogene*, 40(34), 5262–5274. <https://doi.org/10.1038/s41388-021-01933-z>
- Yue, W.-Y., & Chen, Z.-P. (2005). Does vasculogenic mimicry exist in astrocytoma? *The Journal of Histochemistry and Cytochemistry: Official Journal of the Histochemistry Society*, 53(8), 997–1002. <https://doi.org/10.1369/jhc.4A6521.2005>
- Yue, Y., Lou, Y., Liu, X., & Peng, X. (2021). Vasculogenic mimicry in head and neck tumors: A narrative review. *Translational Cancer Research*, 10(6), 3044–3052. <https://doi.org/10.21037/tcr-21-34>
- Zang, M., Hou, J., Huang, Y., Wang, J., Ding, X., Zhang, B., Wang, Y., Xuan, Y., & Zhou, Y. (2021). Crocetin suppresses angiogenesis and metastasis through inhibiting sonic

- hedgehog signaling pathway in gastric cancer. *Biochemical and Biophysical Research Communications*, 576, 86–92. <https://doi.org/10.1016/j.bbrc.2021.08.092>
- Zang, M., Hu, L., Zhang, B., Zhu, Z., Li, J., Zhu, Z., Yan, M., & Liu, B. (2017). Luteolin suppresses angiogenesis and vasculogenic mimicry formation through inhibiting Notch1-VEGF signaling in gastric cancer. *Biochemical and Biophysical Research Communications*, 490(3), 913–919. <https://doi.org/10.1016/j.bbrc.2017.06.140>
- Zantek, N. D., Azimi, M., Fedor-Chaiken, M., Wang, B., Brackenbury, R., & Kinch, M. S. (1999). E-cadherin regulates the function of the EphA2 receptor tyrosine kinase. *Cell Growth & Differentiation: The Molecular Biology Journal of the American Association for Cancer Research*, 10(9), 629–638.
- Zelinski, D. P., Zantek, N. D., Stewart, J. C., Irizarry, A. R., & Kinch, M. S. (2001). EphA2 overexpression causes tumorigenesis of mammary epithelial cells. *Cancer Research*, 61(5), 2301–2306.
- Zhang, J., Liang, H., Yao, H., Qiu, Z., Chen, X., Hu, X., Hu, J., & Zheng, G. (2019). The preparation, characterization of Lupeol PEGylated liposome and its functional evaluation in vitro as well as pharmacokinetics in rats. *Drug Development and Industrial Pharmacy*. <https://doi.org/10.1080/03639045.2019.1569038>
- Zhang, J.-G., Zhou, H.-M., Zhang, X., Mu, W., Hu, J.-N., Liu, G.-L., & Li, Q. (2020). Hypoxic induction of vasculogenic mimicry in hepatocellular carcinoma: Role of HIF-1 α , RhoA/ROCK and Rac1/PAK signaling. *BMC Cancer*, 20(1), 32. <https://doi.org/10.1186/s12885-019-6501-8>
- Zhang, L., Zhang, Y., Zhang, L., Yang, X., & Lv, Z. (2009). Lupeol, a Dietary Triterpene, Inhibited Growth, and Induced Apoptosis Through Down-Regulation of DR3 in

- SMMC7721 Cells. *Cancer Investigation*, 27(2), 163–170.
<https://doi.org/10.1080/07357900802210745>
- Zhang, X., Gao, Z., Chen, K., Zhuo, Q., Chen, M., Wang, J., Lai, X., & Wang, L. (2022). Lupeol inhibits the proliferation and migration of MDA-MB-231 breast cancer cells via a novel crosstalk mechanism between autophagy and the EMT. *Food & Function*, 13(9), 4967–4976. <https://doi.org/10.1039/D2FO00483F>
- Zhang, X., Ruan, Q., Zhai, Y., Lu, D., Li, C., Fu, Y., Zheng, Z., Song, Y., & Guo, J. (2020). Baicalein inhibits non-small-cell lung cancer invasion and metastasis by reducing ezrin tension in inflammation microenvironment. *Cancer Science*, 111(10), 3802–3812. <https://doi.org/10.1111/cas.14577>
- Zhang, Y., Ge, Y., Ping, X., Yu, M., Lou, D., & Shi, W. (2018). Synergistic apoptotic effects of silibinin in enhancing Paclitaxel toxicity in human gastric cancer cell lines. *Molecular Medicine Reports*, 18(2), 1835–1841. <https://doi.org/10.3892/mmr.2018.9129>
- Zhang, Z., & Zhao, Y. (2022). Efficacy of cisplatin in combination with paclitaxel for oral cancer and its effect on cellular immunity. *Tropical Journal of Pharmaceutical Research*, 21(8), Art. 8. <https://doi.org/10.4314/tjpr.v21i8.29>
- Zhang, Z., Imani, S., Shasaltaneh, M. D., Hosseinifard, H., Zou, L., Fan, Y., & Wen, Q. (2019). The role of vascular mimicry as a biomarker in malignant melanoma: A systematic review and meta-analysis. *BMC Cancer*, 19(1), 1134. <https://doi.org/10.1186/s12885-019-6350-5>
- Zhao, G., Han, X., Cheng, W., Ni, J., Zhang, Y., Lin, J., & Song, Z. (2017). Apigenin inhibits proliferation and invasion, and induces apoptosis and cell cycle arrest in human

- melanoma cells. *Oncology Reports*, 37(4), 2277–2285.
<https://doi.org/10.3892/or.2017.5450>
- Zhong, J., He, C., Xu, F., Xu, X., Liu, L., Xu, M., Guo, Z., Wang, Y., Liao, J., & Li, Y. (2020). Lupeol inhibits osteosarcoma progression by up-regulation of HMGA2 via regulating miR-212-3p. *Journal of Orthopaedic Surgery and Research*, 15(1), 374.
<https://doi.org/10.1186/s13018-020-01879-0>
- Zhou, J., Huang, S., Wang, L., Yuan, X., Dong, Q., Zhang, D., & Wang, X. (2017). Clinical and prognostic significance of HIF-1 α overexpression in oral squamous cell carcinoma: A meta-analysis. *World Journal of Surgical Oncology*, 15(1), 104.
<https://doi.org/10.1186/s12957-017-1163-y>
- Zhou, W., Chen, H., Ruan, Y., Zeng, X., & Liu, F. (2021). High Expression of TRIM15 Is Associated with Tumor Invasion and Predicts Poor Prognosis in Patients with Gastric Cancer. *Journal of Investigative Surgery: The Official Journal of the Academy of Surgical Research*, 34(8), 853–861. <https://doi.org/10.1080/08941939.2019.1705443>
- Zhou, Y., & Sakurai, H. (2017). Emerging and Diverse Functions of the EphA2 Noncanonical Pathway in Cancer Progression. *Biological & Pharmaceutical Bulletin*, 40(10), 1616–1624. <https://doi.org/10.1248/bpb.b17-00446>
- Zhou, Y., Cai, W., Li, Y., Jiang, X., Feng, L., Zhu, Q., Liu, Y., Chen, Y., Li, S., Du, B., Lang, F., Wu, P., & Qiu, L. (2019). Correlations between quantitative parameters of contrast-enhanced ultrasound and vasculogenic mimicry in murine tumor model: A novel noninvasive technique for assessment? *Biological Procedures Online*, 21(1), 11.
<https://doi.org/10.1186/s12575-019-0101-5>

- Zhu, Y., Liu, X., Zhao, P., Zhao, H., Gao, W., & Wang, L. (2020). Celastrol Suppresses Glioma Vasculogenic Mimicry Formation and Angiogenesis by Blocking the PI3K/Akt/mTOR Signaling Pathway. *Frontiers in Pharmacology*, *11*.
<https://doi.org/10.3389/fphar.2020.00025>
- Ziello, J. E., Jovin, I. S., & Huang, Y. (2007). Hypoxia-Inducible Factor (HIF)-1 Regulatory Pathway and its Potential for Therapeutic Intervention in Malignancy and Ischemia. *The Yale Journal of Biology and Medicine*, *80*(2), 51–60.
- Zschiesche, W., Schönborn, I., Behrens, J., Herrenknecht, K., Hartveit, F., Lilleng, P., & Birchmeier, W. (1997). Expression of E-cadherin and catenins in invasive mammary carcinomas. *Anticancer Research*, *17*(1B), 561–567.

Conferences/Workshops

Poster presentation

1. Presented Poster entitled “Lupeol Hinders Hypoxia Induced Laminin 5 γ 2 Driven Vasculogenic Mimicry in Oral Squamous Cell Carcinoma in Synergistic Association with Paclitaxel” **Depanwita Saha**, Nabendu Murmu at 41st Annual International Conference of Indian Association For Cancer Research 2022, organized by Amity Institute of Molecular Medicine & Stem Cell Research (AIMMSCR), Amity University Uttar Pradesh, Noida, India from 2nd-5th March, 2022.
2. Presented Poster entitled “*Madhuca indica* inhibits tumor metastasis through regulating EMT and CSC phenotype in *in-vitro* and *ex-vivo* head and neck squamous cell carcinoma model” **Depanwita Saha**, Gaurav Das, Nabendu Murmu in National Science Day organized by Chittaranjan National Cancer Institute, Kolkata on 28th February, 2022.
3. Presented Poster entitled “Lupeol Hinders Vasculogenic Mimicry in Oral Cancer through Downregulation of FAK-pERK1/2-MMP2 Signaling Cascade” **Depanwita Saha**, Nabendu Murmu in 39th Annual Conference of Indian Association For Cancer Research 2020, organized by RGCB, Tiruvananthapuram from 5th-7th March, 2020.
4. Presented Poster entitled “Clinical Significance Of Vasculogenic Mimicry In Oral Cancer And The Role Of Lupeol In Hindering The Process Through Downregulation Of EphA2 Signaling Cascade” **Depanwita Saha**, Nabendu Murmu in IACR 2020 WB chapter at Chittaranjan National Cancer Institute, Kolkata on 11th February, 2020
5. Presented poster entitled “Vasculogenic Mimicry in Oral Cancer: The role of EphA2 signaling pathway”; **Depanwita Saha**, Nabendu Murmu, at 38th Annual Convention of

Indian Association For Cancer Research 2019 organized by PGIMER Chandigarh from 1st-3rd March, 2019.

6. Presented Poster entitled “The expression of cMET, Gab1 and pERK1/2 in Oral Squamous Cell Carcinoma Tissue and Their Association with Vasculogenic Mimicry”; **Depanwita Saha**, Nabendu Murmu, at 2nd Annual Conference on Recent Trends in Cancer Research, Early Diagnosis, Prevention and Therapy organized by Chittaranjan National Cancer Institute, Kolkata on 5th February, 2019.

Workshop attended

1. Pre conference Workshop in IACR 2019 on “Application of ddPCR in Cancer Biology”, organized by PGIMER Chandigarh on 28th February, 2019

List of Publications

1. **Saha D**, Mitra D, Alam N, Sen S, Mustafi SM, Majumder PK, Majumder B, Murmu N. Lupeol and Paclitaxel cooperate in hindering hypoxia induced vasculogenic mimicry via suppression of HIF-1 α -EphA2-Laminin-5 γ 2 network in human oral cancer. *J Cell Commun Signal*. 2022 Sep 5. doi: 10.1007/s12079-022-00693-z. Epub ahead of print. PMID: 36063341.
2. **Saha D**, Mitra D, Alam N, Sen S, MitraMustafi S, Mandal S, Majumder B, Murmu N. Orchestrated expression of vasculogenic mimicry and laminin-5 γ 2 is an independent prognostic marker in oral squamous cell carcinoma. *Int J ExpPathol*. 2022 Apr; 103(2):54-64. doi: 10.1111/iep.12430. Epub 2022 Feb 16. PMID: 35170826; PMCID: PMC8961501.
3. Mitra S, Patra T, **Saha D**, Ghosh P, Mustafi SM, Varghese AC, Murmu N. Sub-chronic cadmium and lead compound exposure induces reproductive toxicity and development of testicular germ cell neoplasia in situ in murine model: Attenuative effects of resveratrol. *J BiochemMolToxicol*. 2022 Jul; 36(7):e23058. doi: 10.1002/jbt.23058. Epub 2022 Apr 1. PMID: 35362238.
4. Ray S, **Saha D**, Alam N, MitraMustafi S, Mandal S, Sarkar A, Majumder B, Murmu N. Exposure to chewing tobacco promotes primary oral squamous cell carcinoma and regional lymph node metastasis by alterations of SDF1 α /CXCR4 axis. *Int J ExpPathol*. 2021 Apr;102(2):80-92. doi: 10.1111/iep.12386. Epub 2021 Mar 3. PMID: 33655604; PMCID: PMC7981595.
5. Bhattacharyya S, Ray S, **Saha D**, Mustafi SM, Alam N, Sarkar A, Murmu N. Chewing tobacco may act as a risk factor for dysplastic transformation of squamous cells in Oral

leukoplakia- A cytochemistry based approach. *Pathol Res Pract.* 2021 Feb; 218:153287. doi: 10.1016/j.prp.2020.153287. Epub 2020 Dec 24. PMID: 33454586.

6. Wamba BEN, Ghosh P, Mbaveng AT, Bhattacharya S, Debarpan M, **Depanwita S**, Saunak MM, Kuete V, Murmu N. Botanical from *Piper capense* Fruit Can Help to Combat the Melanoma as Demonstrated by *In Vitro* and *In Vivo* Studies. *Evid Based Complement Alternat Med.* 2021 Jan 18; 2021:8810368. doi: 10.1155/2021/8810368. PMID: 34007300; PMCID: PMC8100921.



Lupeol and Paclitaxel cooperate in hindering hypoxia induced vasculogenic mimicry via suppression of HIF-1 α -EphA2-Laminin-5 γ 2 network in human oral cancer

Depanwita Saha¹ · Debarpan Mitra¹ · Neyaz Alam² · Sagar Sen² · Saunak Mitra Mustafi³ · Pradip K. Majumder⁴ · Biswanath Majumder^{5,6} · Nabendu Murmu¹ 

Received: 1 June 2022 / Accepted: 17 August 2022

© The International CCN Society 2022

Abstract

Vasculogenic mimicry (VM), defined as an endothelial cell independent alternative mechanism of blood and nutrient supply by dysregulated tumor cells, is associated with poor prognosis in oral squamous cell carcinoma (OSCC). Here we aim to investigate the underlying molecular mechanism of the synergistic effect of phytochemical Lupeol and standard microtubule inhibitor Paclitaxel in reversing the hypoxia induced VM formation in OSCC. The results demonstrated that the hypoxia induced upregulation of HIF-1 α led to augmentation of signaling cascade associated with extracellular matrix remodeling and EMT phenotypes that are mechanistically linked to VM. Induction of HIF-1 α altered the expression of EMT/CSC markers (E-Cadherin, Vimentin, Snail, Twist and CD133) and enhanced the ability of cell migration/invasion and spheroid formation. Subsequently, the targeted knockdown of HIF-1 α by siRNA led to the perturbation of matrigel mediated tube formation as well as of Laminin-5 γ 2 expression with the down-regulation of VE-Cadherin, total and phosphorylated (S-897) EphA2, pERK1/2 and MMP2. We also observed that Lupeol in association with Paclitaxel resulted to apoptosis and the disruption of VM associated phenotypes in vitro. We further validated the impact of this novel interventional approach in a patient derived tumor explant culture model of oral malignancy. The ex vivo tumor model mimicked the in vitro anti-VM potential of Lupeol-Paclitaxel combination through down-regulating HIF-1 α /EphA2/Laminin-5 γ 2 cascade. Together, our findings elucidated mechanistic underpinning of hypoxia induced Laminin-5 γ 2 driven VM formation highlighting that Lupeol-Paclitaxel combination may serve as novel therapeutic intervention in perturbation of VM in human OSCC.

Keywords Hypoxia · Vasculogenic mimicry · HIF-1 α · OSCC · Lupeol · Paclitaxel · Patient derived ex vivo model

✉ Nabendu Murmu
nabendu.murmu@cnci.ac.in

- ¹ Department of Signal Transduction and Biogenic Amines, Chittaranjan National Cancer Institute, 37, S. P. Mukherjee Road, Kolkata 700026, India
- ² Department of Surgical Oncology, Chittaranjan National Cancer Institute, 37, S. P. Mukherjee Road, Kolkata 700026, India
- ³ Department of Pathology, Chittaranjan National Cancer Institute, 37, S. P. Mukherjee Road, Kolkata 700026, India
- ⁴ Department of Cancer Biology, Praesidia Biotherapeutics, 1167 Massachusetts Avenue, Arlington, MA 02476, USA
- ⁵ Departments of Cancer Biology, Molecular Profiling and Molecular Pathology, Mitra Biotech, Bangalore, India
- ⁶ Present Address: Oncology Division, Bugworks Research, C-CAMP, Bangalore, India

Introduction

Oral cancer is one of the leading causes of cancer related mortalities (Sung et al. 2021). Consumption of tobacco (including smokeless tobacco), betel nut chewing, severe alcoholism, poor oral hygiene and human papilloma virus (HPV) infection are the predominant risk factors (Borse et al. 2020). Despite the advances in diagnosis and various treatment modalities, the overall survival of OSCC patients did not improve for more than 50% cases, mostly because of the treatment failure due to the loco-regional recurrence and distant metastasis (Thavarool et al. 2019). The poor survival outcome is also influenced by alternative vascularization strategies associated with resistance in response to anti-angiogenic and anti-neoplastic therapies (Belotti et al. 2021). Hypoxia, one of the most detrimental alterations of the tumor microenvironment mainly in solid tumors

including OSCC, is orchestrated owing to lack of oxygen perfusion in tumor core either due to absence of blood vessels or presence of abnormal blood vessels (Muz et al. 2015) and characterized by overexpression of hypoxia inducible factor-1 alpha (HIF-1 α). The altered metabolism (glycolytic shift) and high acidic microenvironment due to lactate release ultimately promote survival of cancer cells that is linked to resistance towards chemotherapy and radiotherapy (Patel et al. 2020; Pezzuto et al. 2018) and attribute to tumor metastasis (Lee et al. 2020; Zhou et al. 2017). Under hypoxic condition, vasculogenic mimicry (VM) serves as an unique strategy of utilizing oxygen and essential nutrients independent of angiogenesis and programmed these cells to develop aggressive tumor growth (Maniotis et al. 1999; Folberg et al. 2004), leading to tumor invasion, metastasis and poor prognosis of several cancers (Zhang et al. 2019; Mitra et al. 2020; Ren et al. 2019) including OSCC (Hujanen et al. 2021, Wu et al. 2017, Wang et al. 2018b). Although a variety of proteins and tumor micro-environmental factors have been found to contribute VM formation under hypoxic condition in several cancer models including breast cancer (Wang et al. 2018a; Maroufi et al. 2020), hepatocellular carcinoma (Chen et al. 2019; Zhang et al. 2020), lung adenocarcinoma (Fu et al. 2021), melanoma (Li et al. 2019), glioma (Duan et al. 2018), however, their mechanistic involvement in OSCC remains poorly understood. In a hypoxic tumor microenvironment niche, HIF-1 α enhances the differentiation potential of cancer stem cells (CSC) (EmamiNejad et al. 2021) and promotes their phenotypic plasticity to transform cancer cells into more invasive state through epithelial mesenchymal transition (EMT) (Hernández de la Cruz et al. 2020) and remodeling of extracellular matrix (ECM) (Winkler et al. 2020) via degradation of laminin, recruitment of matrix metallo-proteases (Rousselle et al. 2020; Delgado-Bellido et al. 2017) and the formation of PAS +/CD31- infiltrating pseudo-vascular VM network to transport red blood cells and nutrients to the tumor cells (Yue et al. 2021). Previous studies have demonstrated that VM channel forming cells could be fueled by up-regulated expression of VE-Cadherin, EphA2, ERK1/2, MMP2, Laminin-5 γ 2 genes (Hendrix et al. 2001; Hess et al. 2006; Lu et al. 2013; Larson et al. 2014) in several cancer models. However, their active networking in the context of critical nodal role of HIF-1 α has not been established in OSCC. In our earlier study we have depicted the prognostic significance of VM in coordination with Laminin-5 γ 2 expression in OSCC patient cohorts (Saha et al. 2022). Here, we aim to further investigate the mechanistic link between HIF-1 α and Laminin-5 γ 2 in reshaping of ECM and simultaneous formation of VM architecture in OSCC which may be a potential therapeutic intervention in OSCC with high VM propensity.

Since traditional anti-angiogenic therapy could not inhibit the formation of VM due to lack of potential druggable

target, finding new treatment regimens, specifically targeting VM holds a great challenge. To improve prognosis, administration of taxane based drugs such as Paclitaxel in conjunction with the platinum drugs or oncogenic EGFR targeted agent like cetuximab have recently been reported to be effective with lower cytotoxicity and higher tolerability (Ahn et al. 2016; Sawatani et al. 2020) in the treatment of locally advanced OSCC. Paclitaxel is a mitotic inhibitor which stabilizes cytoplasmic microtubules and causes interference of cellular replication, arresting cells from entering to G2/M phases of the cell cycle (Horwitz, 1994). However, its adverse side effects on non-malignant healthy cells remain a safety concern, prompting to develop alternative treatment strategies. Combining the cancer preventive phytochemicals with the conventional chemotherapeutic agents has become an emerging strategy of treating cancer by increasing anti-tumor efficacy and response rate of the anticancer drug and concurrently overcome the drug resistance, dose induced toxicity and adverse side effects (Pezzani et al. 2019; Lee et al. 2020). Hence our next goal is to elucidate the anti-VM efficacy of phytochemical Lupeol which is a pharmacologically active natural triterpene widely found in edible fruits and vegetables (Saleem et al. 2009; Liu et al. 2021) including mango, strawberry, olive, red grapes, white cabbage, cucumber, pepper, tomato and reported to have extensive anti-inflammatory, mutagenesis-inhibiting, anti-neoplastic, anti-arthritis, and anti-diabetic properties in both in vitro and in vivo studies (Bociort et al. 2021; Che et al. 2022; Maleki-nejad et al. 2022). Moreover, data from in vitro (Pitchai et al. 2014; Nyaboke, et al. 2018) and animal studies (Al-Rehaily et al. 2001; Patocka, 2003; Saleem et al. 2009) provided convincing evidences regarding safety profile of Lupeol. In this context, our study aims to explore the possible chemo-sensitization effect of Lupeol in potentiating the conventional chemotherapeutic drug Paclitaxel and their mechanism of action in human OSCC.

Materials and methods

Reagents

A 30 mM stock solution of Lupeol (Sigma, S957712) was prepared by dissolving in warm alcohol followed by dilution with DMSO (Sigma, D2650) at a ratio of 1:1. For all the treatment protocols, the final concentration of DMSO was <0.01%. A 50 mM stock solution of Paclitaxel (Sigma, T1912) was prepared by dissolving in DMSO.

Antibodies

The primary and secondary antibodies used for Western blot (WB) and Immuno-histochemistry (IHC) are as

follows. Rabbit polyclonal anti-HIF1 α (Novus Biologicals, Cat# NB100-479, dilution: 1:500 for WB; 1:100 for IHC), Mouse monoclonal anti-VE-Cadherin (Novus Biologicals, Cat# NB600-1409, dilution: 1:100 for WB; 1:100 for IHC), Rabbit monoclonal anti-EphA2 (Cell signaling technology, Cat# 6997, Clone: D4A2, dilution: 1:1000 for WB; 1:100 for IHC), Rabbit monoclonal anti-pEphA2 (S-897, Cell signaling technology, Cat# 6347, Clone: D9A1, dilution: 1:1000 for WB; 1:100 for IHC), Rabbit monoclonal anti phospho p44/42 MAPK (Erk1/2) (Thr202/Tyr204), from Cell signaling technology, Cat# 4370, Clone: D13.14.4E, dilution: 1:2000 for WB; 1:100 for IHC), Rabbit polyclonal anti Erk1 + Erk2 (Abcam, Cat# ab17942, dilution: 1:1000 for WB), Mouse monoclonal anti-MMP2 (Novus Biologicals, Cat # NB200-114, Clone: 8B4, dilution: 1:1000 for WB; 1:100 for IHC), mouse monoclonal anti-Laminin-5 (Y2 chain) from Merck (Cat # MAB19562, Clone: D4B5, dilution: 1:1000 for WB; 1:100 for IHC), Rabbit monoclonal anti CD-31 or PECAM-1 (Santa Cruz Biotechnology, Cat# sc-1506-R, Clone: M-20, dilution: 1:100 for IHC), Rabbit monoclonal anti-E-Cadherin (Novus Biologicals, Cat# NBP2-67,540, Clone: ST54-01, dilution: 1:1000 for WB; 1:100 for IHC), Mouse monoclonal anti- Vimentin (Santa Cruz Biotechnology, Cat# sc-6260, Clone: V9, dilution: 1:200 for WB; 1:100 for IHC), Mouse monoclonal anti-Snail (Novus Biologicals, Cat# NBP2-50,300, Clone: 20C8, dilution: 1:1000 for WB; 1:200 for IHC), Mouse monoclonal anti-Twist1 (Novus Biologicals, Cat# NBP2-37,364, Clone: 10E4E6, dilution: 1:1000 for WB; 1:200 for IHC), Rabbit polyclonal anti-CD133 (Novus Biologicals, Cat# NB120-16518, dilution: 1:1000 for WB; 1:100 for IHC), Rabbit monoclonal anti -Bcl2 (Novus Biologicals, Cat# NBP2-07,182, Clone: JF104-8, dilution: 1:1000 for WB), mouse monoclonal anti-Bax (Santa Cruz Biotechnology, Cat # sc-7480, Clone: B9, dilution: 1:200 for WB), Mouse monoclonal anti β -Actin (Santa Cruz Biotechnology, Cat# sc-47778, Clone: C4, dilution: 1:200 for WB) were used as primary antibodies in this study. Horseradish peroxidase (HRP) conjugated Goat Anti Rabbit polyclonal IgG (Sigma Aldrich, Cat# A0545) and Rabbit Anti Mouse IgG (Sigma Aldrich, Cat# A9044) were used as secondary antibodies.

Cell lines and culture condition

Human oral squamous cell carcinoma cell lines UPCI: SCC154 (ATCC®CRL-3241™) and UPCI: SCC090 (ATCC®CRL-3239™) were obtained from American Type Culture Collection (ATCC, Manassas, VA, USA). All the cell lines were maintained in Minimum Essential Medium (MEM, Gibco, Life Technologies, USA) supplemented with 10% heat inactivated Fetal Bovine Serum (FBS, Gibco, Life Technologies, USA) and 2 mM of L-glutamine (Thermo-Fisher Scientific) at 37 °C in a humidified incubator with 5%

CO₂. All the experiments were performed after 3rd passage of cell lines which were maintained in an exponential growth phase. Hypoxic condition was stimulated by incubating cells in a hypoxic chamber flushed with a gas mixture of 1% O₂/5% CO₂/94%N₂ and the induction of HIF-1 α expression was assessed by Western blot analysis.

Transfection of siRNA

The ON-TARGETplusSMARTpool siRNA targeting HIF-1 α (siRNA#1: GAACAAAUACAUGGGGAUUA, siRNA#2: AGAAUGAAGUGUACCCUAA, siRNA#3: GAUGGA AGCACUAGACAAA, siRNA#4: CAAGUAGCCUCU UUGACAA) as well as the ON-TARGETplus Non-targeting siRNA (siControl#1: UGGUUUACAUGUCGACUAA, siControl#2: UGGUUUACAUGUUGUGUGA, siControl#3: UGGUUUACAUGUUUUCUGA, siControl#4: UGGUUU ACAUGUUUUCCUA) were purchased from Dharmacon (Horizon). The siRNA dried pellets were re-suspended in RNase free 1X siRNA buffer to prepare 20 μ M stock solutions. The final concentration of 100 nM of HIF-1 α siRNA was used to transfect cells. For transfection, cells were seeded into 6 well plates at 1.5×10^5 cells/well (2 ml) and cultured overnight. The cells (at 50–60% confluency) were transfected with siRNAs using Jetprime (Polyplus) reagents for 48 h according to manufacturer's instructions and then characterized by Western blot to assess the level of silencing of HIF-1 α . The silencing experiments and the downstream assays were performed both under normoxia and hypoxia.

In vitro tube formation assay

Pre-chilled 96 well culture plates were evenly coated with 50 μ l of Matrigel matrix (354262, Corning, USA) and incubated at 37 °C for 30 mins to solidify. Tumor cells (2×10^4 cells/well in 200 μ l) were seeded in the Matrigel coated plates and incubated overnight. In case of transfected cells, after 48 h of transfection, cells were trypsinized and then seeded on the Matrigel coated plate. The VM channels formed were observed under inverted microscope and the images were captured at 100X magnification. The images were analyzed to calculate the tube length and number of tubular junctions using Angiogenesis Analyzer compatible with Image J.

Trans-well migration and invasion assay

The migration and invasion assay were carried out using 24 well plate containing trans-well chambers with the polycarbonate filters of 6.5 mm diameter and 8 μ m pore size (3422, Corning, USA). Cells suspended in 100 μ l of serum free media were seeded in to the upper chambers at a density of 1×10^4 /well for migration and invasion. For the invasion

assay, the growth factor reduced Matrigel (356231, Corning, USA) was diluted with serum-free medium according to the manufacturer's instructions at a ratio of 1:5 and 100 μl /well was added to the upper chambers and incubated at 37 °C for 1 h before seeding cells. The lower chambers were filled with 600 μl of complete media containing 10% FBS as chemo-attractant. After the incubation of 24 h the membranes were fixed with methanol for 15 mins and after washing with PBS the membranes were stained with Giemsa stain. The non-migrating or non-invading cells on the upper surface of the membrane were removed using cotton swab. The number of migrating or invading cells was counted and the images were captured at 100X magnification.

Sphere formation assay

For sphere formation assay, single cell suspension in the tumor sphere media (serum free media supplemented with 1X B27, 20 ng/ml epidermal growth factor, 10 ng/ml basic fibroblast growth factor, 5 $\mu\text{g}/\text{ml}$ insulin, 0.4% FBS) were seeded at a density of 1000 cells/well (200 μl) in a 96-well ultra-low attachment plate (Corning). After one week of incubation, the resulting spheres were observed under inverted microscope and the sphere forming efficiency was determined by dividing the number of oral spheres by the number of cells seeded and the images were captured at 100X magnification.

Cell viability assay

Cell viability was determined by MTT assay. Cells were seeded at a density of 1×10^4 /well (200 μl) in a 96 well plate and exposed to Lupeol (0–200 μM), Paclitaxel (0–150 nM) and Lupeol + Paclitaxel for 48 h under hypoxic condition. Thereafter, 10 μl of MTT solution (2 mg/ml) was added in each well and incubated for 2–4 h at 37 °C. Then 100 μl of DMSO was added to dissolve the formazan crystal and OD was measured at 570 nm using Spectramax i3x microplate reader. The percentage of cell viability was determined with respect to the untreated control.

Determination of combination index (CI)

After the determination of individual and combinatorial inhibitory effect of Lupeol and Paclitaxel, the combination index was calculated according to the method described by Chou et al. (2010). The value of CI implies the quantitative measure of degree of interaction between two drugs. $\text{CI} < 1$ denotes synergistic, $\text{CI} = 1$ denotes additive and $\text{CI} > 1$ denotes antagonistic effects. The dose reduction index (DRI) is the measure of dose reduction of each drug in a synergistic combination of a given level compared with the doses of individual drugs.

Colony formation assay

Colony formation assay was performed as described earlier (Rauth et al. 2016). Approximately 500 cells/well (2 ml) were seeded in a 6 well plate. After overnight incubation, cells were treated with designated doses of Lupeol and Paclitaxel and were grown in fresh medium for another 3 days at 37 °C until the colonies were formed. Cell colonies were fixed with 10% methanol for 15 mins. Colonies were washed with 1X PBS and stained with Harry's hematoxylin. The number of colonies (a single colony denotes > 50 cells) were counted under bright field microscope and photographs were captured at 4X magnification. The percentage of colonies was calculated with respect to the untreated control.

Wound healing assay

Wound healing assay was performed as described earlier (Bhattacharyya et al. 2019). Briefly, cells were seeded at a density of 1×10^6 /well in a 6 well plate. When the cells reached more than 80% confluency, a vertical wound was created through cell monolayer using 200 μl pipette tip. Cellular debris and smooth edges of scratch was removed by washing the cells once and replaced with serum free media containing different concentration of Lupeol and Paclitaxel. Wound closure was observed at different time point and photographs were captured at 4X magnification under bright field microscope. The scratched area was analyzed using Image J software.

Evaluation of apoptosis

Cell apoptosis was detected using Annexin V Apoptosis detection kit (Santa Cruz Biotechnology Inc, sc-4252 AK). Briefly, after treatment of individual and combined doses of Lupeol and Paclitaxel for 48 h, the cells were harvested by centrifugation and dissolved in 1X assay buffer. Cells were then stained with Annexin-V-FITC and Propidium Iodide (PI), incubated at room temperature for 15 mins in the dark and the data were acquired by BD FACSVerserTM flow cytometer. Cells without Annexin V-FITC and PI stains were considered as negative controls. The dual parameter dot plot considering the logarithmic fluorescence intensity of FL1-H (X axis- FITC fluorescence) and FL2-H (Y axis- PI fluorescence) was obtained using FlowJoTM v10 software to determine the percentage of total apoptosis (consisting of early apoptosis and late apoptosis).

Apoptotic cells that undergo DNA degradation were detected using TUNEL assay using TACS -2 TdT-Fluor In-situ Apoptosis detection kit (R&D systems, Cat# 4812-30 K) according to the manufacturer's protocol. After fixation with 3.7% buffered formaldehyde, the cells placed on the sterile coverslips were digested with protease K for 15 mins at room

temperature. The cells were then washed and incubated with TUNEL reaction mix (TdT enzyme solution and labeling solution) for 60 mins at 37 °C in humidified chamber. The cells on the coverslips were mounted on clean glass slides and the TUNEL positive apoptotic cells were detected with fluorescence microscope at 400X magnification.

Western blot analysis

Western blot analysis was performed as described earlier (Rauth et al. 2016). Total cell lysates (50 µg) were resolved by 10% SDS-PAGE and subsequently electro-transferred to Polyvinylidene di-fluoride (PVDF) membrane. After blocking with 5% non-fat dry milk for 1 h at room temperature the membranes were incubated with different dilutions of primary antibodies overnight at 4 °C followed by the exposure with appropriate secondary antibodies conjugated with horse radish peroxidase (HRP) for 1 h at room temperature. The signal was visualized using enhanced chemi-luminescence kit (BioRad) and the resulting bands were acquired using Image Lab 5 software (BioRad). The band density was quantified by Image J software. β -actin was used as a loading control.

Real time PCR

For gene expression analysis total RNA was extracted with Trizol reagent according to manufacturer's protocol. The complementary DNA (cDNA) was synthesized from 2 µg of total RNA using Roche Evoscript Universal cDNA master kit. Quantitative analysis of cDNA amplification was assessed by incorporating SYBR green nucleic acid stain (Roche FastStart Essential DNA Green Master kit) into double stranded DNA. The specific primers for investigating gene expression are as follows: HIF-1 α Forward -5' GTCTGCAACATGGAAGGTATTG-3', HIF-1 α Reverse-5'-GCAGGTCATAGGTGGTTTCT -3', Laminin-5 γ 2 Forward -5'-GATGGCATTCACTGCGAGAAG-3', Laminin-5 γ 2 Reverse 5'-TCGAGCACTAAGAGAACC TTTGG-3', GAPDH Forward- 5'-GTCAACGGATTGTTGTCGTATTG-3', GAPDH Reverse- 5'- TGTAGTTGAGGT CAATGAAGGG-3'. The PCR condition included denaturation at 95 °C for 1 min, Annealing at 52 °C for 1 min and Extension at 72 °C for 2 mins. All the samples were evaluated in triplicates using Roche Light cycler 96. GAPDH was used as an endogenous control. Quantitative evaluation of data was carried out using $2^{-\Delta\Delta CT}$ method and Ct (cycle threshold) values were standardized with respect to GAPDH expression.

Patient derived tumor explant culture

The patient derived tumor explant culture was established as described by Majumder et al. (2015). Fresh OSCC tumor specimens were collected from a total of 5 patients (details mentioned in Supplementary Table 2) immediately after surgical resection from Chittaranjan National Cancer Institute, Kolkata. For each patient, non-heparinized blood was collected and serum was separated and stored at -80 °C for further use. The study was approved by the Institutional Ethics Committee (IEC Ref: A-4.311/53/2014) in accordance with the ethical guidelines of Declaration of Helsinki (1964) and its later amendments. Patients have no history of recurrence, preoperative chemotherapy or radiotherapy. Surgically removed fresh tumor tissues were cut into ~2–3mm³ sections and cultured into 24 well culture plates coated with tumor matrix proteins and RPMI medium (Gibco, Life Technologies, USA) supplemented with 2% autologous serum and 8% FBS. Tumor slices were treated with individual and combinatorial doses of Lupeol and Paclitaxel or with DMSO (vehicle control) for 48 h. The formalin fixed paraffin embedded (FFPE) tumor blocks were then used for histological examination.

Immunohistochemistry/PAS dual staining

Immunohistochemistry staining (IHC) was performed according to the manufacturer's instruction (Millipore, IHC Select DAB150 Immuno-peroxidase secondary detection system kit) on 5-micron sections from the FFPE tumor blocks as per our previously described methods (Saha et al. 2022; Ray et al. 2021; Mitra et al. 2020). Primary antibodies against CD-31 or PECAM-1, HIF-1 α , VE-Cadherin, EphA2, pERK1/2, MMP2, Laminin-5 γ 2, E-Cadherin, Vimentin, Snail, Twist were used for IHC. The final IHC score was determined by considering intensity of staining and proportion (%) of stained cells as described earlier (Saha et al. 2022).

Protein–protein interaction (PPI) and network analysis

For STRING protein–protein interaction (PPI) network analysis (<https://string-db.org>), all input markers were selected from current study and queried in setting that involves full network (type), confidence (edge meaning), multiple active interaction sources/channels in combination spanning text mining, database, experiments, co-expression, neighborhood, gene fusion and co-occurrence. Minimum required interaction score with high confidence or 0.700 was selected for final analysis. We restricted maximum number of interactions only to queried proteins that have been profiled in the study and no additional layer or second shell was added.

Statistical analysis

All the statistical analyses were performed using GraphPad Prism 7 (GraphPad, USA) software. All the experiments were repeated independently three times and the data were recorded as mean \pm SD. One way Analysis of variance (ANOVA) followed by post-hoc comparisons with Tukey test was carried out to assess the significant difference between each treated group and untreated control. $P < 0.05$ was considered as statistically significant.

Results

HIF-1 α escalates VM forming ability in oral cancer in vitro and positively regulates VM associated EphA2/Laminin-5 γ 2 axis

To investigate the role of HIF-1 α in the enhancement of VM formation, the tube forming ability of OSCC cell lines was monitored in 3D tumor culture by stabilizing HIF-1 α under hypoxia and also silencing HIF-1 α expression with HIF-1 α siRNA. The hypoxic condition triggered the formation of vascular architecture (characterized by the interconnected loops and tubular networks) in all the OSCC cell lines. Further, the cells transfected with HIF-1 α siRNA significantly inhibited the tube forming capacity of OSCC cell lines in

both normoxia and hypoxia, demonstrating the fractured tubular structure as well as the significant decrease in the length and number of tubular junctions (Fig. 1a, b). These properties remain unperturbed in the non-transfected cells and control siRNA transfected cells under similar conditions. The expression of VM associated signaling molecules was evaluated following the induced and genetically silenced expression of HIF-1 α using western blot analysis. Under hypoxia, the expression of HIF-1 α protein and its downstream effectors such as VE-Cadherin, EphA2, pEphA2 (S897), pERK1/2, MMP2 and Laminin-5 γ 2 was significantly increased. In contrast, the knock-down of HIF-1 α notably downregulated the expression of these VM associated signaling molecules irrespective of normoxic and hypoxic conditions indicating the role of HIF-1 α in regulating the VM via promoting EphA2/Laminin-5 γ 2 signaling cascade (Fig. 1c). Similarly, the mRNA expression of HIF-1 α and Laminin-5 γ 2 was also markedly reduced in the HIF-1 α silenced cells under normoxia and hypoxia (Fig. 1d).

HIF-1 α regulates VM related aggressive phenotypes and expression of EMT and CSC markers

Since VM is closely associated with the migration and invasion of tumor cells, we subsequently assessed the migratory and invading potential of OSCC cells. Data from trans-well migration and invasion assay in HIF-1 α induced condition

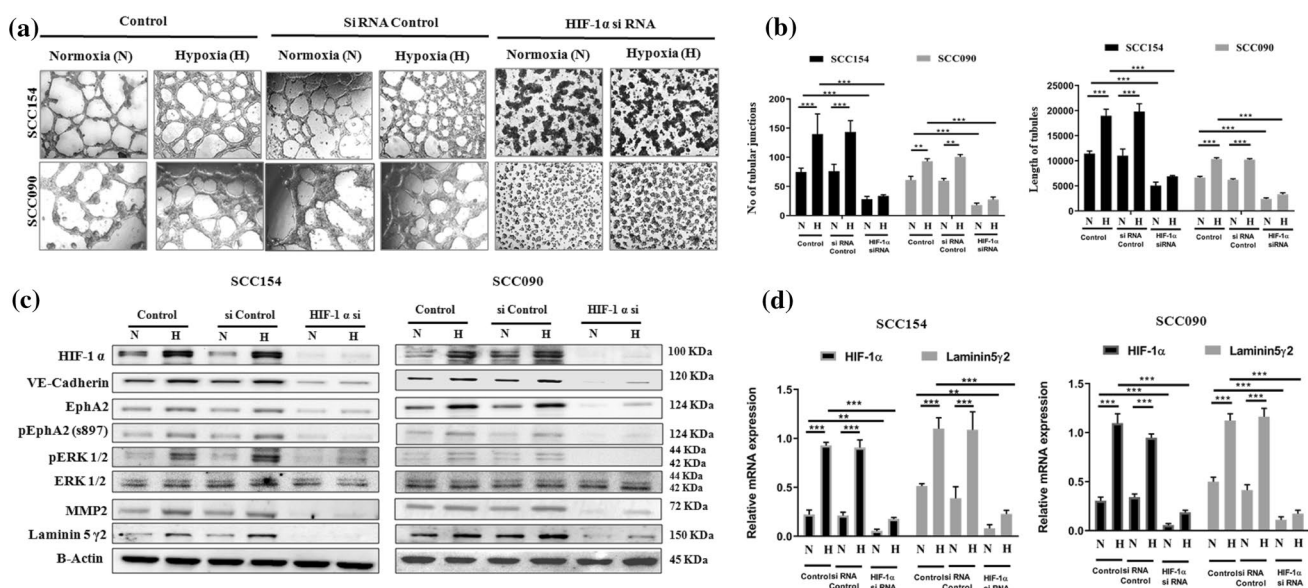


Fig. 1 siRNA against HIF-1 α inhibits vasculogenic mimicry formation and the expression of vasculogenic mimicry related genes in-vitro. **(a)** Effect of silencing of HIF-1 α on the formation of VM in OSCC cells (magnification: 100X) under normoxia and hypoxia. **(b)** Quantification of VM formation with respect to the number of tubular junction and length of tubules in OSCC cells treated with HIF-1 α siRNA under normoxia and hypoxia. **(c)** Effect of silencing of

HIF-1 α on the protein expression of VM related genes. **(d)** Effect of silencing of HIF-1 α on the mRNA expression of VM related genes. Each experiment was performed in triplicates. * P value < 0.05 , ** P value < 0.01 and *** P value < 0.0001 denote statistically significant changes compared to the corresponding control by One Way ANOVA test (P ANOVA < 0.0001) followed by post hoc Tukey's test

and after performing HIF-1 α knockdown revealed that, the induction of hypoxia significantly increased the number of migrating and invading cells, whereas the HIF-1 α siRNA transfected cells exhibited significant decrease in tumor cell migration and invasion through trans-well chambers compared to the non-transfected cells and control siRNA transfected cells. Hypoxia induced HIF-1 α also enhanced the stem like phenotype of tumor cells, characterized by the formation of spherical and non-adherent tumor spheres which was found to be significantly down-regulated in HIF-1 α silenced cells (Fig. 2a, b). Since CSC formation is known to accelerate EMT phenotypic state in some cancers (Mani

et al. 2008), we also delineated the impact of hypoxia driven CSC and EMT phenomenon through HIF-1 α induction. It was found that induction of HIF-1 α resulted in the significant decrease in expression of E-Cadherin (epithelial) and concomitant increase in the expression of CD133 as well as related mesenchymal markers (i.e., Vimentin, Snail and Twist). While evaluating the dysregulated expression of the EMT markers in all the OSCC cell lines, it was found that HIF-1 α siRNA consistently reversed the effect of hypoxia (Fig. 2c).

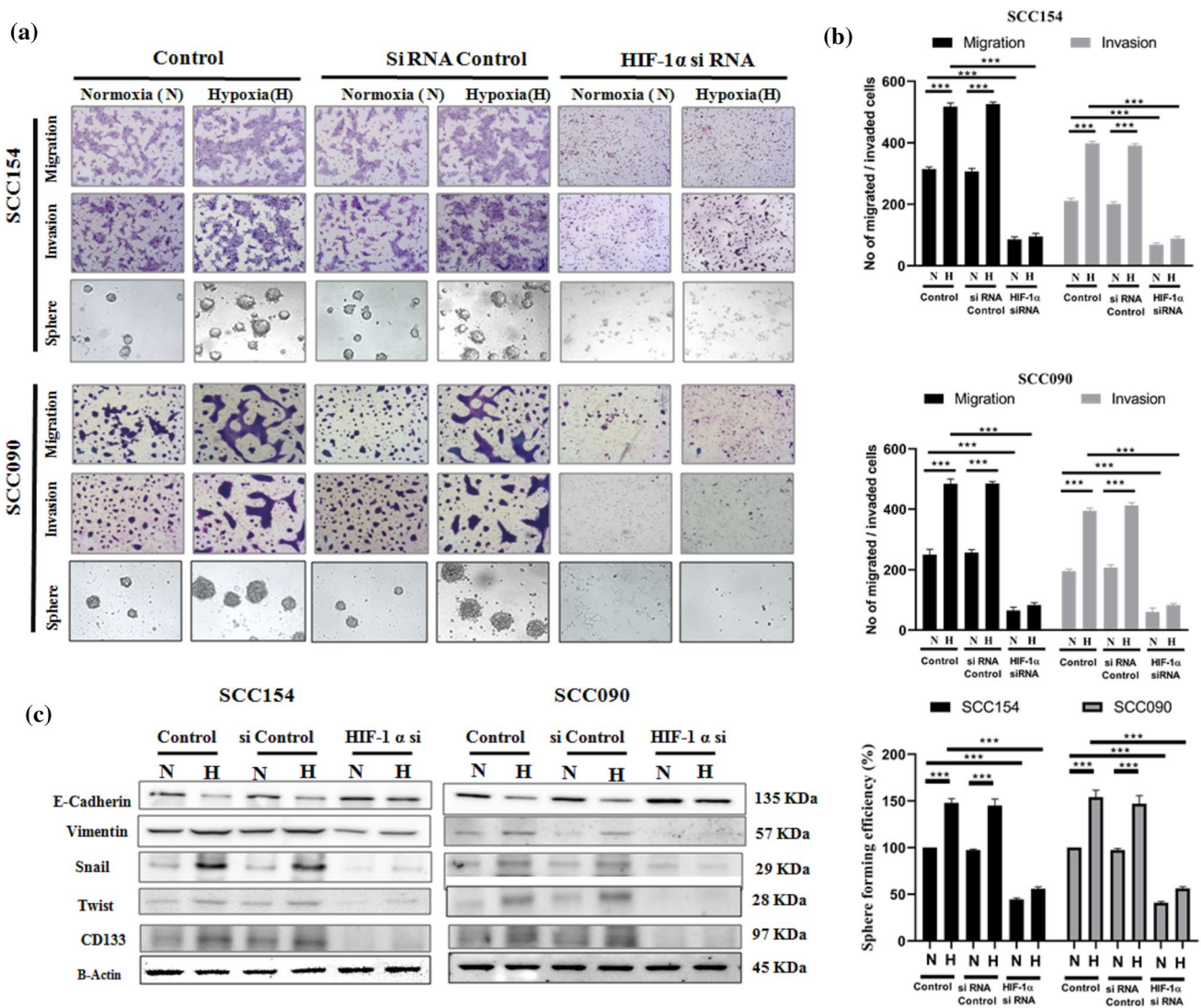


Fig. 2 siRNA targeted against HIF-1 α inhibits trans-well migration, invasion, sphere formation along with the expression of EMT and CSC related genes in vitro. (a) Effect of silencing of HIF-1 α on the trans-well migration, invasion and sphere formation in OSCC cells (magnification: 100X) under normoxia and hypoxia. (b) Quantification of migrated and invaded cells and CSC enriched spheres treated

with HIF-1 α siRNA under normoxia and hypoxia. (c) Effect of silencing of HIF-1 α on the expression of EMT and CSC related proteins. Each experiment was performed in triplicates. * P value < 0.05, ** P value < 0.01 and *** P value < 0.0001 denote statistically significant changes compared to the corresponding control by One Way ANOVA test (P ANOVA < 0.0001) followed by post hoc Tukey's test

Effect of Lupeol and Paclitaxel on the viability and proliferation of OSCC cells under hypoxia

To ascertain that a combinatorial regimen of Lupeol and Paclitaxel offers synergistic effect in perturbation of VM forming cells, we analyzed the data obtained from MTT assay and observed the cytotoxic effect of Lupeol and Paclitaxel on the OSCC cell lines. The dose dependent cytotoxicity of Lupeol did not differ significantly at 24 h and 48 h in both the UPCI: SCC154 and UPCI: SCC090 cell lines. However, treatment with varying doses of Paclitaxel exhibited notable differences in the cell viability at 48 h when compared the same with 24 h. Hence for all the subsequent assays, the treatment duration of 48 h was considered for both of Lupeol and Paclitaxel. Individual treatment of Lupeol attained the IC_{50} value of $79.43 \mu M$

in UPCI: SCC154 cells and $91.25 \mu M$ in UPCI: SCC090 cells during a defined 48 h of treatment window, whereas the treatment of Paclitaxel alone resulted in the IC_{50} value of 83 nM in UPCI: SCC154 cells and 67 nM in UPCI: SCC090 cells. The simultaneous treatment of cells with Lupeol and sub IC_{50} doses of Paclitaxel elicited a stronger inhibitory response on cellular viability compared to their individual treatment (Supplementary Table 1 and Supplementary Fig. 1). The Combination index (CI) value for the combinatorial treatment was found to be 0.737 for UPCI: SCC154 cells and 0.815 for UPCI: SCC090 cells indicating the synergistic effects of Lupeol and Paclitaxel in perturbing cell viability. Finally, the combination of $39.43 \mu M$ of Lupeol + 20 nM of Paclitaxel (for UPCI: SCC154) and $52.58 \mu M$ of Lupeol + 16 nM of Paclitaxel (for UPCI: SCC090) represented the best synergistic inhibition potential (Fig. 3a), which have been designated for

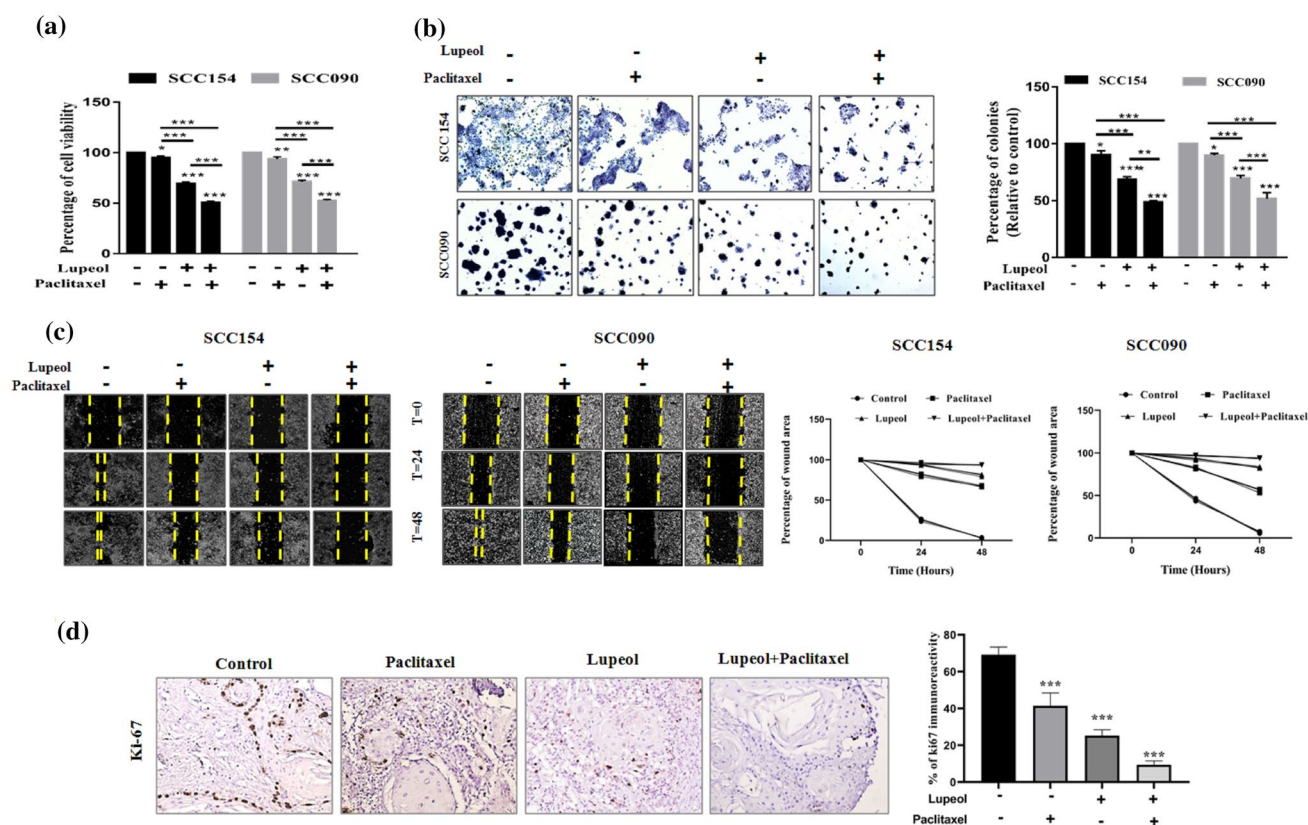


Fig. 3 Effect of Lupeol and Paclitaxel on hypoxia induced cellular proliferation, colony formation and wound healing potential. **(a)** Percentage of cell viability in Lupeol and Paclitaxel treated OSCC cells was measured with respect to the untreated control. **(b)** Individual and combinatorial effect of Lupeol and Paclitaxel was determined on the hypoxia induced colony formation in OSCC cells (magnification: 40X) and quantification of the percentage of colony formation (relative to control) in OSCC cells treated with Lupeol alone and in combination with Paclitaxel was assessed. **(c)** Kinetics of wound closure of OSCC cells treated with Lupeol alone and

in combination with Paclitaxel (magnification: 40X). **(d)** Effect of Lupeol and Paclitaxel on regulating the expression of proliferating marker (Ki-67) in ex vivo platform derived from OSCC was determined by IHC (left, 200X magnification). Comparative analysis of IHC scores among groups has been represented (right). Each experiment was performed in triplicates. * P value < 0.05 , ** P value < 0.01 and *** P value < 0.0001 denote statistically significant changes compared to the corresponding control by One Way ANOVA (P ANOVA < 0.0001) followed by post hoc Tukey's test

further investigations. The combinatorial dose exhibited significantly decreased percentage of colonies (Fig. 3b) and reduced wound healing potential compared to the individual treatment (Fig. 3c).

Lupeol treatment enhances the Paclitaxel induced apoptosis in OSCC cell lines under hypoxia

In order to evaluate whether the anticancer property of Lupeol and Paclitaxel are exerted through inducing apoptotic signal, the rate of apoptosis was quantified by flow cytometry using Annexin V-FITC and PI labelling. In both of the OSCC cell lines; though Lupeol or Paclitaxel individually induced apoptosis, their combinatorial

treatment demonstrated the significant enhancement of the percentage of apoptotic cells (Fig. 4a). In case of UPCI: SCC154 cell line, the total rate of apoptosis was increased by 52.88%. In case of UPCI: SCC090 cells, the same was found to be enhanced by 24.63% through the synergistic combinatorial treatment of Lupeol and Paclitaxel during hypoxic incubation. Moreover, to understand the underlying molecular mechanisms, the protein expression level of the key regulators of apoptosis (i.e., Bax and Bcl2) was investigated. Significantly up-regulated expression of Bax and down-regulated expression of Bcl2 was observed in the cells treated with Lupeol and/or Paclitaxel (Fig. 4b). It is also noteworthy that, the alteration of the apoptotic regulator proteins was found to be more pronounced when

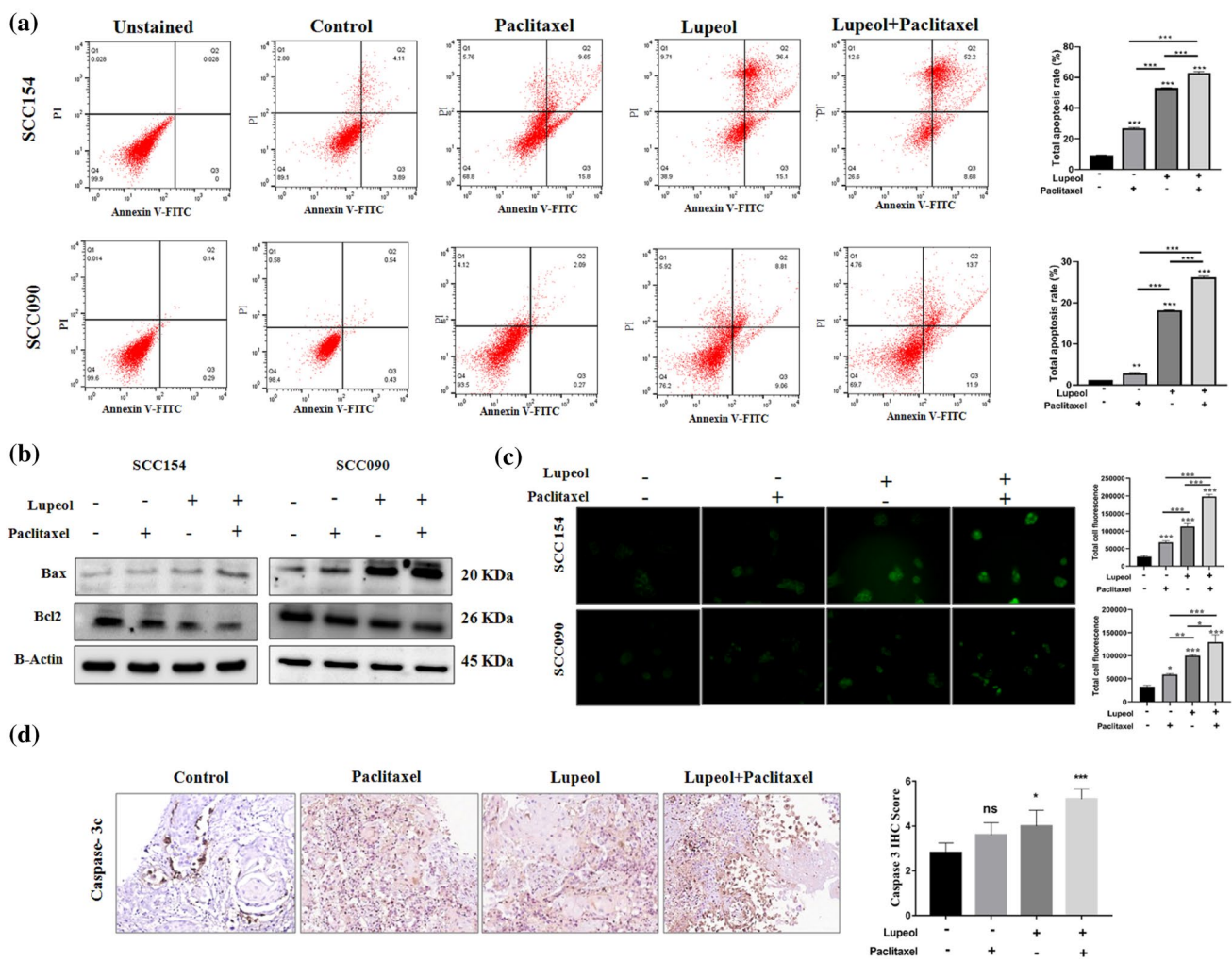


Fig. 4 Effect of Lupeol and Paclitaxel on induction of apoptosis in vitro and ex vivo culture. **(a)** Annexin-V/PI staining indicating total apoptosis rate in OSCC cells treated with Lupeol and Paclitaxel. **(b)** Effect of Lupeol and Paclitaxel on the expression of apoptotic markers. **(c)** TUNEL assay indicating total fluorescence intensity of apoptotic cells following the treatment of Lupeol and Paclitaxel in comparison with untreated control. **(d)** Effect of Lupeol and Paclitaxel

on regulating the expression of apoptotic marker (Caspase-3c) in ex vivo platform of OSCC by IHC (200X magnification, left). Comparative analysis of IHC scores among groups (right). Each experiment was performed in triplicates. **P* value < 0.05, ***P* value < 0.01 and ****P* value < 0.0001 denote statistically significant changes compared to the corresponding control by One Way ANOVA test (*P* ANOVA < 0.0001) followed by post hoc Tukey's test

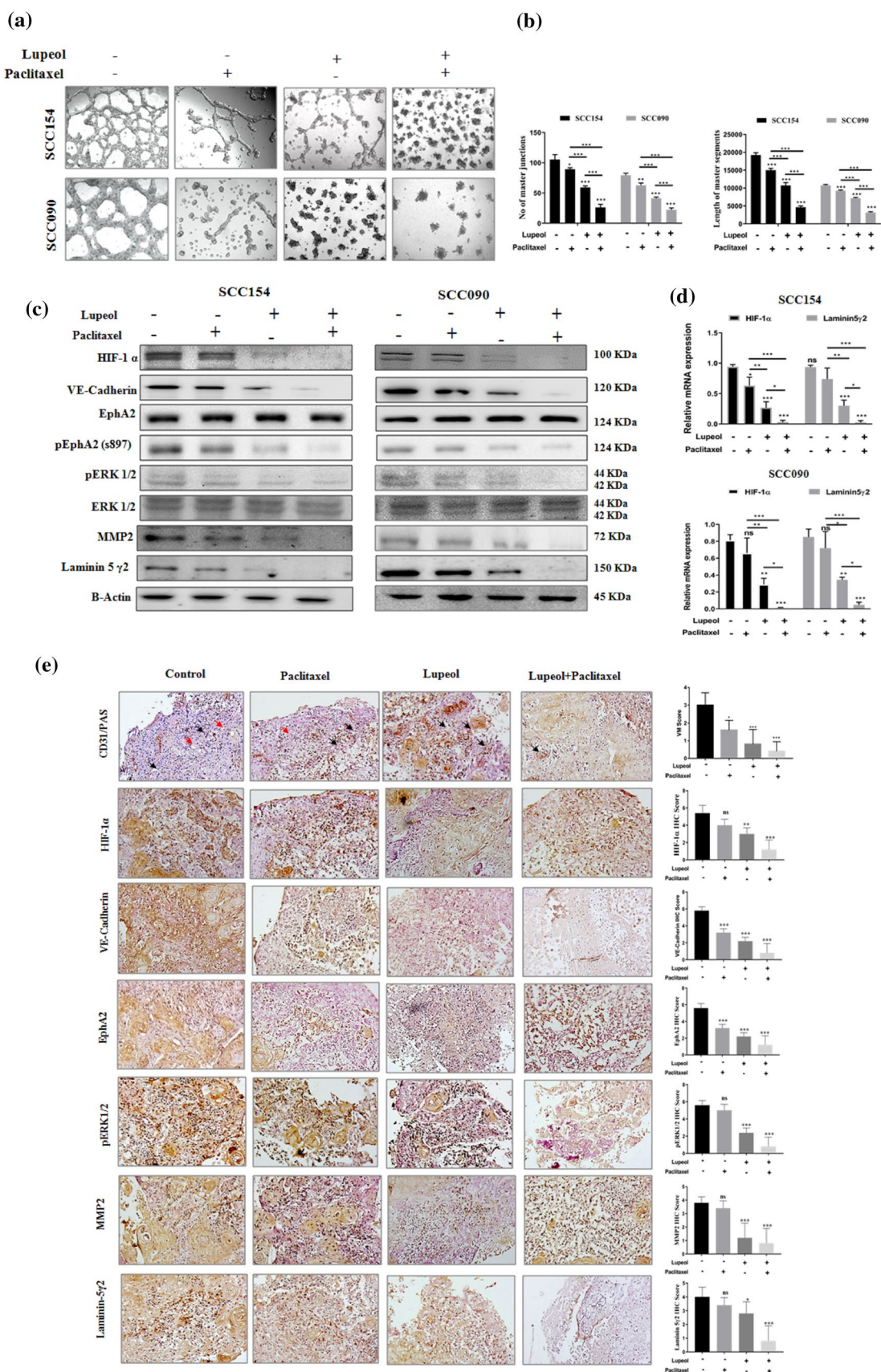


Fig. 5 Effect of Lupeol and Paclitaxel on regulating hypoxia induced VM and the expression of VM related genes in vitro and ex vivo systems. **(a)** Individual and combinatorial effect of Lupeol and Paclitaxel on the hypoxia induced VM formation in OSCC cells (magnification: 100X). **(b)** Quantification of VM formation with respect to number of tubular junction and length of tubules in OSCC cells treated with Lupeol alone and in combination with Paclitaxel. **(c)** Individual and combinatorial effect of Lupeol and Paclitaxel on the protein expression of VM associated genes. **(d)** Individual and combinatorial effect of Lupeol and Paclitaxel was determined by quantifying the mRNA expression of VM associated genes. **(e)** Effect of Lupeol and Paclitaxel on regulating the expression of VM associated genes in OSCC derived ex-vivo platform by IHC staining of markers (200X magnification, left). Red arrows in the CD31/PAS staining indicate PAS positive VM architecture and black arrows indicate endothelial structures. Comparative analysis of IHC scores among groups has been represented (right). Each experiment was performed in triplicates. **P* value < 0.05, ***P* value < 0.01 and ****P* value < 0.0001 denote statistically significant changes compared to the corresponding control by One Way ANOVA test (*P* ANOVA < 0.0001) followed by post hoc Tukey's test

both of the compounds were used together than their individual treatment. TUNEL assay also confirmed significantly increased signal intensity of the apoptotic cells in Lupeol and Paclitaxel treated group (Fig. 4c).

Combined treatment of Lupeol and Paclitaxel hinders the hypoxia induced VM formation and perturbs HIF-1 α /EphA2/ Laminin-5 γ 2 signaling cascade

After ascertaining that hypoxia facilitated VM forming ability of UPCI: SCC154 and UPCI: SCC090 cells (Fig. 1), we further investigated the potential role of Lupeol and Paclitaxel in regulating the hypoxia induced VM forming capacity of these cells (Fig. 5a, b). Significant disruption of VM structures, in conjunction with remarkable reduction of tubular length and numbers were observed in the cells co-treated with Lupeol and Paclitaxel. Though the individual treatment of the compounds notably fractured the in vitro pseudo-vascular architecture, their combinatorial effect is more pronounced affirming their synergistic anticancer potential through mechanistically inhibiting the VM channel formation. To further elucidate the molecular mechanism involved in the reversing effect of Lupeol and Paclitaxel on the hypoxia induced VM formation, the altered expression patterns of HIF-1 α and its downstream signaling components were also investigated. The western blot analysis illustrated the significant down-regulation of hypoxia induced HIF-1 α and its downstream VM associated regulators such as VE-Cadherin, pEphA2 (S-897), pERK1/2, MMP2 and Laminin-5 γ 2 in the cells that were treated with Lupeol alone and in combination with Paclitaxel (Fig. 5c). The synergistic association of Lupeol and Paclitaxel also significantly suppressed the hypoxia

induced upregulation of the mRNA expression of HIF-1 α and Laminin-5 γ 2 indicating their VM inhibiting potential at the transcription level (Fig. 5d).

Synergism of Lupeol and Paclitaxel reverses EMT and CSC phenomenon under the influence of hypoxia

In the Fig. 2, we have investigated that the induction of HIF-1 α enhanced EMT and CSC phenomenon in OSCC cells which displayed a crucial role in the VM formation. Figure 6a depicted a significantly reduced number of migrated and invaded cells in trans-well setting when co-treated with Lupeol and Paclitaxel indicating their indispensable role in regulating VM associated migration and invasion potential. The combinatorial treatment also caused a significant decrease in the sphere forming potential with the down-regulation of CD133 marker. Furthermore, Lupeol alone as well as in combination with Paclitaxel significantly up-regulated the expression of E-Cadherin and consistently down-regulated the expression of mesenchymal markers including Vimentin, Snail and Twist. Together, these data mechanistically substantiate their reversing effect on the hypoxia promoting EMT (Fig. 6b).

Synergistic effect of Lupeol and Paclitaxel on regulating hypoxia induced vasculogenic mimicry in patient derived ex vivo culture

Our findings from the in vitro model motivated us to test the same hypothesis in a more complex but relevant patient tumor derived ex vivo culture system. This model preserves the physiological context of tumor microenvironment and therefore represents a close approximation of native tumor niche state (Majumder et al. 2015). In order to elucidate the efficacy of the combinatorial drugs in ex vivo system, the alteration of VM associated regulators along with the proliferative and apoptotic markers was assessed at 48 h post treatment. Tissue architecture of untreated control exhibited relatively compact tumor cells whereas the Lupeol and Paclitaxel co-treated group was found to have more disintegrated structures. CD31/PAS staining showed a significantly decreased number of VM structures in Lupeol and Paclitaxel treated tumor fragments, compared to the untreated control (Fig. 5e). Lupeol and Paclitaxel treatment group also displayed a significant decrease in the expression of the cell proliferation marker Ki67 (Fig. 3d) as well as VM associated HIF-1 α and its downstream regulators VE-Cadherin, pEphA2 (S-897), pERK1/2, MMP2 and Laminin-5 γ 2, compared to the untreated control (Fig. 5e). The significantly upregulated expression of active Caspase 3c in Lupeol and Paclitaxel treated group confirmed that their augmented anticancer potential is exerted by the induction of apoptosis

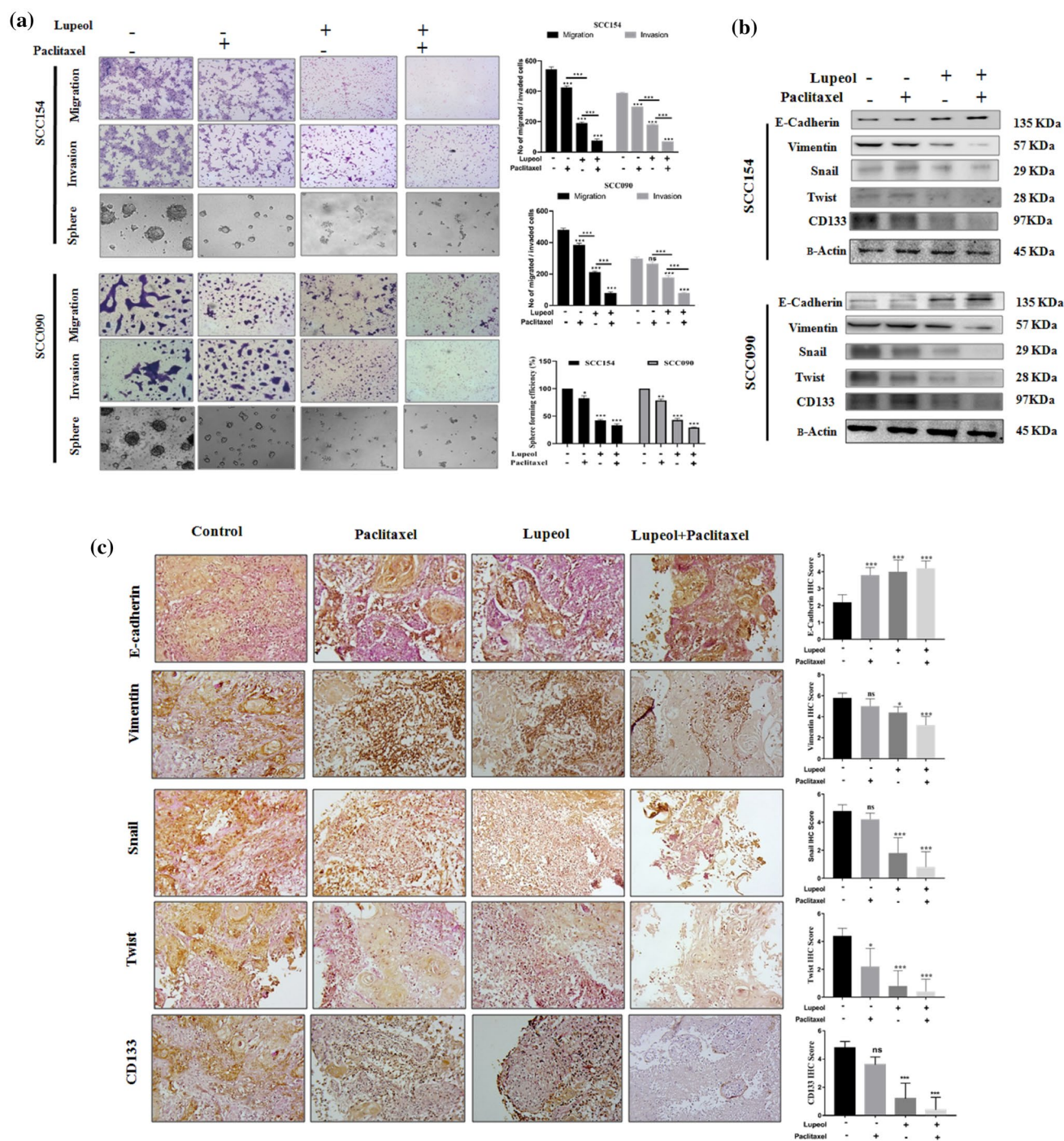


Fig. 6 Effect of Lupeol and Paclitaxel on hypoxia induced migration, invasion, sphere formation along with alteration of EMT and CSC related genes in vitro and ex vivo. **(a)** Individual and combinatorial effect of Lupeol and Paclitaxel on the hypoxia induced transwell migration, invasion and sphere formation in OSCC cells was evaluated (magnification: 100X) and quantification of migrated and invaded OSCC cells and CSC rich sphere forming cells treated with Lupeol alone and in combination with Paclitaxel. **(b)** Individual and combinatorial effect of Lupeol and Paclitaxel on the protein expression of EMT and CSC associated genes in vitro. **(c)** Effect of Lupeol

and Paclitaxel on regulating the expression of VM associated EMT and CSC markers in ex vivo platform of OSCC. IHC staining for expression of markers (200X magnification, left) and comparative analysis of their IHC scores in Lupeol and Paclitaxel treated tissue specimens (right). Each experiment was performed in triplicates. **P* value < 0.05, ***P* value < 0.01 and ****P* value < 0.0001 denote statistically significant changes compared to the corresponding control by One Way ANOVA test (*P* ANOVA < 0.0001) followed by post hoc Tukey's test

(Fig. 4d). Furthermore, the immuno-histochemical profiling of the expression of EMT and CSC markers showed reduced expression of CSC marker CD133 and mesenchymal markers including Vimentin, Snail, Twist and significantly increased expression of the epithelial marker E-Cadherin in the tissue sections treated with Lupeol alone and in combination with Paclitaxel, indicating the potential of this drug combination in disrupting EMT phenomenon in personalized ex vivo setting (Fig. 6c).

PPI analysis of VM interacting proteins

To investigate the functional link among the differentially expressed proteins in the hypothesized network, protein-protein interactions (PPI) were analyzed via STRING. In our

study the STRING analysis identified the main network proteins implicated cellular proliferation, extracellular matrix remodeling, EMT, CSC phenotype and apoptosis. The different grade of association was denoted via confidence level (low-0.150, medium-0.400, high-0.700, highest- 0.900) and edge thickness. Our key network protein HIF-1 α exhibited highest degree of association with Twist (0.979), followed by the same with MMP2 (0.754) and Snail (0.727). Laminin also indicated strong association (0.925) with MMP2 and Caspase 3 (0.907). All other possible associations are depicted in Fig. 7a.

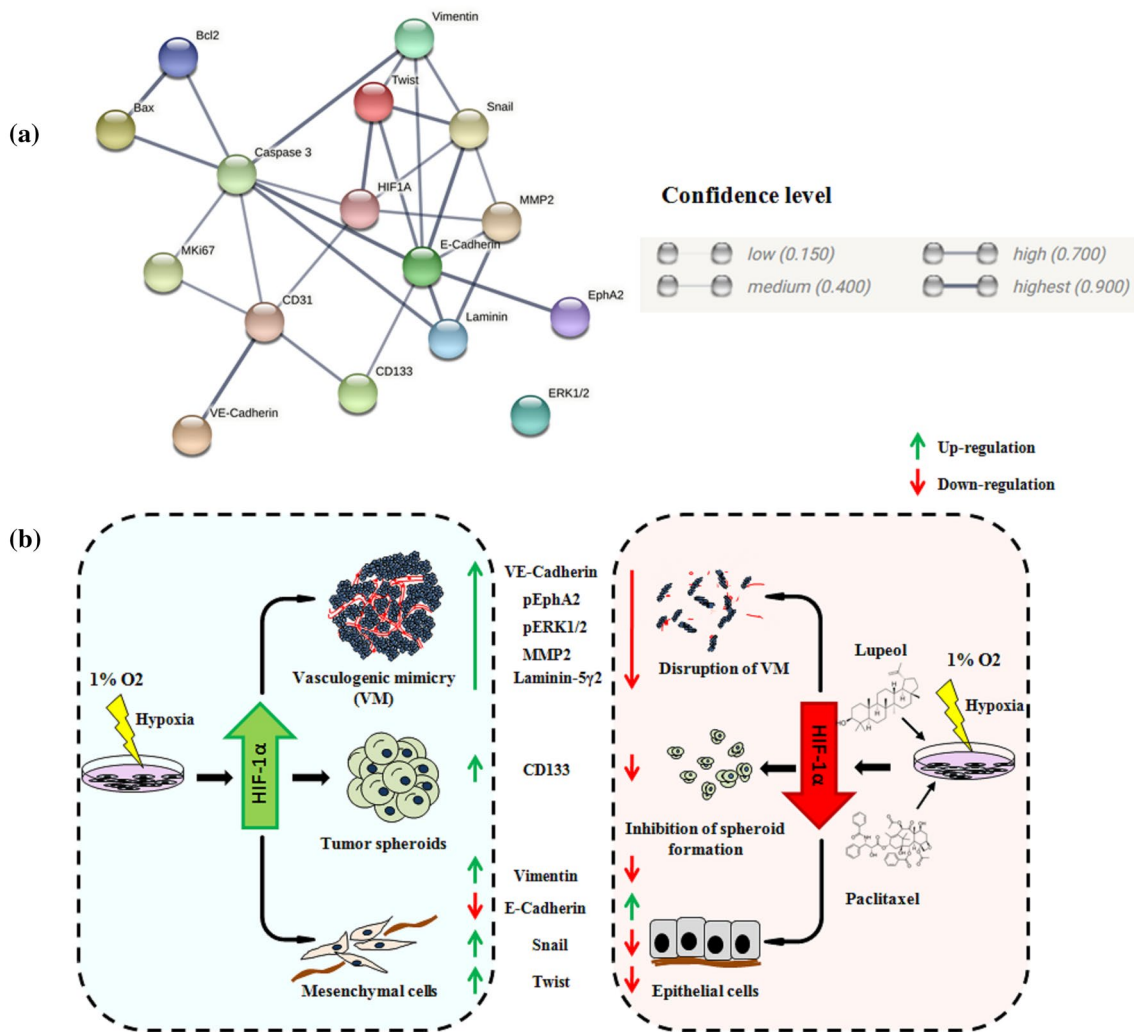


Fig. 7 Model depicting the involvement of HIF1 α and key interacting partners in VM and intervention by Lupeol and Paclitaxel. (a) Protein–protein interaction network analysis using input proteins from the present study on STRING platform showing interacting molecules and confidence level in the network. Legends of confidence level have

been taken from the STRING database. (b) Schematic diagram representing cellular phenotypes, molecular drivers and synergistic effect of Lupeol and Paclitaxel on perturbing hypoxia induced Vasculogenic mimicry in OSCC.

Discussion

Despite the recent advances in tumor biology, the treatment outcome of OSCC patient remains poor. Resistance to anti-angiogenesis and anti-metastatic drugs due to the tumor perfusion through alternative vascularization pathways emerged as a new treatment challenge. VM has been shown to be associated with tumor size, grade, metastasis and poor prognosis in OSCC patients which emphasizes the urgent need for developing novel anti-vascular therapeutic agents that specifically target VM.

Recent studies indicated the prognostic significance of a numbers of VM associated markers including SOX7 (Hong et al. 2021), LGR5 (Wu et al. 2017), ALDH1, Bcl-2, p16 (Wang et al. 2018b), NC11 domain of Collagen XVI (Bedal et al. 2015) in OSCC. However, the molecular mechanisms, underpinning the VM formation, in coordination with other intracellular factors remain elusive. The current study demonstrated an association between hypoxic induction of HIF-1 α and VM formation mainly through modulating the expression of extracellular matrix remodeling protein Laminin-5 γ 2 and elucidated a network that represents the up-regulation of an array of critical players like VE-Cadherin, EphA2, pEphA2 (S-897), pERK1/2 and MMP2. During the siRNA mediated knock-down of HIF-1 α , a disrupted VM formation along with inhibited potential of cellular migration, invasion and stemness was evident under both normoxia and hypoxia in SCC154 and SCC090 cell lines. Hypoxic induction of VM has been reported in lung adenocarcinoma (Fu et al. 2021), hepatocellular carcinoma (Zhang et al. 2020) and breast cancer (Wang et al. 2018a). However, none of the studies have focused upon the hypoxia induced remodeling of ECM components. From these perspectives, our findings suggested a narrative of multifactorial signaling in the hypoxic tumor microenvironment that influences the ECM degradation and metastatic VM formation in OSCC model. We further demonstrated that the hypoxic induction of HIF-1 α augmented EMT in concurrence with stem-like phenotype in OSCC cells through altered expression of E-Cadherin, Vimentin, Snail, Twist and CD133. Previous work by Wang et al. (2019) highlighted the role of VEGFA in hypoxia induced VM formation through regulating EMT and stemness in salivary adenoid cystic carcinoma (SACC). Another study from the same group also indicated the VM forming potential of CD133+ cancer stem like cells in SACC (Wang et al. 2016) highlighting the critical roles of these complementary cellular contexts. The crucial role of EMT in hypoxia induced VM formation has been demonstrated in several other independent studies involving various cancer models (Maroufi et al. 2020, Chen et al. 2019, Li et al. 2019, Wang et al. 2014) covering

diverse indications. However, no evidence supporting hypoxia induced VM formation via EMT has been reported yet in OSCC. From the perspectives of examining therapeutic challenges and opportunities of targeting this key phenotypic cluster, our study also revealed the potential synergistic partnership of Lupeol and Paclitaxel in perturbing the hypoxia induced VM tube formation through the down-regulation of HIF-1 α mediated and Laminin-5 γ 2 driven signaling cascade both in vitro and in patient derived ex vivo system. Several studies have demonstrated that phytochemicals and active compounds from dietary supplements such as green tea extract, hyperforin and silibinin synergistically enhance Paclitaxel response in different cancer models including breast cancer (Barathan et al. 2021), ovarian cancer (Panji et al. 2021), gastric cancer (Zhang et al. 2018). The anticancer activity of Lupeol has been explored in head and neck cancer by inhibiting oncogenic EGFR cascade (Rauth et al. 2016), inducing the intrinsic apoptotic pathway (Bhattacharyya et al. 2017) and downregulating NF- κ B activity (Lee et al. 2007). Though the cytotoxic effect of Lupeol has been studied on various cancer models (Min et al. 2019; Sinha et al. 2019; Malekinejad et al. 2022) the chemo-sensitization potential of Lupeol to amplify the effectiveness of Paclitaxel has not been elucidated yet. To the best of our knowledge, our investigation is the first preclinical study assessing the synergistic potential of Lupeol and common anti-neoplastic drug Paclitaxel in suppressing the vasculogenic mimicry induced by hypoxia both in in vitro and ex vivo OSCC models. Our data comprehensively highlights that Lupeol and Paclitaxel individually exhibited growth inhibitory effects on OSCC cells in a dose dependent manner and the combination index analysis demonstrated that the combination regimen with Lupeol and lower dose of Paclitaxel significantly induced antitumor effects. We have observed synergistic anti-tumor efficacy (CI < 1) with approximately two fold reduction of IC₅₀ dose of Lupeol and four fold reduction of Paclitaxel IC₅₀ dose. The flow cytometric analysis using Annexin-V/PI staining in parallel with fluorescence imaging of TUNEL assay validated that the combined cytotoxic effect of Lupeol/Paclitaxel is causally associated with apoptotic cell death pathway which was consistent with the western blot results showing the alteration of Bax/Bcl2 ratio following the combined treatment of Lupeol and Paclitaxel. Our study further revealed that Lupeol, as a single agent has the potential to inhibit hypoxia induced VM in in vitro and in patient derived ex vivo OSCC model, and its synergistic cooperation with Paclitaxel exhibited an enhanced anti VM effect against OSCC. Earlier the study by Bhattacharyya et al. (2019) indicated the reversing effect of Lupeol on the progression of VM in murine melanoma model by downregulating CD133 expression and Paclitaxel also exhibited an in vitro

VM inhibitory potential in murine glioma model (Liu et al. 2015). However, the exact molecular mechanistic approach that underlines the destruction of VM tubes remained unexplored. In this regard, for the first time our study portrayed that, along with the structural disruption of VM tubes in UPCI: SCC154 and UPCI: SCC090 cell lines, Lupeol decreased the expression of HIF-1 α , leading to the concurrent inhibition of VE-Cadherin, pEphA2 (S-897), pERK1/2, MMP2 and Laminin-5 γ 2. Indeed, its co-treatment with lower dose of Paclitaxel enhanced the down-regulation of key proteins suggesting that Lupeol/Paclitaxel synergism hinders hypoxia induced VM formation in OSCC model and the mechanism may be related to inhibition of HIF-1 α mediated EphA2-Laminin-5 γ 2 axis. Previous studies by Li et al. (2018) and Liu et al. (2018) reported the VM inhibitory effect of Niclosamide and Melatonin in OSCC via up-regulation of miR-124, down-regulation of STAT-3 and through the blockade of ROS reliant AKT/ERK signaling pathways respectively. IL-17F also inhibited the in vitro VM formation in OSCC cells (Almahmoudi et al. 2021). Corresponding to these findings, our study proposed an additional novel therapeutic intervention strategy targeting this potentially actionable perturbation leading to the pseudo-vascular features. Furthermore, our findings also unfolded that, compared to the individual treatment, the combinatorial dose of Lupeol and Paclitaxel revealed pronounced inhibitory effect on the expression of markers related to EMT (Vimentin, Snail, Twist) and CSC (CD133) phenotypes which are critically required for VM formation (Sun et al. 2019; Jue et al. 2017). Consistent with the outcomes of in vitro model, we also demonstrated that a combined treatment of Lupeol and Paclitaxel can proficiently reduce the formation of VM channels in patient derived ex vivo platform via CD31/PAS staining and the immuno-histochemical expression of VM associated markers were also significantly down-regulated in the combination group compared to the individually treated groups. Mechanistically, in this context, the ex vivo data provides key translational insights which will be beneficial for the prediction of therapeutic response in a personalized settings and identifying the most appropriate treatment regimen for individual patients. Collectively, we conjectured from the above findings that Paclitaxel in concert with Lupeol may inhibit hypoxia induced VM formation via down-regulating HIF-1 α -EphA2-Laminin-5 γ 2 cascade and associated EMT and CSC phenomenon in OSCC. Further in vivo investigation in appropriate animal models is critically required to understand their translatability and assess their anti-VM potential for OSCC treatment.

Conclusion

From this study we may conclude that HIF-1 α is a key regulator of OSCC in terms of VM formation and for targeting its downstream signaling components, the synergistic combination of Lupeol and paclitaxel will emerge as a new treatment modality for clinically aggressive oral cancers following evaluation through proper clinical trials in future.

Supplementary Information The online version contains supplementary material available at <https://doi.org/10.1007/s12079-022-00693-z>.

Acknowledgements The study was supported in part by Chittaranjan National Cancer Institute (CNCI), Kolkata, India. Dr. Nabendu Murmu sincerely thanks to Dr. JayantaChakrabarti, Director, CNCI, Kolkata, India for his active support. Ms Depanwita Saha was supported by a Senior Research Fellowship (SRF) from Indian Council of Medical Research (ICMR), Government of India, Sanction No: 3/2/2/112/2022-NCD-III.

Author contributions DS and NM conceptualized and designed the study. DS, DM performed the experiments and analyzed the data. NA, SS supplied tissue specimens. SMM validated the IHC data and provided clinical insights. PKM provided valuable insights into the manuscript. DS, BM and NM drafted the manuscript. BM, PKM and NM reviewed and edited the manuscript. All the authors approved the submitted version of the manuscript.

Funding This work was financially supported by the Science and Engineering Research Board (SERB), Government of India under grant (Project No: EEQ/2016/000345).

Declarations

Conflict of interest Authors declare no conflict of interest.

References

- Ahn MJ, D'Cruz A, Vermorken JB, Chen JP, Chitapanarux I, Dang HQT, Guminski A, Kannarunimi D, Lin TY, Ng WT (2016) Clinical recommendations for defining platinum unsuitable head and neck cancer patient populations on chemoradiotherapy: a literature review. *Oral Oncol* 53:10–16. <https://doi.org/10.1016/j.oraloncology.2015.11.019>
- Almahmoudi R, Salem A, Hadler-Olsen E, Svineng G, Salo T, Al-Samadi A (2021) The effect of interleukin-17F on vasculogenic mimicry in oral tongue squamous cell carcinoma. *Cancer Sci* 112:2223–2232. <https://doi.org/10.1111/cas.14894>
- Al-Rehaily AJ, El-Tahir KEH, Mossa JS, Rafatullah S (2001) Pharmacological studies of various extracts and the major constituent, Lupeol, obtained from hexane extract of *Teclea nobilis* in rodents. *Nat Prod Sci* 7:76–82
- Barathan M, Zulpa AK, Mee Hoong S, Vellamy KM, Vadivelu J (2021) Synergistic effect of hyperforin and Paclitaxel on growth inhibition, apoptotic mediator activation in MCF-7 human breast cancer cells. *J Taibah Univ Sci* 15:918–927. <https://doi.org/10.1080/16583655.2021.2010910>

- Bedal KB, Grassel S, Spanier G, Reichert TE, Bauer RJ (2015) The NC11 domain of human collagen XVI induces vasculogenic mimicry in oral squamous cell carcinoma cells. *Carcinogenesis* 36:1429–1439. <https://doi.org/10.1093/carcin/bgv141>
- Belotti D, Pinessi D, Taraboletti G (2021) Alternative vascularization mechanisms in tumor resistance to therapy. *Cancers (basel)* 13:1912. <https://doi.org/10.3390/cancers13081912>
- Bhattacharyya S, Sekar V, Majumde B, Mehrotra DG, Banerjee S, Bhowmick AK, Alam N, Mandal GK, Biswas J, Majumder PK (2017) CDKN2A-p53 mediated antitumor effect of Lupeol in head and neck cancer. *Cell Oncol (dordr)* 40:145–155. <https://doi.org/10.1007/s13402-016-0311-7>
- Bhattacharyya S, Mitra D, Ray S, Biswas N, Banerjee S, Majumder B, Mustafi SM, Murmu N (2019) Reversing effect of Lupeol on vasculogenic mimicry in murine melanoma progression. *Microvasc Res* 121:52–62. <https://doi.org/10.1016/j.mvr.2018.10.008>
- Bociort F, Macasoi IG, Marcovici I, Motoc A, Grosu C, Pinzaru I, Petean C, Avram S, Dehelean CA (2021) Investigation of lupeol as anti-melanoma agent: an in vitro-in Ovo perspective. *Curr Oncol* 28:5054–5066. <https://doi.org/10.3390/curroncol28060425>
- Borse V, Konwar AN, Buragohain P (2020) Oral cancer diagnosis and perspectives in India. *Sens Int* 1:100046. <https://doi.org/10.1016/j.sintl.2020.100046>
- Che S, Wu S, Yu P (2022) Lupeol induces autophagy and apoptosis with reduced cancer stem-like properties in retinoblastoma via phosphoinositide 3-kinase/protein kinase B/mammalian target of rapamycin inhibition. *J Pharm Pharmacol* 74:208–215. <https://doi.org/10.1093/jpp/rgab060>
- Chen Q, Lin W, Yin Z, Zou Y, Liang S, Ruan S, Chen P, Li S, Shu Q, Cheng B (2019) Melittin inhibits hypoxia-induced vasculogenic mimicry formation and epithelial-mesenchymal transition through suppression of HIF-1 α /Akt pathway in liver cancer. *Evid Based Complement Alternat Med* 2019:9602935. <https://doi.org/10.1155/2019/9602935>
- Chou TC (2010) Drug combination studies and their synergy quantification using the Chou-Talalay method. *Cancer Res* 70:440–446. <https://doi.org/10.1158/0008-5472.CAN-09-1947>
- Delgado-Bellido D, Serrano-Saenz S, Fernández-Cortés OFJ (2017) Vasculogenic mimicry signaling revisited: focus on non-vascular VE-cadherin. *Mol Cancer* 16:65. <https://doi.org/10.1186/s12943-017-0631-x>
- Duan S (2018) Silencing the autophagy-specific gene Beclin-1 contributes to attenuated hypoxia-induced vasculogenic mimicry formation in glioma. *Cancer Biomark* 21:565–574. <https://doi.org/10.3233/CBM-170444>
- Emami Nejad A, Najafgholian S, Rostami A, Sistani A, Shojaeifar S, Esparvarinha M, Nedaenia R, Haghjooy Javanmard S, Taherian M, Ahmadi M (2021) The role of hypoxia in the tumor microenvironment and development of cancer stem cell: a novel approach to developing treatment. *Cancer Cell Int* 21:62. <https://doi.org/10.1186/s12935-020-01719-5>
- Folberg R, Maniotis AJ (2004) Vasculogenic mimicry. *APMIS* 112(7–8):508–525. <https://doi.org/10.1111/j.1600-0463.2004.apm11207-0810.x>
- Fu R, Du W, Ding Z, Wang Y, Li Y, Zhu J, Zeng Y, Zheng Y, Liu Z, Huang J (2021) HIF-1 α promoted vasculogenic mimicry formation in lung adenocarcinoma through NRP1 upregulation in the hypoxic tumor microenvironment. *Cell Death Dis* 12:1–11. <https://doi.org/10.1038/s41419-021-03682-z>
- Hendrix MJ, Sefter EA, Meltzer PS, Gardner LM, Hess AR, Kirschmann DA, Schattman GC, Sefter RE (2001) Expression and functional significance of VE-cadherin in aggressive human melanoma cells: role in vasculogenic mimicry. *Proc Natl Acad Sci U S A* 98:8018–8023. <https://doi.org/10.1073/pnas.131209798>
- Hernández de la Cruz ON, López-González JS, García-Vázquez R, Salinas-Vera YM, Muñoz-Lino MA, Aguilar-Cazares D, López-Camarillo C, Carlos-Reyes Á (2020) Regulation networks driving vasculogenic mimicry in solid tumors. *Front Oncol* 9:1419. <https://doi.org/10.3389/fonc.2019.01419>
- Hess AR, Sefter EA, Gruman LM, Kinch MS, Sefter REB, Hendrix MJ (2006) VE-cadherin regulates EphA2 in aggressive melanoma cells through a novel signaling pathway: implications for vasculogenic mimicry. *Cancer Biol Ther* 5:228–233. <https://doi.org/10.4161/cbt.5.2.2510>
- Hong KO, Oh KY, Yoon HJ, Swarup N, Jung M, Shin JA, Kim JH, Chawla K, Lee JI, Cho SD (2021) SOX7 blocks vasculogenic mimicry in oral squamous cell carcinoma. *J Oral Pathol Med* 50:766–775. <https://doi.org/10.1111/jop.13176>
- Horwitz SB (1994) Taxol (Paclitaxel): mechanisms of action. *Ann Oncol* 5(Suppl 6):S3–6
- Hujanen R, Almahmoudi R, Salo T, Salem A (2021) Comparative analysis of vascular mimicry in head and neck squamous cell carcinoma in vitro and in vivo approaches. *Cancers* 13:4747. <https://doi.org/10.3390/cancers13194747>
- Jue C, Lin C, Zhisheng Z, Yayun Q, Feng J, Min Z, Haibo W, Youyang S, Hisamitsu T, Shintaro I (2017) Notch1 promotes vasculogenic mimicry in hepatocellular carcinoma by inducing EMT signaling. *Oncotarget* 8:2501–2513. <https://doi.org/10.18632/oncotarget.12388>
- Larson AR, Lee CW, Lezcano C, Zhan Q, Huang J, Fischer AH, Murphy GF (2014) Melanoma spheroid formation involves laminin-associated vasculogenic mimicry. *Am J Pathol* 184:71–78. <https://doi.org/10.1016/j.ajpath.2013.09.020>
- Lee TY, Tseng YH (2020) The potential of phytochemicals in oral cancer prevention and therapy: a review of the evidence. *Biomolecules* 10:E1150. <https://doi.org/10.3390/biom10081150>
- Lee TK, Poon RTP, Wo JY, Ma S, Guan XY, Myers JN, Altevogt P, Yuen APW (2007) Lupeol suppresses cisplatin-induced nuclear factor-kappaB activation in head and neck squamous cell carcinoma and inhibits local invasion and nodal metastasis in an orthotopic nude mouse model. *Cancer Res* 67:8800–8809. <https://doi.org/10.1158/0008-5472.CAN-07-0801>
- Li W, Zhou Y (2019) LRIG1 acts as a critical regulator of melanoma cell invasion, migration, and vasculogenic mimicry upon hypoxia by regulating EGFR/ERK-triggered epithelial-mesenchymal transition. *Biosci Rep* 39:bsr20181165
- Li X, Yang Z, Han Z, Wen Y, Ma Z, Wang Y (2018) Niclosamide acts as a new inhibitor of vasculogenic mimicry in oral cancer through upregulation of miR-124 and downregulation of STAT3. *Oncol Rep* 39:827–833. <https://doi.org/10.3892/or.2017.6146>
- Liu K, Zhang X, Xie L, Deng M, Chen H, Song J, Long J, Li X, Luo J (2021) Lupeol and its derivatives as anticancer and anti-inflammatory agents: Molecular mechanisms and therapeutic efficacy. *Pharmacol Res* 164:105373. <https://doi.org/10.1016/j.phrs.2020.105373>
- Liu R, Wang HL, Deng MJ, Wen XJ, Mo YY, Chen FM, Zou CL, Duan WF, Li L, Nie X (2018) Melatonin inhibits reactive oxygen species-driven proliferation, epithelial-mesenchymal transition, and vasculogenic mimicry in oral cancer. *Oxid Med Cell Longev* 2018:3510970. <https://doi.org/10.1155/2018/3510970>
- Liu Y, Mei L, Yu Q, Xu C, Qiu Y, Yang Y, Shi K, Zhang QGH, Zhang Z (2015) Multifunctional tandem peptide modified paclitaxel-loaded liposomes for the treatment of vasculogenic mimicry and cancer stem cells in malignant glioma. *ACS Appl Mater Interfaces* 7:16792–16801. <https://doi.org/10.1021/acsami.5b04596>
- Lu XS, Sun W, Ge CY, Zhang WZ, Fan YZ (2013) Contribution of the PI3K/MMPs/Ln-5 γ 2 and EphA2/FAK/Paxillin signaling pathways to tumor growth and vasculogenic mimicry of gallbladder carcinomas. *Int J Oncol* 42:2103–2115. <https://doi.org/10.3892/ijo.2013.1897>

- Majumder B, Baraneedharan U, Thiagarajan S, Radhakrishnan P, Narasimhan H, Dhandapani M, Brijwani N, Pinto DD, Prasath A, Shanthappa BU (2015) Predicting clinical response to anticancer drugs using an ex vivo platform that captures tumour heterogeneity. *Nat Commun* 6:6169. <https://doi.org/10.1038/ncomms7169>
- Malekinejad F, Kheradmand F, Khadem-Ansari MH, Malekinejad H (2022) Lupeol synergizes with doxorubicin to induce anti-proliferative and apoptotic effects on breast cancer cells. *Daru*. <https://doi.org/10.1007/s40199-022-00436-w>
- Mani SA, Guo W, Liao MJ, Eaton EN, Ayyanan A, Zhou AY, Brooks M, Reinhard F, Zhang CC, Shipitsin M (2008) The epithelial-mesenchymal transition generates cells with properties of stem cells. *Cell* 133:704–715. <https://doi.org/10.1016/j.cell.2008.03.027>
- Maniotis AJ, Folberg R, Hess A, Seftor EA, Gardner LMG, Pe'er J, Trent JM, Meltzer PS, Hendrix MJC (1999) Vascular channel formation by human melanoma cells in vivo and in vitro: vasculogenic mimicry. *Am J Pathol* 155(3):739–752
- Maroufi NF, Amiri M, Dizaji BF, Vahedian V, Akbarzadeh M, Roshanravan N, Haiaty S, Nouri M, Rashidi MR (2020) Inhibitory effect of melatonin on hypoxia-induced vasculogenic mimicry via suppressing epithelial-mesenchymal transition (EMT) in breast cancer stem cells. *Eur J Pharmacol* 881:173282. <https://doi.org/10.1016/j.ejphar.2020.173282>
- Min TR, Park HJ, Ha KT, Chi GY, Choi YH, Park SH (2019) Suppression of EGFR/STAT3 activity by lupeol contributes to the induction of the apoptosis of human non-small cell lung cancer cells. *Int J Oncol* 55:320–330. <https://doi.org/10.3892/ijo.2019.4799>
- Mitra D, Bhattacharyya S, Alam N, Sen S, Mitra S, Mandal S, Vignesh S, Majumder B, Murmu N (2020) Phosphorylation of EphA2 receptor and vasculogenic mimicry is an indicator of poor prognosis in invasive carcinoma of the breast. *Breast Cancer Res Treat* 179:359–370. <https://doi.org/10.1007/s10549-019-05482-8>
- Muz B, de la Puente P, Azab F, Azab AK (2015) The role of hypoxia in cancer progression, angiogenesis, metastasis, and resistance to therapy. *Hypoxia (auckland, N.z.)* 3:83–92. <https://doi.org/10.2147/HP.S93413>
- Nyaboke HO, Moraa M, Omosa LK, Mbayeng AT, Vaderament-Alexe, NN, Masila V, Okemwa E, Efferth T, Kuete V (2018) Cytotoxicity of Lupeol from the Stem Bark of *Zanthoxylum gillettii* against Multi-factorial Drug Resistant Cancer Cell Lines.
- Panji M, Behmard V, Zare Z, Malekpour M, Nejadbiglari H, Yavari S, Nayerpourdizaj T, Safaeian A, Bakhshi A, Abazari O (2021) Synergistic effects of green tea extract and Paclitaxel in the induction of mitochondrial apoptosis in ovarian cancer cell lines. *Gene* 787:145638. <https://doi.org/10.1016/j.gene.2021.145638>
- Patel U, Pandey M (2020) Kannan S (2020) Prognostic and predictive significance of nuclear HIF1 α expression in locally advanced HNSCC patients treated with chemoradiation with or without nimotuzumab. *Br J Cancer* 123:1757–1766. <https://doi.org/10.1038/s41416-020-01064-4>
- Patočka J (2003) Biologically active pentacyclic triterpenes and their current medicine signification. *J Appl Biomed* 1:7–12. <https://doi.org/10.32725/jab.2003.002>
- Pezzani R, Salehi B, Vitalini S, Iriti M, Zuñiga FA, Sharifi-Rad J, Martorell M, Martins N (2019) Synergistic effects of plant derivatives and conventional chemotherapeutic agents: an update on the cancer perspective. *Medicina (kaunas)* 55:110. <https://doi.org/10.3390/medicina55040110>
- Pezzuto A, Carico E (2018) Role of HIF-1 in cancer progression: novel insights. *A Review Curr Mol Med* 18(6):343–351. <https://doi.org/10.2174/1566524018666181109121849>
- Pitchai D, Roy A, Ignatius C (2014) In vitro evaluation of anticancer potentials of lupeol isolated from *Elephantopus scaber* L. on MCF-7 cell line. *J Adv Pharm Technol Res* 5:179–184
- Rauth S, Ray S, Bhattacharyya S, Mehrotra DG, Alam N, Mondal G, Nath P, Roy A, Biswas J, Murmu N (2016) Lupeol evokes anticancer effects in oral squamous cell carcinoma by inhibiting oncogenic EGFR pathway. *Mol Cell Biochem* 417:97–110. <https://doi.org/10.1007/s11010-016-2717-y>
- Ray S, Saha D, Alam N, Mitra Mustafi S, Mandal S, Sarkar A, Majumder B, Murmu N (2021) Exposure to chewing tobacco promotes primary oral squamous cell carcinoma and regional lymph node metastasis by alterations of SDF1 α /CXCR4 axis. *Int J Exp Pathol* 102:80–92. <https://doi.org/10.1111/iep.12386>
- Ren HY, Shen JX, Mao XM, Zhang XY, Zhou P, Li SY, Zheng ZW, Shen DY, Meng JR (2019) Correlation between tumor vasculogenic mimicry and poor prognosis of human digestive cancer patients: a systematic review and meta-analysis. *Pathol Oncol Res* 25:849–858. <https://doi.org/10.1007/s12253-018-0496-3>
- Rousselle P, Scoazec JY (2020) Laminin 332 in cancer: When the extracellular matrix turns signals from cell anchorage to cell movement. *Semin Cancer Biol* 62:149–165. <https://doi.org/10.1016/j.semcancer.2019.09.026>
- Saha D, Mitra D, Alam N, Sen S, Mitra Mustafi S, Mandal S, Majumder B, Murmu N (2022) Orchestrated expression of vasculogenic mimicry and laminin-5 γ 2 is an independent prognostic marker in oral squamous cell carcinoma. *Int J Exp Pathol* 103:54–64. <https://doi.org/10.1111/iep.12430>
- Saleem M (2009) Lupeol, a novel anti-inflammatory and anti-cancer dietary triterpene. *Cancer Lett* 285:109–115. <https://doi.org/10.1016/j.canlet.2009.04.033>
- Sawatani Y, Komiyama Y, Nakashiro KI, Uchida D, Fukumoto C, Shimura M, Hasegawa T, Kamimura R, Hitomi-Koide M, Hyodo T (2020) Paclitaxel potentiates the anticancer effect of cetuximab by enhancing antibody-dependent cellular cytotoxicity on oral squamous cell carcinoma cells in vitro. *Int J Mol Sci* 21:E6292. <https://doi.org/10.3390/ijms21176292>
- Sinha K, Chowdhury S, Banerjee S, Mandal B, Mandal M, Majhi S, Brahmachari G, Ghosh J, Sil PC (2019) Lupeol alters viability of SK-RC-45 (Renal cell carcinoma cell line) by modulating its mitochondrial dynamics. *Heliyon* 5:e02107. <https://doi.org/10.1016/j.heliyon.2019.e02107>
- Sun H, Yao N, Cheng S, Li L, Liu S, Yang Z, Shang G, Zhang D, Yao Z (2019) Cancer stem-like cells directly participate in vasculogenic mimicry channels in triple-negative breast cancer. *Cancer Biol Med* 16:299–311. <https://doi.org/10.20892/j.issn.2095-3941.2018.0209>
- Sung H, Ferlay J, Siegel RL, Laversanne M, Soerjomataram I, Jemal A, Bray F (2021) Global cancer statistics 2020: GLOBOCAN estimates of incidence and mortality worldwide for 36 cancers in 185 Countries. *CA Cancer J Clin* 71:209–249. <https://doi.org/10.3322/caac.21660>
- Thavarool SB, Muttath G, Nayanar S, Duraisamy K, Bhat P, Shringarpure K, Nayak P, Tripathy JP, Thaddeus A, Philip S (2019) Improved survival among oral cancer patients: findings from a retrospective study at a tertiary care cancer centre in rural Kerala. *India World J Surg Oncol* 17:15. <https://doi.org/10.1186/s12957-018-1550-z>
- Wang W, Lin P, Sun B, Zhang S, Cai W, Han C, Li L, Lu H, Zhao X (2014) Epithelial-mesenchymal transition regulated by EphA2 contributes to vasculogenic mimicry formation of head and neck squamous cell carcinoma. *Biomed Res Int* 2014:803914. <https://doi.org/10.1155/2014/803914>
- Wang HF, Wang SS, Zheng M, Dai LL, Wang K, Gao XL, Cao MX, Yu XH, Pang X, Zhang M (2019) Hypoxia promotes vasculogenic mimicry formation by vascular endothelial growth factor A mediating epithelial-mesenchymal transition in salivary adenoid cystic carcinoma. *Cell Prolif* 52:e12600. <https://doi.org/10.1111/cpr.12600>
- Wang SS, Gao XL, Liu X, Gao SY, Fan YL, Jiang YP, Ma XR, Jiang J, Feng H, Chen QM (2016) CD133+ cancer stem-like cells promote migration and invasion of salivary adenoid cystic carcinoma by

- inducing vasculogenic mimicry formation. *Oncotarget* 7:29051–29062. <https://doi.org/10.18632/oncotarget.8665>
- Wang Y, Sun H, Zhang D, Fan D, Zhang Y, Dong X, Liu S, Yang Z, Ni C, Li Y (2018a) TP53INP1 inhibits hypoxia-induced vasculogenic mimicry formation via the ROS/snail signalling axis in breast cancer. *J Cell Mol Med* 22:3475–3488. <https://doi.org/10.1111/jcmm.13625>
- Wang Y, Wang X, Zhang Y, Yu L, Zhu B, Wu S, Wang D (2018b) Vasculogenic mimicry and expression of ALDH1, Beclin1, and p16 correlate with metastasis and prognosis in oral squamous cell carcinoma. *Int J Clin Exp Pathol* 11:1599–1609
- Winkler J, Abisoye-Ogunniyan A, Metcalf KJ, Werb Z (2020) Concepts of extracellular matrix remodelling in tumour progression and metastasis. *Nat Commun* 11:5120. <https://doi.org/10.1038/s41467-020-18794-x>
- Wu Z, Song W, Cheng Z, Yang D, Yu L (2017) Expression of LGR5 in oral squamous cell carcinoma and its correlation to vasculogenic mimicry. *Int J Clin Exp Pathol* 10:11267–11275
- Yue Y, Lou Y, Liu X, Peng X (2021) Vasculogenic mimicry in head and neck tumors: a narrative review. *Transl Cancer Res* 10:3044–3052. <https://doi.org/10.21037/tcr-21-34>
- Zhang JG, Zhou HM, Zhang X, Mu W, Hu JN, Liu GL, Li Q (2020) Hypoxic induction of vasculogenic mimicry in hepatocellular carcinoma: role of HIF-1 α , RhoA/ROCK and Rac1/PAK signaling. *BMC Cancer* 20:32. <https://doi.org/10.1186/s12885-019-6501-8>
- Zhang Y, Ge Y, Ping X, Yu M, Lou D, Shi W (2018) Synergistic apoptotic effects of silibinin in enhancing Paclitaxel toxicity in human gastric cancer cell lines. *Mol Med Rep* 18:1835–1841. <https://doi.org/10.3892/mmr.2018.9129>
- Zhang Z, Imani S, Shasaltaneh MD, Hosseini H, Zou L, Fan Y, Wen Q (2019) The role of vascular mimicry as a biomarker in malignant melanoma: a systematic review and meta-analysis. *BMC Cancer* 19:1134. <https://doi.org/10.1186/s12885-019-6350-5>
- Zhou J, Huang S, Wang L, Yuan X, Dong Q, Zhang D, Wang X (2017) Clinical and prognostic significance of HIF-1 α overexpression in oral squamous cell carcinoma: a meta-analysis. *World J Surg Oncol* 15:104. <https://doi.org/10.1186/s12957-017-1163-y>

Publisher's Note Springer Nature remains neutral with regard to jurisdictional claims in published maps and institutional affiliations.

Springer Nature or its licensor holds exclusive rights to this article under a publishing agreement with the author(s) or other rightsholder(s); author self-archiving of the accepted manuscript version of this article is solely governed by the terms of such publishing agreement and applicable law.

Orchestrated expression of vasculogenic mimicry and laminin-5 γ 2 is an independent prognostic marker in oral squamous cell carcinoma

Depanwita Saha¹ | Debarpan Mitra¹ | Neyaz Alam² | Sagar Sen² |
Saunak Mitra Mustafi³ | Syamsundar Mandal⁴ | Biswanath Majumder⁵ |
Nabendu Murmu¹

¹Department of Signal Transduction and Biogenic Amines, Chittaranjan National Cancer Institute, Kolkata, India

²Department of Surgical Oncology, Chittaranjan National Cancer Institute, Kolkata, India

³Department of Pathology, Chittaranjan National Cancer Institute, Kolkata, India

⁴Department of Epidemiology and Biostatistics, Chittaranjan National Cancer Institute, Kolkata, India

⁵Departments of Molecular Profiling, Cancer Biology and Molecular Pathology, Mitra Biotech, Bangalore, India

Correspondence

Nabendu Murmu, Department of Signal Transduction and Biogenic Amines, Chittaranjan National Cancer Institute, 37, S. P. Mukherjee Road, Kolkata 700026, India.
Email: nabendu.murmu@cnci.ac.in

Present address

Biswanath Majumder, Oncology Division, Bugworks Research, C-CAMP, Bangalore, India

Funding information

This work was financially supported by the Science and Engineering Research Board (SERB), Government of India, under Grant Project No: EEQ/2016/000345.

Abstract

Vasculogenic mimicry (VM), an endothelial cell-independent alternative mechanism of blood supply to the malignant tumour, has long been considered as an adverse prognostic factor in many cancers. The correlation of VM with laminin-5 γ 2 and the assessment of their harmonized expression as an independent risk factor have not been elucidated yet in oral squamous cell carcinoma (OSCC). CD31/PAS staining stratified 116 clinically diagnosed OSCC specimens into VM+ and VM- cohorts. The expression pattern of laminin-5 γ 2 and its upstream modulator MMP2 was evaluated by immunohistochemistry and Western blot. The Kaplan-Meier and Cox regression analyses were performed to assess the survival and prognostic implications. The presence of VM demonstrated a significant correlation with the expression of laminin-5 γ 2 ($p < .001$) and MMP2 ($p < .001$). This pattern was mirrored by the significant upregulation of laminin-5 γ 2 and MMP2 in VM+ cohorts compared with the VM- ones. Furthermore, co-expression of VM and laminin-5 γ 2 was significantly associated with tumour grade ($p = .010$), primary tumour size ($p < .001$), lymph node metastasis ($p = .001$) and TNM stages ($p < .001$) but not with patients' age, gender, tobacco and alcohol consumption habit. Vasculogenic mimicry and laminin-5 γ 2 double-positive cohort displayed a significantly poorer disease-free survival (DFS) and overall survival (OS). Vasculogenic mimicry, laminin-5 γ 2 and their subsequent dual expression underlie a significant prognostic value for DFS [hazard ratio (HR) = 9.896, $p = .028$] and OS [HR = 21.401, $p = .033$] in OSCC patients. Together, our findings imply that VM along with laminin-5 γ 2 is strongly linked to the malignant progression in OSCC and VM and laminin-5 γ 2 coordination emerges as a critical prognostic biomarker for OSCC.

KEYWORDS

co-expression, laminin-5 γ 2, OSCC, prognosis, survival, vasculogenic mimicry

1 | INTRODUCTION

Oral cancer is the 6th most common malignancy in the world.¹ Oral squamous cell carcinoma (OSCC) accounting for over 90% of oral cancers² is one of the most common causes of cancer-related deaths in the developing countries including India and the South-East Asia. The estimated incidence and mortality due to lip, oral cavity cancer in the world are 2.0% and 1.8% respectively.³ Annually 75,000–80,000 new oral cancer cases are being reported in India.⁴ The use of tobacco in various forms including cigarette, bidi, hookah, betel nut and betel quid is the major risk factor for OSCC.⁵ Severe alcoholism, HPV infection, dietary deficiencies and poor oral hygiene are the other common identified risk factors.⁶ Metastasis and postoperative recurrence are the most common reasons for poor 5-year survival⁷ that further increases failure of treatment. There are multiple clinicopathological factors responsible for this poor outcome. Growing tumours survive in the nutrient- and oxygen-deficit state using diverse strategies. In 1999, Maniotis et al.⁸ demonstrated that when blood supply cannot meet the need of rapid tumour growth, some aggressive, metastatic and genetically dysregulated cancer cells mimic the endothelial cells and form pseudovascular channel-like structures called vasculogenic mimicry (VM). It was first described in human uveal melanoma as periodic acid–Schiff (PAS)–positive patterned vascular network and enables the tumours to form matrix-embedded vascular structures carrying plasma and blood cells to fulfil the increasing nutrient and metabolic demands in tumour microenvironment.⁹ Core matrix proteins such as laminin, heparan sulphate proteoglycan and collagens IV and VI have been identified in these patterns.¹⁰ Though vasculogenic mimicry is considered as an established prognostic marker in melanoma,^{11,12} breast cancer,^{13,14} glioblastoma,¹⁵ ovarian cancer,¹⁶ lung cancer,¹⁷ prostate cancer¹⁸ and digestive cancers,¹⁹ the underlying molecular phenotypes inducing it in OSCC and their prognostic significance are poorly understood.

Laminin-5 (Ln-5), a component of extracellular matrix (ECM) adhesion molecules, is expressed predominantly in the epithelial basal membrane structure that promotes static adhesion and hemidesmosome formation.²⁰ However, the cleavage of short arm of $\gamma 2$ subunit of laminin-5 by matrix metalloproteinases (MMPs) such as MMP2 and MT1-MMP leads to its switching from static to migratory form resulting in cell migration and/or invasion.^{21,22} In the context of the molecular mechanism influencing VM, the downstream signalling of VE-cadherin, EphA2 and VEGF choreographs the cleavage of laminin-5 into the pro-migratory $\gamma 2x$ and $\gamma 2'$ fragments through

activated MMP2, implicating the roles of the extracellular matrix remodelling in positively regulating the formation of VM network.²³

Although the differential expression of laminin-5 $\gamma 2$ has been associated with tumour invasion and lymph node metastasis in OSCC^{24,25} and with the poor survival outcome in TCGA database-derived head and neck cancer (HNC) cohorts ($n = 502$),²⁶ its correlation with VM phenotype and the prognostic significance of their coordinated expression have not been elucidated yet. Here, we aim to investigate the phenotypic characteristics of VM structures in OSCC tumour tissues and evaluate the expression of laminin-5 $\gamma 2$ and its upstream modulator MMP2, as well as their correlation in the process of the acquisition of VM structure in OSCC microenvironment. Finally, we have undertaken the survival and risk factor assessment of VM-laminin-5 $\gamma 2$ coordination in a defined patient cohort to enlighten a novel and promising therapeutic target of OSCC.

2 | MATERIALS AND METHODS

2.1 | Patients and tissue samples

The surgical and clinically confirmed OSCC tissue specimens from a sum total of 116 patients (median age: 54 years, range: 28–80 years) were obtained from Chittaranjan National Cancer Institute, Kolkata, during May 2014–April, 2015. Patients with history of recurrence or preoperative chemotherapy and radiotherapy were excluded. Informed written consent was obtained from all the patients prior to specimen collection. The study was approved by the Institutional Ethics committee (IEC Ref: A-4.311/53/2014) in accordance with the ethical guidelines of Declaration of Helsinki (1964) and its later amendments. Tumour-node-metastasis stages were evaluated according to 8th edition of the American Joint Committee on Cancer (AJCC), and tumour grade was classified according to World Health Organization (WHO) standards. For OSCC patients with complete clinicopathological information and follow-up data, the overall survival (OS) time was calculated as the time interval from the date of surgery of the patients to their oral cancer-related death, and disease-free survival (DFS) was noted as the time interval from the date of surgery to the first documentation of local recurrences or distant metastasis. Parameters that are associated with diagnosis, prognosis and treatment of OSCC such as age, anatomic location of primary tumour, histological grade, habit of tobacco and alcohol consumption, tumour size, lymph node metastasis, and TNM stage group have been recorded (Table 1).

2.2 | Immunohistochemistry/PAS dual staining

Immunohistochemistry (IHC) coupled with PAS staining was performed with the primary antibodies against CD31 or PECAM-1 (Santa Cruz Biotechnology, Inc; rabbit monoclonal; clone: M-20, dilution: 1:100), laminin-5 (Y2 chain) (Merck; mouse monoclonal; clone: D4B5, dilution: 1:100) and MMP2 (Novus Biologicals; mouse monoclonal; clone: 8B4, dilution: 1:100) as per previously described methods.^{14,27}

2.3 | Evaluation of vasculogenic mimicry and IHC markers

Vasculogenic mimicry (VM) was identified through the detection of CD31-negative and PAS-positive lumen-like structures surrounded by tumour cells (but not with endothelial cells) with or without red blood cells inside the lumen²⁸⁻³² (Figure 1A). The vascular structures were observed for structural integrity with no incidence of haemorrhage, necrosis or inflammatory cell infiltration in close proximity.³³⁻³⁶ The VM density with respect to the overall vascular density has been assessed according to the modified method described by Weinder et al,³⁷ 1991, Shao et al, 2008,³⁸ and Zhou et al 2019.³⁹ The total number of CD31+ and CD31- lumen-like vascular structures, surrounded by tumour cells or endothelial cells, was considered as the overall vascular density. The areas of highest vascular density were found by observing the slides at 200× magnification. VM vessels were individually counted in 5 randomly selected 200× magnification field. The average percentage of VM has been evaluated relative to the overall vascular density and graded on the basis of following score: 0, negative; 1, <20%; 2, 20-<40%; 3, 40-<60%; and 4, ≥60%. The immunohistochemical score of our studied markers (laminin-5γ2 and MMP2) was determined by considering intensity of staining and proportion (%) of stained cells.⁴⁰⁻⁴⁵ All the staining results were blindly evaluated by two experienced pathologists in a semi-quantitative manner. To account the intra-tumoral heterogeneity of antibody expression, ten randomly selected represented fields (under 400× magnification) from different areas of each slide were evaluated by two qualified pathologists (manual method). The staining intensity was determined on the basis of the following score: 0, negative; 1, mild; 2, moderate; and 3, strong staining, and the percentage (proportion) of positively stained cells per field was scored as follows: 0, <10%; 1, <25% of positively stained cells; 2, <50% of positively stained cells; and 3, >50% of positive cells.⁴⁶⁻⁴⁸ The final immunohistochemical staining score of each sample was determined by summation of staining intensity and percentage (proportion) of positively stained cells, which ranged from 0 to 6. The final staining score 0-3 was considered as negative staining

TABLE 1 Demographic and clinicopathological profile of OSCC patients

Patients' characteristics	n (%)
Age (years)	
<55	62 (53.45)
≥55	54 (46.55)
Gender	
Male	85 (73.28)
Female	31 (26.72)
Tobacco consumption	
Yes	50 (43.10)
No	66 (56.90)
Alcohol consumption	
Yes	10 (8.62)
No	106 (91.38)
Tumour location	
Lip	8 (6.89)
Tongue	17 (14.65)
Buccal mucosa	39 (33.62)
Gingiva	24 (20.69)
Floor of mouth	4 (3.45)
Retromolar trigone (RMT)	5 (4.31)
Others ^a	19 (16.38)
Grade	
Well	73 (62.93)
Moderate	41 (35.34)
Poor	2 (1.72)
Primary tumour status	
T1	64 (55.17)
T2	8 (6.89)
T3	18 (15.52)
T4	26 (22.41)
Lymph node metastasis	
N0	66 (56.89)
N1	27 (23.27)
N2	21 (18.10)
N3	2 (1.72)
TNM stage group	
I (T1N0M0)	50 (43.10)
II (T2N0M0)	5 (4.31)
III (T3N0M0, T1-3N1M0)	23 (19.83)
IV (T4N0M0-T1-4N1-3M0)	38 (32.76)

^aOthers include alveolar mucosa, hard palate and soft palate.

and that of 4-6 was considered as positive staining.^{38,49} The semi-quantitative evaluation of pathologists was further validated by IHC profiler plugin⁵⁰ compatible with ImageJ (Figure S1). To normalize the digital image analysis with the

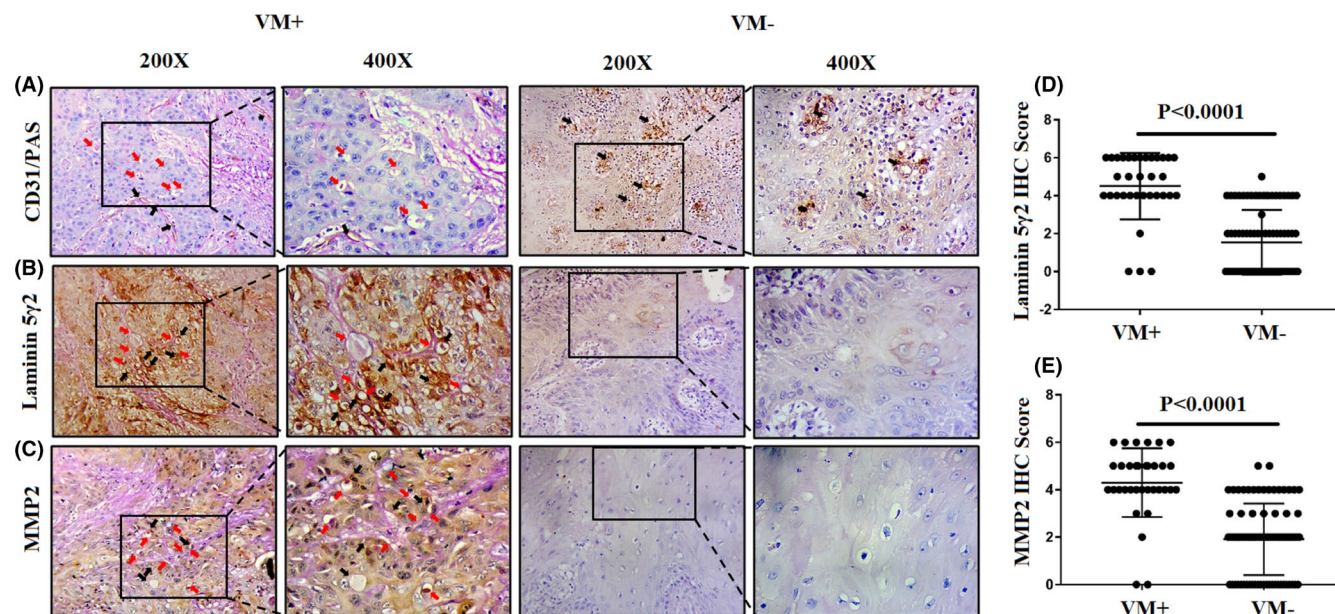


FIGURE 1 (A) CD31-PAS staining showing VM and endothelial structure in OSCC. Red arrows indicate PAS-positive and CD31-negative VM architecture, and black arrows represent endothelial structure showing CD31-positive staining with or without PAS staining (200 \times and 400 \times magnification). Representative images for immunohistochemical status (coupled with PAS staining) of (B) laminin-5 γ 2 and (C) MMP2 in VM-positive and VM-negative OSCC cohorts (200 \times and 400 \times magnification). Red arrows indicate PAS-positive networks, and black arrows indicate specific expression of proteins (B,C). Quantitative analysis of (D) laminin-5 γ 2 and (E) MMP2 expressions was revealed by immunohistochemical scores. The differences between VM-positive and VM-negative groups were calculated by the *t* test ($p < .0001$)

pathologists' manual analysis, the IHC profiler-generated four-tier staining pattern was scored from 0, negative; 1, low positive; 2, moderately positive; and 3, high positive similar to the manual assessment. Further, the total percentage of positive staining (1, low positive; 2, moderately positive; and 3, high positive) was determined from their individual percentage contribution and also scored from 0 to 3 scale in accordance with the pathologists' consideration of score for proportion (%) of stained cells.^{46–48} The final immunohistochemical score (0–6) of each sample was determined by summation of the percentage score of total positive staining and the total intensity score contributed by different degrees of positive staining pattern to harmonize the digital assessment with the manual findings inferring the final score ≤ 3 as negative staining and that of > 3 as positive staining.

2.4 | Western blot

Western blot analysis was performed using 3–5 mg of tissue specimens from few representative samples of both VM+ ($n = 15$) and VM- ($n = 15$) groups as per our previously described methods.⁵¹ Fifty micrograms of total protein extract and appropriate primary antibodies against laminin-5 (γ 2 chain) (Merck; mouse monoclonal; Clone: D4B5, Dilution: 1:100) and MMP2 (Novus Biologicals; mouse monoclonal; Clone: 8B4, Dilution: 1:100) was used. β -Actin was used as a loading control.

2.5 | Statistical analysis

All the statistical analyses were performed using SPSS 17 software (SPSS Inc) and GraphPad Prism version 7.00 software. The chi-squared (χ^2) test was performed to find the associations between clinical-pathological parameters and VM and laminin-5 γ 2, and correlation among laminin-5 γ 2, MMP2 expression and VM was determined by the Spearman correlation test. The *t* test was used to compare two means. Kappa value was calculated to assess the agreement between two pathologists and two methods. The Kaplan–Meier survival analysis followed by the log rank test was used to compare the survival patterns. The multivariate Cox proportional hazard regression model was also used where overall survival (OS) and disease-free survival (DFS) were calculated. $p < .05$ was taken to be statistically significant.

3 | RESULTS

3.1 | Evaluation of VM in OSCC tissue specimens

Vasculogenic mimicry (VM) was identified in 29.31% of OSCC tissue specimens. Based on the CD31/PAS staining, the total patient population was stratified into VM-positive (VM+) and VM-negative (VM-) cohorts (Figure 1A). 34

of 116 (29.31%) cases were VM-positive, and 82 (70.69%) cases were VM-negative.

3.2 | Correlation of VM with the differential expression of laminin-5 γ 2 and MMP2

The immunohistochemical expression of laminin-5 γ 2 and MMP2 was observed in OSCC tumour cell cytoplasm and in tumour stroma. The expression of laminin-5 γ 2 and MMP2 was positively correlated to VM at their individual level ($r = .6642$, $p \leq .001$ and $r = .6201$, $p \leq .001$ respectively), and the expression of laminin-5 γ 2 and MMP2 was also significantly correlated ($r = .5046$ and $p \leq .001$) with each other (Figure S2A–C). The expression pattern of laminin-5 γ 2 and MMP2 in VM-positive and VM-negative cohorts has been represented in Figure 1B,C. The quantitative data indicated the significantly elevated expression of laminin-5 γ 2 and MMP2 in VM-positive cohorts ($p < .0001$; Figure 1D,E). The mean immunohistochemical score of laminin-5 γ 2 and MMP2 in VM-positive cohorts was 4.50 ± 1.75 and 4.29 ± 1.45 (mean \pm SD), respectively, whereas the same for the VM-negative cohorts was 1.74 ± 1.54 and 1.91 ± 1.51 respectively. Figure S1 shows the significantly positive correlation ($R^2 > .9$, $p < .001$) between the IHC scoring of two pathologists and between digital and manual methods. Kappa statistics was used to assess the interobserver and intermethod agreement, which revealed almost perfect strength of agreement ($\kappa = 0.81$ – 1.00) between the scoring of two pathologists and substantial strength of agreement ($\kappa = 0.61$ – 0.80)⁵² between digital and manual methods confirming the reliability of our IHC scoring method. The differential expressional status of the studied markers was also validated through quantitative Western blot analysis (Figure S2D,E), which indicated significantly higher intensity of immunoreactive bands in VM-positive groups compared with the VM-negative ones ($p < .05$).

3.3 | Association of VM and laminin-5 γ 2 with the clinicopathological features

The association of individual and coordinated expression of VM and laminin-5 γ 2 with the clinicopathological characteristics of patients has been summarized in Table 2. The result showed 30 (25.86%) VM–laminin-5 γ 2 double-positive cases, 4 (3.44%) VM-positive laminin-5 γ 2 negative cases, 21 (18.10%) VM-negative laminin-5 γ 2–positive cases and 61 (52.58%) VM–laminin-5 γ 2 double-negative cases. The presence of vasculogenic mimicry in OSCC was significantly associated with tumour grade ($p = .002$),

primary tumour status ($p < .001$), lymph node metastasis ($p = .005$) and TNM stage group ($p < .001$) but not with patient's age, sex and tobacco or alcohol consumption habit. It has been significantly found that 50% (1/2) cohort of the poorly differentiated tumour grade developed VM, whereas 48.78% (20/41) of the moderately differentiated group and 17.80% (13/73) of the well-differentiated group were found to be VM-positive. It is also noteworthy that 59.09% (26/44) patients of T3 and T4 primary tumour status significantly developed VM compared with the T1 and T2 group [11.11% (8/72)]. Similarly, the occurrence of VM was also significantly prevalent in the patients with positive nodal status compared with the negative ones [46% (23/50) vs 16.66% (11/66)], as well as in the patients with TNM stage groups III and IV [47.54% (29/61)] compared with TNM stage groups I and II [9.09% (5/55)]. The positive rate of VM was also significantly associated with the expression of laminin-5 γ 2 in OSCC. 43.9% of the total patients (51/116) showed positive expression of laminin-5 γ 2. Among them, the VM-positive group was found to have significantly increased level of expression of laminin-5 γ 2 [88.23% (30/34)] compared with the VM-negative [25.61% (21/82)] counterparts. Similar to the findings for the association of VM with the clinicopathological features, the positive expression of laminin-5 γ 2 was mostly observed in the patients with T3 and T4 primary tumour status (68.18%, $p < .001$) and TNM stage groups III and IV (57.37%, $p = .002$). Interestingly, the double-positive expressional status of VM–laminin-5 γ 2 was also significantly associated with tumour grade ($p = .010$), primary tumour status ($p < .001$), lymph node metastasis ($p = .00133$) and TNM stage group ($p < .001$) indicating the strong correlation between VM and laminin-5 γ 2 in the pathogenesis of OSCC. In addition to laminin-5 γ 2, we have also found a significant positive association of its upstream modulator MMP2 with VM ($p < .001$; Table S1). In association with the significant positive correlation of MMP2 with VM and laminin-5 γ 2, we have also demonstrated the significant association of MMP2 and VM–MMP2 dual positivity with the other established prognostic features of OSCC (Table S1). These data indicated the deterministic role of laminin-5 γ 2 and its activator molecule MMP2 in the occurrence of VM and progression of OSCC.

3.4 | Correlation of the positive expression of laminin-5 γ 2 and VM with disease-free and overall survival

To understand the collaborative prognostic significance of VM–laminin-5 γ 2, the 5-year survival rate was calculated for total of 116 patients with respect to DFS and OS. After completion of the follow-up (median follow-up

TABLE 2 Association between VM, laminin-5 γ 2 and their dual expression with clinicopathological characteristics of oral squamous cell carcinoma (OSCC)

Patients' characteristics	VM				Laminin-5 γ 2				VM and laminin-5 γ 2 dual expression			
	Positive	Negative			Positive	Negative			Positive	Negative		
	n (%)	n (%)	χ^2	p value	n (%)	n (%)	χ^2	p value	n (%)	n (%)	χ^2	p value
Age (years)												
<55	17 (14.65)	45 (38.79)	0.230	0.632	23 (19.83)	39 (33.62)	2.55	0.110	14 (12.07)	48 (41.38)	0.748	0.387
\geq 55	17 (14.65)	37 (31.89)			28 (24.14)	26 (22.41)			16 (13.79)	38 (32.76)		
Gender												
Male	23 (19.83)	62 (53.45)	0.778	0.378	37 (31.89)	48 (41.38)	0.02	0.875	20 (17.24)	65 (56.03)	0.903	0.342
Female	11 (9.48)	20 (17.24)			14 (12.07)	17 (14.65)			10 (8.62)	21 (18.10)		
Tobacco consumption												
Yes	12 (10.34)	38 (32.76)	1.20	0.274	19 (16.37)	31 (26.72)	1.27	0.260	12 (10.34)	38 (32.76)	0.159	0.690
No	22 (18.96)	44 (37.93)			32 (27.59)	34 (29.31)			18 (15.52)	48 (41.38)		
Alcohol consumption												
Yes	2 (1.72)	8 (6.89)	0.458	0.499	2 (1.72)	8 (6.89)	2.55	0.110	2 (1.72)	8 (6.89)	0.196	0.658
No	32 (27.59)	74 (63.79)			49 (42.24)	57 (49.14)			28 (24.14)	78 (67.24)		
Grade												
Well	13 (11.21)	60 (51.72)	12.6	0.002*	28 (24.14)	45 (38.79)	2.53	0.283	12 (10.34)	61 (52.59)	9.19	0.010*
Moderate	20 (17.24)	21 (18.10)			22 (18.96)	19 (16.38)			17 (14.65)	24 (20.69)		
Poor	1 (0.86)	1 (0.86)			1 (0.86)	1 (0.86)			1 (0.86)	1 (0.86)		
Primary tumour status												
T1	5 (4.31)	59 (50.86)	33.6	<0.001*	17 (14.65)	47 (40.52)	18.5	<0.001*	4 (3.45)	60 (51.72)	30.4	<0.001*
T2	3 (2.59)	5 (4.31)			4 (3.45)	4 (3.45)			3 (2.59)	5 (4.31)		
T3	10 (8.62)	8 (6.90)			12 (10.34)	6 (5.17)			8 (6.89)	10 (8.62)		
T4	16 (13.79)	10 (8.62)			18 (15.52)	8 (6.89)			15 (12.93)	11 (9.48)		
Lymph node metastasis												
N0	11 (9.48)	55 (47.41)	12.9	0.005*	20 (17.24)	46 (39.65)	6.91	0.075	8 (6.89)	58 (50)	15.7	0.001*
N1	14 (12.07)	13 (11.21)			16 (13.79)	11 (9.48)			13 (11.21)	14 (12.07)		
N2	8 (6.89)	13 (11.21)			14 (12.07)	7 (6.03)			8 (6.89)	13 (11.21)		
N3	1 (0.86)	1 (0.86)			1 (0.86)	1 (0.86)			1 (0.86)	1 (0.86)		
TNM stage group												
I+II	5 (4.31)	50 (43.10)	20.6	<0.001*	16 (13.79)	39 (33.62)	9.39	0.002*	4 (3.45)	51 (43.96)	18.9	<0.001*
III+IV	29 (25)	32 (27.59)			35 (30.17)	26 (22.41)			26 (22.41)	35 (30.17)		

TABLE 2 (Continued)

Patients' characteristics	VM			Laminin-5 γ 2			VM and laminin-5 γ 2 dual expression		
	Positive n (%)	Negative n (%)	χ^2	Positive n (%)	Negative n (%)	χ^2	Positive n (%)	Negative n (%)	χ^2
VM									
Positive	-	-	-	30 (25.86)	4 (3.45)	38.3	-	-	<0.001*
Negative	-	-	-	21 (18.10)	61 (52.59)	-	-	-	-

* Significant values i.e. $p < 0.05$ are denoted in bold.

period: 56 months, range: 16–60 months), 36 patients (31.03%) were dead due to local recurrence or metastasis after surgery and 62 (53.45%) patients were alive with the rest being lost to follow-up or died of other diseases unrelated to OSCC and they were considered as censored for further analysis. The Kaplan–Meier plot of DFS and OS in OSCC patients with differential status of VM, laminin-5 γ 2 and their dual existence have been shown in Figure 2. The follow-up data demonstrated that the mean DFS of VM-positive cohort and laminin-5 γ 2-positive cohort was significantly inferior to that of VM-negative (log rank = 92.052, $p < .001$) and laminin-5 γ 2-negative (log rank = 40.575, $p < .001$) cohort; VM–laminin-5 γ 2 double-positive cohort also had significantly worse DFS compared with the respective double-negative cohorts (log rank = 125.283, $p < .001$). The distinguishing DFS rate among these groups was also reflected with the OS time. The mean OS of VM-positive cohort, laminin-5 γ 2-positive cohort and VM–laminin-5 γ 2 double-positive cohort was significantly poorer than that of VM-negative (log rank = 80.363, $p < .001$), laminin-5 γ 2 negative (log rank = 45.209, $p < .001$) and VM–laminin-5 γ 2 double-negative (log rank = 114.464, $p < .001$) cohorts respectively. These findings interpreted that VM and laminin-5 γ 2 either individually or together are important indicators of DFS and OS in OSCC patients. Additionally, we have also found the significant difference in the Kaplan–Meier plot of DFS and OS in the OSCC patients with differential expression of MMP2 and of VM–MMP2 duality (Figure S3).

3.5 | Prognostic impact of paired VM–laminin-5 γ 2 positivity on disease-free and overall survival

Based on the significant findings of univariate analysis, indicating the significance of clinicopathological parameters such as tumour grade, primary tumour status, lymph node metastasis, TNM stage group and occurrence of VM independently, as well as in conjunction with the expression of laminin-5 γ 2 in DFS and OS, the multivariate Cox proportional hazard regression model was applied to assess their role as independent survival risk factors (Table 3). The multivariate analysis revealed that in addition to primary tumour status and lymph node metastasis, the occurrence of VM [hazard ratio (HR): 1.696; 95% CI :1.030–2.791; $p = .038$], positive expression of laminin-5 γ 2 (HR: 1.327; CI: 1.013–1.739; $p = .040$) and VM–laminin-5 γ 2 double-positive status (HR: 9.896; CI: 1.286–76.173; $p = .028$) were proved to be independent risk factors for DFS. Similar to DFS, the occurrence of VM (HR: 3.081; CI: 1.428–6.651; $p = .004$), positive expression of laminin-5 γ 2 (HR: 1.424;

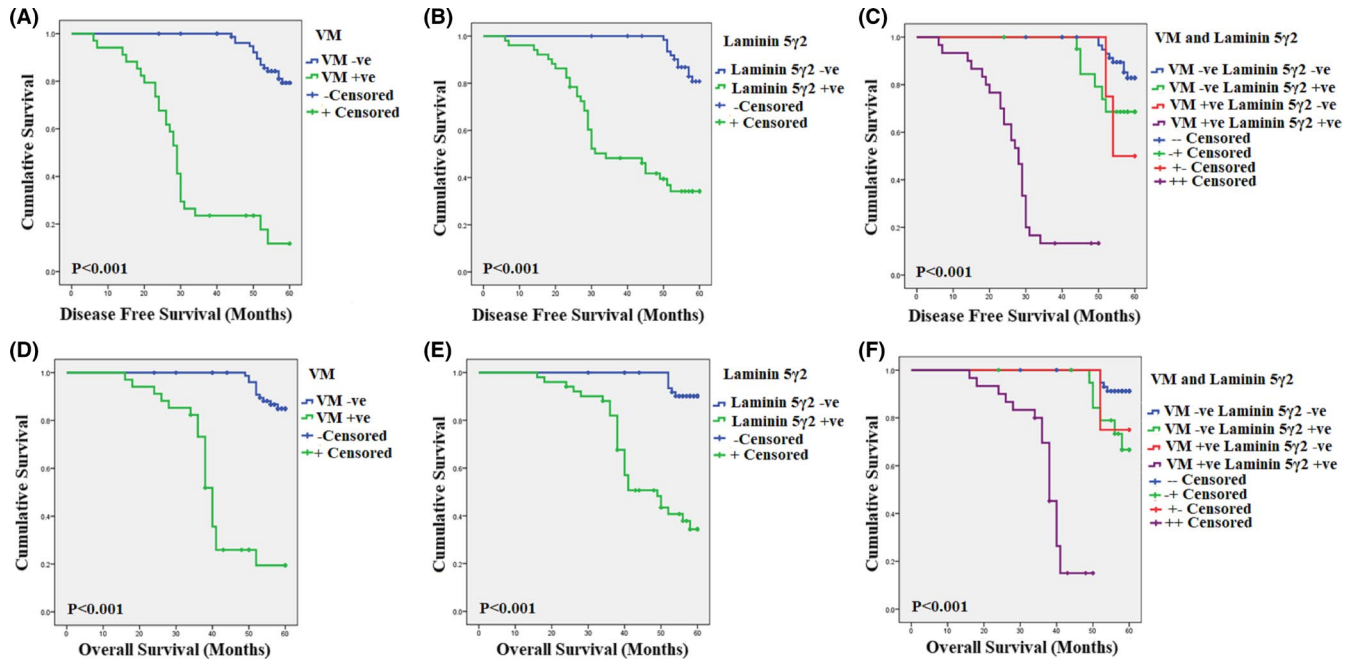


FIGURE 2 Kaplan–Meier analysis of the disease-free survival (DFS) and overall survival (OS) rate of patients with OSCC. DFS of patients in relation to (A) VM, (B) differential expressional status of laminin-5γ2, (C) VM and laminin-5γ2 dual status and OS of patients in relation to (D) VM, (E) differential expressional status of laminin-5γ2, (F) VM and laminin-5γ2 dual status

TABLE 3 Assessment of prognostic factors of disease-free survival (DFS) and overall survival (OS) by multivariate analysis of Cox proportional hazard model

Variables	Disease-free survival (DFS)				Overall survival (OS)			
	HR	p value	95% CI		HR	p value	95% CI	
			Lower	Upper			Lower	Upper
Grade	1.759	0.099	0.900	3.439	1.219	0.625	0.551	2.699
Primary tumour status	1.821	0.003*	1.221	2.717	1.559	0.054	0.992	2.449
Lymph node metastasis	2.944	<0.001*	1.632	5.311	2.865	0.002*	1.478	5.554
TNM stage group	0.307	0.123	0.068	1.379	0.494	0.486	0.068	3.589
VM only	1.696	0.038*	1.030	2.791	3.081	0.004*	1.428	6.651
Laminin-5γ2 only	1.327	0.040*	1.013	1.739	1.424	0.026*	1.043	1.945
VM and Laminin-5γ2 double positive	9.896	0.028*	1.286	76.173	21.401	0.033*	1.276	358.980
MMP2 only	1.091	0.582	0.801	1.485	1.084	0.697	0.721	1.630
VM and MMP2 double positive	1.047	0.951	0.238	4.619	0.282	0.232	0.035	2.251

* Significant values i.e. $p < 0.05$ are denoted in bold.

CI: 1.043–1.945; $p = .026$) and the simultaneous double-positive expression of VM–laminin-5γ2 (HR: 21.401; CI: 1.276–358.980; $p = .033$) were also found to be independent risk factor for OS. In support of the significant findings on the survival endpoints, the positive expression of MMP2 and its co-existence with VM were also considered for the analysis of risk factor assessment, but neither of them proved to be the independent prognostic factor for DFS and OS in our OSCC cohorts.

4 | DISCUSSION

Alternative vascularization influences the poor prognosis of cancer patients,^{53,54} evoking tumour resistance towards anti-angiogenic and anti-neoplastic therapy.⁵⁵ Vasculogenic mimicry is a leading pathological entity representing this state to which prompted us for a more comprehensive evaluation of VM and associated prognostic biomarkers underpinning in OSCC.

In this present study, we have evaluated the correlation of VM with expression of laminin-5 γ 2 in predicting the survival and prognosis of OSCC. We have inferred that the occurrence of VM is significantly prevalent in the poorly differentiated tumour with increased primary tumour size, higher lymph-node metastasis and TNM stage, which reflected the mechanistic link of VM to the invasion and metastasis attributing the aggressive and malignant progression of OSCC. Contextually, commonalities have been observed in other malignant tumours.^{56,57} Laminin-5 γ 2 complements ECM remodelling and is considered to be one of the most common downstream signalling proteins in molecular cascades associated with VM, that is TGF- β ,⁵⁸ VE-cadherin, EphA2, PI3-K⁵⁹ and MMP2.^{60,61} Moreover, laminin receptor integrin β 1-mediated FAK signalling has also been associated with VM-like network formation in human fibrosarcoma cells.⁶² On the contrary, the cooperative interaction between MMP2 and laminin-5 γ 2 has been well established in a number of malignancies including glioblastoma⁵⁸ and aggressive melanoma when cultured on a three-dimensional ECM.⁶³ Our study delineated a significant interrelation of VM, laminin-5 γ 2 and their coordinated alignment with the histological and conventional prognostic parameters such as tumour grade, primary tumour size, lymph node metastasis and TNM stage group highlighting the impact of integrating multiple facets of these markers that may benefit while assessing the risk factors in OSCC. The double positivity of vasculogenic mimicry–laminin-5 γ 2, as well as their individual positive expression, also had the significantly poorer DFS and OS in our study, which may act as a tool to predict a worse prognostic indication. Although a few recent studies indicated the individual prognostic significance of some VM-associated biomarkers including LGR5,⁶⁴ ALDH1, Beclin1, p16⁴⁹ and extracellular IL17-F,⁶⁵ the combinatorial approach of VM with its associated biomarkers^{14,66} is still a less explored area in OSCC. In this context, our investigation confirmed for the first time that both VM and laminin-5 γ 2 in combination provide better prognostic significance with higher statistical power including increased hazard ratio [(HR) = 9.896, p = .028 (DFS) and HR = 21.401, p = .033 (OS)] compared with individual expression of VM [(HR) = 1.696, p = .038 (DFS) and HR = 3.081, p = .004 (OS)] and laminin-5 γ 2 [HR] = 1.327, p = .040 (DFS) and HR = 1.424, p = .026 (OS)]. Collectively, these findings indicate the complementarity of VM and laminin-5 γ 2 as powerful risk factor for DFS and OS in OSCC. Our study also illustrated that in spite of being the upstream modulator of laminin-5 γ 2, MMP2 was not found to be performed as an independent risk factor in association with VM. We further validated the manual quantification data with the inputs from automatic profiler and showed a linear pattern.⁶⁷ Indeed,

digital quantitative pathology is an evolving modality and needs further validation before its routine adoption as stand-alone method. Knowing the therapeutic challenges of late refractory oral malignancies and roles of novel prognostic biomarkers in informed treatment decision, these findings will provide important contextual guidance for defining appropriate clinical strategies.

In conclusion, the study revealed that the expression of the extracellular matrix protein Laminin-5 γ 2 coordinated with VM is significantly associated with tumour grade, primary tumour size, lymph node metastasis and TNM stage. Co-expression of vasculogenic mimicry with laminin-5 γ 2 underlines the independent prognostic impact and correlates with the decreased disease-free and overall survival in OSCC patients. Further validation of these findings in large independent studies would provide important predictive opportunities for better guidance towards effective treatments.

ACKNOWLEDGEMENT

The study was supported in part by the Chittaranjan National Cancer Institute (CNCI), Kolkata, India. Dr Nabendu Murmu sincerely thanks Dr Jayanta Chakrabarti, Director, CNCI, Kolkata, India, for his active support.

CONFLICT OF INTEREST

None.

AUTHOR CONTRIBUTIONS

DS and NM conceptualized and designed the study. DS and DM performed the experiments and analysed the data. NA and SS supplied tissue specimens. SMM validated the data and provided clinical insights. SM interpreted the data and performed statistical analysis. DS, BM and NM drafted the manuscript. BM and NM reviewed and edited the manuscript. All the authors approved the final version of the manuscript.

REFERENCES

1. Borse V, Konwar AN, Buragohain P. Oral cancer diagnosis and perspectives in India. *Sens Int*. 2020;1:100046.
2. Tandon P, Dadhich A, Saluja H, Bawane S, Sachdeva S. The prevalence of squamous cell carcinoma in different sites of oral cavity at our Rural Health Care Centre in Loni, Maharashtra – a retrospective 10-year study. *Contemp Oncol (Pozn)*. 2017;21(2):178-183.
3. Sung H, Ferlay J, Siegel RL, et al. Global Cancer Statistics 2020: GLOBOCAN estimates of incidence and mortality worldwide for 36 Cancers in 185 countries. *CA Cancer J Clin*. 2021;1-121.
4. Mishra N. Oral cancer: a study in retrospection. *Natl J Maxillofac Surg*. 2019;10(1):1-2.
5. Tenore G, Nuvoli A, Mohsen A, et al. Tobacco, alcohol and family history of cancer as risk factors of oral squamous cell carcinoma: case-control retrospective study. *Applied Sci*. 2020;10(11):3896. doi:10.3390/app10113896

6. Khalesi S. A review of head and neck squamous cell carcinoma risk factors with more focus on oral cancer. *J Dent & Oral Disord.* 2016;2(6):1032.
7. Sun L, Chin RI, Gastman B, et al. Association of disease recurrence with survival outcomes in patients with cutaneous squamous cell carcinoma of the head and neck treated with multimodality therapy. *JAMA Dermatol.* 2019;155(4):442-447.
8. Maniotis AJ, Folberg R, Hess A, et al. Vascular channel formation by human melanoma cells in vivo and in vitro: vasculogenic mimicry. *Am J Pathol.* 1999;155(3):739-752.
9. Folberg R, Hendrix MJ, Maniotis AJ. Vasculogenic mimicry and tumor angiogenesis. *Am J Pathol.* 2000;156(2):361-381.
10. Folberg R, Maniotis AJ. Vasculogenic mimicry. *APMIS.* 2004;12(7-8):508-525.
11. Zhang Z, Imani S, Shasaltaneh MD, et al. The role of vascular mimicry as a biomarker in malignant melanoma: a systematic review and meta-analysis. *BMC Cancer.* 2019;19(1):1134.
12. Bhattacharyya S, Mitra D, Ray S, et al. Reversing effect of Lupeol on vasculogenic mimicry in murine melanoma progression. *Microvasc Res.* 2019;121:52-62.
13. Andonegui-Elguera MA, Alfaro-Mora Y, Cáceres-Gutiérrez R, Caro-Sánchez C, Herrera LA, Díaz-Chávez J. An overview of vasculogenic mimicry in breast cancer. *Front Oncol.* 2020;10:220.
14. Mitra D, Bhattacharyya S, Alam N, et al. Phosphorylation of EphA2 receptor and vasculogenic mimicry is an indicator of poor prognosis in invasive carcinoma of the breast. *Breast Cancer Res Treat.* 2020;179(2):359-370.
15. Yue WY, Chen ZP. Does vasculogenic mimicry exist in astrocytoma? *J Histochem Cytochem.* 2005;53(8):997-1002.
16. Yu L, Zhu B, Wu S, et al. Evaluation of the correlation of vasculogenic mimicry, ALDH1, KiSS-1, and MACC1 in the prediction of metastasis and prognosis in ovarian carcinoma. *Diagn Pathol.* 2017;12(1):23.
17. Wang Y, Yang R, Wang X, et al. Evaluation of the correlation of vasculogenic mimicry, Notch4, DLL4, and KAI1/CD82 in the prediction of metastasis and prognosis in non-small cell lung cancer. *Medicine (Baltimore).* 2018;97(52):e13817.
18. Sharma N, Seftor RE, Seftor EA, et al. Prostatic tumor cell plasticity involves cooperative interactions of distinct phenotypic subpopulations: role in vasculogenic mimicry. *Prostate.* 2002;50(3):189-201.
19. Ren HY, Shen JX, Mao XM, et al. Correlation between tumor vasculogenic mimicry and poor prognosis of human digestive cancer patients: a systematic review and meta-analysis. *Pathol Oncol Res.* 2019;25(3):849-858.
20. Giannelli G, Antonaci S. Biological and clinical relevance of Laminin-5 in cancer. *Clin Exp Metastasis.* 2000;18(6):439-443. doi:10.1023/a:1011879900554
21. Malina R, Motoyama S, Hamana S, Maruo T. Laminin-5 gamma2 chain and matrix metalloproteinase-2 expression in the neoplastic changes of uterine cervical squamous epithelium. *Kobe J Med Sci.* 2004;50(3-4):123-130.
22. Rousselle P, Scoazec JY. Laminin 332 in cancer: when the extracellular matrix turns signals from cell anchorage to cell movement. *Semin Cancer Biol.* 2020;62:149-165.
23. Delgado-Bellido D, Serrano-Saenz S, Fernández-Cortés M, Oliver FJ. Vasculogenic mimicry signaling revisited: focus on non-vascular VE-cadherin. *Mol Cancer.* 2017;16(1):65.
24. Yellapurkar S, Natarajan S, Boaz K. Expression of laminin in oral squamous cell carcinomas. *Asian Pac J Cancer Prev.* 2018;19(2):407-441.
25. Ono Y, Nakanishi Y, Ino Y. Clinicopathologic significance of laminin-5 γ 2 chain expression in squamous cell carcinoma of the tongue immunohistochemical analysis of 67 lesions. *Cancer.* 1999;85(11):2315-2321.
26. You GR, Cheng AJ, Lee LY, et al. Prognostic signature associated with radioresistance in head and neck cancer via transcriptomic and bioinformatic analyses. *BMC Cancer.* 2019;19(1):64.
27. Sun B, Qie S, Zhang S, et al. Role and mechanism of vasculogenic mimicry in gastrointestinal stromal tumors. *Hum Pathol.* 2008;39:444-451.
28. Wang W, Lin P, Sun B, et al. Epithelial-mesenchymal transition regulated by EphA2 contributes to vasculogenic mimicry formation of head and neck squamous cell carcinoma. *Biomed Res Int.* 2014;2014:1-10.
29. Liu R, Yang K, Meng C, Zhang Z, Xu Y. Vasculogenic mimicry is a marker of poor prognosis in prostate cancer. *Cancer Biol Ther.* 2012;13(7):527-533.
30. Zhao B, Wu M, Hu Z, et al. Thrombin is a therapeutic target for non-small-cell lung cancer to inhibit vasculogenic mimicry formation. *Sig Transduct Target Ther.* 2020;5:117.
31. Meng J, Chen S, Lei Yy H, et al. Hsp90 β promotes aggressive vasculogenic mimicry via epithelial-mesenchymal transition in hepatocellular carcinoma. *Oncogene.* 2019;38:228-243.
32. You B, Sun Y, Luo J, et al. Androgen receptor promotes renal cell carcinoma (RCC) vasculogenic mimicry (VM) via altering TWIST1 nonsense-mediated decay through lncRNA-TANAR. *Oncogene.* 2021;40:1674-1689.
33. Sun B, Zhang S, Zhang D, et al. Vasculogenic mimicry is associated with high tumor grade, invasion and metastasis, and short survival in patients with hepatocellular carcinoma. *Oncol Rep.* 2006;16(4):693-698.
34. Yu P, Zhu X, Zhu JL, et al. The Chk2-PKM2 axis promotes metabolic control of vasculogenic mimicry formation in p53-mutated triple-negative breast cancer. *Oncogene.* 2021;40:5262-5274.
35. Cheng L, Wang Q, Tao X, et al. FOXM1 induces vasculogenic mimicry in esophageal cancer through β -catenin/Tcf4 signaling. *Diagn Pathol.* 2020;15:14.
36. Shao B, Zhao X, Liu T, et al. LOXL2 promotes vasculogenic mimicry and tumour aggressiveness in hepatocellular carcinoma. *J Cell Mol Med.* 2019;23(2):1363-1374.
37. Weidner N, Semple JP, Welch WR, Folkman J. Tumor angiogenesis and metastasis – correlation in invasive breast carcinoma. *New Engl J Med.* 1991;324:1-8.
38. Shao Z, Zhang WF, Chen XM, Shang ZJ. Expression of EphA2 and VEGF in squamous cell carcinoma of the tongue: correlation with the angiogenesis and clinical outcome. *Oral Oncol.* 2008;44(12):1110-1117.
39. Zhou Y-T, Cai W-W, Li Y, et al. Correlations between quantitative parameters of contrast-enhanced ultrasound and vasculogenic mimicry in murine tumor model: a novel noninvasive technique for assessment? *Biol Proced Online.* 2019;21(1):11.
40. McCarty KS, Szabo E, Flowers JL, et al. Use of a monoclonal anti-estrogen receptor antibody in the immunohistochemical evaluation of human tumors. *Cancer Res.* 1986;46:4244s-4248s.

41. Krajewska M, Krajewski S, Epstein JI, et al. Immunohistochemical analysis of bcl-2, bax, bcl-X, and mcl-1 expression in prostate cancers. *Am J Pathol*. 1996;148(5):1567-1576.
42. Gkouveris I, Nikitakis N, Avgoustidis D, Karanikou M, Rassidakis G, Sklavounou A. ERK1/2, JNK and STAT3 activation and correlation with tumor differentiation in oral SCC. *Histol Histopathol*. 2017;32(10):1065-1076.
43. Wu DH, Wang TT, Ruan DY, et al. Combination of ULK1 and LC3B improve prognosis assessment of hepatocellular carcinoma. *Biomed Pharmacother*. 2018;97:195-202.
44. Kukita A, Sone K, Oda K, et al. Histone methyltransferase SMYD2 selective inhibitor LLY-507 in combination with poly ADP ribose polymerase inhibitor has therapeutic potential against high-grade serous ovarian carcinomas. *Biochem Biophys Res Commun*. 2019;513(2):340-346.
45. Zhou W, Chen H, Ruan Y, Zeng X, Liu F. High expression of TRIM15 is associated with tumor invasion and predicts poor prognosis in patients with gastric cancer. *J Invest Surg*. 2021;34(8):853-861.
46. Sun B, Zhang S, Zhang D, et al. Identification of metastasis-related proteins and their clinical relevance to triple-negative human breast cancer. *Clin Cancer Res*. 2008;14(21):7050-7059.
47. Sun H, Zhang D, Yao Z, et al. Anti-angiogenic treatment promotes triple-negative breast cancer invasion via vasculogenic mimicry. *Cancer Biol Ther*. 2017;18(4):205-213.
48. Dong WW, Li J, Li J, et al. Reduced expression of oestrogen receptor- β is associated with tumour invasion and metastasis in oestrogen receptor- α -negative human papillary thyroid carcinoma. *Int J Exp Pathol*. 2018;99(1):15-21.
49. Wang Y, Wang X, Zhang Y, et al. Vasculogenic mimicry and expression of ALDH1, Beclin1, and p16 correlate with metastasis and prognosis in oral squamous cell carcinoma. *Int J Clin Exp Pathol*. 2018;11(3):1599-1609.
50. Varghese F, Bukhari AB, Malhotra R, De A. IHC Profiler: an open source plugin for the quantitative evaluation and automated scoring of immunohistochemistry images of human tissue samples. *PLoS One*. 2014;5:e96801.
51. Ray S, Saha D, Alam N, et al. Exposure to chewing tobacco promotes primary oral squamous cell carcinoma and regional lymph node metastasis by alterations of SDF1 α /CXCR4 axis. *Int J Exp Pathol*. 2021;102(2):80-92.
52. Landis JR, Koch GG. The measurement of observer agreement for categorical data. *Biometrics*. 1977;33(1):159-174.
53. Cao Z, Bao M, Miele L, Sarkar FH, Wang Z, Zhou Q. Tumour vasculogenic mimicry is associated with poor prognosis of human cancer patients: a systemic review and meta-analysis. *Eur J Cancer*. 2013;49:3914-3923.
54. Hujanen R, Almahmoudi R, Karinen S, Nwaru BI, Salo T, Salem A. Vasculogenic mimicry: a promising prognosticator in head and neck squamous cell carcinoma and esophageal cancer? a systematic review and meta-analysis. *Cells*. 2020;9(2):507.
55. Belotti D, Pinessi D, Tarabozetti G. Alternative vascularization mechanisms in tumor resistance to therapy. *Cancers (Basel)*. 2021;13(8):1912.
56. Yang JP, Liao YD, Mai DM, et al. Tumor vasculogenic mimicry predicts poor prognosis in cancer patients: a meta-analysis. *Angiogenesis*. 2016;19(2):191-200.
57. Zhang J, Qiao L, Liang N, et al. Vasculogenic mimicry and tumor metastasis. *J BUON*. 2016;21(3):533-541.
58. Ling G, Wang S, Song Z, et al. Transforming growth factor- β is required for vasculogenic mimicry formation in glioma cell line U251MG. *Cancer Biol Ther*. 2011;12(11):978-988. doi:10.4161/cbt.12.11.18155
59. Hess AR, Seftor EA, Gruman LM, Kinch MS, Seftor RE, Hendrix MJ. VE-cadherin regulates EphA2 in aggressive melanoma cells through a novel signaling pathway: implications for vasculogenic mimicry. *Cancer Biol Ther*. 2006;5(2):228-233.
60. Lu XS, Sun W, Ge CY, Zhang WZ, Fan YZ. Contribution of the PI3K/MMPs/Ln-5 γ 2 and EphA2/FAK/Paxillin signaling pathways to tumor growth and vasculogenic mimicry of gallbladder carcinomas. *Int J Oncol*. 2013;42(6):2103-2115.
61. Larson AR, Lee CW, Lezcano C, et al. Melanoma spheroid formation involves laminin-associated vasculogenic mimicry. *Am J Pathol*. 2014;184(1):71-78.
62. Kawahara R, Niwa Y, Simizu S. Integrin β 1 is an essential factor in vasculogenic mimicry of human cancer cells. *Cancer Sci*. 2018;109(8):2490-2496. doi:10.1111/cas.13693
63. Seftor RE, Seftor EA, Koshikawa N, et al. Cooperative interactions of laminin 5 gamma2 chain, matrix metalloproteinase-2, and membrane type-1-matrix/metalloproteinase are required for mimicry of embryonic vasculogenesis by aggressive melanoma. *Cancer Res*. 2001;61(17):6322-6327.
64. Wu Z, Song W, Cheng Z, Yang D, Yu L. Expression of LGR5 in oral squamous cell carcinoma and its correlation to vasculogenic mimicry. *Int J Clin Exp Pathol*. 2017;10(11):11267-11275.
65. Almahmoudi R, Salem A, Hadler-Olsen E, Svineng G, Salo T, Al-Samadi A. The effect of interleukin-17F on vasculogenic mimicry in oral tongue squamous cell carcinoma. *Cancer Sci*. 2021;112:2223-2232.
66. Xing P, Dong H, Liu Q, et al. ALDH1 expression and vasculogenic mimicry are positively associated with poor prognosis in patients with breast cancer. *Cell Physiol Biochem*. 2018;49:961-970.
67. Miles GJ, Powley I, Mohammed S, et al. Evaluating and comparing immunostaining and computational methods for spatial profiling of drug response in patient-derived explants. *Lab Invest*. 2021;101(3):396-407.

SUPPORTING INFORMATION

Additional supporting information may be found in the online version of the article at the publisher's website.

How to cite this article: Saha D, Mitra D, Alam N, et al. Orchestrated expression of vasculogenic mimicry and laminin-5 γ 2 is an independent prognostic marker in oral squamous cell carcinoma. *Int J Exp Pathol*. 2022;00:1-11. doi:[10.1111/iep.12430](https://doi.org/10.1111/iep.12430)

Sub-chronic cadmium and lead compound exposure induces reproductive toxicity and development of testicular germ cell neoplasia in situ in murine model: Attenuative effects of resveratrol

Sreyashi Mitra¹ | Tapas Patra² | Depanwita Saha¹ | Paramita Ghosh¹ |
Saunak Mitra Mustafi³ | Alex C. Varghese⁴ | Nabendu Murmu¹ 

¹Department of Signal Transduction and Biogenic Amines (STBA), Chittaranjan National Cancer Institute, Kolkata, India

²E. Doisy Research Center, Saint Louis University, St. Louis, Missouri, USA

³Department of Pathology, Chittaranjan National Cancer Institute, Kolkata, India

⁴Astra Fertility Clinic, Mississauga, Ontario, Canada

Correspondence

Nabendu Murmu, Department of Signal Transduction and Biogenic Amines (STBA), Chittaranjan National Cancer Institute, 37-S.P. Mukherjee Rd, Kolkata 700026, India.
Email: nabendu.murmu@cnci.ac.in

Abstract

Cadmium and lead are widespread, nonbiodegradable heavy metals of perpetual environmental concerns. The present study aimed to evaluate whether sub-chronic exposure to cadmium chloride (CdCl_2) and lead acetate [$\text{Pb}(\text{CH}_3\text{COO})_2$] induces reproductive toxicity and development of testicular germ cell neoplasia in situ (GCNIS) in swiss albino mice. The effects of resveratrol to reverse the metal-induced toxicity were also analyzed. The mice were randomly divided into four groups for metal treatments and two groups received two different doses of each metal, CdCl_2 (0.25 and 0.5 mg/kg) and $\text{Pb}(\text{CH}_3\text{COO})_2$ (3 and 6 mg/kg). The fourth group received oral doses of 20 mg/kg resveratrol in combination with 0.5 mg/kg CdCl_2 or 6 mg/kg $\text{Pb}(\text{CH}_3\text{COO})_2$ for 16 weeks. Toxic effects of both metals were estimated qualitatively and quantitatively by the alterations in sperm parameters, oxidative stress markers, testicular histology, and protein expressions of the treated mice. Pronounced perturbation of sperm parameters, cellular redox balance were observed with severe distortion of testicular histo-architecture in metal exposed mice. Significant overexpression of Akt cascade and testicular GCNIS marker proteins were recorded in tissues treated with CdCl_2 . Notable improvements were observed in all the evaluated parameters of resveratrol cotreated mice groups. Taken together, the findings of this study showed that long-term exposure to Cd and Pb compounds, induced acute reproductive toxicity and initiation of GCNIS development in mice. Conversely, resveratrol consumption abrogated metal-induced perturbation of spermatogenesis, testicular morphology, and the upregulation of Akt cascade proteins along with GCNIS markers, which could have induced the development of testicular cancer.

KEYWORDS

cadmium, lead, male infertility, resveratrol, testicular GCNIS

Abbreviations: Akt, protein kinase B; CdCl_2 , cadmium chloride; CIS, carcinoma in situ; Cox-2, cyclooxygenase 2; GCNIS, germ cell neoplasia in situ; GSH, glutathione; HRP, horse radish peroxidase; MDA, malondialdehyde; NF- κ B, nuclear factor kappa beta; Oct3/4, octamer binding transcription factor 3/4; OS, oxidative stress; PBS, phosphate-buffered saline; $\text{Pb}(\text{CH}_3\text{COO})_2$, lead acetate; ROS, reactive oxygen species.

1 | INTRODUCTION

Cadmium (Cd) and lead (Pb) are ubiquitous environmental toxicants. According to the US Geological Survey, Cd is primarily produced from Asia and the Pacific region.^[1] On the other hand, the highest Pb producing countries are China, Australia, Peru, and United States.^[2] Reported sources of Cd and Pb in the environment include anthropogenic, industrial, agricultural, pharmaceutical, and domestic effluents.^[3] In recent decades, heavy metal contamination has increased dramatically because of their continuous discharge in sewage and untreated industrial effluents. These metals get assimilated in the plant world as they progress through the food chain.^[4] They are nonbiodegradable and have long biological half-lives inside human body, therefore persist in the environment.^[5,6] Compelling data from different parts of the world suggest that environmental and occupational exposure to Cd and Pb compounds significantly induce physiological, biochemical, behavioral dysfunctions^[7-11] and development of a diverse range of cancers^[12,13] in humans as well as in animal models. The International Agency for Research on Cancer (IARC) has classified Cd and its compounds as “carcinogenic to humans” and Pb compounds as “possibly carcinogenic to humans.”^[14,15] Other detrimental health implications of Cd and Pb exposure include development of reproductive toxicity and endocrine disruptions in both male and female subjects.^[16-18]

Several epidemiological reports on the potential association between the detrimental environmental impact on reproduction and the increasing incidence of testicular cancer evoked curiosity among researchers. Studies indicated that men with abnormal semen parameters are at an increased risk of developing germ cell tumors in future.^[19-22] On the other hand, evidence from different parts of the world links oxidative stress to a plethora of acute pathological conditions including reproductive disorders and cancers.^[23,24]

Glutathione (GSH), one of the most abundant low molecular weight nonprotein thiols, modulates physiological levels of ROS and is involved in the cell's oxidative stress response. In living cells, Glutathione exists in reduced (GSH or Glutathione) and oxidized (GSSG or Glutathione disulfide) states. GSH protect cellular components from the damaging effects of oxidative stress by modulating intracellular ROS levels.^[25-27] Studies suggest that glutathione (GSH) synthesis under oxidative stress is regulated by activated Akt.^[28,29] Akt is a well-established regulator of central glucose metabolism and aerobic glycolysis.^[30,31] Aberrant expression of Akt has been reported to play critical role in majority of tumorigenesis and malignancies.^[32,33] Akt and its downstream key signaling proteins, NF- κ B, Cox-2 have been major targets of efficacious therapeutic interventions.^[34-36]

Germ cell neoplasia in situ (GCNIS) is the precursor lesion of malignant testicular germ cell tumors (TGCTs). GCNIS cells express a number of markers including Oct 3/4 and c-Kit.^[37] In early 1990s, KIT expression was first discovered in TGCTs. Subsequent studies showed that KIT was significantly expressed in GCNIS along with other pluripotency markers like OCT3/4.^[38]

Dietary chemo-preventive compounds offer great potential to reduce toxicity and combat cancer development by inhibiting the

carcinogenesis process and inducing antioxidant enzymes.^[39,40] Resveratrol is one such natural polyphenolic compound with potential to alleviate adverse clinical conditions such as cancers, vascular diseases, reproductive disorders, neurodegenerative processes.^[41,42]

The present study aims to explore whether 16-week long sub-chronic exposure to Pb and Cd doses can induce the alterations of semen parameters, testicular histo-architecture, expression of Akt cascade proteins, and the development of GCNIS in swiss albino mice. The efficacy of resveratrol as a chemo-preventive and fertility restorative compound was also evaluated.

2 | MATERIALS AND METHODS

2.1 | Animal care

Five-week-old male Swiss albino mice (*Mus musculus*), weighing 20–25 gm were procured for this study from animal breeding facility of Chittaranjan National Cancer Institute, Kolkata, India and maintained at animal care facility of the institute as per the maintenance guidelines prescribed by the institute and government regulatory body. Mice were housed in well-ventilated wire-mesh cages (five mice/cage). All animals had access to drinking water and standard food pellets under controlled environmental conditions of humidity (60 ± 5%), light (12-h light/dark cycle), and temperature (23 ± 2°C).

2.2 | Ethical clearance of the study

The animal experiments were performed after receiving a written approval from the Institutional Animal Ethics Committee (IAEC), Chittaranjan National Cancer Institute (No: IAEC-1774/NM-3/2015/16) as per the guidelines of the “Committee for the Purpose of Control and Supervision of Experiments on Animals” (CPCSEA) of Govt. of India. The experiments were performed according to the guidelines laid down by the National Institutes of Health guide for the care and use of laboratory animals (NIH Publications No. 8023, revised 1978).^[43]

2.3 | Antibodies and reagents

Rabbit polyclonal primary antibodies against Akt (sc-8312), p-Akt (Ser-473; sc-7985-R), NF- κ B (p50; sc-114), Cox-2 (sc-7951), Oct-3/4 (sc-5279), horseradish peroxidase (HRP)-conjugated goat anti-rabbit secondary antibody (sc-2004) were purchased from Santa Cruz Biotechnologies (Santa Cruz). c-Kit (AF1356) antibody was procured from Novus Biologicals. The immunohistochemistry assay kit (DAB150) was obtained from Merck Millipore, Germany. The GSH/GSSG Ratio Detection Assay kit (ab138881) and Lipid Peroxidation (MDA) Assay kit (ab118970) both were purchased from Abcam. For protein estimation, BCA protein assay kit (Prod # 23225) was procured from Pierce. Western blot bands were visualized using chemiluminescence kit (BioVision ECL Western Blot Substrate).

2.4 | Test chemicals and mode of administration

Crystalline Cd obtained from Sigma-Aldrich (439800) in the form of CdCl_2 was dissolved in physiological saline (0.9% NaCl) immediately before the use. Similarly, Pb obtained from Sigma-Aldrich (316512) in the form of $\text{Pb}(\text{CH}_3\text{COO})_2$ was dissolved in 0.9% NaCl. Both CdCl_2 and $\text{Pb}(\text{CH}_3\text{COO})_2$ solutions were injected to the mice intraperitoneally (i.p.). Resveratrol, commercially available as the trans-isomer (34092, Sigma Aldrich), was suspended in 0.7% carboxymethyl-cellulose (CMC) and administered to mice by oral gavage.

2.4.1 | LD_{50} calculation

Lethal dose 50 or LD_{50} is used to measure acute toxicity of a chemical on living system. The main objective of LD_{50} study was to determine the drug dose which causes death of 50% of the treated animals under the defined conditions of the experiment. An approximate LD_{50} of the CdCl_2 and $\text{Pb}(\text{CH}_3\text{COO})_2$ dose range was determined by using the Probit analysis as described by Litchfield and Wilcoxon.^[44] The experimental design for LD_{50} calculation described below:

Groups	Treatments
Control I	Treated with 0.9% saline
CdCl_2	Alone animals administered with single i.p. injection of various doses of CdCl_2 (0–20 mg/kg body weight)
Control II	Treated with 0.9% saline
$\text{Pb}(\text{CH}_3\text{COO})_2$	Animals administered with single i.p. injection of a dose range (0–200 mg/kg body weight)

Firstly, we found out the least tolerated (100% mortality) and most tolerated dose (0% mortality) of both the metallic compounds in the aforementioned dose range by hit and trial method. After that five doses were selected in between the two determined doses in the dose range for CdCl_2 (0.5, 1, 5, 10, 15 mg/kg body weight) and $\text{Pb}(\text{CH}_3\text{COO})_2$ (5, 25, 50, 100, 150 mg/kg body weight). The selected doses from the dose range for each metallic compound were given intraperitoneally to seven experimental groups of swiss albino mice, with 10 mice in each group ($n = 10$) for the determination of LD_{50} from 0% mortality to 100% mortality. The animals treated with doses were monitored for signs of toxicity for 30 days and during this period any signs of sickness and mortality were recorded. The percentage mortality values are converted into LD_{50} values by the analysis.

2.5 | Experimental design, chemical exposure, and determination of dose regimen

Following a few days of acclimatization, the mice were randomly divided into four different experimental groups for each metal. CdCl_2

treatment groups are divided into four groups (control group [untreated mice], Gr. I [low Cd treatment group], Gr. II [high Cd treatment group], and Gr. III [resveratrol plus Cd treatment group]). Similarly, $\text{Pb}(\text{CH}_3\text{COO})_2$ treatment groups are also divided into four groups (control group [untreated mice], Gr. I [low Pb treatment group], Gr. II [high Pb treatment group], and Gr. III [resveratrol plus Pb treatment group]). Each group consisting of five mice ($n = 5$). The control mice of both the groups received physiological saline (0.9%) for the experimental period of 16 weeks. The selection of experimental doses was based on our experimental data of LD_{50} (Figure S1). Cd-treated mice of Gr. I and Gr. II received the CdCl_2 solution, intraperitoneally, twice per week for 16 weeks at selected doses of 0.25 and 0.5 mg/kg of body weight respectively. These doses are 1/36th and 1/18th of the calculated LD_{50} values of CdCl_2 (9.19 mg/kg body weight). Similarly, the $\text{Pb}(\text{CH}_3\text{COO})_2$ solution was injected intraperitoneally to the experimental male mice twice per week for 16 weeks. The $\text{Pb}(\text{CH}_3\text{COO})_2$ dose regimen was determined to be 3 mg/kg of body weight for Gr. I and 6 mg/kg of body weight for Gr. II, which again are respectively 1/36th and 1/18th of the calculated LD_{50} dose of $\text{Pb}(\text{CH}_3\text{COO})_2$ (108.80 mg/kg body weight). Resveratrol administered to male mice (Gr. III) by oral gavage at a dose of 20 mg/kg of body weight, 5 h before administration of metal doses, twice per week for 16 weeks. The pilot studies were previously performed in our laboratory (data not shown) to observe the effect of resveratrol on mice. The PK/PD information and the dose selection of resveratrol were also based on previously published literature.^[45–50] Twenty-four hours after the administration of the last dose of this experiment, all mice were sacrificed by cervical dislocation. The elaborate dose regimen has been presented in Figure 1.

2.6 | Variation in body weight, weight of testis, and sperm analysis

During the 16 weeks of the treatment period, individual animals from all four groups were weighed at a weekly interval to determine the change in body weight. The testes were excised following the sacrifice of the mice to record the relative changes in weights during the course of the experiment.

2.6.1 | Isolation of testes tissues, sperm cells, and serum from experimental mice

After the cervical dislocation, the testes from each group of mice were excised out for further experiments and divided into parts after the weight measurement. One part of testes with epididymis were then placed in low-retention microcentrifuge tubes containing $1 \times \text{PBS}$ and agitated on an orbital shaker for 10 min to facilitate the swim out of the sperm. The tubes were placed upright on a benchtop and the epididymal tissues were allowed to settle for 10 min. The sperm suspension was removed and an aliquot was taken to ensure purity (~99%) and for counting purposes. The second part of tissue samples was immediately frozen in liquid nitrogen and

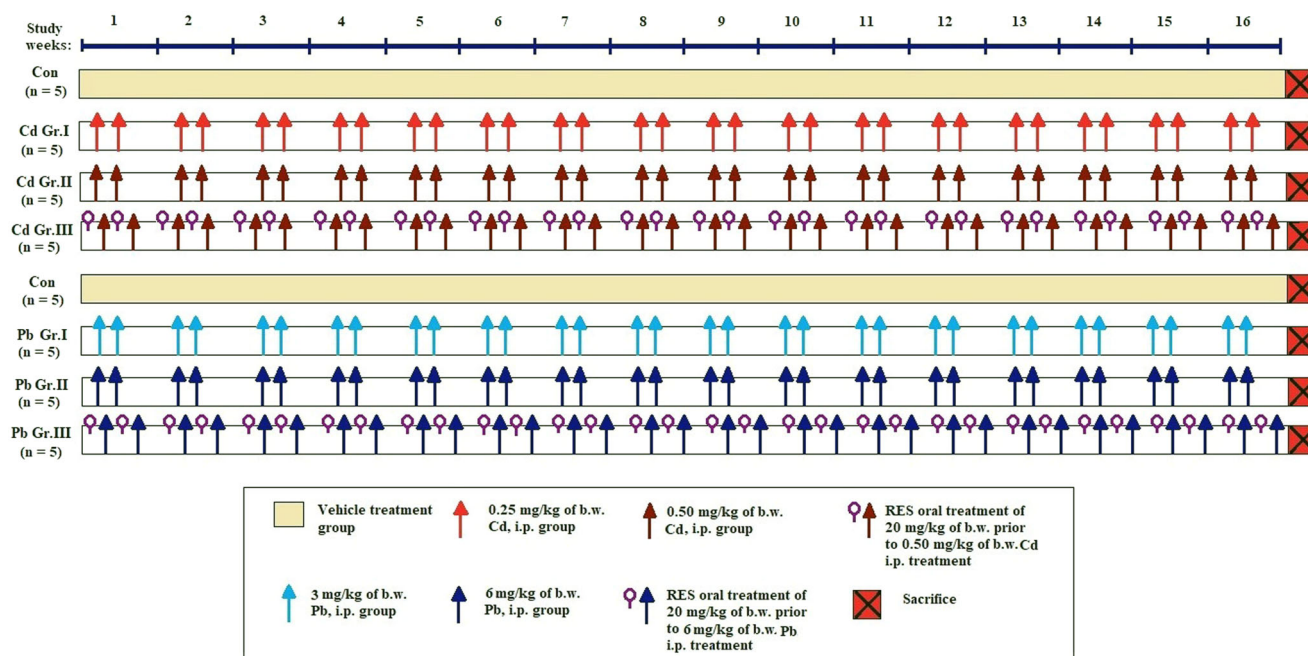


FIGURE 1 Treatment schedule of experimental mice. The schematic representation of 16-week long treatment regimen of experimental mice groups using CdCl_2 and $\text{Pb}(\text{CH}_3\text{COO})_2$ doses separately or in combination with resveratrol. Vehicle treatment group = 0.9% NaCl; Gr. I Cd = CdCl_2 Group I dose, that is, 0.25 mg/kg body weight; Gr. II Cd = CdCl_2 Group II dose, that is, 0.50 mg/kg body weight; Gr. III Cd = CdCl_2 Group III dose, that is, resveratrol 20 mg/kg body weight + CdCl_2 0.50 mg/kg body weight; Gr. I Pb = $\text{Pb}(\text{CH}_3\text{COO})_2$ Group I dose, that is, 3 mg/kg body weight; Gr. II Pb = $\text{Pb}(\text{CH}_3\text{COO})_2$ Group II dose, that is, 6 mg/kg body weight; Gr. III Pb = $\text{Pb}(\text{CH}_3\text{COO})_2$ Group III dose, that is, resveratrol 20 mg/kg body weight + $\text{Pb}(\text{CH}_3\text{COO})_2$ 6 mg/kg body weight. b.w., body weight; Gr., group; i.p., intraperitoneal; kg, kilogram; mg, milligram; RES, resveratrol.

stored at -80°C for the investigation of antioxidant status. The third part of the tissue samples was preserved in formalin for histopathological examination. On the other hand, the fourth part of the testes collected from mice was lysed in western blot lysis buffer and centrifuged for protein analysis. Blood samples were collected by cardiac puncture and aliquot of blood with anticoagulant (heparin) was used to obtain blood plasma for measurement of testosterone.

2.6.2 | Semen collection and epididymal sperm analysis

The sperm suspension obtained from testes and epididymis for further analysis was diluted with 2.9% (w/v) sodium citrate dehydrate solution and thoroughly mixed to determine the sperm density and count.

2.6.3 | Sperm motility assessment

Collected sperm suspensions were flushed in 1 ml of Dulbecco's Modified Eagle Medium (DMEM) in a ratio of 1:1 (1 part sperm suspension and 1 part DMEM). From this suspension, 50 μl was placed on the hemocytometer and each of the four quadrants was observed. A total of 300 spermatozoa were counted by hemocytometer using the improved Neubauer chamber (deep 1/10 mm, LABART, Germany) to estimate sperm motility under light microscope at a magnification of

100x following the protocol by Zamjanis.^[51] The sperm cells were characterized on the following recorded features: forward motility or progressively motile sperms, moving but not making forward progression or nonprogressively motile sperms. Sperm cells were scored as immotile if no flagellar movement was detected.

2.6.4 | Sperm morphological analysis

Anionic dye 0.5% (0.5 g/100 ml) solution of Eosin Y containing 0.9% (0.9 g/100 ml) aqueous sodium chloride was used for staining spermatozoa. Smear was prepared from the supernatant isolated from testis and epididymis, air-dried and stained with Eosin Y stain (Fisher Scientific). This was followed immediately by examination under the microscope at a magnification of 400x. A total of 400 sperm cells from each mice of each group were examined to assess and record the morphological alterations.^[52]

2.7 | Biochemical assays

2.7.1 | Oxidative stress measurement

At the end of the exposure period, after the animals were killed, testes specimens were collected from all experimental groups. Tissues samples were washed in ice-cold 0.9% (w/v) NaCl for redox

status assessment. The tissues were homogenized in Teflon-glass homogenizer with a buffer containing 1.5% potassium chloride to obtain 1:10 (w/v) homogenates. The reduced glutathione (GSH) and malondialdehyde (MDA) levels of the testes tissues of different groups of mice were determined. The tissue homogenates were centrifuged at 18,000 g (4°C) for 30 min to determine reduced glutathione (GSH) levels. Tissue GSH concentrations were measured by a kinetic assay using a dithionitrobenzoic acid recycling method described by Ellman^[53] and were expressed as nmol/mg tissues. Lipid-peroxidation levels were measured according to the method described by Ohkawa et al. using Lipid Peroxidation (MDA) Assay kit. This method was based on estimation of the released malondialdehyde (MDA) molecules which can be quantified colorimetrically (OD = 532 nm). The concentrations of MDA were expressed in nmole of MDA per gram of tissue.^[54]

2.7.2 | GSH/GSSG ratio analysis

GSH/GSSG ratio in the cells of mice testes tissues was determined using GSH/GSSG Ratio Detection Assay Kit (Fluorometric-Green; Abcam #ab138881) according to the manufacturer's protocol. A serial dilution of GSH and GSSG stock standards was prepared, the testes tissue lysates were diluted to 1:80 for the analysis. A one-step fluorimetric reaction of samples was performed by incubating with respective assay buffer for 60 min protected from light. The fluorescence intensity was measured using a spectrofluorometer ($\lambda_{exc} = 490$ nm, $\lambda_{emm} = 520$ nm; SL 174, Elico). GSH was calculated from the standard curve using the formula $GSSG = (\text{total glutathione} - \text{GSH})/2$.

2.7.3 | Testosterone measurement

To determine the effects of Cd and Pb on Leydig cells of testis, plasma was isolated from the blood collected from each experimental group. The plasma testosterone level was assayed using Coat-a-Count Radioimmunoassay kits (Active Testosterone RIA DSL-4000, Diagnostic System Laboratories Inc.) according to manufacturer's protocol. The amount of testosterone was expressed as ng/ml.

2.8 | Histological and protein analysis

2.8.1 | Hematoxylin and eosin staining

To assess the in vivo influence of metal treatment at different doses and the restorative effects of resveratrol on testicular morphology, testes tissues were collected from each group of mice and fixed in 10% (v/v) formaldehyde. The tissues were processed and paraffin blocks were made. Hematoxylin and eosin (H&E) staining was performed following the standard protocols in 3- μ m sections of the blocks to determine the morphological alterations in tissue structures

after treatment. Five slides per group with three repetitions of sample sections from each mouse were analyzed for H&E staining.

2.8.2 | Immunohistochemistry

The testes tissues from control and experimental groups of mice were paraffin embedded. The paraffin-embedded sections of 3 μ thickness were mounted on poly-L-lysine coated slides. The slides were kept in a hot-air oven for 1 h at 56°C and later deparaffinized in xylene for 10 min (three changes). After heat-induced antigen retrieval using 0.01 M citrate buffer (pH 6.0), the slides were treated with 0.3% (v/v) hydrogen peroxide in methanol for endogenous peroxidase blocking. The rest of the procedure was performed according to a standard manufacturer's protocol using an immunohistochemistry (Merck, Millipore) kit. c-Kit antibody was reconstituted at a dilution of 10 μ g/ml for immunohistochemistry as per the manufacturer's protocol (Novus Biologicals). All the antibodies were used in 1:600 dilutions. Five slides per group with three repetitions of sample sections from each mouse were analyzed for histological scoring.

2.8.2.1 | Histological scoring

The slides were examined independently by the pathologist of Chittaranjan National Cancer Institute who examined the clinicopathological characteristics of the experimental tissue sections. Semi-quantitative scoring method was used to evaluate the IHC staining.^[55] Intensity of the staining was scored as 1, 2, 3, and 4 for the negative, weak, moderate and intense staining respectively. The percentage of DAB positive cells per field was evaluated in 10 different fields and scored by qualified pathologist (SM) using the following method: 0 (no expression), 1 (1%–25% expression), 2 (26%–50% expression), 3 (51%–75% expression), and 4 (76%–100% expression). The sum of the stain intensity and positive cell score resulted in the staining index, which was used to determine the final result for each sample low (0–4) and high (5–7).

2.8.3 | Western blot analysis

Testes tissues were collected from each group of mice. To obtain lysates, tissues were suspended into ice-cold lysis buffer (15 mM tris, 2 mM EDTA, 50 mM 2-mercaptoethanol, 20% (v/v) glycerol, 0.1% (v/v) triton X100, 1 mM PMSF, 1 mM sodium fluoride, 1 mM sodium orthovanadate, 1 μ g/ml aprotinin, 1 μ g/ml leupeptin, 1 μ g/ml pepstatin), followed by homogenization and sonication on ice (40 Hz, 65 pulses). The lysates were centrifuged at 13,500 Gx at 4°C for 15 min and the resulting supernatant was collected. Total cellular extracts (50 μ g protein/lane) were subjected to sodium dodecyl sulfate polyacrylamide gel electrophoresis (SDS-PAGE) and electrotransferred to nitrocellulose membranes. The membranes were blocked with 5% (w/v) nonfat dry milk in Tris-buffered saline for 1 h at room temperature. Immuno-antigenicity was detected by overnight incubation of the membrane with the appropriate primary

antibodies, that is, Akt, p-Akt, NF- κ B(p50), and Cox-2 at 1:200 dilution. After being washed, the membranes were incubated with horseradish peroxidase (HRP)-conjugated anti-rabbit secondary antibodies at 1:10,000 dilutions and developed using enhanced chemiluminescence (BioVision ECL western blot substrate) according to the manufacturer's instructions. The immunoreactive bands were analyzed using a densitometer (Bio-Rad, GS 800). β -actin was used as loading control to confirm the equal distribution of protein.

2.9 | Statistical analysis

All experiments were conducted in triplicates. All statistical analyses were performed with the help of Graph Pad Prism 7.0. Descriptive statistical analysis was conducted to calculate the mean with corresponding standard error (SE). One-way analysis of variance (ANOVA) followed by Tukey's post hoc test was performed with the help of critical difference (CD) at 5% (CD5) and 1% level (CD1) to compare different sperm parameters (including morphology, motility, density), cellular level of oxidative stress markers and testosterone levels in different experimental groups. One-way ANOVA was also applied to compare the tissue expression profiles of Akt, NF- κ B(p50), and Cox-2 proteins evaluated by immunohistochemistry and western blot analysis in different experimental mice groups. Tukey's test was used to compare the difference between two specific means after obtaining the significant difference through ANOVA. The analysis of the associations between different experimental parameters was simultaneously performed by multivariate analyses and presented in the form of correlation matrices. $p \leq 0.05$ was considered to be statistically significant in all calculations.

3 | RESULTS

3.1 | Changes in body weight and weight of testes in course of the experiment

The relative bodyweight of the mice was recorded once every week in course of the experimental period of 16 weeks. The data of this record when plotted graphically showed a significant gradual decrease on average body weight of Cd- and Pb-treated experimental groups compared to the control and resveratrol cotreated groups (Figure 2A,B). Significant ($p < 0.0001$) variations in relative testes weight (i.e., testes weight/body weight $\times 100$) were also observed between different CdCl₂ and Pb(CH₃COO)₂ treated experimental groups. However, no variations were recorded in the relative testes weight of control and resveratrol cotreated groups of both the metals (Figure 2C,D).

3.2 | Effects of sub-chronic metal treatment and resveratrol cotreatment on sperm parameters in vivo

Table 1 summarized notable variations in the percentage of epididymal sperm count, total motile sperms, sperm cell density,

and morphologically abnormal sperm cells of four groups of Cd- and Pb-treated mice. Significant ($p < 0.0001$) decline in total sperm count, percentage of motile sperm cells, and percentage of viable sperm cells were observed among mice treated with two different concentrations of CdCl₂ (Gr. I, 0.25 mg/kg and Gr. II, 0.5 mg/kg of body weight) compared to the control group. However, percentage of motile and viable sperm cells remarkably improved in response to cumulative treatment of resveratrol (20 mg/kg of body weight) and CdCl₂ (0.5 mg/kg of body) in Gr. III mice. Conversely, the percentage of average sperm morphological abnormalities notably increased in two CdCl₂-treated groups (Table 1).

The percentage of total sperm count and viable sperm cells showed significant ($p < 0.0001$) decrease and percentage of morphologically abnormal sperm cells showed significant ($p < 0.0001$) increase in case of two different concentrations of Pb(CH₃COO)₂-treated mice groups (3 and 6 mg/kg of body weight). However, no variation was observed in the percentage of motile sperm cells and sperm density of these groups (Table 2).

The staining results of cauda epididymal sperm cells collected from Cd-treated mice showed morphological aberrations including amorphous heads, multiple heads or tails, looped and coiled tails which were summed up as the total percentage of sperm morphological defects. On the other hand, the average percentage of sperm morphological abnormalities significantly reduced in resveratrol cotreated group (Gr. III) (Figure 3A). A similar notable increase in the percentage of sperm morphological anomalies such as bent neck, looped head, folded tails, and blunt hooks was also observed in groups treated with two different doses of Pb(CH₃COO)₂ compared to the control and resveratrol cotreated groups (Figure 3B).

3.2.1 | Variations in the levels of GSH, MDA, and testosterone among different treatment groups

The findings of our studies showed significant variations in the levels of oxidative stress markers of four Cd- and Pb-treated experimental groups. The ANOVA results showed ($F = 51.42$, $p < 0.0001$, $R^2 = 0.906$) notable decrease in the GSH level of testes tissues of mice treated with two different concentrations of CdCl₂ (Gr. I, 2.89 ± 0.087 ; Gr. II, 2.088 ± 0.057) compared to the untreated control group (Con, 3.75 ± 0.153). Conversely, relative increase in tissue GSH levels was recorded in resveratrol cotreated groups (Gr. III, 3.392 ± 0.076). Similar variations were recorded in the tissue GSH concentration of Pb(CH₃COO)₂ treated mice groups ($F = 16.76$, $p < 0.0001$, $R^2 = 0.758$, Con, 3.80 ± 0.090 ; Gr. I, 3.48 ± 0.139 ; Gr. II, 2.94 ± 0.050 ; Gr. III, 3.80 ± 0.097).

On the other hand, MDA is one of the significant markers of lipid peroxidation process which is produced because of increasing oxidative stress. Significantly, elevated levels of MDA was recorded in the testes tissues of both Cd ($F = 37.96$, $p < 0.0001$, $R^2 = 0.876$, Con, 0.979 ± 0.006 ; Gr. I, 1.04 ± 0.050 ; Gr. II, 1.456 ± 0.054 ; Gr. III, 0.969 ± 0.006) and Pb ($F = 8.663$, $p = 0.0012$, $R^2 = 0.618$, Con, 0.979 ± 0.006 ; Gr. I, 0.999 ± 0.026 ; Gr. II, 1.23 ± 0.006 ; Gr. III,

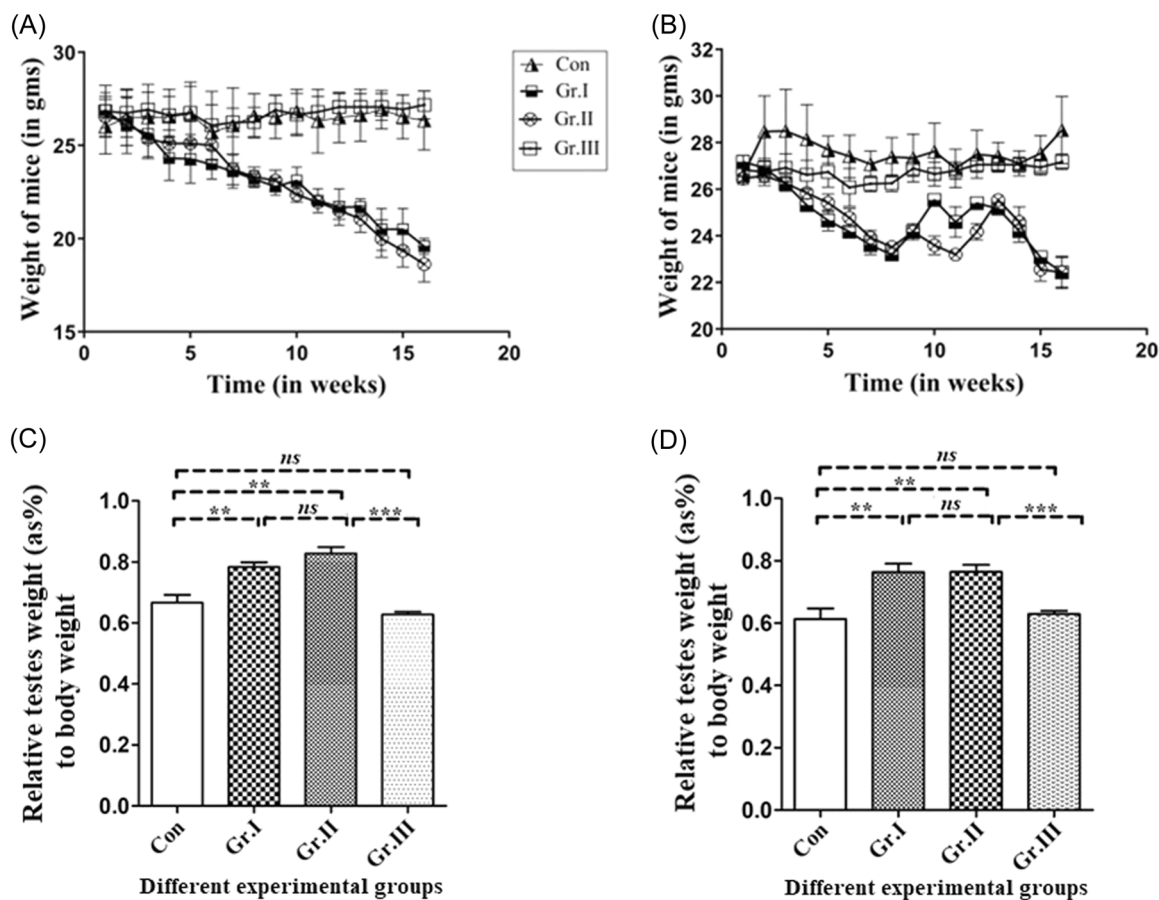


FIGURE 2 Variation in the body weight and relative testes weight in different experimental groups of mice. In course of the 16 weeks of experimental period, body weight of the mice was recorded once every week and the average weight of the testes was measured after the sacrifice of the mice. (A) The plotted line graph represents significant decrease in the average body weight of only CdCl₂-treated group of mice compared to the control and resveratrol cotreated group. (B) The average body weight of only Pb(CH₃COO)₂-treated groups also showed a gradual decrease compared to the control and resveratrol treated group. The relative testes weight (as % to body weight) of (C) CdCl₂ and (D) Pb (CH₃COO)₂-treated mice group varied significantly in four experimental groups. However, the mean weight of the control and resveratrol cotreated group (Gr. III) did not vary significantly. gm, gram; mg, milligram; ns, not significant; **p* < 0.05.

TABLE 1 Variations in different sperm parameters of CdCl₂-treated mice

Variables	Control (n = 5)	Group I (n = 5)	Group II (n = 5)	Group III (n = 5)	CD ₅	CD ₁	F3, F16	<i>p</i> -value
Sperm density	5.8 ± 0.18	5.34 ± 0.37	5.96 ± 0.12	5.38 ± 0.22	0.62	1.00	1.59	0.2300 ^{ns}
Total sperm count (10 ⁶ /ml)	116.2 ± 1.82	94.40 ± 1.98	82 ± 2.07	104.4 ± 1.86	1.6	2.88	56.21	0.000001***
% of motile sperm cells (P + NP)	75.07 ± 1.32	45.62 ± 1.11	11.42 ± 1.32	72.50 ± 1.60	1.29	1.95	75.87	0.000001***
% of viable sperm cells	78.91 ± 0.680	61.75 ± 3.03	50.76 ± 2.64	71.3 ± 0.8	1.44	1.76	34.23	0.000001***
% of morphologically abnormal sperm cells	21.4 ± 0.763	50.79 ± 2.77	65.29 ± 2.35	4.93 ± 1.32	1.01	1.66	185.5	0.000001***

Note: The results are presented as mean ± SE. % of total motile sperm cells = % of progressively motile sperm cells (P) + % of nonprogressively motile sperm cells (NP).

Abbreviations: CD₁, Critical difference at 1% level of significance; CD₅, critical difference at 5% level of significance; F, F statistic; ml, milliliter; ns, not significant; SE, standard error.

****p* < 0.0001.

0.972 ± 0.007) treated mice compared to the control and resveratrol cotreated groups. However, no notable alterations in the levels of plasma testosterone were observed in the Cd (*F* = 0.142, *p* = 0.933, *R*² = 0.025, Con, 1.502 ± 0.170; Gr. I, 1.574 ± 0.076;

Gr. II, 1.59 ± 0.055; Gr. III, 1.51 ± 0.132) and Pb (*F* = 0.118, *p* = 0.947, *R*² = 0.021, Con, 1.53 ± 0.038; Gr. I, 1.584 ± 0.116; Gr. II, 1.598 ± 0.118; Gr. III, 1.576 ± 0.010) treated groups of mice (Figure 4A–F).

TABLE 2 Variations in different sperm parameters of Pb(CH₃COO)₂-treated mice

Variables	Control (n = 5)	Group I (n = 5)	Group II (n = 5)	Group III (n = 5)	CD ₅	CD ₁	F3, F16	p-value
Sperm density	5.94 ± 0.20	5.22 ± 0.24	5.84 ± 0.26	5.5 ± 0.24	0.54	1.03	1.84	0.180 ^{ns}
Total sperm count (10 ⁶ /ml)	111.8 ± 3.94	100.2 ± 2.35	94.2 ± 2.41	105.53 ± 1.58	1.82	2.97	7.660	0.002 ^{**}
% of motile sperm cells (P + NP)	71.094 ± 0.884	66.622 ± 1.728	16.08 ± 2.48	66.792 ± 1.213	1.22	2.06	0.13	0.936 ^{ns}
% of sperm viability	77.2 ± 1.85	62.6 ± 2.37	56.46 ± 363	69.8 ± 0.489	1.47	1.89	14.25	0.000001 ^{***}
% of morphologically abnormal sperm cells	26.74 ± 0.661	35.24 ± 1.88	38.19 ± 2.37	27.03 ± 1.75	0.85	1.5	15.55	0.000001 ^{***}

Note: The results are represented as mean ± SE. % of total motile sperm cells = % of progressively motile sperm cells (P) + % of nonprogressively motile sperm cells (NP).

Abbreviations: CD1, Critical difference at 1% level of significance; CD5, critical difference at 5% level of significance; F, F statistic; ml, milliliter; ns, not significant; SE, standard error.

p < 0.01; *p < 0.0001.

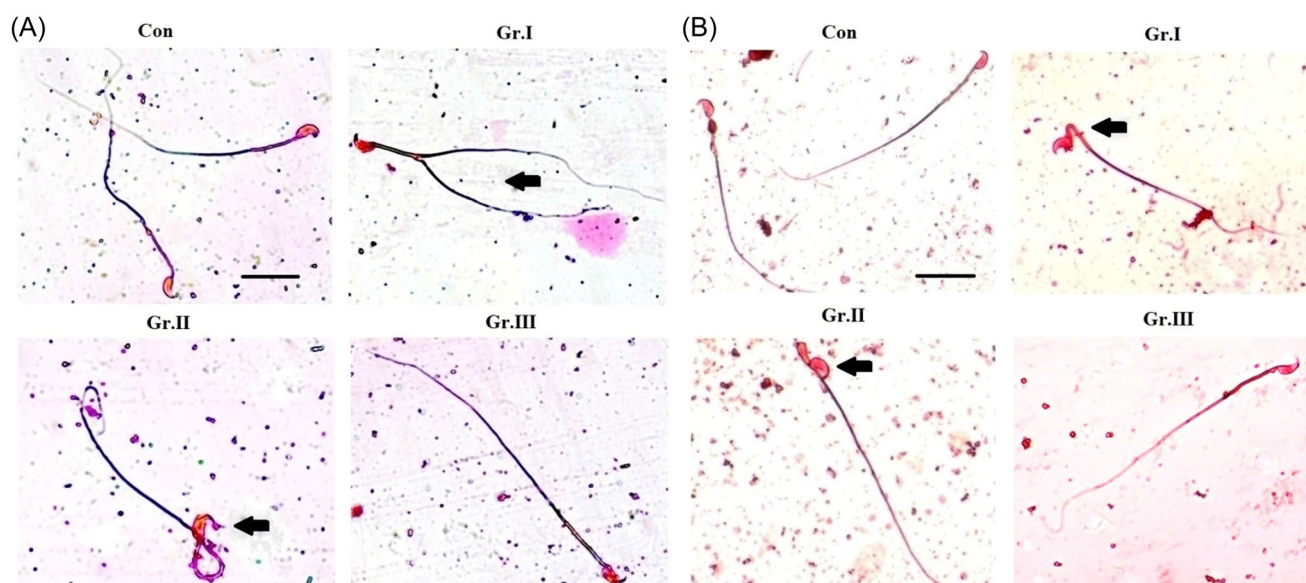


FIGURE 3 Effect of metal treatment separately or in combination with resveratrol on sperm morphological alterations of experimental mice. Experimental mice of both Cd- and Pb-treated sets were divided into four experimental groups. After the sacrifice of mice smears of testes and epididymis were isolated, air-dried, and stained with Eosin Y stain. The photomicrographs of (A) sperm cells of two concentrations of CdCl₂-treated groups (Gr. I, Gr. II) showing significantly high percentage of sperm morphological deformities, such as bifurcated tails and coiled or looped head compared to the sperm cells of control and resveratrol cotreated group (Gr. III). (B) Sperm cells of two Pb(CH₃COO)₂-treated groups showing that with increasing Pb doses, percentage of sperm morphological deformities including bent neck (Gr. I) and looped head (Gr. II) increased relative to the sperm cells of control group or Group III. All images are taken in 400x (inset) magnification. Scale bar corresponds to 50 μm. Con = control group, 0.9% NaCl; Gr. I = CdCl₂ Group I dose = 0.25 mg/kg body weight, Gr. II = CdCl₂ Group II dose = 0.50 mg/kg body weight, Gr. III = CdCl₂ Group III dose = resveratrol 20 mg/kg body weight + CdCl₂ 0.50 mg/kg body weight; Pb(CH₃COO)₂ Group I dose = 3 mg/kg body weight, Pb(CH₃COO)₂ Group II dose = 6 mg/kg body weight, Pb(CH₃COO)₂ Gr. III dose = resveratrol 20 mg/kg body weight + Pb(CH₃COO)₂ 6 mg/kg body weight.

3.2.2 | Variation of GSH and GSSG ratio in the testes tissues of different experimental groups of mice exposed to metals

Glutathione is a tripeptide that exists both in reduced (GSH) and oxidized (GSSG) states. The determination of the GSH:GSSG ratio

is a useful indicator of oxidative stress in cells and tissues. The ratios of GSH and GSSG in mice testes tissues were determined spectrophotometrically with the help of a GSH/GSSG detection assay kit. The experimental evaluations, followed by the one-way ANOVA results showed notable decrease in the ratio of GSH and GSSG levels of mice tissues treated with increasing

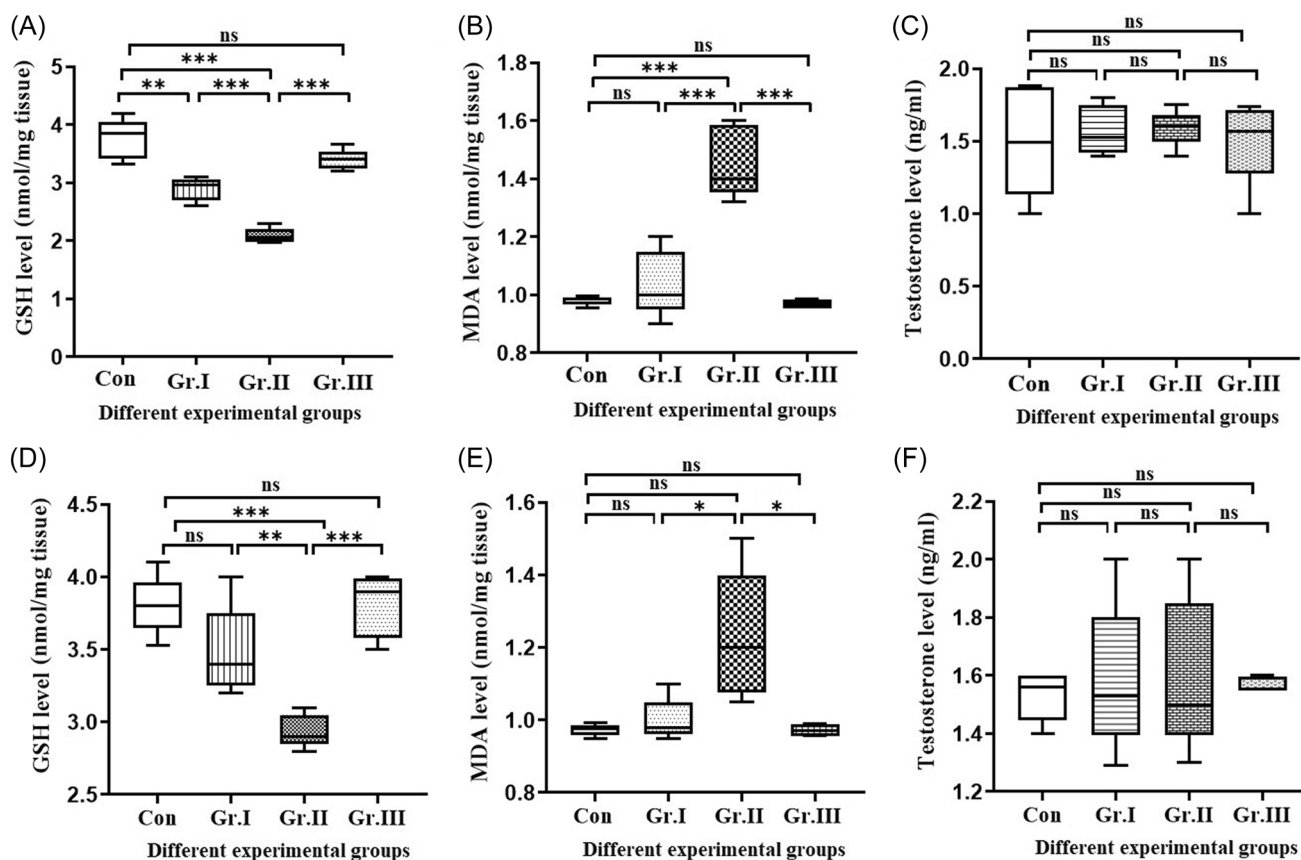


FIGURE 4 Impact of metal and resveratrol treatment on the oxidative stress markers and testosterone levels of experimental mice. At the end of 16th week of experimental period, testes tissue samples were rapidly excised from the sacrificed animals to determine the levels of oxidative stress markers and plasma testosterone. The box and whisker plots represent (A) significant variations in the level of glutathione (GSH) in two different concentrations of CdCl_2 -treated testes compared to the untreated control and resveratrol cotreated group, (B) significant variations in tissue malondialdehyde (MDA) levels of the aforementioned experimental groups, and (C) no notable differences in the plasma testosterone levels of different Cd-treated groups. The representative box and whisker graphs of $\text{Pb}(\text{CH}_3\text{COO})_2$ -treated groups also showing (D) significant alterations in the GSH concentrations of testes tissues of four experimental groups, (E) notable variations in tissue MDA levels of four $\text{Pb}(\text{CH}_3\text{COO})_2$ concentration groups, and (F) no significant variation in the plasma testosterone levels of Pb-treated experimental mice. The variations in oxidative stress markers' levels and testosterone concentrations in testes tissues of different experimental groups were analyzed by one-way analysis of variance test followed by post hoc Tukey's test. The experiments were repeated three times and data is represented as mean \pm SE. ml, milliliter; mg, milligram; nmol, nanomole; ng, nanogram; ns, not significant; SE, standard error; * $p < 0.05$, ** $p < 0.01$, and *** $p < 0.0001$.

concentrations of CdCl_2 compared to the untreated control. However, no significant alterations in the GSH/GSSG ratio was observed in resveratrol coexposed group compared to the control group ($F = 46.68$, $p < 0.0001$, $R^2 = 0.897$; Con, 89.3 ± 7.37 ; Gr. I, 33.27 ± 2.87 ; Gr. II, 21.01 ± 0.92 ; Gr. III, 71.37 ± 4.89) (Figure 5A).

Similar variations in the GSH/GSSG ratio was also measured in the tissues of four experimental mice groups exposed to varied concentrations of $\text{Pb}(\text{CH}_3\text{COO})_2$, individually or in combination with resveratrol ($F = 24.95$, $p < 0.0001$, $R^2 = 0.823$, Con, 70.13 ± 3.21 ; Gr. I, 45.63 ± 3.10 ; Gr. II, 31.47 ± 1.91 ; Gr. III, 56.15 ± 4.39). However, the calculated GSH/GSSG ratio of two different CdCl_2 concentration groups was found to be significantly lower compared to that of $\text{Pb}(\text{CH}_3\text{COO})_2$ -treated groups (Figure 5B).

3.3 | Histopathological alterations of testicular structures in Cd- and Pb-treated mice: Restorative effects of resveratrol

H&E staining of CdCl_2 - and $\text{Pb}(\text{CH}_3\text{COO})_2$ -treated tissues of different groups showed significant alteration of testicular histo-architecture compared to the control groups. The testicular histology of control mice of both the metal groups showed normal histological structures with functioning, mature seminiferous tubules, and complete spermatogenic series. In the low CdCl_2 dose group (Gr. I, 0.25 mg/kg body weight), the architecture of the tissue sections showed morphological derangement along with the disrupted development of spermatogonia, spermatocytes, and differentiating spermatids inside seminiferous tubules. Significant numbers of atypical cells were observed in the tissue sections of

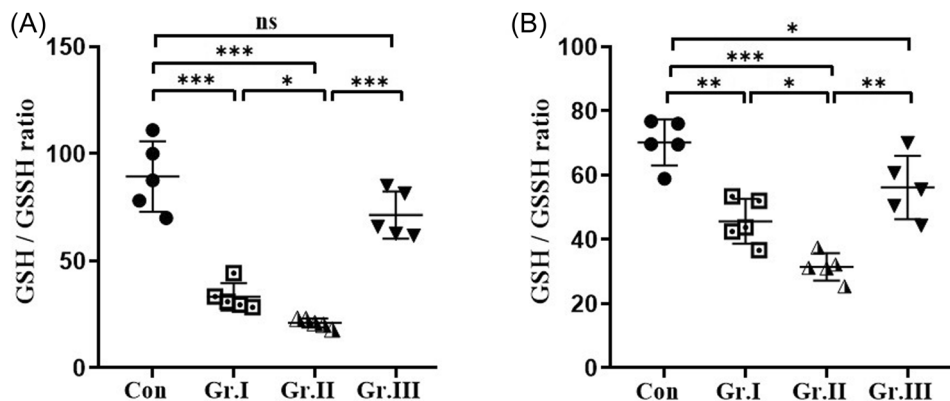


FIGURE 5 Variations in the tissue glutathione/glutathione disulfide (GSH/GSSH) levels in Cd- and Pb-treated mice. The ratio of reduced GSH and GSSG concentrations in the testes tissues of mice, treated with CdCl₂ and Pb(CH₃COO)₂, individually or in combination with resveratrol for 16 weeks were calculated and graphically represented. (A) The graph is showing notable decrease in the tissue GSH and GSSH ratio of mice treated with increasing concentrations of CdCl₂ (Gr. I and Gr. II) compared to the control and resveratrol cotreated testes tissues. (B) Similar variations in the ratio of tissue GSH and GSSH levels of different Pb(CH₃COO)₂-treated groups are represented in this graph. Con = control group, 0.9% NaCl; Gr. I = CdCl₂ Group I dose = 0.25 mg/kg body weight, Gr. II = CdCl₂ Group II dose = 0.50 mg/kg body weight, Gr. III = CdCl₂ Group III dose = resveratrol 20 mg/kg body weight + CdCl₂ 0.50 mg/kg body weight; Pb(CH₃COO)₂ Group I dose = 3 mg/kg body weight, Pb(CH₃COO)₂ Group II dose = 6 mg/kg body weight, Pb(CH₃COO)₂ Gr. III dose = resveratrol 20 mg/kg body weight + Pb(CH₃COO)₂ 6 mg/kg body weight. The variations of GSH and GSSH ratio in testes tissues of different experimental groups were analyzed by one-way analysis of variance test followed by post hoc Tukey's test. The experiments were repeated three times and data is represented as mean ± SE. ns, not significant; **p* < 0.05, ***p* < 0.01, and ****p* < 0.0001. SE, standard error.

treated mice. The seminiferous tubules lost their spherical shape and became elongated. Vacuolization in the luminal parts of some tubules with reduced spermatogenesis was prominent. Interestingly, the high dose of CdCl₂ (Gr. II, 0.50 mg/kg body weight) treated tissue sections showed irregularly shaped nuclei, high nucleus to cytoplasmic ratio, chromatin proliferation, and other aberrant cellular morphology. Moreover, focal crowding of moderately dysplastic cells inside the seminiferous tubule was prominently visible which indicated the possibility of GCNIS development. On the other hand, resveratrol cotreated group (Gr. III, CdCl₂ 0.50 mg/kg + resveratrol 20 mg/kg body weight) showed restored germinal epithelium with distinct, spherical seminiferous tubules (Figure 6A).

Among the Pb-treated groups, the tissue sections of low dose of Pb(CH₃COO)₂ (Gr. I, 3 mg/kg body weight) treated mice showed distortion of the seminiferous tubules and loss of differentiating sperm cells. Edema in interstitial space and nuclear atypia of germ cells were also some of the distinct features observed in these tissue sections. The high Pb(CH₃COO)₂ (Gr. II, 6 mg/kg body weight) treated tissues showed significant morphological derangement in seminiferous tubules. Tubular lumens filled with degenerated germ cells, prominent focal necrosis, and testicular edema were clearly observed in the tissue sections compared to that of the control group. Here also, the resveratrol cotreatment (Gr. III, Pb 6 mg/kg + resveratrol 20 mg/kg body weight) visibly improved testes histo-architecture with redeveloped seminiferous tubules (Figure 6B).

3.4 | Immunohistochemical analysis of Akt cascade proteins in testes tissues of experimental mice

The immunohistochemical studies revealed aberrant expression of Akt and its downstream key proteins NF-κB and Cox-2 in germinal epithelium, sertoli cells, and interstitial cells of the two different CdCl₂ dose-treated tissue sections compared to the untreated control group. Pronounced expressions of the aforementioned proteins were also observed in patches of dysplastic lesions in CdCl₂-treated tissues (Gr. I and Gr. II). Moreover, enhanced immunopositive expression of proteins was recorded in cells, clustered in the form of degenerated clumps inside the tubular lumen of testes tissues of high dose of CdCl₂-treated mice (Gr. II). Distinct nuclear localization of NF-κB(p50) was observed in cells of Gr. II tissues. The key protein of the Akt downstream cascade, that is, Cox-2, showed significant cytoplasmic expressions in germ cells of seminiferous tubules and interstitial tissues. However, weak positive expressions of the above-mentioned proteins were observed in the resveratrol cotreated tissues (Gr. III). The Akt cascade protein expressions recorded by semi-quantitative IHC scoring method and analyzed by ANOVA showed that the mean expression of p-Akt (*F* ratio = 21.06, *p* < 0.0001, *R*² = 0.7980), NF-κB(p50; *F* ratio = 73.27, *p* < 0.0001, *R*² = 0.9322) and Cox-2 (*F* ratio = 220.0, *p* < 0.0001, *R*² = 0.9763) varied significantly among the four experimental groups. Interestingly, intense IHC staining with highest percentage of DAB expression (>76%) of Akt, NF-κB (p50), and Cox-2 proteins was observed in high CdCl₂ (0.5 mg/kg of body weight) treated tissues,

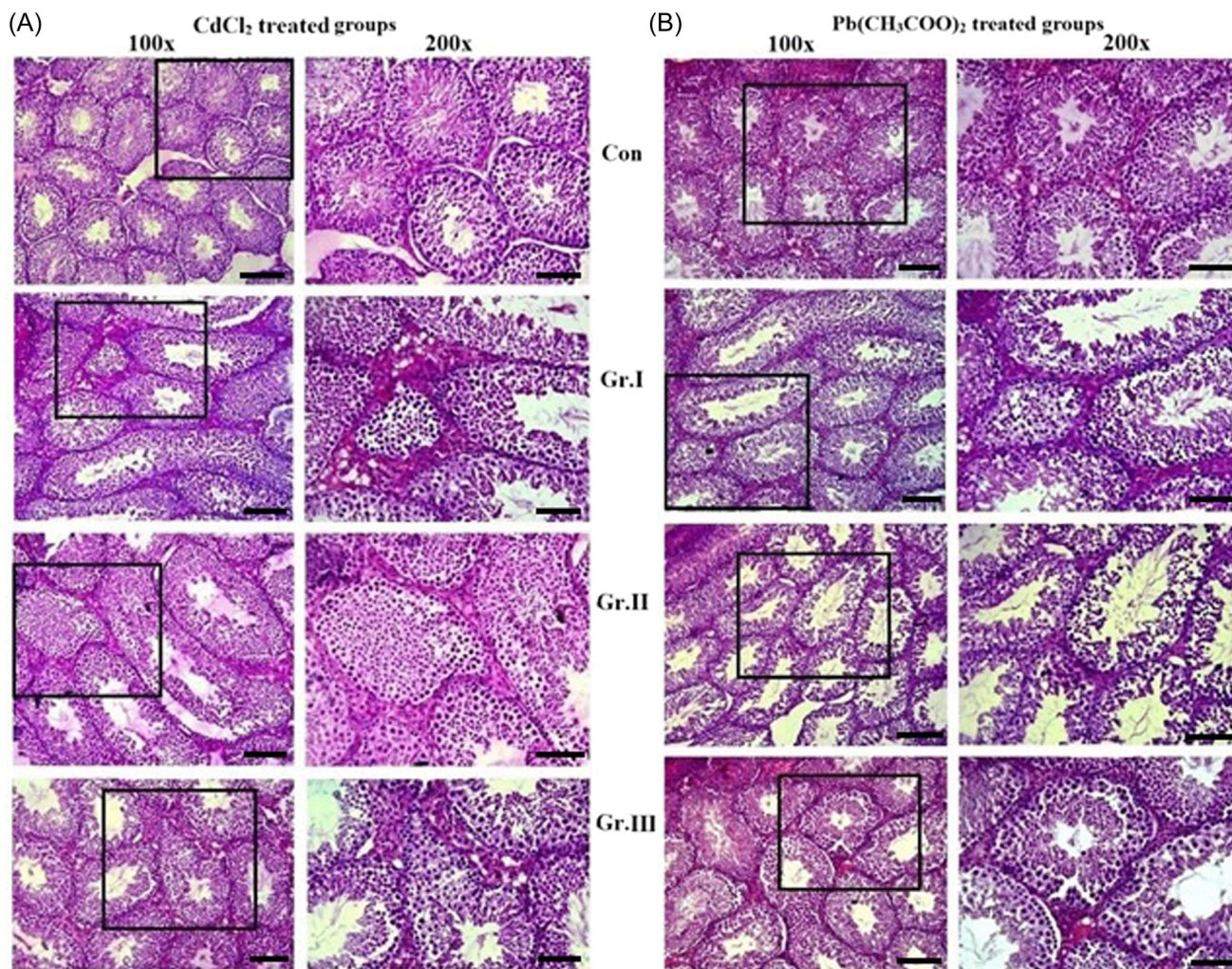


FIGURE 6 Resveratrol confers protection against metal-induced histological alterations in mice testes tissues. The photomicrographs of testes tissue sections of experimental mice after hematoxylin and eosin staining. (A) showing high percentage of histo-architectural derangement in only CdCl_2 -treated mice tissues compared to the control. In high CdCl_2 -treated group (Gr. II), aggregation of dysplastic cells can be observed inside the seminiferous tubules. Restored tissue morphology in the section of resveratrol cotreated group was visible. (B) High percentage of morphological abnormalities including distortion of the shape of seminiferous tubules and loss of differentiating sperm cells can be observed in only $\text{Pb}(\text{CH}_3\text{COO})_2$ -treated testes tissue sections (Gr. I and Gr. II) compared to the control group and the resveratrol cotreated group (Gr. III). All images are taken in 100x and 200x magnification. The boxes outlined with solid black lines are the representative sites in the 100x images. The 200x images are showing high-magnification views of the boxed areas. Scale bar corresponds to 50 μm .

whereas weak to moderate intensity of staining and moderate DAB expression (26%–50%) of proteins was recorded in low CdCl_2 dose group. The untreated control group and the resveratrol cotreated group showed negative and weak DAB expression respectively (Figure 7A).

The $\text{Pb}(\text{CH}_3\text{COO})_2$ -treated mice tissue sections showed similar variations in expression patterns of Akt cascade proteins of four experimental groups. The average protein expression of control and resveratrol cotreated tissue was significantly reduced compared to two $\text{Pb}(\text{CH}_3\text{COO})_2$ -treated groups. The semi-quantitative IHC scores showed that the mean expression of Akt (F ratio = 15.07, $p < 0.0001$, $R^2 = 0.7386$), NF- κB (p50) (F ratio = 70.93, $p < 0.0001$, $R^2 = 0.9301$) and Cox-2 (F ratio = 58.42, $p < 0.0001$, $R^2 = 0.916$) reasonably varied among the four Pb-treated groups of mice (Figure 6B). However, the

intensity of IHC staining and the percentage of DAB expression of Akt cascade proteins recorded in Pb-treated tissues were notably ($p < 0.0001$) lower than the Cd-treated groups (Figure 7B).

3.5 | Assessment of the Akt and downstream signaling proteins by western blot

The results obtained by immunohistochemical analysis were further corroborated by the western blot analysis. The densitometry results showed notable ($p < 0.0001$) overexpression of total Akt, p-Akt, NF- κB (p50), and Cox-2 proteins in testes tissues of mice treated with increasing concentrations of CdCl_2 (Gr. I and Gr. II) compared to the control and resveratrol cotreated group (Gr. III). The ANOVA results

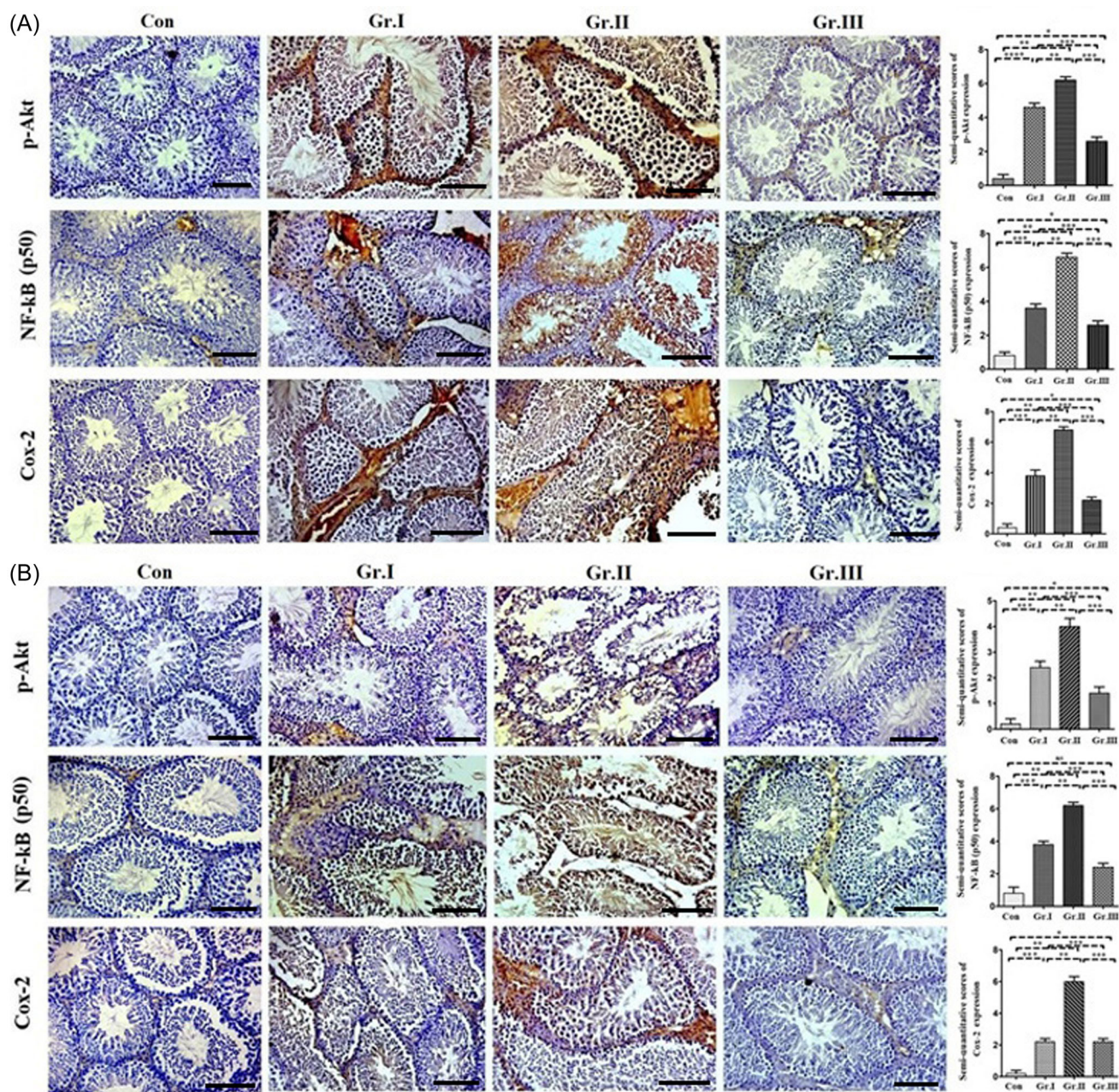


FIGURE 7 Immunohistochemical analysis of Akt cascade proteins in testes tissue sections of different experimental groups. The photomicrographs of immunohistochemical analysis of two different concentrations of CdCl₂ (Gr. I and Gr. II) treated testes tissue sections showing (A) significantly high expression of p-Akt, NF-κβ(p50), and Cox 2 proteins in patches of dysplastic cells and distorted seminiferous tubules compared to the control group and resveratrol coadministered Gr. III tissues. The bar diagrams showing notable ($p < 0.0001$) variations in the IHC scores (which is a sum of staining intensity and percentage of cells with DAB expression) of p-Akt, NF-κβ(p50), and Cox-2 expression of four different CdCl₂-treated groups (control, Gr. I, Gr. II, and Gr. III) calculated by semi-quantitative method. (B) Similar variations in the expression of Akt cascade proteins were recorded in two different concentrations of Pb(CH₃COO)₂ (Gr. I, Gr. II) treated groups compared to the control and Gr. III tissues. The bar diagram represents the IHC scores of p-Akt, NF-κβ(p50), and Cox-2 of four Pb treatment groups (control, Gr. I, Gr. II, and Gr. III). All images are taken in 200x (inset) magnification. Scale bar corresponds to 50 μm. The variations in IHC scores of Akt cascade protein expressions in testes tissues of different experimental groups were analyzed by one-way analysis of variance test followed by post hoc Tukey's test. The experiments were repeated three times and data is represented as mean ± SE. ns, not significant; * $p < 0.05$, ** $p < 0.01$, and *** $p < 0.0001$. SE, standard error.

highlighted on the significant difference (F ratio = 21.43, $p = 0.0004$, $R^2 = 0.889$) between mean expressions of proteins in four CdCl₂ treatment groups (Akt: control, 0.366 ± 0.028 , Gr. I, 0.838 ± 0.031 and Gr. II, 1.306 ± 0.082 , Gr. III, 0.996 ± 0.023 ; p-Akt: control, 0.222 ± 0.0058 ,

Gr. I, 0.852 ± 0.026 , Gr. II, 1.216 ± 0.033 , Gr. III, 0.176 ± 0.0211 ; NF-κβ (p50): control, 0.346 ± 0.008 , Gr. I, 0.786 ± 0.016 , Gr. II, 1.408 ± 0.034 , Gr. III, 0.364 ± 0.010 ; Cox-2: control, 0.28 ± 0.017 , Gr. I, 1.398 ± 0.054 , Gr. II, 1.504 ± 0.028 , Gr. III, 0.474 ± 0.016) (Figure 8A).

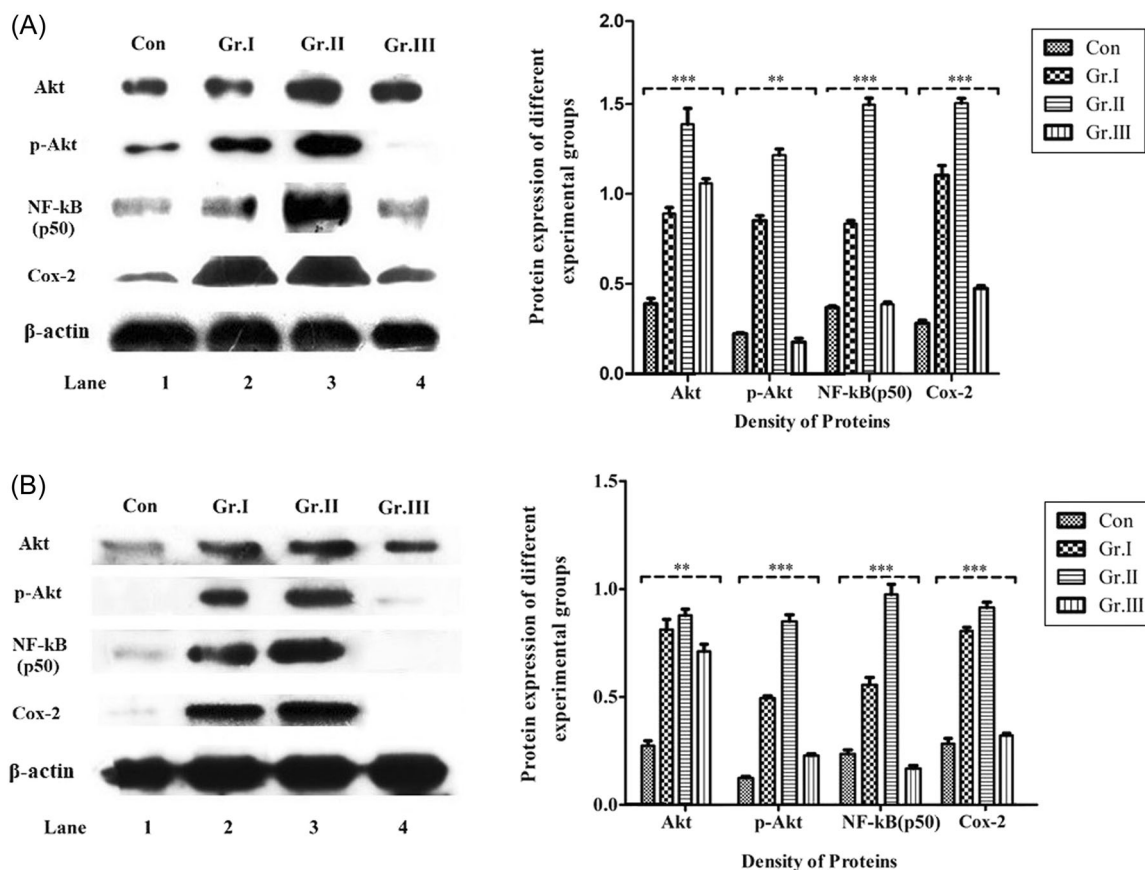


FIGURE 8 Evaluation of Akt cascade protein expressions in tissues of different groups of experimental mice by western blot analysis. The tissue lysates of experimental mice treated with CdCl₂ and Pb(CH₃COO)₂ separately or in combination with resveratrol were subjected to western blot analysis for the quantitative assessment of total Akt, p-Akt, NF-κB(p50), and Cox2 protein expression. The blots were scanned and the intensity of the bands was quantified by densitometry. The representative images of the blots and the respective bar diagram showing (A) notable high expression of total Akt, p-Akt, and downstream proteins NF-κB(p50), Cox2 in Gr. I and Gr. II CdCl₂-treated tissues compared to that of the control group and Gr. III tissues (resveratrol cotreated group). (B) The western blot results of Pb(CH₃COO)₂-treated tissues showing similar but less significant variation in the expression pattern of proteins among four experimental groups compared to the Cd-treated groups. The variations in expression patterns of Akt cascade proteins in testes tissues of different experimental groups were analyzed by one-way analysis of variance test followed by post hoc Tukey's test. The experiments were repeated three times and the data is represented as mean ± SE. β-actin was used as the loading control to confirm equal distribution of proteins. Con = control group, 0.9% NaCl; Gr. I = CdCl₂ Group I dose = 0.25 mg/kg body weight, Gr. II = CdCl₂ Group II dose = 0.50 mg/kg body weight, Gr. III = CdCl₂ Group III dose = resveratrol 20 mg/kg body weight + CdCl₂ 0.50 mg/kg body weight; Pb(CH₃COO)₂ Group I dose = 3 mg/kg body weight, Pb(CH₃COO)₂ Group II dose = 6 mg/kg body weight, Pb(CH₃COO)₂ Gr. III dose = resveratrol 20 mg/kg body weight + Pb(CH₃COO)₂ 6 mg/kg body weight. ns, not significant; **p* < 0.05, ***p* < 0.01, and ****p* < 0.0001. SE, standard error.

On the other hand, the variations in Akt cascade protein expression among the Pb-treated tissues were not as significant as observed in Cd treatment groups. However, ANOVA results suggest (*F* ratio = 4.510, *p* = 0.0393, *R*² = 0.6284) that the average expression of Akt, p-Akt, NF-κβ(p50), and Cox-2 in testes of mice treated with two different doses of Pb(CH₃COO)₂ (Akt: Gr. I, 0.788 ± 0.045 and Gr. II, 0.852 ± 0.028; p-Akt: Gr. I, 0.494 ± 0.011 and Gr. II, 0.85 ± 0.030; NF-κβ(p50): Gr. I, 0.556 ± 0.033 and Gr. II, 1.01 ± 0.003; Cox-2: Gr. I, 0.782 ± 0.016, and Gr. II, 0.914 ± 0.025) was notably higher than the untreated control group (Akt: 0.266 ± 0.021; p-Akt: 0.124 ± 0.007; NF-κβ(p50): 0.236 ± 0.018, and Cox-2: 0.274 ± 0.024). Whereas, the protein expression results of the control groups did not show any notable difference with the results of the resveratrol

cotreatment group (Akt: 0.69 ± 0.032; p-Akt: 0.228 ± 0.008; NF-κβ(p50): 0.168 ± 0.013, and Cox-2: 0.302 ± 0.010) (Figure 8B).

3.6 | Association between overexpression of Akt cascade proteins, altered sperm parameters, and oxidative stress in different experimental groups

The Pearson's correlation results showed significant positive association between increasing expression of Akt cascade proteins, percentage of sperm cell abnormalities, and altered level of oxidative stress marker, GSH, in testes tissues of CdCl₂- and Pb(CH₃COO)₂-treated mice. The correlation between the results of different

experimental parameters of Cd- and Pb-treated mice was represented as correlation matrices. The color of each box represents the level of correlation between the parameters. Blue represented positive correlation, whereas red represented negative correlation. Notable positive ($p < 0.001$) associations were observed between enhanced expressions of Akt cascade proteins and percentage of morphologically abnormal sperm cells. Conversely, significant inverse correlation was recorded between high expression of Akt cascade proteins and the percentage of motile sperm cells as well as tissue GSH concentrations, in two CdCl₂ treatment groups (Gr. I and Gr. II). The represented correlation matrix showed less notable associations between the aforementioned proteins and the sperm parameters among the Pb(CH₃COO)₂-treated mice groups (Figure 9A,B).

3.7 | Variations in testicular carcinoma in situ (CIS) marker protein expressions in Cd-treated tissues

Immunohistochemistry results showed prominent expressions of testicular GCNIS (formerly known as CIS) markers, c-Kit (F ratio = 31.79, $p < 0.0001$, $R^2 = 0.856$) and Oct 3/4 (F ratio = 81.51, $p < 0.0001$, $R^2 = 0.9386$) in testes tissues of mice treated with two different concentrations of CdCl₂ compared to the untreated control group. Additionally, the resveratrol cotreated group did not show any significant expression of the marker proteins. The IHC scores calculated by the semi-quantitative method showed intense IHC staining with highest percentage of DAB expression (>76%) of c-Kit

and Oct 3/4 proteins in high CdCl₂-treated tissues (Gr. II) compared to the other experimental groups. The Gr. III or the resveratrol cotreatment group showed weak staining with very low percentage of DAB expression (<25%). This indicated that prolonged exposure to low doses of Cd compound stimulated an elevated expression of CIS markers, c-Kit and Oct 3/4, in the testes of experimental mice. However, the resveratrol cotreatment effectively suppressed the upregulation of c-Kit and Oct3/4 proteins in Gr. III (Figure 10).

Interestingly, no significant expression of c-Kit (F ratio = 1.41, $p = 0.275$, $R^2 = 0.2096$) and Oct 3/4 (F ratio = 2.24, $p = 0.33$, $R^2 = 0.409$) were observed in two different concentrations of Pb (CH₃COO)₂ treatment groups (Gr. I and Gr. II) compared to the untreated control and resveratrol cotreatment group (Gr. III; Figure 11).

4 | DISCUSSION

The underlying molecular mechanism of metal-induced toxicities in mammalian testes is a result of interactions of a complex network of molecules which is yet to be explored properly.^[56–58] However, testicular changes due to Cd-induced toxicity have been recorded in a variety of animal models at different stages of growth and maturity.^[59] In our previous published study, we observed that a 2 weeks exposure of two different CdCl₂ doses (1.25 mg/kg body weight and 2.5 mg/kg body weight) to mice perturbs semen parameters, testicular histopathology, and EGFR cascade protein

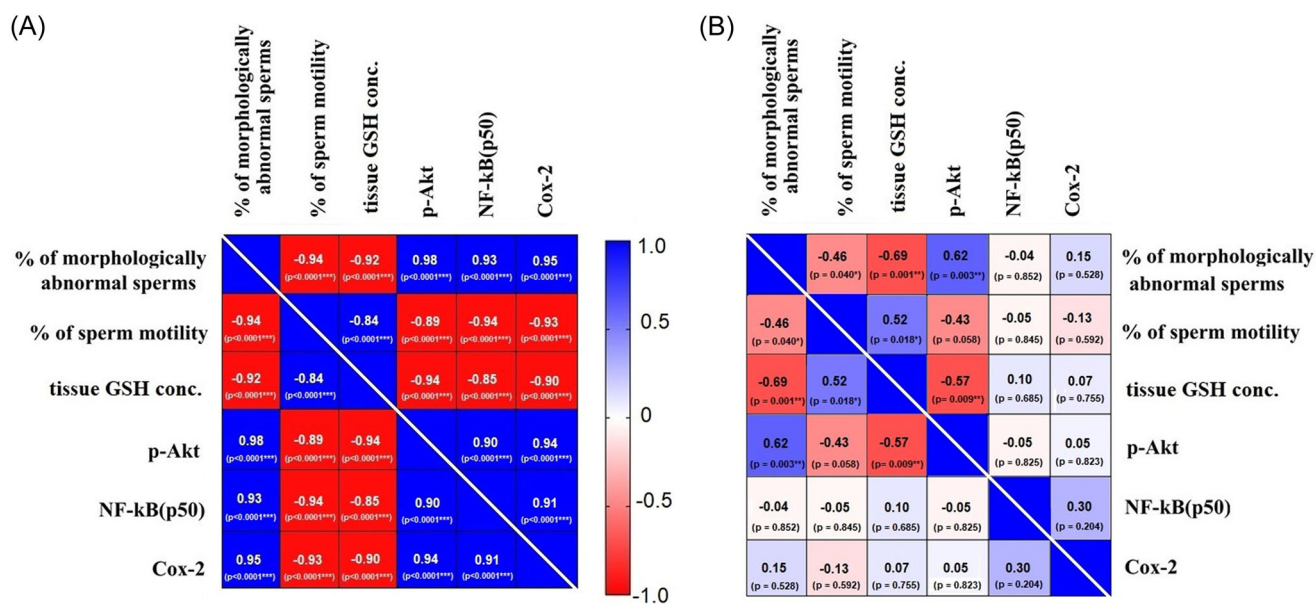


FIGURE 9 Analysis of the associations between different experimental parameters by correlation coefficient matrix. The correlation matrices are representing the association between the upregulation of Akt cascade proteins, alterations in the level of sperm parameters, and oxidative marker, GSH upon a 16-week long, sub-chronic exposure to CdCl₂, and Pb(CH₃COO)₂ doses. The color of each box represents the level of correlation between the analyzed parameters. In this matrix, blue represents positive correlation, red represents negative correlation between the mentioned parameters of (A) different CdCl₂-treated experimental groups and (B) different Pb(CH₃COO)₂-treated groups. The Pearson's correlation coefficient and p values are presented in each box. r = Pearson's correlation coefficient, ns = not significant, % = percentage, conc. = concentration, * $p < 0.05$, ** $p < 0.01$, and *** $p < 0.0001$.

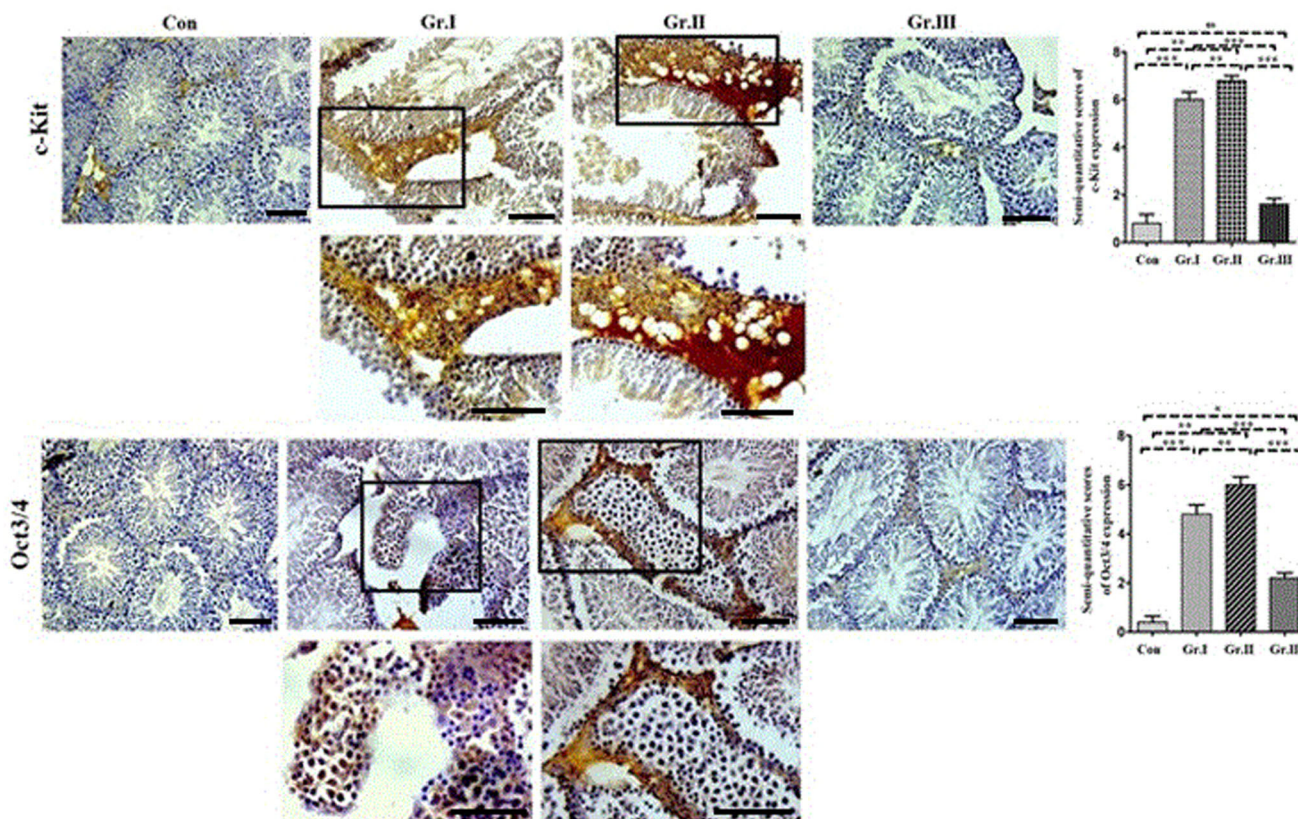


FIGURE 10 Alterations in expression patterns of testicular GCNIS markers in the testes of Cd-treated mice. The overexpression of testicular GCNIS markers, c-Kit, and Oct3/4, were prominent in CdCl₂-treated mice tissues compared to the control group. Resveratrol coadministered tissues did not show any notable expression of the markers. The IHC scores of immuno-positive cells calculated by semi-quantitative method in the tissue sections are graphically represented. All images are taken in 200x (inset) magnification. The boxes outlined with solid black lines are the representative sites of the 200x images. The 400x images represent the high-magnification views of the boxed areas to highlight the expression of proteins in that particular part of the tissue section. Scale bar corresponds to 50 μ m. The variations in IHC scores of c-Kit and Oct3/4 protein expressions in testes tissues of different experimental groups were analyzed by one-way analysis of variance test followed by post hoc Tukey's test. The experiments were repeated three times and data is represented as mean \pm SE. ns, not significant; * p < 0.05, ** p < 0.01, and *** p < 0.0001. SE, standard error.

expression while cotreatment of resveratrol alleviates the toxic effects of the metal.^[60] The findings of this study were consistent with the previous results and elucidated that 16-week long sub-chronic exposure to CdCl₂ doses (0.25 and 0.5 mg/kg of body weight) caused significant alterations of body weight, semen parameters, and oxidative stress levels in testes tissues compared to the untreated control and resveratrol cotreated mice. Similarly, the toxicity of Pb has also been well-documented in mammalian system and the findings showed that exposure to Pb affects libido along with semen parameters in male reproductive system.^[61,62] The results of the present study were in agreement with the previous findings which showed that sub-chronic exposure to Pb(CH₃COO)₂ doses (3 and 6 mg/kg respectively) for 16 weeks, induced significant alterations in all sperm parameters except sperm density and percentage of motile sperm cells of mice compared to the untreated control group.

Increase in the level of cellular oxidative stress and generation of reactive oxygen species (ROS) has been associated with severe pathological conditions which induces compensatory upregulations of antioxidant systems to restore the redox homeostasis.^[63] Among

the enzymatic systems involved in the maintenance of the intracellular thiol-redox balance, glutathione (GSH) is an abundant tripeptide thiol in aerobic cells.^[64] Glutathione peroxidase catalyzes the formation of GSSG from GSH, and glutathione reductase recycles GSSG to GSH. Measuring the GSH/GSSG ratio in pathological tissues is an excellent way to assess cellular redox state.^[65–67] It has been observed that GSH/GSSG ratio is significantly lower in men with abnormal semen parameters.^[68–70] Alterations in the GSH/GSSG index have also been implicated in malignancies of different organs and in cancer cell resistance.^[71–73] Interestingly, our findings highlighted that sub-chronic exposure to low doses of CdCl₂ and Pb(CH₃COO)₂ significantly decreases the intracellular GSH/GSSG ratio which in turn shifts the intracellular redox balance towards acute oxidative stress condition.

The findings of our studies showed that prolonged exposure to metallic compounds [CdCl₂ and Pb(CH₃COO)₂] induced high oxidative stress, which in turn caused testicular histo-architectural degeneration and necrosis. These observations are supported by existing literature.^[74–76] Interestingly, the high dose of CdCl₂-treated

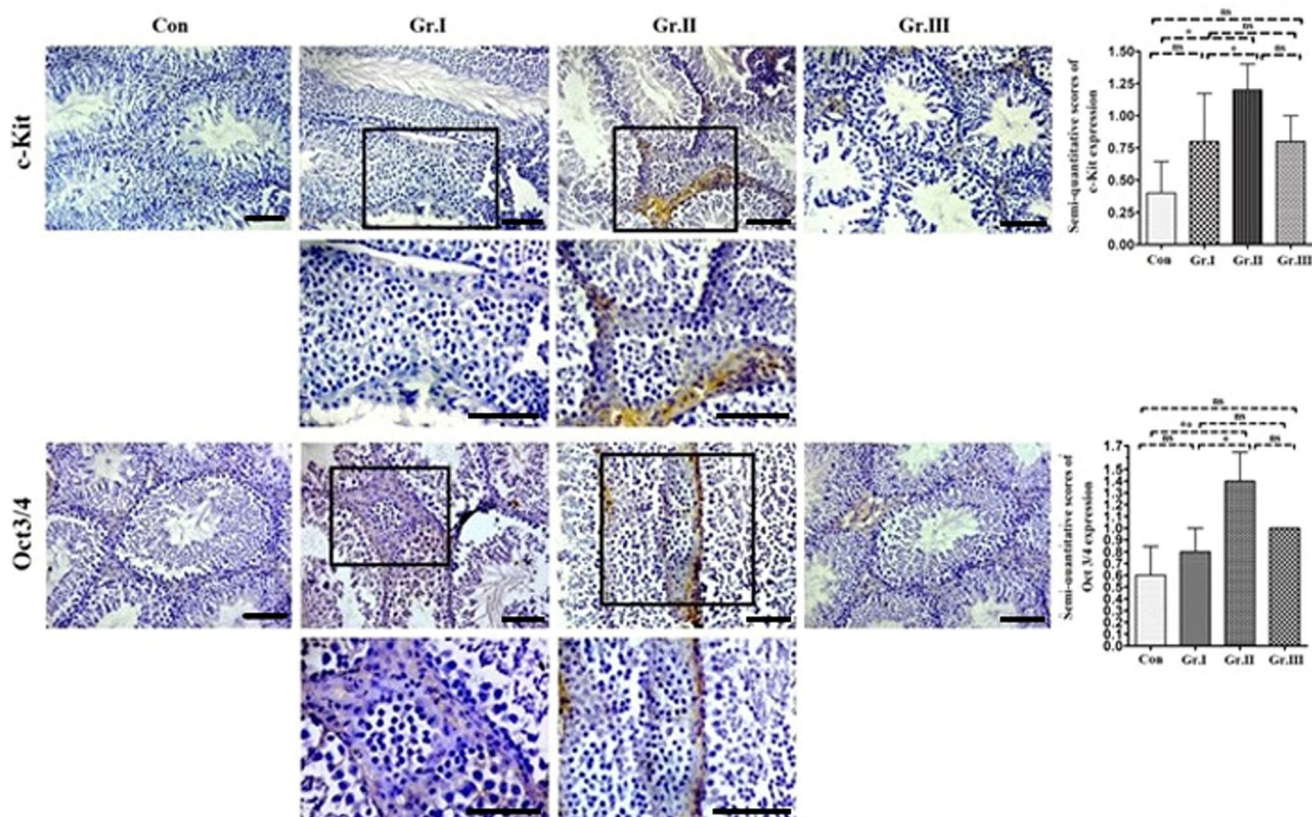


FIGURE 11 Expression patterns of testicular germ cell neoplasia in situ (GCNIS) markers in testes of Pb-treated mice. No significant expression of testicular GCNIS/CIS marker proteins, c-Kit, and Oct3/4, was observed in groups of mice sub-chronically exposed to Pb (CH_3COO)₂ for 16 weeks. The graphical representation of the IHC scores of the marker proteins showing no notable variations in the scores among the experimental groups. All images are taken in 200x (inset) magnification. The boxes outlined with solid black lines are the representative sites of the 200x images. The 400x images represent the high-magnification views of the boxed areas to highlight the expression of proteins in that particular part of the tissue section. Scale bar corresponds to 50 μm . The variations in IHC scores of c-Kit and Oct3/4 protein expressions in testes tissues of different experimental groups were analyzed by one-way analysis of variance test followed by post hoc Tukey's test. The experiments were repeated three times and data is represented as mean \pm SE. ns, not significant; * $p < 0.05$, ** $p < 0.01$, and *** $p < 0.0001$. SE, standard error.

tissue sections showed aberrant cellular morphology, high nucleus to cytoplasmic ratio, and focal crowding of moderately dysplastic cells inside the seminiferous tubule indicating the possibility of GCNIS development. These observations were also in agreement with previous studies.^[77,78]

Cd has been shown to interact with the PI3K/Akt cascade via ROS and non-ROS-mediated pathways.^[79,80] The Akt signaling pathway has been involved in many critical cellular functions, including protein synthesis, proliferation, apoptosis in response to diverse growth factors (such as EGF, VEGF, etc.), hormones, and cytokine stimulation. There is an array of different upstream stimuli of Akt, which can induce activation of Akt signaling cascade.^[81–83] It was a conscious decision to focus on Akt and its downstream proteins NF- κB (p50) and Cox-2 for this study, as there can be several upstream growth factors or stimulators involved in the upregulation of Akt. The binding of growth factor ultimately activates Akt serine/threonine kinases, which successively promotes the induction of downstream target genes including transcription factor NF- κB and

Cox-2. Recent studies indicate that accumulated ROS in cells actively induces the upregulation of NF- κB ,^[84–86] which has been associated with the control of multiple cellular processes including proliferation, metastasis, and upregulation of the downstream key molecule Cox-2.^[87–92] On the other hand, aberrantly activated Akt cascade, primarily caused by the defect of its corresponding phosphatase PTEN, has been implicated in the pathogenesis of multiple critical disorders, including reproductive impairment and different forms of cancers.^[93–95] Our study showed significant inverse associations between activated Akt cascade protein expressions and tissue GSH concentrations of mice exposed to two different concentration of CdCl₂ for 16 weeks. However, less significant associations were observed between the above-mentioned parameters among the Pb (CH_3COO)₂-treated groups. These observations significantly implied that prolonged, sub-chronic exposure to Cd or Pb compounds induced oxidative stress and an increase in the cellular ROS production which leads to the amplification of Akt signaling cascade (a potent modulators of cellular redox balance). The upregulation of

Akt cascade resulted in dysregulation of GSH biosynthesis. On the other hand, histopathological findings of our study highlighted on the focal clumping of atypical dysplastic cells and patches of proliferative lesions inside the seminiferous tubules along with strong positive expressions of Akt cascade proteins in these testes tissue sections of CdCl₂-treated mice groups. Partial necrosis, morphological alteration of seminiferous tubules, and higher than the normal expression of these proteins were also observed in the cross-sections of Pb (CH₃COO)₂-treated testes tissues. The significant morphological alterations and signs of GCNIS development prompted us to further check the expressions of testicular CIS markers c-Kit and Oct3/4 in experimental tissue sections.

TGCTs originate from CIS cells, which are found on the basement membrane of abnormal seminiferous tubules. GCNIS is the pre-cancerous lesion of testes, formerly known as testicular CIS (carcinoma in situ) or ITGGNU (intratubular germ cell neoplasia unclassified). Existing studies suggest that GCNIS consists of neoplastic gonocyte-like germ cells and are common precursors of seminoma and nonseminoma development.^[96,97] Morphologically, the GCNIS or CIS cells resemble primordial germ cells and express number of markers including c-Kit and Oct 3/4. Therefore, c-Kit and Oct 3/4 are identified as testicular CIS markers.^[98–100] The immunohistochemical data of our study showed higher than the normal expression of c-Kit and Oct-3/4 in atypical cell patches of CdCl₂-treated testes tissues compared to the untreated control. In contrast, immunohistochemical results of Pb(CH₃COO)₂-treated tissues

showed basal expression of c-Kit and Oct 3/4 proteins in testes of experimental mice. These findings indicate that prolonged exposure to low doses of Cd compound may lead to the initiation of malignant transformation of testicular cells, while chronic exposure to Pb compound did not induce any noticeable carcinogenic alterations in testicular tissues of Pb-treated mice. Recent findings suggest that Akt and Oct4 are connected by a regulatory circuit which is expressed in embryonic stem cells and plays a significant role in the development of embryonal carcinoma.^[101,102] Another finding suggested that the c-Kit receptor promotes cell survival via activation of Akt-mediated phosphorylation of Bad on Ser136.^[103] However, the precise molecular mechanism by which Akt activation induces Oct3/4 or c-Kit overexpression is yet to be investigated in detail.

Previous in vitro and in vivo investigations highlighted the biological attributes of resveratrol.^[104–106] The antioxidant properties of resveratrol in vivo include inhibition of NADPH oxidase-mediated production of ROS by downregulating the expression of the oxidases.^[107,108] Resveratrol also acts as a potent chemopreventive compound and one of its key molecular targets is Akt.^[109,110] Our previous study showed that a short-term cotreatment of resveratrol with the CdCl₂ markedly improved the sperm quality, distorted testicular histology, and decreased the overexpression of signaling proteins.^[60] Consistently, the results of the present investigation showed that prolonged administration of 20 mg/kg resveratrol with toxic metallic compounds can significantly improve sperm motility, morphology, and density by inducing the biosynthesis

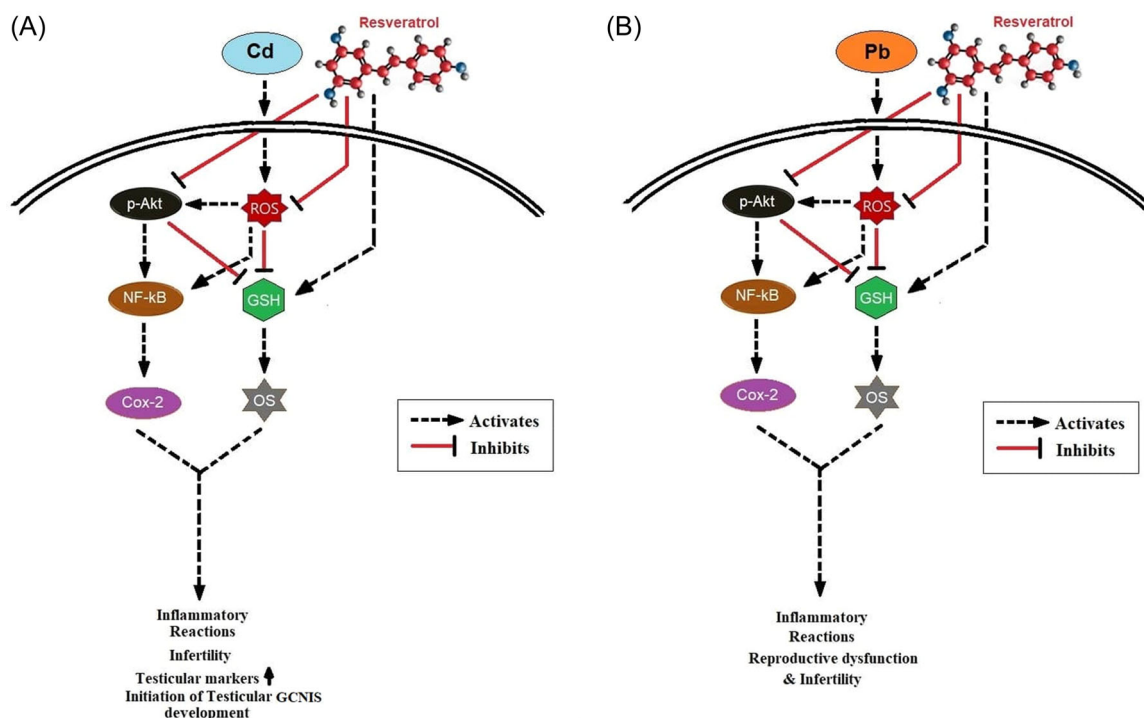


FIGURE 12 The schematic representation of the probable molecular events. (A) The diagrammatic representation of the probable molecular mechanism of action of Cd compound and the mitigative actions of resveratrol treatment against Cd-induced toxicity in testicular tissues of experimental mice. (B) Similar schematic representation of the possible mechanism of action of Pb and resveratrol treatment in testicular tissues of different treatment groups of mice. GCNIS, germ cell neoplasia in situ; OS, oxidative stress; ROS, reactive oxygen species.

of cellular GSH. The existing literature regarding the chemopreventive role of resveratrol also resonated with our observations which showed that it can significantly inhibit the Cd or Pb induced aberrant expression of Akt cascade proteins, consequently reducing the cellular oxidative stress in vivo. Restoration of cellular redox balance resulted in reduced cellular toxicity and suppression of GCNIS development.

5 | CONCLUSION

Taken together, our findings showed that long-term exposure to low concentration of CdCl₂ and Pb(CH₃COO)₂ induced an increased production of cellular ROS, which inhibited the biosynthesis of GSH and stimulated the upregulation of Akt and downstream signaling proteins. In turn, activated Akt reduced the production of cellular GSH, resulting in acute cellular oxidative stress. Significant alterations in cellular redox balance for a long period of time resulted in reduced reproductive capacity and initiation of testicular GCNIS development in treated experimental mice (Figure 12). In contrast, consumption of resveratrol effectively reversed the metal-induced reproductive toxicity and carcinogenicity, restoring oxidative balance in mice testes tissues.

AUTHOR CONTRIBUTIONS

Sreyashi Mitra and Nabendu Murmu conceptualized, formulated the hypothesis, and designed the study. Tapas Patra provided significant insights to formulate the hypothesis. Depanwita Saha and Paramita Ghosh helped in giving doses to experimental animals. Depanwita Saha and Paramita Ghosh helped Sreyashi Mitra to perform the experiments on the animal tissues. Saunak Mitra Mustafi examined and analyzed the histological alterations in mice tissues. Sreyashi Mitra and Tapas Patra performed the statistical analysis. Sreyashi Mitra, Saunak Mitra Mustafi, Tapas Patra, and Alex C. Varghese interpreted the clinical data. Nabendu Murmu, Tapas Patra, and Alex C. Varghese gave valuable inputs in writing the manuscript. Sreyashi Mitra wrote the manuscript. Nabendu Murmu supervised the entire project.

ACKNOWLEDGMENTS

This entire work was funded by institute fund of Chittaranjan National Cancer Institute (CNCI). All the works were performed at Department of Signal transduction and Biogenic Amines (STBA), Chittaranjan National Cancer Institute (CNCI). We sincerely thank Dr. Jayanta Chakraborti, Director, Chittaranjan National Cancer Institute (CNCI), Kolkata for his kind cooperation. We are thankful to everyone associated with this study for their kind cooperation and support.

CONFLICTS OF INTEREST

The authors declare no conflicts of interest.

DATA AVAILABILITY STATEMENT

Data are available in the article's supplementary material.

ORCID

Nabendu Murmu  <http://orcid.org/0000-0002-1311-9479>

REFERENCES

- [1] S. Hossain, G. A. Latifa, *J. Health Pollut.* **2019**, 9(23), 190913.
- [2] H. Abadin, A. Ashizawa, Y.-W. Stevens et al., *Production, Import/Export, Use, and Disposal*, Agency for Toxic Substances and Disease Registry, **2007**.
- [3] Z. He, X. Yang, P. Stoffella, *J. Trace Elem. Med. Biol.* **2005**, 19(2-3), 125-140.
- [4] B. Volesky, M. Sears, R. Neufeld, M. Tsezos, *Recovery of Strategic Elements by Biosorption* **1983**, Wiley-Blackwell, United States, pp. 1749-6632.
- [5] Y. Suwazono, T. Kido, H. Nakagawa, *Biomarkers* **2009**, 14(2), 77.
- [6] M. Azure, R. Archer, K. Sastry, D. Rao, R. Howell, *Radiat. Res.* **1994**, 140(2), 276.
- [7] M. Jaishankar, T. Tseten, N. Anbalagan, B. B. Mathew, K. N. Beeregowda, *Interdiscip. Toxicol.* **2014**, 7(2), 60.
- [8] A. K. Krishna, P. K. Govil, *Environ. Monit. Assess.* **2007**, 124(1-30), 263.
- [9] S. S. Devi, A. R. Biswas, R. A. Biswas, N. Vinayagamoorthy, K. Krishnamurthi, V. M. Shinde, J. G. Hengstler, M. Hermes, T. Chakrabarti, *J. Occup. Environ. Med.* **2007**, 49(11), 1228.
- [10] P. B. Tchounwou, C. G. Yedjou, A. K. Patlolla, D. J. Sutton, *EXS* **2012**, 101, 133.
- [11] D. E. Keil, J. Berger-Ritchie, G. A. McMillin, *Lab. Med.* **2011**, 42(12), 735.
- [12] S. J. Mulware, *3 Biotech.* **2013**, 3(2), 85.
- [13] E. R. Siu, D. D. Mruk, C. S. Porto, C. Y. Cheng, *Toxicol. Appl. Pharmacol.* **2009**, 238(3), 240.
- [14] IARC, *IARC Monographs, Cadmium and Cadmium Compounds*, International Agency for Research on Cancer, Lyon, France **1993**.
- [15] IARC monographs on the evaluation of carcinogenic risks to humans, *Inorganic and Organic Lead Compounds*, International Agency for Research on Cancer **2004**. <http://monographs.iarc.fr/ENG/Monographs/vol87/mono87.pdf>
- [16] S. V. S. Rana, *Biol. Trace Elem. Res.* **2014**, 160, 1.
- [17] J. J. Wirth, R. S. Mijal, *Syst. Biol. Reprod. Med.* **2010**, 56(2), 147.
- [18] P. Rzymiski, K. Tomczyk, P. Rzymiski, B. Poniedziałek, T. Opala, M. Wilczak, *Ann. Agric. Environ. Med.* **2015**, 22(2), 259.
- [19] T. J. Walsh, M. S. Croughan, M. Schembri, J. M. Chan, P. J. Turek, *Arch. Intern. Med.* **2009**, 169(4), 351.
- [20] W. R. Burns, E. Sabanegh, R. Dada, B. Rein, A. Agarwal, *Int. Braz. J. Urol.* **2010**, 36(5), 527.
- [21] R. Jacobsen, E. Bostofte, G. Engholm, J. Hansen, J. H. Olsen, N. E. Skakkebaek, *BMJ* **2000**, 321(7264), 789.
- [22] N. E. Skakkebaek, *Histopathology* **2002**, 41(3A), 2.
- [23] I. Alkan, F. Simşek, G. Haklar, E. Kervancioğlu, H. Ozveri, S. Yalçın, A. Akdaş, *J. Urol.* **1997**, 157(1), 140.
- [24] B. N. Hendin, P. N. Kolettis, R. K. Sharma, A. J. Thomas, Jr., A. Agarwal, *J. Urol.* **1999**, 161(6), 1831.
- [25] D. P. Jones, *Methods Enzymol.* **2002**, 348, 93.
- [26] H. J. Forman, H. Zhang, A. Rinna, *Mol. Aspects Med.* **2009**, 30(1-2), 1.
- [27] L. Cao, D. Waldon, Y. Teffera, *Anal. Bioanal. Chem.* **2013**, 405, 2635.
- [28] E. C. Lien, C. A. Lyssiotis, A. Juvekar, H. Hu, J. M. Asara, L. C. Cantley, A. Toker, *Nat. Cell Biol.* **2016**, 18(5), 572.
- [29] A. Makker, M. M. Goel, A. A. Mahdi, *J. Mol. Endocrinol.* **2014**, 53(3), R103.
- [30] R. L. Elstrom, *Cancer Res.* **2004**, 64(11), 3892.
- [31] R. B. Robey, N. Hay, *Semin. Cancer Biol.* **2009**, 19(1), 25.
- [32] J. R. Testa, A. Bellacosa, *Proc. Natl. Acad. Sci. U.S.A.* **2001**, 98(20), 10983.

- [33] M. Cheung, J. R. Testa, *Curr. Cancer Drug Targets* **2013**, 13(3), 234.
- [34] M. H. Park, J. T. Hong, *Cells* **2016**, 5(2), 15.
- [35] Y. Lin, L. Bai, W. Chen, S. Xu, *Expert Opin. Ther. Targets* **2010**, 14(1), 45.
- [36] A. Greenhough, H. J. Smartt, A. E. Moore, H. R. Roberts, A. C. Williams, C. Paraskeva, A. Kaidi, *Carcinogenesis* **2009**, 30(3), 377.
- [37] F. Pierconti, M. Martini, G. Grande, L. M. Larocca, E. Sacco, D. Pugliese, G. Gulino, P. F. Bassi, D. Milardi, A. Pontecorvi, *Front Endocrinol (Lausanne)* **2019**, 10, 10. <https://doi.org/10.3389/fendo.2019.00512>
- [38] T. Fukawa, H. O. Kanayama, *Int. J. Urol.* **2018**, 25, 337.
- [39] G. Kallifatidis, J. J. Hoy, B. L. Lokeshwar, *Semin. Cancer Biol.* **2016**, 40-41, 160.
- [40] R. Tsobou, P. M. Mapongmetsem, P. Van Damme, *Econ. Bot.* **2016**, 70(2), 145.
- [41] L. G. Carter, J. A. D'Orazio, K. J. Pearson, *Endocr. Relat. Cancer* **2014**, 21(3), R209.
- [42] N. Latruffe, D. Delmas, C. Didier, B. Jannin, P. Dutartre, *Agro. Food Ind. Hi Tech* **2006**, 14.
- [43] National Research Council (US) Committee for the Update of the Guide for the Care and Use of Laboratory Animals, *Guide for the Care and Use of Laboratory Animals*, 8th ed., National Academies Press (US), Washington (DC) **2011**.
- [44] J. T. Litchfield, F. J. Wilcoxon, *J. Pharmacol. Exp. Ther.* **1949**, 96, 9.
- [45] S. Sale, R. D. Verschoyle, D. Boocock, D. J. Jones, N. Wilsher, K. C. Ruparelia, G. A. Potter, P. B. Farmer, W. P. Steward, A. J. Gescher, *Br. J. Cancer* **2004**, 90(3), 736. <https://doi.org/10.1038/sj.bjc.6601568>
- [46] I. M. Kapetanovic, M. Muzzio, Z. Huang, T. N. Thompson, D. L. McCormick, *Cancer Chemother. Pharmacol.* **2011**, 68(3), 593. <https://doi.org/10.1007/s00280-010-1525-4>
- [47] S. Das, H. S. Lin, P. C. Ho, K. Y. Ng, *Pharm. Res.* **2008**, 25(11), 2593. <https://doi.org/10.1007/s11095-008-9677-1>
- [48] A. Shaito, A. M. Posadino, N. Younes, H. Hasan, S. Halabi, D. Alhababi, A. Al-Mohannadi, W. M. Abdel-Rahman, A. H. Eid, G. K. Nasrallah, G. Pintus, *Int. J. Mol. Sci.* **2020**, 21(6), 2084. <https://doi.org/10.3390/ijms21062084>
- [49] M. E. Juan, M. P. Vinardell, J. M. Planas, *J. Nutr.* **2002**, 132(2), 257. <https://doi.org/10.1093/jn/132.2.257>
- [50] F. Y. Özatik, O. Özatik, S. Yiğitaslan, Ç. Ç. Ünel, K. Erol, *Turk. J. Urol.* **2017**, 43(4), 444. <https://doi.org/10.5152/Tud.2017.34101>
- [51] R. Zemjanis *Diagnostic and Therapeutic Techniques in Animal Reproduction* (Eds): R. Zemjanis, The Williams and Wilkins Company, USA **1977**, pp. 139–156.
- [52] C. C. Nascimento, O. A. Junior, V. D'Almeida, *Int. J. Clin. Exp. Pathol.* **2014**, 7(6), 3488.
- [53] G. Ellman, *Arch. Biochem. Biophys.* **1959**, 82, 70.
- [54] H. Ohkawa, N. Ohishi, K. Yagi, *Anal. Biochem.* **1979**, 95(2), 351.
- [55] M. Chevallier, S. Guerret, P. Chossegros, F. Gerard, J. A. Grimaud, *Hepatology (Baltimore, Md.)* **1994**, 20(2), 349.
- [56] R. C. Patra, A. K. Rautray, D. Swarup, *Vet. Med. Int.* **2011**, 2011, 457327. <https://doi.org/10.4061/2011/457327>
- [57] L. Patrick, *Altern. Med. Rev.* **2003**, 8(2), 106.
- [58] R. Toman, P. Massanyi, V. Uhrin, *Trace Elem. Electrolytes* **2002**, 19(3), 114.
- [59] E. R. Siu, D. D. Mruk, C. S. Porto, C. Y. Cheng, *Toxicol. Appl. Pharmacol.* **2009**, 238(3), 240. <https://doi.org/10.1016/j.taap.2009.01.028>
- [60] S. Mitra, S. Bhattacharyya, S. Ray, R. Saha, P. Ghosh, S. Rauth, S. Mandal, S. Banerjee, N. Murmu, *J. Environ. Pathol. Toxicol. Oncol.* **2016**, 35(1), 73.
- [61] S. Telisman, B. Colak, A. Pizent, J. Jurasović, P. Cvitković, *Environ. Res.* **2007**, 105(2), 256. <https://doi.org/10.1016/j.envres.2007.05.011>
- [62] S. Kumar, *Indian J. Occup. Environ. Med.* **2018**, 22(3), 128.
- [63] M. Landriscina, F. Maddalena, G. Laudiero, F. Esposito, *Antioxid. Redox Signal* **2009**, 11(11), 2701.
- [64] A. Meister, *Meth. Enzymol.* **1995**, 251, 3.
- [65] K. Aquilano, S. Baldelli, M. R. Ciriolo, *Front. Pharmacol.* **2014**, 5, 196.
- [66] J. B. Owen, D. A. Butterfield, *Methods Mol. Biol.* **2010**, 648, 269.
- [67] H. Sies, *Redox Biol.* **2015**, 4, 180.
- [68] E. Moretti, L. Micheli, D. Noto, A. I. Fiaschi, A. Menchiari, D. Cerretani, *Oxid. Med. Cell Longev.* **2019**, 2019, 2192093.
- [69] L. Micheli, D. Cerretani, G. Collodel, A. Menchiari, L. Moltoni, A. I. Fiaschi, E. Moretti, *Andrology* **2016**, 4, 456.
- [70] O. Adeoye, J. Olawumi, A. Opeyemi, O. Christiania, *JBRA Assist. Reprod.* **2017**, 22, 61–66. <https://doi.org/10.5935/1518-0557.20180003>
- [71] O. Zitka, S. Skalickova, J. Gumulec, M. Masarik, V. Adam, J. Hubalek, L. Trnkova, J. Kruseova, T. Eckschlager, R. Kizek, *Oncol. Lett.* **2012**, 4(6), 1247.
- [72] S. B. Cheng, H. T. Liu, S. Y. Chen, P. T. Lin, C. Y. Lai, Y. C. Huang, *PLoS One* **2017**, 12(1), 0170016.
- [73] N. Traverso, R. Ricciarelli, M. Nitti, B. Marengo, A. L. Furfaro, M. A. Pronzato, U. M. Marinari, C. Domenicotti, *Oxid. Med. Cell Longev.* **2013**, 2013, 972913.
- [74] Q. Zhu, X. Li, R. S. Ge, *Front. Genet.* **2020**, 11, 527. <https://doi.org/10.3389/fgene.2020.00527>
- [75] A. I. El-Refaiy, F. I. Eissa, *Saudi J. Biol. Sci.* **2013**, 20(3), 265. <https://doi.org/10.1016/j.sjbs.2013.02.004>
- [76] R. A. R. Elgawish, H. M. A. Abdelrazek, *Toxicol. Rep.* **2014**, 1, 795. <https://doi.org/10.1016/j.toxrep.2014.10.010>
- [77] J. J. Martín, R. Martín, J. Codesal, B. Fraile, R. Paniagua, L. Santamaria, *Prostate* **2001**, 46, 11. [https://doi.org/10.1002/1097-0045\(200101\)46:1%3C11::AID-PROS1003%3E3.0.CO;2-K](https://doi.org/10.1002/1097-0045(200101)46:1%3C11::AID-PROS1003%3E3.0.CO;2-K)
- [78] J. Luevano, C. Damodaran, *J. Environ. Pathol. Toxicol. Oncol.* **2014**, 33(3), 183. <https://doi.org/10.1615/jenvironpatholtoxiconcol.2014011075>
- [79] J. Á. F. Vara, E. Casado, de J. Castro, P. Cejas, C. Belda-Iniesta, M. González-Barón, *Cancer Treat. Rev.* **2004**, 30, 193.
- [80] M. Matsuoka, H. Igisu, *Biochem. Biophys. Res. Commun.* **2001**, 282(5), 1120.
- [81] I. E. Ahn, J. H. Ju, S. Y. Lee, J. S. Park, H. J. Oh, H. R. Kim, S. H. Lee, S. H. Park, H. Y. Kim, M. L. Cho, *Scand. J. Immunol.* **2012**, 76(4), 433.
- [82] D. D. Sarbassov, D. A. Guertin, S. M. Ali, D. M. Sabatini, *Science* **2005**, 307(5712), 1098.
- [83] Y. Jing, L. Z. Liu, Y. Jiang et al. *Toxicol. Sci.* **2011**, 125(1), 10.
- [84] G. Gloire, S. Legrand-Poels, J. Piette, *Biochem. Pharmacol.* **2006**, 72(11), 1493.
- [85] M. J. Morgan, Z. G. Liu, *Cell Res.* **2011**, 21(1), 103.
- [86] K. Lingappan, *Curr Opin Toxicol.* **2018**, 7, 81.
- [87] P. J. Barnes, M. Karin, *N. Engl. J. Med.* **1997**, 336, 1066.
- [88] M. H. Park, J. T. Hong, *Cells* **2016**, 5(2), 15. <https://doi.org/10.3390/cells5020015>
- [89] W. Chen, Z. Li, L. Bai, Y. Lin, *Front. Biosci.* **2011**, 16, 1172.
- [90] A. Greenhough, H. J. Smartt, A. E. Moore, H. R. Roberts, A. C. Williams, C. Paraskeva, A. Kaidi, *Carcinogenesis* **2009**, 30(3), 377.
- [91] G.-Y. Liou, P. Storz, *Free. Radic. Res.* **2010**, 44(5), 479.
- [92] V. Aggarwal, H. Tuli, A. Varol, F. Thakral, M. Yerer, K. Sak, M. Varol, A. Jain, M. Khan, G. Sethi, *Biomolecules* **2019**, 9(11), 735.
- [93] A. M. Martelli, C. Evangelisti, M. Y. Follo, G. Ramazzotti, M. Fini, R. Giardino, L. Manzoli, J. A. McCubrey, L. Cocco, *Curr. Med. Chem.* **2011**, 18(18), 2715.
- [94] X.-N. Cao, C. Yan, D.-Y. Liu, J. P. Peng, J. J. Chen, Y. Zhou, C. L. Long, D. W. He, T. Lin, L. J. Shen, G. H. Wei, *Toxicol. Lett.* **2015**, 237(3), 181.


- [95] N. Koundouros, G. Pouligiannis, *Front. Oncol.* **2018**, *8*, 160.
- [96] T. Baroni, I. Arato, F. Mancuso, R. Calafiore, G. Luca, *Front. Endocrinol. (Lausanne)* **2019**, *10*(343), 3389.
- [97] M. Akyüz, R. Topaktaş, A. Ürkmez, O. Koca, M. İ. Öztürk, *Turk. J. Urol.* **2018**, *45*(6), 418. <https://doi.org/10.5152/tud.2018.48855>
- [98] C. E. Høe-Hansen, S. M. Kraggerud, V. M. Abeler, J. Kaern, E. Rajpert-De Meyts, R. A. Lothe, *Mol. Cancer* **2007**, *6*, 12. <https://doi.org/10.1186/1476-4598-6-12>
- [99] G. J. Geijn, R. Hersmus, L. H. Looijenga, *Birth Defects Res. C Embryo Today* **2009**, *87*(1), 96.
- [100] P. Chieffi, *Intractable Rare Dis. Res.* **2017**, *6*(4), 319.
- [101] T. Su, S. Dan, Y. Wang, *Chin. Sci. Bull.* **2014**, *59*, 936.
- [102] Q. W. Zhao, Y. W. Zhou, W. X. Li et al. *Oncol. Rep.* **2015**, *33*(4), 1621.
- [103] S. C. McIver, S. D. Roman, B. Nixon, K. L. Loveland, E. A. McLaughlin, *F1000Res.* **2013**, *2*, 55.
- [104] B. Salehi, A. Mishra, M. Nigam, B. Sener, M. Kilic, M. Sharifi-Rad, P. Fokou, N. Martins, J. Sharifi-Rad, *Biomedicines* **2018**, *6*(3), 91.
- [105] F. A. de Oliveira, W. S. Costa, F. J. B Sampaio, B. M. Gregorio, *Asian J. Androl.* **2019**, *21*(2), 201.
- [106] X. Cui, X. Jing, X. Wu, M. Yan, *Mol. Med. Rep.* **2016**, *14*(5), 4659.
- [107] I. Gülçin, *Innov. Food Sci. Emerg. Technol.* **2010**, *11*, 210.
- [108] N. Xia, A. Daiber, U. Förstermann, H. Li, *Br. J. Pharmacol.* **2017**, *174*(12), 1633.
- [109] D. Li, G. Wang, G. Jin, K. Yao, Z. Zhao, L. Bie, Y. Guo, N. Li, W. Deng, X. Chen, B. Chen, Y. Liu, S. Luo, Z. Guo, *Int. J. Mol. Med.* **2018**, *43*(1), 630–640. <https://doi.org/10.3892/ijmm.2018.3969>
- [110] W. Li, J. Ma, Q. Ma, B. Li, L. Han, J. Liu, Q. Xu, W. Duan, S. Yu, F. Wang, E. Wu, *Curr. Med. Chem.* **2013**, *20*(33), 4185.

SUPPORTING INFORMATION

Additional supporting information can be found online in the Supporting Information section at the end of this article.

How to cite this article: S. Mitra, T. Patra, D. Saha, P. Ghosh, S. M. Mustafi, A. C. Varghese, N. Murmu, *J. Biochem. Mol. Toxicol.* **2022**, e23058. <https://doi.org/10.1002/jbt.23058>

Exposure to chewing tobacco promotes primary oral squamous cell carcinoma and regional lymph node metastasis by alterations of SDF1 α /CXCR4 axis

Sudipta Ray¹ | Depanwita Saha¹ | Neyaz Alam² | Saunak Mitra Mustafi³ | Shyamsundar Mandal⁴ | Aniruddha Sarkar⁵ | Biswanath Majumder⁶ | Nabendu Murmu¹ 

¹Department of Signal Transduction and Biogenic Amines, Chittaranjan National Cancer Institute, Kolkata, India

²Department of Surgical Oncology, Chittaranjan National Cancer Institute, Kolkata, India

³Department of Pathology, Chittaranjan National Cancer Institute, Kolkata, India

⁴Department of Epidemiology and Biostatistics, Chittaranjan National Cancer Institute, Kolkata, India

⁵Department of Head and Neck Oncology, Chittaranjan National Cancer Institute, Kolkata, India

⁶Departments of Cancer Biology, Molecular Pathology and Molecular Profiling, Mitra Biotech, Electronic City, Bengaluru, India

Correspondence

Nabendu Murmu, Department of Signal Transduction and Biogenic Amines, Chittaranjan National Cancer Institute, 37, S. P. Mukherjee Road, Kolkata 700026, India.
Email: nabendu.murmu@cnci.org.in

Funding Information

Sudipta Ray was supported by a Junior Research Fellowship (JRF) from the University Grants Commission, India, Sanction No. F.2-3/2000(SA-I). The funders had no role in study design, data collection and analysis, decision to publish or preparation of the manuscript.

Abstract

A high incidence of oral squamous cell carcinoma (OSCC) is observed in South-East Asian countries due to addictions such as chewing tobacco. Local invasion and distant metastases are primary causes of poor prognosis in OSCC. This study aimed to understand the alterations in metastasis biomarkers, such as stromal cell-derived factor-1 α (SDF-1 or SDF1 α) and its receptor C-X-C chemokine receptor type 4 (CXCR4), in OSCC patient samples that were stratified based on the history of addiction to chewing tobacco. Targeted immunohistochemical staining and Western blotting were performed on primary tumour and metastatic lymph node (LN) tissues in parallel. Overexpression of hepatocyte growth factor (HGF), activated form of its cognate receptor tyrosine kinase, c-Met (p-Met), GRB2-associated-binding protein 1 (Gab1), phospho-protein kinase B (pAkt), nuclear factor kappa B (NF- κ B) and cyclooxygenase-2 (COX-2) were observed in primary tumour and metastatic lymph nodes in both chewer and non-chewer cohorts. Variance analysis showed significant positive correlation between them ($P < .0001$) indicating upregulation of these biomarkers upon ligand-induced activation of c-Met in both tobacco chewers and non-chewers. Significantly higher expressions of SDF1 α and CXCR4 were observed in both primary tumours and metastatic lymph nodes of tobacco chewers ($P < .0001$) and coincided with overexpressed HGF. In contrast, no significant correlation was observed between expression of HGF and that of SDF1 α and CXCR4 in non-chewers. Together, our findings provide important insights into the association of HGF/c-Met and the SDF1 α /CXCR4 axis in lymph node metastasis and to an aetiological link with the habit of chewing tobacco.

KEYWORDS

chewing tobacco, HGF/c-Met pathway, SDF1 α /CXCR4 axis, lymph node metastasis, oral squamous cell carcinoma

1 | INTRODUCTION

Oral squamous cell carcinoma is the most prevalent form of head and neck squamous cell carcinoma (HNSCC) with metastasis and accounts for 50%-70% of total cancer-related mortality.^{1,2} The prime risk factors for the initiation and progression of OSCC include tobacco consumption, alcohol abuse and human papillomavirus (HPV) 16/18 infection.³

Tobacco products are known to increase the risk of various types of cancers including HNSCC, oesophageal and gastric. Worldwide, tobacco is consumed in various forms, smoking of cigarettes being the commonest one. However, another form of tobacco consumption, smokeless tobacco, is especially popular as chewing tobacco in many South-East Asian countries.⁴ This comes in various forms such as chewing tobacco, oral tobacco, dip, spit tobacco and snuff. The World Health Organization (WHO) declared smokeless tobacco as a major and consequential part of the worldwide tobacco problem in 2017. Chewing tobacco is as harmful as smoking tobacco because it contains nicotine and similar tobacco-specific carcinogens including nitrosamines, which are absorbed by the mucous membrane of the mouth and go directly to the bloodstream. This form of smokeless tobacco has been associated with many major health problems - cancer of the oral cavity, oesophagus and pancreas, leucoplakia, gum disease and tooth decay.⁵⁻⁷ Despite significant progress in delineating molecular alterations leading to oral cancer development and progression, in tobacco chewers understanding the biomarkers involved in the molecular mechanisms of cancer development could be a promising approach for early detection, treatment and reducing metastasis.

Despite recent advances in surgery, chemotherapy and radiation therapy, OSCC patients with regional lymph node metastasis have a poor 5-year overall survival (OS) rate in comparison with patients without metastasis.^{8,9} Immediately after initiation, OSCC can spread to the regional lymph nodes in neck and this procedure is accelerated by the lymphatic drainage from the oral fissure.¹⁰⁻¹⁴ Several biomarkers have been shown to be associated with metastasis of OSCC.^{15,16} However, the underlying molecular mechanisms that explicitly drive the migration and invasiveness of OSCC into the adjacent lymph nodes are still not well defined.

Epidermal growth factor receptor (EGFR) pathway is overexpressed in OSCC, which is generally correlated with poor prognosis, invasion and metastasis. Multiple drug targets have been developed against EGFR.¹⁷ While the therapeutic benefit of these targeted modalities in combinatorial setting is evident,¹⁸ there is an unmet need to develop more effective therapies targeting other oncogenic pathways that together orchestrate OSCC pathogenesis. An alternative/parallel oncogenic pathway that has emerged as a potential drug target is c-Met signalling.

HGFR/c-Met is the transmembrane receptor tyrosine kinase (RTK) encoded by N-methyl-N'-nitroso-guanidine human osteosarcoma transforming (*MET*) gene and stimulated by its cognate ligand HGF.¹⁹ In a large number of oral cancer cases, HGF and its receptor c-Met have been reported to be overexpressed.²⁰ In OSCC, overexpression of HGF/c-Met has been clinically correlated with poor prognosis and metastasis to the lymph nodes in the neck region, conferring anti-EGFR therapy resistance. Additionally, this perturbation is contingent upon HPV status.²¹⁻²⁴ In case of oral cancer, HGF is secreted by the tumour-associated fibroblasts (TAFs).²⁵ HGF/c-Met signalling is closely linked to the EGFR cascade in lung cancer, breast cancer, glioblastoma and other malignancies, but the underlying mechanisms have not yet been properly delineated.²⁶⁻²⁹ HGF, depending on context, exhibits its pleiotropic effects by dysregulating various receptor tyrosine kinase signalling cascades that share common downstream nodes, such as phosphatidylinositol 3-kinase/Akt/mitogen-activated protein kinase (PI3K-Akt-MAPK) axis and Janus kinase/signal transducer and activator of transcription (JAK/STAT) pathways. Moreover, NF- κ B-regulated gene expression has been shown to be dependent on the c-Met-mediated recruitment of the PI3K/Akt and non-receptor tyrosine-protein kinase, such as Src, signalling pathways. Furthermore, the spatiotemporal dynamics of the intracellular network involving c-Met is evidenced by its crosstalk with EGFR pathway.^{30,31} The compensatory activation of multiple receptor tyrosine kinases including c-Met is a well-elucidated resistance mechanism in case of anti-EGFR therapy in HNSCC.²⁵ The HGF/c-Met and EGFR signalling pathways converge at both the PI3K/Akt and MAPK nodes, pointing towards the roles for complementary and compensatory mechanisms and therefore space for therapeutic opportunities. In preclinical models and in HNSCC patients, it has been observed that EGFR blockade can be obliterated by c-Met activation.^{32,33} This in turn establishes the fact that therapies that target EGFR can be potentially restricted or even blocked by the activation of the HGF/c-Met pathway. Of note, the DNA-binding and subsequent transcriptional activator functions of NF- κ B are both stimulated by HGF.³⁴ Indeed, activation of NF- κ B is important for tumour development as it controls the gene expression related to cell growth and metastasis.³⁵ For instance, hyperexpression of COX-2 has been linked to the pathogenesis and tumour progression in multiple cancer types including OSCC.³⁶⁻³⁸

The hypoxic condition of a clinically defined oral lesion is often responsible for aberrant activation of the HGF/c-Met and other RTK pathways. Subsequent stimulation of the SDF1 α /CXCR4 cascade promotes metastatic progression of OSCC.³⁹⁻⁴³ C-X-C motif chemokine 12 (CXCL12) or SDF1 α is the known chemokine ligand for CXCR4, a G protein-coupled receptor. It has been shown to play a pivotal role in tumour progression and metastasis in OSCC and other

tumours.⁴⁴⁻⁵⁰ SDF1 α is present in lymph nodes, lungs, bones and livers, suggesting that these sites are contextually most oriented for developing niches for cancer cell metastasis. The underlying hypothesis is that the SDF1 α attracts circulating cells to secondary sites where they can sustain themselves and thus result in metastases.⁴⁷ For the establishment of further metastasis, cancer cells drift out from the metastatic lymph nodes and intravasate into the neo-angiogenic microblood vessels. This latter mechanism in OSCC is thought to be critical because OSCC patients with distant metastases have a high incidence of metastases in the neck lymph nodes.⁴¹ Expression of CXCR4 is regulated by stimuli from the tumour microenvironment (TME), and these include HGF and hypoxia. NF- κ B-promoter interactions under hypoxic conditions and HGF stimulation plays a key role in CXCR4 expression.⁵¹ Within these contexts, our present study aimed to delineate the alterations in the metastasis-related biomarkers in OSCC patients with lymph node metastasis after we segregated the cohorts based on the history of addiction to chewing tobacco.

2 | MATERIALS AND METHODS

2.1 | Sample collection and preparation

A total of 90 cases of primary squamous cell carcinoma diagnosed and subsequently undergoing surgery in Chittaranjan National Cancer Institute (CNCI), Kolkata, India, in the period between 2012 and 2016, were included in the present study. All the patients were divided into two groups: the first group included 45 cases with the habit of only chewing tobacco, and the second group included 45 cases without any history of chewing tobacco or smoking and alcohol abuse. After surgery, the tumour tissue samples and affected metastatic lymph nodes were collected from all the cases. Staging of primary carcinoma cases was done according to the TNM classification based on recommended guidelines by the Union for International Cancer Control (UICC). Relevant clinicopathologic details including the tumour staging and the histologic grading provided by the pathologist were given due consideration. All the cases were selected on the basis of strict inclusion and exclusion criteria. Only histologically confirmed cases of OSCC with more than 30% tumour content, the gingivobuccal complex (ie alveolus, gingivobuccal sulcus, buccal mucosa or retromolar area alone), the floor of the mouth and tongue were selected for this study. Other proliferative lesions such as proliferative verrucous leucoplakia and verrucous carcinomas were excluded. Moreover, patients who had pre-operative chemoradiotherapy or had a history of recurrence were excluded from the study (Supporting Information File S1). The comprehensive data of patients' history are shown in Table 1. After tumour excision, all the

TABLE 1 Comprehensive patient profile

Patient profile	Number of patients (n)	Percentage (%)
Gender		
Male	65	72.22%
Female	25	27.78%
Age		
<40 years	21	23.33%
40-60 years	52	57.78%
>60 years	17	18.89%
Site of origin of carcinoma		
Gingivobuccal complex	68	75.56%
Floor of the mouth	13	14.44%
Tongue	9	10%
Grade of carcinoma		
Well differentiated	73	81.11%
Moderately differentiated	17	18.89%
Habit		
Only chewing tobacco and betel quid	45	50%
No habit	45	50%

specimens were first trimmed and cleanly divided into two sections. One part was routinely fixed in 10% formalin solution for 24 hours, and paraffin blocks were prepared from processed tissues for immunohistochemical analysis. The immediately adjacent part of the corresponding sample was used for preparation of protein lysate for Western blot analysis. Institutional Ethics Committee (IEC) approval was obtained to carry out this study. All work has been carried out in accordance with the Code of Ethics of the World Medical Association (Declaration of Helsinki).

2.2 | Antibodies and reagents

For biomarker evaluation, primary antibodies used against HGF (clone 7-2, Novus Biologicals, NBPI-19182), p-Met (Tyr 1234/1235) (clone D26, Cell Signaling Technology, Cat# 3077s), Gab1 (clone H-198, Santa Cruz Biotechnology, sc-9049), pAkt (Ser-473, Santa Cruz Biotechnology, sc-7985-R), NF- κ B p50 (NF- κ B1 or subunit p50, NLS, Santa Cruz Biotechnology, sc-114), COX-2 (Santa Cruz Biotechnology, sc-7951), SDF-1 α (clone FL-93, Santa Cruz Biotechnology, sc-28876), CXCR4 (clone H-118, Santa Cruz Biotechnology, sc-9046), β -actin (Santa Cruz Biotechnology, sc-7210) and horseradish peroxidase (HRP)-conjugated goat anti-rabbit (Santa Cruz Biotechnology, sc-2004) secondary antibody were used in this study. For detection of chromogenic signal, the immunohistochemistry assay kit (DAB150: IHC Select HRP/DAB Tests, Merck Millipore, Germany)

was used. For Western blot analysis, chemiluminescent detection was performed by using Clarity Western ECL Substrate (Bio-Rad).

2.3 | Immunohistochemistry

Formalin-fixed paraffin-embedded (FFPE) sections (3 μ thickness) were mounted on poly-L-lysine-coated slides. The slides were kept in a hot air oven at 56°C for 30 min and later dipped and deparaffinized in xylene for 10 min (three changes). After antigen retrieval using 0.01 mol/L citrate buffer (pH 6.0), the slides were treated with 3% hydrogen peroxide in methanol for endogenous peroxidase blocking. The rest of the procedure was performed following the standard manufacturer's protocol using immunohistochemistry assay kit. Primary antibodies against HGF, p-Met and COX-2 were used at 1:200 dilution, whereas primary antibodies against Gab1, pAkt, NF- κ B p50, SDF-1 α , CXCR4 and β -actin were used at 1:100 dilution. Binary scoring method was used for immunohistochemistry scoring. Only those cells with DAB positive (brown colour) and that specifically displayed the respective antigens were scored as '1', while those without the brown colour were scored as '0'. Each field was again divided into nine squares, and DAB-positive cells in each of the nine squares were counted under 200X magnification of a brightfield microscope. The sum of total score in the nine squares constituting one field was calculated. The relative expression level of each marker/antigen was calculated as the percentage of DAB-positive cells among total number of cells in each field. Five such random fields were chosen for each antibody in each slide. The final score that was calculated was the average score of all five fields for each marker.⁵²⁻⁵⁴

2.4 | Western blot

Each tissue sample was separately lysed in ice-cold cell lysis buffer (15 mmol/L Tris, 2 mmol/L ethylenediaminetetraacetic acid, 50 mmol/L β -mercaptoethanol, 0.1% Triton X-100, 20% glycerol, 1 mmol/L sodium orthovanadate, 1 mmol/L sodium fluoride, 1 mmol/L phenylmethylsulphonyl fluoride, 1 μ g/mL leupeptin, 1 μ g/mL aprotinin and 1 μ g/mL pepstatin). The whole tissue lysates were first centrifuged at 16912 \times g for 15 minutes at 4°C, and then, the supernatant from each sample was aliquoted in separate tubes. Protein concentration of the samples was measured using Bicinchoninic Acid (BCA) Protein Assay Kit (Thermo Scientific) following the manufacturer's protocol. Total extract (50 μ g protein/lane) of each sample was subjected to sodium dodecyl sulphate-polyacrylamide gel electrophoresis (SDS-PAGE) and then electro-transferred to nitrocellulose membranes. Postblotting, the membranes were incubated in blocking buffer using 5% non-fat dry milk in Tris-buffered

saline (20 mmol/L Tris-HCl and 137 mmol/L sodium chloride, pH 7.5) at room temperature for 1 hour. The membranes were incubated overnight with appropriate primary antibodies for the target proteins (SDF1 α and CXCR4 at 1:200 dilution). Next day, the unbound primary antibody was removed from the membrane using wash buffer (Tris-buffered saline with 0.5% Tween-20). The membranes were incubated with HRP-conjugated goat anti-rabbit secondary antibody (1:10,000 dilution) for 1 hour at room temperature and washed with the same wash buffer to remove any excess unbound secondary antibody. The signal was finally detected by using enhanced chemiluminescence kit following the manufacturer's instructions. The resultant bands were analysed using a densitometer (Bio-Rad, GS 800). β -Actin expression was tested as the loading control, and the expression of all the other proteins was normalized against β -actin.

2.5 | Statistical analysis

All statistical analyses were performed with the help of GraphPad Prism 5.0. To calculate the expression of HGF/c-Met and its downstream proteins, mean and standard error of mean (s.e.m) were calculated. In order to establish the correlation between HGF, c-Met, Gab1, Akt, NF-KB p50 and COX-2, correlation (Pearson's) analysis was performed. Correlation analysis was also performed in order to test the correlation between HGF, SDF1 α and CXCR4 in both tobacco chewers and non-chewers, respectively. One-way analysis of variance (ANOVA) was performed followed by Tukey's test with the help of critical difference (CD) in both tobacco chewer and non-chewer groups. $P \leq .05$ was considered statistically significant for all calculations.

3 | RESULTS

3.1 | Expression of HGF/c-Met and related key proteins

Mainly, two types of cells found in the OSCC tumour sections were considered for evaluation in this study: the tumour cells and the tumour-associated fibroblasts (TAFs) found in the stroma, which constitutes the TME. All the samples, including tumours and metastatic lymph nodes, were first tested for EGFR expression by immunohistochemistry. The protein showed high expression in both the tumour cells and tumour-associated stroma in all cases. Thus, we next proceeded to test the expression status of HGF and activated c-Met in both chewing tobacco users and non-users. HGF is secreted by the TAFs, which then bind to the c-Met receptors present on the tumour cells. HGF and p-Met were also found to be highly expressed in both the tumour cells and tumour-associated stroma in primary tumours, whereas it was highly

expressed in only the tumour cells in the metastatic lymph nodes (Figure 1A and 1B). Gab1 and pAkt showed positive cytoplasmic expression in the tumour cells (Figure 1C and D). The nuclear localization of NF- κ B p50 was found in 37 samples of primary tumour, whereas metastatic lymph nodes showed cytoplasmic expression of NF- κ B p50 indicating its inactive state (Figure 1E). COX-2, the final downstream target of the cascade, showed high cytoplasmic expression in the tumour cells of both primary tumours and metastatic lymph nodes (Figure 1F). No significant difference in the expression pattern of the above-mentioned proteins was observed in tobacco chewers (TC) and non-chewers (NTC).

3.2 | Positive correlation between HGF and its downstream elements in primary tumour and metastatic lymph nodes

In order to understand the downstream cascade of an interactive pathway, correlation analysis was performed. In tobacco chewers, primary tumours showed the expression

(mean \pm s.e.m) of HGF (66.26 ± 0.11), p-Met (61.36 ± 0.10), Gab1 (53.37 ± 0.10), pAkt (55.34 ± 0.10), NF- κ B p50 (65.12 ± 0.13) and COX-2 (63.42 ± 0.09). Similarly, in case of non-chewers, primary tumours were evaluated for the expression (mean \pm s.e.m) of the same set of proteins, that is HGF (64.64 ± 0.09), p-Met (53.57 ± 0.10), Gab1 (54.36 ± 0.10), pAkt (59.54 ± 0.10), NF- κ B p50 (67.50 ± 0.10) and COX-2 (62.37 ± 0.11). ANOVA showed positive correlation among all proteins with very high significance ($P < .0001$) indicating upregulation of all proteins upon activation of c-Met by HGF (Table 2). One-way ANOVA showed that there was significant difference in mean percentage of expression of the different proteins in primary tumour samples of both tobacco chewers ($F_{5,264} = 2556.655894$, $P < .0001$) and non-chewers ($F_{5,264} = 3108.800963$, $P < .0001$). As per the Tukey's critical difference (CD), the mean percentage of expression of HGF was significantly higher and that of Gab1 was found to be significantly lower among all the other proteins ($P < .001$) examined in case of tobacco chewers. While in case of non-chewers, as per CD, the mean percentage of expression of NF- κ B p50 was significantly higher and that of p-Met was

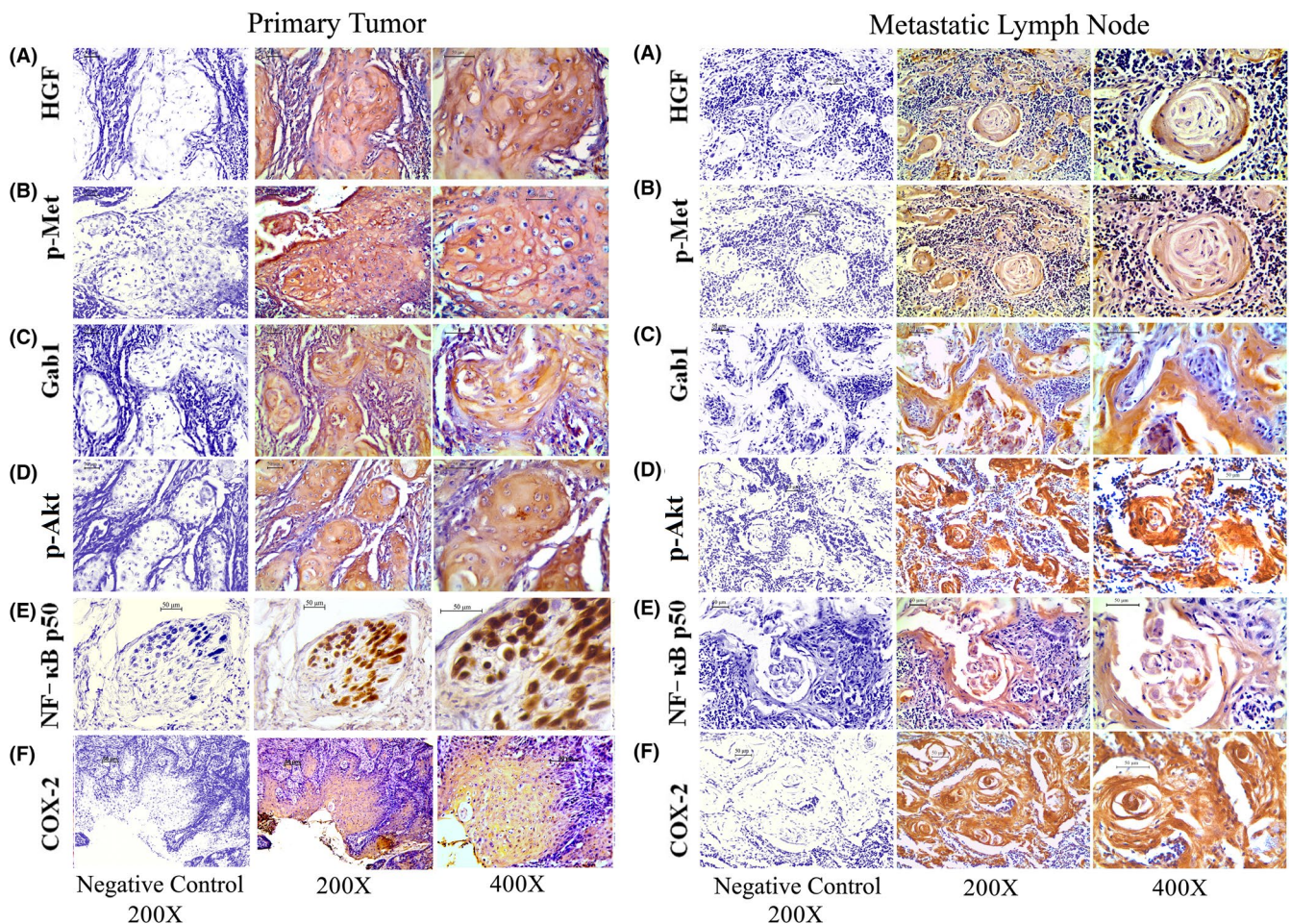


FIGURE 1 Immunohistochemical analysis of the HGF/c-Met cascade in both the primary tumour and metastatic lymph node. Expression for HGF (A), p-Met (B), Gab1 (C), pAkt (D), NF- κ B p50 (E) and COX-2 (F). Each section was compared with a negative control (ie without primary antibody). Images were taken in 200 \times and 400 \times magnifications

TABLE 2 Mean and ANOVA of percentage of expression of HGF and its downstream proteins for primary tumour

	HGF	p-Met	Gab1	pAkt	NF-κB p50	COX-2
Tobacco chewers' profile						
Mean ± sem	66.26 ± 0.11	61.36 ± 0.10	53.37 ± 0.10	55.34 ± 0.10	65.12 ± 0.13	63.42 ± 0.09
Variance	0.509459	0.450664	0.437574	0.46902	0.707102	0.399072
CD	2.24					
Non-chewers' profile						
Mean ± sem	64.64 ± 0.09	53.57 ± 0.10	54.36 ± 0.10	59.54 ± 0.10	67.50 ± 0.10	62.37 ± 0.11
Variance	0.357641	0.441254	0.461687	0.459941	0.471091	0.520412
CD	2.24					

Note: Data are given in mean ± s.e.m and analysed through one-way ANOVA. The tobacco chewer group is compared with the non-chewer group.

TABLE 3 Mean and ANOVA of percentage of expression of HGF and its downstream proteins for metastatic lymph node

	HGF	p-Met	Gab1	pAkt	NF-κB p50	COX-2
Tobacco chewers' profile						
Mean ± sem	61.67 ± 0.10	55.62 ± 0.11	52.67 ± 0.11	59.67 ± 0.09	65.43 ± 0.13	66.55 ± 0.12
Variance	0.473257	0.542584	0.585395	0.39818	0.81002	0.636535
CD	2.24					
Non-chewers' profile						
Mean ± sem	64.43 ± 0.10	63.43 ± 0.11	60.57 ± 0.11	57.72 ± 0.15	64.51 ± 0.11	65.46 ± 0.11
Variance	0.427422	0.558988	0.593331	1.059465	0.562338	0.562
CD	2.24					

Note: Data are given in mean ± s.e.m and analysed through one-way ANOVA. The tobacco chewer group is compared with the non-chewer group.

significantly lower among all the other protein markers analysed ($P < .001$) (Supporting Information File S2).

Indeed, for tobacco chewers, in metastatic lymph nodes, the mean expression (\pm s.e.m) of the HGF pathway biomarkers was determined; data showed the value of HGF (61.67 ± 0.10), p-Met (55.62 ± 0.11), Gab1 (52.67 ± 0.11), pAkt (59.67 ± 0.09), NF-κB p50 (65.43 ± 0.13) and COX-2 (66.55 ± 0.12). Also, for metastatic lymph nodes of non-chewers, the mean expression (\pm s.e.m) of the same proteins was determined and spectrum showed different levels for different proteins, that is HGF (64.43 ± 0.10), p-Met (63.43 ± 0.11), Gab1 (60.57 ± 0.11), pAkt (57.72 ± 0.15), NF-κB p50 (64.51 ± 0.11) and COX-2 (65.46 ± 0.11). ANOVA showed positive correlation among all proteins with very high significance ($P < .0001$), except between HGF and NF-κB (Table 3). One-way ANOVA also showed that there was significant difference in mean percentage of expression of the different pathway proteins in metastatic lymph nodes of both tobacco chewers ($F_{5,264} = 2316.136$, $P < .0001$) and non-chewers ($F_{5,264} = 627.602$, $P < .0001$). As per the CD, the mean percentage of expression of COX-2 was significantly higher, whereas that of Gab1 was significantly lower among all the other proteins ($P < .001$) in case of tobacco chewers. In the case of non-chewers, based on CD, the mean percentage of expression of COX-2 was significantly higher, pAkt was found to show significantly lower expression among all the other proteins

($P < .001$) (Supporting Information File S2). These results indicate that in case of tobacco chewers and non-chewers, Gab1, pAkt, NF-κB and COX-2 show upregulated expression upon activation of oncogenic c-Met pathway by HGF.

3.3 | Perturbed expression of SDF1α/CXCR4 metastatic axis ascribes to chewing tobacco

Aberrant activation of HGF is responsible for induction of the SDF1α/CXCR4 metastatic axis and subsequent entry of circulating tumour cells to the metastasis sites. The lymph nodes of the neck region are the primary sites for metastasis in case of OSCC, and hence, we investigated the alteration in the expression of the metastatic markers in both primary tumours and the affected lymph nodes in patients with confirmed history of chewing tobacco. Immunohistochemistry results demonstrated high cytoplasmic expression of SDF1α (Figure 2A) and high membrane expression of CXCR4 (Figure 2B) particularly in the tumour cells compared with the stroma, in both primary tumours and affected lymph nodes of tobacco chewers. In comparison, the expression levels of both SDF1α and CXCR4 were significantly lower in the primary tumour samples and in metastatic lymph nodes of non-chewers (Figure 2C and D).

Correlation analysis was done in order to check the relationship between the expression status of the three proteins. For tobacco chewers, the marker expression in primary tumours (mean \pm s.e.m) was determined for HGF (66.72 ± 0.13), SDF1 α (67.76 ± 0.14) and CXCR4 (67.24 ± 0.13). In case of non-chewers, in primary tumours, expression (mean \pm s.e.m) was confirmed for HGF (64.93 ± 0.16), SDF1 α (29.84 ± 1.79) and CXCR4 (24.82 ± 1.35). In case of tobacco chewers, there was positive correlation among the three proteins implying that upregulation of HGF induces the subsequent downstream SDF1 α /CXCR4 axis ($P < .001$). However, in case of non-chewers, there was no significant correlation between these three proteins (Figure 3A and B; Table 4). In the case of metastatic lymph nodes, for tobacco chewers, the expression level (mean \pm s.e.m) of the three aforementioned proteins was determined and accordingly showed patterns for all three markers—HGF (61.95 ± 0.14), SDF1 α (64.59 ± 0.10) and CXCR4 (69.87 ± 0.11). For metastatic lymph nodes of non-chewers, the expression level (mean \pm s.e.m) of these three proteins was different: HGF (64.72 ± 0.15), SDF1 α (29.84 ± 2.09) and CXCR4 (28.27 ± 2.15). Consistent with the pattern observed in primary

tumours, metastatic lymph nodes of tobacco chewers showed positive correlation among the three proteins ($P < .001$), highlighting that upregulation of HGF relays its effects to SDF1 α /CXCR4 axis, whereas in case of non-chewers, there was no significant correlation between the three proteins (Figure 3C and D; Table 4; Supporting Information File S3). Together, these data reveal that upregulation of HGF has the ability to lead the activation of metastasis signalling via SDF1 α /CXCR4 axis in OSCC representing the tobacco chewers. In contrast, the SDF1 α /CXCR4 axis is not overtly activated by upregulation of HGF in case of non-chewers.

3.4 | Metastatic risk assessment of chewing tobacco based on perturbation of signalling markers

The differential perturbation of metastatic signalling axis proteins based on their immunohistochemical quantification prompted us to further assess the impact of the potential effects of chewing tobacco on metastatic markers in OSCC patients.

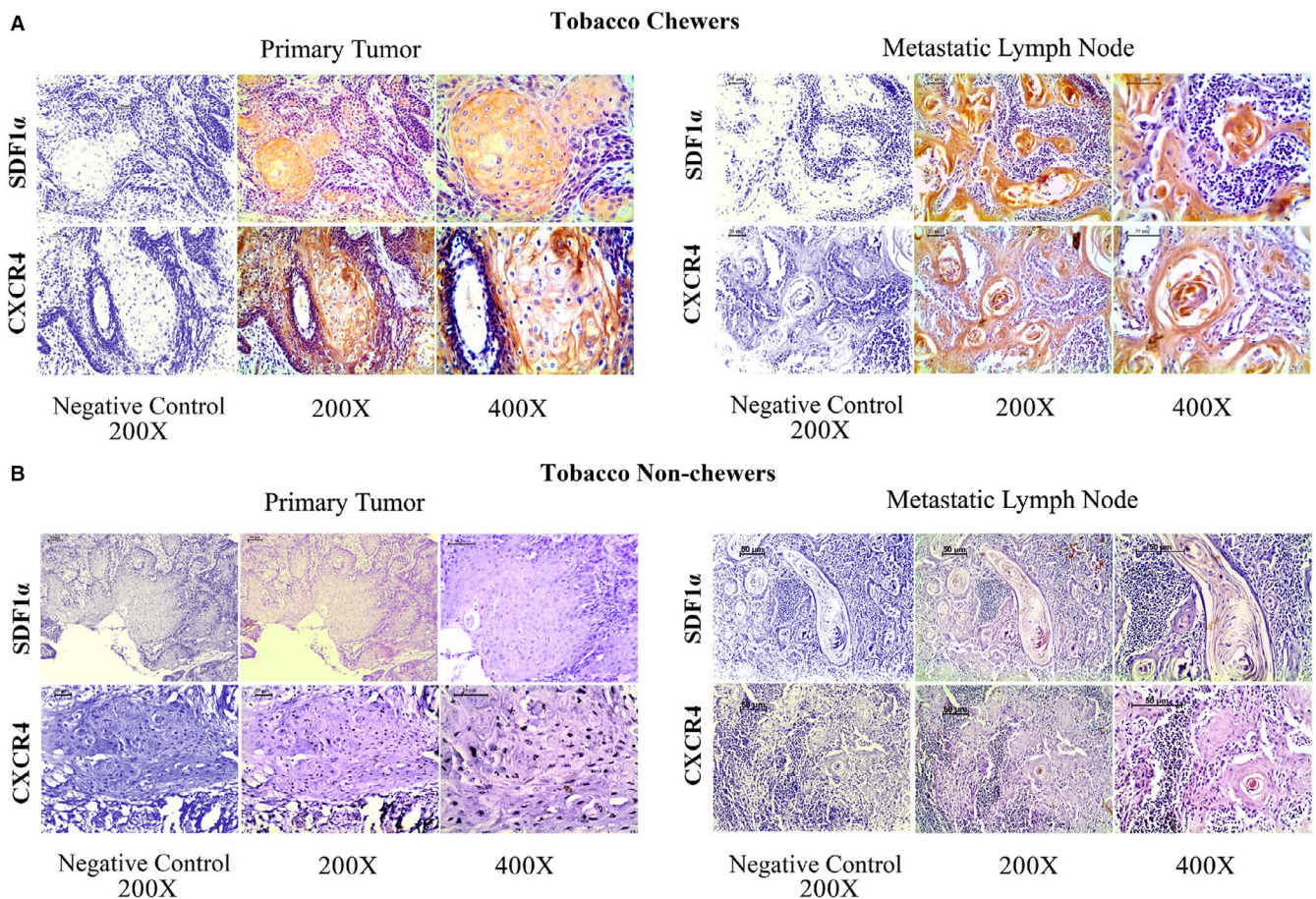


FIGURE 2 Immunohistochemical analysis of the HGF and SDF1 α /CXCR4 axis in primary tumour and metastatic lymph node of both tobacco chewers and non-chewers. In case of tobacco chewers (A), patterns of SDF1 α and CXCR4 expression in both primary tumour and affected lymph node. In non-chewers (B), expression of SDF1 α and CXCR4 in primary tumour and in metastatic lymph node. Each section was compared with a negative control (ie without primary antibody). Image magnifications: 200X, 400X

FIGURE 3 Comparison of HGF/c-Met cascade expression in tobacco chewers and non-chewers. (A) Correlation between HGF, SDF1 α and CXCR4 in primary tumour of tobacco chewers. (B) Correlation between the three proteins in primary tumour of tobacco non-chewers. (C) Correlation between HGF, SDF1 α and CXCR4 in affected lymph node of tobacco chewers. (D) Correlation between the three proteins in metastatic lymph node of tobacco non-chewers

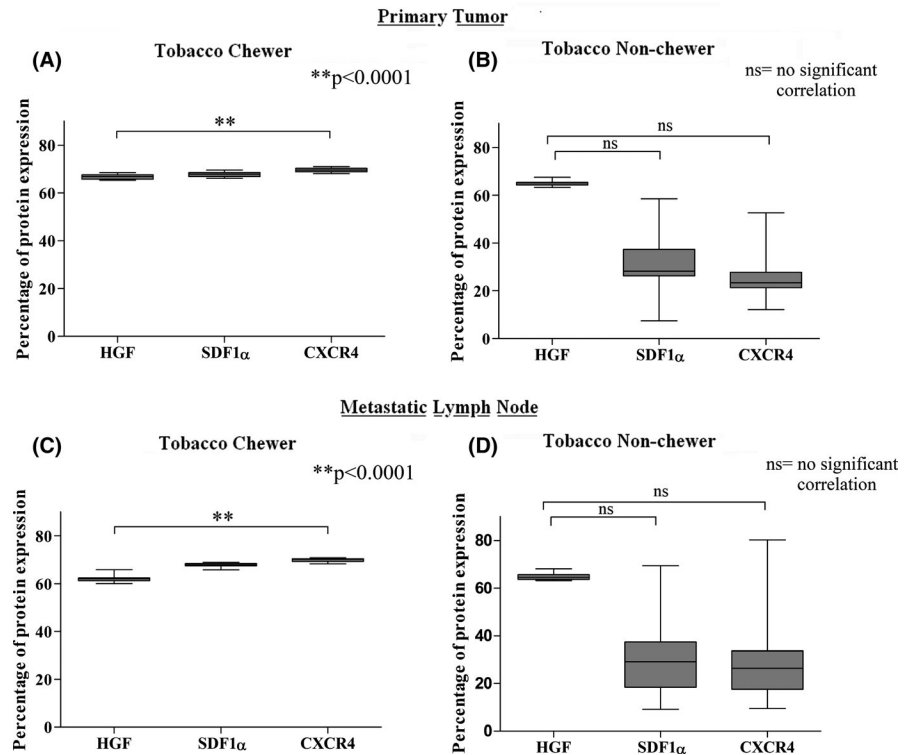


TABLE 4 Mean of percentage of expression of SDF1 α and CXCR4 in tobacco chewers and non-tobacco chewers

	Primary tumour			Metastatic lymph node		
	HGF	SDF1 α	CXCR4	HGF	SDF1 α	CXCR4
Tobacco chewers						
Mean \pm SEM	66.72 \pm 0.13	67.76 \pm 0.14	67.24 \pm 0.13	61.95 \pm 0.14	64.59 \pm 0.10	69.87 \pm 0.11
Median	66.77	67.87	67.25	62.1	64.55	70.2
Range	65.3 - 68.4	66.1 - 69.6	65.8 - 69.0	60.0 - 65.8	63.0 - 66.0	68.3 - 70.9
Non-chewers						
Mean \pm SEM	64.93 \pm 0.16	29.84 \pm 1.79	24.82 \pm 1.35	64.72 \pm 0.15	29.84 \pm 2.09	28.27 \pm 2.15
Median	65.2	28.2	23.4	64.6	29.07	26.3
Range	63.2 - 67.5	7.4 - 58.4	12.1 - 52.6	63.2 - 68.1	9.2 - 69.4	9.5 - 80.3

Note: Data are given in mean \pm s.e.m and analysed through one-way ANOVA. The tobacco chewer group is compared with the non-chewer group for both primary tumour and metastatic lymph node.

The paired t test showed that in primary OSCC samples, the expression of SDF1 α was significantly higher in tobacco chewers in comparison with non-chewers (TC vs NTC – OSCC –msd – $t_{94} = 21.07$, $P < .0001$). In the same way, CXCR4 was significantly higher in chewing tobacco users in comparison with non-users (TC vs NTC – OSCC –msd – $t_{94} = 208.67$, $P < .0001$). In case of metastatic lymph nodes (MLN), the t test analysis revealed that SDF1 α was significantly higher in tobacco chewers in comparison with non-chewers (TC vs NTC – MLN –msd – $t_{94} = 16.63$, $P < .0001$). Similarly, CXCR4 was significantly higher in chewing tobacco users in comparison with non-users (TC vs NTC – MLN –msd – $t_{94} = 19.34$, $P < .0001$) (Supporting Information File S4). The results obtained by immunohistochemistry analysis were further validated by Western blot.

The densitometric analysis demonstrated significantly higher expression of both SDF1 α and CXCR4 in primary tumours and metastatic lymph nodes of tobacco chewers in comparison with non-chewers (Figure 4). Together, these data assert that chewing tobacco initiates lymph node metastasis via the SDF1/CXCR4 and relies on HGF. However, the same pathway markers were not significantly overexpressed in their tobacco non-chewer counterparts.

4 | DISCUSSION

Oral cancer is a major public health issue worldwide. Despite considerable advances in the diagnostic and therapeutic

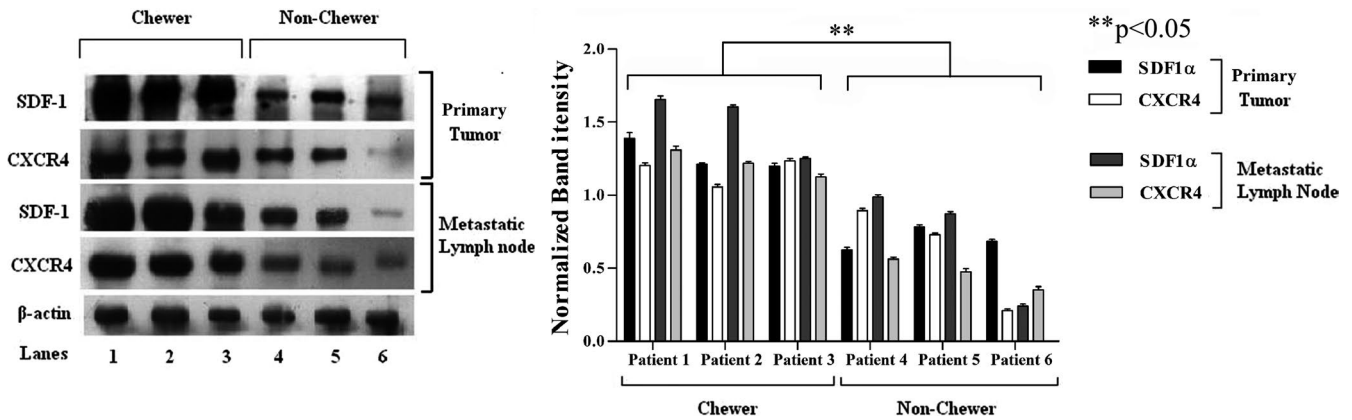


FIGURE 4 Comparison of SDF1 α and CXCR4 expression in tobacco chewers and non-chewers by Western blot. Panel represents protein expression of SDF1 α and CXCR4 (left). The densitometric analysis of expression of SDF1 α and CXCR4 in primary tumour and metastatic lymph node of tobacco chewers and non-chewers. ** denotes statistically significant difference between chewer and non-chewer groups

fronts,⁵⁵ both the incidence and mortality of OSCC have increased over the past decade. In 2018, globally over 18 million new cases of cancer have been diagnosed approximately.⁵⁶ Tobacco-related deaths are hardly properly reported. Worldwide, overuse of tobacco is responsible for every 1 in 10 deaths and this results in over 5 million deaths per year.⁵⁷ The tobacco market in recent years has been captured by chewable and flavoured forms of tobacco, which are locally known as gutka, zarda, khaini, etc.⁵⁸ Gutka contains various other ingredients along with tobacco such as slaked lime, catechu, areca nut, condiments and fragrances.⁵⁹ The fact that it is also being exported to almost 22 countries worldwide confirms its growing usage. In South-East Asia, the demand has escalated so much that it is being sold even to minors in the region.^{60,61} In India, most men <40 years of age use gutka.^{61,62} This chewing tobacco or gutka can be more addictive than smoking tobacco. The most alarming statistics show that more than five million children <15 years of age are addicted to chewing tobacco in India.⁵⁸ It has been reported with strong evidence that chewing tobacco, gutka, betel nut and betel quid are pre-eminent risk factors for oral cancer in India along with other regions of South-East Asia.^{63,64} Many forms of chewing tobacco have become available commercially, and this necessitates the scrutiny of their harmful effects. Widespread use of betel quid, slaked lime and areca nut, with or without tobacco, has been identified as one of the major causes of gingivobuccal OSCC (OSCC-GB) in India.⁶⁵⁻⁶⁷ OSCC-GB patients mostly manifest advanced stage of cancer with high rate of loco-regional metastasis and high rate of mortality.⁶⁸ However, there is paucity of data so far that could provide critical insights into the effect of chewing tobacco on oral cancer at molecular level. The alterations in the genes *EGFR*, *IL8*, *AR*, *ATM*, *BRCA1*, *CDKN1A* and *TP53* have been reported to be associated with nitrosamines and arecoline that are found in chewing tobacco and betel quid.⁶⁹ Additionally, the altered

genes of *TRPM3*, *ARID2*, *MLL4*, *UNC13C* and *USP9X* have been identified by the India Project Team of the International Cancer Genome Consortium (ICGC) to be specifically linked with OSCC-GB.⁷⁰ In an in vitro model, the proliferative and invasive potential of oral keratinocytes has been shown to increase significantly on exposure to chewing tobacco due to overexpression of *ERBB2* and *RABL6* genes.⁷¹ Also when immortal oral keratinocytes are exposed to chewing tobacco, there is alteration in microRNA (miRNA) expression and their target proteins, which are predominantly involved in the initiation and progression of OSCC.⁷² However, a well-defined signalling cascade that is responsible for OSCC-GB and subsequent loco-regional lymph node metastasis has not yet been delineated. In this study, we report the potential biomarkers and their alterations to understand their roles in leading lymph node metastasis in OSCC patients with the habit of chewing tobacco.

Metastasis is one of the most inimical facets of cancer. The presence of lymph node metastasis usually points towards elevated risk of distant metastasis.⁷³ Our study deals with demonstrating the difference in the expression of metastasis-related markers in OSCC in chewing tobacco users in comparison with non-users. This also emphasizes the potential effects of chewing tobacco on the aggressiveness of oral cancer. EGFR is the predominant molecular target, and it is overexpressed in >90% of cases of OSCC. Overexpression of EGFR is clinically related to poor prognosis and elevated risk of metastasis.⁷⁴ The targeted therapies against EGFR have limitations due to the adaptive or acquired resistance developed to the EGFR blockade and owing to other compensatory pathways that are contextually active to bypass anti-EGFR therapy. This highlights the need to develop rationally driven therapies that target other oncogenic pathways involved in pathogenesis of OSCC. The HGF/c-Met signalling is one of the key potential target pathways. Functional proteomic analysis confirmed that in the case of malignant cells, EGFR and

c-Met immunoprecipitate simultaneously in protein extracts, which is not the case for normal hepatocytes. These point towards the fact that the crosstalk between the EGFR and HGF/c-Met pathways is tumour-specific. c-Met may be activated as a result of EGFR activation and crosstalk. Indeed, HGF in turn can transactivate EGFR through amphiregulin and other growth factors.⁷⁵ Thus, in the event of an EGFR blockade, HGF/c-Met pathway can function as an alternative cascade for promoting tumour progression. Activation of the HGF/c-Met pathway stimulates epithelial-mesenchymal transition (EMT), thus inducing the process of invasion, migration and metastasis in OSCC.⁷⁶ Also, the HGF/c-Met and EGFR signalling pathways interact at both the PI3K/Akt and MAPK nodes, pointing towards their ability for imparting compensatory effects.

In this context, we first checked the expression of EGFR in both tumour tissues and metastatic lymph nodes. All the samples demonstrated high membrane expression of activated form of EGFR. High membrane expression of both HGF and activated c-Met was observed in the same region as EGFR. Immunohistochemistry results demonstrated overexpression of HGF/c-Met pathway and its downstream molecules such as Gab1 and phospho-Akt in both primary tumours and metastatic lymph nodes. Nuclear expression of NF- κ B p50 was observed in primary tumours, but cytoplasmic expression was observed in most metastatic lymph nodes indicating its inactive state. The key end product of the pathway, COX-2, was overexpressed in the cytoplasm in both primary tumour tissues and affected lymph nodes. Positive correlation between HGF, p-Met, Gab1, pAkt, NF- κ B and COX-2 with very high significance ($P < .0001$) indicated upregulation of all the downstream proteins, respectively, upon activation of c-Met by HGF. The overexpression of both pEGFR and p-Met in the primary tumour of OSCC and metastatic lymph node suggested the probability that even if the EGFR pathway is inhibited during treatment, activation of c-Met can overcome this blockade. As both the pathways are activated in all the cases, they need to be targeted simultaneously during treatment. In OSCC, overexpression of HGF and c-Met is linked to elevated risk of lymph node metastasis and poor prognosis.⁷⁷ SDF1 α is involved in stem cell proliferation, survival and homing to the bone marrow, via its receptor CXCR4. It has been reported that CXCR4 expression by tumour cells act as chemotactic gradient to organs expressing the ligand SDF-1. Such an endocrine pathway is required for moving CXCR4-positive cancer cells to determine the specific homing sites for metastasis.⁷⁸ In recent years, several pieces of evidence supporting the role of SDF-1/CXCR4 in OSCC progression have been reported. CXCR4 expression is increased in OSCC cells,⁷⁹ while SDF-1 induces invasion and scattering of CXCR4-expressing OSCC cells.^{41,80}

Moreover, overexpression of SDF-1 in lymph nodes strongly suggests local metastasis in OSCC.^{81,82} HGF facilitates Akt phosphorylation and activates CXCR4 via protein kinase C delta (PKC ζ) in cancer cells.⁸³ Furthermore, HGF enhances the ability of SDF1 to promote cancer invasion.⁸⁴ Thus, an interconnection between the HGF/Met axis and the SDF1 α -CXCR4 axis seems to be essential for determining the homing sites in lymph node metastasis. In order to check the difference in the expression of these metastatic markers in OSCC between chewing tobacco users and non-users, we checked the expression status of SDF1 α and CXCR4 in primary tumour and metastatic lymph nodes in both tobacco chewer and non-chewer groups. The results demonstrated significantly high cytoplasmic expression of SDF1 α and high membrane expression of CXCR4 in primary tumour of chewing tobacco users in comparison with non-chewers. Similarly, both the proteins were significantly overexpressed in specific tumour-infiltrated regions of the metastatic lymph nodes of chewing tobacco users. However, there was no significant expression in non-chewers. These results clearly indicate that the HGF/c-Met pathway activation is critical for inducing SDF1 α /CXCR4 axis, which aids in lymph node metastasis in OSCC patients with the habit of chewing tobacco. To our knowledge, this is the first study that reports the critical roles of the HGF/c-Met-stimulated SDF1 α /CXCR4 axis in promoting regional lymph node metastasis in case of OSCC specifically in chewing tobacco users but not in non-users in an Indian patient population. Furthermore, our results clearly indicate that in chewing tobacco users, HGF has specific role in promoting cancer invasion via SDF1 α , thus increasing the aggressiveness of the tumours. These results also imply that in future, the SDF1 α /CXCR4 axis may be used as a specific target to intervene metastasis in OSCC patients with habit of chewing tobacco usage.

Collectively, these findings imply that in case of oral squamous cell carcinoma, HGF/c-Met and SDF1 α /CXCR4 axes facilitate regional lymph node metastasis predominantly among chewing tobacco users, highlight its role in promoting the early molecular events linked to cancer progression, invasion and metastasis and imply its potential prospect of acting as prognostic and stratification biomarkers for the arrest of regional metastasis. Further translational studies and clinical validation of these data are essential before these findings can be taken forward as potential diagnostic biomarkers in OSCC patients segregated based on the history of tobacco usage.

ACKNOWLEDGMENTS

The authors would like to thank Dr Jayanta Chakrabarti, Director, Chittaranjan National Cancer Institute, for providing adequate infrastructure to conduct the research work.

CONFLICT OF INTEREST

The authors declare that they do not have any conflict of interest in this work.

AUTHOR CONTRIBUTIONS

SR and NM designed the experiments; SR and DS performed experiments and analysed the data; NA, SMM and AS provided tissue samples and gave clinical insights; SM interpreted the data and performed statistical analyses of the data; SR, BM and NM interpreted the data and wrote the paper and revised it. The corresponding author NM confirms that all listed authors meet ICMJE authorship criteria and that nobody who qualifies for authorship has been excluded.

ETHICAL APPROVAL

The study has been approved by the Institutional Ethics Committee (IEC) of Chittaranjan National Cancer Institute, Kolkata, India (approval no. CNCI/NM/JP/Mar/10). All the procedures performed in the study were in accordance with the 1964 Helsinki Declaration and its later amendments.

INFORMED CONSENT

Informed consent was obtained from all individual participants included in the study.

ORCID

Nabendu Murmu  <https://orcid.org/0000-0001-8562-9921>

REFERENCES

- Vokes EE, Weichselbaum RR, Lippman SM, Hong WK. Head and neck cancer. *N Engl J Med*. 2010;328:184-194.
- Haddad RI, Shin DM. Recent advances in head and neck cancer. *N Engl J Med*. 2008;359(11):1143-1154.
- Saraiya M, Unger ER, Thompson TD, et al. HPV Typing of Cancers Workgroup. US assessment of HPV types in cancers: implications for current and 9-valent HPV vaccines. *J Natl Cancer Inst*. 2015;107(6):djv086.
- Sreeramareddy CT, Pradhan PM, Mir IA, Sin S. Smoking and smokeless tobacco use in nine South and Southeast Asian countries: prevalence estimates and social determinants from Demographic and Health Surveys. *Popul Health Metr*. 2014;12:22.
- Xue J, Yang S, Seng S. Mechanisms of cancer induction by tobacco-specific NNK and NNN. *Cancers (Basel)*. 2014;6(2):1138-1156.
- International Agency for Research on Cancer. *Smokeless Tobacco and Some Tobacco-Specific N-Nitrosamines - IARC Monographs on the Evaluation of Carcinogenic Risks to Humans*, vol. 89. Lyon, France: IARC Press; 2007.
- National Cancer Institute and Centers for Disease Control and Prevention. *Smokeless Tobacco and Public Health: A Global Perspective*. NIH Publication No. 14-7983. Bethesda, MD: U.S. Department of Health and Human Services, Centers for Disease Control and Prevention, National Cancer Institute; 2014.
- Greenlee RT, Murray T, Bolden S, Wingo PA. Cancer statistics. *CA Cancer J Clin*. 2000;50(1):7-33.
- Fu KF, Silverman S, Kramer AM. Spread of tumor, staging, and survival. In: Silverman S, ed. *Oral cancer*, 4th edn. Ontario: BC Decker; 1998:67-74.
- Mukherji SK, Armao D, Joshi VM. Cervical nodal metastases in squamous cell carcinoma of the head and neck: what to expect. *Head Neck*. 2001;23(11):995-1005.
- Mozzillo N, Chiesa F, Botti G, et al. Sentinel node biopsy in head and neck cancer. *Ann Surg Oncol*. 2001;8(9):103S-105S.
- Zwas ST, Ramon Y. Indirect cervical lymphoscintigraphy in healthy subjects via submucosal cheek injections. *International Journal of Radiation Applications and Instrumentation. Part B. Nucl Med Biol*. 1986;13(6):633-637.
- Ossoff RH, Sisson GA. Lymphatics of the floor of the mouth and neck: anatomical studies related to contralateral drainage pathways. *Laryngoscope*. 1981;91(11):1847-1850.
- Ossoff RH, Bytell DE, Hast MH, Sisson GA. Lymphatics of the floor of the mouth and periosteum: anatomic studies with possible clinical correlations. *Otolaryngol Head Neck Surg*. 1980;88(6):652-657.
- Takes RP, Baatenburg De Jong RJ, Alles MJ, et al. Markers for nodal metastasis in head and neck squamous cell cancer. *Arch Otolaryngol Head Neck Surg*. 2002;128(5):512-518.
- Schmalbach CE, Chepeha DB, Giordano TJ, et al. Molecular profiling and the identification of genes associated with metastatic oral cavity/pharynx squamous cell carcinoma. *Arch Otolaryngol Head Neck Surg*. 2004;130(3):295-302.
- Wieduwilt MJ, Moasser MM. The epidermal growth factor receptor family: biology driving targeted therapeutics. *Cell Mol Life Sci*. 2008;65(10):1566-1584.
- Rajaram P, Chandra P, Ticku S, Pallavi BK, RudreshKB MP. Epidermal growth factor receptor: Role in human cancer. *Indian J Dent Res*. 2017;28(6):687-694.
- Bottaro DP, Rubin JS, Faleto DL, et al. Identification of the hepatocyte growth factor receptor as the c-Met proto-oncogene product. *Science*. 1991;251(4995):802-804.
- Rothenberger NJ, Stabile LP. Hepatocyte growth factor/c-met signaling in head and neck cancer and implications for treatment. *Cancers (Basel)*. 2017;9(4):39.
- Knowles LM, Stabile LP, Egloff AM, et al. HGF and c-Met participate in paracrine tumorigenic pathways in head and neck squamous cell cancer. *Clin Cancer Res*. 2009;15(11):3740-3750.
- Hartmann S, Bhole NE, Grandis JR. HGF/Met signaling in head and neck cancer: Impact on the tumor microenvironment. *Clin Cancer Res*. 2016;22(16):4005-4013.
- Kim CH, Kim J, Kahng H, Choi EC. Change of E-cadherin by hepatocyte growth factor and effects on the prognosis of hypopharyngeal carcinoma. *Ann Surg Oncol*. 2007;14(5):1565-1574.
- Kwon MJ, Kim DH, Park HR, et al. Frequent hepatocyte growth factor overexpression and low frequency of c-Met gene amplification in human papillomavirus-negative tonsillar squamous cell carcinoma and their prognostic significances. *Hum Pathol*. 2014;45:1327-1338.
- Arnold L, Enders J, Thomas SM. Activated HGF-c-Met Axis in Head and Neck Cancer. *Cancers (Basel)*. 2017;9(12):169.
- McDermott U, Pusapati RV, Christensen JG, Gray NS, Settleman J. Acquired resistance of non-small cell lung cancer cells to MET kinase inhibition is mediated by a switch to epidermal growth factor receptor dependency. *Cancer Res*. 2010;70:1625-1634.
- Agarwal S, Zerillo C, Kolmakova J, et al. Association of constitutively activated hepatocyte growth factor receptor (met) with

- resistance to a dual EGFR/Her2 inhibitor in non-small-cell lung cancer cells. *Br J Cancer*. 2009;100:941-949.
28. Breindel JL, Haskins JW, Cowell EP, Zhao M, Nguyen DX, Stern DF. EGF receptor activates MET through MAPK to enhance non-small cell lung carcinoma invasion and brain metastasis. *Cancer Res*. 2013;73:5053-5065.
 29. Mueller KL, Hunter LA, Ethier SP, Boerner JL. Met and c-Src cooperate to compensate for loss of epidermal growth factor receptor kinase activity in breast cancer cells. *Cancer Res*. 2008;68:3314-3322.
 30. Gherardi E, Birchmeier W, Birchmeier C, Vande WG. Targeting MET in cancer: rationale and progress. *Nat Rev Cancer*. 2012;12(2):89-103.
 31. Trusolino L, Bertotti A, Comoglio PM. MET signalling: principles and functions in development, organ regeneration and cancer. *Nat Rev Mol Cell Biol*. 2010;11(12):834-848.
 32. Stabile LP, He G, Lui VW, et al. c-Src activation mediates erlotinib resistance in head and neck cancer by stimulating c-Met. *Clin Cancer Res*. 2013;19(2):380-392.
 33. Krumbach R, Schüler J, Hofmann M, Giesemann T, Fiebig HH, Beckers T. Primary resistance to cetuximab in a panel of patient-derived tumour xenograft models: Activation of Met as one mechanism for drug resistance. *Eur J Cancer*. 2011;47(8):1231-1243.
 34. Müller M, Morotti A, Ponzetto C. Activation of NF- κ B is essential for hepatocyte growth factor-mediated proliferation and tubulogenesis. *Mol Cell Biol*. 2002;22(4):1060-1072.
 35. Bassères DS, Baldwin AS. Nuclear factor-kappaB and inhibitor of kappaB kinase pathways in oncogenic initiation and progression. *Oncogene*. 2006;25(51):6817-6830.
 36. Nasry WHS, Rodriguez-Lecompte JC, Martin CK. Role of COX-2/PGE2 mediated inflammation in oral squamous cell carcinoma. *Cancers (Basel)*. 2018;10(10):pii: E348.
 37. Pannone G, Bufo P, Caiaffa MF, et al. Cyclooxygenase-2 expression in oral squamous cell carcinoma. *Int J Immunopathol Pharmacol*. 2004;17(3):273-282.
 38. Tang DW, Lin SC, Chang KW, Chi CW, Chang CS, Liu TY. Elevated expression of cyclooxygenase (COX)-2 in oral squamous cell carcinoma—evidence for COX-2 induction by areca quid ingredients in oral keratinocytes. *J Oral Pathol Med*. 2003;32(9):522-529.
 39. Uchida D, Begum NM, Almofti A, et al. Possible role of stromal cell-derived factor-1/CXCR4 signaling on lymph-node metastasis of oral squamous cell carcinoma. *Exp Cell Res*. 2003;290:289-302.
 40. Uchida D, Begum NM, Tomizuka Y, et al. Acquisition of lymph node, but not distant metastatic potentials, by the overexpression of CXCR4 in human oral squamous cell carcinoma cells. *Lab Invest*. 2004;84:1538-1546.
 41. Ammar A, Uchida D, Begum NM, et al. The clinicopathological significance of the expression of CXCR4 protein in oral squamous cell carcinoma. *Int J Oncol*. 2004;25:65-71.
 42. Onoue T, Uchida D, Begum NM, Tomizuka Y, Yoshida H, Sato M. Epithelial–mesenchymal transition induced by the stromal cell-derived factor-1/CXCR4 system in oral squamous cell carcinoma cells. *Int J Oncol*. 2006;29:1133-1138.
 43. Uchida D, Onoue T, Tomizuka Y, et al. Involvement of an autocrine stromal cell-derived factor-1/CXCR4 system on the distant metastasis of human oral squamous cell carcinoma. *Mol Cancer Res*. 2007;5:1-10.
 44. Muller A, Homey B, Soto H, et al. Involvement of chemokine receptors in breast cancer metastasis. *Nature (London)*. 2001;410:50-56.
 45. Scotton CJ, Wilson JL, Milliken D, Stamp G, Balkwill FR. Epithelial cancer cell migration: a role for chemokine receptors? *Cancer Res*. 2001;61:4961-4965.
 46. Taichman RS, Cooper C, Keller ET, Pienta KJ, Taichman NS, McCauley LK. Use of the stromal cell-derived factor-1/CXCR4 pathway in prostate cancer metastasis to bone. *Cancer Res*. 2002;62:1832-1837.
 47. Schrader AJ, Lechner O, Templin M, et al. CXCR4/CXCL12 expression and signalling in kidney cancer. *Brit J Cancer*. 2002;86:1250-1256.
 48. Zhou Y, Larsen PH, Hao C, Yong VW. CXCR4 is a major chemokine receptor on glioma cells and mediates their survival. *J Biol Chem*. 2002;277:49481-49487.
 49. Kijima T, Maulik G, Ma PC, et al. Regulation of cellular proliferation, cytoskeletal function, and signal transduction through CXCR4 and c-kit in small cell lung cancer cells. *Cancer Res*. 2002;62:6304-6311.
 50. Hwang JH, Hwang JH, Chung HK, et al. CXCR4 chemokine receptor 4 expression and function in human anaplastic thyroid cancer cells. *J Clin Endocrinol Metab*. 2003;88:408-416.
 51. Matsumoto G, Omi Y, Lee U, Kubota E, Tabata Y. NK4 gene therapy combined with cisplatin inhibits tumour growth and metastasis of squamous cell carcinoma. *Anticancer Res*. 2011;31(1):105-111.
 52. Bhattacharyya S, Mandal S, Banerjee S, Mandal GK, Bhowmick AK, Murmu N. Cannabis smoke can be a major risk factor for early-age laryngeal cancer—a molecular signaling-based approach. *Tumour Biol*. 2015;36(8):6029-6036.
 53. Wang CJ, Huang KE, Sun YC, et al. VEGF modulates angiogenesis and osteogenesis in shockwave-promoted fracture healing in rabbits. *J Surg Res*. 2011;171:114-119.
 54. Wehrhan F, Amann K, Molenberg A, Lutz R, Neukam FW, Schlegel KA. Critical size defect regeneration using PEG-mediated BMP-2 gene delivery and the use of cell occlusive barrier membranes - the osteopromotive principle revisited. *Clin Oral Implants Res*. 2013;24:910-920.
 55. Shaw RJ, McGlashan G, Woolgar JA, et al. Prognostic importance of site in squamous cell carcinoma of the buccal mucosa. *Br J Oral Maxillofac Surg*. 2009;47(5):356-359.
 56. Bray F, Ferlay J, Soerjomataram I, Siegel RL, Torre LA, Jemal A. Global cancer statistics 2018: GLOBOCAN estimates of incidence and mortality worldwide for 36 cancers in 185 countries. *CA Cancer J Clin*. 2018;68:394-424.
 57. World Health Organization & International Union against Cancer. Global action against cancer, Updated edn. World Health Organization; 2005.
 58. Pintos J, Black MJ, Sadeghi N, et al. Human papillomavirus infection and oral cancer: A case-control study in Montreal, Canada. *Oral Oncol*. 2008;44(3):242-250.
 59. Kumar S, Pandey U, Bala N, Tewar V, Oanh KT. Tobacco habit in Northern India. *J Indian Med Assoc*. 2006;104(1): 19-22, 24.
 60. Gupta PC. Mouth cancer in India: A new epidemic? *J Indian Med Assoc*. 1999;97(9):370-373.
 61. Dongre A, Deshmukh P, Murali N, Garg B. Tobacco consumption among adolescents in rural Wardha: Where and how tobacco control should focus its attention? *Indian J Cancer*. 2008;45(3):100-106.
 62. Gupta PC, Warnakulasuriya S. Global epidemiology of areca nut usage. *Addict Biol*. 2002;7(1):77-83.
 63. Mahapatra S, Kamath R, Shetty BK, Binu VS. Risk of oral cancer associated with gutka and other tobacco products: a hospital-based case-control study. *J Cancer Res Ther*. 2015;11(1):199-203.

64. Gupta B, Johnson NW. Systematic review and meta-analysis of association of smokeless tobacco and of betel quid without tobacco with incidence of oral cancer in South Asia and the Pacific. *PLoS One*. 2014;9(11):e113385.
65. IARC Working Group on the Evaluation of Carcinogenic Risks to Humans. Betel-quid and areca nut chewing and some areca-nut-derived nitrosamines - IARC monographs on the evaluation of carcinogenic risks to humans Vol. 85 Lyon, France; 2003.
66. Boffetta P, Hecht S, Gray N, Gupta P, Strad K. Smokeless tobacco and cancer. *Lancet Oncol*. 2008;9:667-675.
67. Gupta PC, Ray CS, Sinha DN, Singh PK. Smokeless tobacco: a major public health problem in the SEA region: A review. *Ind J Pub Health*. 2011;5:199-209.
68. Waldemar RR. Squamous cell carcinoma of the gingivobuccal complex: predictors of locoregional failure in stage III-IV cancers. *Oral. Oncol*. 2009;45:135-140.
69. Yadav DS, Chattopadhyay I, Verma A, et al. A pilot study evaluating genetic alterations that drive tobacco- and betel quid-associated oral cancer in Northeast India. *Tumour Biol*. 2014;35(9):9317-9330.
70. India Project Team of ICGC. Mutational landscape of gingivobuccal oral squamous cell carcinoma reveals new recurrently-mutated genes and molecular subgroups. *Nat. Commun*. 2013;4:2873.
71. Rajagopalan P, Patel K, Jain AP, et al. Molecular alterations associated with chronic exposure to cigarette smoke and chewing tobacco in normal oral keratinocytes. *Cancer Biol Ther*. 2018;19(9):773-785.
72. Bhat MY, Advani J, Rajagopalan P, et al. Cigarette smoke and chewing tobacco alter expression of different sets of miRNAs in oral keratinocytes. *Sci Rep*. 2018;8:7040.
73. Kapoor C, Vaidya S, Wadhwan V, Malik S. Lymph node metastasis: A bearing on prognosis in squamous cell carcinoma. *Indian J Cancer*. 2015;52(3):417-424.
74. Pomerantz RG, Grandis JR. The role of epidermal growth factor receptor in head and neck squamous cell carcinoma. *Curr Oncol Rep*. 2003;5:140-146.
75. Puri N, Salgia R. Synergism of EGFR and c-Met pathways, cross-talk and inhibition, in non-small cell lung cancer. *J Carcinog*. 2008;7:9.
76. De Herdt MJ, Baatenburg de Jong RJ. HGF and c-Met as potential orchestrators of invasive growth in head and neck squamous cell carcinoma. *Front Biosci*. 2008;13:2516-2526.
77. Uchida D, Kawamata H, Omotehara F, et al. Role of HGF/c-Met system in invasion and metastasis of oral squamous cell carcinoma cells in vitro and its clinical significance. *Int J Cancer*. 2001;93(4):489-496.
78. Gelmini S, Mangoni M, Serio M, Romagnani P, Lazzeri E. The critical role of SDF-1/CXCR4 axis in cancer and cancer stem cells metastasis. *J J Endocrinol Invest*. 2008;31(9):809-819.
79. Delilbasi CB, Okura M, Iida S, Kogo M. Investigation of CXCR4 in squamous cell carcinoma of the tongue. *Oral Oncol*. 2004;40(2):154-157.
80. Ishikawa T, Nakashiro K, Hara S, et al. CXCR4 expression is associated with lymph node metastasis of oral squamous cell carcinoma. *Int J Oncol*. 2006;28(1):61-66.
81. Uchida D, Begum NM, Almofti A, et al. Possible role of stromal cell-derived factor-1/CXCR4 signaling on lymph node metastasis of oral squamous cell carcinoma. *Exp Cell Res*. 2003;290(2):289-302.
82. Uchida D, Begum NM, Tomizuka Y, et al. Acquisition of lymph node but not distant metastatic potentials by the overexpression of CXCR4 in human oral squamous cell carcinoma. *Lab Invest*. 2004;84(12):1538-1546.
83. Huang S, Ouyang N, Lin L, et al. HGF-induced PKC ζ activation increases functional CXCR4 expression in human breast cancer cells. *PLoS One*. 2012;7(1):e29124.
84. Tu H, Zhou Z, Liang Q, et al. CXCR4 and SDF-1 production are stimulated by hepatocyte growth factor and promote glioma cell invasion. *Onkologie*. 2009;32(6):331-336.

SUPPORTING INFORMATION

Additional supporting information may be found online in the Supporting Information section.

How to cite this article: Ray S, Saha D, Alam N, et al. Exposure to chewing tobacco promotes primary oral squamous cell carcinoma and regional lymph node metastasis by alterations of SDF1 α /CXCR4 axis. *Int J Exp Path*. 2021;102:80–92. <https://doi.org/10.1111/iep.12386>



Chewing tobacco may act as a risk factor for dysplastic transformation of squamous cells in Oral leukoplakia- A cytochemistry based approach

Sayantana Bhattacharyya^a, Sudipta Ray^a, Depanwita Saha^a, Saunak Mitra Mustafi^b,
Neyaz Alam^c, Aniruddha Sarkar^d, Nabendu Murmu^{a,*}

^a Department of Signal Transduction & Biogenic Amines, Chittaranjan National Cancer Institute, India

^b Department of Pathology, Chittaranjan National Cancer Institute, India

^c Department of Surgical Oncology, Chittaranjan National Cancer Institute, India

^d Department of Head and Neck Oncology, Chittaranjan National Cancer Institute, India

ARTICLE INFO

Keywords:

Chewing tobacco
Oral leukoplakia
EGFR
WNT
Atypia
Dysplasia
Risk factor

ABSTRACT

The use of chewing tobacco is a severe risk factor for oral mucosa related diseases including cancer in India as well as USA, although its relationship with Oral Leukoplakia (OL) or related carcinogenicity is still not clear. This work chose two oncogenic pathway proteins- the Epidermal Growth Factor Receptor and the WNT pathway among leukoplakia patients and established their correlation with the individuals' tobacco chewing habit.

89 fresh patients with OL were selected for the work. The samples were classified based on the individual's tobacco chewing habit. The divided samples were then immunostained with antibodies for both of the EGFR as well as WNT pathway proteins. The samples were further classified based on their proliferation status and the expression of these oncoproteins was also observed. In order to compare the cytological data with histological data, 30 OL patients undergoing biopsy were chosen and immunohistological analysis was performed for the same pathways.

Results showed overexpressing EGFR and WNT pathway proteins in all OL samples. Structurally atypic cells had a tendency to overexpress these oncoproteins. However the immunocytochemistry data could not confirm any positive effect of chewing tobacco on the OL's proliferative state. Statistical data from the immunofluorescence finally revealed the overexpression of both EGFR and WNT pathway proteins on the proliferative population establishing chewing tobacco as a positive risk factor for the onset of OL. Data from biopsy samples followed the same trend of protein expression seen in the cytological samples. Dysplastic zones showed huge overexpression of EGFR and WNT pathway proteins among tobacco chewers. In conclusion, this is the first time report showing the effect of chewing tobacco on the EGFR and WNT pathway in OL and its possible role as a potential risk factor for its proliferative type.

1. Introduction

Oral leukoplakia (OL) is the most common potentially malignant disorder of the oral mucosa [1–3]. According to literature, OL affects from 0.2 % to 11.7 % of the population in India [4]. Such significant differences are due to dissimilarities in the incidence of pathology in the defined age, ethnic and social group. Apart from oral leukoplakia, actinic cheilitis, lichen planus, and erythroplakia are also considered budding pre malignant conditions affecting the oral cavity. These lesions might herald oral squamous cell carcinoma, which is the most common malignancy of the oral cavity. The use of tobacco, including smokeless

tobacco and excessive consumption of alcohol are the prominent risk factors in oral cancer. However, studies among selected group of population (Southern Taiwan) have shown strong correlation between betel quid chewing, tobacco use with that of development of pre cancerous lesions such as leukoplakia and oral submucous fibrosis. Conversely, the occurrence of the disease and alcohol consumption showed weak correlation [5].

The WNT and EGFR pathway has been of immense concern in oral carcinoma cases. The WNT signaling pathway is one of the foremost and evolutionarily conserved pathway that modulates crucial aspects of cell fate determination, cell migration, cell polarity, neural patterning and

* Corresponding author.

E-mail address: nabendu.murmu@cnci.org.in (N. Murmu).

<https://doi.org/10.1016/j.prp.2020.153287>

Received 29 September 2020; Received in revised form 10 November 2020; Accepted 11 November 2020

Available online 24 December 2020

0344-0338/© 2020 Elsevier GmbH. All rights reserved.

organogenesis during embryonic development. The canonical WNT Signaling is initiated by the secreted WNT proteins, which bind to a class of seven-spanning serpentine transmembrane receptors encoded by the frizzled genes [6,7]. This leads to the activation of the receptor resulting into phosphorylation of the dishevelled protein which, through its association with axin, prevents glycogen synthase kinase 3 β (GSK3 β) from phosphorylating critical substrates such as β -catenin [8]. The GSK3 β substrates include the negative regulators axin and APC and β -catenin [9,10]. Unphosphorylated β -catenin escapes recognition by β -TRCP, a component of an E3 ubiquitin ligase, and translocates to the nucleus where it binds to transcription factors such as TCF and LEF [11,12]. Epidermal growth factor receptor (EGFR) is the first discovered type of the family Receptor Tyrosin Kinase (RTK). This pathway leads to cell survival, cell proliferation etc. Aberrant expression of this pathway is linked to many types of cancers. After receptor activation, the protein activates its several downstream targets including Protein Kinase B or AKT [13] which finally leads to overexpression of Prostaglandin-endoperoxide synthase 2 or Cyclooxygenase-2 (COX-2), an inflammatory cytokine that contributes to the development and progression of a variety of cancers, including squamous cell carcinoma of the oral cavity and oropharynx [14].

Malignant cells have a small cytoplasmic amount often with vacuoles [15]. An atypic cell on the other hand is one in which some morphological or architectural change can be noticed in comparison with its normal counterpart. However atypic cells do not always refer to malignancy [16]. Hyperplasia is a condition in which the number of cells increases but microscopically these cells resembles that with the normal cell architecture. The probability of a hyperplastic cell to convert into a malignant one is very rare. Again, hypertrophy is a condition whereby the volume of the cell increases. Although hyperplasia and hypertrophy are two separate conditions, they generally take place together [17]. On the contrary, dysplastic cells are those that show pre-malignant neoplastic conditions. In two previous publications these precancerous changes and altered proliferative status of oral squamous cells have been studied thoroughly and the results showed that both EGFR and WNT pathway proteins are responsible for this premalignant transformation. It was found out that EGFR is expressed in leukoplakia regardless of dysplasia, but the protein's positivity was found to be more frequent in lesions sited in areas of high cancer risk [18]. On the other hand, nuclear translocation of the canonical WNT pathway protein, WNT3 and β -Catenin was accounted for progression of dysplasia in oral leukoplakia [19]. These two independent pathways were not only found to play the key role in oral premalignancy but scientists revealed a highly sophisticated molecular cross-talk between these two pathways in advanced stage of oral malignancy [20,21]. It was found out that EGFR regulates β -catenin location, stability, and transcriptional activity whereas β -Catenin inhibition alters the fucosylation status of EGFR. Keeping these particulars in mind, the main aim of the project was to draw a correlation between the classic morphological alterations in oral leukoplakia patients, the expression of several oncoproteins (i.e. the EGFR and WNT pathway), proliferative status of the cells and the habit of tobacco chewing.

2. Materials and methods

2.1. Patient samples

A sum total of 89 patients with fresh incidence of oral leukoplakia were chosen for the work. Patients with additional complications including oral infections and prior treatment histories were excluded from the work. Squamous cell layers were scraped from the patients using sterilized cytobrush and the samples were divided into two parts-one part was used for morphological identification of the samples whereas the other part was used for immunocytochemical analyses. The demographic data for patients along with their addiction habit are attached in Table 1. To check the proteins' expression status in

Table 1

Demographic data of OL patients. The entire population has been sub- divided into two groups based on the experiments carried out. The top panel represents the "Swab samples" pool and the later panel represents patients undergone for both swab sample collection as well as "Biopsy samples" group.

Swab samples				
Age group (Years)	35–45 (47)		45–55 (31)	55–65 (11)
Sex	Male (48)		Female (41)	
Addiction (Chewing tobacco)	Positive (66)		Negative (23)	
Leukoplakia site	Buccal mucosa (34)	Hard palate (31)	Soft palate (22)	Gingiva (02)
Biopsy samples				
Age group (Years)	35–45 (3)		45–55 (9)	55–65 (6)
Sex	Male (13)		Female (5)	
Addiction (Chewing tobacco)	Positive (10)		Negative (8)	
Leukoplakia site	Buccal mucosa (14)	Hard palate (2)	Soft palate (2)	Gingiva (0)

histological sections 18 OL patients from the pool undergoing biopsy was selected. These samples were divided into two sub- groups as well; one part of which was used for immunohistochemistry and the other part was kept for quantitative western blot analyses (Demographic data given in Table 1). All procedures performed in the study involving human participants were in accordance with the ethical standards of the institutional research committee and with the Helsinki declaration (1964) and its later amendments or comparable ethical standards.

2.2. Antibodies and reagents

Antibodies against EGFR (sc-373746), pAKT1/2/3 (sc-514032), NF- κ B p50 (sc-8414), COX-2 (sc-376861), WNT (sc-514531), APC (sc-9998), GSK-3 β (sc-373800), β -catenin (sc-7963) and Ki-67 (sc-15402) were purchased from SantaCruz Biotechnologies (California, USA). FITC and PE tagged secondary antibodies (anti- mouse, sc-516140 and anti-rabbit, sc-3753) were also purchased from SantaCruz Biotechnologies (California, USA). For immunocytochemistry IHC Select® HRP/DAB, 150 Test was purchased from Merck (Darmstadt, Germany). All the stains used for differential staining techniques (Haematoxylin, EA50 and Orange G) were purchased from Merck (Darmstadt, Germany).

2.3. Classification of the squamous cell population

To differentiate between normal cellular structure and atypia, Papanicolaou staining (PAP) staining was performed in all samples. The cell smears were first fixed on glass slides using methanol. Next the slides were dipped in Harri's Haematoxylin for 5 min and rinsed for 2 min under running tap water. The slides were then dipped in Orange G staining solution (specifically stains Keratin) for 5 min followed by ten dips in 90 % ethanol (differentiating agent). In the next step the slides were dipped in EA50 (Eosin Azure 50, containing Eosin and Light Green SF Yellowish) for 5 min and dipped in 90 % ethanol 10 times. The slides were finally dipped in 100 % ethanol for 5 min, followed by 10 dips in xylene and mounted using DPX mountant. All samples were photographed under 20X and 40X magnification using Bright Field Microscope (Leica DM1000, Germany).

For micronuclei detection in the cells, Feulgen staining was performed. DNA hydrolysis was first done by placing the slides in 1 N HCl at 60 °C for 8 min. The cells were next placed in the Schiff's reagent and incubated for 1 h 30 min in dark. The cells were next rinsed with sulphurous acid followed by counterstaining by Light Green SF Yellowish. The slides were finally mounted using DPX and observed under bright field microscope (Leica DM1000, Germany) in 100X magnification.

2.4. Immunocytochemistry

The entire experiment was performed followed by standard protocol mentioned in the Immunoperoxidase Secondary Detection System (DAB150, Merck Millipore). The slides were first treated with citrate buffer for antigen retrieval (microwave method) followed by endogenous peroxidase blocking. For primary antibodies, all samples were treated with anti- EGFR, pAKT1/2/3, NF- κ B p50, COX-2, WNT, APC, pGSK-3 β and β -catenin antibodies respectively. After staining with DAB, the smears were counterstained with Mayer's hematoxylin and photographed using bright- field microscope under 40X magnification (Leica DM1000, Germany).

2.5. Immunohistochemistry

Thin sections of 4 μ m each was made from the FFPE biopsy tissue blocks and were de-waxed in xylene and rehydrated in graded alcohols. Endogenous peroxidase was quenched (using 3 % H₂O₂ solution in Methanol) followed by heat-induced epitope retrieval in citrate buffer (0.01 mol/L; pH 6.0). Immunohistochemical staining (IHC) for was performed by incubating the tissue sections for 1 h at room temperature, using the same primary antibodies followed by DAB (3, 3'-Diaminobenzidine) detection method according to the manufacturer's protocol (DAB 150 Kit, Merck).

2.6. Immunofluorescence staining

For quantitative identification of the expression status of the EGFR and WNT pathway proteins on the proliferative cell population, double immunofluorescence staining was performed using all the aforementioned antibodies along with Ki-67 -a well established marker for cellular proliferation. After incubation with the universal blocking buffer (1 % BSA, 0.1 % cold fish skin gelatin, 0.5 % Triton X-100, 0.05 % sodium azide in 0.01 M PBS, pH 7.2–7.4) for 1 h, the cells were incubated with primary antibodies for 1 h at room temperature in a moist chamber. After incubation with the FITC (sc-516140) and PE (sc-516141) tagged secondary antibodies followed by thorough wash with PBS, the samples were mounted with 90 % glycerol and observed under Fluorescence microscope (Leica DM 4000B).

2.7. Western Blot

With the purpose of estimating the presence and quantification of the proteins, western blot was done on the supernatants of the patient biopsy samples. Tissue lysates were produced by homogenizing and sonicating the samples in western blot lysis buffer (15 mM Tris, 2 mM EDTA, 50 mM 2-Mercaptoethanol, 20 % Glycerol, 0.1 % Triton X100, 1 mM PMSF, 1 mM Sodium Fluoride, 1 mM Sodium Orthovanadate, 1 μ g/mL Aprotinin, 1 μ g/mL Leupeptin, 1 μ g/mL Pepstatin) at room temperature. Fifty microgram of total cell lysates (TLC) were separated on a 10 % sodium dodecyl sulphate- polyacrylamide gel SDS-PAGE, and blotted onto nitrocellulose membranes, blocked in TBS-T (0.1 % Triton in 1xTBS) and probed with primary antibodies (EGFR and WNT pathway) overnight at 4 °C. The membranes were then incubated with the appropriate horseradish peroxidase- conjugated secondary antibodies. The immunoreactive protein bands were developed by enhanced chemiluminescence kit (BioVision ECL Western Blot Substrate, USA) and analyzed by a densitometer (Bio Rad, GS 800, USA) for quantification.

2.8. Scoring and Statistical analyses

For histological scoring, binary scoring technique was used. Each cell showing DAB positive color was scored as '1' whereas cells with no brown precipitate were counted as '0'. Each field was subdivided into nine squares under 40X magnification, and the number of DAB positive cells in each small square was counted. All statistical analyses were

performed with the help of Epi Info (TM) 3.5.3 which is a trademark of the Centre for Disease Control and Prevention (CDC), NIH, USA. To calculate the expression of EGFR and WNT pathway proteins, mean and standard error (s.e.) were calculated. For establishing the correlation between the EGFR and WNT pathway proteins, correlation analysis was performed. Risk factor analysis was also performed using the microscopic score comparing with the patients' tobacco chewing habit.

3. Results

3.1. Classification of the squamous cell population

PAP staining revealed two distinct types of squamous cells in all patients' samples. Cells with normal cellular characteristics of the squamous epithelium were marked as 'normal' whereas cells with morphological changes (neoplastic type) were marked as 'atypia' (Supplementary Fig. 1). In order to determine the altered expressional status of the EGFR and WNT pathway proteins, cells from each sample was sub divided into these two classes and their expression status were compared.

3.2. Alteration in the EGFR and WNT pathway proteins

Immunocytochemistry revealed overexpression of the key EGFR pathway proteins both in normal cells as well as atypic cells among tobacco chewers (Fig. 1A). However, although tobacco non chewers had high expression of the pathway proteins in the atypic cells among non tobacco users, their expression on the normal cells among non tobacco chewers were at basal level. On the other hand, there was very little or no expression of the WNT (Fig. 1B) pathway proteins among non tobacco chewers in normal cells, but comparatively higher expression of all the proteins were found in all atypia cases indicating this pathway's probable participation in tobacco induced early carcinogenesis from leukoplakia. To check if the samples collected from cytobrush represent true data, immunohistochemistry (IHC) was also performed in the same patients' biopsy samples. IHC revealed identical expression pattern for both EGFR (Fig. 2A) and WNT (Fig. 3A) pathway (Except GSK-3 β) among tobacco chewers and non chewers. Western blot from Biopsy samples confirmed the findings after densitometric evaluation (Figs. 2B and 3 B). Statistical analysis showed positive correlation among all the pathway proteins (i.e. EGFR, pAKT1/2/3, NF- κ B and COX-2 for the EGFR pathway and WNT, APC and β -catenin for the WNT pathway). p-value <0.05 was considered to be significant for all cases.

3.3. Effect of chewing tobacco on the proliferative cell population

To check the proteins' expression on proliferating cells from OL samples, immunofluorescence staining was performed using the proliferation marker Ki- 67. Results showed positive expression of both cascade proteins among tobacco users with respect to the patients with no history of chewing tobacco (Fig. 4). The results remained the same when the only Ki- 67 positive population was considered.

3.4. Comparative evaluation and risk factor analysis

From the entire pool of immunocytochemistry data, the cells from each patient were classified into two further groups- total population expressing the EGFR and WNT pathway proteins and atypic cells expressing these proteins' among tobacco chewers and non chewers. Results revealed marked downregulation of both the EGFR and WNT pathway proteins among tobacco non- chewers for the total population. On the other hand, among the atypic population, no such correlation was observed (Fig. 5A). For risk factor analysis, initially the KI-67 positive population was chosen and the expression profile of the EGFR and WNT pathway proteins was assayed. Although the atypic population did not show any significant effect of chewing tobacco on the

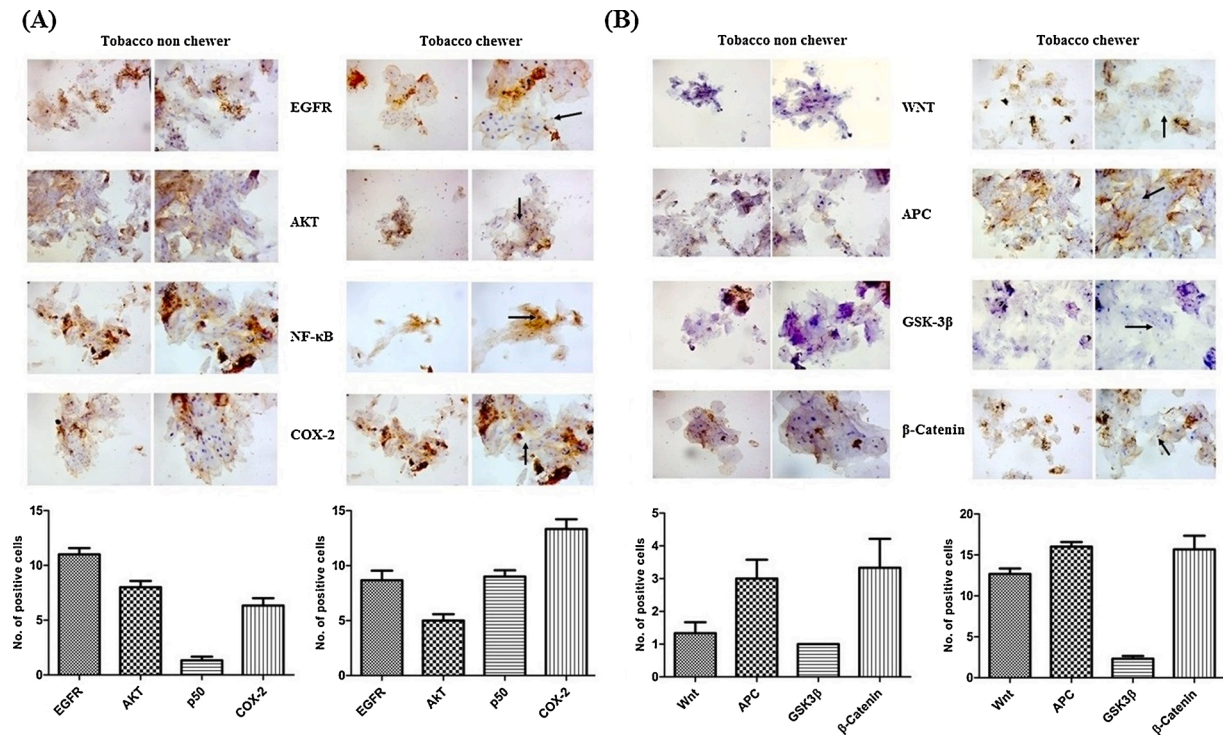


Fig. 1. Expression profiling of the EGFR and WNT pathway proteins in OL swab. Immunocytochemistry was performed for both the EGFR and WNT pathway proteins in all OL samples. Results showed relatively higher expression of the proteins among tobacco chewers in normal cells. In the atypic population, the EGFR pathway had a mixed expression pattern. Upon quantification, it was revealed that although the normal morphology population had noticeably higher expression of the proteins, the atypic population too had higher expression among tobacco chewers (A). The WNT pathway proteins showed huge upregulation of WNT, APC and β-Catenin with downregulated GSK-3β among the tobacco chewing population in normal cells. Atypic cells showed similar protein expression pattern among the tobacco chewers although the difference of percentage positivity of the proteins remained minor (B).

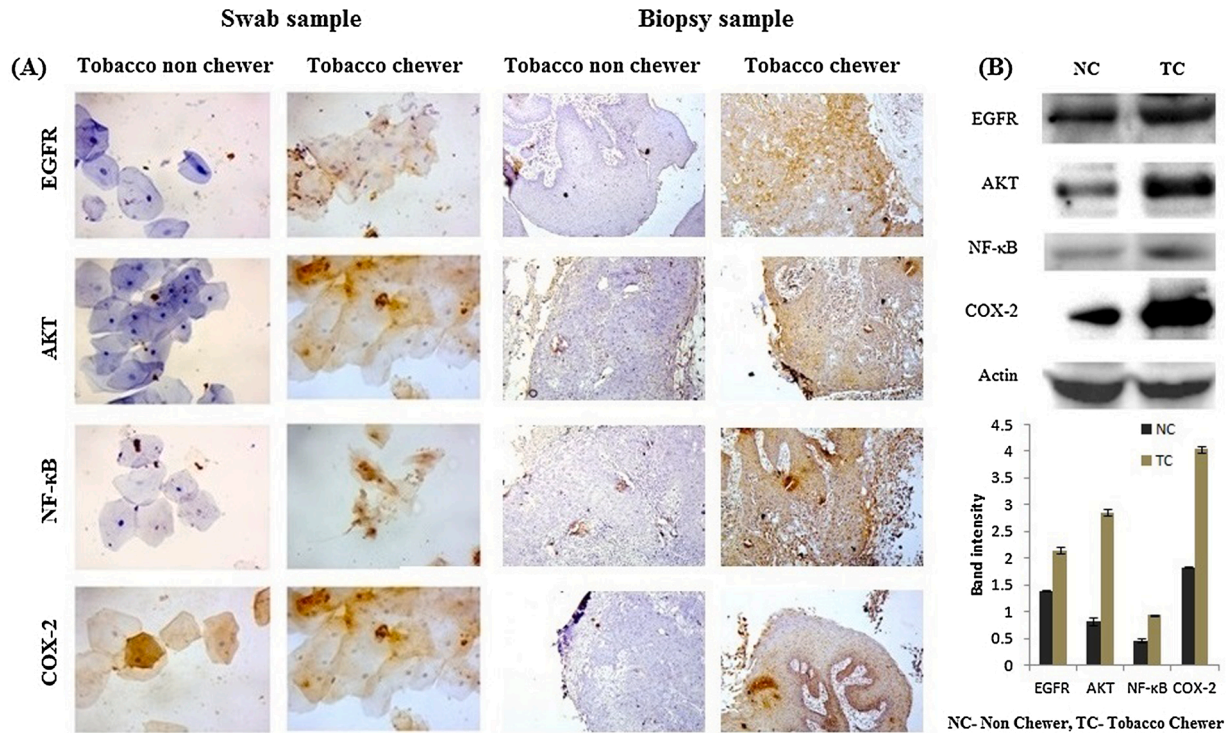


Fig. 2. Comparative profiling of the EGFR pathway proteins in both OL swabs and biopsies. Immunohistochemistry of the biopsy samples showed huge upregulation of the EGFR pathway proteins in the dysplastic zones suggesting these pathways' roles in the cells' proliferative state (A). Swab data of the same patients showed identical expression pattern supporting the results of cytobrush- isolated squamous cells. Data from western blot also showed an overall upregulation of all the proteins in the tobacco chewing population (B) with respect to the non- chewers.

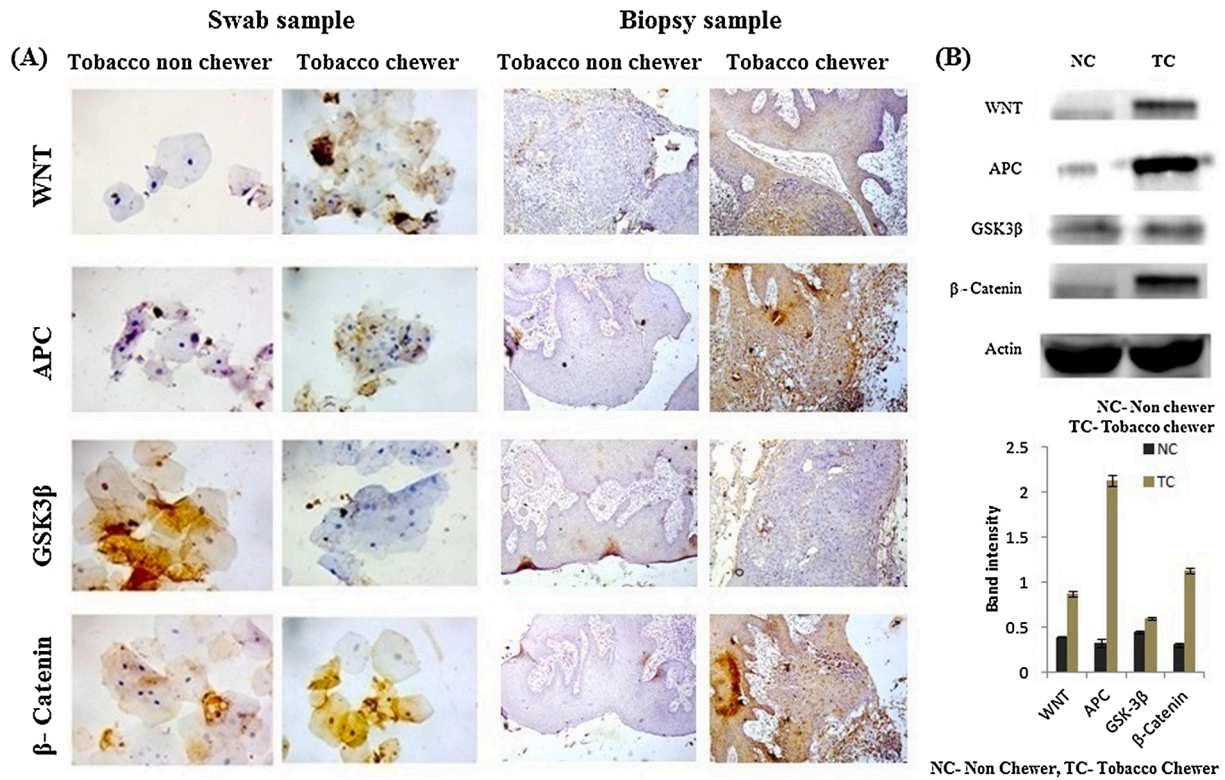


Fig. 3. Comparative profiling of the WNT pathway proteins in both OL swabs and biopsies. Immunohistochemistry of the biopsy samples showed upregulated WNT pathway proteins in the dysplastic zones. Swab data of the same patients showed identical expression pattern supporting the results of cytobrush- isolated squamous cells (A). Data from western blot also showed an overall upregulation of all the proteins in the tobacco chewing population (B) with respect to the non- chewers.

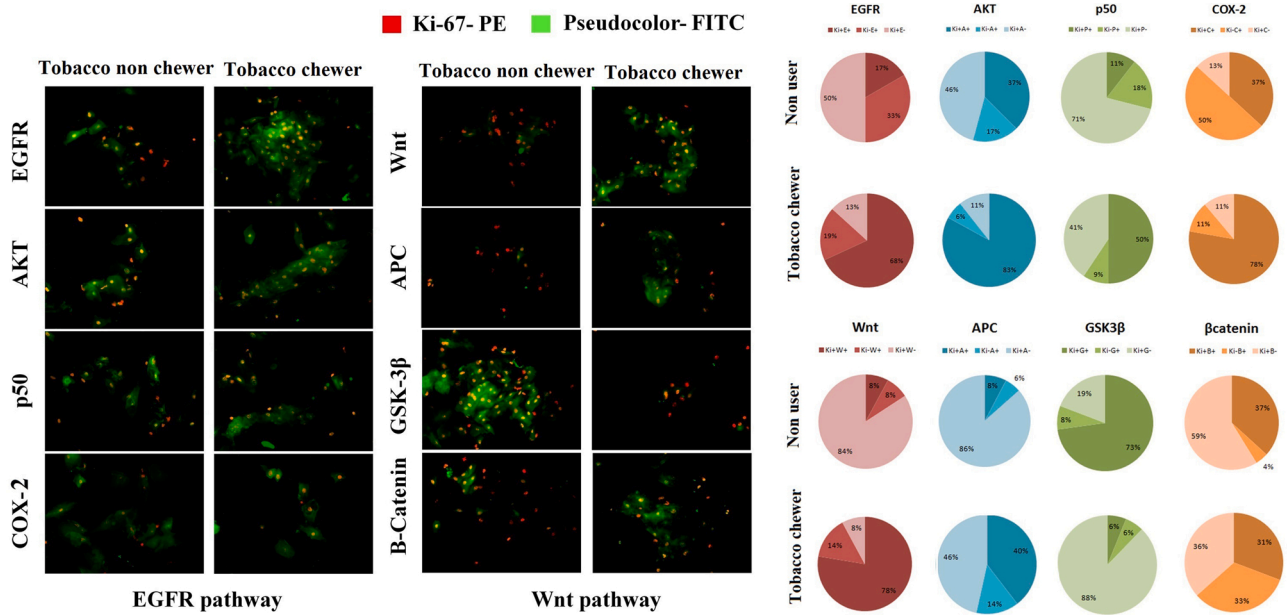


Fig. 4. Molecular profiling of the EGFR and WNT pathway proteins in proliferative cells. To check the expression pattern of both the EGFR and WNT pathway proteins among the proliferative cell population in OL samples, immunofluorescence staining was done. Data showed comparatively higher expression of EGFR cascade expression among tobacco chewers with respect to non chewers. On the other hand, the WNT pathway proteins showed similar upregulation for WNT and APC with marked downregulation of GSK3β among the tobacco chewers whereas the non chewers had relatively lower expression of WNT and APC and upregulation of GSK3β. However, β-Catenin did not show any significant expression among both the tobacco chewers and non chewers.

proteins' expression, KI-67 positive population clearly showed a rise in the mentioned proteins among the tobacco chewer population (Fig. 5B). For risk factor analysis the average expression for all proteins were first calculated and protein expression higher than the average was

considered as "high" expression and expression lower than the average was considered as "low". Data showed that, among the tobacco chewers population, the entire WNT pathway proteins had significant odds ratio (OR) except GSK3β which made tobacco chewing a risk factor for the

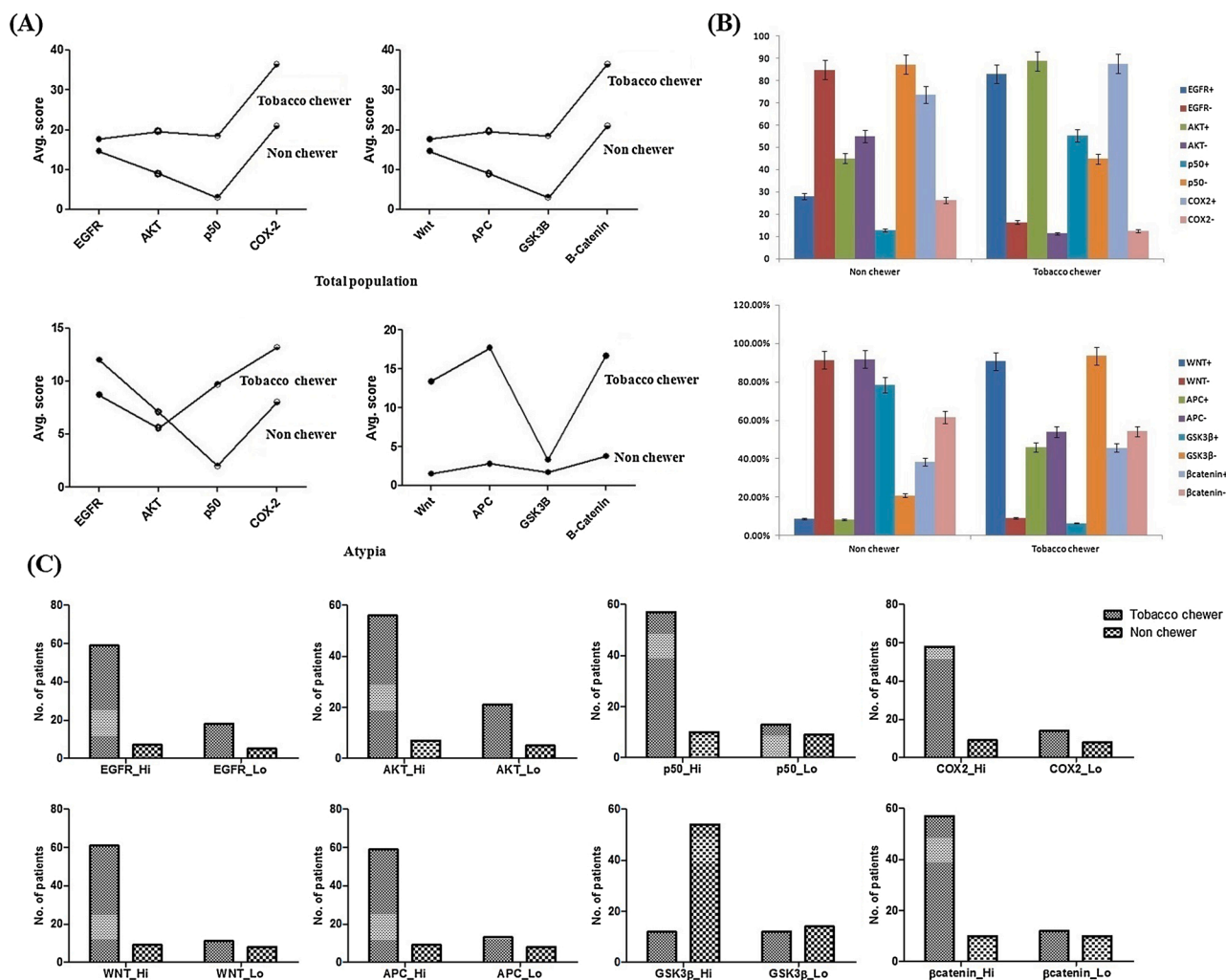


Fig. 5. Risk factor analysis of chewing tobacco among OL patient samples. Immunocytochemistry data from the total population showed an overall upregulation of both the EGFR and WNT pathway proteins among tobacco chewers. However the atypic population did not show any significant correlation (A). For further investigation, the population was again divided among tobacco chewers and non chewers but this time, only the proliferative cells were chosen. Result from the second set showed huge upregulation of both pathway proteins among tobacco chewers (B) and risk factor analysis revealed upregulation of both these pathways as a positive risk for the occurrence of OL ($p < 0.05$).

upregulation of the entire WNT signal cascade (C). The OR range for all proteins were between 0.2593 (for β -Catenin) to 4.929 (for WNT). The p value was significant (<0.05) for all cases except EGFR and AKT (Table 2).

4. Discussion

According to the National Cancer Institute (NCI) Dictionary of cancer terms, “pre-malignancy” describes a condition that is likely to become cancer. However, besides being a well-known premalignant lesion, the definition for OL changes with time based on the current findings and their understanding. The hallmark of Histopathological aspects of leukoplakia is epithelial hyperplasia and surface hyperkeratosis. Additional epithelial dysplasia, if present may range from mild to severe. However, there is no molecular profiling for the cells participating in OL and their altered expression based on environmental carcinogens. This work first time showed the significance of the EGFR as well as the WNT pathway proteins in different cases of OL. Our work also showed the independence of these proteins’ expression based on their morphological difference. The expression pattern did not show any direct significance for either of the atypic or the normal population.

Tobacco companies have played a mammoth role in advertising within the sports industry since the beginning. As a result, the use of

chewing tobacco has become a common habit among school goers in USA [22,23]. In India, although two states have already banned the marketing of chewing tobacco, the entire country is still submerged in this noxious addiction. Low socio-economic status is found to be significantly associated with increased use of chewing tobacco among males and females in India [24]. A severe lack of knowledge and awareness is thought to be the key reason for the higher usage of tobacco in this country [25]. Although there were previous studies deciphering the effect of chewing tobacco on the onset of oral carcinogenesis, this work shows the significance of this habit on the formation of OL, if any. From a molecular signaling based approach, we chose to observe the expression pattern of the two most cited signaling pathways related to oral carcinogenesis i.e. the EGFR and the WNT pathway [26,27]. The experiments revealed significant upregulation of most of the proteins among tobacco chewers suggesting its ability to trigger oral carcinogenesis. Results also showed chewing tobacco to be a significant risk factor for the upregulation of the EGFR and WNT pathway proteins among the dysplastic cell population in OL tissues.

OL has long been considered as risk factor for the development of oral cancer [18]. Although the etiology is not fully explored, these lesions are often associated with carcinogenic exposures, particularly in Southeast Asia, betel nut [5]. The contribution of chewing tobacco has also been observed in some studies [28,29]. However, all of these studies

Table 2

Risk factor analysis for chewing tobacco in OL. Data from fluorescence staining was quantified using the percentage number of proliferating cells showing positive expression for the EGFR and WNT pathway proteins. Results showed positive odds ratio with significant p value suggesting chewing tobacco as a positive risk factor for the overexpression profile of the EGFR and WNT pathway proteins in OL.

Risk factor for	Cases (n)	Control (n)	OR	95 % CI	P value
EGFR Hi	59 (66.29 %)	7 (7.86 %)	2.341	0.6618, 8.283	0.1782 (ns)
EGFR Lo	18 (20.22 %)	5 (5.61 %)			
AKT Hi	56 (62.92 %)	7 (7.86 %)	1.905	0.5442, 6.667	0.3078 (ns)
AKT Lo	21 (23.59 %)	5 (5.61 %)			
P50 Hi	57 (64.04 %)	10 (11.23 %)	3.946	1.335, 11.66	0.0099 (**)
P50 Lo	13 (14.60 %)	9 (10.11 %)			
COX-2 Hi	58 (65.16 %)	9 (10.11 %)	3.683	1.205, 11.26	0.0176 (*)
COX-2 Lo	14 (15.73 %)	8 (8.98 %)			
WNT Hi	61 (68.53 %)	9 (10.11 %)	4.929	1.563 15.55	0.0040 (**)
WNT Lo	11 (12.35 %)	8 (8.98 %)			
APC Hi	59 (66.29 %)	9 (10.11 %)	4.034	1.308, 12.44	0.0113 (*)
APC Lo	13 (14.60 %)	8 (8.98 %)			
GSK3 β Hi	12 (13.48 %)	54 (60.67 %)	4.750	1.621, 13.92	0.0029 (**)
GSK3 β Lo	14 (15.73 %)	12 (13.48 %)			
β -Catenin Hi	57 (64.04 %)	10 (11.23 %)	0.2593	0.096, 0.699	0.0059 (**)
β -Catenin Lo	12 (13.48 %)	10 (11.23 %)			

were either retrospective or case- control study that deals with only the incidence of the disease. The classical swab testing has recently gained its focus after the recent work published in the Journal of American Medical Association (JAMA) based on the current Covid testing methods [30]. This work used the expression profile of oncoproteins for the first time for determining the likelihood of OL samples (cytological as well as histological) to turn into neoplasms, based on the individual's tobacco chewing habit.

Author statement

All persons who meet authorship criteria are listed as authors, and all authors certify that they have participated sufficiently in the work to take public responsibility for the content, including participation in the concept, design, analysis, writing and revision of the manuscript.

Authorship contribution

Category 1- Conception and design of study: Sayantan Bhattacharyya, Rishav Mitra, Saunak Mitra Mustafi, Nabendu Murmu.

Category 2- Drafting the manuscript: Sayantan Bhattacharyya, Rishav Mitra, Sudipta Ray, Nabendu Murmu.

Category 3- Approval of the version of the manuscript to be published (the names of all authors must be listed): Sayantan Bhattacharyya, Rishav Mitra, Sudipta Ray, Saunak Mitra Mustafi, Neyaz Alam, Nabendu Murmu.

Funding

This project was funded by Chittaranjan National Cancer Institute Intramural Fund (File Number: A-4.145/13) and Department of Science and Technology (DST) INSPIRE (IVR Number: 201400105038), India.

Declaration of Competing Interest

The authors declare that there are no conflicts of interest.

Acknowledgement

We are grateful to Dr. Jayanta Chakraborty, Director, Chittaranjan National Cancer Institute (CNCI) for supporting the entire project.

Appendix A. Supplementary data

Supplementary material related to this article can be found, in the online version, at doi:<https://doi.org/10.1016/j.prp.2020.153287>.

References

- [1] B.W. Neville, T.A. Day, Oral cancer and precancerous lesions, *CA Cancer J. Clin.* 52 (July–August (4)) (2002) 195–215.
- [2] Elisabeth R.E.A. Brouns, Jacques A. Baart, Elisabeth Bloemena, Hakki Karagozoglu, Isaäcvander Waal, The relevance of uniform reporting in oral leukoplakia: definition, certainty factor and staging based on experience with 275 patients, *Med Oral Patol Oral Cir Bucal.* 18 (January (1)) (2013) e19–e26.
- [3] Ma C. Haya-Fernández, J.V. Bagan, J. Murillo-Cortes, R. Poveda-Roda, C. Calabuig, The prevalence of oral leukoplakia in 138 patients with oral squamous cell carcinoma, *Oral Dis.* 10 (2004) 346–348.
- [4] S. Silverman, K. Bhargava, L.W. Smith, A.M. Malaowalla, Malignant transformation and natural history of oral leukoplakia in 55518 industrial workers of Gujarat, *India, Cancer* 38 (1976) 1790–1795.
- [5] C.H. Lee, Y.C. Ko, H.L. Huang, Y.Y. Chao, C.C. Tsai, T.Y. Shieh, L.M. Lin, The pre-cancer risk of betel quid chewing, tobacco use and alcohol consumption in oral leukoplakia and oral submucous fibrosis in southern Taiwan, *Br. J. Cancer* 88 (2003) 366–372.
- [6] P. Bhanot, M. Brink, C.H. Samos, J.C. Hsieh, Y. Wang, J.P. Macke, D. Andrew, J. Nathans, R. Nusse, A new member of the frizzled family from *Drosophila* functions as a Wingless receptor, *Nature* 382 (July (6588)) (1996) 225–230.
- [7] P. Polakis, WNT signalling and cancer, *Cold Spring Harb. Perspect. Biol.* 4 (May (5)) (2012) a008052, <https://doi.org/10.1101/cshperspect.a008052>.
- [8] H. Yamamoto, S. Kishida, M. Kishida, S. Ikeda, S. Takada, A. Kikuchi, Phosphorylation of axin, a WNT signal negative regulator, by glycogen synthase kinase-3 β regulates its stability, *J. Biol. Chem.* 274 (April (16)) (1999) 10681–10684.
- [9] B. Rubinfeld, I. Albert, E. Porfiri, C. Fiol, S. Munemitsu, P. Polakis, Binding of GSK3 β to the APC- β -catenin complex and regulation of complex assembly, *Science* 272 (1996 May (5264)) (1996) 1023–1026.
- [10] C. Yost, M. Torres, J.R. Miller, E. Huang, D. Kimelman, R.T. Moon, The axis-inducing activity, stability, and subcellular distribution of beta-catenin is regulated in *Xenopus* embryos by glycogen synthase kinase 3, *Genes Dev.* 10 (June (12)) (1996) 1443–1454.
- [11] J. Behrens, J.P. von Kries, M. Kühl, L. Bruhn, D. Wedlich, R. Grosschedl, W. Birchmeier, Functional interaction of beta-catenin with the transcription factor LEF-1, *Nature* 382 (August (6592)) (1996) 638–642.
- [12] M. Molenaar, M. van de Wetering, M. Oosterwegel, J. Peterson-Maduro, S. Godsave, V. Korinek, J. Roose, O. Destree, H. Clevers, XTcf-3 transcription factor mediates beta-catenin-induced axis formation in *Xenopus* embryos, *Cell* 86 (August (3)) (1996) 391–399.
- [13] Kwang-Yu Chang, Shan-Yin Tsai, Shang-Hung Chen, Hsiao-Hui Tsou, Chia-Jui Yen, Ko-Jiunn Liu, Hsun-Lang Fang, Hung-Chang Wu, Bin-Fay Chuang, Shao-Wen Chou, Careen K. Tang, Shyun-Yeu Liu, Pei-Jung Lu, Ching-Yu Yen, Jang-Yang Chang, Dissecting the EGFR-PI3K-AKT pathway in oral cancer highlights the role of the EGFR variant III and its clinical relevance, *J. Biomed. Sci.* 20 (1) (2013) 43, <https://doi.org/10.1186/1423-0127-20-43>, 2013; Published online 2013 Jun 27.
- [14] Walaa Hamed Shaker Nasry, Juan Carlos Rodriguez-Lecompte, Chelsea K. Martin, Role of COX-2/PGE2 mediated inflammation in oral squamous cell carcinoma, *Cancers (Basel)* 10 (2018 October (10)) (2018) 348, <https://doi.org/10.3390/cancers10100348>. Published online 2018 Sep 22.
- [15] A.I. Baba, C. Cătoi, Comparative Oncology, The Publishing House of the Romanian Academy, Bucharest (RO), 2007.
- [16] O. Driemel, R. Dahse, A. Berndt, H. Pistner, S.G. Hakim, L. Zardi, T.E. Reichert, H. Kosmehl, High-molecular tenascin-C as an indicator of atypical cells in oral brush biopsies, *Clin. Oral Investig.* 11 (March (1)) (2007) 93–99. Epub 2006 Nov 17.

- [17] M. Ebina, T. Takahashi, T. Chiba, M. Motomiya, Cellular hypertrophy and hyperplasia of airway smooth muscles underlying bronchial asthma: a 3-d morphometric study, *Am. Rev. Respir. Dis.* 148 (1993) 720–726.
- [18] Daniela C. Ribeiro, Frederico O. Gleber-Netto, Sílvia F. Sousa, Vanessa F. Bernardes, Mauro H.N. Guimarães-Abreu, Maria C.F. Aguiar, Immunohistochemical expression of EGFR in oral leukoplakia: association with clinicopathological features and cellular proliferation, *Med. Oral Patol. Oral Cir. Bucal* 17 (September (5)) (2012) e739–e744, 2012.
- [19] Kosei Ishida, Satoshi Ito, Naoyuki Wada, Hiroyo Deguchi, Tsuyoshi Hata, Masaru Hosoda, Tsutomu Nohno, Nuclear localization of beta-catenin involved in precancerous change in oral leukoplakia, *Mol. Cancer* 6 (2007) 62, <https://doi.org/10.1186/1476-4598-6-62>, 2007; Published online 2007 Oct 9.
- [20] C. Lee, H. Hung, P. Hung, et al., Epidermal growth factor receptor regulates β -catenin location, stability, and transcriptional activity in oral cancer, *Mol. Cancer* 9 (2010) 64, <https://doi.org/10.1186/1476-4598-9-64>.
- [21] Kevin Brown Chandler, Khalid A. Alamoud, Vanessa L. Stahl, Bach-Cuc Nguyen, VinayK. Kartha, Manish V. Bais, Kenichi Nomoto, Takashi Owa, Stefano Monti, MariaA. Kukuruzinska, Catherine E. Costello, β -Catenin/CBP inhibition alters epidermal growth factor receptor fucosylation status in oral squamous cell carcinoma, *Mol. Omics* 16 (2020) 195–209.
- [22] M.M. Walsh, J. Ellison, J.F. Hilton, M. Chesney, V.L. Ernster, Spit (smokeless) tobacco use by high school baseball athletes in California, *Tob. Control* 9 (June (Suppl 2)) (2000) ii32–ii39, https://doi.org/10.1136/tc.9.suppl_2.ii32.
- [23] M.M. Walsh, J.F. Hilton, V.L. Ernster, C.M. Masouredis, D.G. Grady, Prevalence, patterns, and correlates of spit tobacco use in a college athlete population, *Addict Behav.* 19 (July–August (4)) (1994) 411–427.
- [24] A. Singh, L. Ladusingh, Prevalence and determinants of tobacco use in India: evidence from recent Global Adult Tobacco Survey data, *PLoS One* 9 (12) (2014), e114073.
- [25] J.S. Thakur, R. Paika, Determinants of smokeless tobacco use in India, *Indian J. Med. Res.* 148 (July (1)) (2018) 41–45, https://doi.org/10.4103/ijmr.IJMR_27_18.
- [26] T. Sasahira, T. Kiritani, Hallmarks of cancer-related newly prognostic factors of oral squamous cell carcinoma, *Int. J. Mol. Sci.* 19 (August (8)) (2018) 2413.
- [27] S.G. Shiah, Y.S. Shieh, J.Y. Chang, The role of WNT signaling in squamous cell carcinoma, *J Dent Res.* Feb 95 (2) (2016) 129–134.
- [28] K. Niaz, F. Maqbool, F. Khan, H. Bahadar, F. Ismail Hassan, M. Abdollahi, Smokeless tobacco (paan and gutkha) consumption, prevalence, and contribution to oral cancer, *Epidemiol. Health* 39 (March 9) (2017) e2017009.
- [29] S. Sharma, L. Satyanarayana, S. Asthana, K.K. Shivalinges, B.S. Goutham, S. Ramachandra, Oral cancer statistics in India on the basis of first report of 29 population-based cancer registries, *J. Oral Maxillofac. Pathol.* 22 (January–April (1)) (2018) 18–26.
- [30] Denise J. McCulloch, Ashley E. Kim, Naomi C. Wilcox, Jennifer K. Logue, Alex L. Greninger, Janet A. Englund, Helen Y. Chu, Comparison of unsupervised home self-collected midnasal swabs with clinician-collected nasopharyngeal swabs for detection of SARS-CoV-2 infection, *JAMA Netw Open.* 3 (July (7)) (2020) e2016382, <https://doi.org/10.1001/jamanetworkopen.2020.16382>. Published online 2020 Jul 22.

Research Article

Botanical from *Piper capense* Fruit Can Help to Combat the Melanoma as Demonstrated by *In Vitro* and *In Vivo* Studies

Brice E. N. Wamba,^{1,2} Paramita Ghosh,¹ Armelle T. Mbaveng ,² Sayantan Bhattacharya,¹ Mitra Debarpan,¹ Saha Depanwita,¹ Mustafi Mitra Saunak,³ Victor Kuete ,² and Nabendu Murmu ¹

¹Department of Signal Transduction and Biogenic Amines, Chittaranjan National Cancer Institute, 37, S.P. Mukherjee Road, Kolkata 700026, India

²Department of Biochemistry, Faculty of Science, University of Dschang, Dschang, Cameroon

³Department of Pathology, Chittaranjan National Cancer Institute, 37, S. P. Mukherjee Road, Kolkata 700026, India

Correspondence should be addressed to Victor Kuete; kuetevictor@yahoo.fr and Nabendu Murmu; nabendu.murmu@cnci.org.in

Received 25 September 2020; Revised 16 November 2020; Accepted 16 December 2020; Published 18 January 2021

Academic Editor: Saheed Sabiu

Copyright © 2021 Brice E. N. Wamba et al. This is an open access article distributed under the Creative Commons Attribution License, which permits unrestricted use, distribution, and reproduction in any medium, provided the original work is properly cited.

Piper capense belongs to Piperaceae family and has long been used as a traditional medicine to treat various diseases in several parts of Africa. The present study aims to investigate the effect of *Piper capense* fruit extract (PCFE) alone and in combination with dacarbazine on metastatic melanoma cell line B16-F10 and *in vivo* in C57BL/6J mice. Cytotoxic effects of PCFE alone and in association with dacarbazine on B16-F10 cells were studied by 3-(4, 5-dimethylthiazol-2-yl)-2, 5-diphenyl tetrazolium bromide (MTT) assay and colony formation assay. Wound healing assay, immunofluorescence staining, and western blot analysis were performed to evaluate the individual and combined effect of PCFE and dacarbazine on epithelial-mesenchymal transition (EMT). For *in vivo* studies, C57BL/6J mice were subcutaneously injected with B16-F10 cells (5×10^5 cells/mL), and the effect of PCFE and dacarbazine was studied on tumor development. The alteration of EMT was evaluated by targeting E-cadherin, vimentin, and CD133 in PCFE alone and in combination with dacarbazine-treated tumor tissues by western blot analysis. Phytochemical screening of PCFE reveals the presence of certain secondary metabolites. Our results showed that PCFE alone and in association with dacarbazine has a good activity in preventing B16-F10 melanoma cell progression and clonogenicity. This extract also regulated EMT. *In vivo* results showed that PCFE (100 mg/kg body weight) reduced tumor size in C57BL/6J mice along with the decrease in the expression of vasculogenic mimicry (VM) tubes as well as an improvement in the qualitative and quantitative expression of markers involved in EMT. Our study suggests that PCFE may be useful for managing the growth and metastasis of melanoma.

1. Introduction

Cancer is increasingly recognized as a critical public health problem worldwide, specifically in some parts of Africa where people are poor and do not have the financial means to obtain adequate treatment even though the survival rates are lower compared to other countries [1].

The latest World Health Organization (WHO) global data show 18.1 million new cases and 9.6 million cancer deaths in 2018 [2]. It is recognized as the leading and the second leading cause of death, respectively, in economically

developed and developing countries [3]. WHO Bulletin in 2018 reports 15769 cases of cancer detected against 10533 cases of deaths or more than half of the incidence in Cameroon [2]. There are more than a hundred different cancers depending on the organ affected. Malignant melanoma is the most aggressive form of skin cancer. About 96480 new cases of melanoma have been diagnosed (57220 in men and 39260 in women) and 7230 cases of death (4740 in men and 2490 in women) from this disease in the United States in 2019 according to the work of Siegel et al. [4]. Melanomas which are not of epithelial origin develop from

neural crest-derived pigmented melanocytes [5]. In Africa and more particularly in Cameroon, its incidence in 2018 has been estimated at 148 cases against 89 cases of death [2].

These growing burdens in developing countries are caused by not only etiological factors [6] but also risk factors such as genetics, population growth and ageing, urbanisation, and the adoption of new lifestyles (smoking, alcoholism, and lack of physical exercise). This has led to a rapid increase in incidence, environmental pollution, lack of preventive measures, delay in diagnosis, and a deficit of health workers trained in oncology. If adequate measures are not taken quickly, cancer mortality will continue to increase at the same rate as incidence [7, 8]. The scientific community, in its quest to find ways and means to reduce the morbidity and mortality rate associated with this disease, has set up several treatment strategies. These strategies include chemotherapy, radiotherapy, and surgery which are the most important and have given rise to the hope of eradicating this disease, though it was later on discovered that cancer cells were capable of developing resistant mechanisms to overcome the lethal action of conventional drugs (chemotherapy) given that it is the most widely used treatment method.

Cancer can be subdivided into several types according to the causal agent and the affected organ. Melanoma is particularly common among Caucasians, especially Northern and North-Western Europeans, living in sunny climates. There are higher rates in Oceania, North America, Europe, Southern Africa, and Latin America. This geographic pattern reflects the primary cause, ultraviolet light (UV) exposure in conjunction with the amount of skin pigmentation in the population. A crucial conundrum that goes hand in hand with tumor aggressiveness and poor prognosis of patients is drug resistance. Many tumors, especially melanoma, have the tendency to show resistance against various chemotherapeutic drugs that make the treatment difficult at best [9]. Although the general mode of action for drug resistance is thought to be achieved by the ATP-binding cassette (ABC) transporter system [10] present in the cancer stem cell (CSC) population, the molecular signalling is different in melanoma. Dacarbazine, a potent alkylating agent, is considered the gold standard for melanoma treatment. But the response rate of the drug is only 15–20% [11], and the possible mechanism of evasion is mediated by the upregulation of interleukin-8 (IL-8) and vascular endothelial growth factor (VEGF) expressions, two major proteins that regulate angiogenesis, drug resistance, and tumor cell growth by an autocrine mechanism [12–14].

Besides being the most widely used chemotherapeutic agent for eliminating malignant melanoma, the response rate and duration of dacarbazine treatment are disappointing due to the resistant property of the cells and it is still uncertain whether combination therapies are superior to the single-agent dacarbazine [15, 16] in various randomized phase III studies. In 2018 in Africa, melanoma of skin cancer caused 6629 new cases and 4143 deaths [2].

Cancer cells have developed resistance to existing conventional drugs over time, but also signs of toxicity have been observed; for example, doxorubicin, a widely used

chemodrug, causes renal and cardiac toxicity [17–20], and 5-fluorouracil, a common chemotherapeutic agent, is known to cause myelotoxicity and cardiotoxicity [21, 22]. All of these justify the urgency in the search for naturally occurring anticancer drugs with fewer side effects and designed to overcome the resistance problem. Several studies have already been carried out with plant extracts in relation to melanoma cell line B16-F10; for example, Pandey [23], showed the *in vivo* antitumor potential of extracts from the different parts of *Bauhinia variegata* Linn. Rajasekar et al. [24] showed the anticancerous effect of *Lithospermum erythrorhizon* extract *in vitro* and *in vivo*. Uscanga-Palomeque et al. [25] showed the inhibitory effect of *Cuphea aequipetala* extracts on melanomas *in vitro* and *in vivo*. In coherence with these findings, a keen interest in a Cameroonian pharmacopoeia plant called *Piper capense* from the Piperaceae family was taken into consideration due to its therapeutic virtues, most especially in the treatment of several illnesses like cancer when used in the form of formulation [26, 27]. *Piper capense* L. is traditionally used in Cameroon to treat cancers [28]; the aerial part of *Piper capense* L. is traditionally used in the Comoro Islands for diarrhoea and cough [29], with their traditional use in South Africa for the treatment of wounds, vaginal discharge, infertility, sore throat, and tongue sores. Both the aerial part and the plant roots when boiled are also used against malaria in Kenya [30]. Nevertheless, its *in vitro* cytotoxic activity on several types of cancer cell lines, notably methanolic extract against CCRF-CEM leukemia cell lines (inhibitory concentration 50% (IC₅₀): 6.95 µg/mL), HL60 (IC₅₀: 8.16 µg/mL), HL60AR (IC₅₀: 11.22 µg/mL), and CEM/ADR5000 (IC₅₀: 6.56 µg/mL), breast adenocarcinoma cell lines MDA-MB231 (IC₅₀: 4.17 µg/mL) and MDA-MB231/BCRP (IC₅₀: 19.45 µg/mL), colon carcinoma cell lines HCT116 p53+/+ (IC₅₀: 4.64 µg/mL) and HCT116 p53-/- (IC₅₀: 4.62 µg/mL), glioblastoma cell lines U87MG (IC₅₀: 13.48 µg/mL) and U87MG.ΔEGFR (IC₅₀: 7.44 µg/mL), has been demonstrated [28, 31]. The activities of *P. capense* MeOH and aqueous extracts against *Mycobacterium tuberculosis* and *C. albicans* with minimal inhibitory concentrations (MICs) of 512 µg/mL and 0.56 µg/mL, respectively [32, 33], have been demonstrated.

Despite all these studies and the results found in the literature, no report on *Piper capense* extract on melanoma cell lines has been documented *in vitro* as well as *in vivo*. Hence, this work aims to evaluate the *in vitro* and *in vivo* anticancer effects of the methanol extract of PCFE alone and in combination with dacarbazine on B16-F10 murine melanoma.

2. Material and Methods

2.1. Collection and Identification of Plant Material. The fruits of *Piper capense* Linn (Piperaceae) were purchased from the Dschang City main market, in the Menoua Division of the West Region of Cameroon. The plant was subsequently identified and authenticated at the National Herbarium of Cameroon (NHC) by Mr. Fulbert Tadjouteu, Yaoundé, where a sample was deposited and registered under reference number 6018/SRF-Cam.

2.2. Preparation of the PCFE. The plant was cleaned and ground and the powder obtained was macerated in methanol in the proportions 1 : 3 (m/v) for 48 hours at room temperature followed by filtration using Whatman No.1 paper. The filtrate obtained was concentrated using a rotary evaporator under reduced pressure (BÜCHI R-200) at 40°C where the crude extract was obtained. The extract was thereafter lyophilized and stored at -20°C for future use.

2.3. Chemicals, Antibodies, and Cell Line. 3-(4,5-Dimethylthiazol-2-yl)-2, 5-diphenyl tetrazolium bromide (MTT) (Merck) has been used for the revelation of viable cells, Dimethylsulfoxide (DMSO) (Merck) was used to dissolve the formazan crystals formed, Dulbecco's modified Eagle medium (DMEM) and high glucose culture medium supplemented with fetal bovine serum (FBS) (Gibco) were used for the cultivation and maintenance of the B16-F10 cell line, and penicillin/streptomycin (Invitrogen) was used for the preparation of culture media; 4', 6-diamino-2-phenylindole (DAPI) (LB097-10MG) was purchased from HIMEDIA Laboratories (Mumbai, India) and used as a nuclear counterstain; dacarbazine was purchased from Celon Laboratories (Telangana State, India) and used as reference chemotherapeutic drug.

The aqueous solution of dacarbazine was freshly prepared and exposed to sunlight at least one hour before any experiment to activate the chemotherapeutic drug.

Antibodies vimentin (mouse IgG1; NBP2-32910) and CD133 (rabbit IgG; NB120-16518) were purchased from Novus Biologicals (10730 E. Briarwood Avenue Centennial, CO 80112); E-cadherin (rabbit IgG; sc-7870), β -actin (rabbit IgG; sc-47778), and CD31 (mouse IgG) (sc-1506) were purchased from Santa Cruz Biotechnology (Bergheimer Str. 89-2, 69115 Heidelberg, Germany, Europe). All secondary antibodies (anti-mouse IgG-HRP: sc-2031, anti-rabbit IgG-HRP: sc-2004, and anti-mouse IgGk BP-PE: sc-516141) were purchased from Santa Cruz Biotechnology (Bergheimer Str. 89-2, 69115 Heidelberg, Germany, Europe). For periodic acid-Schiff staining (PAS), periodic acid was purchased from Merck (Massachusetts, USA); Schiff's reagent and hematoxylin were purchased from SRL (India).

2.4. Cell Culture. The cell line B16-F10 murine melanoma was obtained from the National Centre for Cell Science (NCCS), Pune, India. It was cultured and maintained in Dulbecco's modified Eagle medium (DMEM) and a high glucose culture medium supplemented with 10% fetal bovine serum (FBS) and 1% penicillin/streptomycin in an incubator at 37°C in an atmosphere containing 5% CO₂. All experiments were carried out after three passages.

2.5. Phytochemical Screening of *Piper capense*. The main classes of secondary metabolites, alkaloids (Mayer's tests), sterols (Salkowski's test), polyphenols (ferric chloride test), tannins (gelatin test), saponins (foam test), flavonoids (aluminum chloride test), triterpenes (Liebermann-Burchard's test), and anthraquinones

(Borntrager's test), have been investigated following the phytochemical methods as described in [34, 35].

2.6. In Vitro Evaluation

2.6.1. MTT Assay. The assay was carried out following the experimental protocol described in [36]. Briefly, 100 μ L of culture medium at a density of 1×10^4 cells per well in a 96-well plate was exposed to 100 μ L increasing concentrations of PCFE (10–1000 μ g/mL) for 24 hours. 10 μ L of 5 mg/mL MTT (3-(4, 5-dimethylthiazol-2-yl)-2, 5diphenyltetrazolium bromide) was added to each well and incubated for 2 hours at 37°C. After incubation, 100 μ L DMSO was added to each well and the absorbance was measured at 570 nm using a microtitre plate reader (Tecan Infinite M200). Results were expressed as a percentage of viable cells as compared to 100% representing control cells. The IC₅₀ value was calculated using nonlinear regression (curve fit) followed by log (inhibition) vs. response equation in GraphPad Prism software. The amount of drug was plotted on the X-axis as the log of drug concentration and OD was plotted on the Y-axis.

2.6.2. Clonogenic Assay. B16-F10 cells were seeded at a very low number (500 cells in 2 mL/well) in six-well plates. After 24 h, they were treated with the optimum concentration of PCFE (100 μ g/mL) alone and in combination with dacarbazine at 1000 μ g/mL [37] and incubated for 72 hours. The colonies were fixed with methanol and stained with Harry's hematoxylin. The number of colonies defined as >50 cells/colony was counted under the bright field of a light microscope (Leica DM1000, Germany) at 200x magnification [38].

2.6.3. Wound Healing Assay. The wound healing assay was performed in a 6-well plate following the experimental protocol described in [39]. 2 mL of B16-F10 cells was cultured in DMEM without serum to minimize cellular proliferation. Wounds were generated by scratching the 90% confluent cell monolayer with a sterile 200 μ L pipette tip. The unattached cells were washed away with PBS, and cells were treated with PCFE (100 μ g/mL) alone and in combination with dacarbazine (1000 μ g/mL) diluted in DMEM. Images of the wounds were acquired every 24 h under a phase-contrast microscope. The scratch area was measured using Wound Healing Tool in Image J software and relative scratch closure was calculated as the average length of the relative scratch gap based on the change in the scratch area at time zero.

2.6.4. Immunofluorescence Staining (IFS). For immunofluorescence analysis, 2 mL of B16-F10 cells in DMEM culture media was seeded on coverslips in six-well plates and cultured overnight. Cells were treated with PCFE (100 μ g/mL) alone and in combination with dacarbazine (1000 μ g/mL) for 24 h. The coverslips were fixed with methanol and incubated for 1 hour with 1 : 400 dilution of primary antibody against vimentin, E-cadherin, and CD133 followed by incubation with goat anti-mouse IgG-FITC (green) and goat anti-mouse IgG-PE (red) at 1 : 300 dilutions [40]. Coverslips were

mounted with glycerol, and images were captured with a fluorescence microscope (Leica DM4000 B, Germany).

2.6.5. Western Blot Analysis. Briefly, 2 mL of B16-F10 cells was seeded in six-well plates and treated with individual and combination doses of PCFE (100 µg/mL) and dacarbazine for 24 hours. After incubation, treated cells were lysed in cold western blot lysis buffer (15 mM Tris, 2 mM EDTA, 50 mM 2-mercaptoethanol, 20% glycerol, 0.1% Triton X-100, 1 mM PMSF, 1 mM sodium fluoride, 1 mM sodium orthovanadate, 1 µg/mL aprotinin, 1 µg/mL leupeptin, and 1 µg/mL pepstatin) for 5 minutes at room temperature. Cell lysates were sonicated and centrifuged at 13500 rpm for 15 minutes. Protein samples (50 µg per lane) were thereafter resolved on a 10% sodium dodecyl sulfate-polyacrylamide gel (SDS-PAGE), blotted onto nitrocellulose membranes, blocked in TBS-T (0.1% Triton in 1xTBS), and probed with primary antibodies (E-cadherin, vimentin, CD133, and actin) overnight at 4°C. The membranes were incubated with the appropriate horseradish peroxidase-conjugated secondary antibodies. The immunoreactive protein bands were developed by an enhanced chemiluminescence kit (BioVision ECL Western Blot Substrate) and the immunoreactive bands were analyzed by using Image Lab software (Bio-Rad, GS 800) [41].

2.7. In Vivo Evaluation

2.7.1. Experimental Animals. The male mice of strain C57BL/6J (aged 4-5 weeks; weight 22–25 g) were reared in the Animal House Department of the Chittaranjan National Cancer Institute in appropriate conditions with an alternating light-dark cycle of 12 hours and controlled temperature (22 ± 2°C). They were fed with a standard mouse diet and received water and feed ad libitum. The mice were acclimatized for seven days before being divided into different subgroups according to well-defined criteria before the onset of each experiment. The distribution of the mice was based on their body weight and tumor size as well. The animals were treated according to the recommendations of the Institutional Animal Ethics Committee (IAEC) of the Chittaranjan National Cancer Institute, Kolkata, just as the protocols used in this study were approved by this committee (Project no. IAEC-1774/NM-14/2019/9; 25.06.2019).

2.7.2. Evaluation of the Effect of PCFE and Dacarbazine on Tumor Development in Mice. To check the effect of PCFE on solid melanoma tumor tissue, B16-F10 cells were administered in C57BL/6J mice. Five- to six-week-old C57BL/6J mice were subcutaneously injected with 2.5×10^4 B16-F10 cells (in 200 µL of PBS) into the right dorsolateral flanks. Treatment with the PCFE began once the tumors were visible and reached an average volume of 50 to 70 mm³. Animals were separated into six different groups (5 mice per group) receiving PCFE 50, 100, 150, 200, and 250 mg/kg body weight (b.w.), respectively, and control group. The choice of doses ≤250 mg/kg was made on the basis of the results of the acute and subchronic toxicity studies of PCFA

carried out by Wamba and collaborators which highlighted in their work the nontoxic effects of PCFE at a dose of 250 mg/kg b.w./day and the toxic effects of PCFE at high doses [42]. After 15 days of intraperitoneal treatment, tumor size was determined and animals were sacrificed by cervical dislocation [43]. Tumors were collected for further analysis.

2.7.3. Combination Treatment. In order to check the effect of dacarbazine alone and in combination with PCFE in solid melanoma tumor, the experiment was designed in 5 groups. The first group was treated with dacarbazine at 80 mg/kg body weight [37]; second, third, and fourth groups were treated with different doses of PCFE 100, 150, and 200 mg/kg b.w., respectively, along with dacarbazine, and the fifth group was considered as a control. The treatment was carried out over a period of seven days; on the 8th day, all animals were sacrificed. After determining the size of the tumor for each treatment group, the tumor tissues of the different groups were treated specifically for further experiments.

2.7.4. CD31 Immunohistochemistry with PAS Staining for Identification of VM Tubes. Formalin-fixed paraffin-embedded (FFPE) sections (5 µm) were kept in xylene for 20 minutes at 55°C and later dipped and deparaffinised in xylene for 10 min (3 changes). The tissue sections were rehydrated with various grades of alcohol. For CD31 expression, an immunohistochemistry study was performed according to the standard protocol as mentioned in the immunoperoxidase secondary detection system (DAB 150, Merck Millipore). After staining with DAB, the tissues were incubated with a freshly prepared periodic acid solution (5 mg/mL) for 15 min at room temperature [44]. The slides were treated with Schiff base for 20–30 min in dark and counterstained with Harris hematoxylin. Pink stained VM tubes in the sections were photographed using a bright-field microscope (Leica DM1000, Germany).

2.7.5. Qualitative and Quantitative Estimation of the Markers that Play a Key Role in the VM. A qualitative analysis was made with the aid of immunofluorescence staining following the experimental protocol previously described [40]. The tissues were rehydrated with different grades of alcohol, blocked with a blocking buffer solution (1% bovine fetal serum (FBS), and incubated separately with primary antibodies anti-E-cadherin and anti-vimentin, followed by treatment with secondary antibodies marked PE and FITC. 4', 6-Diamino-2-phenylindole (DAPI) (1 mg/mL; 1:10000) was used for nuclear staining. After mounting the slides, images were captured using a Leica BM 4000B fluorescence microscope (Germany). The alteration of EMT was evaluated by targeting E-cadherin, vimentin, and CD133 in PCFE alone and in combination with dacarbazine-treated tumor tissues. The mice melanoma tissues were homogenized and lysed (UP200S) in a western blot lysis buffer and centrifuged at 13500 rpm for 15 minutes (Thermo Scientific Biofuge Stratos). The lysate thus obtained was separated on SDS-PAGE and probed with desired primary and secondary antibodies.

2.7.6. CD31 Immunohistochemistry with PAS Staining for Identification of Microvessel Density. To evaluate microvessel density for angiogenic activity in PCFE and dacarbazine-treated tumor tissues, CD31 immunohistochemistry with PAS staining was performed according to the standard protocol previously described [45]. The diameters of the microvessel were measured and their numbers were estimated after skeletonization of the endothelium in three different fields using ImageJ software.

2.8. Statistical Analysis. Statistical analyses were performed with GraphPad Prism 5 software. Representative data from three independent experiments are shown as mean value \pm SEM. One-way analysis of variance (ANOVA) followed by post hoc Tukey's test was used to determine the significance of the difference between mean values relative to the control. The p value was calculated to determine significant differences (p value < 0.05).

3. Results

3.1. Qualitative Phytochemical Composition of PCFE. The results of the phytochemical screening reported in Table 1 revealed the presence of alkaloids, polyphenols, saponins, tannins, and sterols in the plant extract while secondary metabolites such as anthraquinones, flavonoids, and triterpenes were absent in the plant extract.

3.2. PCFE Inhibits the Proliferation of B16-F10 Melanoma Cell Line

3.2.1. MTT Assay. To investigate the role of PCFE and dacarbazine on B16-F10 melanoma cells, MTT assay was performed. B16-F10 cells were treated with increasing concentrations of PCFE (10 to 1000 mg/mL) for 24 hours and subjected to MTT assay. The result showed a decrease in the viability of B16-F10 cells as compared to the control (Figure 1(a)). The IC_{50} value of treated B16-F10 cells was calculated to be 47.38 μ g/mL (Figure 1(b)).

3.2.2. Colony Formation Assay. To further confirm the cytotoxicity of PCFE on melanoma cells, colony formation assay was performed. Cells were treated with single and combined doses of PCFE and dacarbazine for 24 hours. Result revealed that PCFE alone and in combination with dacarbazine significantly ($p < 0.0001$; F ratio = 244.3; $R^2 = 0.989$) decreased the number of colonies in B16-F10 cells up to 35% and 12%, respectively (Figures 1(c) and 1(d)).

3.3. PCFE Inhibits EMT in B16-F10 Melanoma Cells

3.3.1. Wound Healing Assay. Wound healing assay showed that PCFE (100 μ g/mL) and dacarbazine (1000 μ g/mL) decreased the invasion and migration of the B16-F10 melanoma cells. However, PCFE treatment and combination treatment inhibit wound healing after 48 hours (Figure 2).

TABLE 1: Phytochemical composition of PCFE.

Chemical classes	<i>Piper capense</i> extract
Extractive yield (%)	12.80
Alkaloids	+
Anthraquinones	-
Flavonoids	-
Polyphenols	+
Saponins	+
Tannins	+
Sterols	+
Triterpenes	-

(+): present; (-): absent; yield is obtained by the ratio of the mass of the extract to the methanol obtained to the mass of the plant powder.

3.3.2. Immunofluorescence Staining. In order to evaluate the effect of PCFE and dacarbazine on EMT of B16-F10 cells, immunofluorescence assay was performed. Fluorescence intensity was quantified and represented as a percentage of intensity. The results revealed that PCFE at a concentration of 100 μ g/mL downregulates the expression of the vimentin and upregulates E-cadherin protein expression in B16-F10 cells. However, treatment with dacarbazine (1000 mg/mL) showed strong immunopositive expressions of vimentin and no detectable E-cadherin expression in B16-F10 cells. Conversely, in the combination treatment (PCFE 100 μ g/mL and dacarbazine 1000 μ g/mL), detectable expressions of E-cadherin and moderate immunopositive expression of vimentin were observed (Figure 3(a)).

3.3.3. Western Blot Analysis. Western blot analysis was performed to evaluate the expression of E-cadherin, vimentin, and CD133. The results obtained showed a significant decrease in the expression of the vimentin ($p < 0.0001$; F ratio = 51.86; $R^2 = 0.9511$) and CD133 ($p < 0.0001$; F ratio = 33.74; $R^2 = 0.9268$) proteins compared to the control (Figure 3(b)). However, the expression of vimentin with dacarbazine treatment was not statistically significant with the control (calculated by Tukey's multiple comparison test) (Figure 3(c)). But we observed significant downregulation with PCFE alone at a concentration of 100 μ g/mL and in association with dacarbazine. Conversely, we observed a significant increase in the expression of E-cadherin protein ($p < 0.0001$; F ratio = 102.4; $R^2 = 0.9746$) at different treatment concentrations compared to the progressive control as described progressively with effective upregulation at the treatment dose corresponding to the association between PCFE and dacarbazine. PCFE extract alone or in association with dacarbazine used in this work results in a downregulation of vimentin and CD133 proteins and an upregulation of the E-cadherin protein compared to the control (Figures 3(b) and 3(c)).

3.4. Antitumoral Activity of PCFE and Dacarbazine on B16-F10 Melanoma in Mice

3.4.1. PCFE Reduces Tumor Size in B16-F10 Melanoma Mice. An increase in tumor size was observed in animals treated with dacarbazine (4.0 \times 4.3 cm²) compared to control

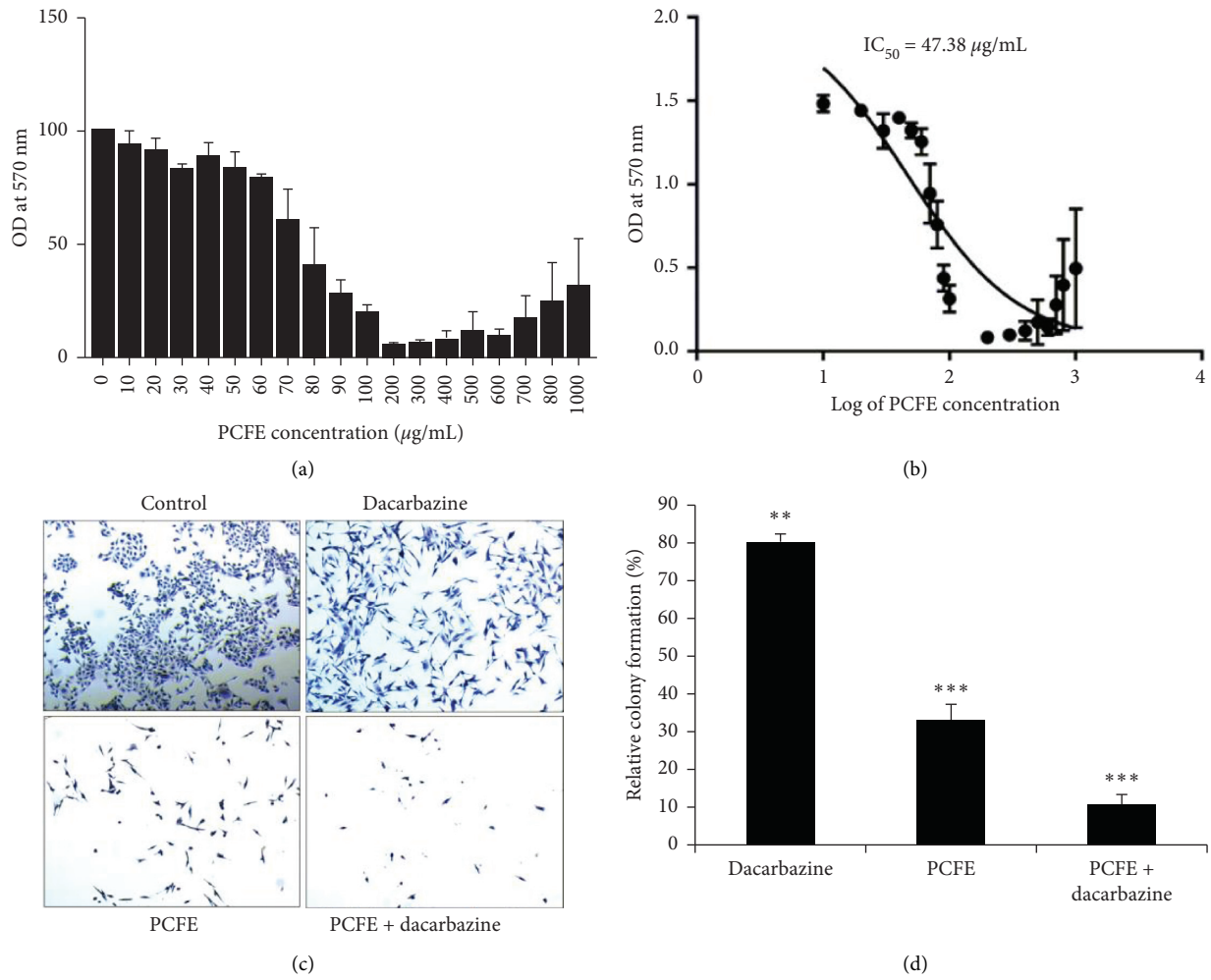


FIGURE 1: Cytotoxic effect of PCFE in B16-F10 cells. The percentage viability of PCFE-treated B16-F10 cells was calculated as OD of the drug-treated sample/OD of the nontreated sample $\times 100$ (a). IC_{50} of melanoma cells treated with increasing concentration of PCFE was calculated as 47.38 $\mu\text{g/ml}$ (b). PCFE alone and in combination with dacarbazine significantly induced inhibition of colony formation and development of B16-F10 cells *in vitro* (c, d). Statistical significance of each treatment group with untreated control is analyzed by one-way ANOVA test ($p_{\text{ANOVA}} < 0.0001$) followed by post hoc Tukey's test. Data are represented as mean \pm SD of triplicate determinations from their independent experiments with * p value < 0.05 , ** p value < 0.01 , and *** p value < 0.0001 versus untreated control and among each group.

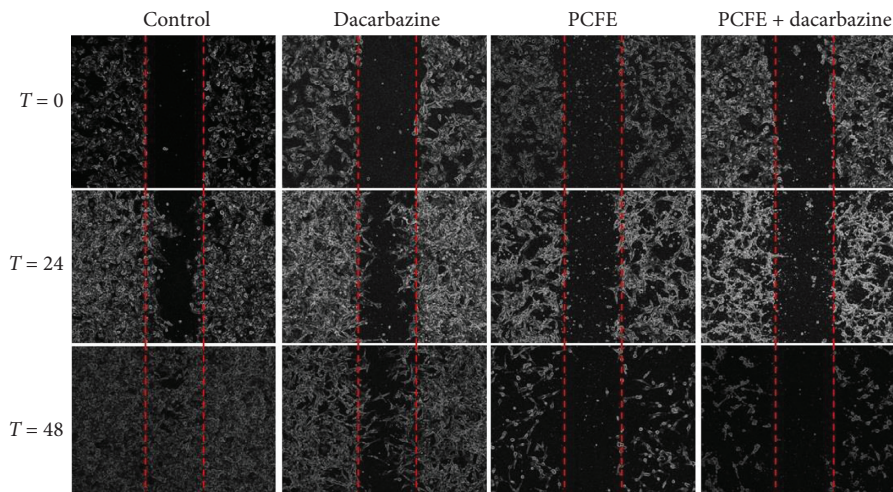


FIGURE 2: Antimigratory effect of PCFE on B16-F10. PCFE alone and in combination with dacarbazine prevents cell migration as compared to the control.

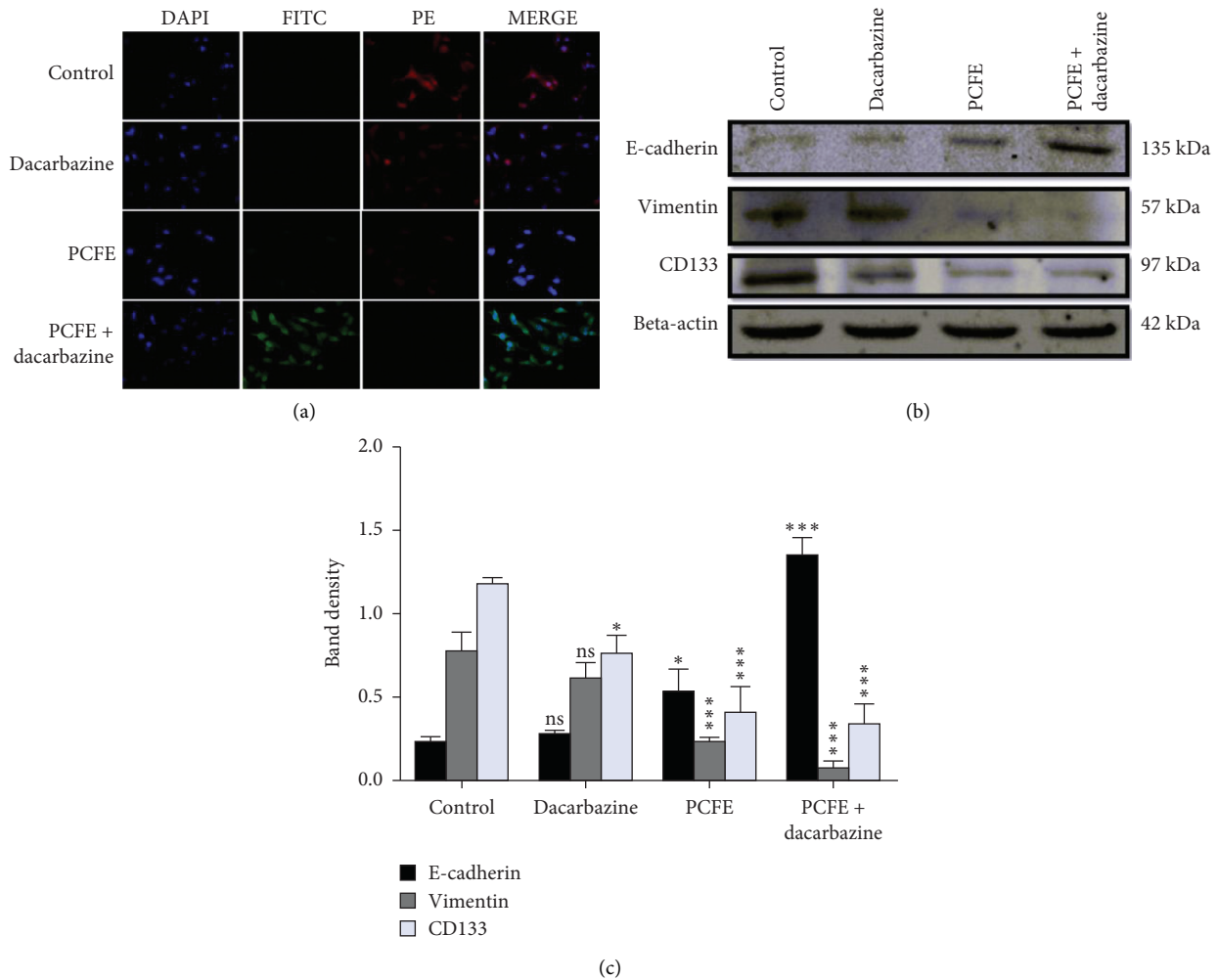


FIGURE 3: PCFE treatment modulates the expression of EMT markers *in vitro*. PCFE alone and in combination with dacarbazine upregulates the expression of FITC-tagged (green) E-cadherin and downregulates PE-tagged (red) vimentin of B16-F10 cells as compared to the untreated control (a). Western blot analysis and densitometric plot also showed significant upregulation of E-cadherin and downregulation of vimentin as well as CD133 (b, c). Statistical significance of each treatment group with untreated control is analyzed by one-way ANOVA test ($p_{ANOVA} < 0.0001$) followed by post hoc Tukey's test. Data are represented as mean \pm SD of triplicate determinations from their independent experiments; ns: not significant, * p value < 0.05 , ** p value < 0.01 , and *** p value < 0.0001 versus untreated control and among each group.

animals ($3.3 \times 3.1 \text{ cm}^2$). In contrast, there was a remarkable decrease in tumor size in animals treated with different doses of PCFE: 50 mg/kg ($2.4 \times 2.6 \text{ cm}^2$), 100 mg/kg ($0.8 \times 1.0 \text{ cm}^2$), 150 mg/kg ($1.0 \times 1.1 \text{ cm}^2$), 200 mg/kg ($1.6 \times 1.7 \text{ cm}^2$), and 250 mg/kg ($2.4 \times 2.5 \text{ cm}^2$). PCFE at different concentrations in combination with dacarbazine at 80 mg/kg showed remarkable inhibition in tumor size: dacarbazine + 100 mg/kg dose ($1.1 \times 1.3 \text{ cm}^2$), dacarbazine + 150 mg/kg dose ($1.9 \times 1.8 \text{ cm}^2$), and dacarbazine + 200 mg/kg dose ($2.8 \times 2.5 \text{ cm}^2$). PCFE at the dose of 100 mg/kg b.w. showed maximum antitumor effect alone in melanoma mice as well as in combination with dacarbazine at 80 mg/kg b.w. (Figures 4(a) and 4(b)).

3.4.2. PCFE Inhibits the Formation and/or Development of Vasculogenic Mimicry. CD31-PAS immunohistochemistry results of dacarbazine-treated tumor tissue isolated from

mice melanoma showed enormous VM tubes. However, different doses of PCFE alone and in combination with dacarbazine treatment showed inhibition of vasculogenic mimicry tubes (CD31 negative/PAS positive). 100 mg/kg b.w. doses of PCFE alone and in the presence of dacarbazine showed a significant decrease in the tumor size and therefore a decrease in the number of tubes at different doses of treatment (Figures 5(a) and 5(b)).

3.4.3. Qualitative and Quantitative Effect of PCFE and Dacarbazine on the Expression of the Markers that Play a Key Role in the VM and EMT. The immunofluorescence carried out on the corresponding tissue sections, each at a precise dose, made it possible to demonstrate the effect of different doses of PCFE alone and in association with dacarbazine on protein expression. These proteins are involved in the heart of

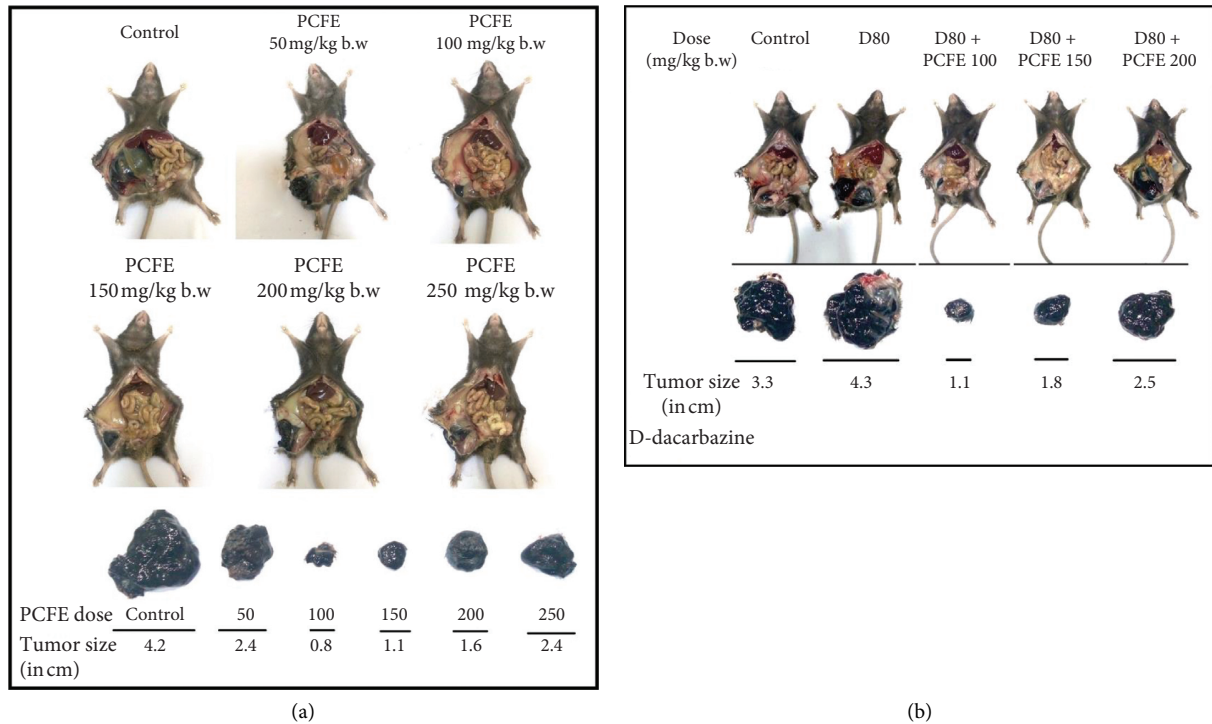


FIGURE 4: PCFE alone and in combination with dacarbazine causes a decrease in tumor size of B16-F10 melanoma mice. The treatment of melanoma mice with various doses of PCFE alone (a) and in combination with dacarbazine (b). PCFE alone at 100 mg/kg b.w. and in combination with dacarbazine showed a maximum decrease in tumor size as compared to the untreated control and other treatment regimes.

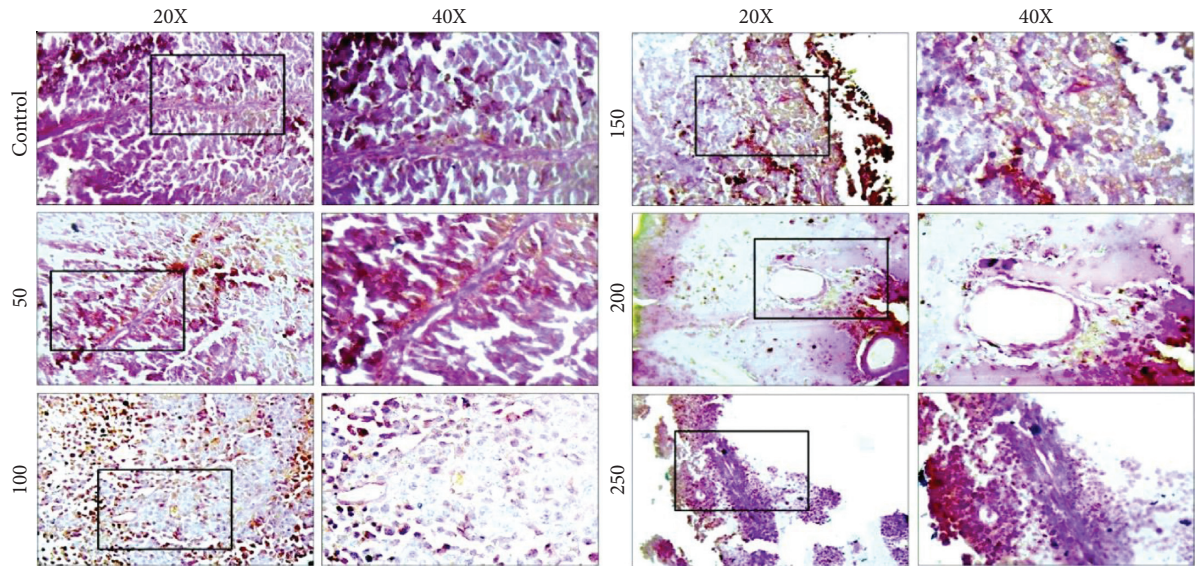
EMT, especially in the inhibition of the expression of vimentin (progressive reduction of the red color) and activation of the expression of E-cadherin (progressive increase in green color), dose dependently in groups of animals treated with PCFE compared to the control group (infected and untreated group). 100 mg/kg dose of PCFE was found to be the dose with the best ability to regulate the expression of these proteins both when administered individually and in combination with dacarbazine (Figure 6(a)). Similar results were obtained from western blot analysis of mice melanoma tumor lysates treated with different doses of PCFE which showed significant downregulation of CD133 ($p < 0.0001$; F ratio = 70.74; $R^2 = 0.963$) and vimentin ($p < 0.0001$; F ratio = 152; $R^2 = 0.982$) and upregulation of E-cadherin expression ($p < 0.0001$; F ratio = 158.1; $R^2 = 0.983$) (Figures 6(b) and 6(c)). However, a better regulation was observed in terms of expression at the dose of 100 mg/kg individually and in combination with dacarbazine (Figure 6(d)).

3.4.4. Effect of PCFE and Dacarbazine on Microvessel Density. This test was performed in order to evaluate the effect of different doses of PCFE on the antigenic vessels present in the tumors collected from different groups of animals. The treatment of animals with the PCFE resulted in a progressive and significant decrease in the number and diameter of the different antiangiogenic vessels in different groups of animals tested and those treated more intensely treated with the 100 mg/kg dose (Figures 7 and 8).

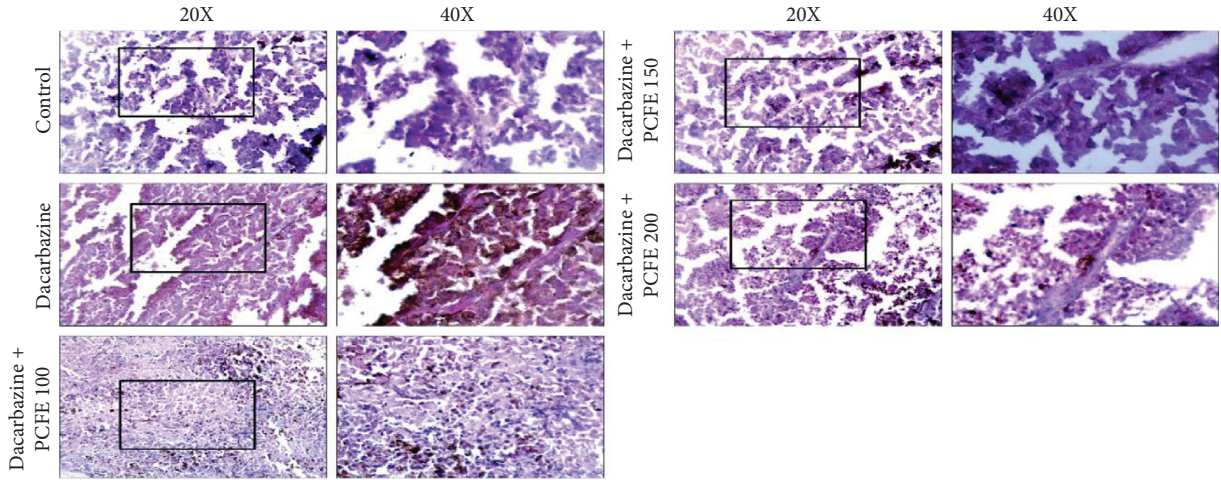
4. Discussion

According to the International Agency for Research on Cancer (IARC) in 2018, the global cancer burden was estimated at 18.1 million for new cases against 9.6 million cancer deaths. Both metastatic and nonmetastatic melanomas have over time developed resistance to conventional anticancer drugs, which are nowadays classified as a public health hazard with reference to their relatively high mortality rate. There is therefore an urgent need to find new effective, low-toxicity substances, and given that phytochemicals are a poorly explored field makes it an unexplored gold mine for researchers. *Piper capense* is a food plant used in Cameroon and other countries in the world in the preparation of dishes and also for its therapeutic virtues [46, 47]. This plant species found in the natural flora of Cameroon has already been the subject of several *in vitro* studies on its anticancer activities on several cancer cell lines [28, 48]. Nevertheless, no reports in the literature have so far shown activities of this plant on melanoma both *in vitro* and *in vivo*, hence the essence of this work.

Several classes of secondary metabolites in plants are known to have cytotoxic and antitumor activities, including alkaloids, polyphenols, saponins, tannins, and sterols [49, 50]. The presence of alkaloids, polyphenols, saponins, tannins, and sterols in the methanol extract of *Piper capense* may justify its anticancer activities *in vitro* and *in vivo* observed in this work. The phytochemical screening results obtained in this study corroborate those of Fankam et al. [51].

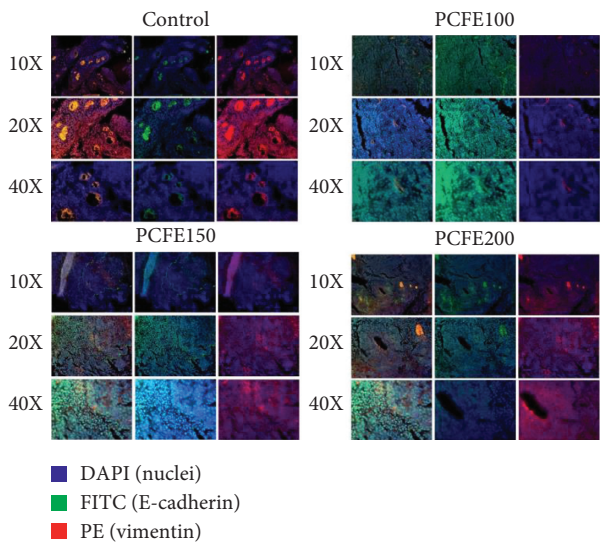


(a)

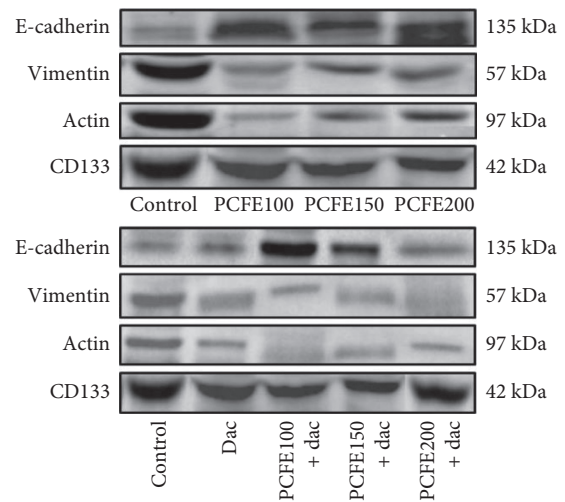


(b)

FIGURE 5: Effect of PCFE on the development of vasculogenic mimicry. CD31-PAS immunohistochemistry result showed PCFE alone (a) and in association with dacarbazine (b) inhibits the formation and development of vasculogenic mimicry in B16-F10 melanoma mice.



(a)



(b)

FIGURE 6: Continued.

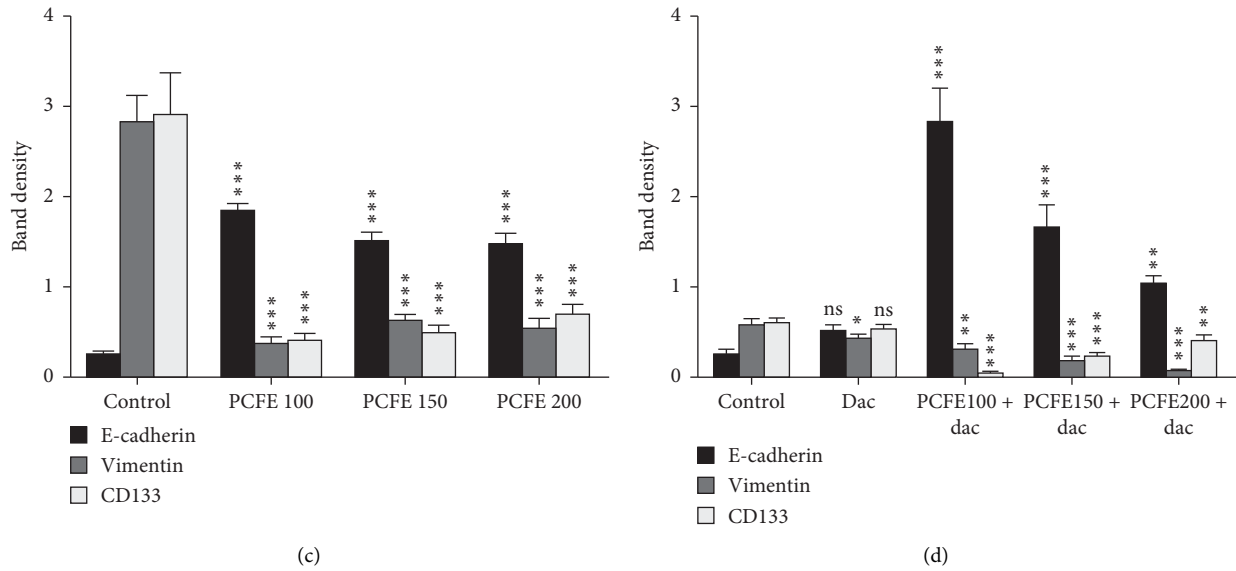


FIGURE 6: Qualitative and quantitative effect of PCFE on the expression of the markers that play a key role in the VM and EMT. Immunofluorescence study with various individual treatments of PCFE and in combination with dacarbazine in mice melanoma tumor sample showed an increase in the expression of E-cadherin and decrease in vimentin (a). Western blot analysis (b) and its densitometry plot (c, d) also showed significant upregulation of E-cadherin and downregulation of vimentin and CD133 in tumor tissue lysate of mice melanoma. Statistical significance of each treatment group with untreated control is analyzed by one-way ANOVA test ($p_{ANOVA} < 0.0001$) followed by post hoc Tukey's test. Data are represented as mean \pm SD of triplicate determinations from their independent experiments with * p value < 0.05 , ** p value < 0.01 , and *** p value < 0.0001 versus untreated control and among each group.

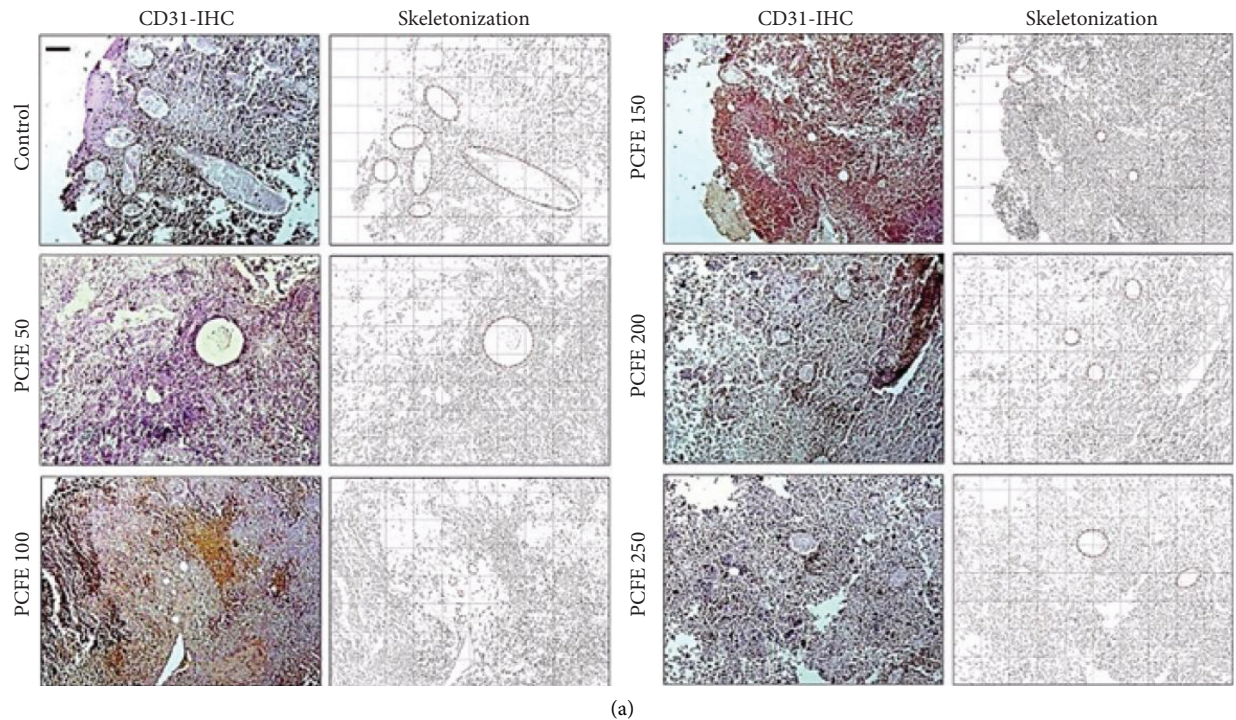


FIGURE 7: Continued.

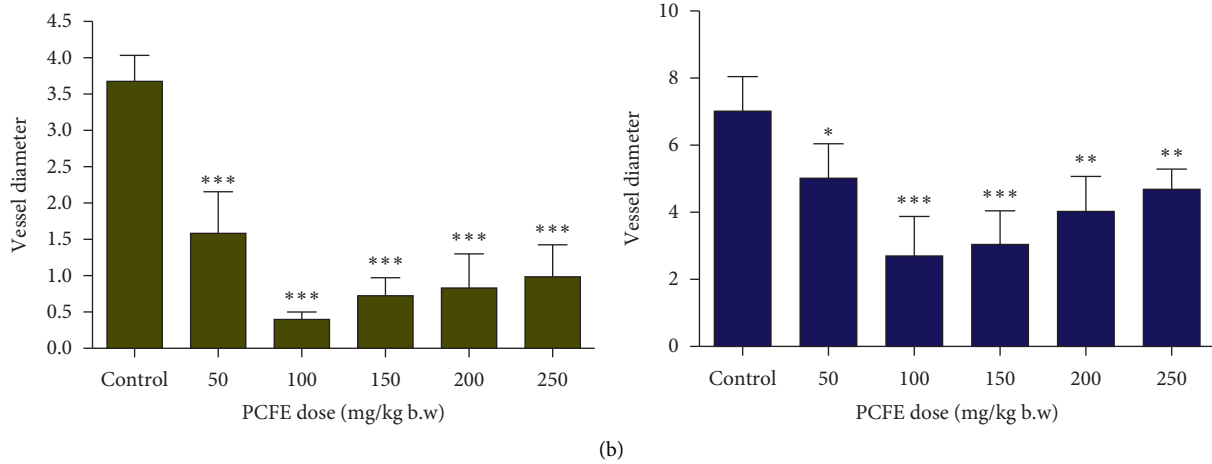


FIGURE 7: Effect of PCFE on microvessel density. PCFE alone at different doses effectively reduces microvessel size and density in B16-F10 melanoma mice.

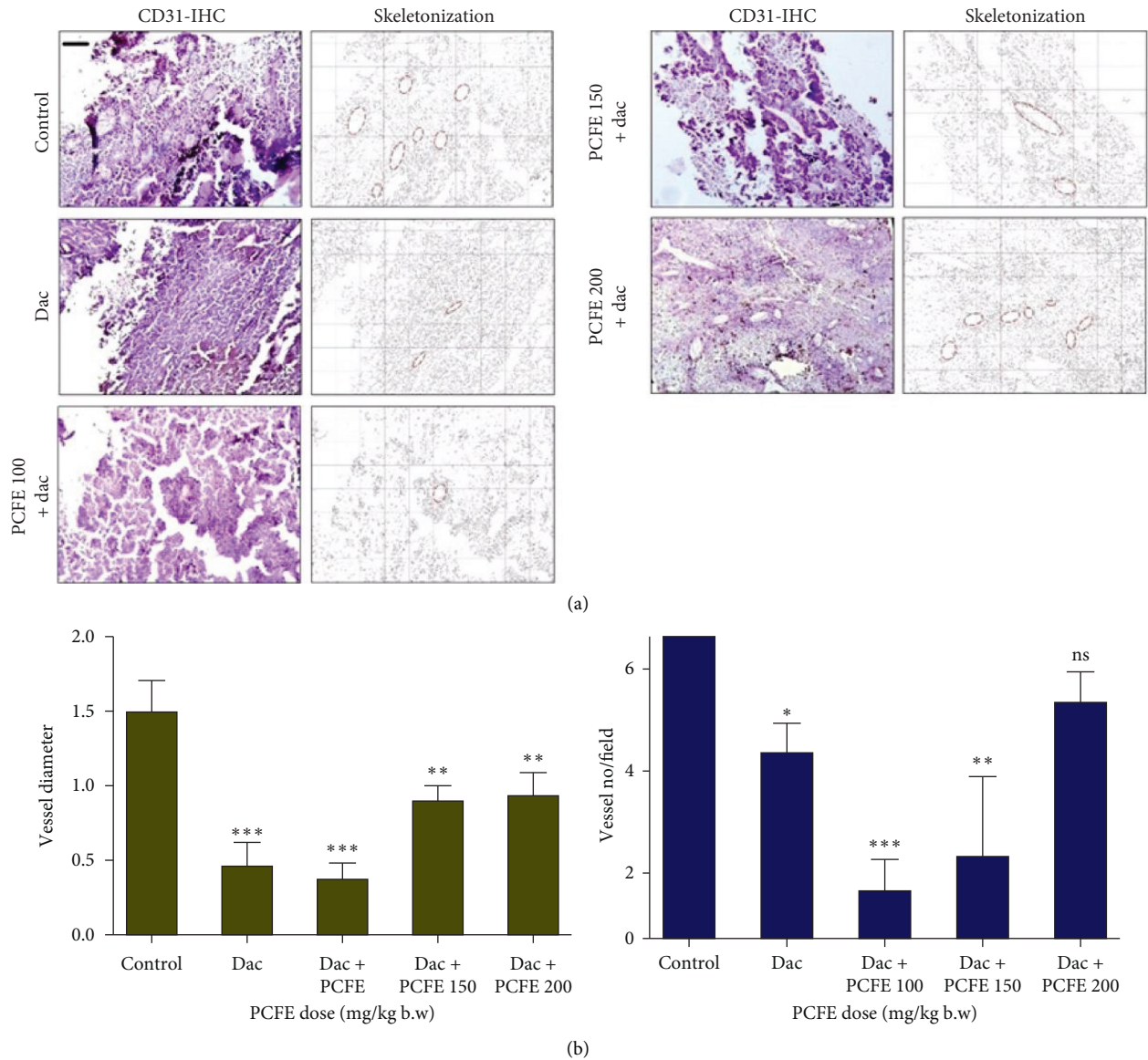


FIGURE 8: Effect of PCFE in association with dacarbazine on microvessel density. PCFE at different doses in combination with dacarbazine effectively reduces microvessel size and density in B16-F10 melanoma mice.

Research on new drugs focuses on substances targeting a specific metabolic pathway or acting on a molecular target with a key role in the survival of cancer stem cells (CSCs), especially those with the ability to restore the expression of proteins involved in EMT. Epithelial-mesenchymal transition is a cellular process in which cells lose their epithelial characteristics and acquire mesenchymal characteristics. EMT has been associated with various tumor functions, including tumor initiation, malignant progression, tumor tenacity, tumor cell migration, metastasis, and treatment resistance [52, 53] and is often defined by downregulation of the epithelial marker E-cadherin and upregulation of the mesenchymal markers vimentin and CD133 [54].

The results obtained in this work show the ability of PCFE to induce a cytotoxic effect on B16-F10 cells and the ability of PCFE alone and in combination with dacarbazine to prevent and/or inhibit colony formation and also for the inhibition of wound healing of B16-F10 melanoma cells and to the reversal of markers involved in EMT by modification of their expression *in vitro*. All these activities could be attributed to the presence of various secondary metabolites with proven anticancer activity in this plant extract [55]. Many works have demonstrated the antiproliferative effect of secondary metabolites such as alkaloids, phenolic compounds, and triterpenes [28, 56, 57]. PCFE alone and in combination with dacarbazine-induced shrinkage of tumor size in animals by inhibiting the development of VM tubes and microvessel density. It also restored the expression of proteins involved in EMT (downregulation of CD133 and vimentin markers and upregulation of E-cadherin) both *in vitro* and *in vivo*. These activities could be due to the presence of the secondary metabolites endowed with anticancer activity in the extract. These results corroborate those of other previous works that have shown that spices possess cytotoxic activities either by induction of apoptosis or by cell cycle arrest at a specific phase [28, 58] and action on EMT markers *in vitro* and *in vivo* [59–61].

The work done by Woguen et al. [48] on the evaluation of the phytochemical composition of essential oil of fruits of *P. capense* by GC-MS revealed the presence of two major compounds (β -pinene and (*E*)-caryophyllene) with good cytotoxic activities. β -Pinene and (*E*)-caryophyllene are compounds belonging to the class of phenolics and terpenoids, respectively; the latter were identified in PCFE. Phenolics and terpenoids are classes of secondary metabolites with antiproliferative and antitumor activities [48, 56]. The presence of these classes of metabolites in PCFE may account for the *in vitro* and *in vivo* anticancer activities observed in this study.

Some compounds like piperine found in alkaloids having anticancer activities *in vitro* and *in vivo* as documented in the literature are also found in plants belonging to the genus *Piper* and the species *Piper nigrum*, *Piper longum*, and *Piper capense* [61–63]. In view of the above, the similarities between the results with the methanol extract of *Piper capense* obtained in this study and those with piperine obtained in other studies lead us to suggest that alkaloids (one group of secondary metabolite highlighted in PCFE) could also be responsible for the activities observed in this study. The

results of this study showed the capacity of PCFE to inhibit the formation and development of VM tubes which are indeed neoformed vessels which play a role in supplying the cancerous cells with nutrients at the level of the primary tumor [64]. The inhibition of the development of these VM tubes by PCFE accompanied by the restoration of the expression of proteins involved in EMT could justify the decrease in the size of the tumor because it lacks a supply route. Also, the antiangiogenic activities of this plant extract were observed in this study as shown previously [65]. These aforementioned activities demonstrate and sufficiently justify the antiproliferative activity of PCFE and could be due to the possible presence of alkaloids in this plant.

The work of Greenshields et al. [66] demonstrates the ability of piperine to inhibit the growth of triple breast cancer xenografts in immune-deficient mice corroborating the results of this study which was carried out on moles of mice of C57BL/6J strains with melanomas. Makhov et al. [67] showed a remarkable effect of the association of an anticancer agent (docetaxel) with piperine through the improvement of the antitumor activity in the xenograft model of human castration-resistant prostate cancer. This is consistent with the results obtained in our study given that a remarkable improvement in the activity of dacarbazine (conventional chemotherapeutic drug of melanoma) administered in association with the PCFE was noted both *in vitro* and *in vivo*. A justification for this activity could be due to the possible presence of one or many active compounds that can be found in the different groups of secondary metabolite that we have highlighted in PCFA.

5. Conclusion

In conclusion, this study, which is the first of its kind to evaluate the anticancer activity of the methanol extract of *Piper capense* fruit against melanoma *in vitro* and *in vivo*, clearly demonstrates the ability of PCFE to inhibit cell proliferation alone and in combination with dacarbazine *in vitro*, to induce the shrinkage of the melanoma tumor size in mice by modification of expression of the markers involved in EMT through downregulation of CD133 and vimentin markers and up-regulation of the E-cadherin marker *in vivo* in melanoma models with the best effect at 100 mg/kg b.w. These results coupled with those in the literature indicate that the *Piper capense* plant is a very good candidate plant for the formulation of phytomedicines in the treatment of melanoma. One of the limitations of this study is the characterization of the phytochemical constituents and mostly the bioactive as well as potentially toxic constituents of the tested methanol extract. However, this work is ongoing and constitutes the aim of our further investigations.

Abbreviations

PCFE:	<i>Piper capense</i> fruit extract
MTT:	3-(4, 5-Dimethylthiazol-2-yl)-2, 5-diphenyl tetrazolium bromide
EMT:	Epithelial-to-mesenchymal transition
DAB:	3,3'-Diaminobenzidine

DMEM: Dulbecco's modified Eagle medium
 FBS: Fetal bovine serum
 VM: Vasculogenic mimicry
 MIC: Minimal inhibitory concentration
 ABC: ATP-binding cassette
 CSC: Cancer stem cell
 IC₅₀: Inhibitory concentration 50%
 WHO: World Health Organization.

Data Availability

All data generated or analyzed during this study are included in this published article.

Ethical Approval

All the experimentation was carried out in strict accordance with the established guidelines on the use of experimental animals (Project no. IAEC-1774/NM-14/2019/9; 25.06.2019).

Conflicts of Interest

VK is an Associate Editor in *Evidence-Based Complementary and Alternative Medicine*; all the other authors declare that there are no conflicts of interest.

Authors' Contributions

BENW, PG, VK, and NM conceptualized the study, formulated the hypothesis, and designed the study. DS, DM, and ATM gave valuable inputs in designing the experiments. BENW, PG, DM, and DS interpreted the data. BENW, VK, and NM wrote the manuscript. ATM, VK, and NM supervised the entire project. BENW, PG, DM, DS, SMM, ATM, VK, and NM read and approved the final version of the manuscript.

Acknowledgments

This study was supported by the Chittaranjan National Cancer Institute, Kolkata, India. The authors acknowledge Department of Science and Technology (DST) RTF-DCS (DCS/2018/000060), Government of India, for funding this project and Dr. Jayanta Chakrabarti, Director, Chittaranjan National Cancer Institute (CNCI), Kolkata, India, for his active support.

References

- [1] D. A. Vorobiof and R. Abratt, "The cancer burden in Africa," *South African Medical Journal = Suid-Afrikaanse Tydskrif Vir Geneeskunde*, vol. 97, no. 10, pp. 937–939, 2007.
- [2] International Agency for Research on Cancer (IARC), *Latest Global Cancer Data: Cancer Burden Rises to 18.1 Million New Cases and 9.6 Million Cancer Deaths in 2018*, Press Release, London, UK, 2020.
- [3] A. L. Torre, F. Bray, L. R. Siegel, J. Ferlay, J. Lortet-Tieulent, and A. Jemal, "Global cancer statistics," *A Cancer Journal for Clinicians*, vol. 65, pp. 87–108, 2012.
- [4] R. L. Siegel, K. D. Miller, and A. Jemal, "Cancer statistics, 2019," *CA: A Cancer Journal for Clinicians*, vol. 69, no. 1, pp. 7–34, 2019.
- [5] P. Prasad, A. Vasas, J. Hohmann, A. Bishayee, and D. Sinha, "Cirsiliol suppressed epithelial to mesenchymal transition in B16F10 malignant melanoma cells through alteration of the PI3K/akt/NF- κ B signaling pathway," *International Journal of Molecular Sciences*, vol. 20, no. 3, p. 608, 2019.
- [6] P. Aubry and B.-A. Gaüzère, "Les cancers dans les pays en développement actualités," 2016.
- [7] A. Jemal, F. Bray, M. M. Center, J. Ferlay, E. Ward, and D. Forman, "Global cancer statistics," *CA: A Cancer Journal for Clinicians*, vol. 61, no. 2, pp. 69–90, 2011.
- [8] ALIAM (Alliance des Ligues francophones Africaines et Méditerranéens), "Les cancers en Afrique Francophone," *Ligue Nationale Contre le Cancer (France)*, vol. 13, pp. 1–36, 2017.
- [9] M. Zigler, G. J. Villares, D. C. Lev, V. O. Melnikova, and M. Bar-Eli, "Tumor immunotherapy in melanoma," *American Journal of Clinical Dermatology*, vol. 9, no. 5, pp. 307–311, 2008.
- [10] M. Dean, T. Fojo, and S. Bates, "Tumour stem cells and drug resistance," *Nature Reviews Cancer*, vol. 5, no. 4, pp. 275–284, 2005.
- [11] D. C. Lev, A. Onn, V. O. Melinkova et al., "Exposure of melanoma cells to dacarbazine results in enhanced tumor growth and metastasis *in vivo*," *Journal of Clinical Oncology*, vol. 22, no. 11, pp. 2092–2100, 2004.
- [12] D. C. Lev, M. Ruiz, L. Mills, E. C. McGary, J. E. Price, and M. Bar-Eli, "Dacarbazine causes transcriptional up-regulation of interleukin 8 and vascular endothelial growth factor in melanoma cells: a possible escape mechanism from chemotherapy," *Cancer Cell*, vol. 8, pp. 299–309, 2005.
- [13] O. Casanovas, D. J. Hicklin, G. Bergers, and D. Hanahan, "Drug resistance by evasion of antiangiogenic targeting of VEGF signaling in late-stage pancreatic islet tumors," *Cancer Cell*, vol. 8, no. 4, pp. 299–309, 2005.
- [14] G. H. Goren, R. Halaban, and G. Neufeld, "Human melanoma cells but not normal melanocytes express vascular endothelial growth factor receptors," *Biochemical and Biophysical Research Communications*, vol. 190, pp. 702–708, 2005.
- [15] M. R. Middleton, J. J. Grob, N. Aaronson et al., "Randomized phase III study of temozolomide versus dacarbazine in the treatment of patients with advanced metastatic malignant melanoma," *Journal of Clinical Oncology*, vol. 18, no. 1, p. 158, 2000.
- [16] M. R. Middleton, P. Lorigan, J. Owen et al., "Randomized phase III study comparing dacarbazine, BCNU, cisplatin and tamoxifen with dacarbazine and interferon in advanced melanoma," *British Journal of Cancer*, vol. 82, pp. 1158–1162, 2010.
- [17] A. Avilés, N. Arévila, J. C. Díaz Maqueo, M. J. Nambo, R. Garcia, and M. J. Nambo, "Late cardiac toxicity of doxorubicin, epirubicin, and mitoxantrone therapy for Hodgkin's disease in adults," *Leukemia & Lymphoma*, vol. 11, no. 3–4, pp. 275–279, 1993.
- [18] E. Leo, R. Arletti, F. Forni, and R. Camerani, "General and cardiac toxicity of doxorubicin-loaded gelatin nanoparticles," *Farmaco*, vol. 52, pp. 385–388, 1997.
- [19] S. Kilickap, E. Akgul, S. Aksoy, K. Aytemir, and I. Barista, "Doxorubicin-induced second degree and complete atrio-ventricular block," *Europace*, vol. 7, no. 3, pp. 227–230, 2005.

- [20] L. Manil, P. Couvreur, and P. Mahieu, "Acute renal toxicity of doxorubicin (adriamycin)-loaded cyanoacrylate nanoparticles," *Pharmaceutical Research*, vol. 12, no. 1, pp. 85–87, 1995.
- [21] J. S. Macdonald, "Toxicity of 5-fluorouracil," *Oncology*, vol. 13, pp. 33–34, 1999.
- [22] G. Rexroth and V. Scotland, "Cardiac toxicity of 5-fluorouracil," *Medizinische Klinik*, vol. 89, pp. 680–688, 1994.
- [23] S. Pandey, "In Vivo antitumor potential of extracts from different parts of *Bauhinia variegata* linn. Against B16-F10 melanoma tumour model in C57BL/6 mice," *Applied Cancer Research*, vol. 37, p. 33, 2017.
- [24] S. Rajasekar, D. J. Park, C. Park et al., "In vitro and in vivo anticancer effects of Lithospermum erythrorhizon extract on B16F10 murine melanoma," *Journal of Ethnopharmacology*, vol. 144, no. 2, pp. 335–345, 2012.
- [25] A. C. Uscanga-Palomeque, P. Zapata-Benavides, S. Saavedra-Alonso et al., "Inhibitory effect of *Cuphea aequipetala* extracts on murine B16-F10 melanoma *in vitro* and *in vivo*," *BioMed Research International*, vol. 11, 2019.
- [26] Y. W. Xin, W. D. Qi, and C. Y. Han, "Traditional chinese medicine for treating respiratory cancer," 2009.
- [27] T. C. Chen, "Observation of the medicine made by oneself in treating with 97 cases with gastric diseases," *Practice of Medical Technology*, vol. 15, pp. 593–594, 2008.
- [28] V. Kuete, L. P. Sandjo, B. Wiench, and T. Efferth, "Cytotoxicity and modes of action of four Cameroonian dietary spices ethno-medically used to treat Cancers: *echinops giganteus*, *Xylophia aethiopica*, *Imperata cylindrica* and *Piper capense*," *Journal of Ethnopharmacology*, vol. 149, no. 1, pp. 245–253, 2013.
- [29] A. M. Kaou, V. Mahiou-Leddet, S. Hutter et al., "Antimalarial activity of crude extracts from nine African medicinal plants," *Journal of Ethnopharmacology*, vol. 116, no. 1, pp. 74–83, 2008.
- [30] A. Koch, P. Tamez, J. Pezzuto, and D. Soejarto, "Evaluation of plants used for antimalarial treatment by the Maasai of Kenya," *Journal of Ethnopharmacology*, vol. 101, no. 1–3, pp. 95–99, 2005.
- [31] V. Kuete, B. Krusche, M. Youns et al., "Cytotoxicity of some Cameroonian spices and selected medicinal plant extracts," *Journal of Ethnopharmacology*, vol. 134, no. 3, pp. 803–812, 2011.
- [32] E. M. Tekwu, T. Askun, V. Kuete et al., "Antibacterial activity of selected Cameroonian dietary spices ethno-medically used against strains of *Mycobacterium tuberculosis*," *Journal of Ethnopharmacology*, vol. 142, no. 2, pp. 374–382, 2012.
- [33] V. Steenkamp, A. C. Fernandes, and C. E. J. Van Rensburg, "Screening of Venda medicinal plants for antifungal activity against *Candida albicans*," *South African Journal of Botany*, vol. 73, no. 2, pp. 256–258, 2007.
- [34] J. B. Harbone, *Phytochemical Methods: A Guide to Modern Techniques of Plant Analysis*, Chapman & Hall, London, UK, 1973.
- [35] H. M. P. Poumale, R. Hamm, Y. Zang, Y. Shiono, and V. Kuete, "Coumarins and related compounds from the medicinal plants of Africa," in *Medicinal Plant Research in Africa: Pharmacology and Chemistry*, V. Kuete, Ed., vol. 1, pp. 261–300, Elsevier, Oxford, UK, 2013.
- [36] T. Mossmann, "Rapid colorimetric assay for cellular growth and survival: application to proliferation and cytotoxicity assays," *Journal of Immunological Methods*, vol. 65, pp. 55–63, 1983.
- [37] S. Bhattacharyya, D. Mitra, S. Ray et al., "Reversing effect of Lupeol on vasculogenic mimicry in murine melanoma progression," *Microvascular Research*, vol. 121, pp. 52–62, 2019.
- [38] N. A. P. Franken, H. M. Rodermond, J. Stap, J. Haveman, and C. Van Bree, "Clonogenic assay of cells *in vitro*," *Nature Protocols*, vol. 1, no. 5, p. 2315, 2006.
- [39] C.-C. Liang, A. Y. Park, and J.-L. Guan, "In vitro scratch assay: a convenient and inexpensive method for analysis of cell migration *in vitro*," *Nature Protocols*, vol. 2, no. 2, p. 329, 2007.
- [40] C. Wählby, F. Erlandsson, E. Bengtsson, and A. Zetterberg, "Sequential immunofluorescence staining and image analysis for detection of large numbers of antigens in individual cell nuclei," *Cytometry*, vol. 47, no. 1, pp. 32–41, 2002.
- [41] F. A. Bhat, G. Sharmila, S. Balakrishnan et al., "Quercetin reverses EGF-induced epithelial to mesenchymal transition and invasiveness in prostate cancer (PC-3) cell line via EGFR/PI3K/Akt pathway," *The Journal of Nutritional Biochemistry*, vol. 25, no. 11, pp. 1132–1139, 2014.
- [42] B. E. N. Wamba, A. T. Mbaveng, G. M. Tazoho, and V. Kuete, "Botanical from the medicinal spice, *Piper capense* is safe as demonstrated by oral acute and subchronic toxicity investigations," *Heliyon*, vol. 6, 2020.
- [43] Vertebrate Animal Research, "AVMA guidelines for the euthanasia of animals: 2013 edition," 2013.
- [44] M. J. C. Hendrix, E. A. Seftor, R. E. B. Seftor et al., "Regulation of uveal melanoma interconverted phenotype by hepatocyte growth factor/scatter factor (HGF/SF)," *American Journal of Pathology*, vol. 152, no. 4, pp. 855–863, 1998.
- [45] N. C. Munshi and C. Wilson, "Increased bone marrow microvessel density in newly diagnosed multiple myeloma carries a poor prognosis," *Seminars in Oncology*, vol. 28, no. 6, pp. 565–569, 2001.
- [46] N. Ahmad, H. Fazal, B. H. Abbasi, S. Farooq, M. Ali, and M. A. Khan, "Biological role of *Piper nigrum* L. (Black pepper): a review," *Asian Pacific Journal of Tropical Biomedicine*, vol. 2, pp. 1945–1953, 2012.
- [47] I. A. Oyemitan, "Chapter 27- african medicinal spices of genus *Piper capense*," in *Medicinal Spices and Vegetables from Africa*, pp. 581–597, Elsevier Inc: Academic Press, London, UK, 2017.
- [48] V. Woguem, F. Maggic, H. P. D. Fogang et al., "Antioxidant, antiproliferative and antimicrobial activities of the volatile oil from the wild pepper *Piper capense* used in Cameroon as a culinary spice," *Natural Product Communications*, vol. 8, pp. 1791–1796, 2013.
- [49] A. Kinghorn, "Plant secondary metabolites as potential anticancer agents and cancer chemopreventives," *Molecules*, vol. 5, no. 12, pp. 285–288, 2000.
- [50] R. B. Birudu and M. J. Naik, "Anticancer properties of secondary metabolites of medicinal plants in carcinoma," *British Biomedical Bulletin*, vol. 2, pp. 662–668, 2014.
- [51] A. G. Fankam, V. Kuete, K. I. Voukeng, J.-R. Kuiaté, and J.-M. Pages, "Antibacterial activities of selected Cameroonian spices and their synergistic effects with antibiotics against multidrug-resistant phenotypes," *BMC Complementary and Alternative Medicine*, vol. 11, p. 104, 2011.
- [52] M. A. Nieto, R. Y.-J. Huang, R. A. Jackson, and J. P. Thiery, "EMT: 2016," *Cell*, vol. 166, no. 1, pp. 21–45, 2016.
- [53] B. D. Craene and G. Berx, "Regulatory networks defining EMT during cancer initiation and progression," *Nature Reviews Cancer*, vol. 13, no. 2, pp. 97–110, 2013.
- [54] A. Puisieux, T. Brabletz, and J. Caramel, "Oncogenic roles of EMT-inducing transcription factors," *Nature Cell Biology*, vol. 16, no. 6, pp. 488–494, 2014.
- [55] V. Kuete, O. Karaosmanoglu, and H. Sivas, "Chapter 10- anticancer activities of african medicinal spices and

- vegetables,” in *Medicinal Spices and Vegetables from Africa*, pp. 271–297, Academic Press, London, UK, 2017.
- [56] Y.-L. Chen, S.-Z. Lin, J.-Y. Chang et al., “*In vitro* and *in vivo* studies of a novel potential anticancer agent of isochaihulactone on human lung cancer A549 cells,” *Biochemical Pharmacology*, vol. 72, no. 3, pp. 308–319, 2006.
- [57] A. T. Mbaveng, F. Damen, İ. Çelik, P. Tane, V. Kuete, and T. Efferth, “Cytotoxicity of the crude extract and constituents of the bark of *Fagara tessmannii* towards multi-factorial drug resistant cancer cells,” *Journal of Ethnopharmacology*, vol. 235, pp. 28–37, 2019.
- [58] V. Kuete, L. P. Sandjo, A. T. Mbaveng, M. Zeino, and T. Efferth, “Cytotoxicity of compounds from *Xylopia aethiopica* towards multi-factorial drug-resistant cancer cells,” *Phytomedicine*, vol. 22, no. 14, pp. 1247–1254, 2015.
- [59] A. M. D’Alessandro, A. Mancini, A. R. Lizzi et al., “Crocus sativus stigma extract and its major constituent crocin possess significant antiproliferative properties against human prostate cancer,” *Nutrition and Cancer*, vol. 65, pp. 930–942, 2013.
- [60] H. Jikihara, G. Qi, K. Nozoe et al., “Aged garlic extract inhibits 1,2-dimethylhydrazine-induced colon tumor development by suppressing cell proliferation,” *Oncology Reports*, vol. 33, no. 3, pp. 1131–1140, 2015.
- [61] J. Zheng, Y. Zhou, Y. Li, D.-P. Xu, S. Li, and H.-B. Li, “Spices for prevention and treatment of cancers,” *Nutrients*, vol. 8, no. 8, p. 495, 2016.
- [62] M. Pedersen, B. Metzler, G. Stafford, J. Van Staden, A. Jäger, and H. Rasmussen, “Amides from *piper capense* with CNS activity—a preliminary SAR analysis,” *Molecules*, vol. 14, no. 9, pp. 3833–3843, 2009.
- [63] P. Umadevi, K. Deepti, and D. V. R. Venugopal, “Synthesis, anticancer and antibacterial activities of piperine analogs,” *Medicinal Chemistry Research*, vol. 22, no. 11, pp. 5466–5471, 2013.
- [64] L. Qiao, N. Liang, J. Zhang et al., “Advanced research on vasculogenic mimicry in cancer,” *Journal of Cellular and Molecular Medicine*, vol. 19, no. 2, pp. 315–326, 2015.
- [65] R. Folberg, M. J. C. Hendrix, and A. J. Maniotis, “Vasculogenic mimicry and tumor angiogenesis,” *American Journal of Pathology*, vol. 156, pp. 61–381, 2000.
- [66] A. L. Greenshields, C. D. Doucette, K. M. Sutton et al., “Piperine inhibits the growth and motility of triple-negative breast cancer cells,” *Cancer Letters*, vol. 357, no. 1, pp. 129–140, 2015.
- [67] P. Makhov, K. Golovine, D. Canter et al., “Co-administration of piperine and docetaxel results in improved anti-tumor efficacy via inhibition of CYP3A4 activity,” *The Prostate*, vol. 72, no. 6, pp. 661–667, 2012.